Aeolian Dune Development and Evolution on a Macro-tidal Coast with a Complex Wind Regime, Lincolnshire coast, UK

by

Anne-Lise Montreuil

Doctoral Thesis

Submitted in partial fulfillment of the requirements
for the award of
Doctor of Philosophy of Loughborough University

July 2012

Abstract

Coastal foredunes are natural aeolian bedforms located landward of the backshore and which interact continuously with the beach. Traditionally, coastal dunes have been associated with onshore winds, however they can be found under more complex wind regimes where offshore winds are common – such as the UK East coast, Northern Ireland and New Zealand. This research investigates the ways in which foredune-beach interactions occur under a complex wind regime at a range of overlapping temporal and spatial scales and is innovative in that it explicitly links small-scale processes and morphodynamic behaviour to large scale and long-term dynamics. The study area is the north Lincolnshire coast, East England.

Detailed observations of airflow at three locations under varying wind regimes revealed considerable spatial variations in wind velocity and direction, however it was possible to determine a general model of how foredune topography deflected and modified airflow and the resultant geomorphological implications (i.e. erosion and deposition). During direct offshore and onshore winds, airflow remained attached and undeflected; and distinct zones of flow deceleration and acceleration could be identified. During oblique winds airflow was deflected to become more parallel to the dune crest.

The field sites used are characterized by a seasonal erosion/accretion cycle and a series of increasingly complex models was developed and tested to determine whether it was possible to predict sand volume changes in the foredune-beach system based on a limited number of variables. The model predictions were tested against detailed digital terrain models at a seasonal timescale. The model prediction that best matched the observed (surveyed) sand volume changes included wind speed, direction, grain size, fetch effect controlled by beach inundation and angle of wind approach was accurate to within ±10% for 18 out of 48 tests at the seasonal scale and 6 out of 12 tests over periods of >5 years. A key variable influencing foredune-beach sand volume is the magnitude and frequency of storm surge events and this was not factored in to the model, but may explain the model-observation mismatch over the medium-term on two occasions.

Over the past 120 years historical maps and aerial photographs indicate long-term foredune accretion of approximately 2 m year^{-1} at the three study sites (1891-2010). At this timescale, rates of coastal foredune accretion reflect the low occurrence of severe storm surges and suggest rapid post-storm recovery. The morphological response of the foredune-beach morphology is considered to be a combination of controlling and forcing factors. Process-responses within the system, associated with nearshore interactions and sediment transfer from the littoral drift, are compiled into a multi-scale morphodynamic model.

Important to match appropriate dataset to scale of research question or management plan being explored. In the case of management, long-term records of past activity are necessary to predict the future but also to understand natural responses of system to short-term impact such as storm surge.

Key words: coastal dunes, foredune-beach system, morphodynamics, temporal and spatial scales, wind regime, storm surge, macro-tidal beach, north Lincolnshire.

Research Output

Montreuil, A.L. and Bullard, J.E., submitted. A 150 year record of coastline dynamics within a large-scale sediment cell: eastern England, Geomorphology.

Montreuil, A.L. and Bullard, J.E., 2011. Meso-scale foredune development on a macro-tidal coast with a complex wind regime, Journal of Coastal Research, SP 64, 265-268.

Montreuil, A.L. and Bullard, J.E., 2011. Aeolian dune development and evolution on a macro- tidal coast with a complex wind regime, Lincolnshire coast, UK, Journal of Coastal Research, SP 64, 269-272.

Montreuil, A.L. and Bullard, J.E., 2010. Using high resolution ground survey and LIDAR data to monitor embryo dune development in a conservation area, North Lincolnshire (UK). In: European Association of Remote Sensing Laboratories Symposium, 30th Symposium. UNESCO, 457-461. [Conference proceedings].

Acknowledgements

Contents

Table of Figures

Table of Tables

Chapter 1. Introduction

1.1. Scope and Rationale of Thesis

On many wave dominated sandy beaches, coastal dunes are present. They are natural aeolian bedforms developed at the interface of terrestrial, marine and atmospheric systems (Pye, 1983). Dunes are very dynamic and complex geomorphological features playing significant roles in protecting the coast from storm erosion and risk of flooding (Claudino-Sales et al., 2008, Houser et al., 2008). They are also of great importance from the perspectives of nature conservation, recreation and tourism (Pye and Neal, 1994). On macro-tidal coasts, it is common to have well-developed coastal dune landscapes comprising primary and secondary foredunes strongly interacting with the beach; and established dunes often separated by dune slacks located further inland (Figure 1.1).

A)

B)

Figure 1.1. (A) aerial photographs of coastal dunes along the North Lincolnshire coast in 2010, (B) ground photograph at Brickyard Lane, North Lincolnshire.

In this study, sand dunes formed at the top of the backshore zone by aeolian sand deposition within vegetation are described as 'foredunes' (Hesp, 1988). They are actively coupled to nearshore processes such as wave run-up (vertical displacement of the still water level), storm surge, and tidal excursions, and have a dynamic inter-relationship with the beach (Bauer and Sherman, 1999). Coastal foredunes are the integrated result of a suite of morphological processes and sedimentary responses, which are controlled by factors affecting foredune-beach systems over a wide spectrum of spatial and temporal scales (Sherman, 1995).

The formation of coastal foredunes usually requires strong and prevailing onshore winds, an ample supply of sediment suitable for aeolian transport and the presence of vegetation to trap sand. Until recently, most research has considered that offshore winds contribute a negligible amount of sediment to coastal dune systems, however they can also be found under more complex wind regimes where offshore winds are common – such as the UK East coast, Northern Ireland (e.g. Lynch et al., 2008) and New Zealand (Hesp, 2005).

In comparison with those associated with onshore winds, coastal dunes forming under complex wind regimes that include not only an onshore component, but also significant offshore and alongshore components have received little research attention. The aim of this thesis is to improve understanding of the ways in which foredune-beach interactions occur under a complex wind regime at a range of overlapping temporal and spatial scales.

1.2. Coastal Geomorphic Systems

Coastal processes and landforms can be considered within the framework of the geomorphic system. This consists of several nested and hierarchical compartments, each with its own temporal and spatial scale (Kroon, 1994); interactions take place within and across the different scales and these determine the form and functioning of the geomorphic system (De Boer, 1992). Spatial and temporal scales are coupled, with the result that they are smaller in lower-order compartments and larger in higher-order compartments (Figure 1.2).
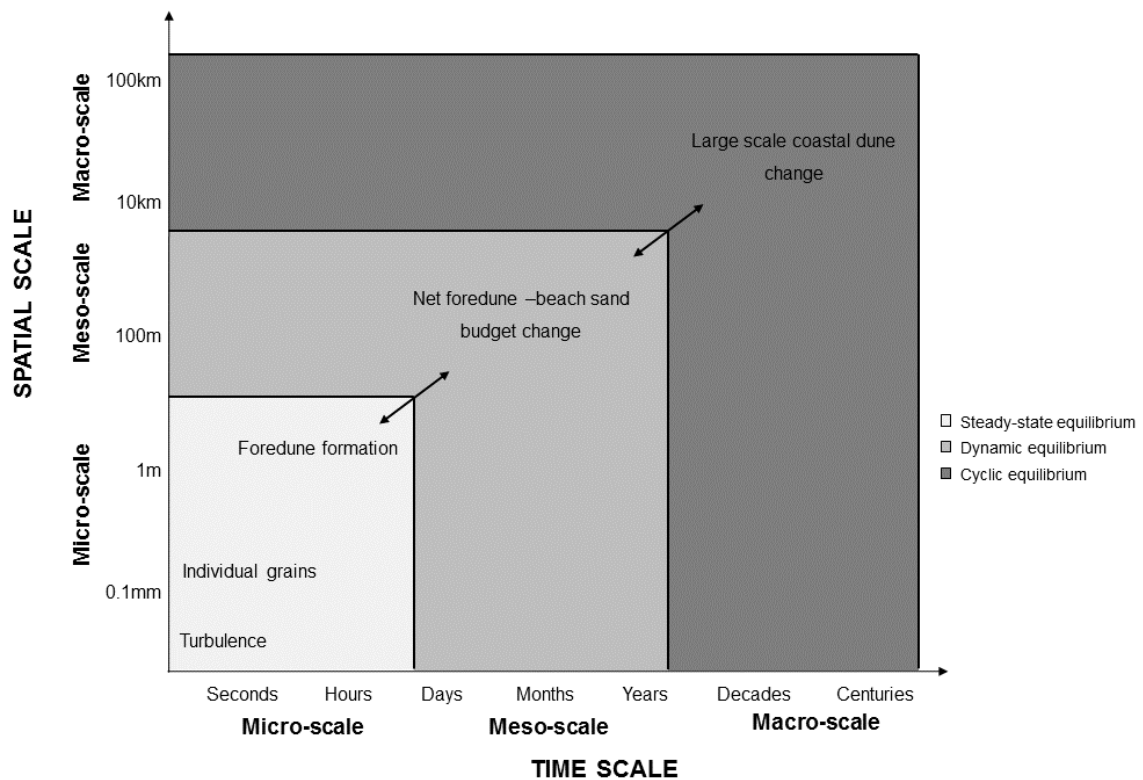
Figure 1.2. Temporal and spatial scales of dune morphology. Arrows indicate the feedbacks between compartments.

Wright and Thom (1977) were the first to apply a systems approach to the examination of coastal morphological change, coastal processes and feedback between different components. They thus introduced the term coastal morphodynamics, defined as a mutual adjustment between the coastal system and environmental conditions such as sediment supply from terrestrial and marine sources, regional geology, which defines the space for coastal evolution, and the external forcing factors which provide the energy (winds, tides, waves) required to stimulate morphological change. At defined scales, aero/hydro-dynamic (fluid) processes, sand transport, and morphology interact

3

and adjust mutually and thus morphodynamic systems can be identified within each compartment (Figure 1.3).

Feedback mechanisms between morphology and energy (fluid dynamics) are fundamental in a morphodynamic system, and play a critical role in governing its evolution (Phillips, 1992). A geomorphic system can be considered both to retain an equilibrium morphology and undergo a progressive change in morphological equilibrium over time (Summerfield, 1991). A negative feedback may reinforce the system to preserve an equilibrium state, but coastal systems rarely attain this state because the variations in dynamic forcing often last a shorter time span than the duration of the relaxation time of the morphology. This effect is more significant at larger temporal and spatial scales, where the interactions between process-response are slow and long-term than at small scales, where a dynamic equilibrium can be reached. Depending on the scale of study, the same process or phenomenon may also be just noise, a component in the morphodynamic interaction process, or an extrinsic condition (De Vriend, 1991). The relationships between the compartments can be difficult to distinguish because the scale dimensions between one level and the next can differ significantly.

Figure 1.3 illustrates the relationships among sediment processes, flow and geomorphological form. For example, airflow processes result from the energy input by wind, which is then transferred to aeolian sand transport. Sand transport causes morphological change, which in turn influences airflow processes. The same feedback processes can be applied to hydro-dynamic processes driven by wave and currents. However throughout most geomorphic systems such interactions between aero-dynamics, sediment transport and morphology are typically non-linear; Baas (2002) describes the coastal system in particular as a nonlinear, dissipative, complex system because wind and wave energy are dissipated in the coastal zone. In addition, relaxation time referred to above is one of two time lags that affect the rate of response of the coastal geomorphic system to forcing factors. Relaxation time is described by De Boer (1992) as corresponding to the interval over which the morphology adjusts to the flow dynamics. It is proportional to the morphological inertia within a system, and is dependent on the intensity of flow processes and the quantity of sediment involved in the morphological adjustments (Kroon, 1994). The second lag is determined by

reaction time, the interval between the change in the force and the beginning of observable morphological change.
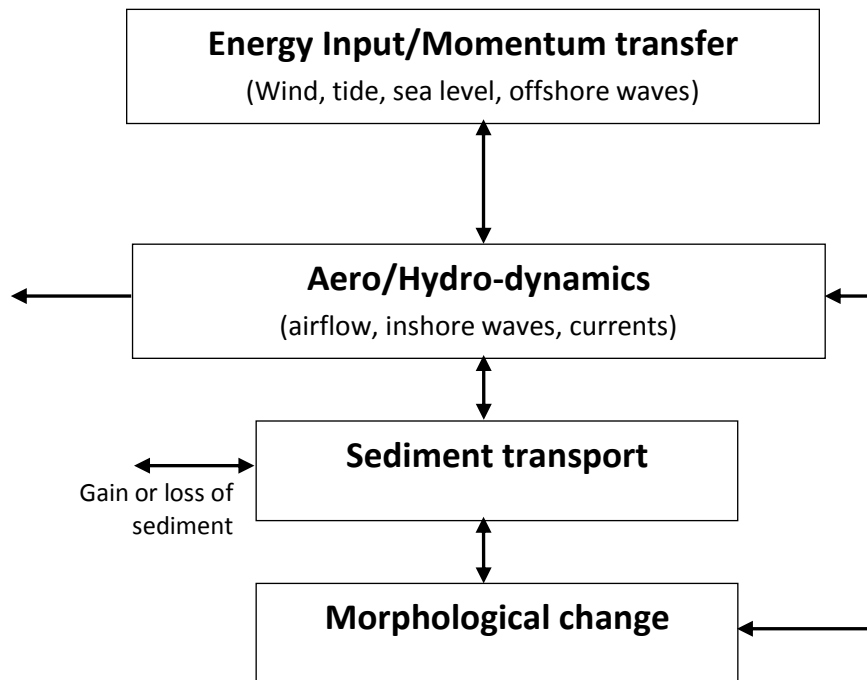
Figure 1.3. Coastal morphodynamic system.

Theoretical approaches to understanding coastal foredune-beach systems at various scales, and linking between different scales are discussed in section 1.6.

1.3. Coastal Dune Systems

1.3.1. Coastal Dune Formation

Coastal dune formation can be initiated in different ways, but dunes generally start to develop near the drift line above the spring high tide on a beach. They form where constructive waves encourage accretion of sand and when energetic/strong onshore winds move dry sands from the shore to the backshore of the beach. The sand is carried until the wind velocity decreases below the transport threshold or surface roughness increases (decreasing wind erosivity) and is deposited against topographic obstacles such as tidal litter, driftwood, or clumps of vegetation on the backshore (Goldsmith, 1985, Hesp, 2002).

Many well-developed dune systems are developed on the downwind margins of oceanic basins. They originated when sea-level was lower and/or when sediment availability was greatest and are often associated with paraglacial coasts. Thus, most of the old dunes in Europe have formed from shelf material that has migrated onshore during the Late-Pleistocene and which was reworked by marine processes during, and following, the Holocene marine transgression (Pye and Neal, 1993, Orford, 2000, Wilson et al., 2001). Similarly, some modern dunes in Western Europe were formed during the Little Ice Age (e.g. Clarke et al., 2002).

The growth and morphology of dunes depends on sand availability controlled by patterns of erosion and accumulation, airflow characteristics and rates of aeolian sand transport (Bird, 2000).

1.3.2. Coastal Dune Morphology

Coastal dunes are generally classified into two main types: primary and secondary dunes (Psuty, 1989). Figure 1.4 illustrates a coastal dune associated with its determinants of formation namely sand-transporting winds, sediment supply and accommodation space.
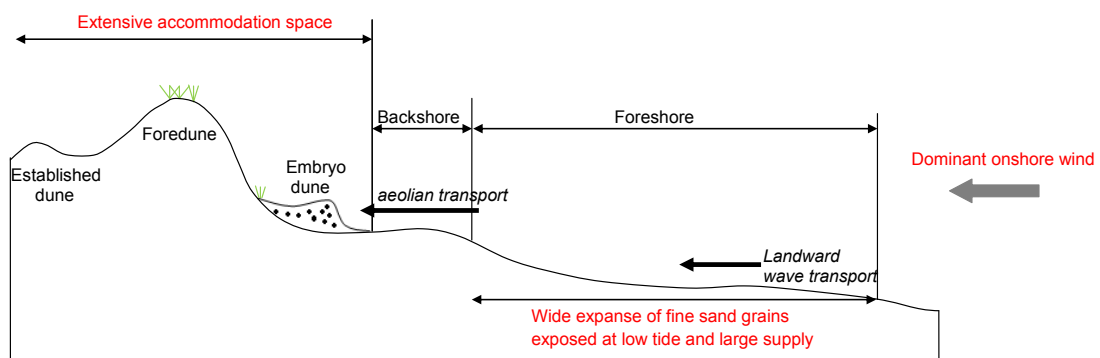
Figure 1.4. Basic components of coastal dune system.

Primary dunes are located landward of the backshore, and can be significantly affected by wave processes (e.g. wave run-up, storm erosion) (Bauer and Sherman, 1999). They include embryo dunes and incipient foredunes (i.e. primary foredune) and interact with the beach as a complex system (Figure 1.5). Embryo dunes are small, often ephemeral dunes approximately 1-2 m high present on the backshore, where aeolian sand has become trapped within the vegetation (Hesp, 1981, 1983). Ongoing accretion can occur following the establishment of pioneer plant species, enabling the embryo

dunes to grow upward and merge to form incipient primary foredunes, which are actively developing shore-parallel and often discontinuous foredunes formed by aeolian deposition within vegetation (Hesp, 1988).
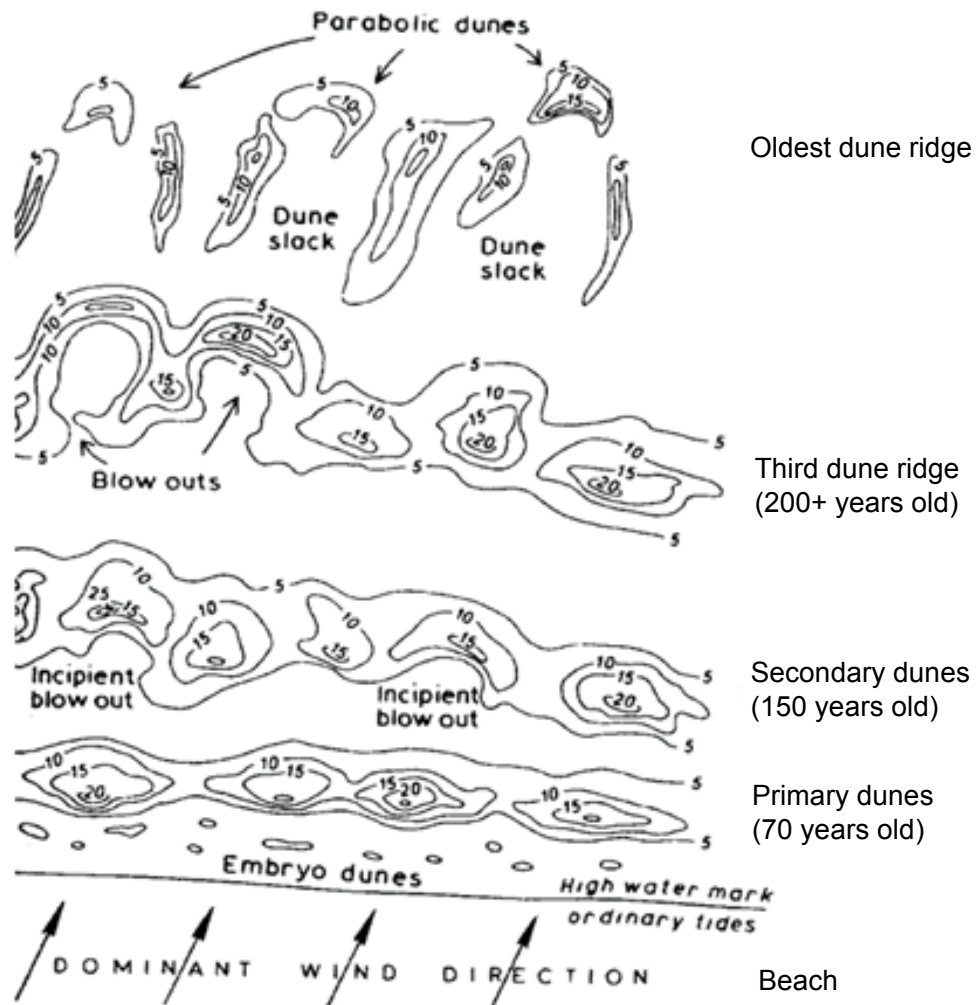
Figure 1.5. Sequential development of the dune ridges in a dune system (Pethick, 1984).

Over time, primary foredunes coalesce and become secondary foredunes, characterized by the presence of successive and mature plant communities (e.g. woody plant species) (Hesp, 1991) and also by their morphological complexity, height, width, age and spatial location (Figure 1.5). Secondary dunes are thus present landward of primary foredunes; they are isolated from deposition and accretion from nearshore processes through coastal propagation of a new incipient foredune which itself may develop to form an established dune (Hesp, 2002). Secondary dunes are frequently stabilized and composed of multiple parallel and vegetated dune ridges sequenced by dune slacks (Carter et al., 1990, Hesp, 1991).

1.3.3. Factors Controlling Dune Formation

The fundamental prerequisites for foredune formation are a strong and favourable wind capable of transporting available sand from the beach to a suitable accommodation space (Pye, 1983, Carter, 1988, Hesp, 2002). Important secondary factors that may influence or modify the size and shape of the coastal dunes include sea-level change, energetic wave, tide environment and vegetation cover (Pye and Tsoar, 1990, Pye, 1993, Hesp, 2002). Figure 1.6 presents the major factors influencing foredune formation and morphology.
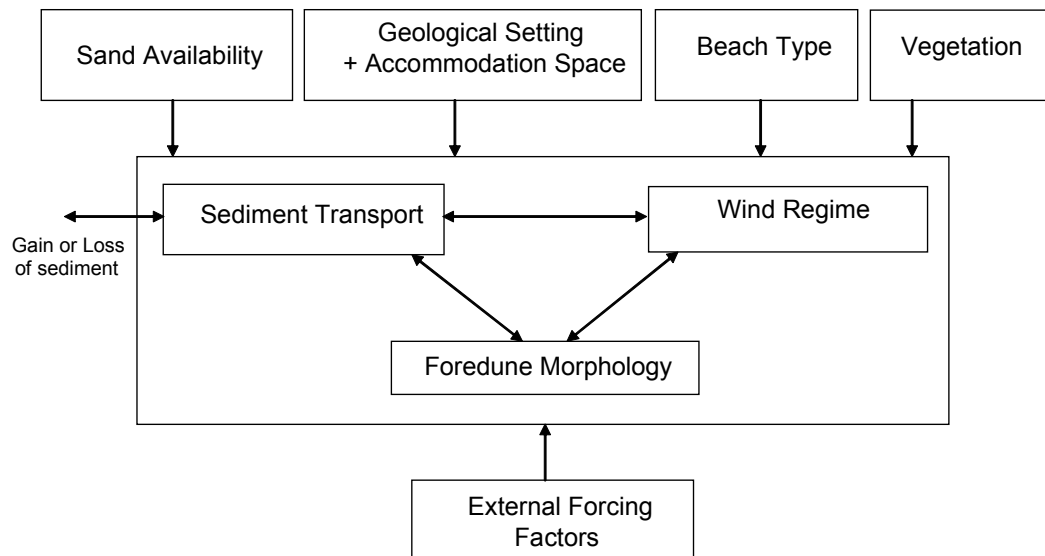
Figure 1.6. Summary diagram of the main factors influencing coastal dune formation.

A. Wind regime: velocity and direction

Foredune formation is controlled by the wind speed, which is the essential driving force for transporting sand from the beach (Sherman and Hotta, 1990). Wind directional variability determines subsequent foredune evolution (Randwell, 1972). The optimal wind conditions for foredune development are a dominant onshore wind direction and speed that exceed the threshold velocity for sand transport (Bagnold, 1941).

Wind direction plays a critical role in sediment supply because it determines the effective beach width, or fetch distance (Davidson-Arnott and Law, 1990). The main sand supply is the dry beach, the width of which varies according to tide. Winds approaching the foredunes at an oblique angle will travel across a wider stretch of dry beach, increasing the potential for sand transport, compared with those approaching

directly onshore (Bauer and Davidson-Arnott, 2002). The wind also transfers energy to waves, playing an important role in the persistence and evolution of coastal dunes by modifying the source of sand available for aeolian transport and modifying the landforms directly through erosion.

B. Sand supply and coastal processes

Foredune formation and development are controlled by the rate and the rhythms of sediment supply. The littoral/longshore drift plays a significant role in carrying sediment provided by both coastal and fluvial systems. Houser and Mathew (2011) report that the foredune development on wide, low-angled dissipative beaches is mainly controlled by the availability of sediment rather than the transport potential.

During extreme storm activity, storm waves dissipate their energy through foredune erosion releasing sand, which may be transported to the shoreface or nearshore zone (Aagaard et al., 2004). This in turn causes, waves to break earlier, reducing the amount of energy available to erode the backshore and the foredunes (Masselink et al., 2006). After fair weather conditions, usually in summer months, sand often returns to the beach driven by constructive waves, and then aeolian processes may renew foredune formation and development (Davidson-Arnott and Law, 1990, Psuty, 1990, Ruz and Meur-Férec, 2004).

Furthermore, the shape and size of the available accommodation space along the coastline play a significant role in determining the area available for sediment accumulation (Pye, 1993, Hesp, 2004) and provide a location protected from wave erosion in which dunes can be built (Aagaard et al., 2007). As a consequence, progradational coasts are optimal for foredune development (Carter, 1988). Jackson et al. (2005) suggest that inherited geological factors are likely to be play a more important role in determining beach morphology than contemporary dynamics and will affect nearshore wave transformations, sediment abundance and accommodation space.

C. Secondary factors

Whilst wind regime and sediment supply are the main determinants of coastal dune formation, a range of other secondary factors can also influence dune characteristics. These include changing sea level, vegetation characteristics, wind-wave climate, storm surge frequency and magnitude, and anthropogenic activities (Pye et al., 2007). At regional and long time scales of centuries to millenia, sea level rise or fall may have a significant impact on coastal dune system behaviour, and morphology (Carter et al., 1989, Clemmensen et al., 1996). Sea level change redistributes coastal sediment over large zones and can control local levels of wave attack. During a period of rising sea level, coastal erosion is highly amplified, releasing a large quantity of sediment. This material may be transported along the coast and under an appropriate wind regime may accumulate to build a series of foredunes, which may in turn develop to form a dune plain over time (Carter, 1988, Davidson-Arnott and Law, 1996). However, a rising sea level also reduces the beach width for sand transport and so may cause foredune erosion and landward migration. In contrast, during falling sea level, sediment is released from the continental shelf and may move onshore, increasing the beach width and hence potential sand supply to the foredunes. The most favourable condition for foredune formation is a slowly falling sea level (Carter, 1991). Sea level change can also influence ground water table levels which in turn determine the base level for deflation within the coastal dune field.

Vegetation is a vital factor in foredune formation and stabilisation, since it helps in constructing sand dunes by trapping wind-blown sediment, and plant roots and rhizomes can bind sediment, stabilizing it. The drag effect imposed by vegetation on airflow can also control the dune form itself. Short and Hesp (1982) classify established foredunes into five morpho-ecological stages based on the proportion of vegetation cover. This ranges from foredunes dominated by plants (fixed, linear ridges) to those with no plants (free, transverse blowouts, barchanoid dunes); partially-vegetated dunes have transitional morphologies characterised by fragmented topography (Figure 1.7). Each foredune stage corresponds to "a modal morphology typical of a range of morphologies […] and vegetation cover" occurring around that stage (Hesp, 1988, p20).
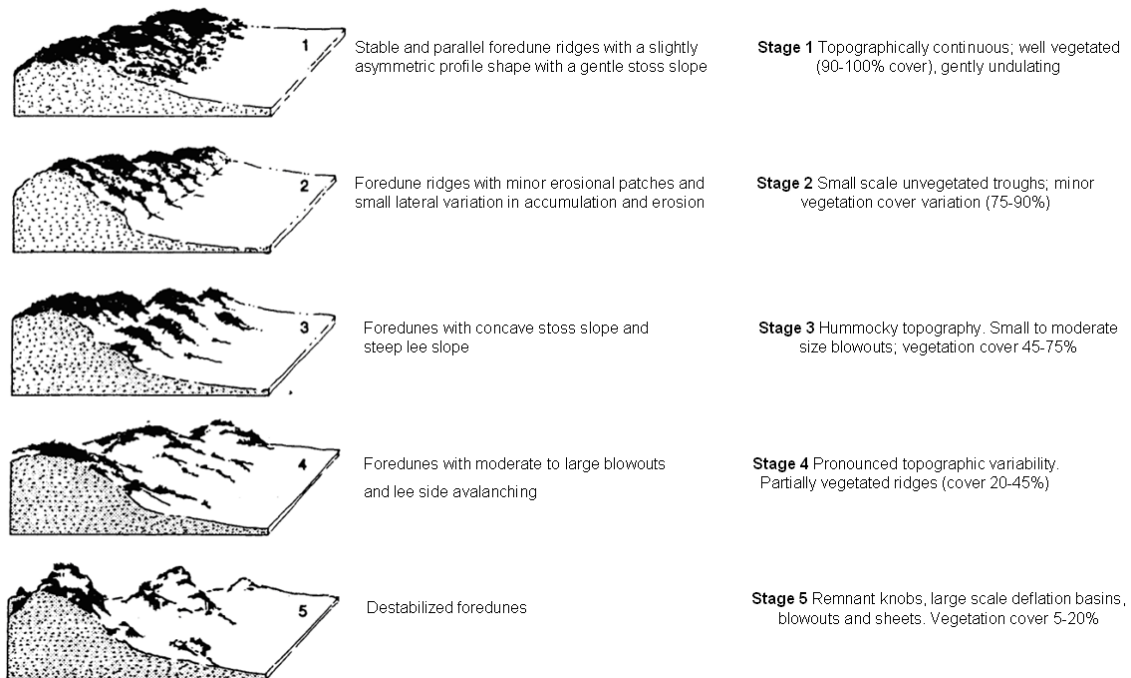
Figure 1.7. Morphological classification of coastal dunes based on the proportion of vegetation (modified from Short and Hesp, 1982).

The development and morphology of coastal dunes are highly controlled by the nature of the pioneer plants including mode of colonization, morphology, resistance to sand blasting and salt tolerance, and other characteristics (Trenhaile, 1997). During foredune formation and development, different plant communities will succeed each other. As a result, further inland sand-fixing plants will be substituted for sand-trapping plants. In consequence, vegetation is a distinct coastal dune feature, playing a crucial role in dune morphology and mobility.

1.4. Foredune-Beach Interactions

Foredunes and beaches are two environments "strongly coupled and mutually adjusted" (Sherman and Bauer, 1993, p413). Sediment exchanges between foredune and beach systems are governed by complex and continuous feedback mechanisms. A number of conceptual models of coastal dune development has been proposed over the last few years. Short and Hesp's (1982) model relates the modal morphodynamic beach state to the morphology of coastal dunes (Table 1.1). This conceptual model mainly focuses on spatial relations, however it implicitly includes time.

Table 1.1. Summary of Short and Hesp's (1982) conceptual model relating beach morphodynamic states and coastal dune dynamics.

	Modal nearshore morphodynamic state		
	Dissipative	**Intermediate**	**Reflective**
Frequency and height of wave attack	Low (<1 m)	Moderate	High
Sand transport rates	High	Moderate to Low	Low
Dominant coastal dunes	Large-scale transgressive dune sheets	Parabolic dunes and blowouts	Linear foredune scarping with small blowouts
Foredune size	Large (15-30 m high and >100 m wide)	Moderate to Small	Small (<10 m high and <50 m wide)
Beach mobility index	Low	Low to Moderate	Low
Potential frequency (>100 years) of total foredune destruction	Moderate	Low to high	Low

Short and Hesp's classification states that onshore aeolian sand transport rates are potentially the greatest from a dissipative beach, moderate from an intermediate beach and lowest from reflective beaches. The reasons are that a dissipative beach is wide with a low slope, and presents a larger beach width, abundant and finer sediment (Jackson and Cooper, 1999, Saye et al., 2005, Lynch et al., 2006) whilst reflective beaches are typically steep and narrow leading to greater flow disturbance and a shorter fetch. Additionally, foredune erosion by waves occurs less frequently on dissipative beaches than on reflective beaches. A wide beach may reduce the impact of storm surge activity by an increased dissipation of wave energy compared with a reflective and narrow beach. It eventually might favour the formation of a new foredune by protecting colonizing vegetation (Saunders and Davidson-Arnott, 1990) and hence

by generating a source area for aeolian sand supply to the foredune (Davidson-Arnott and Law, 1996). Therefore, the tendency of the dissipative beach is to be a relatively stable system with a low frequency of shoreline accretion-erosion events and spatially continuous, parallel, back-beach dune ridge scarps (Short and Hesp, 1982). Sherman and Bauer (1993) reported that a dissipative beach may receive 140% more sand than a reflective one. Thus, flat and wide dissipative beaches give rise to the optimal conditions for the development of large and vegetated foredunes. Such foredunes develop over extended time scales and so reach equilibrium in their morphology only over the longer term. By contrast, intermediate and reflective beach systems are often characterized by moderate or low sediment supply; foredunes may be eroding and associated with blowouts due to wave scarping processes and rip-currents. On intermediate and reflective beaches, this suggests that the level of wave energy is likely to be a more important factor in determining beach and foredune instability than the wind. Consequently, to model foredune development and evolution it is crucial to consider sediment exchanges between foredune and beach and the impacts of nearshore processes (Bauer and Sherman, 1999, Houser, 2009).

At the time scale spanning from 1-year to decades, Psuty (1992) found that foredune development is dependent on the availability of sediment from the beach, and from transported material from eroded coastal cliffs, estuaries and other sources. He proposed a model in which foredune development is linked to variations in the availability of sediment from the beach, which is in turn controlled by sediment supply from littoral drift (Figure 1.8).
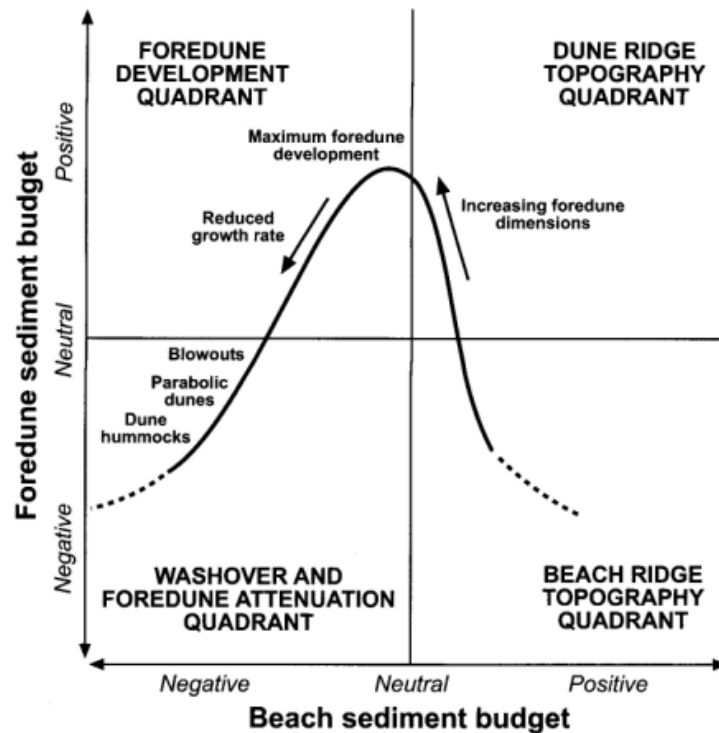
Figure 1.8. Morphologic evolution of the foredune depending on the foredune-beach sediment budget (Psuty, 1992).

Psuty (1992) claims that optimal conditions for foredune development occur when the beach sediment budget is neutral or slightly negative and the dune sediment budget is positive. Beach erosion and retreat may benefit the foredune sediment budget by destroying stabilizing vegetation on the seaward dune faces and re-exposing sediments to aeolian processes (Hesp, 1988). However, sediment supply to the foredune corresponds to a loss from the beach, and thus over the longer time period (years and decades) foredune development necessitates a net positive provision of beach sediments by aeolian processes; otherwise a negative feedback cycle occurs through narrowing of the beach, scarping and eroding the dune by wave action (Psuty, 1988). An increasingly negative beach supply interrupts the development of foredunes but promotes the formation of hummock dunes and blowouts which may become larger over time (Hesp, 1999). Nonetheless, a positive beach sediment budget affects the way in which the continuous propagation of the shoreline sets a limit to the amount of sand that can accumulate on a foredune. Hence, extremely rapid beach accretion leads to the development of low foredune ridges. Psuty's model identifies four possible situations of sediment budget in foredune-beach systems and thus it represents a continuum of phases at both temporal and spatial scales, in which foredune development is the consequence of the changing combination of beach and foredune

14

sediment availability. Sherman and Bauer (1993) expanded Psuty's (1992) model to include steady-state sediment budgets for foredune-beach systems, with little alteration in sediment volume. Recently, Houser (2009) proposed a synchronization model of transport and supply events for which the foredune development is quasi-periodic in response to changes in the beach and shoreface/nearshore state, and further predictable by considering it within the beach-nearshore system.

As a result of these interactions, foredune-beach systems are very active geomorphological systems and continuously evolve over time. Foredune development and evolution may take place over a medium (from year to decadal scale) or a long (century scale) time scale. Medium term coastal changes are often controlled by specific micro-scale triggers (days) via storm surge events. A severe surge storm or a sequence of surge storms can dramatically erode the foredune over a short period of hours, while its recovery is often much slower, taking place over several years (Thom and Hall, 1991, Anfuso, et al., 2007). The foredune accretion process is typically much less rapid than erosion and as a result, severe storms can produce more significant morphological foredune changes than are achieved during many years of non-storm conditions (Morton et al., 1995). Coastal dune morphologies change through a succession of morphological states in which, at any time they may be aggrading, eroding, or in equilibrium over a short time period. They are thus controlled by flexible and dynamic constraints of sand supply and aeolian transport between foredune and beach.

1.5. Dynamics of Foredune-Beach Systems under Offshore Winds

The efficiency of onshore winds is widely recognized for foredune formation, and many researchers have considered offshore winds as a negligible contributor of sand to foredune-beach systems (e.g. Sarre, 1989, Nordstrom et al., 1996, Arens, 1997). This is due to low sediment input into the system caused by the sheltering effect of the foredune, resulting in an incident wind speed dropping below the threshold necessary for the entrainment of sediment (Gares et al., 1993). Nevertheless, recent studies indicate that offshore winds can play an important role in foredune-beach system evolution through aeolian sand transport and may contribute to the system

maintenance by recycling sand to the backshore for incipient foredune growth, and infilling erosion scarps (Walker et al., 2006, Lynch et al., 2009). Nordstrom et al. (1996) found that the foredune affects offshore sand transport with rapid and spatial transitions along the foredune-beach profile. The authors suggested that offshore transport cannot occur on the seaward side of the foredune due to its topographic effect. Wal and McManus (1993) also found that offshore winds contribute directly and indirectly to the foredune. The recent studies of Hesp (2005) and Lynch et al. (2008, 2009, 2010) underscore the potential of offshore airflow as a important process in foredune-beach system, describing the occurrence of well-developed foredunes related to the operation of large scale flow separation cells that locally reverse the prevailing offshore wind and cause onshore movement of sediment. Such micro-scale airflow and sand processes are discussed in further detail in Chapter 3.

Although offshore winds are now recognized in coastal dune formation, the relationship or balance, amongst different wind components is still poorly understood. These include not only onshore and offshore winds but also alongshore winds which move sand along the coastline parallel or sub-parallel to the foredune-beach interface. The implications for foredune development of the coupling and interaction of foredune-beach processes at different temporal and spatial scales are still not well-understood, particularly in macro-tidal environments. At present, most research on foredune-beach interactions has concentrated on micro- or meso-tidal beaches (e.g. Davidson-Arnott and Law, 1990, Nordstrom et al., 1996, Hesp et al., 2005, Lynch et al., 2008, Delgado-Fernandez and Davidson-Arnott, 2011). Nonetheless, macro-tidal beaches are characterised by a distinct set of attributes which is expected to influence foredune-beach interactions in different ways. For example, this type of beach usually has wide and flat intertidal zones (tidal range >4 m), which are likely to promote aeolian sand transport because fetch is unlikely to be a limiting factor. However, the tidal zone is often wet due to tidal inundation and also the presence of intertidal bars may reduce the benefit of having a wide 'feeder' zone due to the often water-filled troughs (runnels) that separate them (Anthony et al., 2009).

1.6. Theoretical Approaches to Understanding Coastal Foredune-Beach Systems

The temporal dynamics of the foredune-beach system can be considered at scales from fractions of a second to centuries, while the spatial scales of this system reflect the behaviour of single sediment grains up to individual foredunes to whole coastlines. In this thesis, micro-scale is defined as time and space scales from seconds to days (short-term) and millimetres to hundreds of metres respectively (Figure 1.9). Micro-scale research thus focuses on the processes of sediment transport by wind and provides an insight into specific details of dune geometry or characteristic spacing (Sherman and Bauer, 1993). However, it provides relatively little information about the dynamics of foredune evolution. Meso-scale is defined here as from days to decades (medium-term) and hundreds of metres to less than ten kilometres, emphasizing the gross sediment fluxes and net budgets for foredune development. Finally, the macro-scale encompasses decades to centuries (long-term) and larger than tens of kilometres. Macro-scale studies concentrate on coastal dune evolution in relation to sea level changes (Carter, 1991, Sherman and Bauer, 1993, Hesp, 2002), and the influences of geological and sedimentary processes within the coastal cell (Sherman and Bauer, 1993).
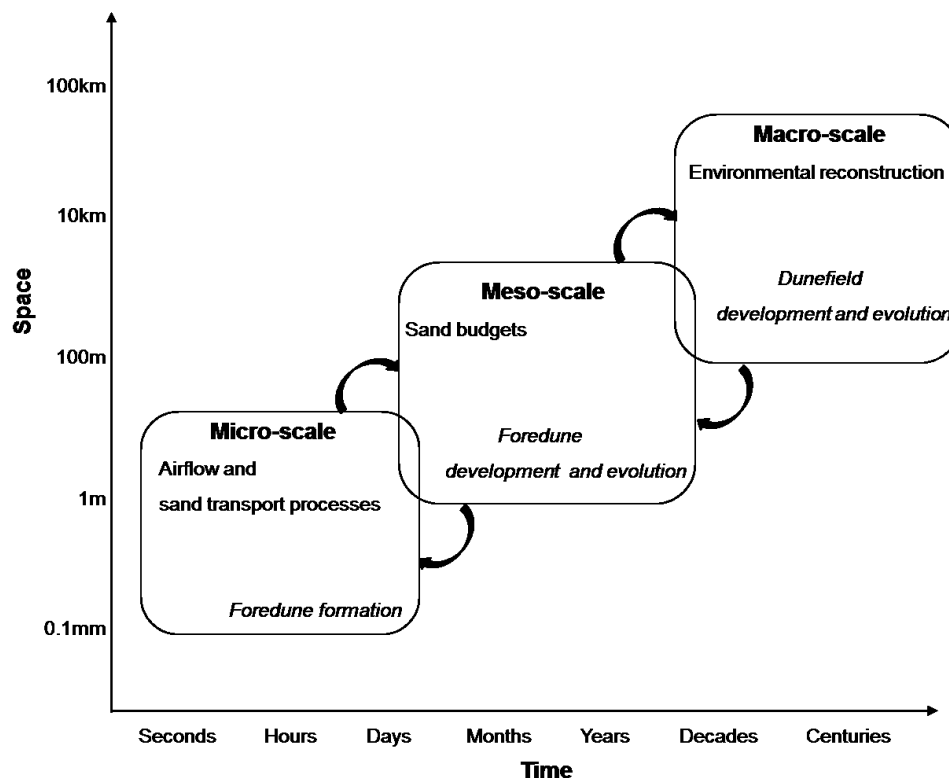
Figure 1.9. Primary scale relationships within a coastal geomorphologic system with a hierarchy of temporal and spatial scale compartments. Arrows represent the process-response feedbacks.

Many studies of foredune dynamics have been restricted to single scales and compartmentalised, inhibiting the development of a better understanding of the whole coastal dune system. The character of processes and form responses differs within the micro-, meso-, and macro-scale domains, which presents a challenge when attempting to extrapolate findings (Horn, 2002). To link the scales, three-pronged approaches were suggested by Sherman (1995, p339) for coastal dune study: "identification of key controls on dune development [systemic approach], measurement of those controls [synoptic approach], and synthesis of data describing past and present conditions [synthesis approach] and used as calibration points will improve the viability of coastal dune models [...] and the reliability of predictions across a range of geomorphological scales". According to Sherman's approach, together systemic and synoptic approaches presume that the formation of coastal dunes is predictable with an understanding of processes over the shorter time scales, and can be predicted through the application of the principles of physics and fluid dynamics. This involves obtaining simultaneous field or laboratory measurements of a completely specified sediment transport system in order to quantify relationships and calibrate models. The synthetic approach operates over longer time scales; it starts with the foredune itself and attempts to reconstruct the processes and environment history. The intent of the synthetic approach is to identify the events and conditions that contribute most significantly to foredune development and morphological changes over meso- to macro-scales.

Bauer and Sherman (1999) also present two common but divergent research strategies into foredune dynamics. The mechanistic-reductionist approach is concerned essentially with short-term process measurements of aero-dynamics and aeolian sediment transport in the complex system. The holistic-constructivist approach includes large and long-term studies of sequential foredune development and morphological equilibrium relationships. However, both research strategies are significant and necessary because they make it possible to gain complementary perspectives on coastal dune system behaviour.

To achieve increased understanding of coastal dune system dynamics, all temporal and spatial scales should be considered. However, this is a major problem and challenge in coastal dune system studies, as well as in other geomorphological systems (Sherman, 1995, Phillips, 2003). One of the main adopted strategies is up-scaling through the use of process-based sediment transport models, so that findings

from one spatial and temporal scale are integrated to another (Terwindt and Wijnberg, 1991). The results of this research can differ by several orders of magnitude due to the large differences in scales and the inherent nonlinear behaviour of coastal geomorphological environments (Sherman et al., 1998). Consequently, process-based understanding of a coupled foredune-beach system necessitates mining research from diverse sources covering a spectrum of temporal and spatial scales.

1.7. Aim and Objectives

The aim of the present study is to improve understanding of the ways in which foredune-beach interactions occur under a complex wind regime at a range of overlapping temporal and spatial scales. More specifically, the objectives are, for a single coastal dunefield:

(1) Identify near-surface airflow processes operating on the beach and dunes under different wind regimes (onshore, offshore, alongshore) at the micro-scale;

(2) Use the findings from (1) to develop a conceptual model describing the patterns of sand transport and deposition under different wind conditions;

(3) Compare seasonal measured and predicted rates of sediment supply in order to define the roles of different wind directions in dune formation at the meso-scale;

(4) Generate a time series of digital terrain models of the dunefield and of historical foredune position to determine the annual changes and long-term evolutionary tendency and to investigate the relative importance of different external factors in driving those changes;

5) Up-scale from micro- to macro-scales to contribute to the wider understanding of the foredune-beach geomorphological system.

1.8. Research Approach

As is typical of geomorphological systems, the study of coastal dune landforms has essentially been scale dependent, because research methodologies have been scale dependent (Sherman, 1995). However, recent advances in aeolian and geospatial science offer significant potential for more robust multi-scale integrations of aeolian coastal dune system dynamism and development at a range of spatial and temporal scales (Thomas and Wiggs, 2008, Woolard and Colby, 2002). The study investigates coastal dune system dynamics over a range of temporal and spatial scales in a macro-tidal environment along the north Lincolnshire coast in England (Figure 1.10). This present research will complement the multi-scale studies which have been carried out on the intertidal ridges and runnels characterizing macro-tidal beaches along this coast (Masselink and Anthony, 2001, Kroon and Masselink, 2002, Van Houwelingen et al., 2006, 2008). A framework of four main strategies with appropriate methodologies is adopted for identifying, measuring and developing integrative syntheses of foredune-beach interactions at different spatio-temporal scales (i.e. using systematic, synoptic and synthetic approaches). High resolution airflow and sediment transport measurements provide information concerning micro-scale processes (seconds to a day); seasonal topographic surveys and environmental monitoring stations are used to determine meso-scale (season to a year) foredune-beach interactions. The establishment of reliable predictions of potential rates of foredune sediment supply is used to try and bridge the gap between micro- and meso-scale interactions. Analysis of topographic profiles, aerial photographs and LIDAR data collected with a frequency from years to decades, in conjunction with an investigation of external forcing factors, provide an insight into meso-scale coastal development and evolution. The investigation from meso- to macro-scales (decades to a century) is undertaken by reconstructing the long-term evolution of the foredunes in relation to historic external forcing factors and synoptic weather climate. An advantage of the chosen site (discussed further in Chapter 2) is that one of the longest data sets of topographic beach elevation and oceanographic measurements in the UK is available make such a long-term investigation possible.

Sherman (1995) addressed the issue of scale dependent discontinuities existing at the conceptual boundaries. In this study, the approach of overlapping temporal and spatial scales bridges the scale boundaries, which makes it possible to up-scale process-responses within the coastal dune system. Additionally, the viability of the approach is supported by the fact that micro-scale process effects could last for longer timescales

(Sherman, 1995), and thus control the general evolution of the foredune system. The up-scaling is also considered by making rational assumptions and reasoning about which factors are important or unimportant, thus improving the tractability of a number of issues. For instance, when investigating the meso-scale foredune evolution, airflow processes and other environmental factors controlling aeolian sand transport processes can be ignored in large part because they can be subsumed within the sediment budget calculations (Sherman and Bauer 1993). The overall approach is to deliver a reliable, interpretable and comprehensive coastal dune system representation across micro- to macro-scales. The approach will be simple, when compared with one that includes all the separate components, in that it will only include the key factors and process-response.
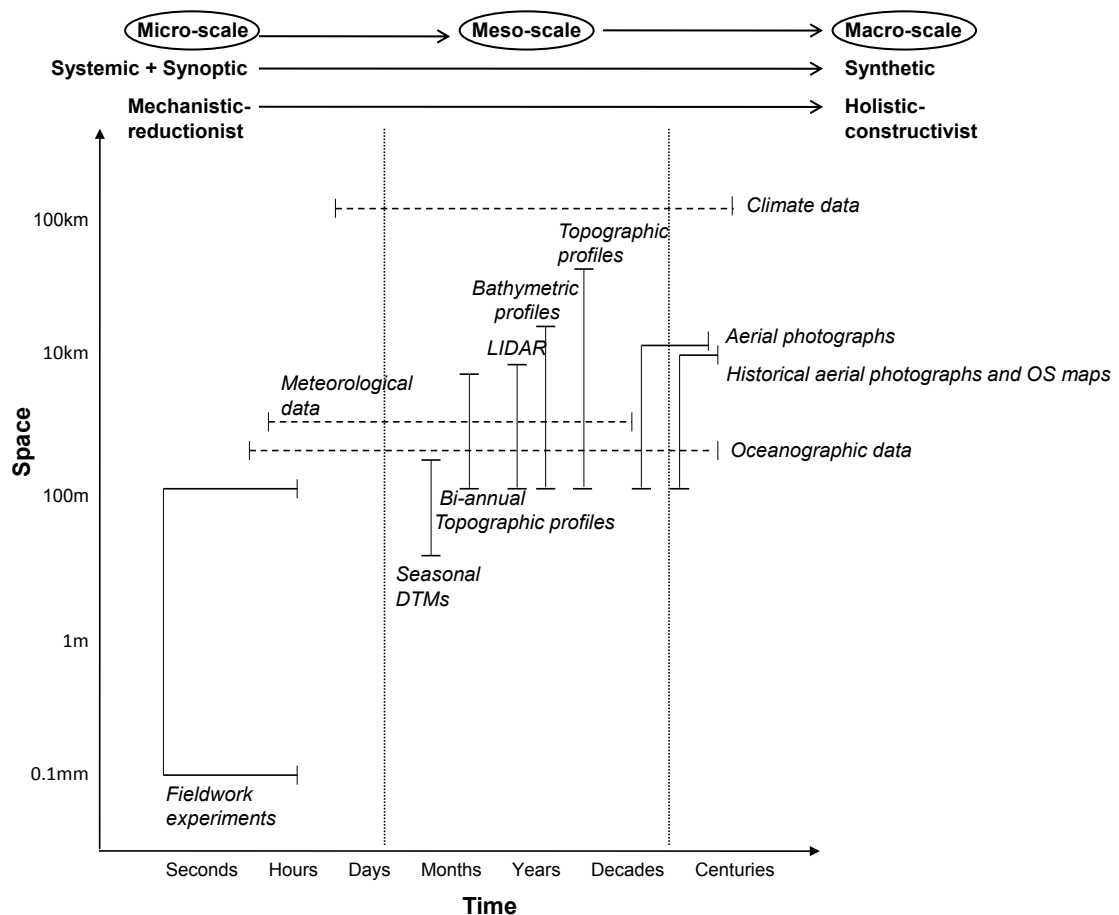
Figure 1.10. Schematic showing the research approach linked to the different methodologies applied. As the spatio-temporal scales of interest increase, the approach changes from synoptic to synthesis (Sherman, 1995), or from mechanistic-reductionist to holistic-constructivist (Bauer and Sherman, 1999).

1.9. Outline of the Thesis

The introduction provides a prologue to the thesis, giving a general overview of the coastal geomorphological system, coastal dune formation, morphology and its controlling factors, it describes the research aims, objectives, presents the project approach and strategies and explains the layout of the thesis. Chapter 2 describes the coastal geomorphology, meteorology and oceanography of north Lincolnshire where the study was carried out at three sites with distinct morphological characteristics. Chapter 3 examines micro-scale airflow and sediment transport processes in order to identify the near-surface airflow properties at the three sites under different wind conditions. Chapter 4 presents the seasonal results of morphometric and volumetric changes of the foredune-beach systems based on ground topographic surveys. These were related to seasonal environmental, meteorological, and oceanographic conditions during the monitoring year-period, in order to investigate the response of morphology to these factors. This is followed by a simple approach to modelling seasonal sand supply into the foredune-upper beach system (Chapter 5). Meso-scale foredune evolution at the three selected sites is discussed next, based on ground topographic survey profiles, aerial photographs and LIDAR surveys (Chapter 6). Chapter 7 examines the long-term foredune evolution over a ~120 year period, and investigates the inter-linkages between coastline and nearshore long-term behaviour within the whole sediment cell with sea level and climate forcing trends. Chapter 8 embeds the findings of the preceding chapters in an up-scaling model of the foredune-beach morphodynamics; and also presents the concluding comments of the thesis.

Chapter 2. Study Area

The research aims and objectives detailed in Chapter 1 will be addressed in relation to a field site in the United Kingdom, but it is anticipated that many of the findings and outcomes will be applicable or transferable to other similar sites worldwide.

2.1. UK Coastal Dunes

Coastal dunes occur extensively around the Western Europe coastline. They are very common in the United Kingdom (Figure 2.1 and Table 2.1); dune type and morphology vary considerably in relation to their sedimentation, climatic setting both past and present, and ecological parameters. Although some UK coastal dune systems occupy areas of more than 5 km^2, they are more often smaller (Doody, 1991). The UK coastal dune systems have a scattered distribution and range in size from 2-21 km^2 in England, 1.25-17 km^2 in Wales and 0.75-17.8 km^2 in Scotland with additional small dunefields on offshore islands. Coastal dune height depends on the environmental setting and ranges from 1 m to more than 20 m (Pye et al., 2007).

The largest coastal dune systems occur on the west coasts where the prevailing westerly winds reinforce the dominant onshore winds, allowing well-vegetated foredunes to develop. However they are also present on the east coast, notably in Northumberland, Lincolnshire and East Anglia, where the wind regime is more complex and prevailing offshore winds and dominant onshore winds are in opposition. Regardless of wind regime, the most well-developed coastal dunefields are associated with the dissipative beaches characteristic of macro-tidal environments with a mean spring range of greater than 4 m.

Coastal dunes always changing, 40% eroding, 30% experiencing stability and nearly 30% prograding of the UK dune frontages (Pye, 2007, SNH, 2000), changes in sea level and storminess likely to affect the rate and nature of these changes and the same trend is occurring in Western Europe. Predicted regional changes in sea-level and storminess are likely to accelerate this erosion in the next century making it likely that coastal management strategies will need to be adapted. To maximize the success of such strategies they will need to be based on sound understanding of coastal dune processes. This research contributes to this understanding by investigating the interaction of beach and dune processes and landforms over a range of temporal and spatial scales.
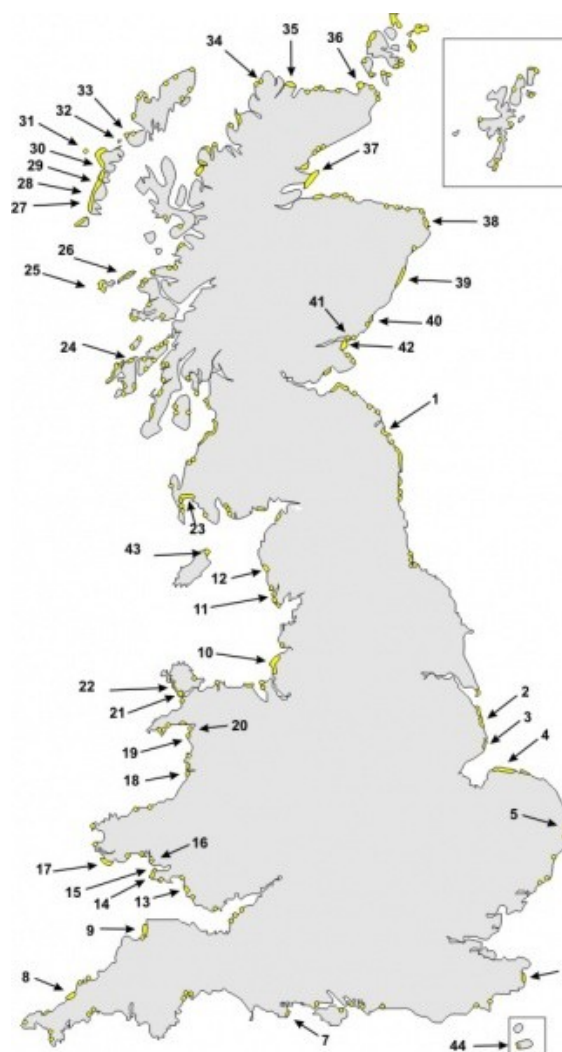
Figure 2.1. Location of the main coastal dune systems in the United Kingdom (Doody, 1991).

Table 2.1. Major coastal dune localities in England – numbers refer to locations shown in Figure 2.1 and other important sites are listed in Appendix 2.1 (Doody, 1991).

Site	Location	Size (km^2)	Habitats
1	North Northumberland Dunes	5.54	Sand flats
2	Saltfleetby-Theddlethorpe	3.67	Saltmarshes and sand beaches
3	Gibraltar Point	2.79	Saltmarshes and sand beaches
4	North Norfolk Coast	7	Beaches plus sand flats
5	Winterton	3	Beaches plus sand flats
6	Sandwich and Pegwell Bay	4.8	Saltmarshes and sand beaches
7	Studland Heath	2.04	Saltmarshes
8	Penhale	5.42	Sand beaches
9	Braunton Burrows	8.8	Sand beaches
10	Sefton Coast	21.09	Beaches plus sand flats
11	North Walney	3.4	Sea inlets
12	Drigg Point	3.44	Saltmarshes and beaches plus sand flats

Over geological timescales, the evolution of the UK coast has been primarily driven by changes in (relative) sea level. At the end of the glacial maximum, around 18,000 years ago, eustatic sea level began to rise rapidly from c. 120 m below present sea level, attaining its present level around 4000 years ago (Fairbanks, 1989). The effect of this sea-level rise on the UK coastline must be considered in combination with the uplift and subsidence effects associated with glacio-isostatic fluctuations, in particular isostatic rebound of the formerly glaciated areas in the northern of England. Associated with the solid geology, the drift geology has played an important role, and is primarily a legacy of the most recent (the Devensian) and penultimate (the Wolstonian) glaciations. Over the deglaciation period, large amounts of glacial and paraglacial sediments, composed of different sediment sizes from mud to boulders, were left behind by the retreating glaciers (Balson and Jeffrey, 1991). The coarser material was likely deposited on the present-day continental shelf, then moved onshore during the post-glacial transgression and integrated to the beach, and other coastal features (Orford et al., 2002). Nowadays most of the marine sediment source has been depleted and offshore sediment supply to the coast by natural processes has been strongly reduced. In contrast, much of the material that was deposited on the present-day land is still present (Bray and Hooke, 1997). On the east coast, the finer material of these eroded glacially-derived sediments (mud and silt) are being left on saltmarshes and tidal flats near estuaries, or are driven by tidal currents to the southern North Sea (Robinson, 1968). The coarser fractions, mainly composed of sand and gravel, are incorporated into the littoral system and transported along the coast. The present Lincolnshire coastline is entirely composed of superficial deposits and has formed during the last 10,000 years. During this period, boulder clay covered the ancient Chalk wave cut platform (Brampton and Bevan, 1987). Until the 13th century, the coastline was protected from extreme marine action and floods by offshore banks of morainic material, however the breaching of this barrier led to a rapid coastal recession corresponding to the present-day coastline position (Posford-Duvivier, 1996). The coastline was then exposed to the open sea and wave and tidal conditions in the North Sea have continued to adjust the coastline over the following centuries.

2.2. Morphological Setting

The convex north Lincolnshire coast extends c. 16 km from Donna Nook to Mablethorpe (Figure 2.2). This east facing coast forms the southern part of the ebb-tidal delta of the Humber estuary (Pethick, 2001). It comprises a relatively recent low lying coastal plain composed of superficial deposits which were produced by the retreat of the last ice sheet covering Northern Europe (Swinnerton, 1936, Robinson, 1984, Brampton and Bevan, 1987).

Historical relics of offshore and nearshore sand banks are present from Donna Nook to the north of Mablethorpe, and there is also a subtidal bank along the study coast. The intertidal zone is 500-2500 m wide characterized by multiple-intertidal bar and trough (ridge-runnel) systems (Masselink and Anthony, 2001). It is predominantly controlled by tidal and wave energy conditions, and the input of sediment, allowing the formation of sediment stores in the form of ebb-tidal deltas (Van Houwelingen, 2005). The north Lincolnshire coast has experienced a long-term accretion (King, 1972, Halcrow, 1988, Montreuil and Bullard, 2011). The width of the coastal plain attains its maximum in the northern part of the study area and progressively decreases toward the south.

Coastal foredune development is variable along this coast. In the southern part where the intertidal beach is relatively narrow (<1 km), well-developed and regular (secondary) foredune ridges are present (Figure 2.3). By contrast, foredunes are low and isolated fronting saltmarsh or located on top of gravel ridges in the northern part.

This thesis is concerned with coastal dunes along the north Lincolnshire coast, and attention is focused on three sites along Theddlethorpe beach which is classified as a National Nature Reserve and Site of Special Scientific Interest (SSSI). These sites from the north to the south are referred to as Brickyard Lane (BL), Theddlethorpe St Helens (TSH), and Mablethorpe North End (MNE) (Figure 2.2). They have been selected for their particular morphological characteristics and environmental characteristics. Within the study area, the inland zone consists of established dunes and landwards of these the area is under agriculture.

Figure 2.3 shows typical foredune-beach profiles at the three sites. All vertical heights are referenced to Ordnance Datum Newlyn (ODN) corresponding to the mean sea level (MSL). Here, and throughout the thesis foredune-beach profiles are plotted with considerable vertical exaggeration to highlight topographic features.
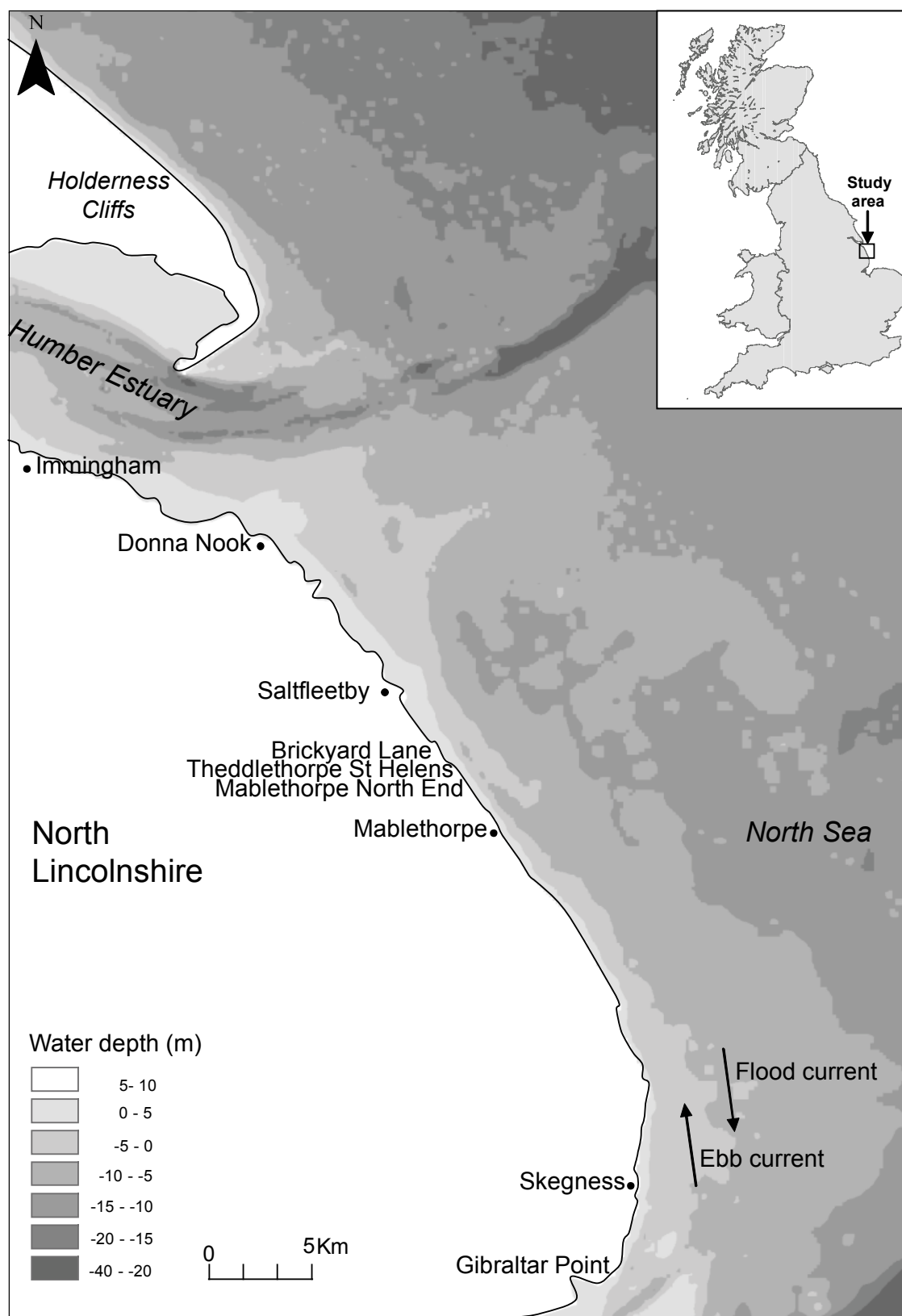
Figure 2.2. Map of the study area.

BL lies 3 km to the south of Saltfleetby saltmarsh. At this point on the coast the beach is flat and can exceed 600 m width above the ODN contour in places; the beach is characterized by intertidal ridge and runnel morphology. Landward of the beach, the coastal foredunes are morphologically characterized by a convex-concave-convex-concave profile composed of two shore parallel and regular ridges (Figure 2.3A). Secondary foredunes, located inland, are c. 5 m high above ODN and are distinguished by a very dense vegetation cover dominated by Marram grass (*Ammophila arenaria)* up to 1 m tall which contrasts with the short (~0.10 m high) pioneer plants on the primary foredune. The primary foredune is relatively low (approximately 4 m above ODN) and wide (approximately 8 m) with a very gentle seaward slope of 4°.

At the TSH site, the beach is around 300 m wide between the reach of the highest astronomical tide and ODN, and is extended seaward by the presence of intertidal ridges and runnels (Figure 2.3B). Landward of the beach are well-established, regular foredunes about 150 m wide with a height of less than 6 m and with a seaward slope of 8°. The morphology of the foredune is characterized by a convex-concave-straight profile. Since 2005, scrub management has been carried out to remove the invasive Sea Buckthorn species (*Hippophae rhamnoides*) on these established dunes. A distinctive feature of this site is the presence of a small field of embryo dunes on the upper beach, situated between the ridge and runnel system and the established foredunes. These reach a height of up to 4.6 m above ODN (1.4 m above the beach surface) and the whole field of embryo dunes consists of a large patch c. 210 m x 65 m, and a small patch c. 150 m x 35 m located 80 m to the North. The embryo dunes are irregular in morphology, and at high spring tide the upper beach between the established foredunes and the embryo dunes is occasionally inundated by the sea. Both the foredunes and embryo dunes are densely vegetated with Marram grass.

MNE site is the most southerly site. The beach is relatively narrow, up to 200 m wide (distance between the reach of the highest astronomical tide and ODN), and exhibits a barred intertidal morphology comprising several sets of ridges and runnels (Figure 2.3C). Well-developed coastal foredunes are present and densely vegetated by Marram grass. High secondary foredunes approximately 7 m high and 50-75 m wide have a fairly steep seaward slope of 7°. On the seaward side, they are joined by a ramp to the irregular incipient primary foredunes which have a height of up to 3.5 m. The morphology of the foredune profile is described as convex-ramp-concave-straight.
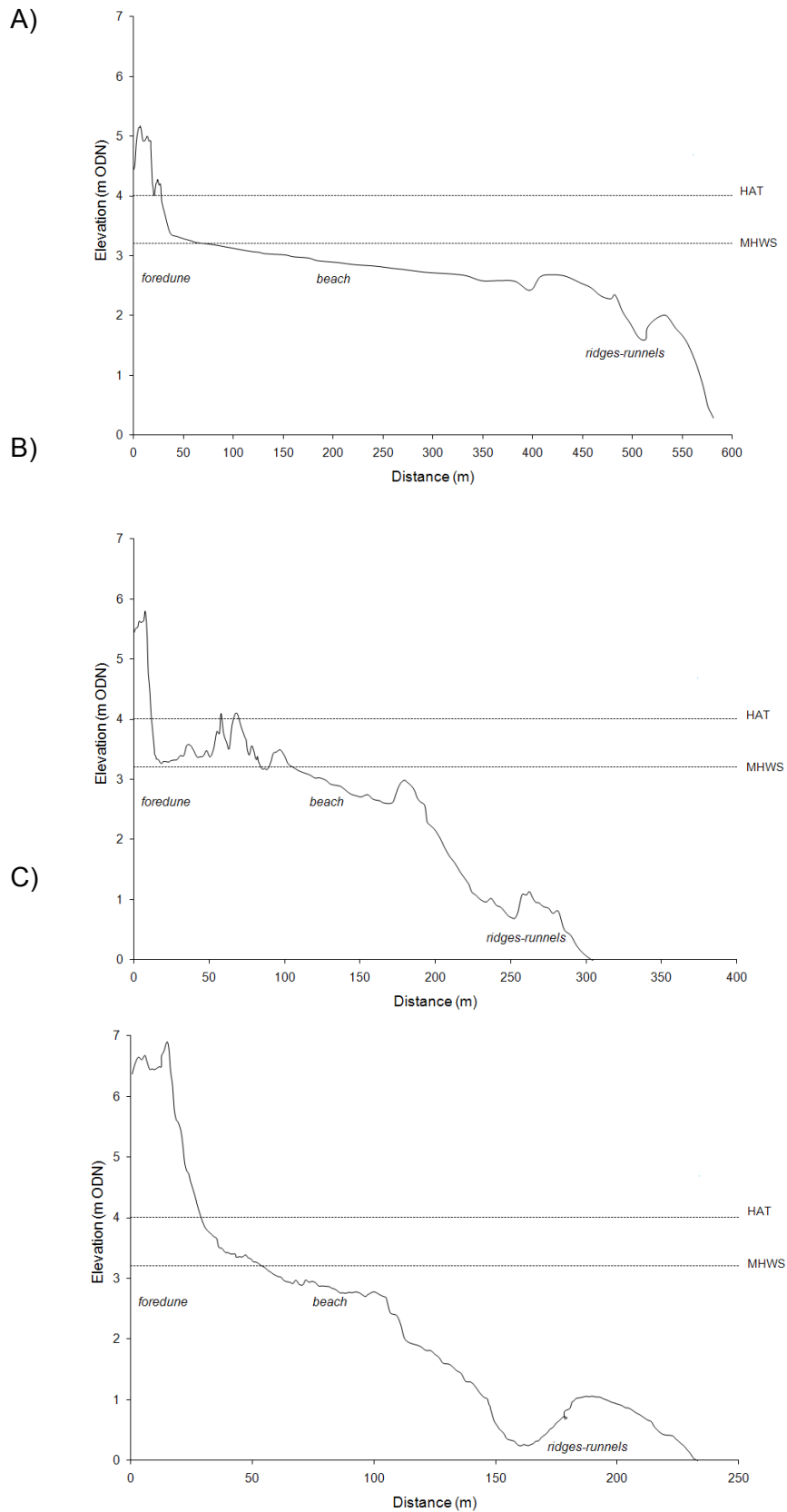
Figure 2.3. Typical foredune-beach profiles at the three sites: (A) BL, (B) TSH and (C) MNE. The water levels shown are the highest astronomical tide (HAT) and the mean high water springs (MHWS).

2.3. Foredune-Beach Sediments

The foredune and beach sediments at the three sites described above were sampled to determine their overall characteristics and also to monitor whether they changed significantly from season to season. Sand transport is influenced by grain size, which is primarily related to the mass/surface ratio of the grains. Bagnold (1941) reported that quartz grains with a diameter c. 80 µm are optimal for transport. Particles smaller than this necessitate stronger wind velocities due to higher cohesion forces between grains, and larger grains provide greater resistance caused by their greater mass/surface ratio. Therefore, the grain size distribution is an important parameter influencing aeolian sand transport. Before collecting the sediment samples, visually discernible and representative geomorphological units were identified across the foredune-beach at each study site (Table 2.2 and Figure 2.4). Sediment samples were collected five times over the seasonal monitoring periods from October 2009 to October 2010. Sample locations were surveyed using a Real Time Kinematic global positioning system (RTK-GPS) with accuracies of ±10 mm horizontally and ±20 mm vertically (Trimble, 2009) during October 2009 (survey 1) ensuring that sediment samples were taken from identical positions in subsequent seasons.

Table 2.2. Geomorphological units in the foredune-beach system.

Unit	Morpho-sedimentary features	Sample sites
Foredune	Secondary foredune crest (SFC)	Top and seaward side of the secondary foredune
	Secondary foredune toe (SFT)	Bottom of the seaward secondary foredune
	Primary foredune crest (PFC)	Top and seaward side of the primary foredune
	Primary foredune toe (PFT)	Junction between primary foredune and beach face
Upper beach	Upper beach (UB)	Top of the tidal beach with no direct connection to the foredune slope
Beach	Middle-beach (MB)	Centre of the tidal beach
	Lower-beach (LB)	Seaward of the tidal beach and landward of the first intertidal ridges

A)

B)

C)
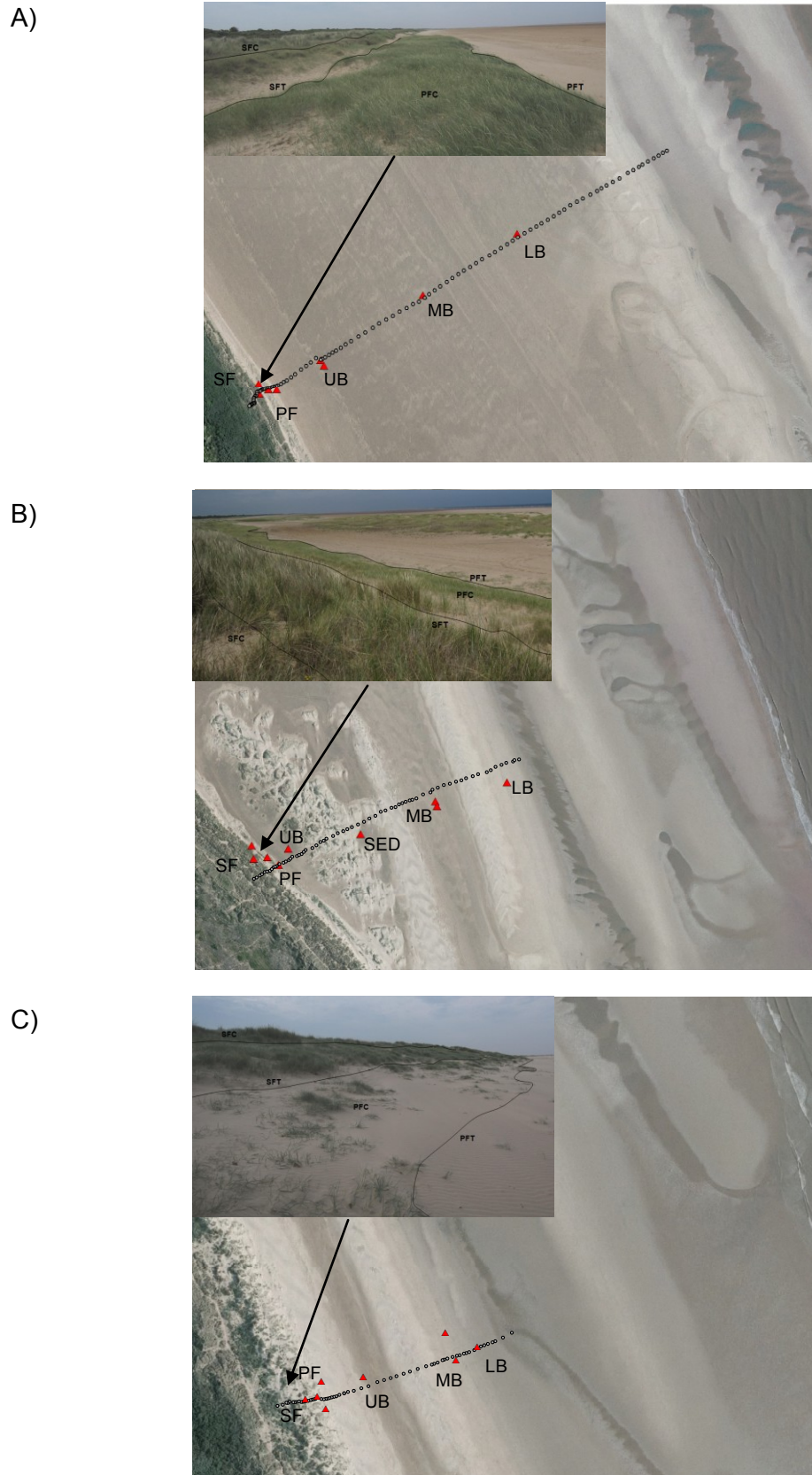
Figure 2.4. Morphological features observed in the field across the secondary foredune (SF), primary foredune (PF) and beach system at: (A) BL, (B) TSH and (C) MNE sites. The inset ground photograph shows the foredune sub-units. See Table 2.1 for explanation of abbreviations.

Sediment samples were collected by scraping a surface layer approximately 5 mm thick from the sand surface for each sub-unit. Sediment size and sorting was measured using a laser diffraction particle size analyser (model: Coulters LS200) recommended for grain size measurements (Bott and Hart, 1990). The mean value of all the temporal samples was calculated for each study site. Seasonal sediment characteristics in the foredune unit are also presented.

At all three sites, the foredunes and beaches are composed of well to very-well sorted fine to medium sand typically ranging from 100-600 µm (Figure 2.5) (based on the Udden-Wentworth classification, 1922). However spatial variations in textural characteristics exist.
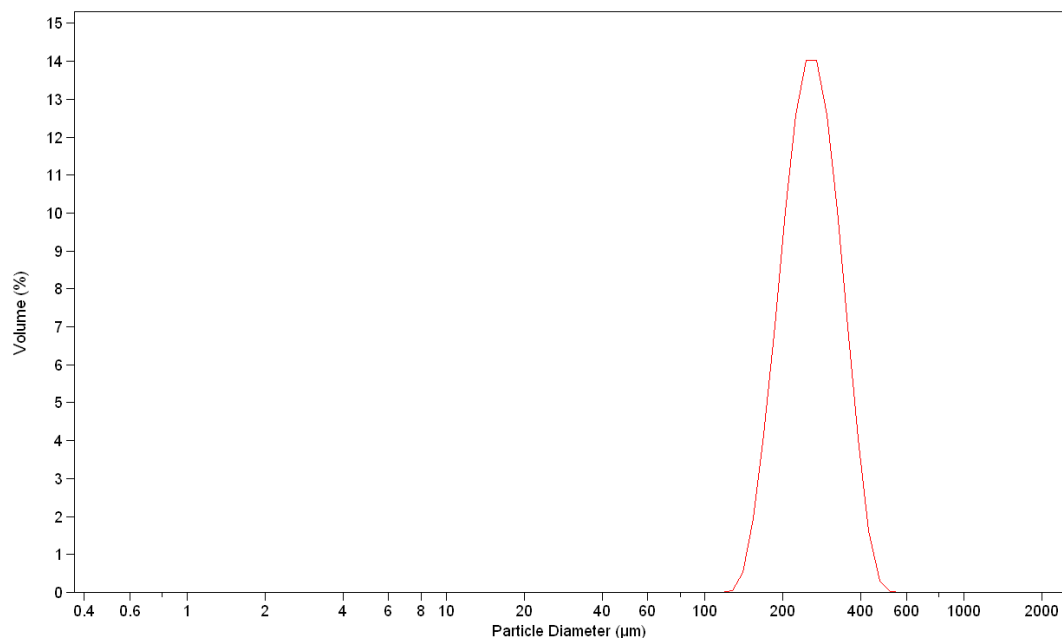
Figure 2.5. Typical size distribution curve of the sediment sample.

The seasonal average of the grain size D_{50} ranged from 253.4-277 µm, and the mode from 245.6-266.6 µm across the foredune-beach system at BL (Table 2.3). The grain size D_{50} on the beach (256.4 µm) is slightly finer than the average over the foredune units (265.8 µm) where the largest particles are found on the secondary foredune toe (Figure 2.6 and Table 2.3). Van Houwelingen (2005) also found an increase in grain size from the intertidal bars to the backshore with an important textural break at the MSL. In contrast, the mean D_{50} in the foredune units at the TSH and MNE sites is 2.2 µm and 7.4 µm finer respectively than that on the middle and lower beach units (Tables 2.5 and 2.7). Figures 2.7 and 2.8 clearly show a progressive decrease in grain size from the beach to the foredune units. The sediment size distributions across the foredune-beach system at all three sites suggest a spatial variation in wind sorting which is likely to both cause and reflect differences in aeolian sand transport rate between sub-units (e.g. Nordstrom et al., 1996).

Seasonal variation in grain size in the foredune unit was relatively small at the three sites, ranging from 257.3-271 µm at BL (Table 2.4), from 250.1-261.1 µm at TSH (Table 2.6) and from 250.3-258.9 µm at MNE (Table 2.8). This suggests a homogeneous sediment suite in the foredune unit over the seasonal monitoring periods.
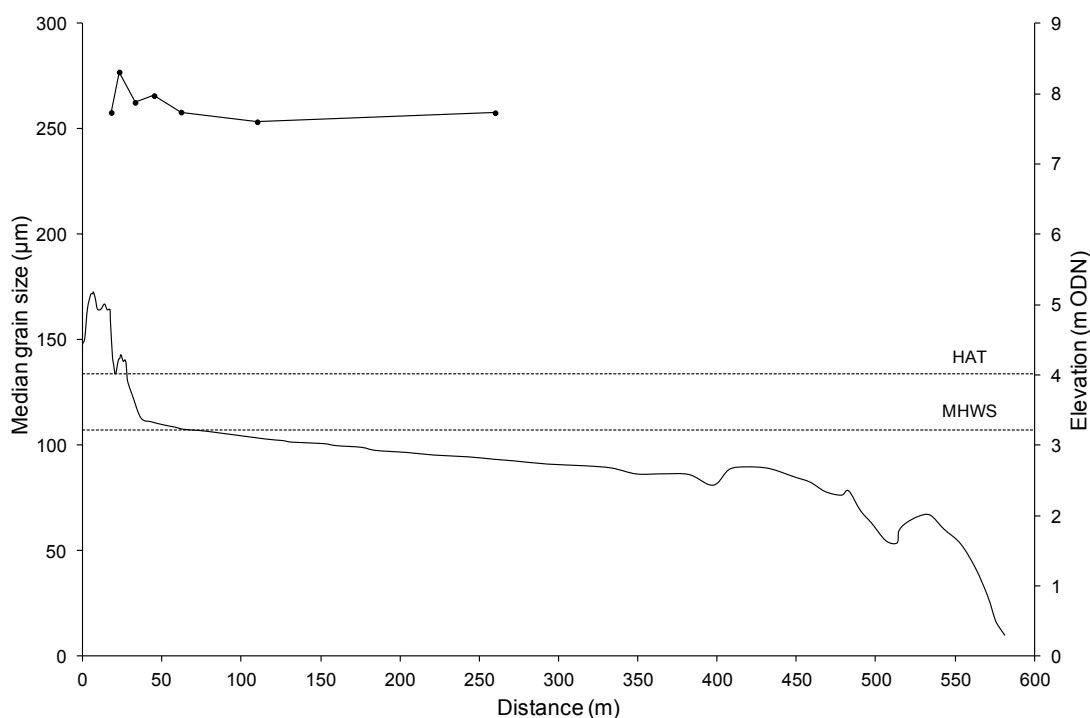
Figure 2.6. Cross-shore spatial variability in the average median sediment size (D_{50}) for all samples at each sub-unit over the seasonal surveys (line with circle marks) along a typical topographic profile at BL.

Table 2.3. Average statistical parameters of grain size (µm) distributions in the sub-units at BL over the seasonal surveys.

	SFC	SFT	PFC	PFT	Average foredune unit	UB	MB	LB
Range	255-265	262-286	252-282	249-279	**249-286**	256-262	233-260	250-264
D_{50}	257.8	277	262.6	265.8	**265.8**	258	253.4	257.7
Mode	245.6	266.6	249	254.8	**244**	247.6	257	243.6
SD*	1.34	1.35	1.34	1.35	**1.35**	1.35	1.52	1.35

*SD: standard deviation

Table 2.4. Temporal variability in sediment size (D_{50}) within the foredune unit at BL over the seasonal surveys.

	Survey				
Average of the foredune unit	Autumn 2009	Winter	Spring	Summer	Autumn 2010
D_{50} (µm)	271	265.3	268.8	257.3	266.9
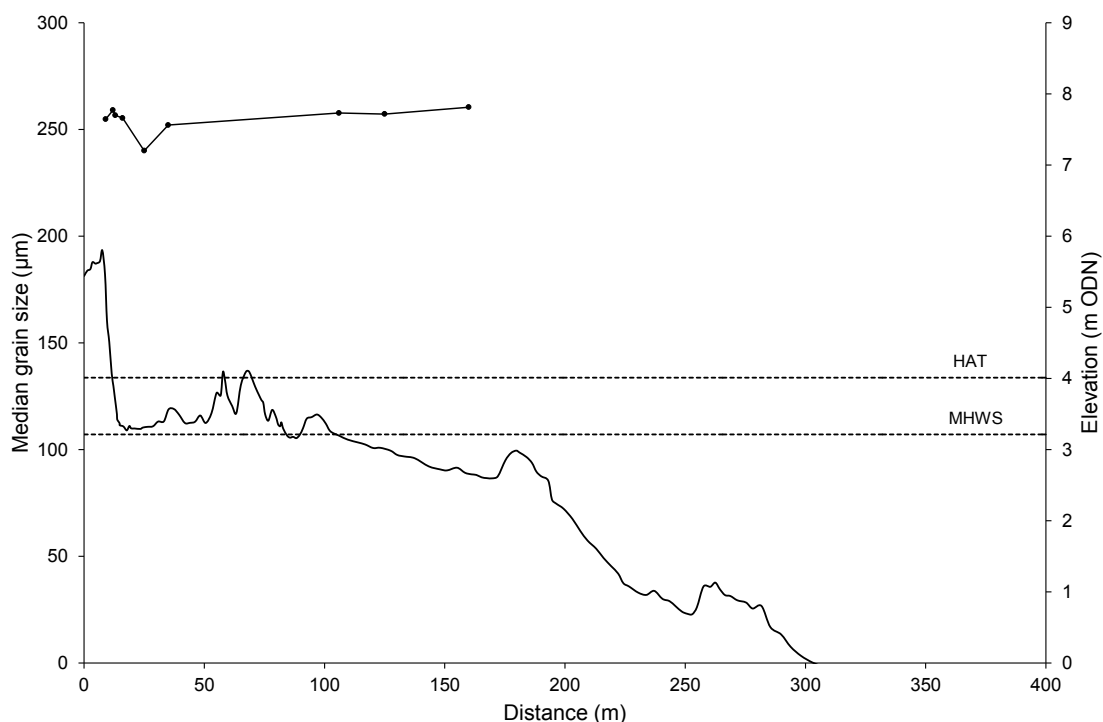
Figure 2.7. Cross-shore spatial variability in the average median sediment size (D_{50}) for all samples at each sub-unit over the seasonal surveys (line with circle marks) along a typical topographic profile at TSH.

Table 2.5. Average statistical parameters of grain size (µm) distributions in the sub-units at TSH over the seasonal surveys.

Unit	SFC	SFT	PFC	PFT	Average foredune unit
Range	248-272	251-270	246-262	246-266	**246-272**
D_{50}	254.8	259	256.6	255.3	**256.6**
Mode	200.8	205.6	259.4	251.4	**229.3**
SD*	1.03	1.03	1.28	1.32	**1.17**
Unit	UB	Landward embryo dunes	Seaside embryo dunes	MB	LB
Range	238-242	246-254	253-261	241-251	253-269
D_{50}	240	252	257.6	257.2	260.4
Mode	245	245	258.3	245	261
SD*	1.28	1.29	1.28	1.27	1.30

*SD: standard deviation

Table 2.6. Temporal variability in sediment size (D_{50}) within the foredune unit at TSH over the seasonal surveys.

| Average of the foredune unit | Survey | | | | |
	Autumn 2009	Winter	Spring	Summer	Autumn 2010
D_{50} (µm)	261.1	254	250.1	256.3	261
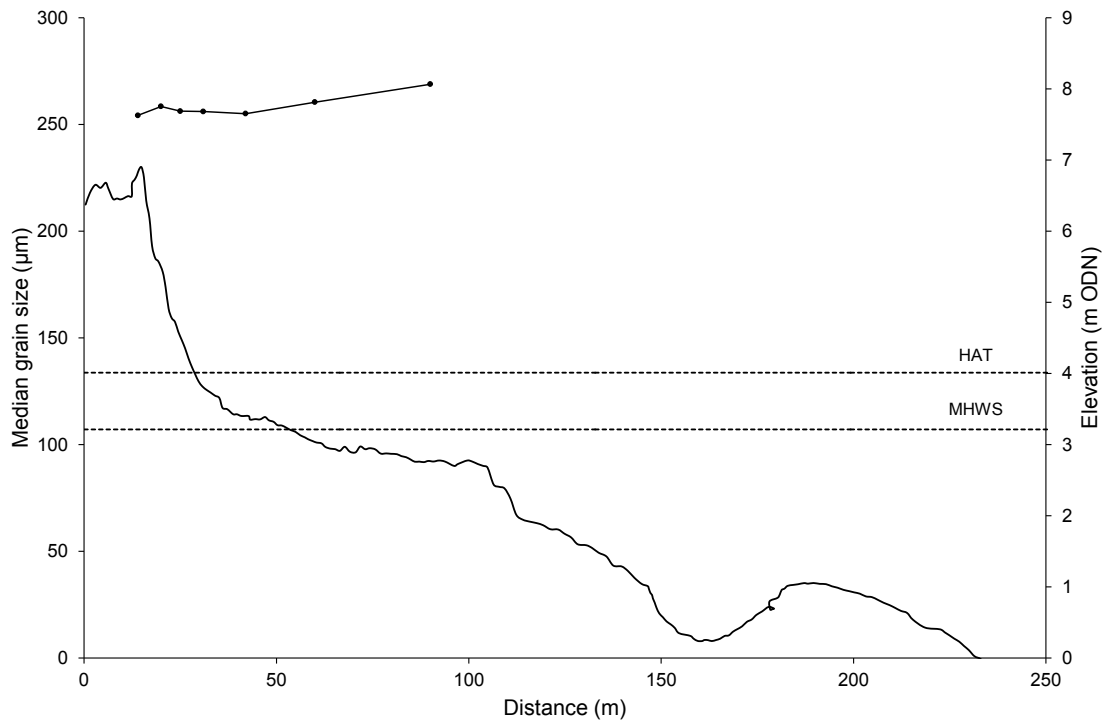
Figure 2.8. Cross-shore spatial variability in the average median sediment size (D_{50}) for all samples at each sub-unit over the seasonal surveys (line with circle marks) along a typical topographic profile at MNE.

Table 2.7. Average statistical parameters of grain size (µm) distributions in the sub-units at MNE over the seasonal surveys.

	SFC	SFT	PFC	PFT	Average foredune unit	UB	MB	LB
Range	240-265	238-263	248-263	250-260	**238-265**	252-263	244-273	255-292
D_{50}	254.2	258.4	256.2	256	**256.2**	255	258.4	268.8
Mode	248.2	243.6	253	251.4	**249.05**	259.4	256.2	266.4
SD*	1.28	1.28	1.28	1.28	**1.28**	1.28	1.28	1.32

*SD: standard deviation

Table 2.8. Temporal variability in sediment size (D_{50}) within the foredune unit at MNE over the seasonal surveys.

	Survey				
Average of the foredune unit	**Autumn 2009**	**Winter**	**Spring**	**Summer**	**Autumn 2010**
D_{50}	250.3	256.8	258.9	258.9	256.5

2.4. Environmental Conditions

2.4.1. Wind

The nearest meteorological station to the three field sites is located at Donna Nook (Figure 2.2) which is 12 km to the north-north-west. Hourly wind data for Donna Nook were obtained from the British Atmospheric Data Centre website (BADC, 2009). Hourly measurements of wind speed and direction are estimated from 10 minute scans and 36 direction sectors (centred on 10° intervals). Meteorological instruments are mounted at a height of 8 m above the ground surface and all the land between the sites and Donna Nook is less than 5 m above the ground. This suggests the data are also likely to be representative of conditions at the field sites. Donna Nook station has monitored hourly wind conditions, and daily atmospheric pressure since 1st January 1993. The unit of measurement for wind speeds is the knot, and values are recorded to the nearest whole unit, however these were converted into m s^{-1} for this study (1 knot=0.515 m s^{-1}).

In this study, wind regime is classified in terms of onshore (0°-<150°), offshore (180°-<330°), and alongshore (150°-170°; 330°-350°) direction components based on the coastline orientation of 160°-340° (Figure 2.9). Highly oblique winds are likely to deflect parallel to the crestline (Arens et al., 1995, Walker et al., 2009), so winds with an incident angle of ≤10° were considered as alongshore components.
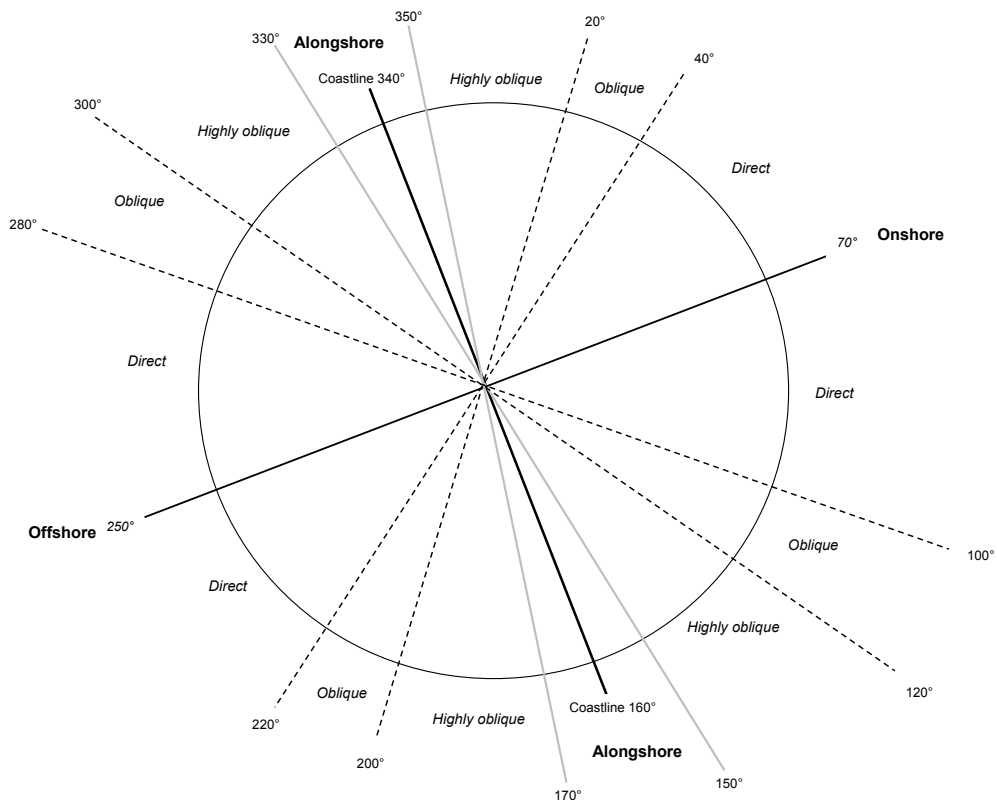
Figure 2.9. Schematic diagram of the classification of wind components.

Along this coast, winds prevail from the southwest, and thus are mainly offshore (Figure 2.10A). Wind speeds are modest (<8 m s^{-1}) for the majority of the time (73%) (Figure 2.10B). The wind regime is very consistent at the Lincolnshire coast from year to year. During winter months, however, the development of high pressure systems over the British Isles and the North Sea can lead to prolonged strong northwesterly and easterly winds, corresponding to the maximum fetch (Steers et al., 1979).

A)

B)
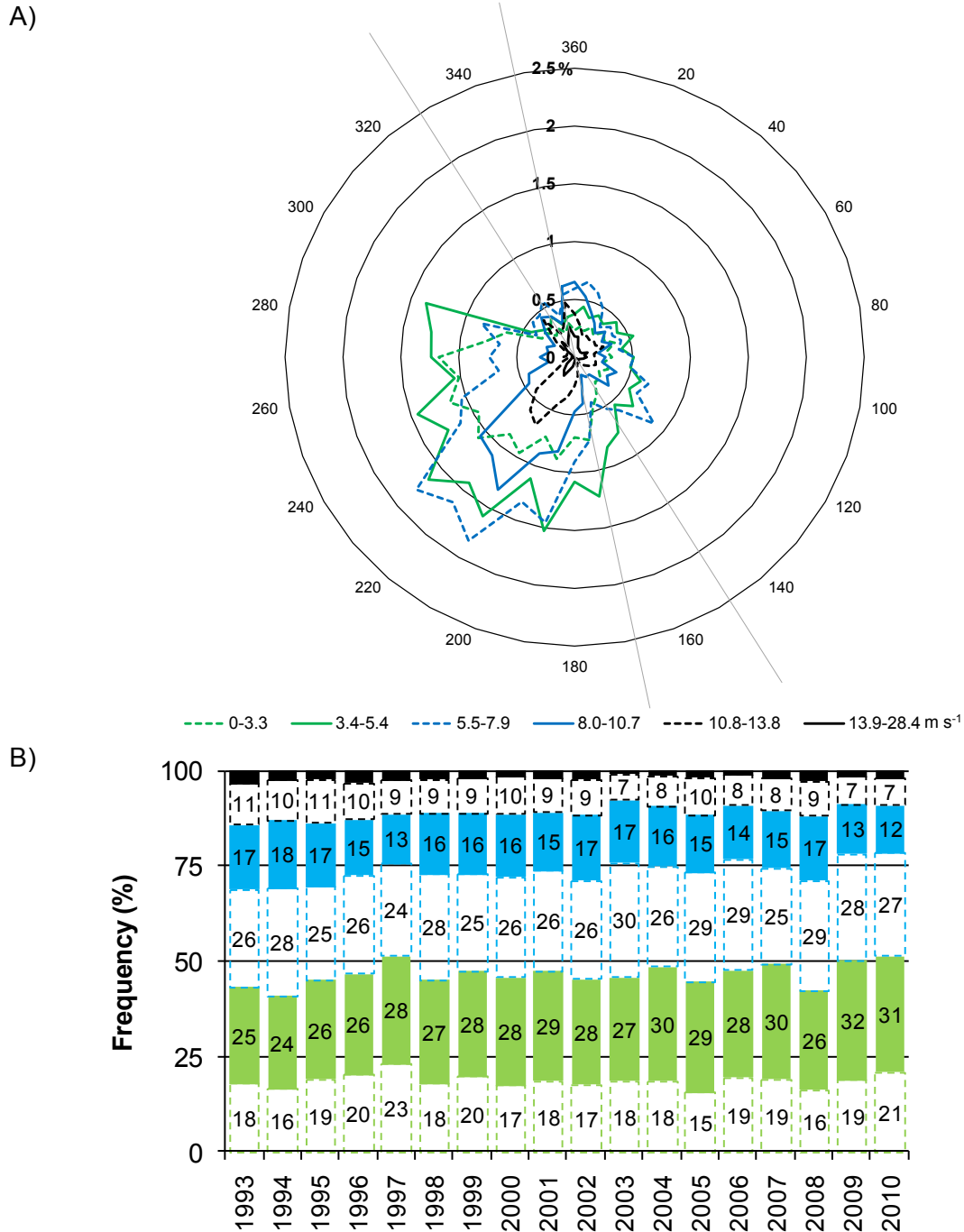
Figure 2.10. Wind conditions along the North Lincolnshire for the period 1993-2010 with direction centred on 10° intervals: (A) annual wind roses for different wind speeds, (B) annual wind speed frequencies.
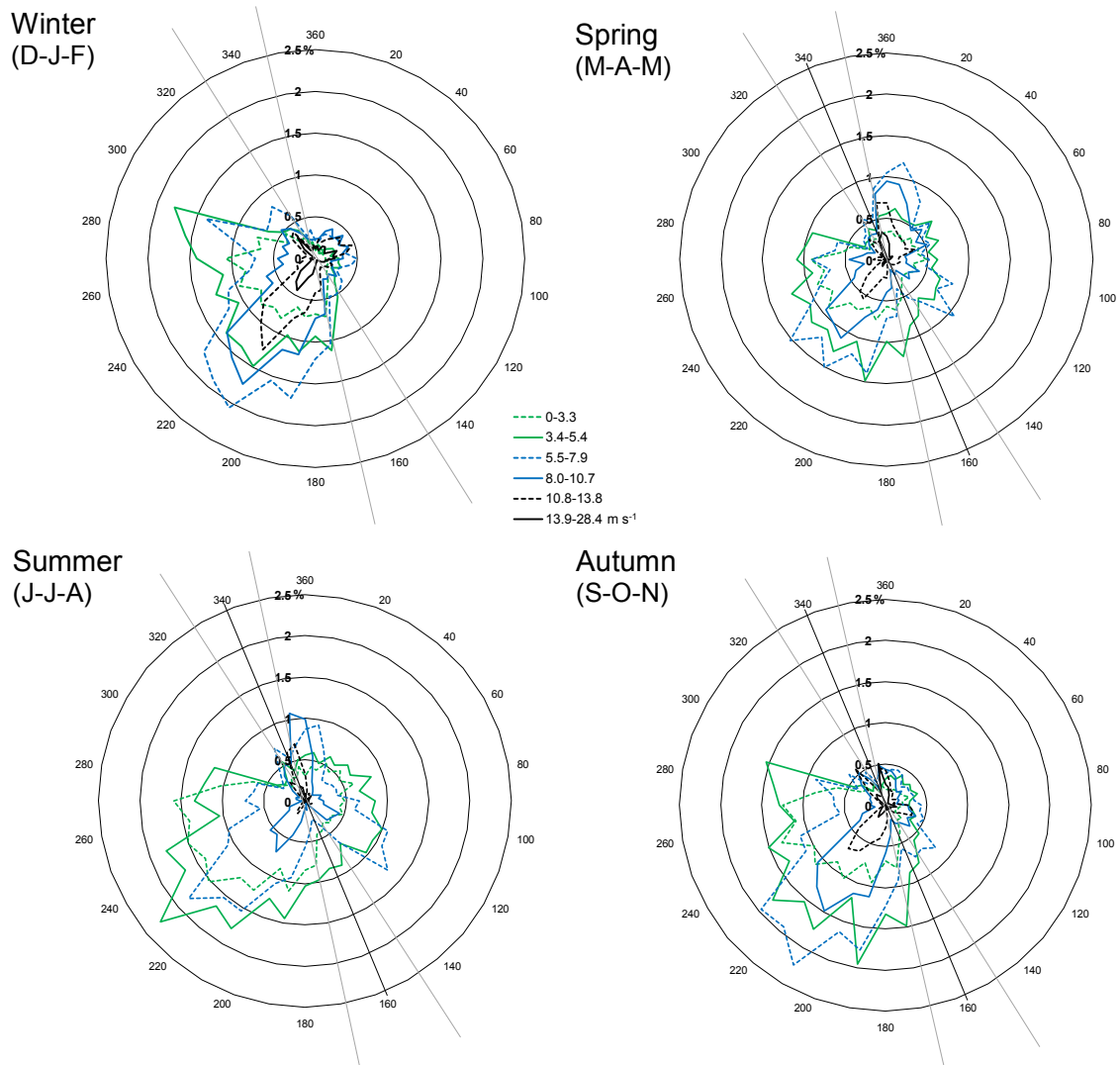
Figure 2.11. Seasonal wind roses for Donna Nook between 1993-2010.

Additionally, wind regime varies seasonally (Figure 2.11). Modest wind speeds (<8 m s^{-1}) occur most of time, and especially in summer. During this season, mean wind speed is 5.2 m s^{-1}, dominated by offshore winds with a frequency of 52%. Strongest winds (≥13.9 m s^{-1}) are recorded in winter for 5% of time, and can be directed either offshore or onshore. However the prevailing wind direction is offshore during the winter (67%), while onshore winds blow 21% of the time. Figure 2.11 shows clearly the pronounced seasonality in spring, when onshore winds blow more frequently (37%) with a mean speed of 7.6 m s^{-1}. The autumn is characterized by a similar wind regime to that in winter with offshore winds 62% occurring of the time. Around 3% of autumn winds are ≥13.9 m s^{-1}. Alongshore winds are very consistent from season to season, blowing between 12% and 14% of the time in each season.

2.4.2. Temperature and Precipitation

Temperature and precipitation were only recorded at the nearby weather station at Skegness, located c. 20 km south of the study area (Figure 2.2). The climate in the region is typically temperate oceanic with a mean annual temperature of 10.4°C and rainfall of 671 mm (Figure 2.12). Figure 2.13 shows that the rainfall is abundant from September to December.
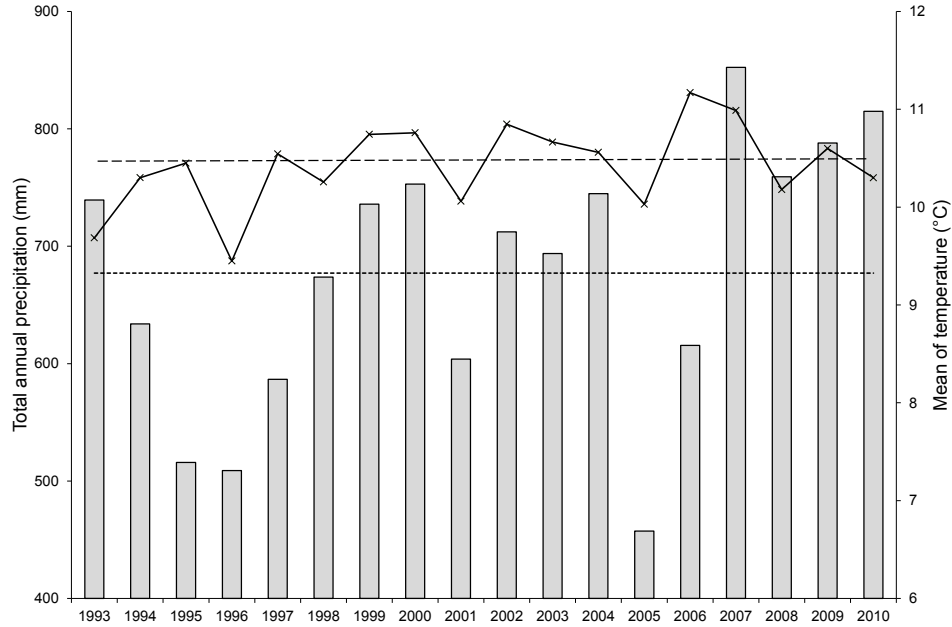
Figure 2.12. Annual average of local precipitation conditions (grey bars) and temperature (black line). Dotted and dashed lines correspond to the mean of precipitation and temperature respectively from 1993-2010.
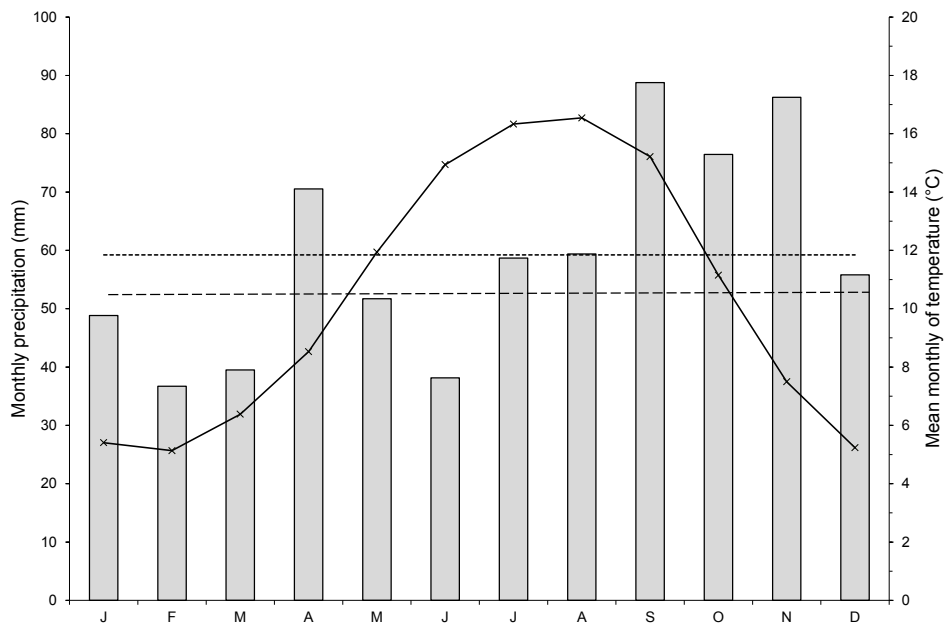
Figure 2.13. Monthly precipitation (grey bar) and mean monthly temperature (black line) from January 2010 to December 2010. Dotted and dashed lines correspond to the annual mean of precipitation and annual temperature respectively from 1993-2010.

2.4.3. Tide

Water levels have been recorded at Immingham tide gauge since 1956 (situated c. 65 km north of the study sites) (Figure 2.2). However, it is located at the entrance to the Humber estuary and may therefore not be representative of the open coastline. To evaluate the utility of this long-term tide gauge, a statistical comparison was undertaken between data from Immingham and Ingoldmells, a contemporary open sea tide gauge located south of the study area.

The north Lincolnshire coast is characterised by macro-tidal and semi-diurnal tides (Davies, 1964). The mean spring and neap tidal ranges are 6 m and 2.86 m respectively. Table 2.9 presents the tidal levels based at Skegness.

Table 2.9. Tidal levels at Skegness, expressed in metres above ODN. Statistics are derived from POLTIPS 3 software developed by the National Oceanography Centre Liverpool (NOC, 2009). Abbreviations: HAT – Highest Astronomical Tide; MHWS – Mean High Water Spring; MHW– Mean High Water; MHWN – Mean High Water Neap; MLWN – Mean Low Water Neap; MLW – Mean Low Water; MLWS – Mean Low Water Spring; LAT – Lowest Astronomical Tide.

HAT	MHWS	MHW	MHWN	MLWN	MLW	MLWS	LAT
4.09	3.21	2.46	1.70	-1.09	-1.85	-2.59	-3.57

The tidal cycles are slightly asymmetrical with the flood lasting around 5.9 hours and the ebb tide lasting 6.5 hours, except during neap tide conditions when energy and duration are similar between the flood and ebb flows. Tidal currents usually flow southward during the flood and northwards during the ebb (Admiralty Tidal Stream Atlas, 1962). The tidal residual current is directed to the south (Motyka, 1986) and is moderate (>1 m s^{-1}) with a stronger energy in winter than in summer (Simpson, 1993).

Long-term tidal water level records at Immingham were supplied by the UK Tide Gauge Network, part of the British Oceanographic Data Centre. Water level at Immingham has been recorded since 1956, so a long record is available, with the exception of 1959-1962. Hourly measurements were acquired for the period 1956-1992 and the average data completeness was greater than 75% for all years. For the period 1993-2010, 15-minute records were available with an average of completeness of 98%. All data are reported relative to Admiralty Chart Datum (ACD) and were converted to ODN using corrections given on the BODC website (2009) (ACD=3.75 m below ODN at Skegness).

Immingham is located 65 km north of the study sites and in the entrance to the Humber estuary. Fifteen minute measurements of water levels were compared at Immingham and a local tide gauge at Ingoldmells; and this was only based on the high water levels because it was expected that the shortcomings would be more easily depicted (Table 2.10). Ingoldmells is a recently installed secondary tide gauge (April 2003- December 2010), and located on an open coast, 16 km south of the MNE site. Hence it is more likely to represent the water level conditions at the study site.

Table 2.10. Statistics summary of the difference of high water level records between Immingham and Ingoldmells tide gauges (n samples=46).

Mean	Maximum	Minimum	SD
0.06	0.16	0	0.04

The calculated average difference of high water level measurements recorded at the two sites was 0.06 m. This suggests that Immingham records provide a reasonable indicator of water level along the open coast and was thus used in this research due to the longer available record.

2.4.4. Storm surge

Storm surges occur due to the frictional stress of strong onshore winds which cause the water level to be raised (Pond and Pickyard, 1983). These strong winds are generated by the passage of low pressure systems which also cause a rise in sea level through the inverse barometer effect (i.e. a 1hPa decrease in atmospheric pressure raises the sea level of c. 1 cm). When this temporary increase in sea level occurs in conjunction with strong onshore winds water level can rise by several metres.

Large surges in water level, defined as the difference between observed and astronomical water level, show a distinct seasonal pattern along this coast. During the summer, the surge level is generally positive and less than 0.2 m whereas it often exceeds 0.5 m in winter (Van Houwelingen et al., 2006). The most severe storm surges occurred in 1953 and 1978 (King and Barnes, 1964, Brampton and Bevan, 1987), and these significantly affected the Lincolnshire coast (Robinson, 1953, 1981). This result of a combination of high tidal level and energetic wave activity is also known as a storm tide. Such tides are caused by deep depressions tracking eastward toward the North Sea and moving around the North Sea basin in an anticlockwise circulation. Consequently surge levels increase along the east coast of England caused by the

funnelling effect as the surge travels south. The 1-in-50 year storm surge residual is approximately 2.5 m (Southgate and Beltran, 1998).

2.4.5. Waves

Wave conditions along the fetch-limited Lincolnshire coast are strongly controlled by the prevailing wind direction and speed. Offshore wave conditions are characterised by 50% and 10% exceedence significant wave heights of 0.5 m and 1.5 m respectively; and a modal wave period of less than 4 seconds (Department of Energy, 1989). Wave conditions also display seasonal variations – the monthly averaged significant offshore wave height during winter months is 2.5 m, whereas in summer it is 1.2 m. Inshore wave heights at the coast are about two-three times smaller than the offshore wave height (Van Houwelingen, 2005) due to the influence of the subtidal and nearshore banks. These act to reduce wave activity and longshore drift. The 1-in-100 year significant wave height is estimated to be 7.4 m at a distance of 3 km from the coast (Posford-Duvivier, 1996). The largest wave and the dominant wave direction are strongly influenced by the swell component approaching from the north to east quadrant (i.e. longest wind fetch). This increases coastline exposure to wave energy to the south, resulting in a net southerly littoral drift of beach material (Pye, 1995).

During the monitoring period for this study, 30-minute offshore wave measurements were collected at the Dowsing wave buoy (55 km from the coast and at a water depth of 22 m). Inshore wave conditions are undoubtedly more representative of the conditions at the coast, however local inshore wave records were not available during this period. Further it would not have been possible accurately to simulate the inshore waves through the use of a hydrodynamic model (e.g. MIKE21, SWAN) forced over a detailed bathymetric grid and the offshore wave records from the Dowsing offshore wave buoy due to the absence of a recent and detailed bathymetric survey.

2.4.6. Sediment Transport Processes

Longshore sediment transport is directed towards the south and is mainly driven by littoral drift and by flood residual currents landward of the innermost sand banks (Pye, 1995). The southerly sediment transport is subordinate to the cross-shore exchange of sediment (Halcrow, 1988). Sediment transport studies in the southern North Sea have found that suspended sediment transport rates are approximately two orders of magnitude higher than those of bedload transport, and the former is influenced by seasonal and short-term variations in water movements (Dyer and Moffat, 1998). During winter periods associated with energetic events, suspended sediment

concentrations are several times greater than those during summer (ABP, 1996). Additionally, Van Houwelingen et al. (2006) found that longshore sediment transport plays a major role in the intertidal bar dynamics along the North Lincolnshire coast.

2.5. Geomorphological Sub-units within the Foredune-Beach System

2.5.1 Elevation Data Collection and Control

Detailed topographic surveys were carried out using an RTK-GPS system (Trimble R6 GPS), composed of a base station (transmitter) and a minimum of one rover (receiver). It is currently one of the most direct and best topographic data collection systems for coastal dune monitoring, especially when morphology is complex (Navarro et al., 2011). RTK-GPS system requires that the base station remains at a point of known coordinates, which was located at the L2D1 benchmark, the nearby Environment Agency (EA) GPS station (approximately 240 m inland from the MNE site). Once the base station was placed, the survey was performed in kinematic mode. In this case, the receiver was connected with an antenna that was deployed on top of a surveying rod and carried by an operator. At each site a temporary fixed benchmark was established in the secondary foredunes and its location determined relative to the permanent EA benchmark. During the monitoring period topographic profiles were measured aligned to the relevant benchmark at each site.

The horizontal and vertical errors for each topographic data point were computed and reported by the GPS controller and stored with the positional information. Errors for the walking survey data represent the total error relative to the base station. The horizontal error ranged from 0.004-0.010 m and averaged 0.007 m relative to the referenced base station. The vertical error ranged from 0.006-0.041 m and averaged 0.026 m.

2.5.2. Delimitation of Geomorphological Sub-Units

Although the interaction of beach and dune land units is important, most previous studies have found it useful, and often necessary to sub-divide these units to assess their dynamics (Nordstrom et al., 1996, Miccadei et al., 2011). Such an approach has been successfully applied to determine the relationships between coastal dune and beach morphology and also to quantify shoreline evolution (e.g. Halcrow, 1988, Saye et al., 2005, Thomas et al., 2011). For this study, specific reference levels, determined by the intersection of the coastal profile with a specific vertical elevation, were used to

divide the foredune and the active aeolian beach system into units and sub-units at each site (Table 2.11) and then evaluated.

Table 2.11. Foredune and active aeolian beach sub-units, tidal reference and topographic control level boundaries *Land: from the fixed benchmark.

Units	Foredune		Beach		
Sub-units	Secondary foredune	Primary foredune	Upper beach	Middle beach	Lower beach
Level boundaries	Land*-HAT	HAT-z=3.5 m	z=3.5 m-MHWS	MHWS-z=3 m	z=3 m-MHW

The non-parametric statistical Pettitt test (Pettitt, 1979) was used to confirm and evaluate the objectivity of the sub-units delimited from the tidal reference and topographic contour levels. The Pettitt test is based on the Mann Whitney test and identifies significant thresholds in a spatial sequence of measurements by assessing the null hypothesis of an absence of change (Pettitt, 1979). This test was applied to the topographic cross-shore profiles undertaken in survey 1 (autumn 2009) using a RTK-GPS system for each site. The null hypothesis was the absence of a change-point in the sequence of elevation measurements (Xi) along the cross shore profile of size N, and the change point was the distance (d) separating two sub-sequences with significant differences of the sum of ranks. The statistic $U_{d,N}$ considers that for each distance (d) with a value between 1 and N the two samples X_i and X_j, for i=1 at distance d and for j=d+1 at N, are issued from the same population. The value that is tested is the maximum, in absolute value of $U_{d,N}$ defined as (Pettitt, 1979):

$$U_{d,N} = \sum_{i=1}^{d} \sum_{j=d+1}^{N} D_{ij}$$

Eq 2.1

with D_{ij}=sgn(X_i-X_j) and sgn(X)=1 if X>0, 0 if X=0 and -1 if X<0.

If the null hypothesis is rejected, an estimate of the change-point distance is provided by the moment (*d*) that corresponds to the maximum of the absolute value of $U_{d,N}$.

It has been successfully applied in previous studies to identify morphological structures and zone boundaries in sequences of data (e.g. Lassettre et al., 2008, Toone, 2009). To first evaluate the use of the tidal reference and contour levels as a robust basis from which to delineate sub-units within the foredune-beach system, the test was used to identify significant (p<0.05) morphological changes along the cross-shore topographic profiles in autumn 2009.
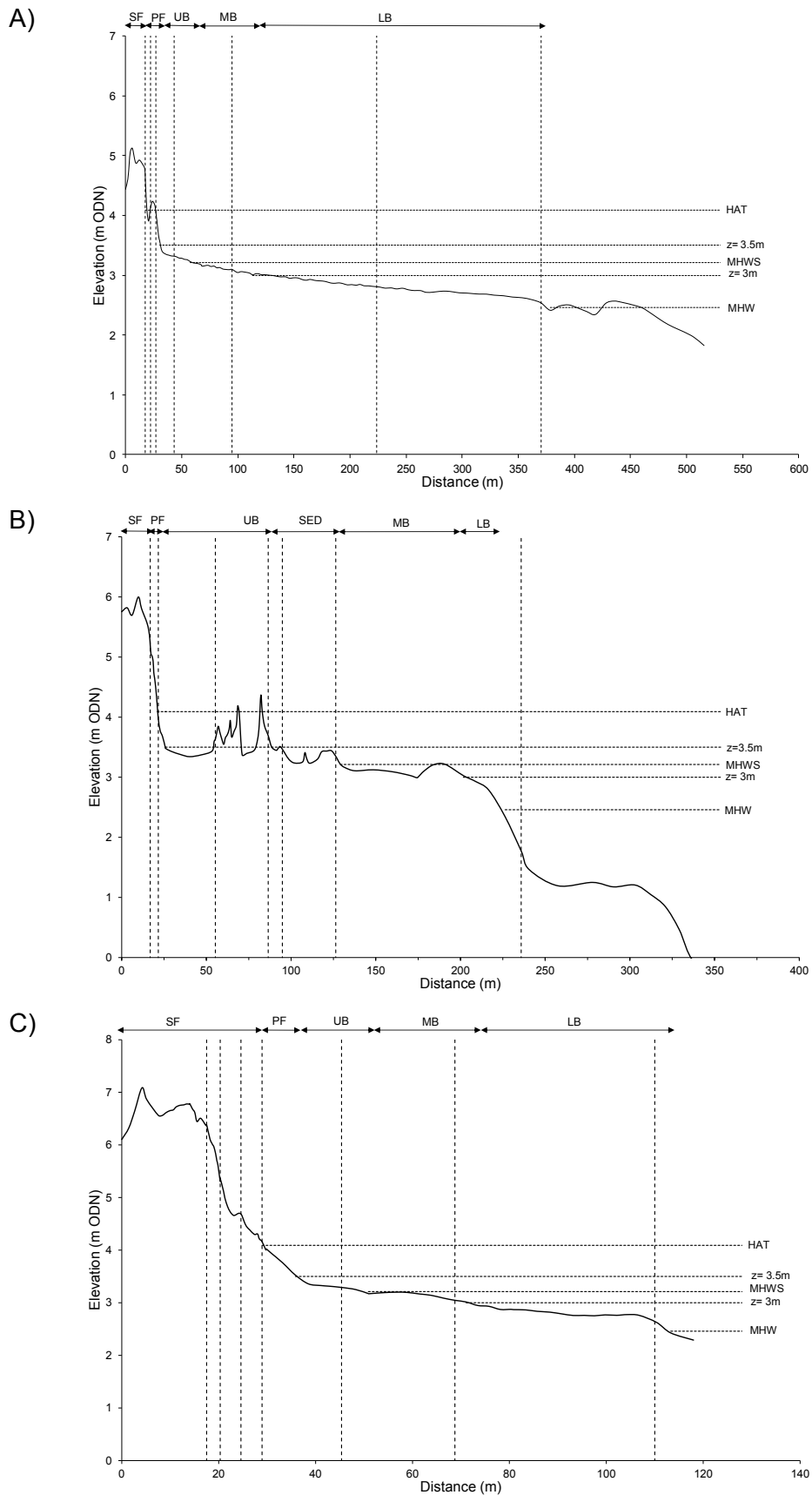
Figure 2.14. Significant (p<0.05, Pettitt test) morphological/distance changes (dashed vertical lines) along topographic foredune-beach profiles in autumn 2009 at: (A) BL, (B) TSH and (C) MNE. Top arrows indicate sub-units assessed by tidal reference and contour level.

Figure 2.14 shows that the statistical thresholds identified for the topographic profiles (in autumn 2009) at each site and the sub-unit boundaries delimited by tidal reference and contour levels differ from several metres on the beach. This difference is mainly due to a relatively flat morphology so that it is unlikely to affect the investigations. At TSH, the complexity of the beach morphology hides any clear relationships (Figure 2.14B). Results also indicate that the number of significant statistical thresholds was more important than the delimited sub-units along the secondary and primary foredunes. These thresholds correspond well to the foredune morphological features visually identified in the field, so that they were further used to segment foredune unit into sub-units such as SFC, SFT, PFC, and PFT (Table 2.12). The results of the Pettit test analysis are sufficient to validate the use of tidal reference and contour levels and field foredune morphology identification. It also underscores that the tidal reference and contour levels can provide an objective means of identifying morphological sub-units boundaries along foredune-beach profile.

The difficulty of identifying the position of the foredune toe has been previously recognized (e.g. Guillén et al., 1999, Ruessink and Jeuken, 2002, Pye and Blott, 2008). It theoretically corresponds to a transition point between the beach and the mainland, and is often, in practice, taken as the position of the highest waterline or the position of the maximum storm surge level (Van de Graaff, 1990). However the foredune toe can also be defined using a morphological criterion, where its position is characterized by the contact of the steep foredune face with the gentle upper beach slope. This may be clearly discernible in the field at any one particular time, but the foredune toe position varies on a wide range of temporal and spatial scales, and has been suggested to be a 2-3 m wide zone (Guillén et al., 1999), rather than a discrete line in long-term coastline studies (Battiau-Queney et al., 2003). In this study, a representative foredune toe evolution from season to decades is needed, where morphological changes caused by local and instantaneous processes occurring immediately before the topographic or aerial survey are not relevant. Therefore, the objective approach of defining the foredune toe based on a constant reference level of z=3.5 m is considered more useful and can also be applied simply and repeatedly at the three different morphological sites from micro- to macro-scales.

Table 2.12. Delimitation of the foredune and active aeolian beach system for the different research scales. ***Boundaries identified in the field and used only for seasonal scale.**

Research scale	Unit	Sub-unit	Boundaries	Morphological features
Micro-scale	Foredune	Secondary foredune crest (SFC)	Landward-HAT	Top and seaward side of the secondary foredune
		Secondary foredune toe (SFT)		Junction between the secondary foredune front and primary foredune
		Primary foredune crest (PFC)	HAT-z=3.5 m	Top and seaward side of the primary foredune
		Primary foredune toe (PFT)		Junction between primary foredune and beach face
	Upper beach	Upper beach (UB)	z=3.5m-MHWS	Top of the tidal beach with no direct connection to the foredune slope
	Beach	Middle beach (MB)	MHWS-z=3 m	Centre of the tidal beach
		Lower beach (LB)	z=3 m-MHW	Bottom of the tidal beach and landward of the first intertidal ridges
At THS site	Beach	Seaward side of the embryo dune field (SED)	z=3.5 m against embryo dune-MHWS	Seafront of the embryo dune field
Meso- and Macro-scales	Foredune		Landward-z=3.5 m Landward-foredune toe*	Vegetated foredune slope-toe
	Upper beach		z=3.5 m-MHWS foredune toe*-MHWS	Junction between foredune and beach face
	Beach		MHWS-MHW*	Lower beach
			MHWS-ODN	Lower beach
			ODN-z=-1 m	Intertidal beach composed of upper ridge-runnel system

2.6. Characteristics of Spatio-Temporal Data

The study approach of spatio-temporal overlapping necessitates the collection of a diverse range of data from a variety of sources spanning micro- to macro- scales. The temporal resolution, spatial cover, and representation of the data records collected over different timescales are summarized in Table 2.13.

Table 2.13. Characteristics of the data records used in this thesis over different time and spatial scales.

	Data records	Temporal resolution	Spatial cover
Micro-scale	Field experiments	1 min	mm-m
Meso-scale	Field topographic terrain models and profiles	Season	m
	EA topographic profiles	Bi-annual	m
	EA bathymetric profiles	Years	m
	Airborne topographic data (LIDAR)	2001 and 2007	m-km
	Meteorological data	1 hour	>1 km
	Oceanographic data: water level records	15 min (recent years) 1 hour (historical)	>1 km
	Oceanographic data: wave records	30 min	>1 km
Macro-scale	Aerial photographs	Years	m-km
	OS maps	Decades	m-km
	Climate records	1 day	>1 km

Coastal morphological changes and external forcing factor trends are investigated using a broad variety of methods and data sets depending on the study time spans.

Chapter 3. Micro-scale airflow and sand transport processes

3.1. Introduction

The physics of aeolian sand transport have been widely studied; key approaches include laboratory (wind tunnel) experiments, field experiments in both desert and coastal environments, and more recently computer modelling and computational fluid dynamics (e.g. Svasek and Terwindt, 1974, Jackson, 1976, Frank and Kocurek, 1996a, 1996b, Van Boxel et al., 1999, Wiggs, 1993, Wiggs et al., 1996, Bórowka and Rotnicki, 2001, Walker and Nickling, 2002, Hesp et al., 2005, Lynch et al., 2008, 2009, Parson et al., 2004a, 2004b).

As discussed in Chapter 1, it is the cumulative operation of aeolian sand transport processes at the micro-scale (i.e. micro-event scale process) that leads to the development and geomorphological characteristics of dune forms. The purpose of this chapter is to identify near-surface airflow processes operating within the foredune-beach system under different wind regimes (onshore, offshore, alongshore) at the micro-scale. Specifically, the objectives are to:

(1) Characterize airflow and aeolian sediment transport patterns within the foredune-beach system at three sites under a range of different wind regimes (speed and direction);

(2) Determine the key factors influencing the observed airflow and sediment transport patterns;

(3) Identify and evaluate the implications of (1) and (2) for the geomorphic development of the foredune-beach systems;

(4) Use the micro-scale data to develop a conceptual model of the relationship between wind regime and aeolian sediment distribution that can be scaled-up and used to predict meso- and macro-scale behaviour of the foredune-beach system.

3.2. Coastal Sand Dune Processes

The formation and development of coastal dunes are a response to a physically complex series of processes associated with sand transport by wind (Sherman and Hotta, 1990). Wind velocity essentially determines the sand transporting capacity of the wind whilst wind direction controls the distribution of the sediment (Kocurek and Lancaster, 1999). Foredune growth occurs when sediment is transported from the beach to the foredune and retained there. Aeolian sand transport across the foredune-beach system is highly variable, mainly due to the presence of a broad suite of environmental factors, acting at different spatial and temporal scales (e.g. Gares, 1988, Jackson and Cooper, 1999, Davidson-Arnott and Bauer, 2009).

3.2.1. Aeolian Sand Transport Processes

As previously mentioned in section 1.3.3, wind is the essential driving force in aeolian sand transport as it shears the ground surface (i.e. the wind slides over the ground). The initial picture to describe the phenomena is a flat surface formed by sand grains over which air flows. The wind exerts a drag force on the surface grains, resulting from the horizontal momentum transfer from the air to the grains (Figure 3.1).
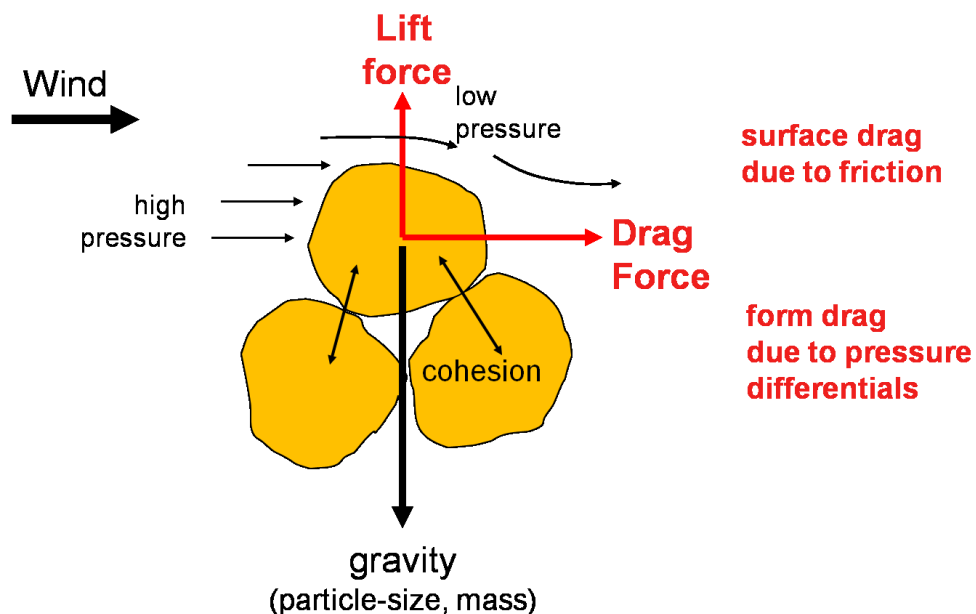
Figure 3.1. Forces acting on a surface grain. Drag force acts parallel to the surface, and is proportional to the friction velocity squared.

When the wind reaches a threshold velocity known as the fluid/static threshold, the sand grains are entrained and begin to move by drag and lift forces. The fluid threshold is dependent on the turbulent structure of the boundary layer resulting from coherent structures such as bursts and sweeps (Lyles and Kraus, 1971). However, two forces act on the grain movement besides the horizontal force due to the wind: gravity and the resistance of the air (drag) (Figure 3.1).

Once entrainment has started, a second transport phenomenon can take place at wind speeds lower than the fluid threshold (Figure 3.2). Under normal conditions, if gravitational force is greater than the lift and drag forces then the particle in the wind will return to the surface. If the surface is hard, the sand grain will rebound when impacting the ground surface. However over a surface composed of similar sand grains resting loosely on one another, the impacting grain can transfer energy to the loose sand grains, ejecting some of them upwards into the airstream. If the wind speed is high enough, the energy transferred from the wind to the particles is equal to the energy lost at the impact and the motion is sustained. The descending grains bring down energy from above, which means that less energy is needed to maintain movement, and it can carry on at a lower overall wind speed than before. Thus, the impact threshold at which grain movement can be maintained is about 80% of the static threshold (Bagnold, 1941, Anderson and Haff, 1988).

The wind lifts, accelerates, and transmits kinematic energy to the grains, which travel following trajectories of different lengths and heights depending on the initial velocity at which the sand grain leaves the surface and also on surface characteristics. This process is known as saltation and grains typically follow a steep upward trajectory and shallow downward trajectory. Arens and Van der Lee (1995) suggest that the resulting sand cloud is limited to the lowest 0.25 m above the surface on a beach, and the content of sand in the wind decreases exponentially with height.
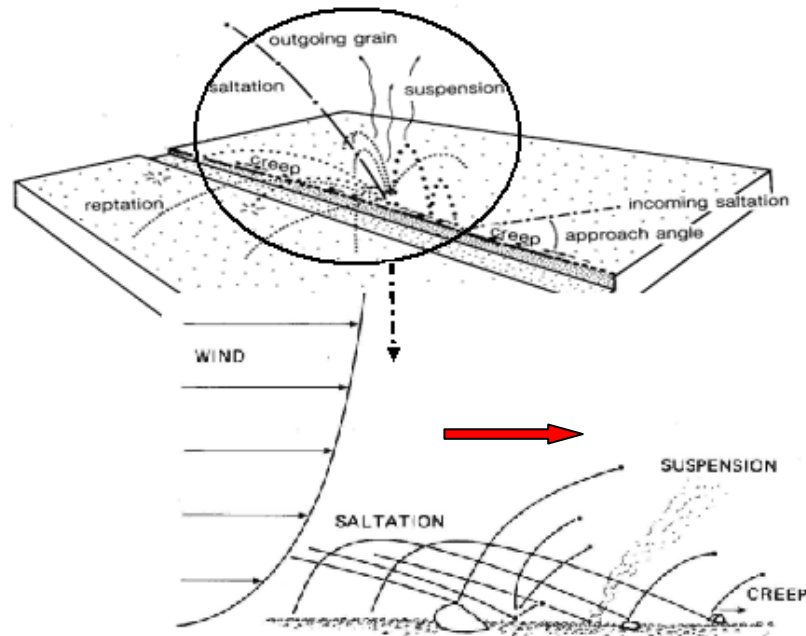
Figure 3.2. Different modes of grain transport, and illustrating the cascade effect (Livingstone and Warren, 1996 and modified by author). Red arrow indicates the wind direction.

Most sediment transported by the wind travels by saltation, which in turn can initiate two other modes of transport, which contribute to the total aeolian transport: these are suspension and surface creep (Figure 3.2). The suspension transport is the motion of usually smaller grains, lifted from the ground by turbulent eddies, and transported over longer distances, without any interaction with the sand bed. Surface creep includes the rolling of large grains driven by the impact of smaller grains in saltation and the rolling of these grains into holes formed by the saltation impacts (Livingstone and Warren, 1996). The proportion of the total amount of sand moved by creep is however relatively small, consequently the most important processes on a sandy beach is saltation.

The amount of sand transported over time q(t) is controlled by a series of environmental factors and process variables (a_1-a_n) defining both the input of energy to the system and the capability of the system to respond to that energy (Jackson and McCloskey, 1997).

$$q(t) = f(a_1, a_2, a_3, \dots)$$

Eq 3.1.

These variables include at a minimum wind velocity (determining shear stress velocity), fetch distance and surface characteristics such as grain size.

Sand transport occurs when the threshold of shear velocity of cohesionless sediment on a horizontal surface is exceeded. The threshold shear velocity (U_{*t}) can be determined using Bagnold's equation (1941):

$$U_{*t} = A \times [gd\left(\frac{\rho_s - \rho}{\rho}\right)]^{1/2}$$

Eq 3.2.

Where A is an empirical constant of proportionality with a value of 0.1 at the onset of sand movement (Bagnold, 1954) for grain sizes larger than 0.1 µm diameter; ρ_s is the density of sand particles (2650 kg m^{-3}, for quartz); ρ is the density of air (1.22 kg m^{-3}); g is the gravitational acceleration (9.81 m s^{-2}); d is the mean sand grain diameter. In this study, d is equivalent to 260 µm corresponding to the D_{50} of the grain size collected from the foredune unit during field surveys. Although the seasonal D_{50} of the grain size ranges between 250.1 µm at TSH and 271 µm at BL, the calculation of U_{*t} is very similar (difference of <0.005 m s^{-1}).

Studies suggest the transition from fluid to impact threshold velocity takes place in less than 1 second (Pye and Tsoar, 1990) but for this thesis fluid velocity was calculated in order to estimate the threshold condition of sand entrainment. Over longer periods of time this may result in an under-estimate of the total amount of sand in transport.

The region of flow that is near to the surface and retarded by frictional effects is referred as the boundary layer. Theoretical considerations of the boundary layer concept and the 'law of wall' highlight the significance of fundamental quantities that describe the capability of the system to respond. Under steady and uniform airflow conditions, the lower portion of a time-averaged wind speed profile over a flat surface can be described by a log-linear increase in wind velocity with height above the roughness length mainly controlled by surface characteristics. The logarithmic portion of the boundary layer has been described by Kármán-Prandtl in the 'law of wall' equation:

$$U_t = \frac{U_{*t}}{K} \times \ln\left(\frac{Z}{Z_0}\right)$$

Eq 3.3.

Where U_t is the wind speed at a given height Z (in this case 2.4 m high); K is von Karman's constant of 0.41; and Z_0 is the roughness length.

Although the roughness length (Z_0) is a critical and variable factor depending on the actual ground surface and other environmental conditions, its average value of 0.02m, determined from wind velocity profiles of the foredune sub-units for each experiment, was used. Hence, the threshold shear velocity for Z_0 is calculated to be 0.235 m s^{-1}, corresponding to a wind velocity of 2.75 m s^{-1} at 2.4 m height.

3.2.2. Factors Controlling Sand Transport

The factors influencing aeolian sand transport were discussed in section 1.3.3. These can be divided into two types, according to whether they influence 1) the wind field, or 2) sand supply. Their potential effects on sand transport are presented in this section.

A. Wind regime

Speed, direction and turbulence structures within the wind profile fluctuate rapidly and extensively in both space and time. For instance using high resolution field measurements, Davidson-Arnott and Bauer (2009) found that maximum wind velocities on a beach typically exceed the average velocity by a factor two or greater, and that the minimum velocities can be less than half the average, within only 1-minute of record. Aeolian sand transport rate varies on an equally short timescale, and therefore it is a short-term process (Arens, 1996a). Wind tunnel and field experiments have indicated that the rate of sand transport by wind rapidly responds to changes in wind velocity, and that unsteadiness or gustiness in the wind record is reflected in similar fluctuations in the instantaneous sand transport rate on a timescale of 1-2 seconds (Butterfield, 1991, McKenna et al., 2000). The spatial and temporal response of the system to wind gustiness, speed-up and turbulence eddies (Bauer et al., 1998, Wiggs et al., 2004b, Baas, 2007, Davidson-Arnott and Bauer, 2009) is therefore complicated by the difference in the response time for sand entrainment and for adjustment of the wind velocity profile to changes in the mass of sand being transported (Owen, 1964, Anderson and Haff, 1991, Arnold, 2002). Typically, wind speed fluctuates around the threshold of movement, and sand transport is intermittent with long periods of zero sand transport punctuated by short or long bursts of sand motion when wind exceeds the threshold (Stout and Zobeck, 1997, McKenna Neuman et al., 2000, Bauer et al., 2009). This type of fluctuation gives rise to features such as aeolian sand streamers (Baas, 2008).

B. Fetch distance

The fetch effect refers to the progressive increase in sand transport in the wind direction, with distance downwind from a zone of no sand transport (e.g. leading edge of the inundated beach/shoreline) to an erodible surface (Davidson-Arnott and Law, 1990, Gillette et al., 1996, Jackson and Norsdtrom, 1998, Bauer et al., 2009). The fetch distance is defined for a given wind direction as the distance to the shoreline in the wind direction. Figure 3.3 defines the parameters relative to the fetch. On a beach, the maximum available fetch (Fm) is dependent on the beach width (W), and the angle of wind approach from shore perpendicular (α), and can be estimated from the cosine law (Chepil et al., 1964):

$$Fm = \frac{W}{\cos(\alpha)}$$

Eq 3.4.

The critical fetch (Fc), however, refers to the wind-parallel distance between the shoreline and the point downwind at which maximum sand transport is reached (Davidson-Arnott and Dawson, 2001). Bauer and Davidson-Arnott (2002) suggest a theoretical framework to model sediment supply within which the interactions of beach geometry, the wind approach angle (i.e. cosine effect) and critical fetch distance can be quantified.

Fetch is partly controlled by the beach width which is in turn is governed by beach slope, tidal range, and wave characteristics; and partly by the wind direction regulating fetch distances and wave run-up (Nordstrom and Jackson, 1993, Bauer et al., 2009, Delgado-Fernandez and Davidson-Arnott, 2011). Tidal range is an important factor for fetch distance in macro-tidal environments because it influences the water table located near the beach surface and thereby re-defines the boundaries within which aeolian transport system occurs (Meur-Férec and Ruz, 2002). On beaches such as that studied here features such as intertidal ridges and runnels can reduce or segment the aeolian fetch and interrupt sand transport paths (Vanhée et al., 2002, Anthony et al., 2009).

Estimates of the Fc distance necessary to attain maximum sediment transport vary from <20 m (Svasek and Terwindt, 1974) to 200 m (Davidson-Arnott et al., 2008). The critical fetch distance reflects that over which a fully developed saltation cloud can form balanced against changes in the nature of the surface over which the air is flowing caused by micro-topography, surface moisture, surface crust development and

sediment sorting (Gillette et al., 1996). As a result, fetch effect may be considered as a controlling variable that incorporates the specific influences of a large range of physical parameters that govern the amount of sand supply into coastal dune systems (Bauer et al., 2009). In this thesis, Fc is not measured so that the assumption is a fully saturated flow over the whole fetch distance (F_1-F_3). The effect of this assumption will be discussed in Chapter 5.
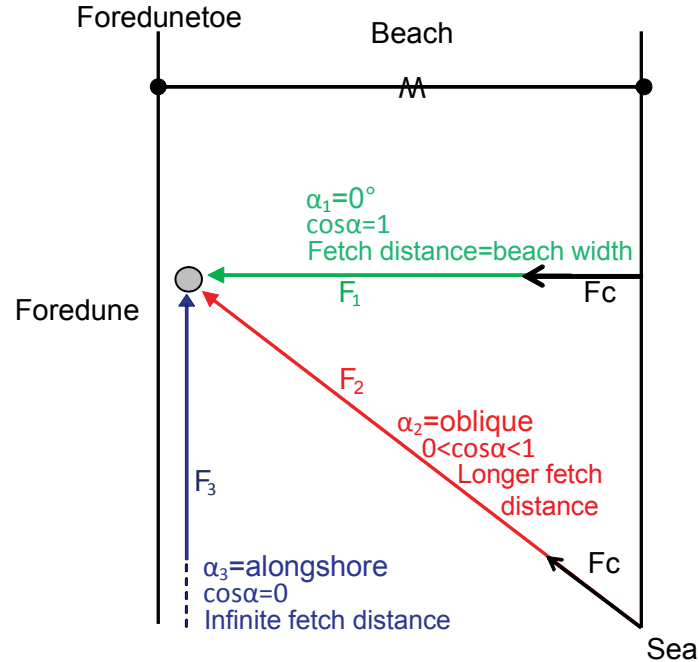
Figure 3.3. Definition of fetch distance and influence of wind direction in a foredune-beach system. The fetch distances are a function of the width of the beach (W), the angle of the wind approach (α) at the circle: fetch distance is equal to the beach width when the wind blows direct onshore (F_1), and increases during oblique onshore winds (F_2). When the wind blows parallel to the foredune (F_3), the fetch is assumed to be infinite but sand transport into the foredune tends towards zero. The critical fetch distance (Fc) is identical for any wind direction in the theoretical case where the entire surface of the beach is uniform. The critical fetch length augments with increasing surface moisture content, so that the maximum rate of sand transport is small on a wet beach and the distance over which the maximum equilibrium rate of transport develops is longer.

C. Surface characteristics

C.1. Surface moisture

Surface moisture is a significant factor controlling both the threshold of sand movement and the aeolian transport rate (Davidson-Arnott and Law, 1996, Davidson-Arnott et al., 2008). Interaction between particles in moist sediment is increased by capillary forces, which result in the existence of water wedges that form at the contact point of the grain, and by adhesion forces determined by the molecular absorption of water onto the surface of the grain (McKenna Neuman and Nickling, 1989). These forces combine to retain water in the sediment matrix increasing the resistance of surface particles to

entrainment (Belly, 1964, Wiggs et al., 2004a). Estimates of the surface moisture content above which sand transport cannot take place vary considerably, but a moisture content greater than 10% is generally agreed to significantly reduce sand flux (Sherman and Lyons, 1994, Wiggs et al., 2004a).

Moisture sources on a beach include groundwater seepage, tidal variation and precipitation. During rainfall events, rain splash can have an impact similar to that of saltation bombardment by dislodging and ejecting particles into the airstream (e.g. Cornelis et al., 2004). This can therefore cause enhanced aeolian transport. However for this study, all fieldwork was conducted during dry weather conditions so only surface moisture content was accounted for.

C.2. Particle size distribution

A number of sediment characteristics affect particle entrainment, including density, textural variation and shape (Logie, 1982, Jensen and Sorensen, 1986, Nickling and McKenna Neuman, 1995, Van der Wal, 1999). At the study sites, all sediments were > 80 µm diameter and samples were > 90% quartz (see section 2.3).

C.3. Vegetation

The presence of vegetation has a strong effect on sand transport by protecting the surface via direct cover of the surface resulting in a decrease of wind speed above the surface (additional drag). This restricts sand entrainment, traps particles and most significantly extracts momentum from the airflow (Wolfe and Nickling, 1993). The extent of these effects depends on the plant species present, and their density (Buckley, 1987, Hesp, 1989, Arens, 1996b, Hesp, 2002).

C.4. Summary of supply-limiting factors

Table 3.1 summarises the impact of various controlling factors on foredune development at the micro-scale.

Table 3.1. Summary of how different factors influence aeolian sand transport. In most cases symbol (+/-) indicates whether an increase in the factor will increase (+) or decrease (-) potential sand transport.

Primary factors	Atmospheric conditions	Sediment characteristics	Secondary factors		
			Surface	Topography	Other factors
Sand supply (+)	Precipitation (-/+)	Size (-/+)	Moisture content (often-/+)	Surface roughness (-)	Vegetation cover (-)
Wind speed (+)	Evaporation (+)	Density (-)	Surface crusts (-)	Slope upward (-) Slope downward (+)	
Turbulence (+)	Air temperature (+/-)	Texture and shape: Roundness(+) Angularity (-)	Tide: High (-) Low (+)	Micro-features (-)	
Wind direction (+/-)	Air pressure (-)	Shericity (+/-)	Fetch distance (+)		

3.2.3. Airflow Structure over the Foredune

Relationships between foredune topography and near-surface airflow influence the foredune-beach system through airflow-form interactions. These result in secondary flow effects such as topographic forcing, modifying the distribution of wind speed and surface shear stress over the foredune; and topographic steering, a redirection of airflow in the lee of the foredune, that can be significantly different from the incident wind direction (Mikkelsen, 1989, Arens et al., 1995, Lynch et al., 2010). Flow-form interactions will differ between onshore and offshore winds due to the contrasts in topography and vegetation cover encountered by the wind.

As airflow approaches a foredune, near-surface pressure rises due to increased (positive) pressure gradient (Figure 3.4A [on the left], Figure 3.4B [on the right]). A flow stagnation zone of diminished wind speeds and shear stresses occurs at the foredune toe, where potential sand deposition may take place (Wiggs, et al., 1996, McKenna-Neuman, et al., 1997, Walker and Nickling, 2002). Where this zone coincides with vegetation cover, flow stagnation effect is likely to increase (Rasmussen, 1989, Arens et al., 1995). Despite a decrease in velocity near the base of the windward slope, shear is still maintained due to the curvature effect on the airflow, which enhances sand transport potential at the up-wind dune base (Wiggs et al., 1996).

Along the windward foredune slope, airflow is compressed and topographic flow acceleration associated with speed-up occurs in response to a declining (negative) pressure gradient toward the foredune crest (Jackson and Hunt, 1975, Arens et al., 1995, Hesp et al., 2005). This causes a significant drop in pressure as flow is compressed and accelerates to the foredune crest, increasing surface shear stress and potential sand transport (Lancaster, 1985, McKenna Neuman et al., 1997, 2000, Walker, 2000). Generally, oblique winds approaching a foredune deflect toward crest-normal (Svasek and Terwindt, 1974, Rasmussen, 1989, Arens et al., 1995). This effect is amplified when incident angles are between 30° and 60° to the dune crestline (Mikkelsen, 1989) because topographic airflow acceleration augments the foredune-normal component of local flow vectors up the windward slope. Highly oblique winds (less than 30°) are typically deflected parallel to the dune crestline (Mikkelsen, 1989, Walker et al., 2009). As airflow travels over the foredune, the isovels (i.e. lines of equal wind velocity) are compressed at the crest, increasing potential sand transport capacity. Flow expansion and deceleration over the foredune crest depend on the

slope profile, specifically the crest height and lee slope width. Sand accumulation can occur in this downwind zone due to wind speed deceleration (Arens et al., 1995) (Figure 3.4A [on the left] and 3.4B [on the right]).

A) **Offshore winds**
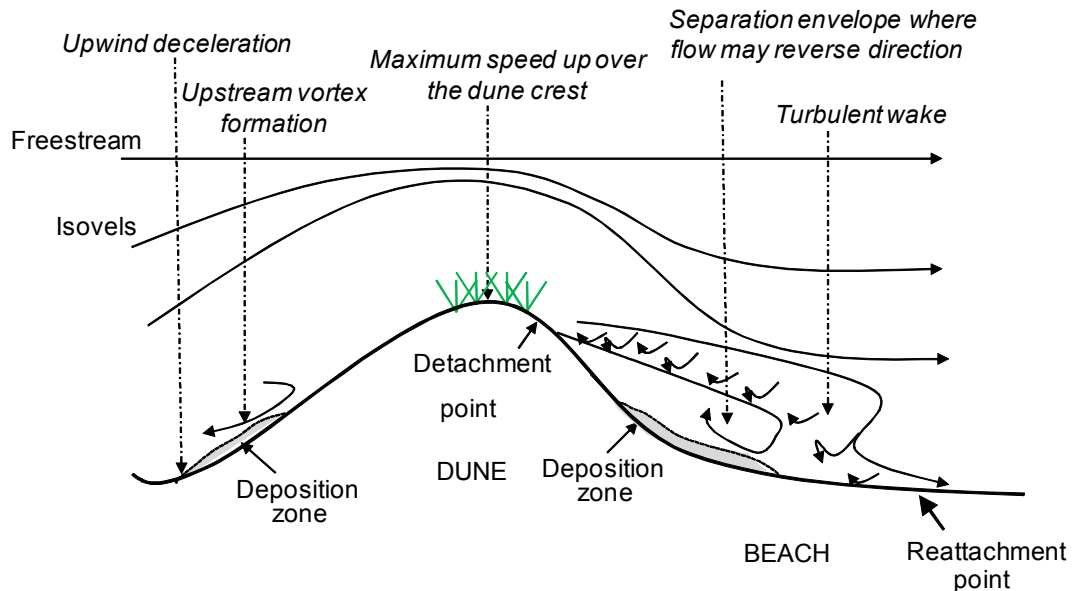
B) **Onshore winds**
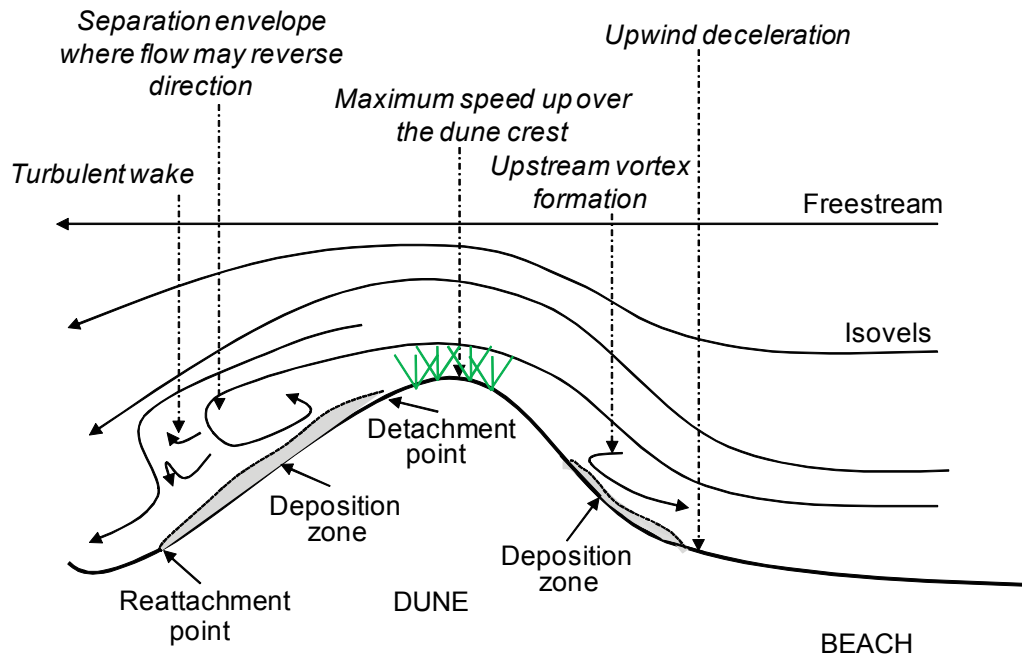
Figure 3.4. Schematic of idealized airflow over a foredune with: (A) offshore winds, (B) onshore winds.

There are three types of secondary lee side airflow (Figure 3.5): attached and undeflected flow, attached and deflected flow, and separated flow (Sweet and Kocurek, 1990, Walker and Nickling, 2002). Which one occurs is primarily dependent on foredune shape (described by the aspect ratio, h/L where h is the foredune height and L is the distance from the crest to h/2) and the incident angle of the wind (Figure 3.5B). Attached and undeflected lee side airflow occurs when wind approaches at an angle less than 10° from crest normal and the lee slope angle is below 20°. Oblique wind incident angles between 10° and 70°, or 70° and 90° for aspect ratios below 0.2 under stable atmospheric conditions, result in attached flow with crest-parallel deflection in the foredune lee. Incident wind angles above 70° for dunes with an aspect ratio above 0.2 promote separated flow with a recirculation cell, while below 0.2 flow separation only takes place with unstable thermal atmospheric conditions (Figure 3.4A [on the right], Figure 3.4B [on the left]).

A)

B)
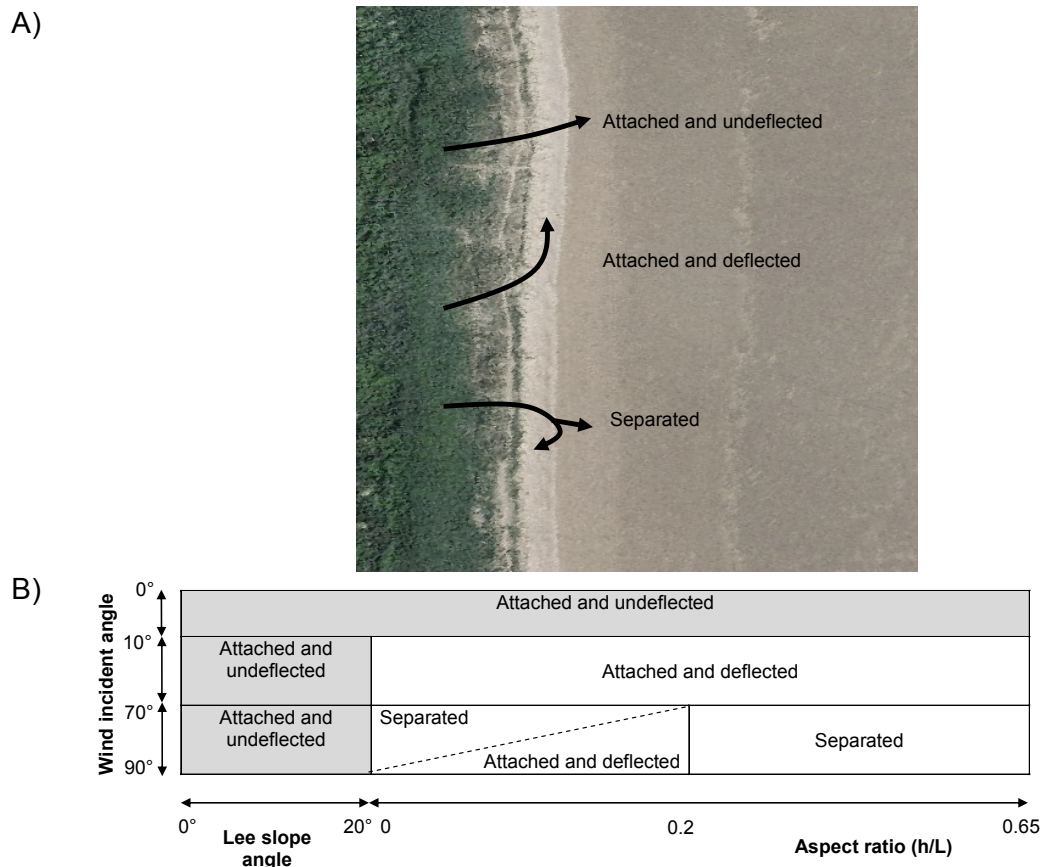
Figure 3.5. (A) Description of secondary lee side airflows illustrated for offshore winds, (B) model of their patterns over a foredune as function of wind approach, dune shape (h/L), and lee slope angle (modified from Sweet and Kocurek, 1990).

Each type of secondary lee flow is characterized by wind velocity decelerations and a significant variability of wind direction and/or speed, caused by the occurrence of turbulence (Arens et al., 1995, Walker and Nickling, 2003). Thus, each type of lee flow can be assumed to influence sand transport in different ways (Lynch et al., 2008). In general, the attached airflows are expected to be able to entrain sand in the lee of a foredune if velocities exceed the transport threshold. While reverse airflow combined with airflow separation may result in a process capable of moving sediment counter to the primary direction of airflow (Lynch et al., 2008). Separated flow will transport minimal or no sand on the leeward side, and be characterised by an increase in turbulence.

Recent coastal research has highlighted the role of lee-side airflow in coastal foredune development. Hesp (2005) identified the potential of offshore winds in dune formation describing large climbing dunes (~150 m high) in the lee of bedrock cliffs that are directly attributed to large-scale lee side re-circulation cells. Lynch et al. (2009) report sediment deposition at the foredune toe under offshore winds and suggest this is due to airflow modification due to the morphology (Lynch et al., 2010). These findings have highlighted the importance of secondary airflow patterns in foredune morphodynamics, and especially in dune maintenance and post-storm recovery.

3.3. Methodology

3.3.1. Experimental Set-up

A. Wind data

Aeolian field experiments require at a minimum the deployment of a static reference mast and a mobile mast, which is further described below. A series of one-day field experiments was conducted during a single week in each season at Brickyard Lane (BL), Theddlethorpe St Helens (TSH) and Mablethorpe North End (MNE) sites (Table 3.2).

Table 3.2. Field day experiments.

Site	Experiment	Day	Dominant wind direction
BL	Exp-1	13/10/2009	Oblique onshore
	Exp-2	28/01/2010	Oblique offshore
	Exp-3	28/04/2010	Highly oblique offshore
	Exp-4	07/07/2010	Direct offshore
TSH	Exp-1	15/10/2009	Oblique onshore
	Exp-2	27/01/2010	Oblique offshore
	Exp-3	29/04/2010	Highly oblique offshore
	Exp-4	08/07/2010	Direct offshore
MNE	Exp-1	14/10/2009	Highly oblique offshore
	Exp-2	26/01/2010	Oblique onshore
	Exp-3	27/04/2010	Highly oblique onshore
	Exp-4	06/07/2010	Direct offshore

In total, twelve experiments were carried out, focusing on the geomorphological sub-units along the foredune-beach at the three study sites previously defined in Chapter 2: the secondary foredune crest (SFC), secondary foredune toe (SFT), primary foredune crest (PFC), primary foredune toe (PFT), upper beach (UB), middle beach (MB) and lower beach (LB) and seaward embryo dunes (SED) at TSH (Figure 3.6).

Recent research suggests the intertidal ridge and runnel system reduces or segments the fetch distance and hence aeolian sand transport due to high surface moisture content and bedform control associated with the development of wave-and tide-generated ripples (Vanhée et al., 2002, Anthony et al., 2009). In this study, it was assumed that a little sand transport took place between the intertidal ridge-runnel system and the foredune-beach at the micro-scale. Aeolian sand transport is the main process over the upper beach above the MHW elevation (2.46 m), representing a transitional limit between foredune and shoreline related and wave and tidal driven processes (Masselink and Short, 1993, Haxel and Holman, 2004).
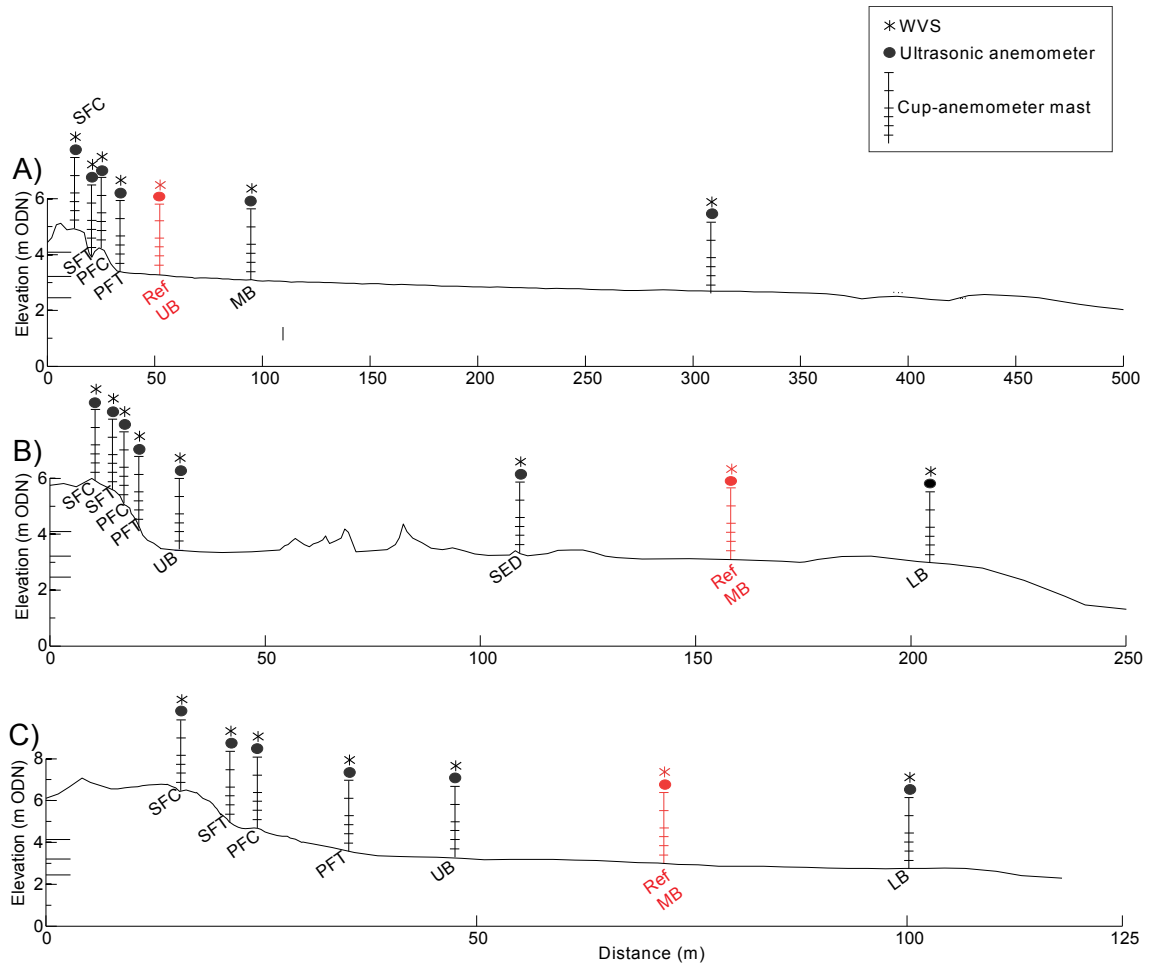
Figure 3.6. Instrument mast locations and sub-units of the foredune-beach profile at: (A) BL, (B) TSH and (C) MNE. On the left axis, the horizontal lines indicate HAT (top), MHWS (centre) and MHW (bottom). WVS=wind vane sample, see text for details.

In autumn 2009 (Exp-1), the reference mast was deployed on the SFC at all the sites, however vegetation on the dune can make it hard to interpret the reference conditions. For subsequent experiments, the reference mast was deployed on the flat unvegetated upper beach at BL and in the middle of the beach at the TSH and MNE sites (Figure 3.6). The reference mast comprised a vertical array of Vector A-100R three cup anemometers mounted at 0.22 m, 0.50 m, 0.80 m, 1.20 m and 1.70 m heights and a RM Young 5013 wind monitor at 2.4 m above the surface. All these mechanical anemometers were calibrated using wind tunnel measurements to certify the wind speed readings.

Wind direction was recorded at a height of 0.50 m with a wind vane (Vector W 200P) and at 2.4 m with a wind monitor (Figure 3.7). Manufacturer ratings are that direction measurements are accurate to ±2° in steady winds. Wind speed measurements are

accurate to ±0.1 m s^{-1} over the range 0.3-10 m s^{-1} (Campbell Scientific, 2009). A further identical array of instruments was mounted on a mobile mast, which was deployed for periods of at least 20-minutes at each sub-unit. All instruments were oriented normal to the wind direction and each mast was connected to a Campbell Scientific CR800 datalogger for recording wind velocity and direction data every 10 seconds which was then averaged over 1-minute periods.

Near-surface turbulent flow is defined as a series of vortices of different sizes superimposed on mean flow and on each other (Tennekes and Lumley, 1972). Turbulent vortices transport air, momentum, temperatures and other properties. If, on average, the air moving downward has a greater horizontal velocity than the air moving upward, this suggests a downward flux of horizontal momentum corresponding to the Reynold stress (Van Boxel et al., 2004). This strongly influences sand transport dynamics. Turbulence was measured using an ultrasonic anemometer (CSAT3 Campbell Scientific). This wind sensor is composed of three fixed pairs of non-orthogonal transducers, recording the three dimensional wind at high frequency, based on the transit time of ultrasonic acoustic signals (Figure 3.7). An ultrasonic anemometer was placed at the reference station and the mobile mast at 0.80 m above the surface. All ultrasonic anemometers were aligned to true horizontal and orientated into the prevailing wind. Three-dimensional wind velocities were sampled at 1 Hz, and the records were directly transferred to the datalogger. Low frequency oscillations with a periodicity of several minutes should be detected as well as short gusts/turbulence with a minimum duration of 1 second. However, structures of the smallest duration will not be measured (Walker, 2005). The accuracy of the wind speed is ≤ ±1% RMS (root-mean-square) with a resolution of 0.01 m s^{-1}; and the directional accuracy is ≤ ±1° RMS with a directional resolution of 1° (Campbell Scientific, 2007).
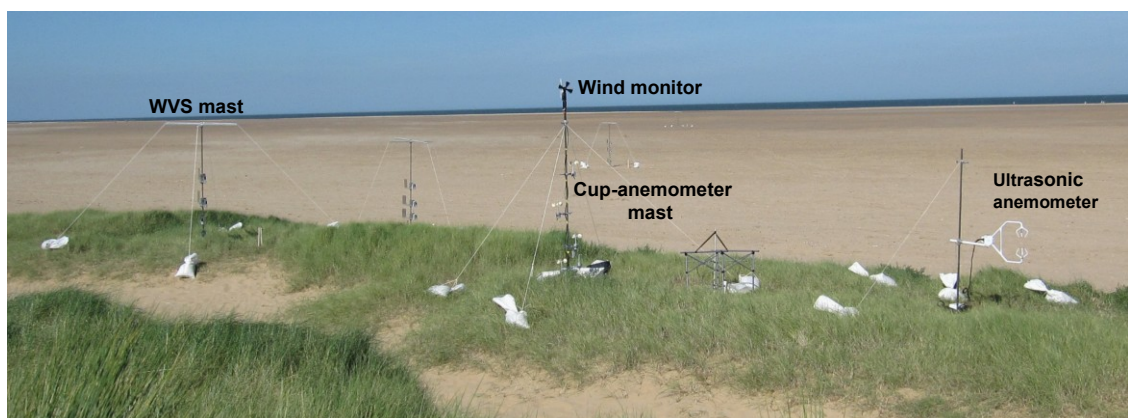
Figure 3.7. Typical field instrument mast deployment.

B. Aeolian sand transport measurements

Aeolian sand transport was measured using fixed masts of four self-orientating Wind Vane Samplers (WVS) (Fryrear, 1986) at each sub-unit (Figures 3.6, 3.7). These were modified to include a rain hood (Shao et al., 1993). The traps have an opening of 0.001 m^2 and whilst only 40% efficient, they have the advantage of constant efficiency for a wide range of wind speeds (Goossens and Offer, 2000). The WVS were mounted at the same elevation as the cup anemometers and the mast placed at a distance of 3 m from the wind measurement masts to minimise airflow disturbance. The weight of trapped sand from the WVS sand traps was converted to a rate of transport in g m^{-1} h^{-1}.

C. Surface, vegetation characteristics and beach fetch measurements

Surface moisture content of the ground surface was measured using a Type ML2x Theta probe (Delta-T Devices, 1999). This impedance probe is a robust and reliable method of recording near-surface moisture (Atherton et al., 2001, Yang and Davidson-Arnott, 2005). The probe was calibrated for the local sediment characteristics as described by Yang and Davidson-Arnott (2005). Calibration relationships were developed from linear regression of measured gravimetric moisture content versus probe output (1110 mV is equivalent to 100% moisture content). In the field, surface moisture content was measured at 2 hour intervals at each sub-unit. Surface sediment samples were collected at each sub-unit and as described in section 2.2.

Estimates of the vegetation cover, height, and plant species characteristics were made using a quadrat of 1 m × 1m during each experiment. Ideally vegetation flexibility, porosity, and lateral cover would also have been made (Ranwell, 1972) but this was not possible due to time constraints. There was little seasonal variation in vegetation cover, so only average vegetation cover is presented in Figure 3.8.

The distance of potential maximum fetch distance for each experiment was estimated using Eq 3.4 which incorporated the day experiment average wind direction measured at the reference mast and the lowest tide level predicted during the experiment. Additionally, seaward aspect ratio was calculated for each experiment in relation to wind direction (defined in section 3.2.5). Landward sides of the secondary foredunes are flat fields, so it was considered that the landward aspect ratio was small (<0.01) and unlikely to disturb the airflow. Further the vegetation cover on the landward side is 100% and tall (> 1m) so that this will prevent much sand transport in the back dunes.
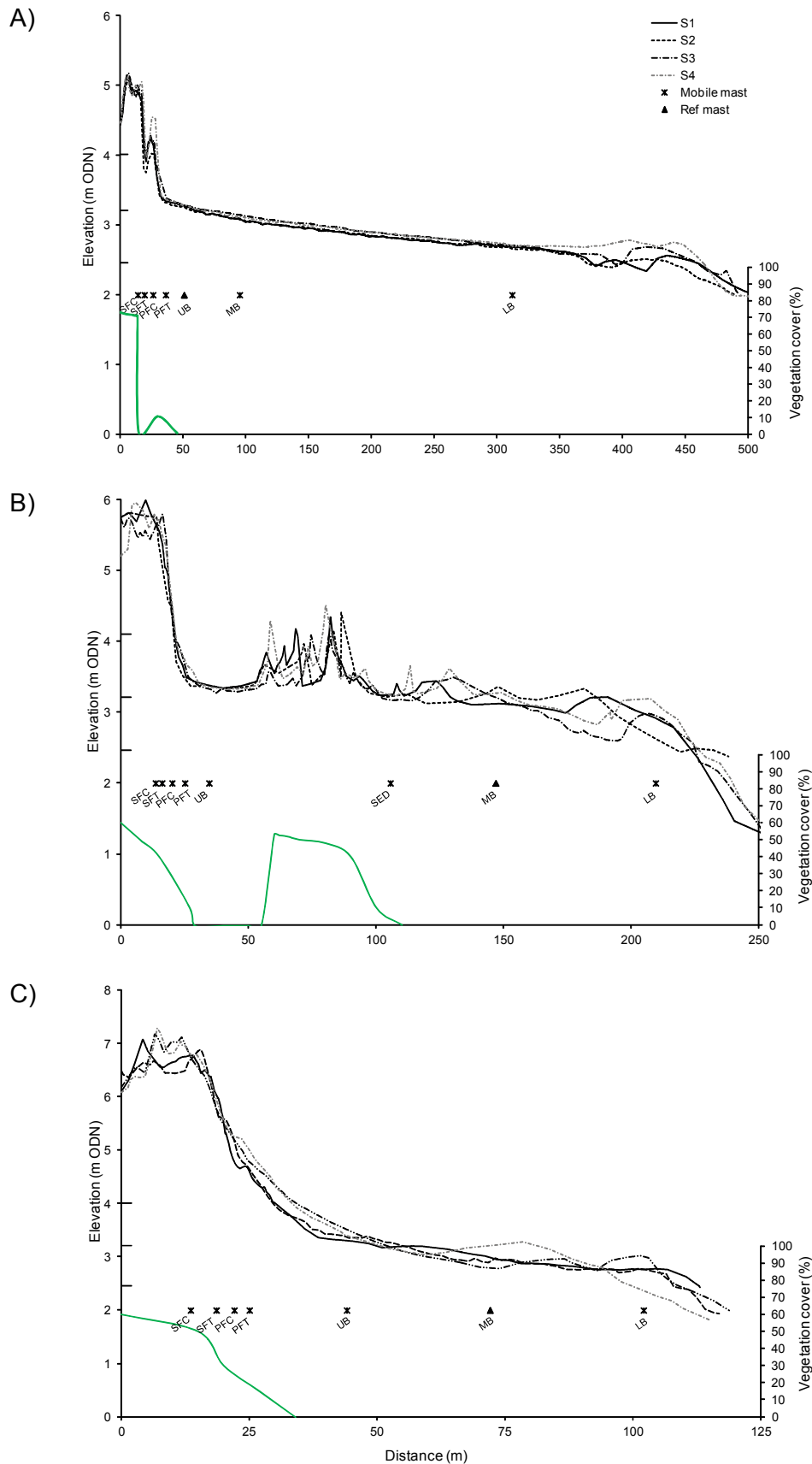
Figure 3.8. Field deployment along the seasonal topographic profiles at: (A) BL, (B) TSH and (C) MNE; and average of vegetation cover surveys (Green line). The horizontal ticks on elevation axis indicate HAT (top), MHWS (centre) and MHW (bottom).

3.3.2. Wind Field Data Analysis

In each sub-unit, sampling duration was a minimum of 20-minutes, which was statistically long enough to measure net horizontal wind regime and also to capture a few of the largest turbulent eddies characterizing the airflow (Van Boxel et al., 2004, Leenders et al., 2005).

A. Wind-cup and -vane data handling and analysis

Wind velocity variations were investigated along the foredune-beach profile. Data on mean wind velocity from the mobile mast were normalized against the reference station data and used to calculate the fractional speed-up ratio (δ_S) as defined by Jackson and Hunt (1975):

$$\delta_S = \frac{U_m}{U_{ref}}$$

Eq 3.5.

Where U_m is the velocity at height z on the mobile mast, and U_{ref} is the velocity at height z at the reference station. Thus, where δ_s=1 wind speed at a given height is the same at both mobile and reference masts. Values of δ_s<1 (δ_s>1) indicate relative decrease (increase) in wind speed at the mobile mast.

The RM Young Wind monitor at 2.4 m height is not a self-aligned vane. For each experiment, the angle of the horizontal plane between the incoming wind vector and geographical north was recorded for the reference mast and at each 20-minute recording for the mobile mast. This was used to correct the wind monitor measurements by calculating the difference between true geographic direction and the datalogger records and applying an adjustment to the data sets. The wind direction accuracy is assumed to be ±10°. Due to the difference in equipment accuracy and difficulties with orientating the vanes on top of the masts (differences of ±10° due to improper orientation are probable), only relative patterns should be compared. Wind direction was compared between the mobile and reference masts recording at the same height.

B. Ultrasonic anemometer data procedures and analysis

Complex turbulent flow is ubiquous in aeolian environments, and its characterization is important for sand transport because instantaneous peaks in velocity components that exceed time-averaged shear velocity above a surface may be sufficient to entrain sand grains (Walker, 2005). Turbulent vortices often lead to velocity fluctuations in all directions. The instantaneous wind velocity above a ground surface can be characterized by three orthogonal components horizontal/streamwise (u), spanwise (v) and vertical (w); and each component can be split by Reynolds averaging (Reynolds, 1895) into a mean part (denoted by overline) and a fluctuating part (denoted by a prime):

$$u = \bar{u} + u'$$
$$v = \bar{v} + v'$$
$$w = \bar{w} + w' \qquad \qquad \text{Eq 3.6.}$$

By definition, $\bar{w}$ is equal to zero.

Although airflow should be considered in three dimensions, the most important velocity fluctuations are in the uw plane because they contribute most to shear stress and they are used for the detection and characterization of coherent structures in the turbulent boundary layer (Willmarth and Lu, 1972). Thus, characterization of u- and w-components are usually considered to be directly related to sediment transport dynamics, and therefore are used to determine the surface shear stress using the Reynolds stress (RS) approach (Kaimal and Finningan, 1994):

$$RS = -\rho \overline{u'w'}$$

Eq 3.7.

Where ρ is the density of air, and time-average RS describes the covariance ($\overline{-u'w'}$) (m^2 s^{-2}) between u'- and w'- velocity components.

Physically, RS is the time-averaged vertical flux of horizontal momentum at a point generated by diverging velocity fluctuations within the airflow. As a surrogate, the kinematic Reynolds stress (RS_k) is frequently used (Chapman et al., 2012):

$$RS_k = -\overline{u'w'}$$

Eq 3.8.

such that the surface shear stress (u_{*RSk}) (m s^{-1}) can be estimated by:

$$u_{*RSk} = \sqrt{|\overline{u'w'}|}$$

Eq 3.9.

Despite the normally distributed u- and w- components, Reynolds stress captures the average vertical flux of horizontal streamwise momentum. The turbulence structures are crucial in geophysical flows because they are related to sediment transport dynamics (Jackson, 1976, Leeder, 1983). Nevertheless, the relationships between sediment transport and quadrant analysis rely on the assumption that the ultrasonic anemometer is parallel to the bed plane and that the mean vertical velocity, normal to the surface, is equal to zero; thus w'>0 indicates a motion away from the surface and is associated with sediment suspension whereas w'<0 is related with bed load transport as it indicates a motion of fluid towards the surface (Leeder, 1983; Williams et al., 1989).

Observed 3-D velocity data were rotated for yaw and pitch to correct for potential ultrasonic misalignment to local streamlines (Van Boxel et al., 2004, Walker, 2005). The yaw rotation aligns the u-component parallel to the surface in the wind direction (ω), while the pitch rotation orientates the u-component into the direction of the sloping streamlines with w-component perpendicular to the streamlines and was corrected using the arctangent function (Appendix 3.1). This realignment transforms wind speed and direction from Cartesian coordinates into Polar coordinates. The roll-rotation, to orient the v-component along the stream surfaces and w-component perpendicular to the stream surface, was omitted due to the uncertainties that arise in this dimension after pitch and yaw corrections over complex terrain (Van Boxel et al., 2004, Lee and Baas, 2012). Given that the average v-component was zero ($\bar{v}$=0) no further analysis of this component was carried out. The remaining velocity data were partitioned into a time average part ($\bar{u}, \overline{w}$) and a turbulent fluctuating part (u', w') from which the time-

averaged shear velocity (u_{*RSk}), a direct product of turbulent momentum flux, was determined.

Steadiness of horizontal airflow (CV) (dimensionless) was measured using the coefficient of variance which has been described as a turbulence proxy (Walker and Nickling, 2003):

$$CV = \frac{\sigma}{\bar{u}}$$

Eq 3.10.

Where σ and $\bar{u}$ are the standard deviation and the mean of horizontal wind velocity respectively during the 20-minute experiment.

The variation in wind direction and wind speed variability are combined in the CV and made it possible to infer the level of turbulence in the airflow (Lynch et al., 2010). For example, an increase of turbulence structures (unsteady airflow) associated with onshore-directed airflow suggests airflow separation. The CV calculated at the different sub-units was then normalized by the CV values at the reference mast where the streamwise airflow would be expected to be steady. A normalized CV value >1 (<1) suggests an unsteady (steady) airflow usually associated with turbulence structures.

3.4. Results

Wind speed, direction, turbulence and other variables such as fetch distance and surface moisture are examined by sub-unit and by site for each experiment day and presented here with relation to wind direction (i.e. measurements taken during offshore, oblique offshore and onshore winds). Due to differences in equipment accuracies and orientation correction, only relative variations in wind angle of approach and patterns are compared. The wind direction measured at 2.4 m high was assumed to reflect the regional wind direction (i.e. undisturbed airflow).

The angle of approach of the wind will affect the precise topography over which air flows and the dune aspect ratio encountered. For this reason, the topographic profile aligned parallel to the wind direction was extracted from digital terrain models of the beach measured on the same field week experiment (see Chapter 4). The angle of approach of wind varies from near direct onshore/offshore to very oblique flow. From Figure 3.3 when wind approaches at an angle the topography and beach fetch distance will need to be adjusted, and additionally the aspect ratio of the foredunes will change. For example, at MNE if wind blows perpendicularly offshore the seaward aspect ratio of the dunes is 0.167 and the distance between the middle beach anemometer and the benchmark is 72 m. However, if wind blows obliquely offshore at an angle of 187° the seaward aspect ratio changes to 0.060 and the middle beach anemometer would be 159 m from the benchmark. In all cases the topography over which the wind flows is adjusted for angle of approach using the cosine equation (Eq. 3.4). The DTMs do not extend far enough seawards to generate a full beach profile so that the relative position of the seaward most measurements is indicative rather than absolute (i.e. from the upper beach to lower beach masts). Where reported, the aspect ratio is the value adjusted for wind direction and coastline orientation.

3.4.1. Direct Offshore Winds

Table 3.3 presents the meteorological and beach environmental conditions measured at the three study sites during direct offshore winds recorded during the summer survey (Exp-4).

Table 3.3. Characteristics of meteorological and beach environmental conditions during direct offshore winds at the three study sites. U=mean wind speed at 2.4 m high; WD=wind direction at 2.4 m high; α=incident angle relative to foredune normal; T=mean air temperature; Seaward foredune (F) slope; Fmax=maximum potential fetch distance and UL for unlimited; aspect ratio of the seaward side (dimensionless).

Site	Day	U (m s^{-1})	WD (°)	α (°)	T (°C)	F slope (°)	Fmax (m)	Aspect ratio	Rain
BL	Exp-4: 07/07/2010	5.23	230 [Direct offshore]	20	27	3.78	UL	0.016	no
TSH	Exp-4: 08/07/2010	4.11	242 [Direct offshore]	12	26	7.80	UL	0.036	no
MNE	Exp-4: 06/07/2010	3.28	264 [Direct offshore]	14	24	10.04	UL	0.167	no

Figure 3.9A shows that at BL the time-averaged wind speed on the middle and lower beach are higher at all measurement elevations compared to the reference mast on the upper beach, while that measured on the foredunes was lower. This reflects a general flow stagnation as the airflow passes over the foredunes followed by a re-equilibrium on the beach. The velocity reduction observed immediately to the lee side of the foredune is what would be expected for offshore winds. Specifically, near-surface airflow progressively increases as it passes over the SFC, SFT, and the PFC, but decelerates over the PFT. Near-surface speed (0.22 m) increases over the lower foredune ranging from δ_S 0.29 at SFC to 0.63 at PFC. This reflects a flow stagnation encountered by offshore winds and drag imposed by vegetation roughness on the secondary foredune; and also that the airflow has started to recover at PFC. The upper portion of all the profiles show uniform and linear shape. Although wind speed was above sand transport threshold only a very small amount of material was trapped, and in only two locations (SFT: 0.079 g m^{-1} h^{-1}; PFT of 0.05 g m^{-1} h^{-1}). None of the other WVS trapped sand, and this was probably due to high beach moisture content (up to 35.6% on the middle beach) (Figure 3.9D).
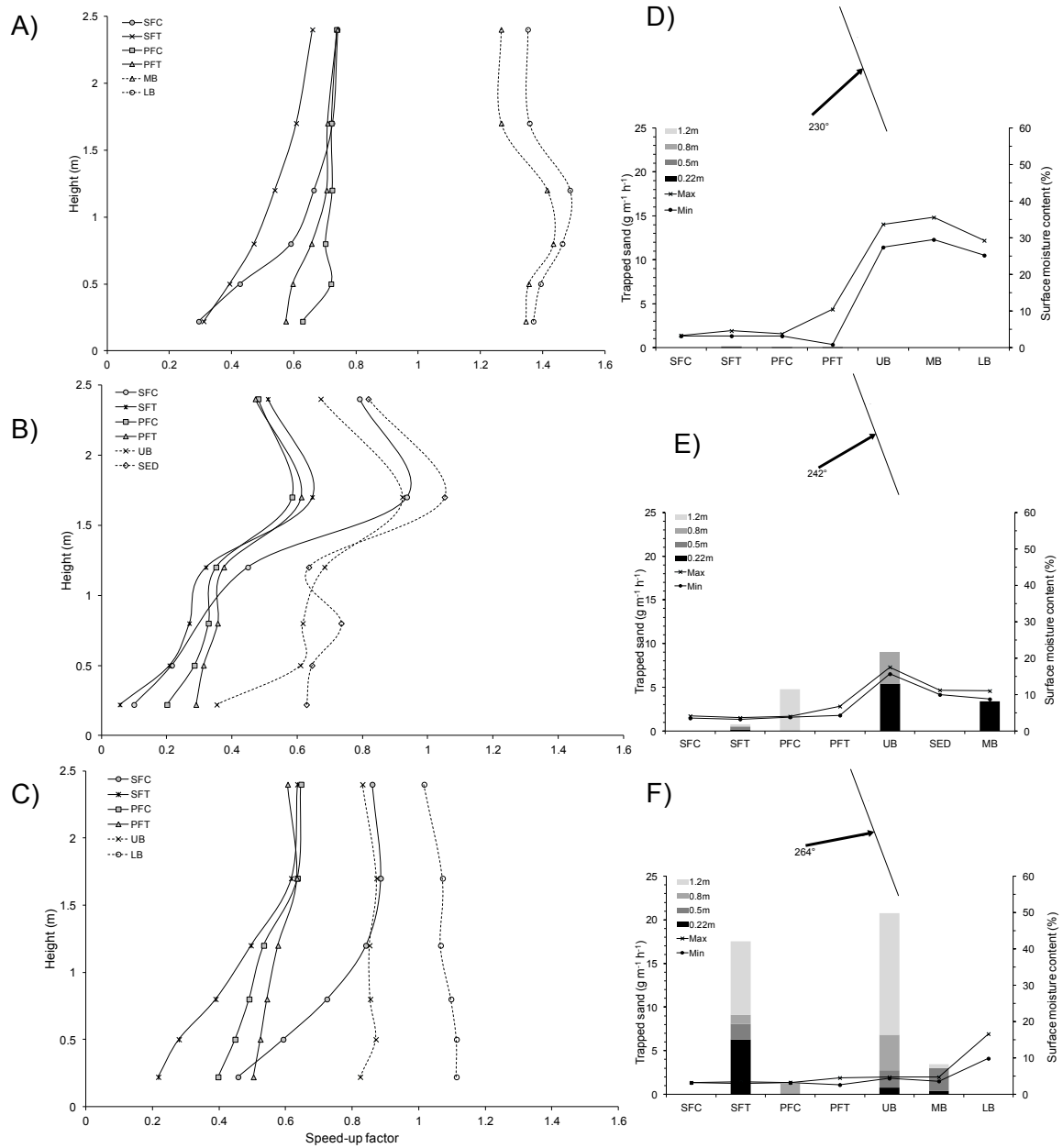
Figure 3.9. Time-averaged speed-up profiles over the foredune-beach during direct offshore winds at: (A) BL, (B) TSH and (C) MNE; trapping rate of sand and moisture content over the profile at: (D) BL, (E) TSH, and (F) MNE. Insert: line represents coastline and arrow shows the wind direction at the reference mast.

Figure 3.9B indicates complex velocity profiles at TSH. All wind speeds measured over the foredunes were lower than those on the middle beach (reference mast). Near-surface airflow generally increases as it passes over the SFT, SFC, PFC and over the PFT. This indicates a flow stagnation effect due to wind speed reduction immediately in the lee-side of the foredune. This was more pronounced at the SFT ($0.056 \, \delta_S$ at 0.22 m high), whereas an increase of airflow occurred at the PFT ($0.29 \, \delta_S$ at 0.22 m high). These results show the near-surface airflow starts to recover over the primary foredune. In general, windflow at all sub-units linearly increases up to 1.2 m with steeper slopes at the upper portions, indicating an increase of fluid shear above the

vegetation canopy. The upper profiles show acceleration at 1.7 m high, ranging from δ_S of 0.58 at PFC to 1.05 at SED. This probably indicated a wake of flow generating a zone of relatively high turbulence. At the end of the experiment at TSH, the sand traps on the SFC, SED, and PFT were empty indicating that no sand transport occurred (Figure 3.9E). Sand transport was measured at the higher sand trap of the PFC (4.79 g m^{-1} h^{-1}) but very little trapping occurred at the SFT. Although the moisture content was relative high (from 15.6-17.5%) on the upper beach, maximum sand transport occurred there with a rate of 5.37 g m^{-1} h^{-1} at 0.22 m high and 3.69 g m^{-1} h^{-1} at 0.80 m high, while less transport rate occurred on the middle beach (3.37 g m^{-1} h^{-1}).

At MNE, all the speed-up profiles were lower at all elevation measurements compared to the reference station on the middle beach (Figure 3.9C). Near-surface airflow decreases as it passes over the SFC, however progressively accelerates at the PFC, PFT and over the UB. At the PFT, the speed-up is 0.502 δ_S at 0.22 m high, however a lower value was expected due to the flow expansion, so surface roughness may have inhibited this effect. No sand was trapped at SFC, PFT and LB (Figure 3.9F). A maximum sand transport was measured on the dry UB and SFT sub-units that had not been submerged during the previous high tide. Interestingly, the greatest sand transport rate for both these sub-units was at the top traps (1.20 m), suggesting the occurrence of effective suspension transport. Little sand was trapped at PFC and MB, although the surface moisture content only ranged from 3.6-4.7%.

During direct offshore wind, wind directional variability was low in all sub-units at BL (Figures 3.10A, B). Streamwise flow steadiness values (normalized CV, refer to section 3.3.2.B) exceed 1 in near surface flow over the foredunes, indicating an unsteady flow likely to be associated with turbulence structures (Figure 3.10C). Turbulence in the lee of the secondary foredune caused a rise in variability up to 1.7 on the SFT. However, as expected, CV values decreased toward the beach, indicating steady airflow. Figure 3.10D is a summary of the flow structures and changing transport capacity of the wind from sub-unit to sub-unit. Comparing one anemometer reading with the adjacent downwind measurements, a positive sign indicates increase in potential sand transport capacity and negative sign indicates a decrease. At BL, sand transport capacity is reduced on the downwind (lee) slopes of the dunes (under offshore winds), the seaward slope is likely to feature in deposition while the airflow recovers on the beach to produce transport.
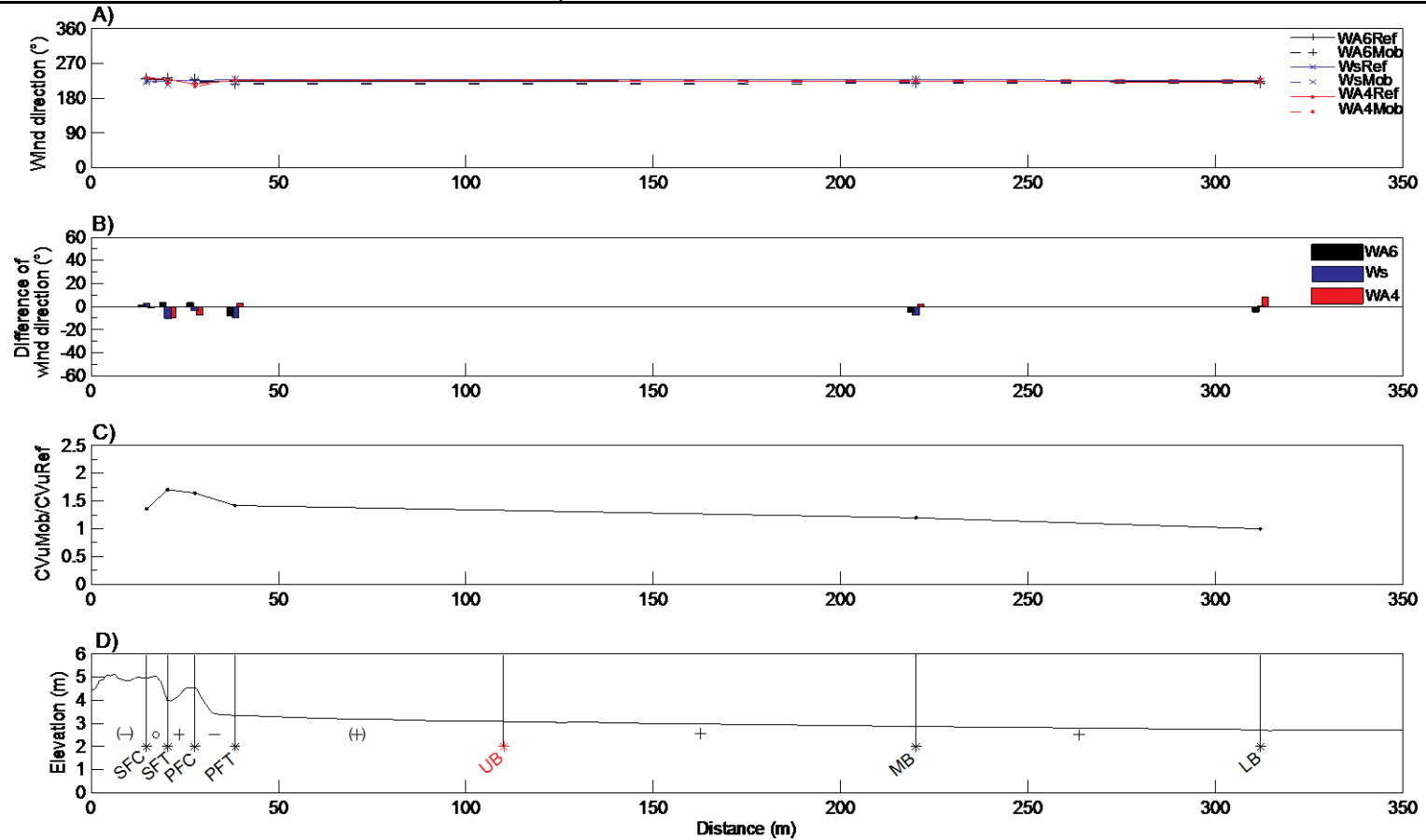
Figure 3.10. Wind regime at BL during direct offshore wind (Exp-4) in relation to topographic profile: (A) wind direction for reference (Ref) and mobile (Mob) anemometers at 0.50 m high (WA4), at 0.80 m high using an ultrasonic (Ws) and 2.4 m high (WA6); (B) variability in wind direction where the zero line corresponds to the average record at the reference mast; (C) flow steadiness, normalized CV; and (D) transport capacity model estimated from the speed-up factor measurement at the lowest anemometer. The symbol (+) corresponds to an increase of speed-up compared to the downwind sub-unit measurement, while the inverse corresponds to (-), and the equivalence to (o). Red and black annotations indicate the position of the reference and mobile mast respectively.

77

Overall wind direction at TSH was 242°, variability in wind direction was greater over the foredunes and for the near-surface airflow at 0.50 m and 0.80 m high than on the beach. In general, turbulence was higher over the foredune compared with the beach (Figure 3.11C). The normalized CV values of SFC and UB display relatively steadiness of the airflow, while high values were recorded at SFT, PFC and PFT. This indicates an increase of turbulence in the lee of the secondary foredune, which drastically declines after passing the primary foredune crest. Although the airflow was steady at the SED, it is likely to be disturbed over the embryo dunes. Figure 3.11D shows as the wind approaches the secondary foredune toe transport capacity is negative. However sand transport is likely to occur at the other sub-units, and in particular at the PFC where the development of turbulence could transfer additional energy. Relatively high amounts of trapped sand on the UB suggest that the greatest transport capacity is likely to occur at this sub-unit, which was characterized by effective fetch distance, low surface moisture content and fine sediment grains (range 238-242 μm see Table 2.5). Although sand was not trapped on the SED, transport capacity was positive with a relative steady airflow after re-emerging from the vegetated embryo dunes likely due to the distance of c.8 m between the mast position and the seawardmost embryo dune field, allowing a resetting of the airflow.
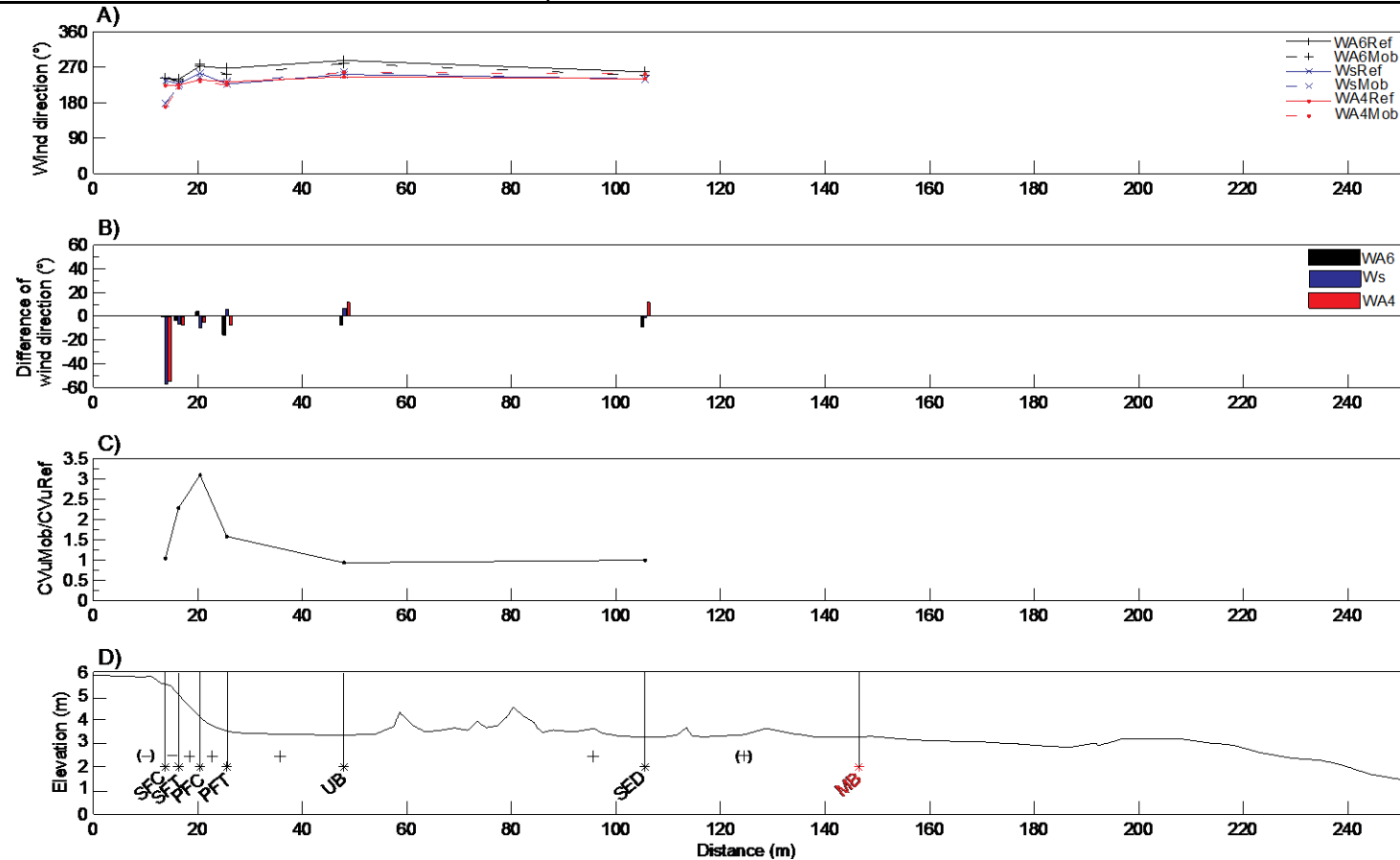
Figure 3.11. Wind regime at TSH during direct offshore wind (Exp-4) in relation to topographic profile: (A) wind direction for reference (Ref) and mobile (Mob) anemometers at 0.50 m high (WA4), at 0.80 m high using an ultrasonic (Ws) and 2.4 m high (WA6); (B) variability in wind direction where the zero line corresponds to the average record at the reference mast; (C) flow steadiness, normalized CV; and (D) transport capacity model estimated from the speed-up factor measurement at the lowest anemometer. The symbol (+) corresponds to an increase of speed-up compared to the downwind sub-unit measurement, while the inverse corresponds to (-), and the equivalence to (o). Red and black annotations indicate the position of the reference and mobile mast respectively.

Figures 3.12A, B shows noteworthy variability in wind direction on the SFT at MNE ranging from 19° at 2.4 m (254°) to 15° at both 0.80 m and 0.50 m (252°-253°). The same trend with a lower magnitude occurred at the PFC, while a slight variability was recorded at the PFT. This illustrates that the airflow is steered normal to the foredune, mainly caused by the straight ramp slope topography between secondary and primary foredunes (Figure 3.12D). Results also suggest that the effect of variations in wind direction was greater in the upper-portion of the airflow, perhaps due to topographic sheltering caused by the secondary foredune. Airflow is steady to prevail over the SFC (0.95), but more turbulent at the SFT with the greatest normalized CV value of 2.4 (Figure 3.12C). This however declines to c. 1.5 at PFC, PFT to become steady at UB. Figure 3.12D illustrates that transport capacity was only limited over the secondary foredune, as previously observed at the two other sites. However turbulence generated over the SFT is likely to play a significant role, as suggested by the relatively high sand transport rates recorded there (Figure 3.9F). Positive transport capacity is likely to take place over the primary foredune and beach sub-units.

Figure 3.12. Wind regime at MNE during direct offshore wind (Exp-4) in relation to topographic profile: (A) wind direction for reference (Ref) and mobile (Mob) anemometers at 0.50 m high (WA4), at 0.80 m high using an ultrasonic (Ws) and 2.4 m high (WA6); (B) variability in wind direction where the zero line corresponds to the average record at the reference mast; (C) flow steadiness, normalized CV; and (D) transport capacity model estimated from the speed-up factor measurement at the lowest anemometer. The symbol (+) corresponds to an increase of speed-up compared to the downwind sub-unit measurement, while the inverse corresponds to (-), and the equivalence to (o). Red and black annotations indicate the position of the reference and mobile mast respectively.

81

Table 3.4 presents the shear stress velocities calculated from the ultrasonic anemometers at 0.80 m high for each sub-unit during direct offshore winds. These were derived from the 20-minute averaged u'- and w'-components (section 3.3.2.B) presented in Appendix 3.2. Results at BL show the time-averaged shear stress velocity gradually increases from 0.78 m s^{-1} at the SFC to 0.93 m s^{-1} at the PFT, and then decreases at the beach sub-units. The average shear stress velocity (U_{*RSk}) was relatively uniform over the foredune sub-units at TSH ranging from 0.71 m s^{-1} at the SFC to 0.64 m s^{-1} at the PFC, but greater than on the flat middle beach (Reference mast).

Table 3.4. Summary of the time-averaged surface shear stress velocity (u_{*RSk}) at the reference (Ref) and mobile (Mob) masts estimated from the ultrasonic at 0.80 m high during direct offshore winds.

				u_{*RSk}				
	Ref	Mob		Ref	Mob		Ref	Mob
BL	Mean	Mean	**TSH**	Mean	Mean	**MNE**	Mean	Mean
Exp-4			**Exp-4**			**Exp-4**		
SFC	0.69	0.78	SFC	0.46	0.71	SFC	0.43	0.47
SFT	0.57	0.71	SFT	0.49	0.65	SFT	0.37	0.41
PFC	0.67	0.88	PFC	0.49	0.64	PFC	0.49	0.56
PFT	0.74	0.93	PFT	0.51	0.68	PFT	0.60	0.66
MB	0.67	0.63	UB	0.46	0.60	UB	0.47	0.50
LB	0.68	0.60	SED	0.46	0.55	LB	0.54	0.48

At MNE, unsteady airflow over the foredune observed in Figure 3.12C does seem to be enough to enhance the conveyance of momentum toward the surface of the foredunes as it protrudes into the atmospheric layer because the velocity of shear stress was relatively low over the foredunes ranging from 0.41 m s^{-1} to 0.66 m s^{-1}.

3.4.2. Oblique Offshore Winds

Oblique offshore winds occurred during five of the field experiments. The meteorological and beach environmental conditions measured at the three study sites during oblique offshore winds are summarized in Table 3.5. Figure 3.13 presents the time-averaged speed-up profiles, rate of trapped sand and moisture content at the three sites.

Table 3.5. Characteristics of meteorological and beach environmental conditions during oblique offshore winds at the three study sites. U=mean wind speed at 2.4 m high; WD=wind direction at 2.4 m high; α=Incident angle relative to foredune normal; T=mean air temperature; Seaward foredune (F) slope; Fmax=maximum potential fetch distance and UL for unlimited; aspect ratio of the seaward side (dimensionless); u_t below sand transport threshold. *1h before end of experiment.

Site	Day	U (m s^{-1})	WD (°)	α (°)	T (°C)	F slope (°)	Fmax (m)	Aspect ratio	Rain
BL	Exp-2: 28/01/2010	5.51	280 [Oblique]	30	6	2.58	UL	0.015	yes*
	Exp-3: 28/04/2010	4.73	185 [Highly oblique]	65	18	1.83		0.013	no
TSH	Exp-2: 27/01/2010	6.30	280 [Oblique]	30	6	4.75	UL	0.035	no
	Exp-3: 29/04/2010	2.18 [below u_t]	290 [Highly oblique]	40	20	4.92	UL	0.029	no
MNE	Exp-1: 14/10/2009	2.80	187 [Highly oblique]	63	15	3.49	UL	0.060	no
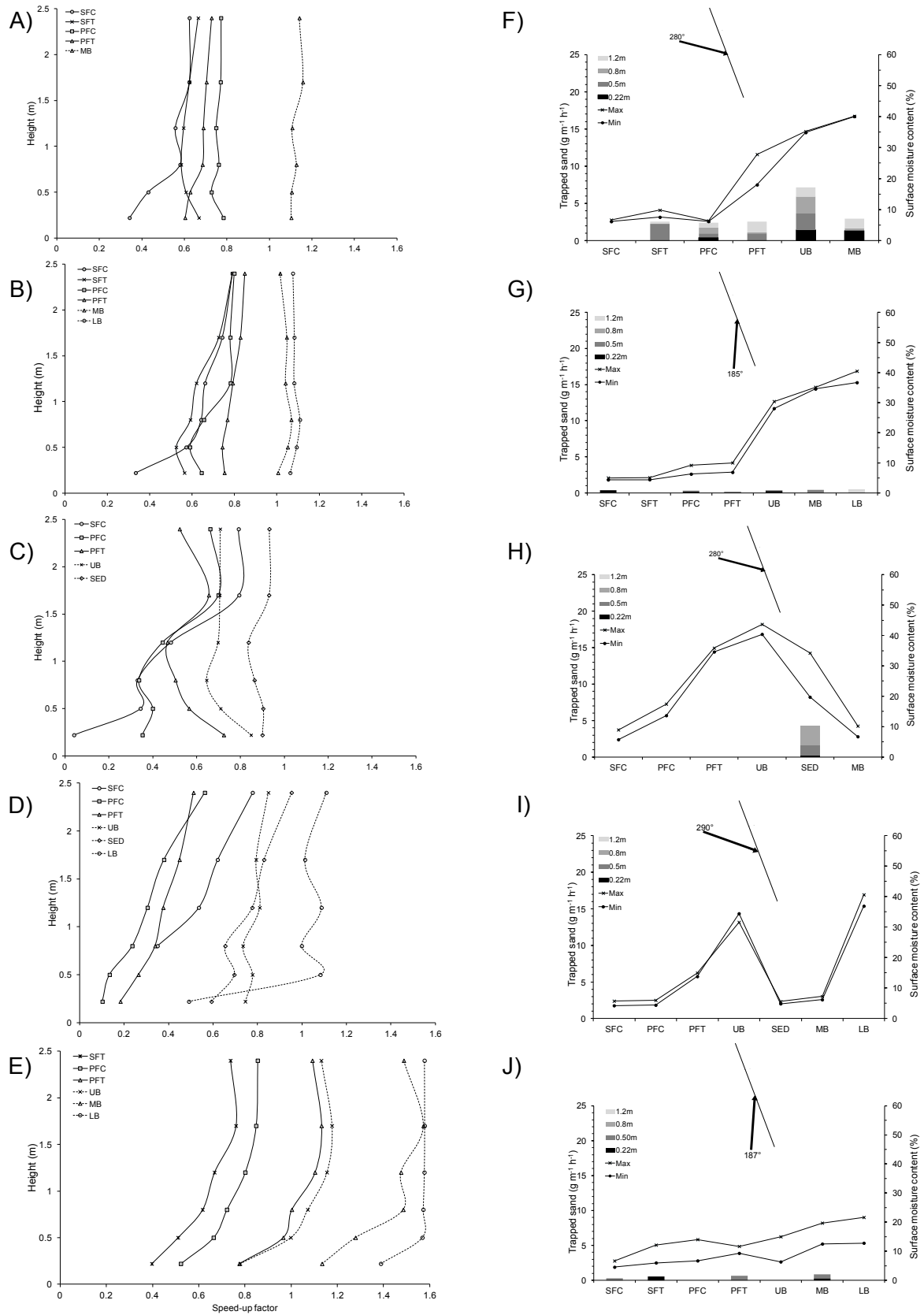
Figure 3.13. Time-averaged speed-up profiles over the foredune-beach during oblique offshore winds at: (A) and (B) BL, (C) and (D) TSH and (E) MNE; trapping rate of sand and moisture content over the profile at: (F) and (G) BL, (H) and (I) TSH and (J) MNE. Insert: line represents coastline and arrow shows the wind direction at the reference mast.

During oblique offshore winds (WD: 280° and α: 30° incident angle) at the BL site, all time-averaged wind speeds over the foredunes were lower than those on the beach (Figure 3.13A). The lower portion of the SFC profile shows the greatest deceleration of 0.34 δ_S and 0.43 δ_S at 0.22 m and 0.50 m high respectively, due to the high vegetation cover over this unit (>70%). Near-surface airflow accelerates as it passes over the SFT and PFC, but decelerates over the PFT. The upper-portion of all the profiles from 0.80 m to 2.40 m is largely invariant. Sand transport was measured at all the sub-units, except at the SFC (Figure 3.13F). The greatest amount of total sand collected for all traps was 7.17 g m^{-1} h^{-1} on the UB, and where the maximum sand transport rate was 2.27 g m^{-1} h^{-1} in the trap at 0.80 m. Sand transport rate was relatively similar on the SFT, PFC, PFT, ranging from 2.40 to 2.57 g m^{-1} h^{-1}, however it varies with trap height. Although high moisture surface content was recorded of 40.1% at the MB (Figure 3.13F), trapped sand was captured, and likely supplied by localised dry sand patches on the foreshore. Rain one hour before the end of the experiment may have reduced sand transport.

Figure 3.13B shows the foredune velocity profiles were slower compared to the reference mast at BL during highly oblique offshore winds (WD: 185° and α: 65°) while the middle and lower beach speed-up profiles were slightly faster at all measurement elevations. Specifically, near-surface airflow is subject to a high stagnation effect on the SFC, however it accelerates over the SFT, PFC the PFT and over the beach. Interestingly, the magnitude of this effect at 0.22 m high (0.34 δ_S) was similar to the values recorded during oblique (Exp-2) and direct offshore wind (Exp-4) experiments. The speed-up profile of the SFC shows a complex shape with a maximum of 0.66 δ_S at 1.20 m, while the upper-portion of the other profiles has a linear and constant shape. Additionally, the whole profile on the PFT was characterized by a uniform shape and acceleration trend during highly oblique offshore wind conditions, contrasting with the deceleration during less oblique or direct offshore winds. This is perhaps caused by a less abrupt angle of wind approach (α: 65°) limiting the flow stagnation effect. Figure 3.13G illustrates that blown sand was trapped at all sub-units in the lowest trap with the exception of the SFT. However sand transport rate was very low, ranging from 0.36 g m^{-1} h^{-1} at SFC to 0.13 g m^{-1} h^{-1} at PFT.

During relatively strong and oblique offshore wind (WD: 280°), near-surface airflow accelerates as it passes over the PFC, PFT, UB and SED at TSH site (Figure 3.13C). Near the surface, the reduction of wind speed on the well-vegetated SFC was much more pronounced than at the PFC, due to the drag imposed by a high vegetation density. Results also indicate a complex shape of the lower portion of all the foredune profiles, contrasting with the linear shape of the upper portion between 1.7 and 2.4 m high. In contrast, the upper portion of the profiles at the UB and SED were uniform and linear, resulting in a clear difference between the foredune and beach profiles. Sand transport was only measured at the SED, although rates were moderate at 0.26 g m^{-1} h^{-1}, 1.39 g m^{-1} h^{-1} and 2.62 g m^{-1} h^{-1} in the three lowest traps respectively. Sand transport may have been limited to this location because other sites had a higher surface moisture content that will dampen entrainment, but it is also the case that the highest wind speeds were recorded at the SED (Figure 3.13H).

Distinct airflow speed-up profiles could be observed over the foredune-beach profile at TSH during highly oblique offshore and low wind conditions (Table 3.5, and Figure 3.13D). The two lowest anemometers at SFC were not working due to technical problems. As the near-surface airflow passed the secondary foredune, a significant deceleration occurred at the PFC, but acceleration dominated over the PFT and UB following by a flow reduction at SED and LB. Greater decelerations occurred in the lower portion of the profiles on the PFC, where speed-up values were 0.10 δ_S at 0.22 m and 0.14 δ_S at 0.50 m, and its profile slope steepens compared to the other beach profiles. This thus indicated an increase in fluid shear above the plant canopy height at SFC. Flow acceleration dominated the lower beach at all measurement points except at 0.22 m elevation, likely caused by local topographic features disturbing the lowest portion of the airflow. No sand transport was measured mainly due to low wind speeds during the experiment (Figure 3.13I).

Figure 3.13E shows the speed-up ratio profiles at MNE during highly oblique offshore winds (WD: 187° and α: 63°), where a distinct trend is observed between the different sub-units. Wind speed increases as it passes over the SFT, PFC, PFT, and the beach sub-units. Speed-up values for the PFT and UB were remarkably similar and especially at 0.22 m (~0.80 δ_S) and 0.50 m (>0.97 δ_S) measurement elevations. This indicates a flow acceleration immediately in the lee side of the secondary foredune, which may have been amplified by the foredune slope topography (i.e. ramp). Although, the average wind speed was slightly higher than at TSH during the Exp-3, sand transport was recorded (Figure 3.13J). This could be explained by a larger fetch associated with

an average highly oblique winds fluctuating parallel to the foredune during the experiment at MNE. However no sand was trapped at PFC, UB and LB probably due to the presence of micro-topographic features combined with a low wind speed conditions.

Both figures 3.14A, B and 3.15A, B present the wind regime during oblique offshore winds at BL. Variability of wind direction is high ranging from 43° at SFC to 26.7° at SFT for Exp-2; and from 39° at SFC to 17.6° at PFT for Exp-3. The same trend is generally observed at 0.80 m high, and decreases to the beach. These results suggest a topographic steering (deflection) of the airflow parallel to the foredune which then decreases gradually on the beach. This effect increases with the obliquity of the regional wind direction. The presence of dense vegetation on the secondary foredune crest may also have amplified this steering effect. However the effect of variation in wind direction was not observed at the beach sub-units for oblique and highly oblique winds. In general, the normalized CV values exceeded just 1 over the foredunes for both experiments, suggesting there a slightly unsteady airflow but becoming steady over the beach (Figures 3.14C, 3.15C) The maximum normalized variability in the horizontal velocity was 1.36 at PFC and 1.30 at PFT for oblique and highly oblique offshore winds respectively, however these values are much lower than those recorded during direct offshore winds (Figure 3.9A). This may indicate that the airflow was less affected by the topographic forcing due to oblique incident wind direction which is likely to limit the topographic forcing effect over the foredunes.
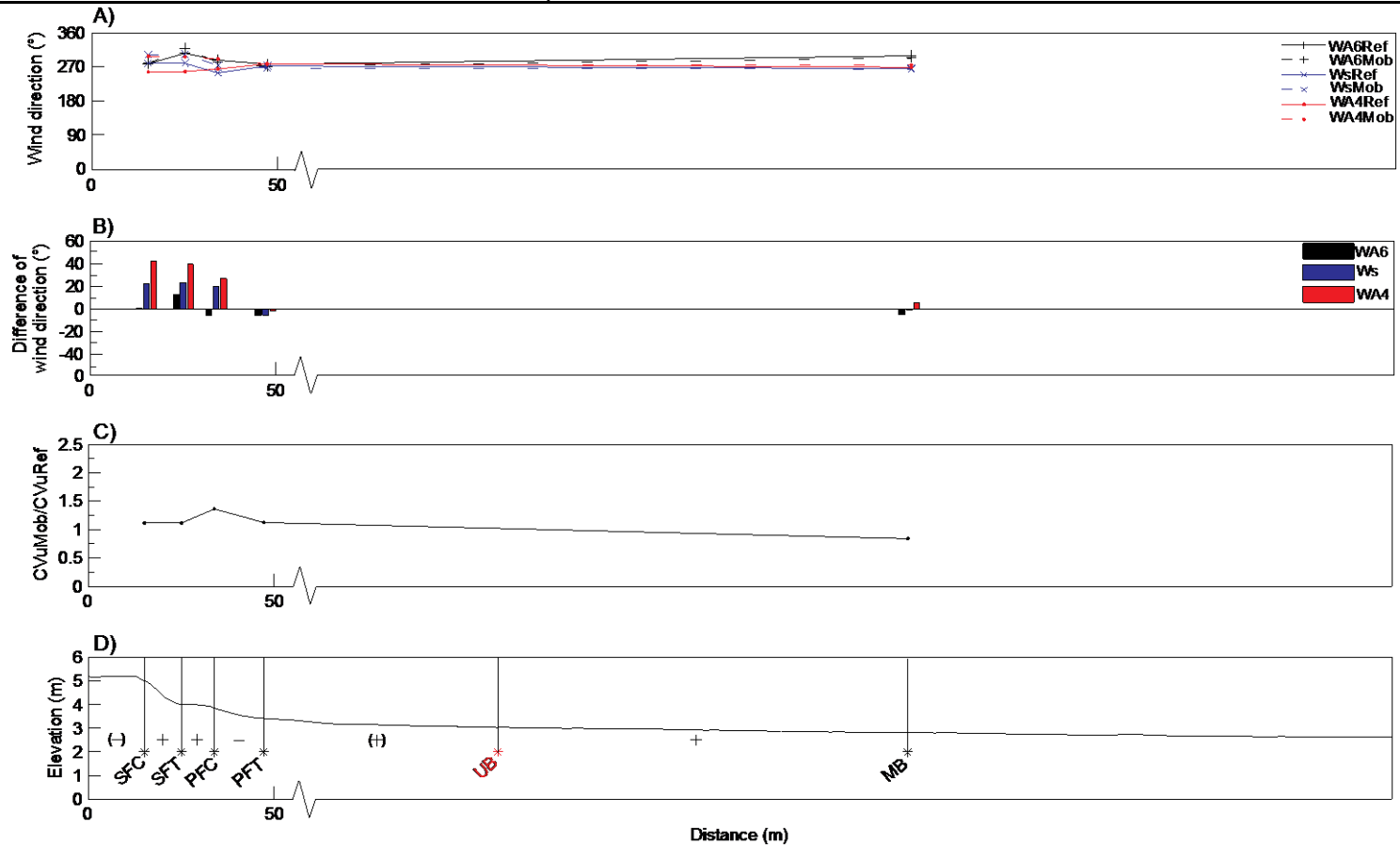
Figure 3.14. Wind regime at BL during oblique offshore wind (Exp-2) in relation to topographic profile: (A) wind direction for reference (Ref) and mobile (Mob) anemometers at 0.50 m high (WA4), at 0.80 m high using an ultrasonic (Ws) and 2.4 m high (WA6); (B) variability in wind direction where the zero line corresponds to the average record at the reference mast; (C) flow steadiness, normalized CV; and (D) transport capacity model estimated from the speed-up factor measurement at the lowest anemometer. The symbol (+) corresponds to an increase of speed-up compared to the downwind sub-unit measurement, while the inverse corresponds to (-), and the equivalence to (o). Red and black annotations indicate the position of the reference and mobile mast respectively.

Figure 3.15. Wind regime at BL during highly oblique offshore wind (Exp-3) in relation to topographic profile: (A) wind direction for reference (Ref) and mobile (Mob) anemometers at 0.50 m high (WA4), at 0.80 m high using an ultrasonic (Ws) and 2.4 m high (WA6); (B) variability in wind direction where the zero line corresponds to the average record at the reference mast; (C) flow steadiness, normalized CV; and (D) transport capacity model estimated from the speed-up factor measurement at the lowest anemometer. The symbol (+) corresponds to an increase of speed-up compared to the downwind sub-unit measurement, while the inverse corresponds to (-), and the equivalence to (o). Red and black annotations indicate the position of the reference and mobile mast respectively.

Figure 3.16 and 3.17 summarise the wind regime during oblique offshore winds at TSH. For both experiments wind directional variability is high over the foredunes (up to 31°) however under slightly oblique offshore winds (280°), the wind direction stabilises over the flat beach whereas under highly oblique winds (290°) direction remains variable on the UB and on the seaward side of the embryo dunes. For slightly oblique winds, this suggests a parallel airflow deflection on the lee side of the foredunes. However no clear trend could be depicted during highly oblique winds, mainly due to low wind speed conditions. Figures 3.16C and 3.17C show that airflow was unsteady over the foredunes for both experiments (normalized CV value >1), however the seawardmost measurement mast recorded a steady airflow. For slightly oblique winds, the normalized CV values were relatively similar over the foredune sub-units, while these values increase as the airflow passes the SFC, PFC to attain its maximum on the PFT (2.07) during highly oblique winds. The pattern of sand transport capacity was generally the same over the foredune-beach with the exception being at the SED (Figures 3.16D, 3.17D). During the highly oblique experiment, the transport capacity was negative at the SED, probably caused by the presence of embryo dunes causing a deceleration of the airflow.
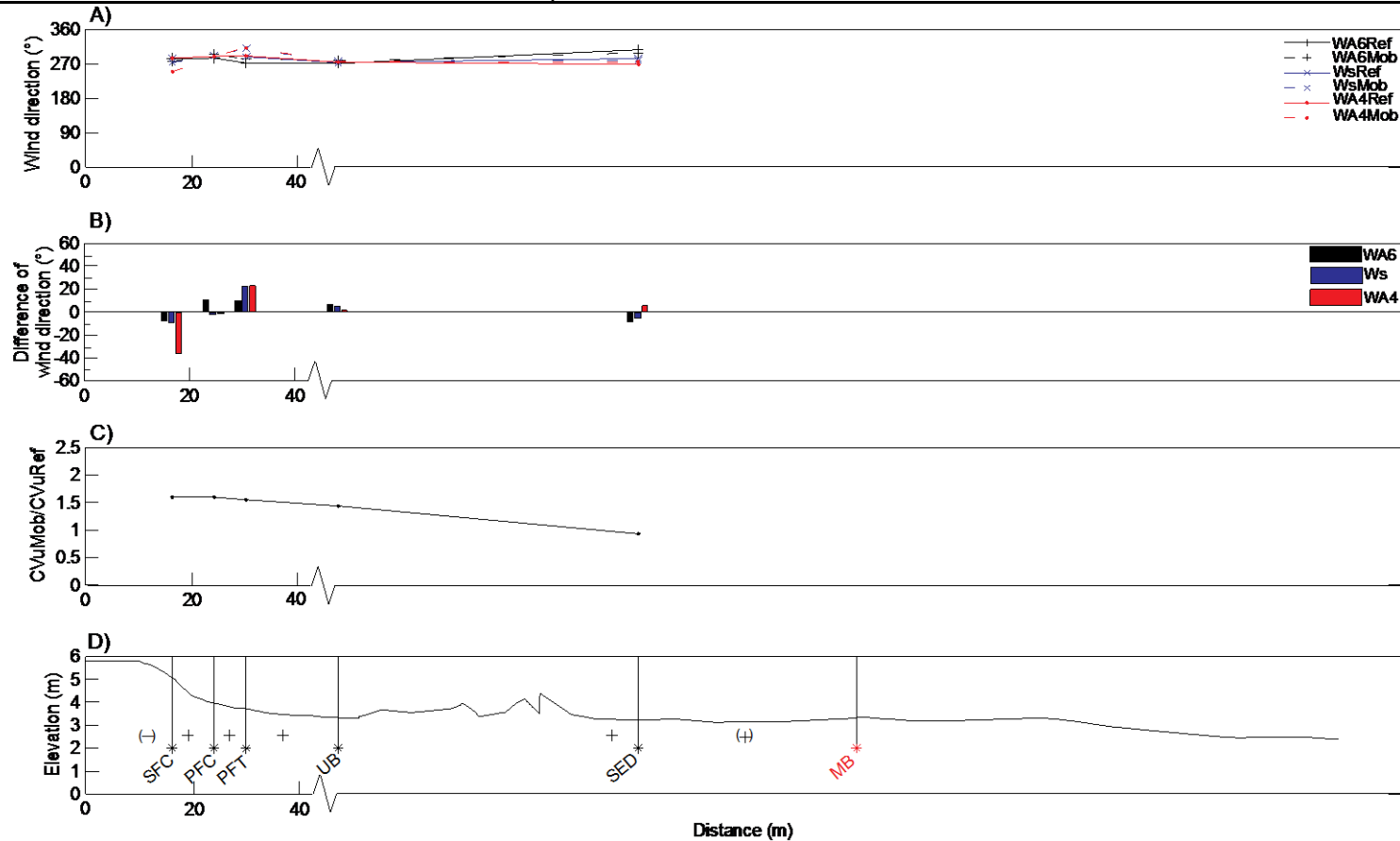
Figure 3.16. Wind regime at TSH during oblique offshore wind (Exp-2) in relation to topographic profile: (A) wind direction for reference (Ref) and mobile (Mob) anemometers at 0.50 m high (WA4), at 0.80 m high using an ultrasonic (Ws) and 2.4 m high (WA6); (B) variability in wind direction where the zero line corresponds to the average record at the reference mast; (C) flow steadiness, normalized CV; and (D) transport capacity model estimated from the speed-up factor measurement at the lowest anemometer. The symbol (+) corresponds to an increase of speed-up compared to the downwind sub-unit measurement, while the inverse corresponds to (-), and the equivalence to (o). Red and black annotations indicate the position of the reference and mobile mast respectively.

Figure 3.17. Wind regime at TSH during highly oblique offshore wind (Exp-3) in relation to topographic profile: (A) wind direction for reference (Ref) and mobile (Mob) anemometers at 0.50 m high (WA4), at 0.80 m high using an ultrasonic (Ws) and 2.4 m high (WA6); (B) variability in wind direction where the zero line corresponds to the average record at the reference mast; (C) flow steadiness, normalized CV; and (D) transport capacity model estimated from the speed-up factor measurement at the lowest anemometer. The symbol (+) corresponds to an increase of speed-up compared to the downwind sub-unit measurement, while the inverse corresponds to (-), and the equivalence to (o). Red and black annotations indicate the position of the reference and mobile mast respectively.

High variability of the upper and near surface wind direction occurred over the foredune sub-units at MNE (Figures 3.18A, B). The maximum difference in wind direction of 31° was measured at the bottom wind vane on the SFT (180°) compared to the reference mast (211°), while it is slightly lower for the two other vanes. These results show a parallel deflection of the airflow as observed at the two other sites. Figure 3.18C displays a high normalized CV value of 1.43 at PFC, while it ranged from 0.52 to 0.80 at the other sub-units. This suggests a steady airflow over the foredune-beach during oblique offshore winds, which then becomes turbulent as it passes the primary foredune crest. Figure 3.18D indicates an increase of transport capacity as the airflow passes over the primary foredune crest.
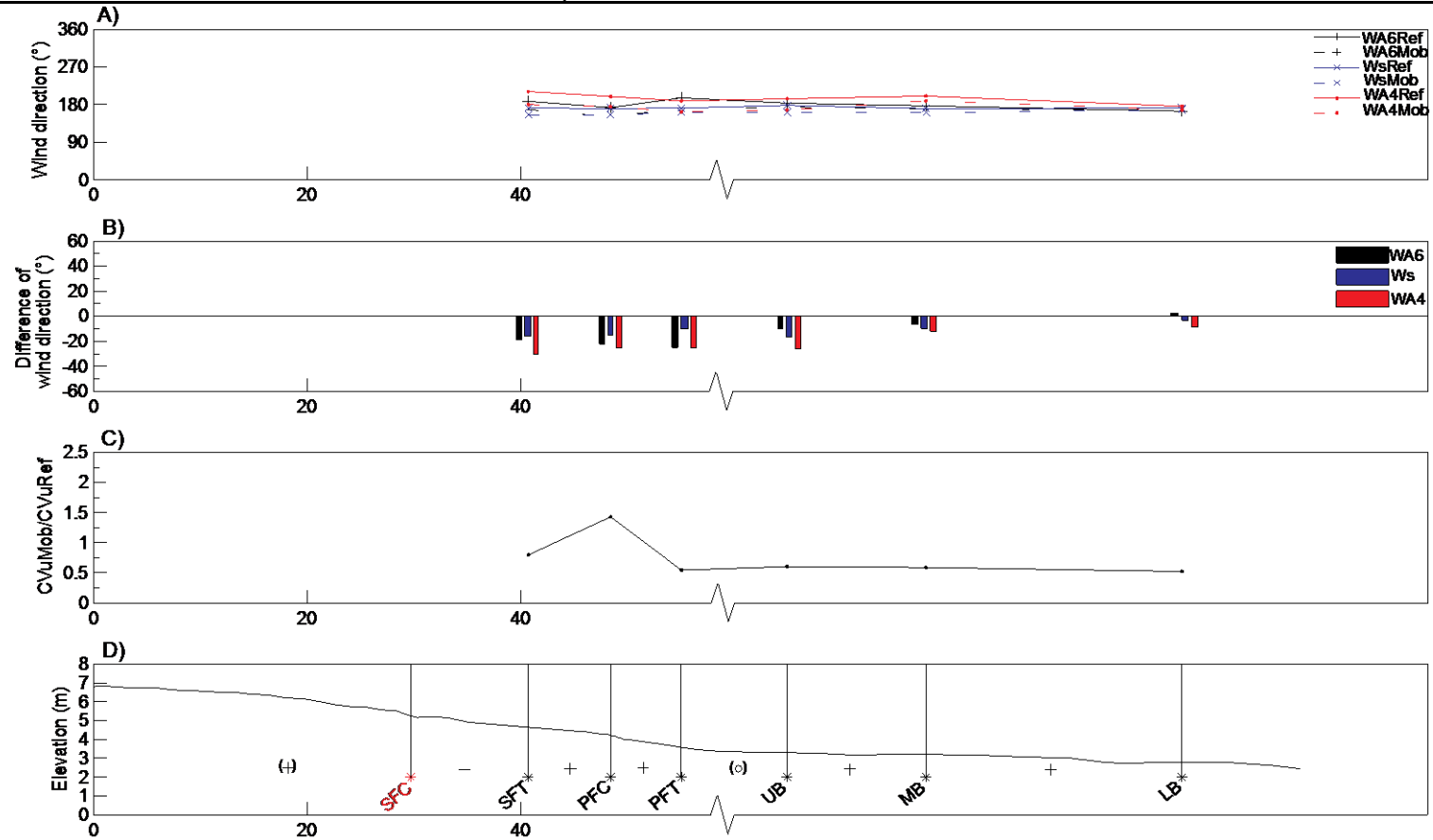
Figure 3.18. Wind regime at MNE during highly oblique offshore wind (Exp-1) in relation to topographic profile: (A) wind direction for reference (Ref) and mobile (Mob) anemometers at 0.50 m high (WA4), at 0.80 m high using an ultrasonic (Ws) and 2.4 m high (WA6); (B) variability in wind direction where the zero line corresponds to the average record at the reference mast; (C) flow steadiness, normalized CV; and (D) transport capacity model estimated from the speed-up factor measurement at the lowest anemometer. The symbol (+) corresponds to an increase of speed-up compared to the downwind sub-unit measurement, while the inverse corresponds to (-), and the equivalence to (o). Red and black annotations indicate the position of the reference and mobile mast respectively.

Table 3.6 presents the time-averaged u_{*RSk} along the foredune-beach sub-units; and derived from u'- and w'-components during oblique offshore winds (Appendix 3.3). Results show higher u_{*RSk} on the foredunes, ranging from 0.57 m s^{-1} on the SFT to 0.67 m s^{-1} at the PFC, than on the upper beach (Reference mast) at BL during oblique offshore winds. The development of turbulence structures observed over the foredunes (Figure 3.14C) may have enhanced conveyance of momentum to the surface. During highly oblique offshore winds, a similar trend occurred however the maximum u_{*RSk} was reached at the SFT at BL (0.92 m s^{-1}) where the normalized CV was above 1 (Figure 3.15). For slightly oblique winds (Exp-2), values of u_{*RSk} were much greater over the foredune sub-units at TSH (up to 0.87 m s^{-1} at the SFC) than at the reference mast (0.57 m s^{-1}), and decreased toward the middle beach (Reference mast). Similar patterns were observed at TSH during oblique offshore winds, however u_{*RSk} values at the foredune sub-units for Exp-2 (above u_t) were nearly twice those during for Exp-3 (below u_t). For both experiments, the greatest u_{*RSk} is associated to a high normalized CV value. Similar values of u_{*RSk} occur over the foredune and beach at MNE, ranging from 0.27 m s^{-1} to 0.33 m s^{-1}. The results appear to support a lack of generation of turbulence structures over the foredune-profile, but these may not have been detected due to low wind speed conditions.

Table 3.6. Summary of the time-averaged surface shear stress velocity (u_{*RSk}) at the reference (Ref) and mobile (Mob) masts estimated from the ultrasonic at 0.80 m high during oblique offshore winds.

				u_{*RSk} (m s^{-1})					
	Ref	Mob		Ref	Mob		Ref	Mob
BL	Mean	Mean	**TSH**	Mean	Mean	**MNE**	Mean	Mean
Exp-2			**Exp-2**			**Exp-1**		
SFC	0.43	0.63	SFC	0.57	0.87	SFT	0.40	0.33
SFT	0.42	0.57	PFC	0.57	0.72	PFC	0.38	0.33
PFC	0.48	0.67	PFT	0.59	0.75	PFT	0.32	0.33
PFT	0.49	0.53	UB	0.65	0.68	UB	0.30	0.31
MB	0.35	0.33	SED	0.50	0.58	MB	0.37	0.32
SFC	0.68	0.82	SFT	0.21	0.23	LB	0.36	0.27
BL			**TSH**					
Exp-3			**Exp-3**					
SFT	0.77	0.92	PFC	0.34	0.44			
PFC	0.60	0.73	PFT	0.34	0.45			
PFT	0.56	0.68	UB	0.33	0.42			
MB	0.41	0.38	SED	0.36	0.45			
LB	0.36	0.36	LB	0.37	0.32			

3.4.3. Onshore Winds

Table 3.7 reports the meteorological and beach environmental conditions measured at the study sites during onshore winds.

Table 3.7. Characteristics of meteorological and beach environmental conditions during onshore winds at the three study sites. U=mean wind speed at 2.4 m high; WD=wind direction at 2.4 m high; α=Incident angle relative to foredune normal T=mean air temperature; Seaward Foredune (F) slope; Fmax=maximum potential fetch distance; aspect ratio of the seaward side (dimensionless); u_t below sand transport threshold.

Site	Day	U (m s^{-1})	WD (°)	α (°)	T (°C)	F slope (°)	F max (m)	Aspect ratio	Rain
BL	Exp-1: 13/10/2009	2.34 [below u_t]	135 [Highly oblique]	65	16	1.26	1600	0.014	no
TSH	Exp-1: 15/10/2009	1.10 [below u_t]	118 [Oblique]	48	15	3.60	810	0.027	no
MNE	Exp-2: 26/01/2010	1.86 [below u_t]	94 [Direct]	24	5	6.67	298	0.127	no
	Exp-3: 27/04/2010	5.12	133 [Highly oblique]	63	21	3.38	880	0.039	no

Figure 3.19A shows time-averaged speed-up ratio profiles recorded at BL during weak onshore winds (WD: 135° and α: 65°). Wind profiles across the beach are all very similar. As airflow reaches the PFT, velocity decreases to c. 80% of the wind speeds recorded at the beach. As it travels over the PFC and SFC near-surface wind speeds continue to decrease, however at 0.80 m high accelerations occur, and uniform and linear profiles characterize the upper profiles. Although the potential maximum fetch distance was larger than 1600 m, blown sand was only trapped at the PFT in the lowest trap (11.92 g m^{-1} h^{-1}) mainly due to low wind speed conditions during the experiment (Figure 3.19E).
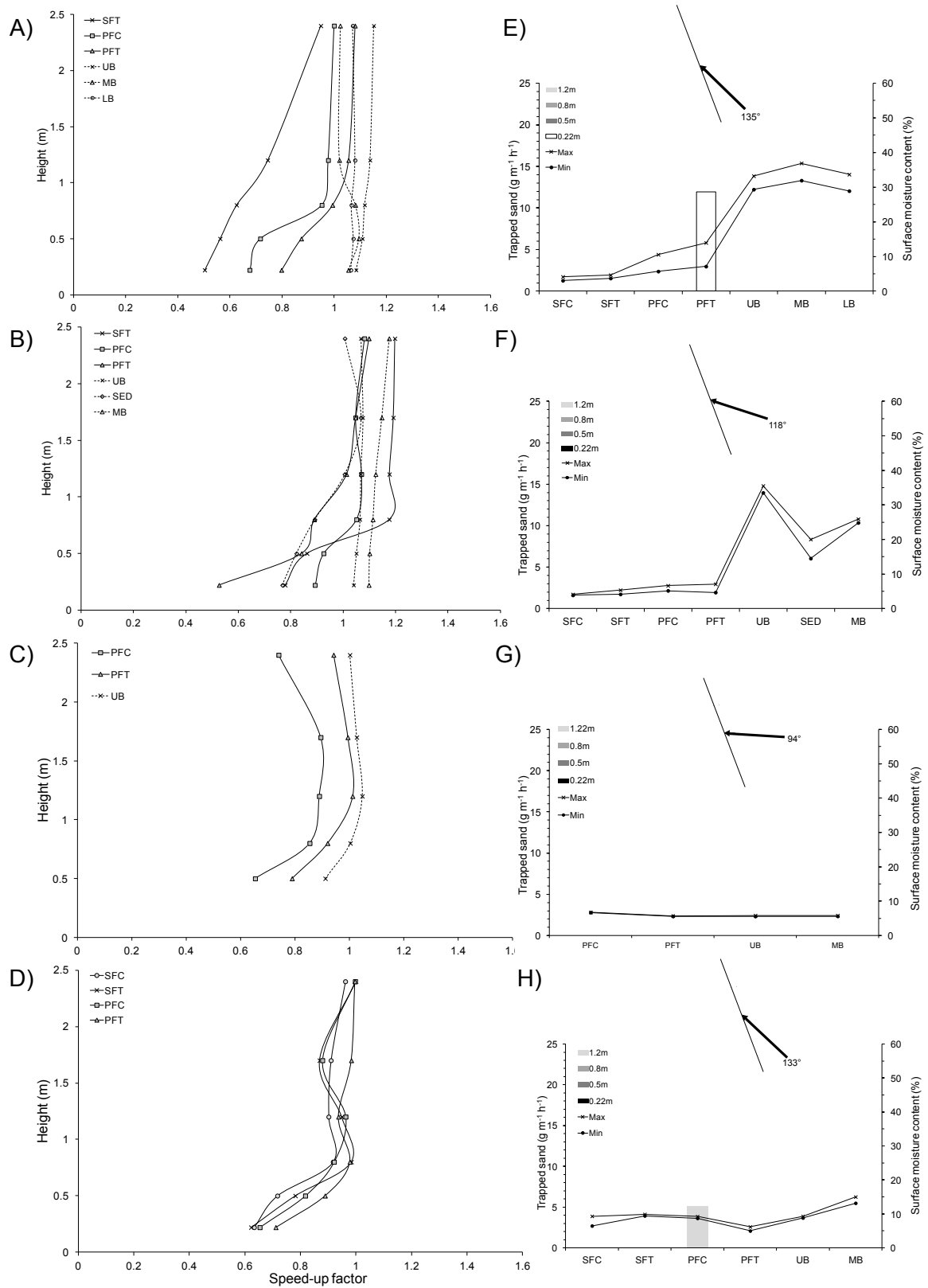
Figure 3.19. Time-averaged speed-up profiles over the foredune-beach during onshore winds at: (A) BL, (B) TSH and (C), (D) MNE; trapping rate of sand and moisture content over the profile at: (E) BL, (F) TSH and (G), (H) MNE. Insert: line represents coastline and arrow shows the wind direction at the reference mast.

The lower (below 1.2 m high) and upper portions for the foredune speed-up profiles at TSH under oblique onshore winds are different, however the latter was similar to that at BL (Figures 3.19A, B). Results also show near-surface airflow significantly decelerates over the PFT and then increases over the PFC, but it finally reduces at SFT. The presence of the embryo dune field does not seem to disturb the airflow up to 0.50 m high at the SED mast located at c.7 m of the seawardmost of embryo dunes (Figure 3.21D). While deceleration was observed at the lowest anemometer height on the SED mainly due to the sparse vegetation. After passing over the embryo dune field, results show near-surface airflow recovers at the UB mast distant of 19 m from the landward embryo dunes. No sand transport was measured during the experiment, mainly due to low wind speeds (Figure 3.19F).

Figure 3.19C displays speed-up profiles measured at MNE during weak and direct onshore winds (WD: 94° α: 24°). The lowest anemometers at the mobile mast were not working due to technical problems. Results show that the airflow decreases as it passes over the beach, PFT and PFC. The greatest wind reductions were 0.65 δ_S and 0.79 δ_S at 0.50 m high for PFC and PFT respectively, caused by vegetation. A distinct kink is evident in the foredune profiles at 0.80 m high, corresponding to the top of the vegetation canopy. Above the kink, the profile slopes decrease, indicating less airflow disturbance. At the end of the experiment, no trapped sand was measured, primarily due to low wind speed conditions and even so it would have been restricted by limited fetch distance.

Due to a technical problem with the cup-anemometer at 0.80 m, data from the ultrasonic anemometer record at the same height was used for all the sub-units at MNE during highly oblique onshore winds. Near-surface airflow decelerates as it passes over the PFT, PFC, SFT and SFC at MNE during relatively strong oblique onshore winds (Figure 3.19D and Table 3.7). This indicates a flow stagnation effect due to wind speed reduction immediately upwind of the primary foredune and extending up to the secondary foredune toe. The upper-portion of the SFC and PFT speed-up profiles are relatively uniform and linear, while slight decelerations of 0.87 δ_S on the SFT and 0.88 δ_S on the PFC occurred at the measurement elevation of 1.70 m. This suggests the entire vertical wind profiles were affected (up to 1.70 m) after the passage of the airflow over the primary foredune toe, however it rapidly re-stabilized at the top of the secondary foredune. Despite a beach fetch up to 880 m and wind velocity above sand transport threshold, Figure 3.19H shows that no sand trapping occurred except at the

PFC in the trap 1.20 m height (5.04 g m^{-1} h^{-1}). This could be caused by the moist sediment over the foredunes (surface moisture content up to 9.9%).

Wind direction was steady and invariant over the beach and then foredune units at BL during (highly oblique) onshore winds (Figures 3.20A, B). The normalized CV values were less than 1 across the foredune-beach, reflecting the occurrence of steady horizontal airflow (Figure 3.20C). Figure 3.20D illustrates positive and similar transport capacity characterized the beach sub-units, whilst a gradual decrease of sand transporting capacity can be distinguished at the foredune sub-units. The greatest potential sand transport rate may occur in the PFT.

Figures 3.21A, B show a relatively invariant wind direction over the foredune-beach at TSH, with the exception of the lowest measurement (0.50 m high) at SED and SFT where average incident flow conditions deviated by 52° and 44° respectively. This was probably caused by the vegetation canopy at the SED and the topography at the SFT. Airflow was steady over the beach up to the PFT, while normalized CV values up to 1.25 were recorded at the SFT and PFC, indicating development of turbulence within these sub-units. Figure 3.21D indicates that the transport capacity varies spatially, with a positive trend at MB, UB, PFC, while the opposite trend occurs at the SED, PFT and SFT. A positive potential sand transport rate at the SED would be expected due to the effective beach fetch distance, but the opposite occurred, probably due to the presence of local topographic features (seaward embryo dunes, beach ramp) and micro-topography (ripples), disturbing the stability of the near-surface airflow.
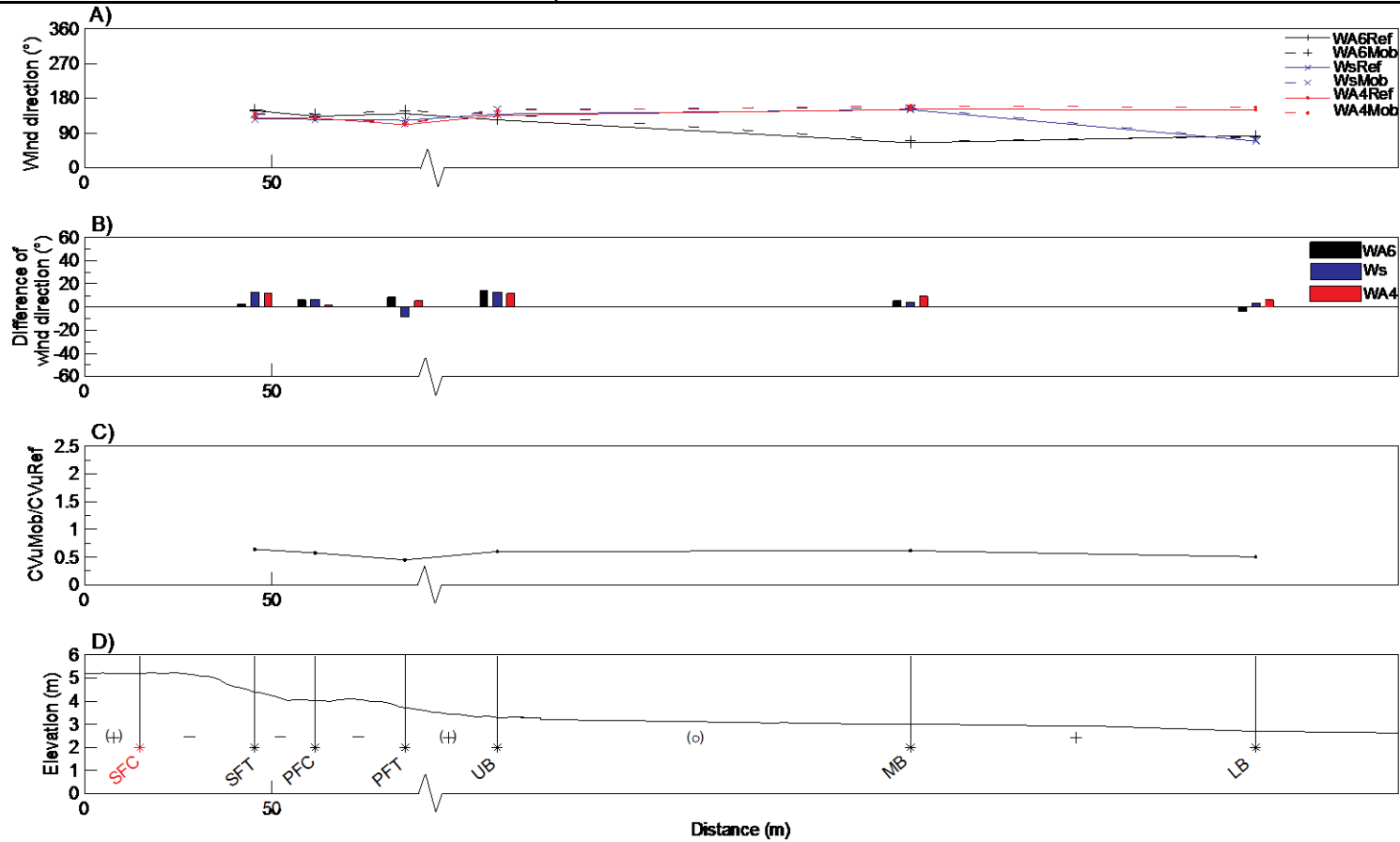
Figure 3.20. Wind regime at BL during (highly) oblique onshore wind (Exp-1) in relation to topographic profile: (A) wind direction for reference (Ref) and mobile (Mob) anemometers at 0.50 m high (WA4), at 0.80 m high using an ultrasonic (Ws) and 2.4 m high (WA6); (B) variability in wind direction; (C) flow steadiness, normalized CV; and (D) transport capacity model estimated from the speed-up factor measurement at the lowest anemometer. The symbol (+) corresponds to an increase of speed-up compared to the downwind sub-unit measurement, while the inverse corresponds to (-), and the equivalence to (o). Red and black annotations indicate the position of the reference and mobile mast respectively.
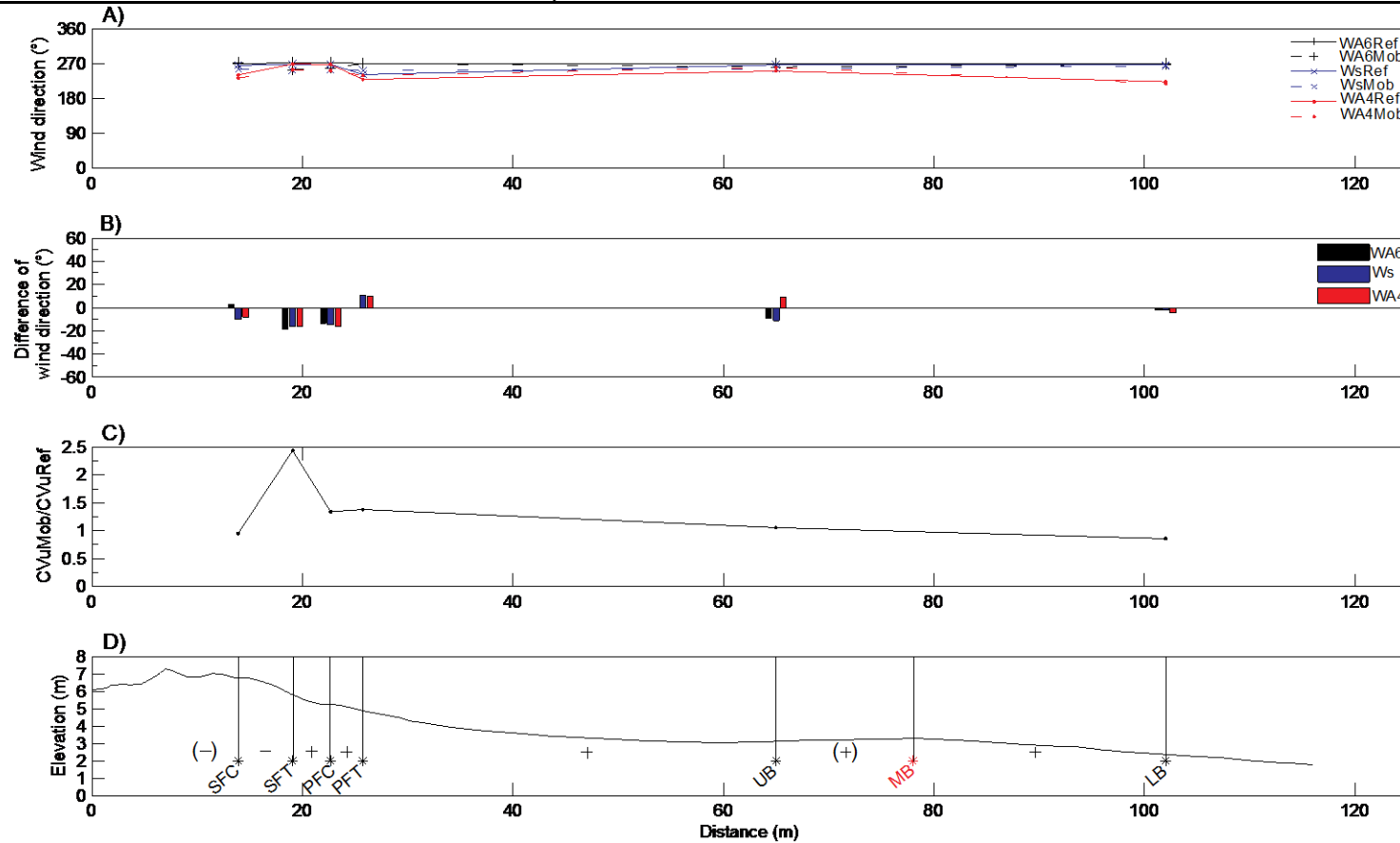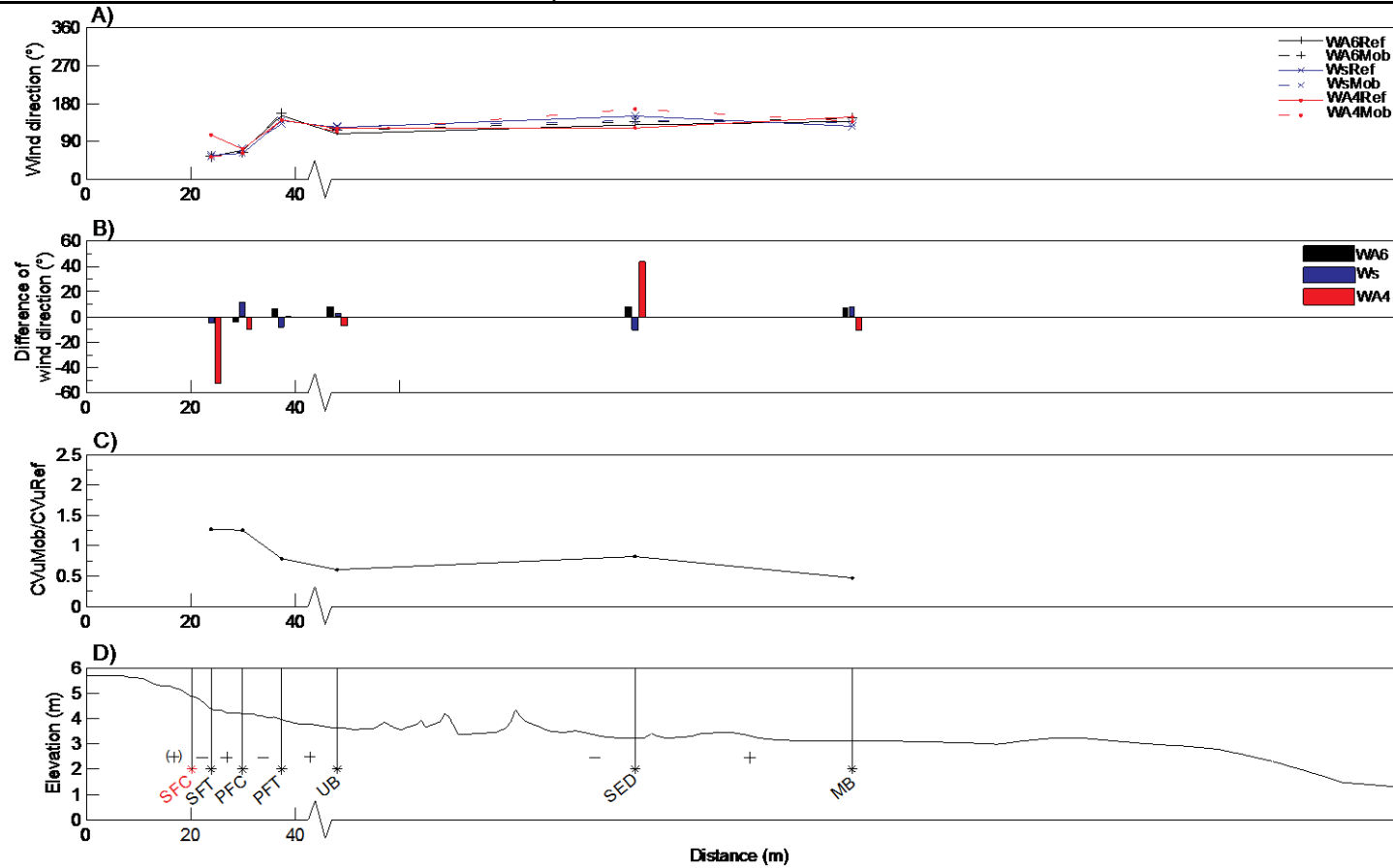
Figure 3.21. Wind regime at TSH during oblique onshore wind (Exp-1) in relation to topographic profile: (A) wind direction for reference (Ref) and mobile (Mob) anemometers at 0.50 m high (WA4), at 0.80 m high using an ultrasonic (Ws) and 2.4 m high (WA6); (B) variability in wind direction where the zero line corresponds to the average record at the reference mast; (C) flow steadiness, normalized CV; and (D) transport capacity model estimated from the speed-up factor measurement at the lowest anemometer. The symbol (+) corresponds to an increase of speed-up compared to the downwind sub-unit measurement, while the inverse corresponds to (-), and the equivalence to (o). Red and black annotations indicate the position of the reference and mobile mast respectively.

Figure 3.22 presents the wind regime at MNE during direct onshore winds. Wind direction was generally invariant, with the exception of the lowest anemometer on the PFC at MNE (deviation of 17° compared to the reference mast) due to the disturbances caused by vegetation. Near-surface airflow was also steady across the foredune-beach (Figure 3.22C). Figure 3.22D shows a positive transport capacity over the beach. Negative transport capacity characterizes the foredune sub-units, however clear airflow processes and interactions may have been overwhelmed by the low wind speed conditions.

During highly oblique onshore winds, Figure 3.23A, B shows a variability of wind direction across the foredunes at MNE. Wind direction at 0.50 m high shifts from 23° at the PFC to 21° at the PFT. This reflects a slight parallel deflection of the airflow. The presence of vegetation is further likely to affect airflow at the SFC, where a shift up to 15° was recorded at 0.50 m high between the mobile and reference masts. Figure 3.23C shows that the airflow was unsteady on the PFC (1.35) and SFC (1.46), contrasting with the results of oblique onshore winds (Exp-2) (Figure 3.22C). The obliquity of the wind approach may decrease the net effect of streamline compression but cause a mixing of steady and unsteady flows with additional deceleration effects due to the presence of sparse vegetated hummocks along the foredune slope. Figure 3.23D indicates a negative sand transport capacity on the primary and secondary foredune sub-units despite an effective beach fetch (c. 880 m). Although the wind speed was low during the experiment, sand was trapped at the PFC where turbulence structures were observed which may have favoured sand transport along the foredune slope.
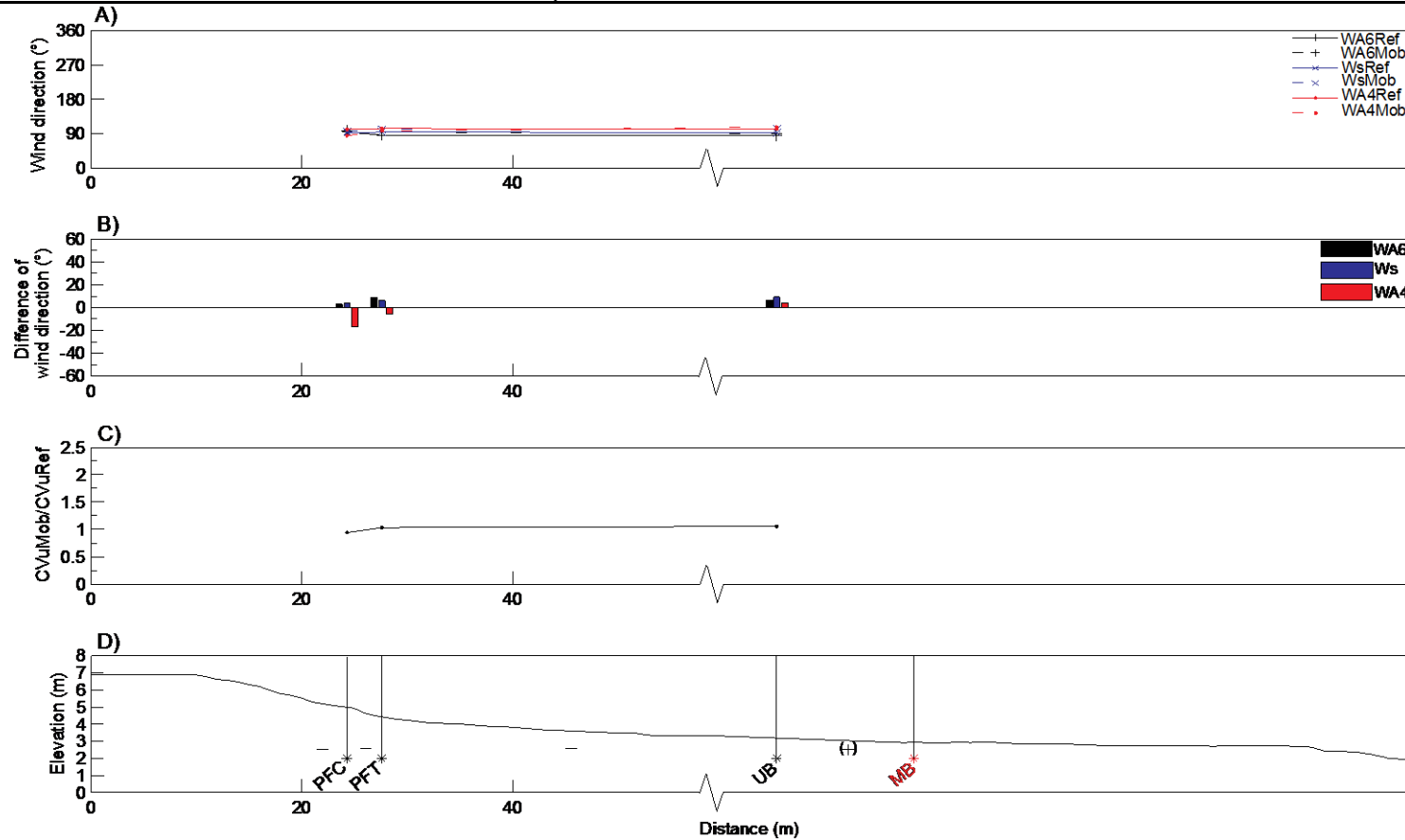
Figure 3.22. Wind regime at MNE during direct wind (Exp-2) in relation to topographic profile: (A) wind direction for reference (Ref) and mobile (Mob) anemometers at 0.50 m high (WA4), at 0.80 m high using an ultrasonic (Ws) and 2.4 m high (WA6); (B) variability in wind direction where the zero line corresponds to the average record at the reference mast; (C) flow steadiness, normalized CV; and (D) transport capacity model estimated from the speed-up factor measurement at the lowest anemometer. The symbol (+) corresponds to an increase of speed-up compared to the downwind sub-unit measurement, while the inverse corresponds to (-), and the equivalence to (o). Red and black annotations indicate the position of the reference and mobile mast respectively.

Figure 3.23. Wind regime at MNE during highly onshore wind (Exp-3) in relation to topographic profile: (A) wind direction for reference (Ref) and mobile (Mob) anemometers at 0.50 m high (WA4), at 0.80 m high using an ultrasonic (Ws) and 2.4 m high (WA6); (B) variability in wind direction where the zero line corresponds to the average record at the reference mast; (C) flow steadiness, normalized CV; and (D) transport capacity model estimated from the speed-up factor measurement at the lowest anemometer. The symbol (+) corresponds to an increase of speed-up compared to the downwind sub-unit measurement, while the inverse corresponds to (-), and the equivalence to (o). Red and black annotations indicate the position of the reference and mobile mast respectively.

Table 3.8 presents the time-averaged u_{*RSk} along the foredune-beach sub-units; and derived from u'- and w'-components (Appendix 3.4). The u_{*RSk} results of the measured foredune-beach units at BL were lower than at the reference mast partly due to its location at the SFC during onshore winds. A gradual increase of u_{*RSk} occurs as the airflow flows from the beach to SFC (reference mast), however the values were lower than at the reference mast. Generally, the same trend took place at TSH where the reference mast was located on the SFC. An increase of u_{*RSk} was also observed across the foredune-beach with the exception at SED. No substantial difference in u_{*RSk} was observed between the mobile and reference masts at MNE during direct and low speed conditions. For highly oblique onshore winds, the measurements were limited to the foredune sub-units, but results suggest greater shear stress on the foredune sub-units compared to the upper beach.

Table 3.8. Summary of time-averaged of surface shear stress velocity (u_{*RSk}) using the ultrasonic at 0.80 m high at the reference (Ref) and mobile (Mob) masts during onshore winds.

				u_{*RSk} (m s^{-1})				
BL	Ref Mean	Mob Mean	**TSH**	Ref Mean	Mob Mean	**MNE**	Ref Mean	Mob Mean
Exp-1			**Exp-1**			**Exp-2**		
SFT	0.48	0.40	SFT	0.24	0.22	PFC	0.10	0.11
PFC	0.43	0.27	PFC	0.22	0.19	PFT	0.14	0.16
PFT	0.44	0.27	PFT	0.16	0.19	UB	0.17	0.19
UB	0.41	0.21	UB	0.20	0.18			
MB	0.30	0.18	SED	0.25	0.20		Ref Mean	Mob Mean
LB	0.26	0.16	LB	0.22	0.14	**MNE Exp-3**		
						SFC	0.33	0.46
						PFC	0.32	0.37
						PFC	0.33	0.44
						PFT	0.35	0.40

3.5. Discussion

Airflow over the foredune is influenced by topographic forcing and steering effects which are responsive to changes in the speed and direction of the incident airflow (e.g. Borówka and Rotnicki, 2001, Walker et al., 2006, 2009, Lynch et al., 2010). The adjustments of horizontal and vertical wind speed, and direction were analysed to investigate the airflow-morphology interactions, with the incident wind approach separated into direct offshore, oblique offshore and onshore winds. During the field experiments, wind speeds were generally low. This meant that sediment transport measurements in relation to wind speed were patchy, because wind rarely exceeded the required threshold velocity. However variation in relative wind velocity from sub-unit to sub-unit can be used to infer likely patterns of flow acceleration and deceleration and hence potential sand entrainment and deposition – this is referred to as changing potential sand transport capacity (e.g. Kocurek and Lancaster, 1999).

3.5.1. Topographic Forcing Effects

During direct offshore winds, both topographic forcing and surface shear stress modify wind profiles. Near-surface wind speed decreases in the lee of the foredunes at the three sites during direct offshore winds, as expected from Figure 3.4A. Deceleration was the greatest at the foredune toe sub-units. Flow stagnation was generally combined with unsteady airflow (normalized CV value >1). The airflow gradually recovers and becomes steady as it passes from the UB towards the beach. At TSH, however a topographic forcing effect due to the presence of embryo dunes re-affected the airflow causing it to decelerate.

A clear contrast in net horizontal airflow dynamics is observed between direct and oblique offshore winds with increasing of obliquity of flow. Streamwise wind speed and steadiness of the flow increase during oblique winds because the pressure stagnation effect imposed by the foredune is less abrupt (i.e. foredune appears less steep to incident wind flow), resulting in less deceleration on the lee side. The foredune toe stagnation effect also decreases with increasing obliquity of flow. This suggests that speed-up is receptive to changes in the angle of the incident wind angle approach, indicating strong relationships between streamwise velocity and the angle of incident wind.

During onshore winds, wind speed decreases at the three sites from the beach to the foredunes, where flow deceleration was generally the most pronounced at the foredune toe (Figure 3.19). This effect, resulting in potential sediment deposition, was expected because when airflow approaches the foredune, near-surface pressure rises due to an increase of positive pressure gradient (Figure 3.4B). As previously presented in section 3.2.5, streamline compression and topographic flow acceleration usually characterize the airflow along the windward stoss slope. In this study, the deceleration effect was only observed over the foredunes at the three sites, perhaps due to the combined effects of flow deceleration at the PFT and an increase of vegetation roughness drag. The most pronounced deceleration was at BL where the remarkably distinct PFT and SFT sub-units act as 'dead' flow zones. This was also observed at Walker et al.'s (2009) West site characterized by a concave-convex foredune profile where they suggested streamwise velocity and steadiness are not responsive to topographic forcing at the foredune toe mainly due to the prevailing flow stagnation effect. For highly oblique onshore winds, the velocity reduction over the foredunes at MNE was less than during slightly oblique onshore winds (Figure 3.19D). Here the pressure stagnation flow imposed by the foredune is less abrupt resulting in less flow deceleration in the foredune toe and lower stoss regions (Hesp et al., 2005).

3.5.2. Topographic Steering Effects

The wind direction is critical to understanding airflow dynamics over the foredune-beach (e.g. Walker and Nickling, 2002, Lynch et al., 2008). During direct offshore winds, no variability in wind direction for incident flow ranging from 12° to 20° was observed between the reference mast and monitored foredune-beach sub-units at the three sites, suggesting flow attachment with no deflection in the lee side of the secondary foredune. This agrees with Sweet and Kocurek's model (1990) (Figure 3.5B).

Oblique offshore winds (incident angle ranging from 30°-65° relative to shore normal equivalent to 25°-60° from the crestline) changed direction by deflecting towards crest-parallel in the lee of the secondary foredune crest (aspect ratio ranging from 0.013 to 0.06) at all three study sites. This topographic steering also occurs over the foredune with the greatest effect occurring closer to the surface (from 0.22 m to 0.80 m); and increases with the obliquity of the regional wind direction. The results agree with Sweet and Kocurek's model (1990) for incident wind between 10°-70° from the crestline, and lee aspect ratio of less than 0.2. In general, near-surface airflow deflection was greater

at the top of the secondary foredune, gradually decreased toward the primary foredune crest and was generally absent on the flat beach at the three sites. Therefore flow vectors were deflected alongshore, resulting in transport pathways with a greater effective fetch (maximum potential fetch) for sand transport than those determined by regional wind. Further, highly oblique winds at BL suggest that the 'boundary' of the deflection zone expands to the seaward side of the PFT, however this was not observed at TSH during such highly oblique winds. Although this offshore pattern and steering is documented over dunes (Sweet and Kocurek, 1990, Arens et al., 1995, Bórowka and Rotnicki, 2001, Lynch et al., 2010), this present study may be the first to document alongshore deflection in areas of airflow recovery. It might also be expected that attached airflow on the lee side of the foredune would be subject to vegetation drag effects, favouring flow deflection. Walker et al. (2006) found that the occurrence of differential airflow deflection with height above the surface on the stoss slope was likely due to drag at the canopy level.

Secondary airflow patterns resulting from oblique offshore winds were thus inferred to have been attached and deflected at the three study sites. The results of this thesis are in agreement with Arens et al. (1995) who observed a parallel deviation of the airflow over a vegetated foredune of 9 m height (site 2) during offshore winds. The authors underscored that the deflection was never opposite to the regional wind direction. However separation and reversal flow has been recently observed by Lynch et al. (2009, 2010) at a site characterized by a steep foredune seaward slope (25°) and height of 11.4 m resulting in a high aspect ratio of 0.8 (site 1).

For onshore winds, no clear evidence of topographic steering is observed at the three sites. However a slight parallel deflection was observed at MNE during Exp-3, likely due to a combination of relatively high wind speed (U=5.12 m s^{-1}), highly oblique wind (α: 63° equivalent to angle of 33° relative to the dune crestline) and smooth foredune topography (Figure 3.23D). This agrees with previous research which has shown that oblique onshore wind (less than 30°) is steered alongshore on the beach (Mikkelsen, 1989, Arens et al., 1995, Walker et al., 2006, 2008).

3.5.3. Airflow Turbulence and Sediment Transport

The turbulent characteristics of airflow are significant, since these establish the erositivity of wind (i.e. facilitating momentum exchange toward the ground surface). Wiggs et al. (1996) measured Reynolds stress over a dune in a wind tunnel, and found that a significant portion of the total shear stress at the dune toe and crest may be

transferred by streamline curvature which modifies the stability and turbulent structure of the airflow. Thus, additional surface shear stresses to the airflow can be conveyed from the streamline curvature over the foredune. Concave streamline curvature and streamwise acceleration both increase surface shear stress, in contrast convex curvature and deceleration reduce it (Livingstone and Warren, 1996, Wiggs et al., 1996). The magnitude of the shear stress velocity also depends on the morphology of the foredune, the level of streamline curvature, and the degree of streamwise velocity. Relationships between shear stress velocity (u_{*RSk}), controlled by near-surface airflow properties, fluctuating u'- and w'-components (presented in Appendices 3.2, 3.3, 3.4) and vegetation were investigated (Table 3.9).

Table 3.9. Pearson correlation table between surface shear stress velocity (u_{*RSk}) and airflow properties measured from the mobile ultrasonic anemometer over the foredune-beach (based on 64 records): mean, maximum, minimum of u- and v-components; maximum, minimum, standard deviation of u'- and v'-components; vegetation factor corresponding to the seasonal vegetation cover. Significant values are in bold.

	U mean	U max	U min	W max	W min	W max	u' max	u' min	u' st	w' max	w' min	w' st	Veg
u_{*RSk}	0.31	0.36	0.23	0.74	-0.75	0.74	**0.96**	**0.90**	**0.85**	**0.92**	**0.93**	**0.81**	0.23

Shear stress velocity was strongly correlated to fluctuating u'- and w'-components (r>0.9; p<0.05). While it was moderately related to the vertical airflow (w-component) (r=0.75; p<0.05) and uncorrelated with horizontal airflow (u-component) (r<0.36; p<0.05). This reinforces the significant role of turbulence structures for sand entrainment and transport, and the necessity of integrating this factor into sand transport models for a better prediction of sand supply to the foredune. Walker et al. (2009) highlighted that in terms of turbulence generation, vertical velocity fluctuations play a significant role in transporting horizontal momentum from outer flow toward the surface through vertical turbulent eddies. Fluvial research has shown that sediment entrainment and transport are controlled by burst and sweep activity (u'<0 and w'>0; u'>0 and w'<0) (e.g. Jackson, 1976, Robert et al., 1996, Kostaschuk et al., 2008). Recently, Chapman et al. (2012) carried out high frequency (32Hz) measurements of turbulent airflow over a foredune during oblique onshore conditions. They observed a high activity of outward and inward interaction (u'>0 and w'>0; u'<0 and w'<0) at the upper crest likely leading to sediment deposition. However the lower stoss slope was dominated by sweep and ejection activity, the authors report that this could explain how sand is supplied to the windward slope through a region subject to flow stagnation.

Moreover, Bauer et al. (2008) reported that sand transport is related to wind speed and also shear stress velocity, which are difficult to differentiate under field conditions. Further explorations between turbulent airflow dynamics and near surface shear stress patterns over the foredune from higher temporal resolution (>1 Hz) measurements are required for a better understanding of aeolian dune morphodynamics. No relationship in this study was noted between shear stress velocity and the presence of vegetation (Table 3.9). However, recently Walker et al. (2006) observed turbulence in the plant canopy during sand transport events, suggesting distinct near-surface turbulent periodicity caused by plant-airflow interactions. Although research has been carried out on the dynamic between vegetation and turbulent airflow (e.g. Neumeier, 2007, Coastes and Folkard, 2009, Siniscalchi et al., 2012), it is still not well-understood, particularly with regards to the control of marram grass vegetation-generated turbulence on surface shear stress and sand transport.

3.5.4. Implications for Geomorphic Processes

Table 3.10 summarizes the potential sand transport capacity models derived from the near-surface airflow patterns (speed-up profiles) during different wind conditions at the three sites. Positive values mean that wind speed increases between one unit and the next and therefore potential transport capacity increases. Conversely negative values mean wind speed is slowing between one unit and the next so transport capacity decreases and deposition would be expected.

Table 3.10. Summary of transport capacity models during offshore and onshore wind conditions at the three sites. The symbol (+) corresponds to an increase of speed-up compared to the downwind sub-units measurement, while the inverse corresponds to (-), and the equivalence by (o).

		Sub-units							
	Site	SFC	SFT	PFC	PFT	UB	SED	MB	LB
Direct offshore	BL	-	o	+	-	+		+	+
	TSH	-	-	+	+	+	+	+	
	MNE	-	-	+	+	+		+	+
Oblique offshore	BL	-	+	+	-	+		+	
	TSH	-		+	+	+	+	+	
Highly oblique offshore	BL	-	+	+	+	+		+	+
	TSH	-		+	+	+	-	+	-
	MNE	+	-	+	+	o		+	+
Direct	MNE			-	-	-		+	
Oblique onshore	TSH	+	-	+	-	+	-	+	
Highly oblique onshore	BL	+	-	-	-	+		o	+
	MNE	o	-	-	-			+	

Direct offshore winds may be capable of transporting sand over the beach at all three sites. Deceleration at the primary foredune toe at BL (convex-concave-convex-concave foredune profile), and secondary foredune toe at TSH (convex-concave-straight) and MNE (convex-ramp-concave-straight) decreases sand transport capacity and is likely to result in deposition. Results in this study agree with Nordstom et al. (1996) that found that the 'lee-of-dune-zone' is subjected to the sheltering effect of the dune resulting in a airflow 'muting/dead transport zone' at the seaward side of foredune; and its extent depends on wind speed and offshore direction (Arens, 1994). However, as previously demonstrated, turbulence can lead to the opposite effect. The airflow may be gradually less disrupted by the foredune as it travels seaward and recover sufficiently to allow sand transport across the beach. However, sand is likely to be deposited mainly due to the high surface moisture content and micro-topography on the lower beach or intertidal zone where it may be temporally stored and re-transported inland during effective onshore conditions. At TSH, the embryo dunes on the upper beach at TSH are likely to reduce sand transport toward the beach by trapping transported sand and also by segmenting the fetch distance, however the magnitude of this effect depends on the angle of the wind approach. The same effect is expected under onshore wind conditions.

For oblique offshore winds, sand transport capacity increases from the SFT to the beach at the three sites (Table 3.10). As previously described, topographic steering effects through deflecting airflow parallel to the foredunes occurred. Under relatively slow sand-transporting winds, sand deposition would be expected on the foredunes, however for stronger sand-transporting winds alongshore sand transport would take place parallel to the foredunes.

Under onshore winds, sand transporting capacity generally decreases from the beach to the SFT at the three sites (Table 3.10). This suggests sand deposition on the seaward side of the foredunes, however the airflow accelerates over the SFC which may encourage sand to reach the crest and possibly to be transported further inland. Arens (1996a) found that dune topography forces the airflow to move upward, allowing some sediment to pass up the vegetated dune slope and towards the crest by a suspension/jettation process.

Winds orientated parallel to the foredune are the most efficient ones for sand entrainment and transport due to long fetch distances (Nordstrom and Jackson, 1993, Arens, 1996a, Wal and McManus, 1993, Ruz and Meur-Férec, 2004). Unfortunately, no seasonal experiment was carried out during winds strictly parallel to the foredune. Arens (1996a) suggested that although the fetch distance and sand source can be considered infinite during alongshore winds, sand supply to the foredune is limited or null. However recent studies have suggested that alongshore winds can contribute to the growth of the foredune by enabling substantial amounts of aeolian transport, even with a high surface moisture content, due to long fetch distances (Lynch et al., 2008, Delgado-Fernandez, 2011). Along the present study area, there is no doubt that sand transport takes place during alongshore winds above the threshold velocity. Although alongshore wind does not transfer sand directly into the foredunes, it is a significant component because rather than sand being lost offshore it moves laterally and hence is retained on the beach, and would be available to supply the foredunes when conditions are favourable (Hesp, 2002, Walker et al., 2006, Lynch et al., 2010).

Finally, the results show that important key factors regulate both the occurrence and the magnitude of sand transport at the three sites. Although wind speed above the threshold velocity is fundamental for sand transport processes, wind direction controls how the sand is distributed. Results also explicitly acknowledge the key role played by the controlling factors such as morphology, surface moisture content, fetch distance (i.e. fetch effect depends on the angle of wind approach and water level) and vegetation in determining sand transport process-response across the foredune-beach system. Turbulence plays an important role in sand grain entrainment and transport (e.g. Arens, 1996a, Sterk et al., 1998, Chapman et al., 2012). This present study has indicated the potential implications of turbulence structures for sand transport dynamics on the seaward side of foredunes.

3.6. Conclusion

- Foredune topography causes spatial variability in the velocity and direction of airflow resulting in secondary flow patterns that can contribute to sand dune morphological development.

- A decrease in wind speed is observed at the secondary foredune toe under both offshore and onshore winds at all sites. This effect decreases with the obliquity of the wind approach angle. A decrease in wind speed at the primary foredune toe was observed at BL only.

- Foredunes with a seaward aspect ratio below 0.167 experience attached and undeflected airflow during direct offshore and onshore winds. Topographic steering of near-surface winds produces local flow vectors that are significantly different in direction and magnitude from the regional oblique offshore winds at the three sites. These incident winds are initially deflected parallel to the foredune in the lee side slope, and finally deflected back towards the approach direction at the beach. This topographic steering effect was also generally associated with unsteady airflow that progressively decreases toward the beach. Because sand transport pathways follow these streamwise vectors, oblique offshore winds can contribute to foredune maintenance, where the transport threshold velocity is exceeded.

- At the three sites, wind regime (speed and direction), beach width, fetch effect, vegetation and moisture content can be considered key factors when linking micro- scale sand transport to predict the meso- and macro- scale behaviour of the foredune-beach system.

Chapter 4. Seasonal Foredune-Beach morphodynamics

4.1. Introduction

Having described the importance of micro-scale process interactions in the foredune-beach system in Chapter 3, this chapter moves up a scale to focus on the morphodynamics of the north Lincolnshire coastal dunes on a seasonal timescale.

Foredune development may take place over a timescale from seasons to years. However some external forcing factors, particularly storm surge events which typically only last a few hours, can significantly alter the sand budget within the foredune-beach system and influence its evolution (Sanderson et al., 1998, Vasseur and Héquette, 2000, Pye and Blott, 2008). Theoretical and experimental studies of the processes of foredune erosion under storm surge conditions show the role of different factors such as morphology, sedimentology and hydrodynamics (Vellinga, 1982, Carter et al., 1990, Claudino-Sales et al., 2008, Houser et al., 2008). Van de Graff's study (1986) was the first to demonstrate that the submersion parameter, corresponding to the extreme water level at the coast, due to conjunction of the surge peak with astronomical tide level, was the primary factor involved in foredune erosion. Whilst wave factors also determine the destructive potential of a storm, storm surge controls how far inland the storm waves can penetrate.

The severity of coastal foredune erosion does not only depend on storm surge characteristics, but also on both the beach and shoreface state conditions. Vellinga (1982) reported that as the initial beach profile steepened, storm surge erosion increased, thus influencing the volume of material eroded from the foredune. The author found that the bulk of eroded foredune sand was deposited only a short distance (150-200 m) from the foredune and was likely to be returned to the foredune by onshore aeolian sand transport. Laboratory experiments and field observations further indicated that foredune erosion and beach profile changes are small until the water level rises to the upper beach and the foredune toe (Van de Graaff, 1986, 1994, Ruz and Meur-Férec, 2004), which then starts to be exposed to storm waves (Hughes, 1983). Therefore there is a critical elevation above which waves have the greatest impact on the foredune. However the storm surge at a particular location may change significantly over a short distance due to the effect of run-up controlled by interactions with local nearshore bathymetry and beach profile. Research applying a model-based

approach has shown the importance of the impact of run-up on the foredune front (Overton and Fisher, 1988, Ruggiero et al., 2001). The total foredune retreat, related to the volume of sand eroded, is controlled by the frequency and intensity of each run-up event and its height exceeding the foredune toe (Overton and Fisher, 1988).

The complexities of the external forcing factors and also controlling parameters of sand transport make it difficult to predict changes in the foredune budget based on formulae derived from empirical data collected at a timescale of minutes to hours (Sherman et al., 1998), and the results of any extrapolation of such findings to longer timescales is often extremely tenuous (e.g. Davidson-Arnott and Law, 1990). The most common technique for circumventing the problem of daily versus seasonal studies is through detailed topographic profiling or three-dimensional surveys of landforms, repeated at regular intervals in order to monitor foredune-beach morphological and volumetric changes (e.g. Arens, 1995, Anthony et al., 2006, Navarro et al., 2011). Comparison of such repeat surveys enables quantification of the actual changes in sand budget and may also provide insights into processes and patterns of sand dispersal within the foredune-beach system driven by controlling and forcing factors. The overall aim of this chapter is to obtain a data set of time-stamped morphological information which can be used to test and validate the up-scaling model from micro- to meso-scale that will be developed in Chapter 5. The assessment of the morphological changes in the foredune-beach system is undertaken from season to season at the three sites described in Chapter 2. The focus is on identifying changes in the amount of sediment stored within the foredune and beach units and how this varies during the year. The main driver of high magnitude, rapid morphological change – as discussed in Chapter 2 and above – is suggested to be storm surges. The occurrence and potential impact of these events on the foredune-beach system are investigated. The specific research objectives are to:

(1) Determine whether the morphology of the foredune-beach system changes at the seasonal timescale;
(2) Identify any spatial variability in these changes amongst the three sites;
(3) Determine the main meteorological factors controlling these morphological changes;
(4) Quantify the magnitude and frequency of storm surge events during the research period and explore the extent to which these can account for the morphological changes identified in (1).

4.2. Methodology

4.2.1. Meteorological and Environmental Conditions

Wind frequency distribution was calculated for four seasonal periods, corresponding to the elapse time between the field surveys, to produce wind roses. Several statistics were calculated for each survey period, such as average and maximum wind speed for the three wind components: onshore (0°-<150°), offshore (180°-<330°) and alongshore (150°-170°; 330°-350°). In addition, other environmental variables were analysed over the seasonal periods in order to explore their potential influence on the transport of sand to the foredunes. These included total precipitation, mean temperature, precipitation/temperature ratio, all recorded locally at Skegness weather station and the frequency of occurrence of seawater inundation above 3.21 m (MHWS), 3.5 m, and 4 m between seasonal surveys.

4.2.2. Seasonal Topographic Surveys

Recent topographic surveying technology enables spatio-temporal analysis of the monitored foredune-beach system at a high resolution. Two-dimensional cross-shore profiles and more recently three-dimensional Digital Terrain Model (DTM) surveys have been widely used to estimate foredune budget changes over short (order of days) to medium (order of months to a few years) timescales, and also to explore processes and patterns of sand distribution within foredune-beach systems (e.g. Andrews et al., 2002, Anthony et al., 2006). Topographic survey monitoring was carried out at approximately 3-month intervals over the course of a year (Table 4.1), using an RTK-GPS with a horizontal error of ±0.007 m and vertical of ±0.026 m.

Table 4.1. Summary of the seasonal topographic surveys.

Survey	Season	Date	Number of days between surveys
Survey 1 (S1)	Autumn	16th October 2009	initial
Survey 2 (S2)	Winter	25th January 2010	101
Survey 3 (S3)	Spring	26th April 2010	86
Survey 4 (S4)	Summer	5th July 2010	70
Survey 5 (S5)	Autumn	19th October 2010	106

At each field site an area of interest (AOI) was defined for the seasonal topographic surveys. A two-dimensional profile was aligned to the benchmark (described in Chapter 2) and crossed the centre of the AOI, oriented perpendicular to the foredune crest, extending as far as possible towards the sea. This profile was surveyed during each field season. To enable a more detailed examination of volumetric changes in the foredune-beach system, and to identify any spatial variation in sand budget within the AOI, the foredune-upper beach section of the AOI was surveyed in detail in three-dimensions so that digital terrain models could be constructed. This is the critical zone where exchanges between the dune and beach are most likely to be detected. Whilst ideally this three-dimensional survey would extend further seawards, the constraints of completing the survey between tides made this impossible.
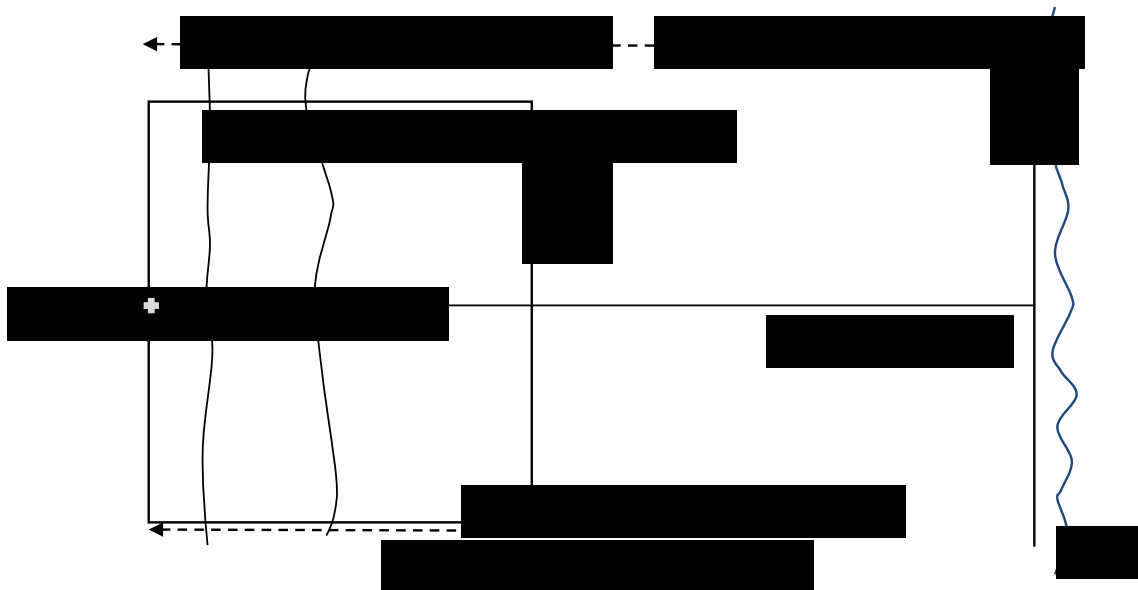
Figure 4.1. Sketch of the topographic data acquisition.

A. Profile data

Seasonal topographic surveys were conducted along profiles from the benchmark to the tidal beach around MHW (2.46 m) at all three sites. During surveying, heights were recorded at 2 m intervals and at obvious changes in micro-morphology. The topographic profiles were further linearly interpolated to 0.1 m. Analysis of seasonal cross-shore morphological change was carried out with reference to a set of standard morphological indicators (Halcrow, 1988, Saye et al., 2005, Thomas et al., 2011). These were applied in the foredune, upper beach and lower beach units previously defined in section 2.5 (Table 4.2).

Table 4.2. Definitions of indicators to characterize the seasonal foredune-beach system.

Indicator	Definition
Secondary foredune crest (m ODN)	Highest elevation of the secondary dune crest
Primary foredune toe (m ODN)	Elevation of the base of the seaward primary foredune slope
Primary foredune toe distance (m)	Position of the foredune toe Objective approach: Position of z=3.5 m contour
Upper beach width (m)	Distance between position of z=3.5 m contour and MHWS contour
Lower beach width (m)	Distance between MHWS and MHW contour
Slope of the foredune (°)	Height difference between foredune toe and secondary foredune crest divided by their distance
Slope of the beach (°)	Height difference between MHW and foredune toe divided by their distance
Volume of the foredune ($m^3 m^{-1}$)	Sand volume between the benchmark and the primary foredune toe
Volume of the upper beach ($m^3 m^{-1}$)	Sand volume between the position of z=3.5 m contour and MHWS contour
Volume of the lower beach ($m^3 m^{-1}$)	Sand volume between MHWS and MHW contours

Quantification of changes in sand budget are based on the method of 'vertical surface calculation'. Seasonal topographic profiles were not only used to quantify the seasonal variability, but also to determine statistical relationships between indicators.

It should be noted that the cross-shore profile approach only measures two-dimensional changes in elevation along a distance. It is a static measure of a foredune-beach system showing only the form of the coastal features and the changes normal to the foredune crest at a specific position (Andrews et al., 2002). As demonstrated in Chapter 3, aeolian sand transport controlled by the wind speed and direction are spatially variable; the two-dimensional cross-shore profiles are oriented perpendicular to the coastline and therefore will not reflect the full range of conditions to which the coastline has been subjected between surveys. For this reason, the three-dimensional DTMs are likely to be a better representation of overall change in sediment budget.

The procedure of volumetric analysis assumes that the core layer of the foredune units are sand deposits composed of entirely aeolian particles, which is unlikely. However this assumption makes it possible to carry out objective and repeatable volumetric calculations in order to compare sediment budget changes and dynamics in the foredune-beach system.

B. DTM data

A series of five detailed topographic surveys was conducted using a RTK-GPS system connected with four receivers at each study site during the seasonal monitoring period. The survey sizes were a compromise between the necessity of covering both the overall area of dynamic dune units up to the established dunes and the transition between the foredune and the upper beach, resulting in surveyed areas of cross-shore dimension above MHWS of approximately 50 m; and alongshore of 100 m at Brickyard Lane (BL) and Theddlethorpe St Helens (TSH), and 98 m at Mablethorpe North End (MNE). Survey points were located every 2 m and at obvious breaks in slope to produce a high density sampling grid to maximize the accuracy of the sediment budget calculations.

All DTMs were generated using ArcView 9.3 (GIS) software (Spatial Analyst and 3D Analyst). The in-built kriging option was used to interpolate between survey points; this is a geostatistical method determining the quality of predicted elevation points in terms of an estimation of variance through the creation of a semivariogram (Burrough and McDonnell, 1998). In order to create the DTMs, it was necessary to interpolate among the field-surveyed points to generate a three-dimensional model. To assess the most useful and accurate spatial resolution of the DTM a series of tests was run using different derived grid cell sizes. The determination of the grid cell size was based on the results of the comparative analysis of the residuals error (Andrews et al., 2002) through the Geostatistical wizard tool in ArcView. The equidistant grid with pixels 1 m ×1 m was found to be the optimum size for the dense surveyed point sampling and provided accurate representation of the overall shape of the foredune-upper beach. Overall, the mean of the root-mean-square error (RMSE) calculated between the interpolating DTMs and their respective field survey point data was around 3 cm, so that the final error of the DTM was ± 3 cm.

The DTMs were used to identify and quantify the morphodynamic changes related to ODN (≈0 m) using the definitions given in Table 4.2. Over the successive surveys, net total sand budget was calculated and coupled with the percentage of seasonal contribution relative to the net overall budget change, which is an important indicator of the degree of morphological mobility (Anthony et al., 2006). Difference DTMs were also produced between each survey in order to visualise the morphological changes, and to determine areas of deposition, erosion or no change. As an aid to interpretation, as they are presented each DTM includes the 3.5 m and HAT (4.09 m) contour lines; these separate the secondary foredune sub-unit, primary foredune sub-unit and upper beach and provide a common point of comparison from season to season. In order to compare the sites, the annual net sand budget change at each site was normalised by dividing the net budget change by the DTM surface.

4.2.2. Seasonal Forcing Factors Influencing the Morphological Changes of the Foredune-Beach System

The forcing factor analysis was focused on the potential energetic storm surge events which may influence the seasonal morphological changes of the foredune-beach system. Previous research suggests that the determination of the threshold of wind speed at which a morphological event occurs depends on the scale of the study (e.g. Stout, 1998). Long-term shoreline evolution research has focused on extreme storm events with a wind speed exceeding 14 m s^{-1}. However in this seasonal investigation, the threshold was reduced to 10 m s^{-1} in order to track the episodic events capable of causing foredune erosion. Time series of hourly measurements of wind speed and direction at Donna Nook weather station were analysed.

In association with the meteorological investigation, time series of water level and offshore wave activity were analysed in order to characterize the marine hydro-dynamic conditions. Given that the morphology of the foredune and beach is the result of atmospheric and marine conditions, the data series for forcing factors starts from the 1st July 2009, three and half months prior to survey S1, and continues through to 18th October 2010 (S5), encompassing the entire monitoring period. To identify the potential foredune eroding events, the storm surges occurring between successive seasonal surveys were extracted. For understanding seasonal changes, a storm surge was defined as the occurrence of onshore and/or landward-directed alongshore (wind blowing from 350°- 150°) winds ≥ 10 m s^{-1} associated with a water level ≥ 3.5 m. This

water level corresponds to the average vertical position of the primary foredune toe along the DTMs at each site over the entire monitoring period.

For further analysis, meteorological and marine records for each extracted storm surge event were averaged over the storm duration. This was because the sampling frequency for the forcing factor variables differs. Under storm conditions, energetic waves are usually associated with a maximum wave run-up, corresponding to the vertical displacement of the water level and consisting of a steady component (wave set-up) and fluctuating component (wave up-rush). Wave run-up is a significant process in causing and/or promoting foredune erosion. Ruggiero et al. (2001) found that the run-up for dissipative beaches depends on the beach slope, and wave parameters:

$$R_{2\%}^{T} = 0.27 \sqrt{SH_s \frac{gT_p^{\,2}}{2\pi}}$$

<div align="right">Eq 4.1.</div>

where $R_{2\%}^{T}$ is the wave run-up height exceeded by 2% of the run-up events (m), S represents beach slope (tan β), H_s is the significant wave height measured in deep water (m), g is the gravitational acceleration (m s^{-2}) and T_p represents peak wave period (sec).

For each extracted storm surge, a mean run-up was calculated by considering the local beach slope of the previous and post seasonal topographic profiles at each site. Then, wave run-up and observed water level were summed to determine the maximum total water levels. By examining mean sea level atmospheric pressure at Donna Nook station and synoptic pressure charts, the associated storm system was identified and the storm was recorded for the analysis of storm pathways.

Along a macro-tidal beach, foredune erosion impact is governed by the water level reached during the storm surge, which is dependent on the tidal and surge amplitudes in addition to wind speed and direction (Ruz and Meur-Férec, 2004). Wave height is also a significant parameter because when a storm coincides with high tides, the waves undergo less attenuation and are likely to reach and attach higher up on the

beach profile. Zang et al. (2001) suggest that a parameter of the storm tide should be incorporated into a storm erosion potential index to reflect the storm impact on the coastline. Potential foredune eroding events were here evaluated by using a storm erosion susceptibility index (SESI). It has been successfully applied to estimate the impact of storm surges on coastal erosion along macro-tidal beaches in the North of France (Chaverot et al., 2005). This dimensionless index combines the intensity of storm event (I) determined using the height of the observed water level above the foredune toe (3.5 m), the offshore water significant wave height (Hs) and the storm duration (D).

$$SESI = I \times H_S \times D$$

<div align="right">Eq 4.2.</div>

Additionally, a maximum SESI was also calculated by considering the total water level, corresponding to the observed tidal water level and the estimated mean run-up. Previous research reports that foredune morphology exhibits a strong dependence on the frequency of storm surge events (e.g. Guillén et al., 1999, Christiansen and Davidson-Arnott, 2004). The cumulative effects of storm surge groups, even those with a weak intensity, may often exceed the damage of one severe storm (Ferreira, 2005, Claudino-Sales et al., 2008). Bryant (1987) demonstrated that the cumulative storm index ('seasonal' and 'annual storm index') had a clear relationship with the coastline position. It thus allows the foredune-beach system to be regarded as the result of the `integration and combination' of the forcing events with a natural 'discharge' factor occurring during fair weather conditions (Bryant, 1987). Foredune erosion is thus more likely to be related to the cumulative effect of storm events (i.e. group of storm surges) between two successive surveys; for this reason the seasonal cumulative SESI was determined for observed and total water level at each site.

$$CumulSESI = \sum (I \times H_S \times D)$$

<div align="right">Eq. 4.3.</div>

To evaluate the role played by forcing factors in foredune-beach morphological changes, statistical analysis was carried out using Principal Component Analysis (PCA), which makes it possible to correlate the diachronics at short-term of the beach-dune system with the forcing factors recorded during the storm surge events over the seasonal periods. PCA has been described as a powerful and robust technique and has been commonly used in meteorology and coastal sciences to identify dominant

patterns of change (e.g. Orford et al., 1999, Short and Trembanis, 2004, Suanez and Stéphan, 2006, Houser et al., 2008). It provides insight into the multivariate structure of interrelated data by reducing their dimensionality (Jolliffe, 2002), so that it makes it possible to transform a large number of variables into linearly independent sources of "information" (referred to as components). PCA statistically measures and displays individually the relationship between n-observations (storm surges) on p-variables (forcing factors records and sand volume measurements) which could be represented as n points plotted in p-component axes constructed in p-dimensional space (Rogerson, 2004). A strong relationship is defined by the distance between points or axes, referring to the eigenvalues/scores defined as the variances of the principal components. The component axes are sorted from high to low and monotonically decrease relative to their eigenvalues, so that the largest values reflect the greatest variance (i.e. retaining the greatest amount of information). It is often considered that after the second components, variables become meaningless. In this analysis, the focus was on potential eroding events which were examined by evaluating the relationship between the forcing factor conditions during the storm surges and the volumetric changes of the foredune-upper beach system. The latter is represented by DTM volumes (e.g. DTMVol-MNE- at the specific study site) as well as volumes derived from the cross-shore profiles for foredune, upper beach and lower beach units (e.g. PROFdune, PROFupbeach, PROFbeach) for each study site. Based on the identification of the storm surges, nine meteorological and marine components were considered, these were wind speed (Wspd), wind direction (Wdir), and atmospheric pressure (Press), the water level (WatLevel), duration of the observed water level exceeding 3.5 m (Time), significant wave height (Hs), wave peak period (Pk), and the total maximum water level considering the mean run-up at each study site (e.g. RunUpWat-MNE). PCA analyses were undertaken to determine the relationships of external forcing factors with both the overall sand budgets of the upper beach-dune system, and cross-shore volumetric changes of the foredune and beach units. This statistical analysis also makes it possible to compare the seasonal and spatial trends at the three sites.

4.3. Results

4.3.1. Meteorological and Environmental Conditions

The total frequency of the winds occurring between the seasonal surveys is shown in Figure 4.2. Over the S1-S2 period (autumn-winter), offshore wind was prevailing (55.76%) with an average wind speed of 5.94 m s^{-1}. Onshore winds accounted for 26.94% of observations during this time, and included the maximum wind speed which was 19.53 m s^{-1}. Alongshore winds occurred 17.3% of the time – one third as often as offshore winds. Mean and maximum wind velocity were lower for all direction groups in S2-S3 compared with S1-S2. Onshore, offshore and alongshore winds accounted, respectively for 35.91%, 48.08%, and 16.01% of these winds. Thus, the prevailing wind was offshore between the winter and spring period. Over the S3-S4 (spring and summer period), onshore winds were prevalent (47.70%) with an average and maximum wind speed of 6.9 m s^{-1} and 14.95 m s^{-1} respectively. However, the strongest wind of 16.46 m s^{-1} was recorded amongst the alongshore components, which occurred 15.29% of the time. Offshore winds accounted for 37.01% with the lowest average speed recorded over the monitoring period. Over the S4-S5 period (summer-autumn), offshore winds were prevalent (58.66%), with an average wind speed of 5.14 m s^{-1}. The highest average wind speed of 7.25 m s^{-1} was recorded for onshore winds, which occurred 27.10% of the time. The occurrence of alongshore winds (14.24%) was half that of onshore winds.

A) S1-S2
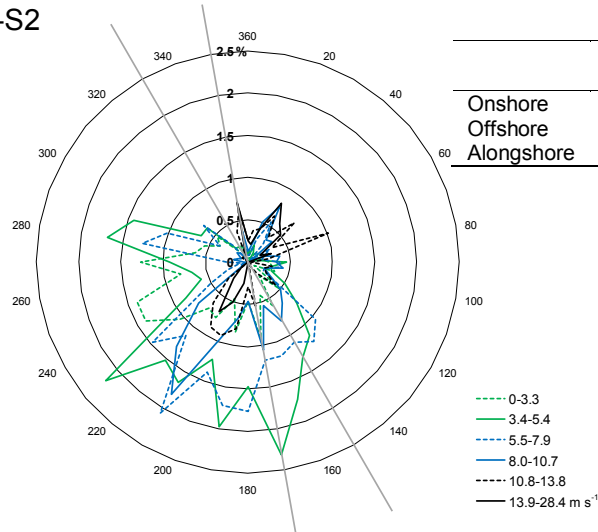
	Freq (%)	Mean (m s⁻¹)	Max (m s⁻¹)
Onshore	26.94	9.45	19.53
Offshore	55.76	5.94	17.99
Alongshore	17.30	7.69	16.45

B) S2-S3
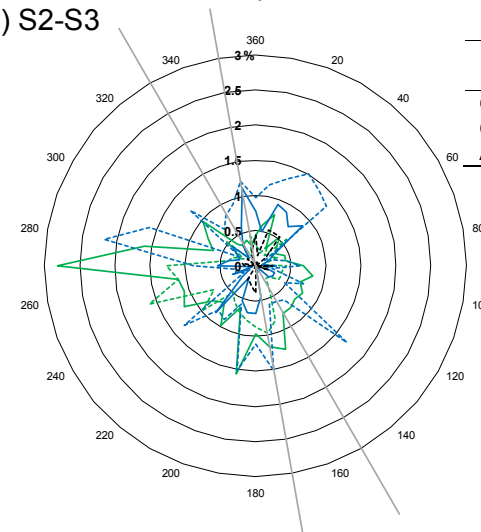
	Freq (%)	Mean (m s⁻¹)	Max (m s⁻¹)
Onshore	35.91	6.78	14.40
Offshore	48.08	5.27	13.37
Alongshore	16.01	5.78	11.83

C) S3-S4
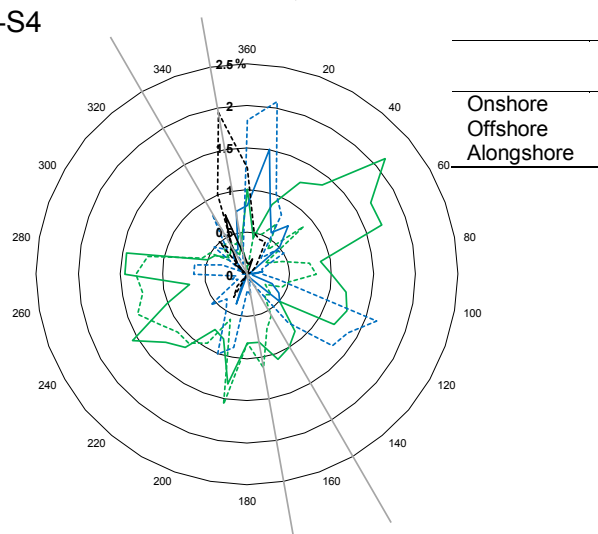
	Freq (%)	Mean (m s⁻¹)	Max (m s⁻¹)
Onshore	47.70	6.90	14.95
Offshore	37.01	4.36	14.90
Alongshore	15.29	6.17	16.46

D) S4-S5
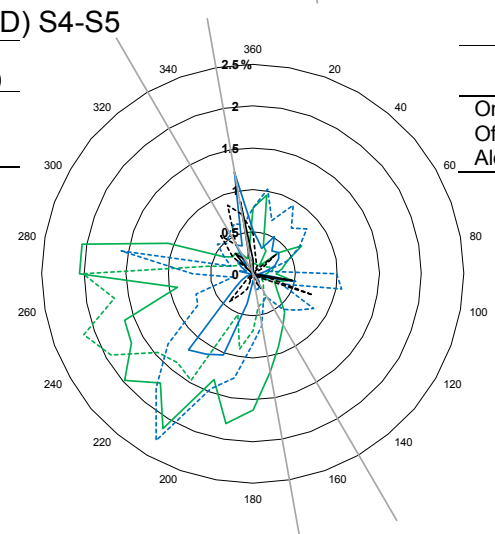
	Freq (%)	Mean (m s⁻¹)	Max (m s⁻¹)
Onshore	27.10	7.25	18.00
Offshore	58.66	5.14	16.98
Alongshore	14.24	7.24	18.51

Legend:
- 0-3.3
- 3.4-5.4
- 5.5-7.9
- 8.0-10.7
- 10.8-13.8
- 13.9-28.4 m s⁻¹

Figure 4.2. Wind roses for winds occurring between each seasonal survey: (A) autumn-winter (S1-S2), (B) winter-spring (S2-S3), (C) spring-summer (S3-S4) and (D) summer-autumn (S4-S5). Legend for all wind roses as shown in (A).

Figure 4.3 and Table 4.3 summarise local environmental conditions recorded at Skegness weather station over the whole monitoring period. There is a clear seasonal variation with autumn-winter being wetter and colder than the spring-summer months.
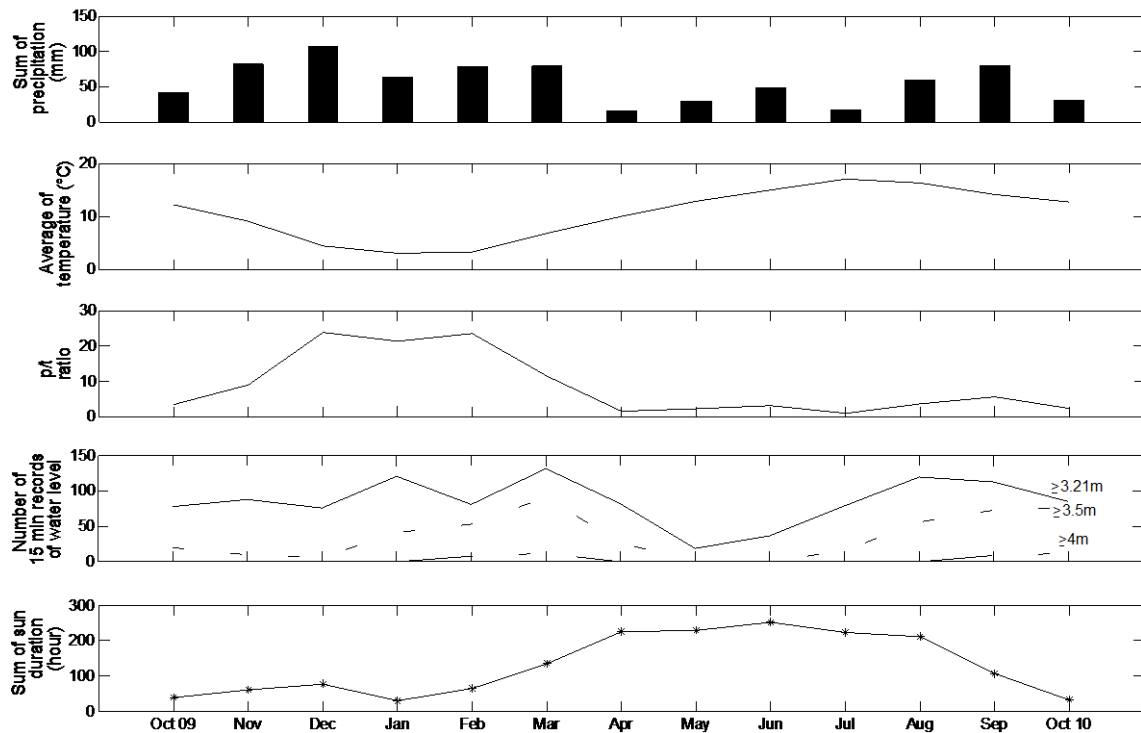
Figure 4.3. Time series of environmental variables over the monitoring seasonal periods recorded at Skegness.

Table 4.3. Summary of the environmental variables at Skegness station.

Period	Total precipitation (mm)	Mean temperature (°C)	P/T ratio	Frequency of seawater inundation (%)		
				≥3.21 m	≥3.5 m	≥4 m
S1-S2 [Autumn-Winter]	287.30	7.19	39.96	3.36	0.61	0
S2-S3 [Winter-Spring]	173.40	5.87	29.56	4.08	2.04	0.24
S3-S4 [Spring-Summer]	85	14.25	5.97	3.01	0.30	0
S4-S5 [Summer-Autumn]	187.40	16.13	11.62	4.31	2.08	0.20

126

Over S1-S2, the greatest amount of precipitation was measured (287.3 mm) and this was concurrent with a low mean temperature to give a high precipitation/temperature ratio (39.96). Frequency of seawater inundation $\geq$ 3.21 m (MHWS) occurred 3.36% of the time, $\geq$ 3.5 m just 0.61% of the time, and the elevation of 4 m was not exceeded. Between the winter-spring period, the total precipitation and mean temperature were both lower. However the frequency of seawater inundation was generally greater due to the occurrence of the vernal equinox on 20th March 2010. Heights $\geq$3.21 m, $\geq$3.5 m and $\geq$4 m were exceeded 4.08%, 2.04% and 0.24% of the time respectively. The spring-summer period (S3-S4) was characterized by low precipitation (85 mm) and a mean temperature of 14.25°C so that the precipitation/temperature ratio was low (5.97). The frequencies of seawater inundation were also the lowest during this monitoring period. Over the summer-autumn period, the total precipitation was 187.4 mm with a high mean temperature. The frequencies of seawater inundation above 3.21 m, 3.5 m and 4 m occurred for 4.31%, 2.08% and 0.2% of the time respectively. Compared with the other seasons, these frequencies were high, which was likely due to the occurrence of the autumnal equinox on 23rd September 2010.

4.3.2. Seasonal Topographic Surveys

A. Brickyard Lane (BL)

Figure 4.4 shows the seasonal topographic profiles from landward of the secondary foredune across the entire beach down to the lower beach (i.e. MHW level=2.46 m). The zones of active change, derived from the standard deviation computation for successive changes for all surveys at BL site are within the foredune and on the lower beach.

Along the profile, the main morphological change took place in the foredune zone (from 0-35 m) and the tidal beach zone where the ridges and runnels occur (from 360-490 m). Specifically, Figure 4.4B illustrates that the maximum standard deviation of 0.408 m was recorded on the secondary foredune slope (17.3 m). However, it is relatively low, suggesting the overall changes in foredune-beach profile are minor (Figure 4.4B).
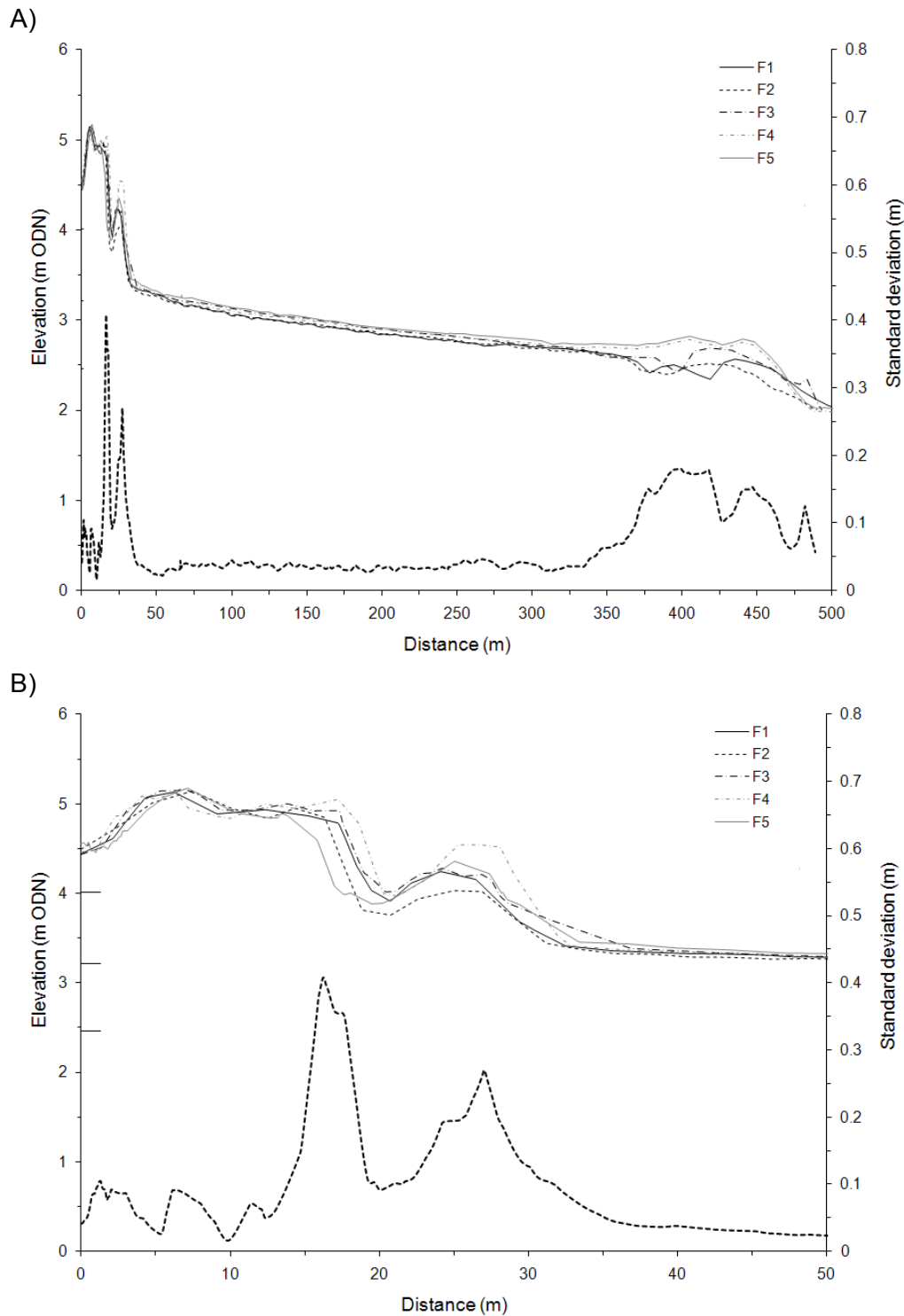
Figure 4.4. Seasonal cross-shore profiles at BL: (A) full profile of foredune and lower beach, (B) expanded section of foredune-upper beach. Dashed line represents the standard deviation computed from all surveys defining the zone of greatest morphological change. The small horizontal lines indicate HAT (top), MHWS (middle) and MHW (bottom).

For the total monitoring period, accretion occurred on the foredune and in the upper beach units with a total net sand gain of 6.45 m^3 m^{-1} $year^{-1}$ and 60.03 m^3 m^{-1} $year^{-1}$ respectively (Table 4.4). Overall the volume of the foredune changed very little, however the shape of the dune changed and became wider with the primary foredune toe advancing seawards by 1.1 m. Cumulative gross mobility of the beach budget, corresponding to budget changes relative to the net overall budget change, was nearly six times greater than the foredune. However negative volume changes were recorded in surveys S3 and S5, leading to a total negative net change of -159 m^3 m^{-1} over the 12-month monitoring period.

Seasonal and difference DTMs are shown in Figure 4.5. Over the S1-S2 period (October 2009-January 2010), the overall site experienced a relatively minor sand loss of -51.12 m^3. The DTM of difference shows erosion occurred seaward of the HAT contour, while sand accretion is shown to its landward side. Morphology was relatively stable near the 3.5 m contour and on the upper beach. Between January and April 2010 (S2-S3), the DTM showed a gain of 191.08 m^3 overall. The DTM of difference indicates that the greatest negative elevation changes occurred in small patches up to 0.25 m high landward of the HAT. By contrast, accretion can be seen in the north and also between the seaward side of the HAT and 3.5 m contour levels. However, the upper beach seemed to lose sand volume in the south. From late April to early July 2010 (S3-S4), further accretion of 138.96 m^3 took place at the site and was generally localized from landward of the HAT and 3.5 m contour levels, while the upper beach appeared to be relatively stable. Between the S4 and S5 period (July-October 2010), the overall site experienced a significant accretion of 259.08 m^3, which mainly occurred landward of the HAT, while to seaward the beach was relative stable with patches of erosion. Over the 12-month monitoring period, BL site underwent a net sand gain of 538 m^3 which seemed largely to have occurred between the secondary and primary foredunes. Normalised annual net budget, obtained by dividing the total volume change by the DTM size, corresponded to a gain of 0.14 $m^3 m^2$ $year^{-1}$.

Table 4.4. Summary of the morphometric and volume indicators for the seasonal cross-shore profiles at BL site.

Survey date	Elevation secondary foredune crest (m)	Elevation primary foredune toe (m)	Distance primary foredune toe (m)	Distance z=3.5m contour (m)	Upper beach width (m)	Lower beach width (m)	Slope foredune (°)	Slope upper beach (°)	Volume foredune (m³ m⁻¹)	Volume upper beach (m³ m⁻¹)	Volume lower beach (m³ m⁻¹)
S1: 16th Oct 2009	5.13	3.46	31.9	31.4	28	339.7	3.72	0.12	143.05	92.23	1107.72
S2:25th Jan 2010	5.13	3.48	30.9	30.7	26	314.8	4.06	0.12	137.36	85.24	1161.35
S3:26th Apr 2010	5.18	3.42	36.2	34.9	33.3	388.5	3.43	0.12	160.79	109.05	1110.65
S4:5th Jul 2010	5.13	3.47	32.4	32.2	32.6	399	3.66	0.12	142.58	107.64	1135.83
S5:19th Oct 2010	5.18	3.50	33	33	46.3	330.7	3.72	0.12	149.50	152.26	948.69
Total net change	0.05	0.04	1.1	1.6	18.3	-69			6.45	60.03	-159.03
Cumulative gross mobility									54.25	76.83	316.65

A) Survey 1: 16th Oct 2009   B) Survey 2: 25th Jan 2010   C) Survey3: 26th Apr 2010   D) Survey4: 5th Jul 2010   E) Survey5: 19th Oct 2010

Fixed DTM size: 3805 m²

F) 16th Oct 2009 - 25th Jan 2010
(101 days)

G) 25th Jan - 26th Apr 2010
(86 days)

H) 26th Apr - 5th Jul 2010
(70 days)

I) 5th Jul - 19th Oct 2010
(106 days)

Volume changes: -51.12 m³
NVC: -0.013 m³ m⁻²

Volume changes: 191.08 m³
NVC: 0.05 m³ m⁻²

Volume changes: 138.96 m³
NVC: 0.037 m³ m⁻²

Volume changes: 259.08 m³
NVC: 0.068 m³ m⁻²

Figure 4.5. Seasonal DTMs (A-E) and differential DTM budget changes (F-I) of the foredune-upper beach at BL. NVC: Normalised volume changes, obtained by dividing budget volume changes by survey DTM size. The HAT and 3.5 m contours are represented by the black line on the left and right respectively. To emphasize the seasonal morphological changes, a distinct scaling legend was produced for each difference DTMs.

B. Theddlethorpe St Helens (TSH)

At TSH site, the seasonal profiles indicate that the foredune unit, the embryo dune field and the lower beach were the main active zones (Figure 4.6). The standard deviation of height change was nearly 0.3 m for the former and latter, while it exceeded 0.53 m for the embryo dune field.

A)
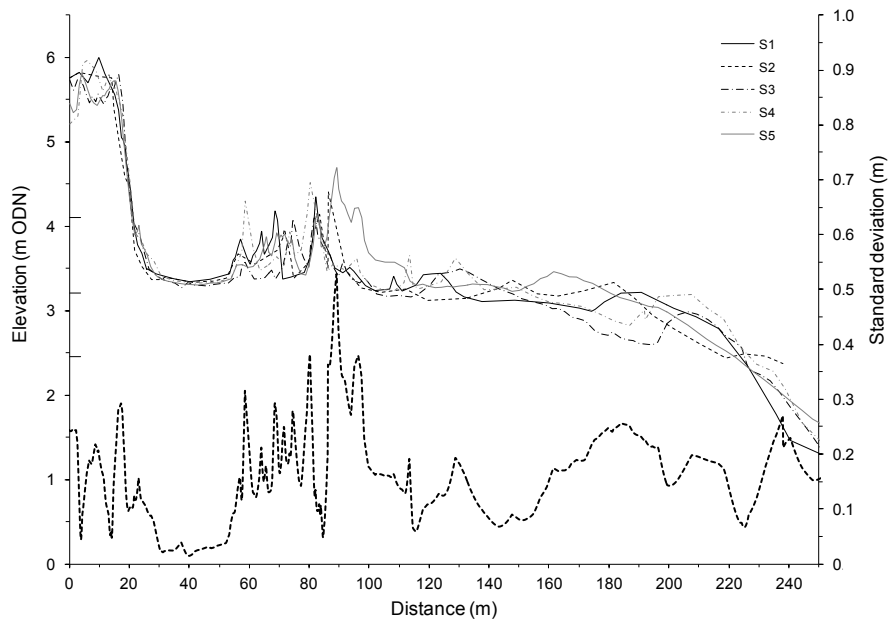
B)
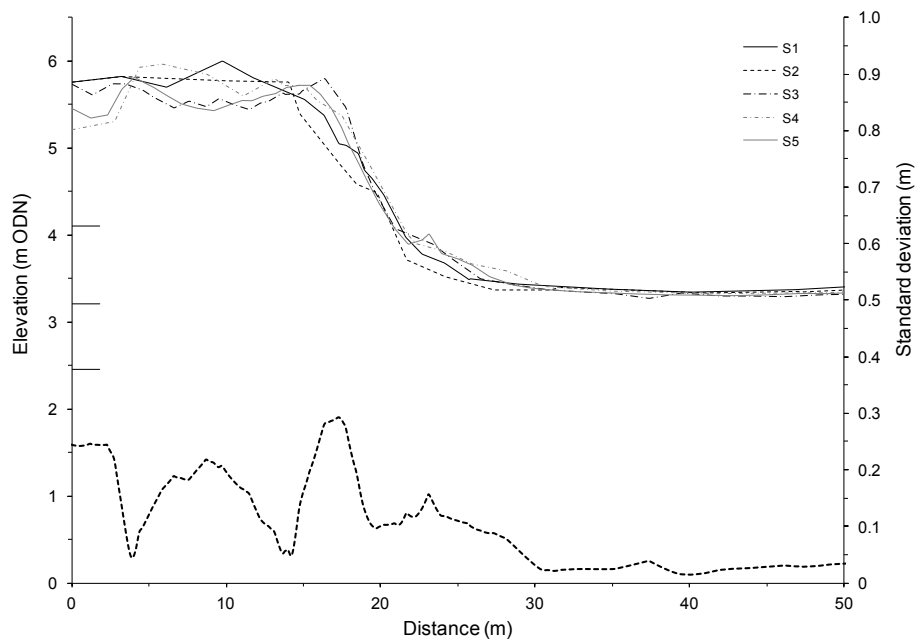
Figure 4.6. Seasonal cross-shore profiles: (A) along the foredune and lower beach at TSH site, (B) along the foredune-upper beach. Dashed line represents the standard deviation computed from all surveys defining the zone of greatest morphological change. The small horizontal lines indicate HAT (top), MHWS (middle) and MHW (bottom).

132

Results show that the secondary foredune crest and primary foredune toe experienced a slight decrease in elevation, but the latter also advanced seaward by 4.4 m (Table 4.5). Over the monitoring period, the shape of the foredune has thus become shorter and wider. From S1 to S4, the foredune and the lower beach showed similar behaviour, each undergoing a continuous accretion with a greatest sand volume of 150.71 m^3 m^{-1} and 240.16 m^3 m^{-1} respectively recorded in the summer survey (S4). In contrast, there was erosion of both the lower beach and foredune between S4-S5. The upper beach unit underwent erosion in autumn-spring 2009 (S1-S3) and accretion in summer and autumn 2010 (S4-S5). Over the monitoring period, the total net changes were relatively small in all units. However, the cumulative gross mobility was significant for upper beach and lower beach units reaching 327.58 m^3 m^{-1} and 257.52 m^3 m^{-1} respectively (Table 4.5), so that a redistribution of sand within the monitored foredune-upper beach units was more likely to have occurred than an additional supply of sand. The cumulative gross mobility of the foredune suggests that its sand gain was likely supplied from the beach units over the study period.

Figure 4.7 shows that the overall foredune-upper beach lost -470 m^3 of sand between the survey S1-S2 (October 2009 and January 2010). This mainly occurred at two spots between the HAT and 3.5 m contours. The spring survey (S3) indicated erosion was still taking place resulting in a net negative budget change of -178.56 m^3. The DTM of difference showed a contrast between erosion and accretion zones. Negative morphological change occurs landward of the embryo dunes on the upper beach, whereas accretion primarily occurred in the area between the first foredune and the corridors between the embryo dunes. This tendency of very distinct corridors of sand gain and loss was noticed in the field, and is easily detectable from the difference DTM. From late April to early July (S3-S4), the site experienced a net sand gain of 264.22 m^3 across the whole area with positive elevation changes of nearly 0.5 m. Accretion was about uniform across the whole of the upper beach. In contrast, erosion took place over the last survey (S5), with a net sand loss of -160.03 m^3 within the DTM limits. The corresponding DTM of difference highlights negative elevation changes at the landward side of the HAT contour, while the seaward side was characterized by a patchwork of areas of difference in sand loss and stability. Over the monitoring period, TSH experienced a net sand loss of -544.37 m^3 $year^{-1}$ corresponding to erosion of -0.16 m^3 m^{-2} $year^{-1}$ however the annual gross mobility was twice as important attaining 1072.81 m^3 $year^{-1}$.

Table 4.5. Summary of the morphometric and volume indicators for the seasonal cross-shore profiles at TSH site.

Survey date	Elevation secondary foredune crest (m)	Elevation primary foredune toe (m)	Distance primary foredune toe (m)	Distance z=3.5m contour (m)	Upper beach width (m)	Lower beach width (m)	Slope foredune (°)	Slope upper beach (°)	Volume foredune (m³ m⁻¹)	Volume upper beach (m³ m⁻¹)	Volume lower beach (m³ m⁻¹)
S1:16th Oct 2009	5.88	3.49	32.5	31.4	158.6	34.9	8.87	0.46	134.19	528.68	102.45
S2:25th Jan 2010	5.77	3.37	38.3	30.7	148.1	45	7.86	0.34	142.50	498.98	133.67
S3:26th Apr 2010	5.67	3.34	43.6	34.9	103.1	79.3	8.31	0.23	143.37	351.85	222.99
S4:5th Jul 2010	5.79	3.35	43.7	32.1	108.9	77.4	7.80	0.23	150.71	379.24	240.16
S5:19th Oct 2010	5.72	3.43	36.9	29.9	143.3	41.8	8.81	0.40	144.43	502.60	120.35
Total net change	-0.16	-0.07	4.4	-1.5	-15.3	6.9			10.24	-26.08	17.90
Cumulative gross mobility									22.8	327.58	257.52
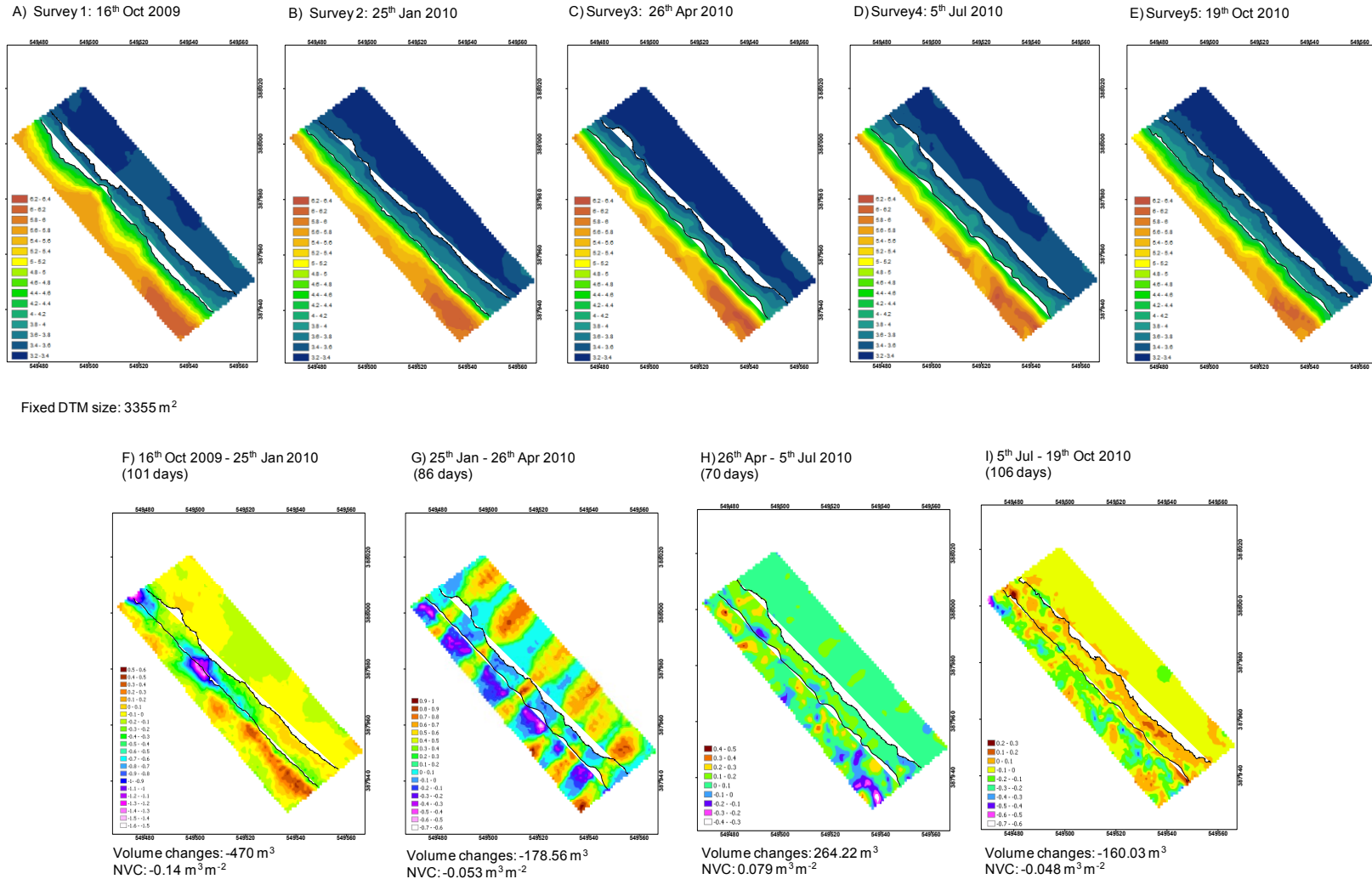
Figure 4.7. Seasonal DTMs (A-E) and differential DTM budget changes (F-I) of the foredune-upper beach at TSH. NVC: Normalised volume changes, obtained by budget volume changes by dividing survey DTM size. The HAT and 3.5 m contours are represented by the black line (left) and the dashed line (right) respectively. To emphasize the seasonal morphological changes, a distinct scaling legend was produced for each difference DTMs.

135

C. Mablethorpe North End (MNE)

Figure 4.8 shows the seasonal topographic profiles and the zones with important morphological changes at MNE site.

A)

B)
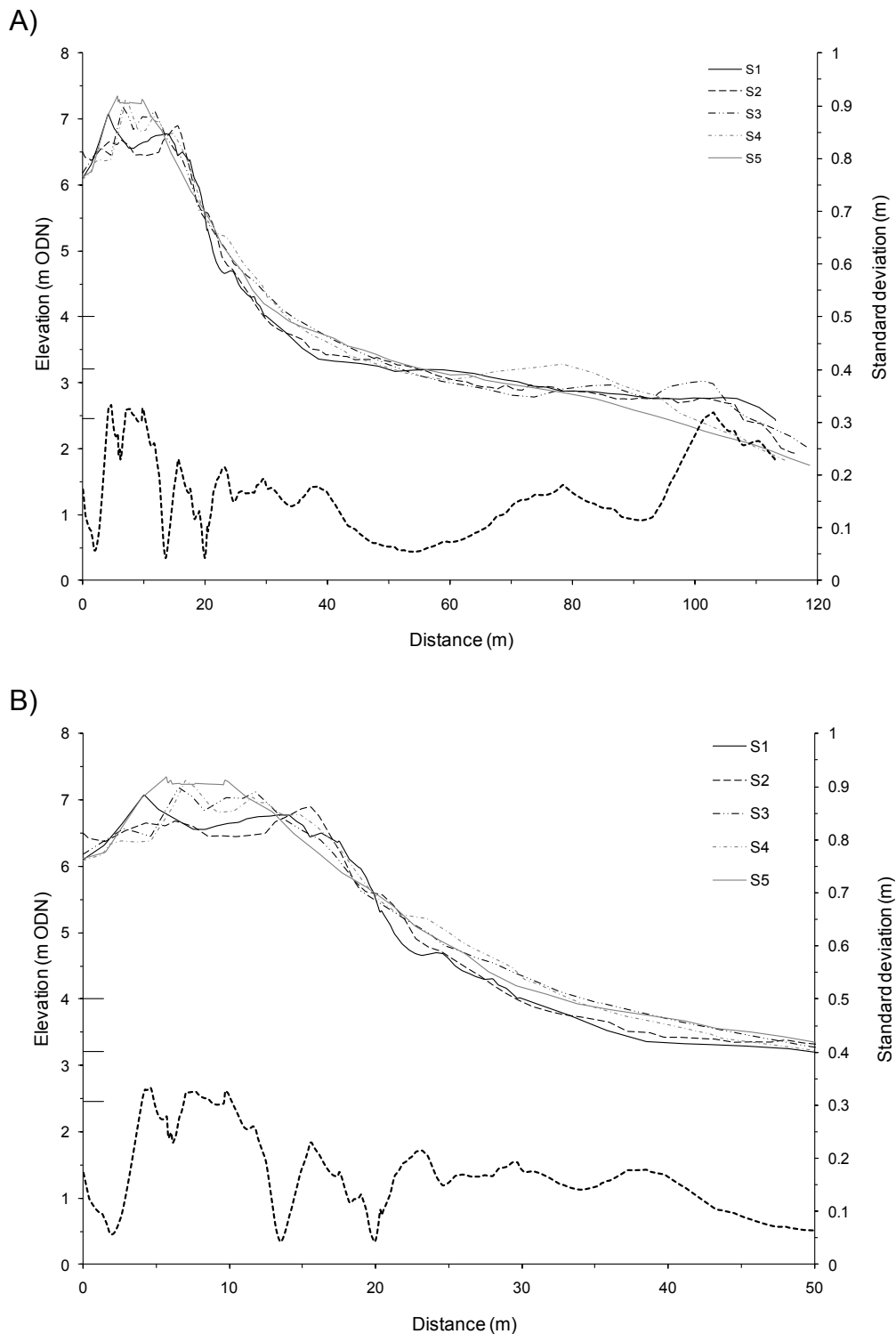
Figure 4.8. Seasonal cross-shore profiles: (A) along the foredune and lower beach at MNE site, (B) along the foredune-upper beach. Dashed line represents the standard deviation computed from all surveys defining the zone of greatest morphological change. The small horizontal lines indicate HAT (top), MHWS (middle) and MHW (bottom).

136

Over the entire profile, most morphological variation took place at the top (from 3.4-12.5 m) and seaward slope (from 15-16.5 m) of the secondary foredune sub-units, within the primary foredune sub-units (from 22.3 m to 40 m, and on the lower beach of the profile (from 97-110 m), for which the changes reach approximately ±0.2 m. During the monitoring period there was an increase of 0.8 m in height of the secondary foredune crest, while the primary foredune was mainly characterized by a positive horizontal change associated with its seaward advance of 12 m (Table 4.6). Thus, the shape of the foredune unit has become higher and wider over the monitoring period.

Between surveys S1 and S2, the foredune unit experienced a net sand gain of 59.32 m^3 m^{-1}, and a slight accretion of 7.38 m^3 m^{-1} was recorded at the upper beach unit (Table 4.6). In contrast the lower beach underwent a slight erosion of -31.59 m^3 m^{-1}. The spring survey (S3) indicated that the foredune and upper beach were affected by erosion with a net sand loss of -14.98 m^3 m^{-1} and -4.02 m^3 m^{-1} respectively, associated with a retreat of more than 1 m of the foredune toe. Between S3 and S4 surveys, a slight accretion of 6.29 m^3 m^{-1} took place in the foredune unit, resulting in a decrease of its slope, while slight sand losses dominated in the beach units and were associated with a steepening of the beach slope. In autumn 2010 (S5), the survey showed a slight decrease in foredune sand volume of -3.35 m^3 m^{-1} but this was much larger for the lower beach corresponding to a sand loss of -35.84 m^3 m^{-1}. The upper beach unit was relatively stable. Over the monitoring period, the cumulative gross mobility of the foredune and beach units were greater than their respective total net changes. However, foredune and both beach units showed opposite behaviour at this site. The foredune underwent a net accretion of 47.28 m^3 m^{-1} $year^{-1}$ which was nearly twice as much sand material as was lost along the entire beach profile. It is possible therefore that half of the sand deposited on the beach was transported directly to the foredune. The rest was transported alongshore to adjacent sites.

Table 4.6. Summary of the morphometric and volumetric indicators for the seasonal cross-shore profiles at MNE.

Survey date	Elevation Secondary foredune crest (m)	Elevation Primary foredune toe (m)	Distance Primary foredune toe (m)	Distance z=3.5 m contour (m)	Upper beach width (m)	Lower beach width (m)	Slope foredune (°)	Slope upper beach (°)	Volume foredune (m³ m⁻¹)	Volume upper beach (m³ m⁻¹)	Volume lower beach (m³ m⁻¹)
S1:16th Oct 2009	6.76	3.53	35.8	36.3	13.9	63.3	7.97	0.69	198.14	45.91	184.11
S2:25th Jan 2010	6.75	3.50	38.7	38.5	15.9	53.2	7.97	0.80	257.46	53.29	152.52
S3:26th Apr 2010	7.02	3.46	37.6	44.4	14.3	56.9	6.84	0.75	242.48	49.27	165.61
S4:5th Jul 2010	7.04	3.47	42.9	42.3	7.4	49.2	6.28	0.86	248.77	24.59	150.14
S5:19th Oct 2010	7.56	3.43	47.8	45.8	7.7	39.5	5.14	1.09	245.42	24.84	114.30
Total net change	0.81	-0.09	12.0	9.5	-6.2	-23.8			47.28	-21.07	-69.81
Cumulative gross mobility									83.94	36.33	95.99

The seasonal monitoring topographic data and budget changes for the foredune-upper beach site are summarized in Figure 4.9. In January 2010 (S2), the overall foredune-upper beach DTM shows a net accretion of 567.81 m^3, this is mainly located landward of the HAT contour. In general, the seaward side was characterized by relative stability and accretion zones. Between S2-S3, there was a net sand loss of -227.08 m^3 over the site. The erosion zones were located on the upper beach, and up to 10 m landward of the HAT contour. The most important negative elevation changes also occurred along the landward limit of the DTM. These changes were observed in the field, and were associated with areas of rabbit holes which result in unstable and collapsing ground. The S4 survey (summer) showed that accretion was taking place within the DTM limit with a net sand gain of 235.32 m^3 landward of the HAT contour, while the upper beach exhibited a slight sand loss. In October 2010 (S5), net sand accumulation of 582.96 m^3 occurred in the overall site. DTM comparison revealed an accumulation located from 15 m landward of the HAT to the upper beach. However erosion dominated along the landward limit of the DTM and there are several patches where significant negative elevation changes up to -0.72 m occurred. This may be explained by the summer anthropogenic erosion (i.e. high trampling pressure by pedestrians) and exacerbated by the rabbit activity. Pedestrian walking and trampling can have significant impacts in foredunes by altering morphology and surface characteristics due to mainly the destruction of the vegetation (Eastwood and Carter, 1981, Hesp, 2002). The gross mobility of the MNE site was 1613.17 m^3 $year^{-1}$ over the surveyed period and was accompanied by a total net accretion attaining nearly 1160 m^3 $year^{-1}$ (corresponding to normalised annual net accretion of 0.22 $m^3 m^{-2} year^{-1}$) which mainly was localized in the foredune. This indicated that the sand supply was deposited and then stored in the foredune unit over the monitoring period.

A) Survey 1: 16th Oct 2009   B) Survey 2: 25th Jan 2010   C) Survey3: 26th Apr 2010   D) Survey4: 5th Jul 2010   E) Survey5: 19th Oct 2010

Fixed DTM size: 5250 m²

F) 16th Oct 2009 - 25th Jan 2010 (101 days)   G) 25th Jan - 26th Apr 2010 (86 days)   H) 26th Apr - 5th Jul 2010 (70 days)   I) 5th Jul - 19th Oct 2010 (106 days)

Volume changes: 567.81 m³
NVC: 0.108 m³ m⁻²

Volume changes: -227.08 m³
NVC: -0.043 m³ m⁻²

Volume changes: 235.32 m³
NVC: 0.045 m³ m⁻²

Volume changes: 582.96 m³
NVC: 0.111 m³ m⁻²

Figure 4.9. Seasonal DTMs (A-E) and differential DTM budget changes (F-I) of the foredune-upper beach at MNE. NVC: Normalised volume changes, obtained by budget volume changes by dividing survey DTM size. The HAT and 3.5m contours are represented by the black line on the left and right respectively. To emphasize the seasonal morphological changes, a distinct scaling legend was produced for each difference DTMs.

4.3.3. Comparison of Geomorphological Units amongst Sites

A series of statistical tests was conducted to explore whether there are any relationships between morphological changes occurring in different geomorphological units. For example, is there a relationship between foredune height and width? This was achieved by calculating Pearson's correlation coefficient between pairs of variables.

Table 4.7 summarises the correlation coefficients between various morphological indicators and some of these correlations are visualised in Figure 4.9.

Table 4.7. Correlation table between various morphometric indicators characterizing the foredune-beach system morphology ($p<0.05$, Pearson correlation coefficient): (1) Elevation of the secondary foredune crest; (2) elevation of the primary foredune toe; (3) distance of the primary foredune toe; (4) distance of the z=3.5 m contour; (5) width of the upper beach; (6) width of the lower beach; (7) slope of the foredune; (8) slope of the beach; (9) volume of the foredune; (10) volume of the upper beach; and (11) volume of the lower beach. Correlations above ±0.9 are in bold, and negative correlations between foredune indicators and upper beach or lower beach unit indicators above ±0.5 are in italic.

		1	2	3	4	5	6	7	8	9	10	11
		Elev SFC	Elev PFT	Dist PFT	Dist 3.5m	Wid UB	Wid LB	Slope F	Slope B	Vol F	Vol UB	Vol LB
1	Elev SFC	■	-	-	-	-	-	-	-	-	-	-
2	Elev PFT	0.16	■	-	-	-	-	-	-	-	-	-
3	Dist PFT	0.65	-0.56	■	-	-	-	-	-	-	-	-
4	Dist 3.5m	0.86	0.15	0.61	■	-	-	-	-	-	-	-
5	Wid UB	-0.33	-0.51	-0.02	-0.62	■	-	-	-	-	-	-
6	Wid LB	*-0.74*	0.19	-0.62	-0.38	-0.34	■	-	-	-	-	-
7	Slope F	0.40	-0.23	0.36	-0.01	0.60	*-0.88*	■	-	-	-	-
8	Slope B	**0.98**	0.24	0.59	0.83	-0.32	-0.72	0.38	■	-	-	-
9	Vol F	0.89	0.30	0.52	**0.92**	*-0.62*	-0.45	0.11	0.89	■	-	-
10	Vol UB	-0.33	-0.52	-0.01	*-0.61*	**0.91**	-0.35	0.61	-0.32	*-0.62*	■	-
11	Vol LB	*-0.74*	0.20	*-0.64*	-0.40	-0.35	**0.99**	*-0.88*	-0.72	-0.46	-0.36	■

There are strong positive correlations between lower beach width and volume (r=0.99), foredune width and volume (r=0.92), and upper beach width and volume (r=0.91) (p<0.05; n=15) (Table 4.7). Strong correlations are also found between the relative position of the z=3.5 m contour and both the secondary foredune crest height and total foredune volume. This supports the earlier use of the z=3.5 m contour as the seaward boundary of the foredune unit. Interestingly, the correlations between foredune indicators (secondary foredune crest elevation, distance of z=3.5m contour, volume) and upper beach and beach unit indicators were negative.

Figure 4.10 separates the data into results from each of the three sites so that any differences in the relationships between variables at different geographical locations can be identified. The coefficient of determination (R^2) of morphometric indicators was calculated per study site (Wheater and Cooke, 2000). Results should be interpreted with care due to low n samples (n=5).

Figure 4.10A indicates that the secondary foredune crest elevation and position of the z=3.5 m contour are quite strongly associated at BL and MNE, while only a very weak correlation appears at TSH. The same trends occur between foredune unit indicators (Figure 4.10D). In contrast, it appears that stronger relationships occur between foredune unit indicators and upper beach or beach unit indicators at TSH (Figure 4.10B, C, E, F, G), while relationships are generally lower for the two other sites and especially at BL. Results also show a high variability in the correlations between sites, mainly due to their distinct morphological characteristics within the foredune-beach system.
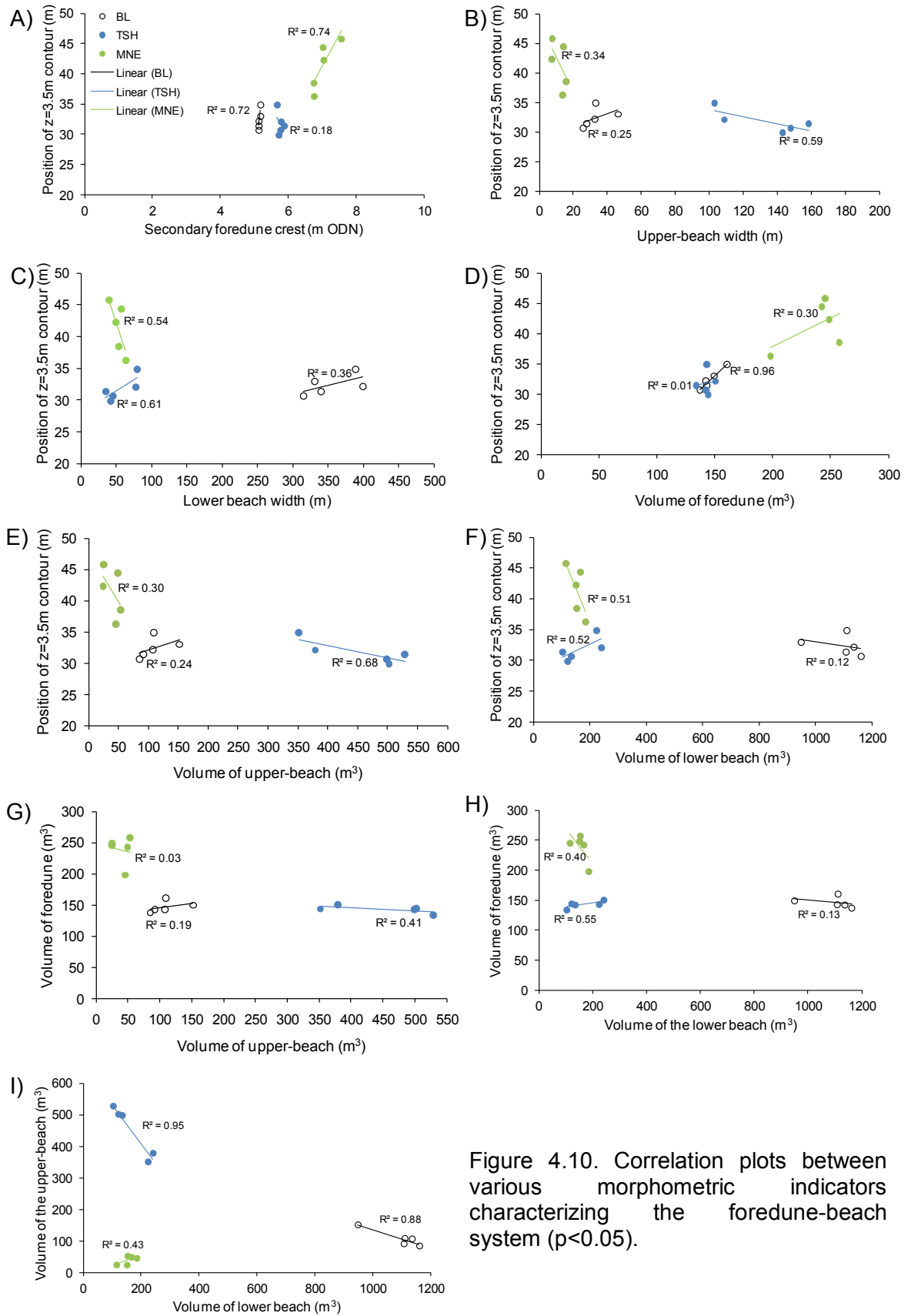
Figure 4.10. Correlation plots between various morphometric indicators characterizing the foredune-beach system (p<0.05).

4.3.4. Forcing Factors

Figure 4.11 illustrates time series of wind, water level and offshore wave characteristics over the whole monitoring period, and shows that winds were predominantly from offshore and with a speed below 10 m s $^{-1}$.

The average offshore wave height and peak period were 1.17 m and 6.5 s respectively with a dominant North direction. Eight potential morphological events were registered between July 2009 and October 2010 (Table 4.8). However only six storm surges occurred, characterized by a water level reaching at least 3.5 m coincident with onshore winds $\geq$ 10 m s $^{-1}$. These potential foredune eroding events presented different degrees of severity depending on both their meteorological and marine hydro-dynamic conditions, and also the length of time during which measured high water level exceeds the threshold of 3.5 m.

No storm surges occurred between July and October 2009 (pre-S1 survey); and between S3-S4 surveys period. In these cases, the potential morphological event was defined as the highest observed water level. During summer 2009 (pre-S1 survey), calm conditions prevailed with a mean wind speed of 5.5 m s $^{-1}$ blowing from south-south-west (190°). For this period, the only event with the potential to have a morphological impact on the foredunes took place in late September when a high water level reaching 3.84 m occurred although the mean wind speed was 6.4 m s $^{-1}$ blowing landward oblique alongshore (330°).
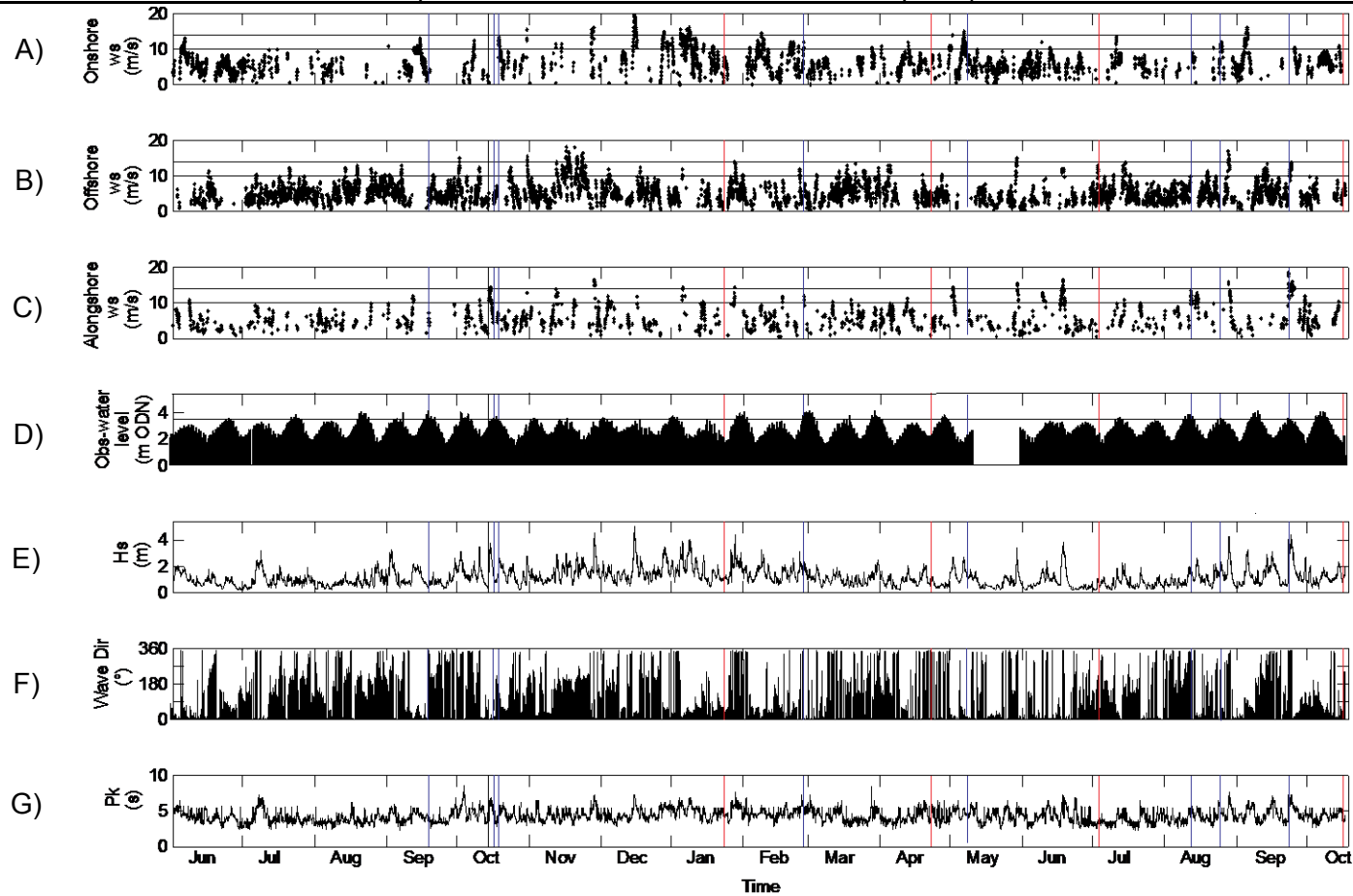
Figure 4.11. Time series of meteorological and marine conditions recorded from 1st June 2009 to 19th October 2010. (A) onshore, (B) offshore and (C) alongshore wind speed records from the Donna Nook station in which the horizontal lines represent the threshold of 10 m s^{-1} (bottom) and 14 m s^{-1} (top), (D) measured and adjusted water level at Skegness in which the horizontal line indicates the threshold of 3.5 m (not functioning tide gauge from 12th to 31st May), (E), (F) and (G) offshore wave height, direction and period respectively. Timing of surveys, storm surge and other potential morphodynamic events are indicated by vertical lines in red, blue and dashed blue lines respectively.

Table 4.8. Characteristics of the storm surge and other potential morphologic events over the monitoring period. * Duration of observed high water level >=3.5m (hour); ** Offshore significant wave height; *** Total water level corresponding to the observed water level associated with the mean run-up calculated from the beach slopes derived from the pre- and post-survey profiles.

Event	Date	Wind speed (m s^{-1})	Wind direction (°)	Observed water level (m)	Time* (hour)	Surge (m)	Wave height ** (m)	Wave period (s)	Wave direction (°)	Total water level*** at BL	Total water level*** at TSH	Total water level*** at MNE	Atmosph. pressure (hPa)
1	20/09 05:00	6.52	330	3.92	-	0.09	0.87	3.65	338	3.98	4.01	4.06	1021.6
	Survey 1: Autumn 2009 (initial morphological state)												
2	17/10 04:00	10.62	350	3.52	0.75	-0.01	2.68	9.16	23	3.76	3.87	4.13	1031.6
3	20/10 06:00	11.57	130	3.56	1	-0.09	1.92	6.52	126	3.69	3.77	3.92	1001.2
	Survey 2: Winter 2010												
4	28/02 06:00	10.29	20	3.57	0.5	0.27	1.56	8.34	6	3.80	3.73	4.02	985.5
	Survey 3: Spring 2010												
5	29/04 19:00	3.26	150	3.69	-	0.25	0.37	10.94	342	3.80	3.85	4.03	1006.0
	Survey 4: Summer 2010												
6	13/08 20:00	11.32	350	3.54	1	0.02	0.97	6.93	6	3.64	3.69	3.88	1016.5
7	26/08 07:00	11.19	60	3.58	1	0.17	1.56	9.10	177	3.71	3.84	4.09	1008.0
8	24/09 18:00	15.43	350	3.52	0.75	0.36	3.67	10.09	180	3.82	3.97	4.48	1011.5
	Survey 5: Autumn2010												

Over the S1-S2 surveys (autumn period), the extreme wind speed threshold of 14 m s^{-1} was frequently exceeded (Figure 4.11A). Two events with potential to impact foredune morphology occurred successively on 17th October and 20th October 2009 with an observed water level of 3.5 m and a wind speed slightly higher than 10 m s^{-1}(Table 4.8) For the first of these, the synoptic situation indicates that the low pressure system was generated from the North-east of Europe (Appendix 4.1A). Meteorological and oceanographic conditions were characterized by a landward-directed alongshore wind direction (350°), an average wave height of 2.68 m and peak period of 9 s. This generated run-up ranging from 0.23 m to 0.61 m at the sites, and resulted in a total water level of 3.76 m at BL, 3.87 m at TSH and at 4.13 m at MNE. The second storm surge was generated by a low pressure (971hPa) above the North Atlantic (Appendix 4.1B). Wave run-up was only 0.14 m at BL site and 0.37 m at MNE site due to a lower wave height and period, however this event was dominated by a relatively direct onshore wind (130°) and had a longer duration which makes it more likely to cause erosion in the foredune-upper beach system.

Between the surveys S2-S3 (January and April 2010), events with a wind speed threshold of 10 m s^{-1} were often attained (Figure 4.11A). A major storm surge was recorded on 28th February 2010, characterized by a North-easterly wind (20°) with a mean wind speed of 10.3 m s^{-1} and a low atmospheric pressure of 985.5hPa. The synoptic situation shows that the British Isles were surrounded by three low pressures present above Scotland, Norway and France (Appendix 4.2A). This event occurred during a spring high water level and a relatively high surge of 0.27 m was measured. Hence, persistent oblique onshore winds with unlimited wave fetch, which were likely to induce a high wind/wave set up associated with a maximum run-up, resulted in a total water level reaching an elevation of 3.80 m at BL, 3.73 m at TSH and 4.02 m at MNE. Between the late April survey and early July 2010 (S3-S4 surveys), no storm surges occurred, however the highest water level, recorded on 29th April 2010, reached 3.69 m with a weak wind blowing onshore. Water level measurements were missing from 12th May to 31st May 2010, however no strong onshore winds were recorded over this period, so storm surges are unlikely to have occurred. Fair weather conditions were prevalent and no storm surge was measured over this period and until mid-August 2010. However two successive storms occurred on 13th August and 26th August with similar characteristics such as an average of wind speed up to 11 m s^{-1}, and a water level reaching 3.5 m high. The potential foredune impacts are likely to have been higher during the second of these events due to a direct onshore wind and a higher

wave height than the preceding event. However the synoptic situations for both of these events (Appendix 4.3A, B) indicated that the low pressures are not fully developed so that the atmospheric pressures were above 1000hPa with low gradients (i.e. wide spacing between the isobars). On 24th September, a major storm surge took place due to two depressions above England and the North Sea associated with a relatively high pressure gradient caused by the squeezing of anticyclones present above Iceland and central Europe (Appendix 4.3C). This occurred during a spring high tide with observed water level reaching 3.52 m, surge level of 0.36 m, and a mean wind speed greater than 15.4 m s^{-1}. Offshore waves reached a height of 3.67 m and a period of 10.09 s, producing significant run-up along the coast. Thus, the total water level elevation likely attained was 3.82 m at BL, 3.97 m at TSH, and 4.48 m at MNE.

Over the monitoring seasonal periods, the assessment of the impacts of the storm surges on the morphological changes in foredune-upper beach system was undertaken at the three sites through the seasonal cumulative of erosion susceptibility index (SESI) (Figure 4.12). Over the surveys S1-S2 (autumn-winter 2009), relatively high cumulative SESI values were measured for the observed water level and total water level. Foredune-upper beach systems were subject to a volume loss of -51.12 m^3 at BL and -470 m^3 at TSH. However the high water levels did not affect the foredune-upper beach units at MNE. Volume changes varied spatially at the three sites over the successive seasons between the surveys S2 and S4, but the cumulative SESI values were low. Over the autumn period (S4-S5) significant foredune accretion of 259.08 m^3 and 582.96 m^3 occurred at BL and MNE respectively, while this period coincided with the highest cumulative SESI. This unexpected result is likely due to occurrence of constructive aeolian sand transport events. The high water levels however affected the foredune-upper beach system at the TSH site where a negative volume change of -160.03 m^3 was measured. The results indicate no clear relationships between the SESI values and the volume changes of the foredune-upper beach system at the three sites over the seasonal surveys.

Figure 4.12. Volume changes in foredune-upper beach system associated with SESI at: (A) BL, (B) TSH and (C) MNE, and the seasonal cumulative storm susceptibility index (SESI) for water level recorded and potential maximum reached water level. The scales of the right axes are not the same. Legend in (A).
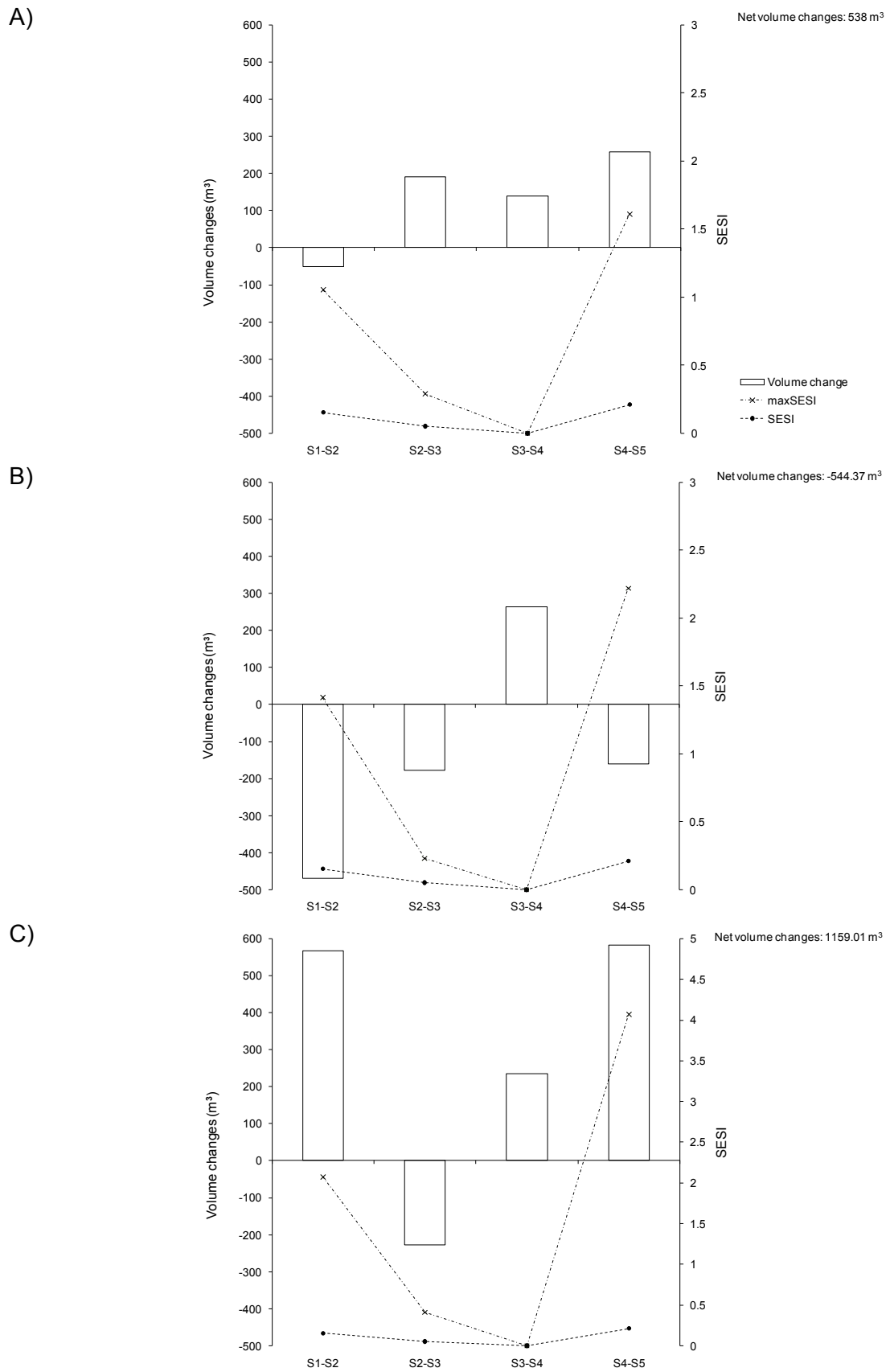
In order to investigate the role played by external forcing factors in foredune-beach morphological changes, a statistical analysis was carried out using Principal Component Analysis (the total variances), where the PC1 explains the largest part of the observed variance.

Table 4.9. Results of the PCA analysis with the eigenvalues of the considered variables.

Variables	All sites		BL		TSH		MNE	
	PC1	PC2	PC1	PC2	PC1	PC2	PC1	PC2
Wind direction (Wdir)	-0.05	-0.52	0.07	-0.98	0.48	0.84	-0.11	0.95
Wind speed (Wspd)	-0.57	0.31	0.37	-0.06	-0.50	0.56	-0.61	0.01
Atmospheric pressure (Press)	0.23	0.32	-0.21	-0.70	0.43	0.52	0.19	-0.68
Water level (WatLevel)	-0.68	-0.67	-0.34	-0.30	0.89	-0.30	0.70	-0.37
Surge	-0.10	-0.33	0.41	-0.07	0.08	0.35	0.00	0.01
Total water level BL (RunUpWat-BL)	-0.38	0.49	0.18	0.13				
Total water level TSH (RunU pWat-TSH)	-0.53	0.13			-0.33	0.44		
Total water level MNE (RunUpWat-MNE)	-0.61	0.17					-0.62	-0.04
Offshore wave height (Hs)	-0.32	0.23	0.09	-0.23	-0.29	-0.50	-0.37	-0.18
Wave period (Pk)	-0.53	0.23	0.39	0.26	-0.52	-0.16	-0.51	0.24
Wave direction (Hdir)	-0.31	0.77	-0.04	-0.19	0.78	0.50	0.33	0.32
Time	-0.66	0.46	0.34	0.17	-0.64	0.44	-0.72	0.24
DTM Volume BL (DTMVol-BL)	-0.89	-0.29	0.99	0.03				
DTM Volume TSH (DTMVol-TSH)	-0.99	0.02					-0.99	0.00
DTM Volume MNE (DTMVol-MNE)	0.67	-0.72			0.98	-0.07		
Dune profile Volume (PROFdune)			0.49	0.47	0.54	0.27	0.54	0.39
Upper beach profile Volume (PROFupbeach)			0.99	0.02	0.43	0.61	0.70	0.16
Beach profile Volume (PROFbeach)			-0.95	0.10	-0.34	-0.63	0.98	0.02
Score	**0.77**	**0.13**	**0.69**	**0.15**	**0.64**	**0.26**	**0.83**	**0.09**

Table 4.9 presents combined data from all three sites and shows the first two Principal Components (PCs) accounting for 77% and 13% respectively, and representing 90.01% of the total variance present within the original 15 variables. This thus gives a reasonably good approximation to the relative positions of the observations. The highest scores for the external forcing variables were for total water level (from -0.68 to -0.38), wind speed (-0.57) and measured high water duration of the storm surge event (-0.66). Good relationships are also observed between these external forcing factors, offshore wave height, wave period and foredune sand volume (Figure 4.13A). These forcing factors clearly structure the first component for the total sand volume for the foredune-upper beach derived from the DTMs at the three sites. This could also be observed for the volume of foredune determined by the topographic profile at BL and MNE (Figure 4.13B, D). The PC1 score was high at MNE (83%) and BL (69%), while it were lower at TSH (64%) where the relationships between forcing factors and morphological changes was less pronounced (Figure 4.13C). The volumes of upper beach and lower beach at BL and MNE were associated with a high PC1 score (>0.7), indicating that the pattern of the PC1 can be largely ascribed to the seasonal behaviour of the upper and lower beach units influenced by the occurrence storm surges. Interestingly, opposite correlation was generally found between the volume of the foredune and lower beach determined by the topographic profiles at BL and MNE sites (Figure 4.13B, D). However, no clear relationship can be depicted at TSH where these variables are associated with overlapping PC1 and PC2 components so that it is unclear whether the first or the second PC explains the largest part of the observed variance. Another possibility can also be that the first and second PCs are a mixture of the true underlying pattern (North et al., 1982). Furthermore, the dispersion of individual morphologic events results in the absence of any seasonal relationships, while it was expected that there would be a difference between winter-spring and summer-autumn storm surges (Figure 4.13). This could be explained by the occurrence of other dynamic processes between the surveys.

1: 20th Sept 2009   5: 29th Apr 2010
2: 17th Oct 2009   6: 13th Aug 2010
3: 20th Oct 2009   7: 26th Aug 2010
4: 28th Feb 2010   8: 24th Sept 2010
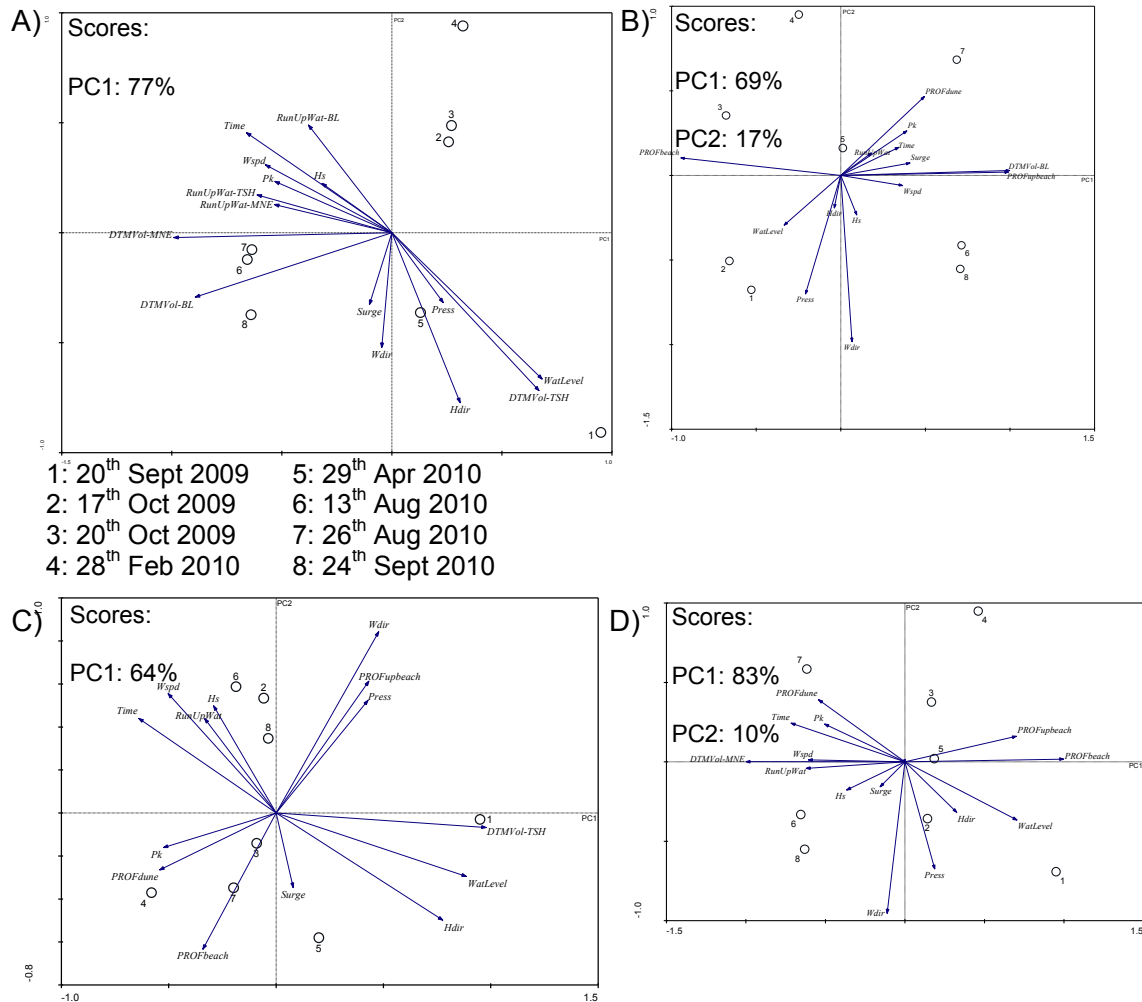
Figure 4.13. Statistical analysis (PCA) of sand budget and external forcing factor conditions recorded over the monitoring period (p<0.05). (A) applied to the foredune-upper beach sand volume derived from the DTM at each study site; and applied to the volumes for foredune, upper and lower beach at: (B) BL, (C) TSH and (D) MNE.

152

4.4. Discussion

4.4.1. Seasonal and Spatial Morphological Changes in the Foredune-Beach Systems

The key factor controlling foredune-beach dynamics is the sediment budget, primarily determined by aeolian sediment transport and the occurrence of storm surges (Arens, 1996b, Hesp, 2002, Delgado-Fernandez, 2011). The morphological change and pattern of the foredune-beach system proved to be variable at the three sites punctuated by the occurrence of storm surge events. Foredune accretion took place at BL and MNE almost throughout the seasonal monitoring periods. The greatest amount of morphological change of the foredune-upper beach at BL occurred in the form of accretion between S4-S5, while further south at MNE the greatest accretion was observed between S1-S2 and S4-S5 (Figure 4.14). There is a notable contrast between these two sites and the central TSH site where net erosion occurred during three out of the four survey periods.

At the three study sites, the seasonal topographic profiles illustrated that the upper and lower beach budget fluctuations were generally greater than the changes in the foredune units (Tables 4.4, 4.5, 4.6). Over the course of the year, the amount of sand gained within the foredune units at BL and MNE was equivalent to 4.06% and 67.70% respectively of the total sand lost from the lower beach unit. This suggests that rather than being sequestered by the lower beach unit, some of the sand supplied from the shoreface to the beach is directly transferred to the foredune unit and the remainder is transported alongshore, and/or nearshore during storm conditions. Both high sand input and gross mobility of the foredune at MNE underscores very active process-interactions within the foredune-beach system which could be favoured by the ramp dune morphology. Differences in morphodynamics between the three sites are, over seasonal scales, likely to be determined by the controlling factors of aeolian sand transport and local environmental conditions.

Figure 4.14. Seasonal changes (bar) of the foredune-upper beach derived from the DTMs at: (A) BL, (B) TSH and (C) MNE. The line is seasonal percentage contribution to the cumulative budget change (100%).
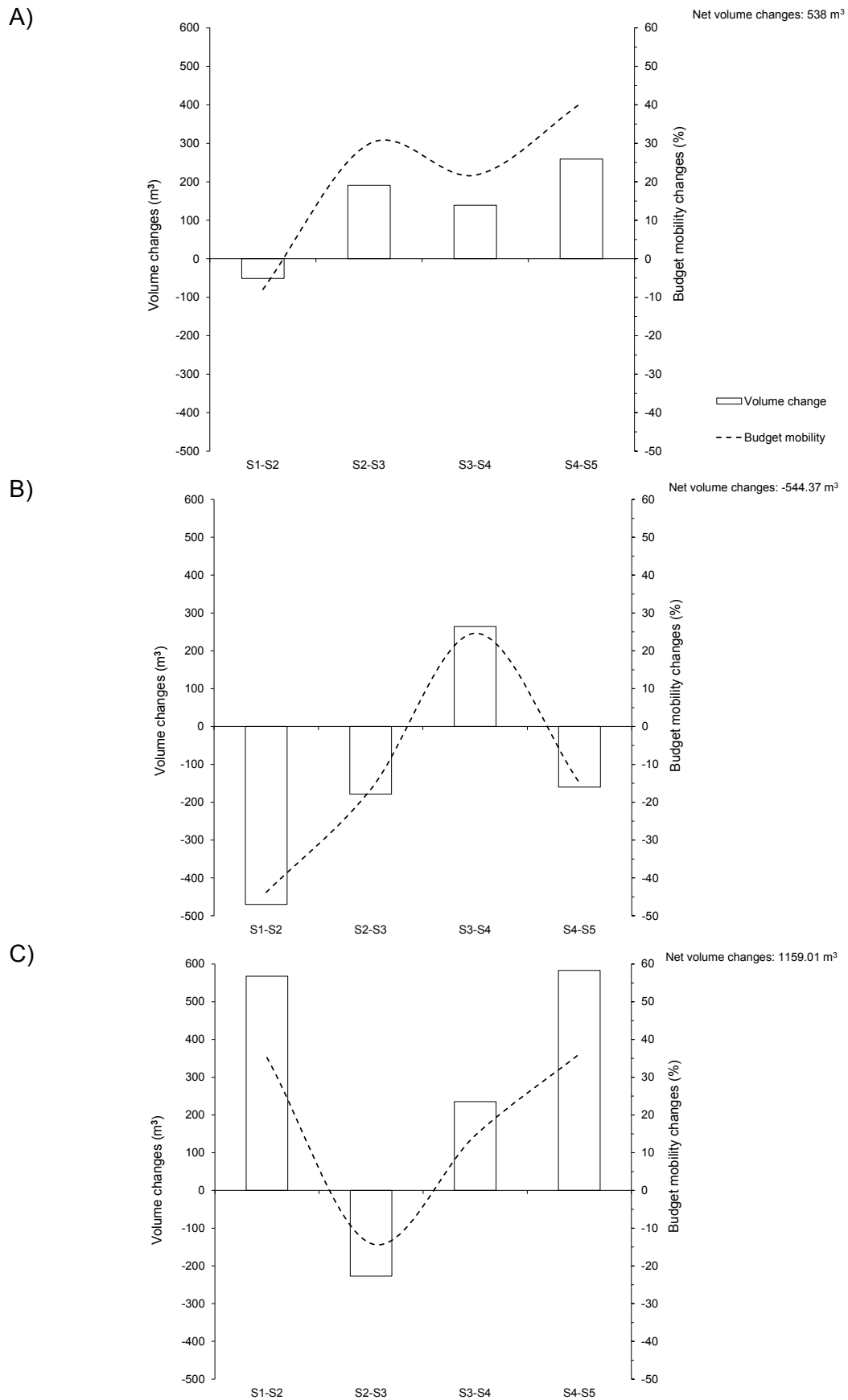
Use of morphometric indicators has emphasized the temporal and spatial variability of the foredune-beach system. The main findings demonstrate unsurprisingly a positive correlation between the increase in width and gain in sand volume within both the foredune and beach units. Interestingly, an opposite correlation appears between foredune morphology and upper beach or lower beach volume. Also, stronger relationships were found between foredune morphometric indicators at the BL and MNE sites, whereas foredune morphology at TSH was mainly associated with upper beach or lower beach volume indicators. It thus appears that the foredune at the latter site is likely to be more influenced by changes in the upper beach and lower beach. The relationships for the foredune-beach morphological system obtained agree with Saye et al. (2005) who found general relationships between beach morphology, dune morphology and erosion/accretion status in different coastal dune systems along UK. The authors also found that beach morphology between MHW and HAT influences the morphological trend of the foredunes, which often exhibit the same patterns.

As previously described in section 1.4, Psuty (1992) presents a model in which foredune development is dependent on the local availability of sediment from the beach. Foredune growth is maximized at times of slightly negative beach sediment budget (Figure 1.8). However a long-term beach sediment budget deficit results in beach lowering and frontal dune erosion, while a positive beach sediment budget leads to foredune accretion (Psuty, 1988, 1992). This study is consistent with Psuty's model, foredune development was observed in response to slightly negative beach sediment budget at BL and MNE ('Foredune development quadrant'). Although the model does not describe the current morphological state of the foredune-beach system at TSH, the embryo dunes can be considered as a temporary sand storage on the upper-beach (positive beach budget) which then may benefit foredune growth ('Beach ridge topography quadrant').

Over the whole monitoring period, the relative foredune sand budget changes were similar whether using the DTM or cross-shore profile approaches, however differences were observed at the seasonal scale. This is likely attributable to the spatial variability of the storm surge impacts along the foredunes. Also, coastal processes, and especially aeolian sand transport, are not two-dimensional deterministic processes quantified by systematic measurements along predetermined profiles (Baas, 2007). It thus illustrates the stochastic three-dimensional spatial variability of aeolian sediment transport at the seasonal scale.

4.4.2. Wind and Marine Forcing Factors

Over the seasonal monitoring periods, wind regimes displayed a pronounced seasonality in the meteorological and marine forcing factors. Modest winds (<8 m s^{-1}) occurred most of the time and particularly in summer, while stronger winds (≥13.9 m s^{-1}) blew in autumn-winter (S1-S2) and summer-autumn (S4-S5). The prevailing wind direction was offshore (with the exception of S3-S4), but the foredune-upper beach system underwent positive morphological changes at the three study sites. This suggests that episodic onshore winds were likely to be constructive events. As demonstrated in Chapter 3, oblique offshore winds (30°-65° relative to shore normal) are capable of supplying sand directly to the foredune. Direct offshore winds and alongshore winds could also have potentially caused remobilisation of sand from landward of the foredune to the beach resulting in a temporary positive beach sediment budget, before finally being re-incorporated to the foredune by onshore winds. This is consistent with Wal and McManus (1993) who found that positive sediment budget is the result of a combined interplay between onshore and offshore winds, and that the latter contributes both directly and indirectly to the foredune development.

In general, results agree with the classic seasonal foredune equilibrium system with a cycle of autumn-winter erosion occurring during storm surges and summer sand accretion reported in previous research (Carter et al., 1990, Arens, 1996b, Ruz and Meur-Férec, 2004, Suanez and Stéphan, 2006). Along the study coast, a storm surge occurs at high tide coinciding with a strong onshore wind principally blowing from the north to the east (longest wave fetch) generating significant wave heights. Further Ruz and Meur-Férec (2004) suggested that aeolian sand transport and foredune-upper beach development in a macro-tidal environment are strongly governed by the magnitude and frequency of occurrence of high water levels. The authors found that the winter storm surge associated with high water levels occurring in spring tides can completely annul sand gains from summer accretion.

Over the autumn-winter 2009 period (S1-S2), the cumulative SESI was relatively high (Figure 4.12), due to the occurrence of two successive storm surges induced by strong onshore winds and spring high water level with energetic offshore waves, causing a loss of sand from the foredune-upper beach system at both BL and TSH sites, while coastal dunes at MNE accreted. However, three storm surge events took place over the last seasonal survey period (S4-S5), for which the cumulative SESI attained greater

values. Specifically, the highest potential erosion events occurred on 24th September 2010 during the autumnal equinox period. For this seasonal period, the cumulative SESI predicted severe foredune erosion along the coast. However foredunes had accreted at the BL and MNE sites, and a slight erosion occurred at TSH, suggesting no or low impacts of the successive storm surges. Storm surge impacts depend on the magnitude, frequency and duration of such events, but also on the antecedent beach state (Morton, 2002). The level of impacts can have a significant effect on the nature and rate of foredune post-recovery (Saunders and Davidson-Arnott, 1990). A relatively low magnitude storm surge event may cause slight foredune impacts therefore post-storm recovery would be rapid and the impacts not recorded in the survey. Timing between storm surge event(s) and survey is also a key aspect in the foredune post-recovery.

Although mechanisms for offsetting some of the volumetric loss, and hence SESI value through aeolian transport into the foredune took place, this may have been combined with energetic nearshore processes (swash sand deposition) and perhaps associated with onshore sand transporting winds and a large fetch to drive sand from the shoreface to the foredune-upper beach system. This process was observed by Anthony et al. (2009) who suggested that the tidal beachface can supply an important source of sand when the beach is in accretion and characterized by filled intertidal runnels, increasing the length of the fetch. High wind speed events can generate aeolian sand transport on the flat beach at low tide, and also a large swash deposition of sand at high tide (Anthony et al., 2006). However as the upper beach flat becomes flooded by the large spring tides combined with water level reinforced by the run-up due to onshore storm surges, aeolian sand transport ceases. Furthermore, Anthony et al. (2006) observed a limitation of sand exchanges between the upper beach and foredune due to the segmentation of the fetch by the barred intertidal beach morphology immediately adjacent to the foredune slope. However on the Lincolnshire coast, this effect is reduced because there is a large distance between the upper beach and the landward runnel ranging from c. 115 m at MNE to c. 360 m at BL.

The PCA analysis mainly indicated the importance of the total water level associated with high onshore wind speeds, relatively important offshore wave height and period and measured high water duration of storm surge as key controlling factors in the foredune morphodynamic changes. These relationships were clear at BL and MNE

sites, but not at TSH site. This may be explained by the spatial variability of the storm surge affecting the foredunes along the coast and also the potential role of the embryo dunes on the upper beach for reducing erosion. In general, seasonal tendency was not thus clearly observed because the potential storm surge foredune impacts may have been offset by sand supply to the foredune during favourable conditions. These results also emphasize that the morphological changes on the foredune-upper beach depend on the occurrence of factors and process-interactions that act at different temporal scales such as episodic storm surge event disturbances (1-day) and post-storm recovery (months). As argued by Houser (2009), foredune sand supply results from the synchronization between transport potential and the availability of sediment in the beach. In the north of France, Ruz and Meur-Férec (2004) observed that 'optimal' transport conditions (strong onshore wind events) occurred during the winter and spring seasons, while sand accumulation in the foredune was only recorded during the summer period. The high transport potential during the energetic wind seasons was associated with an increase in storm surges that caused a lowering of the upper beach and a foredune scarp erosion. Sand was transferred towards the lower beach and nearshore zone and deposited as bars. Following storm surge events, the upper beach was characterized by a planar, low-angle morphology and the foredune toe could be reached by waves during successive but smaller high tides. The upper beach was inundated during these periods, limiting aeolian sand transport and thus foredune development. However foredune accretion occurred during the summer season when the beach and backshore had recovered, and only moderate aeolian sand transport took place.

Foredune development and storm-recovery result from the spatial and temporal coupling of aeolian and nearshore processes (Christiansen and Davidson-Arnott, 2004, Houser, 2009). Sedrati and Anthony (2008, 2007) further reported that littoral drift reinforced by large waves and strong wind forcing during storm conditions can strongly influence fluctuations in sediment budget on the upper beach and intertidal zone. They observed that severe storm surges can induce positive morphological change on the upper beach. Delivery of sand to the foredune is governed by a specific combination of transport potential and sand availability supplied by the shoreface. This is further discussed in Chapter 8.

In this study, the purpose of the PCA analysis was to reveal the temporal and spatial patterns between morphological changes and external forcing factors in order to reduce the number of factors considered in the foredune sand supply model. It was expected that the variables with the greatest influence on foredune morphology would be the same at all three sites, however this was not the case, and at individual sites the most important variables changed from season to season. In addition, the PCA only focused on high magnitude, low frequency storm surge events, whereas the data suggest that low to moderate magnitude, higher frequency processes such as Aeolian sand transport have a greater influence on foredune morphology. For this reason, storm surges were not included in the model in Chapter 5 whereas efficient sand transporting winds are.

4.5. Conclusion

- Along this coast, wind regimes displayed a pronounced seasonal variability. This controls the morphology of the foredune-beach system, which is characterized by an apparently classical seasonal cycle of autumn-winter erosion occurring during storm surges and summer sand accretion. This seasonal morphological pattern seems to be less clear for the TSH site.

- During the seasonal monitoring, coastal dunes experienced a net sand gain along the BL and MNE sites. An opposite behaviour occurred for the foredune-upper beach system at TSH site due to the presence of embryo dunes on the upper beach.

- Correlation analysis between various morphometric indicators showed relationships between foredune morphology and the beach unit status (upper beach and lower beach). However differences in morphological dynamics within the foredune-beach system amongst the three sites are primarily controlled by the availability of sand supply and local morphological characteristics.

- Morphological changes of the foredune-upper beach depend on interacting processes that act at different temporal scales: episodic storm surge and seasonal controlling factors.

Chapter 5. Modelling sediment supply to the foredune-upper beach

5.1. Introduction

After investigating the role of near-surface airflow and sand transport processes in the dynamics of the foredune-beach system in Chapter 3 and deriving an accurate dataset of time-stamped seasonal morphological changes in Chapter 4, this chapter attempts to develop a model for up-scaling from micro- to meso-scale process-responses. In particular, the focus is to identify the role of different wind regimes that control the foredune morphological changes at the seasonal and annual periods. This would make it possible to establish a link between short-term aeolian sand transport events and medium-term foredune development.

As outlined in Chapters 1 and 3, most research on coastal dune development has either focused on measuring airflow and sand transport processes at the micro-scale or on determining the morphology and development of foredunes at the meso-scale. A few researchers have attempted to correlate sand supply, using conventional instantaneous transport rate equations (e.g. Bagnold, 1941, Kadib, 1964, Hsu, 1974, Lettau and Lettau, 1977), with foredune development at scales spanning days to months (e.g. Sarre, 1989, Wal and McManus, 1993, Arens, 1997, Bórowka and Rotnicki, 2001). Several studies have also attempted to estimate sand input by integrating transport rate equations in relation to standard climatic records such as hourly wind speed and direction, and precipitation (e.g. Fryberger and Dean, 1979, Illenberger and Rust, 1988, Lynch et al., 2008).

The resulting predictions are, however, often substantially different to observed values of sand deposited into the foredunes (e.g. Sarre, 1989, Gomes et al., 1992, Davidson-Arnott and Law, 1990, Van der Wal, 2000, Navarro et al., 2011). The difficulties associated with identifying and quantifying all the variables contributing to aeolian sand entrainment, transport and deposition across the different spatial and temporal scales make predicting sand input to the foredunes very challenging (e.g. Nickling and Davidson-Arnott, 1990). However, Delgado-Fernandez (2011) recently reports that a good prediction of sediment input into the coastal dunes at the meso-scale, based primarily on wind speed and direction, can be achieved by accounting for relationships between the main supply-limiting factors.

160

This aim of this chapter is to explore whether it is possible to develop a model that can be used reliably and widely to predict sediment supply to coastal dunes in macro-tidal environments where the main controlling variables are wind regime and water level. Accurate models that facilitate such explicit linkages between micro- and meso-scales are desirable because they can provide a more complete explanation of interactions between processes and responses of coastal dune development at timescales of relevance to coastal management and potential coastal response to environmental change. Although the problems of scale linkage have been previously highlighted, this chapter will attempt to overcome some of them by integrating key controlling factors of sand transport identified in Chapter 3 into a meso-scale foredune sediment supply model. The specific objectives of the chapter are to:

(1) Simplify the wind regime and use it to calculate maximum potential sand transport;

(2) Quantify the impact of wind direction and water level (tide) on potential sand transport;

(3) Use data from (1) and (2) to develop a model of potential sand supply to the foredune-beach system;

(4) Run the model in (3) to predict sand transport in the beach-dune system at timescales comparable with the seasonal field surveys detailed in Chapter 4;

(5) Compare the model predictions of changes in sand volume with the measured volumes and evaluate its performance.

Thinking a head to the overall aims of the thesis, the challenge is to try and restrict data inputs to the model to those which are likely to be available at all time scales, from micro- to macro-scales.

5.2. State of Art in Modelling Sand Transport

A number of empirical equations linking sand transport rate to the wind velocity have been proposed based on wind tunnel experiments (e.g. Bagnold, 1941; Kawamura, 1951) and also on coastal field measurements (e.g. Svasek and Terwindt, 1974, Illenberger and Rust, 1988, Sarre, 1989). More complex aeolian sand transport (q) (kg m^{-1} s^{-1}) formulae relate sediment flux to shear velocity and a range of other variables such as grain size, grain density, and air density (e.g., Bagnold, 1941, Kawamura, 1951, Kadib, 1964, Lettau and Lettau, 1977, White, 1979). Typically sand transport flux is proportional to the shear velocity cubed (q$\propto$u^3) over and above the threshold velocity at which sand begins to move.

The instantaneous sand transport rate equation of Bagnold (1941) has been the most widely and successfully employed (Sherman and Li, 2011) so it will be used as a basis in this study. This equation is based on fluid mechanics and boundary layer theory applied to the aeolian saltation system. It has a theoretical foundation with a functional form given by:

$$q(t) = f(C, g, D, d, \rho, \rho_S, u_*)$$

<div align="right">Eq. 5.1</div>

Where q is the sediment flux defined as the mass of sediment transported per unit cross-sectional area of flow per unit time (t); C is Bagnold's semi-empirical dimensionless coefficient; d is the grain diameter; D is the reference grain diameter; ρ is air density; ρ_s is sediment density, g is the gravitational acceleration; and u$_*$ is the shear stress velocity.

Bagnold derived a set of predictive relations which were calibrated and tested using detailed empirical measurements from wind tunnel and field experiments. He calculated the weight of the sand which moves along a line of unit width past a fixed point, during a unit of time, over a surface of loose sand and under the influence of steady wind conditions. The calculated flux corresponds to sand transport over the whole height of the wind tunnel, including surface creep, and in the ideal case where the wind speed varies with the logarithmic height. Sand transport rate equations are only validated under 'ideal' conditions such as a steady and uniform wind flow, flat and unvegetated dry surface, well sorted sand and a fully loaded saltation layer. As

previously mentioned (see section 3.2.2), these 'ideal' conditions are rarely present in coastal environments due to the large range of limiting factors.

In general, large discrepancies over both short- (minutes) and longer- (months) time periods have been found between equilibrium model predictions and measured rates of transport in the field; the latter are frequently lower than those predicted by formulae due to environmental complexity (Sarre, 1987, Sherman and Hotta, 1990, Sherman et al., 1998, Bauer et al., 2009). For example, Goldsmith et al. (1990) predicted an annual sand supply along the coast of Israel of 170% greater than the actual measured rates. Conventional equations provide an estimate of a potential sand transport rate corresponding to an average of a sequence of temporally adjusting flows. One of the primary problems in attempting to predict sediment input to coastal dunes over periods of weeks to years is to determine an appropriate set of equations that incorporate the complexities of primary variables. Also, it is not always immediately apparent which discrepancies are due to the inadequacies of the sediment transport equations and which to the manner in which they have been incorporated. Additionally, most researchers have focused on identifying the influence of each factor individually on aeolian sand transport, whilst their relative significance and combined effects are still unclear at the meso-scale (Bauer and Sherman, 1999). It is also worth noting that, whilst equations are often judged to be inadequate representations of natural processes, it is also very challenging to accurately measure rates of sand transport in the field with which to compare model output (e.g. Bauer et al., 1996, Ellis et al., 2009).

5.3. Methodology

5.3.1. Modelling Assumptions

The methodology used was to estimate the potential rates of sand supply based on the capacity of the wind to transport material at each study site over the seasonal periods using readily available data from weather and tide gauge stations. Potential sand transport is defined as the maximum transport, assuming that all winds above the threshold can move sand; in other words, disregarding all environmental variables which reduce aeolian sand transport. The main assumption of the modelling approach was that the primary environmental factors of wind speed and fetch control both the frequency and the magnitude of transport events. Whilst wind speed determines the likelihood of sand transport, fetch is assumed to determine sediment supply and incorporates variables such wind direction and beach inundation. The model also assumes that potential sand supply is the same – vegetation on foredunes is likely to limit offshore sand supply (discussed further in section 5.5.3). At the meso-scale, the prediction of sand transport can better be estimated by improving our understanding of the importance, and the synergistic behaviours, of key controlling factors. The procedure adopted in this study was to simplify the way in which this synergistic behaviour is modelled and not to focus on individual factors.

5.3.2. Modelling Approaches and Data

In the context of a steady wind blowing over an ideal surface and large sediment availability, the amount of saltating particles within the saltation cascade increases exponentially to a maximum condition (Bauer and Davidson-Arnott, 2002), mirroring saturation of the system where the momentum flux of the wind is transferred to the sand and when the sand transport rate is independent of the downwind distance from a zone of no sand transport (Shao and Raupach, 1992). Instantaneous sand transport equations are usually applicable to the equilibrium situation that exists beyond the downwind distance. As previously mentioned, Bauer and Davidson-Arnott (2002) presented a theoretical framework to determine sediment supply to the foredunes which considers geometric tradeoffs between the wind angle approach (cosine effect), beach width and the fetch effect (see section 3.2.2.B). Due to the foredune-beach geometry, wind loses its effectiveness to input sand to the foredune when the wind becomes more oblique as a function of the cosine of the wind angle (i.e. cosine effect) (Davidson-Arnott and Dawson, 2001), so that wind directions 340° and 160° were considered unable to transport sand from the beach to the dunes. The relationship

between angle of wind approach and beach width determines the available fetch distance between the swash limit on the beach and the vegetated foredune.

In this study, all the model approaches incorporate wind speed and grain size. Grain size is taken to be the D_{50} of sand sampled from the foredune unit collected at the end of each season (see section 2.3) which was assumed to be representative of the sand transported during the preceding season. Four approaches based on Bagnold's sediment transport equation (Eq 5.2) were derived to predict the total sand transport rate across a fixed foredune segment (Figure 5.1). The models Q_{T1} and Q_{T2} take account of the wind direction classes; the latter excludes direct alongshore winds (i.e. shore parallel to the foredune) because there is no sand input to the foredunes. As in Q_{T1}, the model Q_{T3} also considers all the wind direction classes, however it excludes effective transporting winds that occur when the whole beach is inundated. The model Q_{T4} is similar to Q_{T3}, except that direct alongshore transporting winds are excluded. The boundaries of the models are therefore the inundation of the beach and direct alongshore winds.
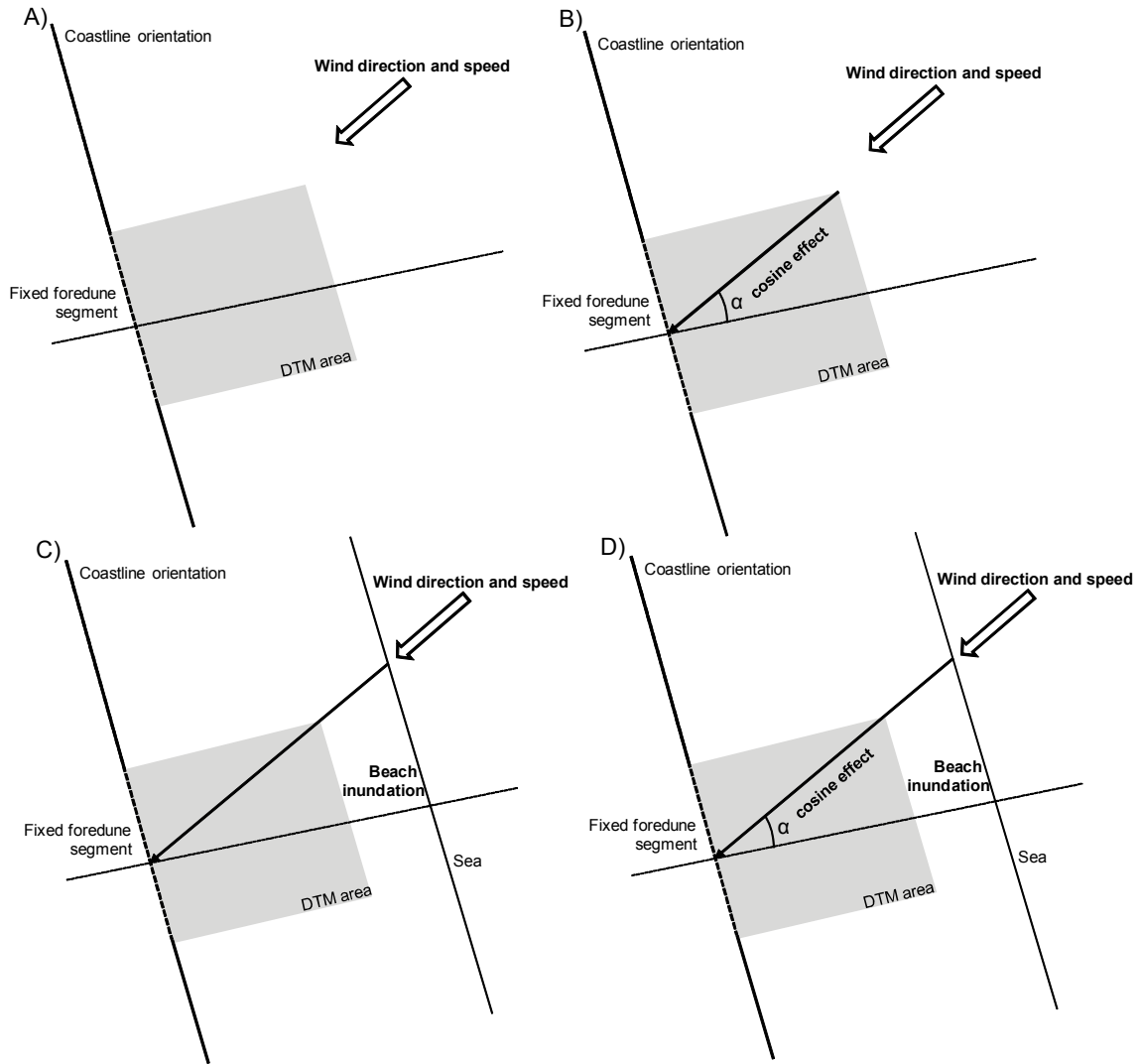
Figure 5.1. Conceptualization of foredune sand supply rate approaches: (A) Q_{T1}, (B) Q_{T2}, (C) Q_{T3} and (D) Q_{T4}.

For all four models, mean hourly wind records at Donna Nook were grouped into velocity classes above the threshold of sand transport (8 m s^{-1}): 8.0-10.7 m s^{-1}; 10.8-13.8 m s^{-1}; 13.9-28.4 m s^{-1} and divided into 36 sector directions which centred on 10° intervals (e.g. 10°, 20°). The frequency distribution of the wind speed-direction component was calculated for each interval and class over each seasonal period, corresponding to the elapsed time between the seasonal field experiments. In the third and fourth models, it was assumed that foredune sand supply cannot occur when the sea covers the upper beach. Adjusted water level records along the study area, measured every 15-minutes at Immingham adjusted at Skegness (refer section 2.4.3.), were processed in order to find intervals with low and high water level that affect the beach dimensions. A water level of 3.21 m (MHWS) was considered to be the height at which no sand transport from beach to foredune could occur because the whole beach

was inundated. Hence, all potential sand supply events were extracted for times when the water level was lower than MHWS contour level. These conditions were assumed to represent an effective fetch distance for the supply of blown sand to the foredune, if steady-state sand transport conditions are achieved. For the S3-S4 period, the observed water level data was missing from 12th May to 31st May 2010, and as a substitute, the astronomical water level at Skegness was used. Table 5.1 shows the impact of excluding different categories of ineffective winds. As a comparison, wind data used in the Q_{T1} approach are shown in Figure 4.2, and the effective winds under Q_{T4} are presented in Figure 5.2.

Table 5.1. The impact on the frequency of effective and ineffective winds of different model approaches where Q_{T1} includes all winds, Q_{T2} excludes alongshore winds, Q_{T3} excludes winds occurring when water level ≥MHWS and Q_{T4} excludes alongshore winds and winds occurring when water level ≥MHWS.

Period		Frequency of effective winds (%)			Frequency of ineffective winds (%)
	Model	Onshore	Offshore	Alongshore	
S1-S2	Q_{T1}	14.36	12.59	5.39	67.66
	Q_{T2}	14.36	12.59	4.29	68.76
	Q_{T3}	13.93	12.45	5.13	68.49
	Q_{T4}	13.93	12.45	4.15	69.47
S2-S3	Q_{T1}	9.64	7.45	3.02	79.89
	Q_{T2}	9.64	7.45	2.29	80.62
	Q_{T3}	9.43	7.25	2.97	80.35
	Q_{T4}	9.43	7.25	2.34	80.98
S3-S4	Q_{T1}	10.13	2.52	6.04	81.31
	Q_{T2}	10.13	2.52	3.97	83.38
	Q_{T3}	9.35	1.73	5.24	83.68
	Q_{T4}	9.35	1.73	3.46	85.46
S4-S5	Q_{T1}	7.32	7.52	5.93	79.23
	Q_{T2}	7.32	7.52	4.35	80.81
	Q_{T3}	6.80	7.49	5.89	81.41
	Q_{T4}	6.80	7.49	4.30	85.71

Figure 5.2 also shows that the effective winds were the most frequent over the S1-S2 period (autumn). The greatest frequency of high onshore and offshore wind speed (≥13.9 m s^{-1}) occurred in S1-S2 for 3.17% and 1.77% and in S4-S5 for 0.71% and 0.52% respectively.

A) S1-S2
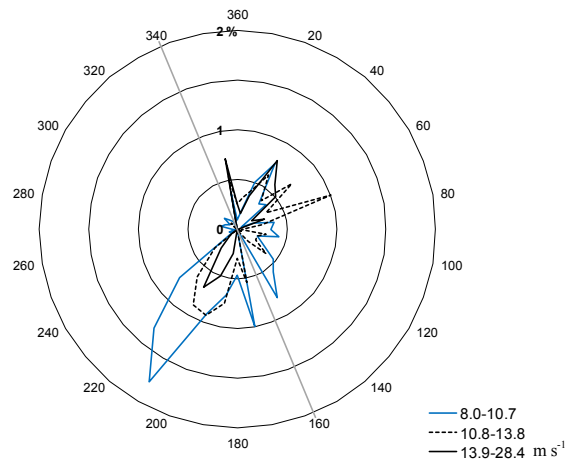
B) S2-S3
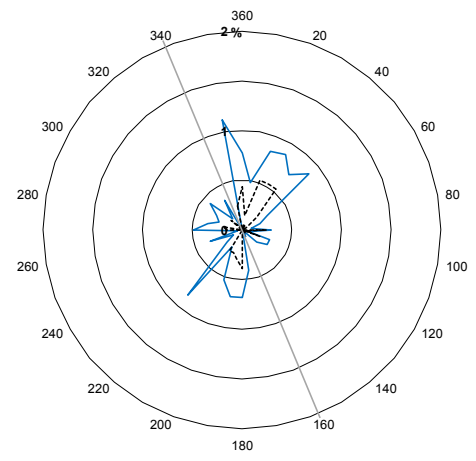
C) S3-S4
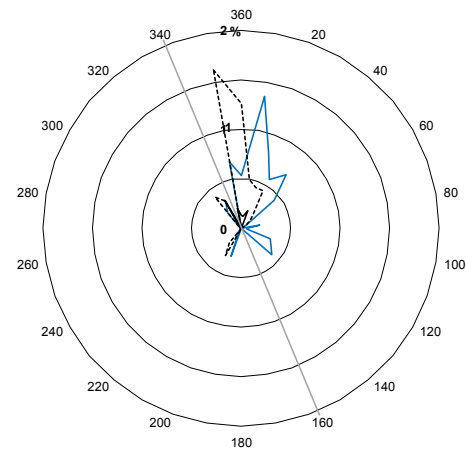
D) S4-S5
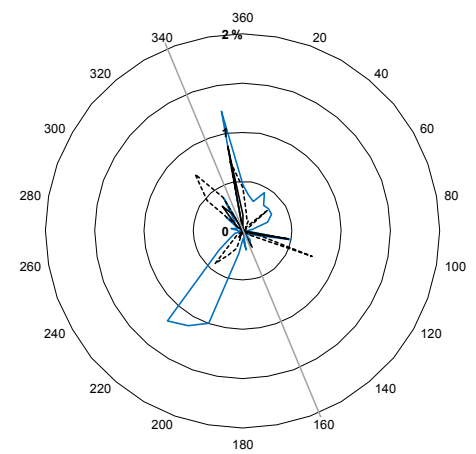
Figure 5.2. Seasonal wind roses of effective winds under Q_{T4} approach. Grey line indicates the coastline orientation. To compare with Q_{T1} data see Figure 4.2.

5.3.3. Prediction of the Potential Foredune Sand Supply

One of the key elements of the potential sand transport equation is the threshold shear velocity of cohesionless sediment on a horizontal surface (U_{*t}) given by Bagnold's equation (1941) (see Eq 3.2). In this study, the threshold velocity was estimated before the start of the saltation transport process (fluid threshold) using the Karman-Prandtl equation (Eq 3.3 with Z is equal to 8 m). In general, studies have used the fluid threshold shear velocity to filter sand transport events (e.g. Pye and Tsoar, 1990, Vespremeanu-Stroe and Preoteasa, 2007, Navarro et al., 2011). However, it is recognized that this would underestimate the calculation of the potential amount of sand supply, so it should be considered as potential minimum value. The fluid threshold shear velocity for Z_0, for roughness length of 1/30th of the D_{50} grain size collected from the foredune unit at the three sites during field surveys, is 0.235 m s^{-1}, corresponding to a wind velocity of 7.884 m s^{-1} at Donna Nook station (8 m high). For model calculations this was adjusted to 8 m s^{-1} in order to facilitate analysis. This threshold was used to filter wind time series and thus extract potential sand transport periods. After determining the threshold velocity, the next step applied for each approach was to estimate the potential aeolian sand transport rate (q) for each wind speed and direction classes according to the equilibrium equation derived by Bagnold (1941):

$$q = C \sqrt{\frac{d}{D}} \left(\frac{\rho}{g}\right) u_*^3$$

Eq. 5.2

Where q is the instantaneous sand transport rate (kg m^{-1} s^{-1}); C is the Bagnold's semi-empirical dimensionless coefficient (1.8 for naturally well-sorted sands); d is the D_{50} grain diameter (μm); D is the reference grain diameter of 250 μm used for the wind tunnel experiment; ρ is the air density (1.22 kg m^{-3}); g is the gravitational acceleration (9.81 m s^{-2}); u_* is the shear velocity (m s^{-1}).

Shear velocity was given by re-arranging the law of the wall, eq. 3.3:

$$u_* = \frac{U_{DN} \times K}{\ln\left(\frac{Z_{DN}}{Z_0}\right)}$$

Where U_{DN} is the wind speed recorded at Donna Nook at height Z_{DN} of 8 m; K is von Karman's constant (0.41).

From the wind frequency distribution, sand transport rate was determined for each 10° direction based on equation (5.2), in which shear velocity u_* was computed by using the actual mean wind velocity for each sector (U_{DN}) (Pearce, 2005). To incorporate wind records (hour) and water level records (15-minutes) into the same equation, it was necessary to convert to a common time period, so that all the measurements of potential sand transport (q in kg m^{-1} s^{-1}) were in seconds. Application of the wind frequency distribution yields the total sand supply Q_b per wind sector in m^3 m^{-1} by summation of all calculated transport rates q:

$$Q_b = \frac{1}{\rho_s} \sum_{i=1}^{n_b} q$$

Eq. 5.3

Where n_b is the total number of seconds for wind sector (b) and ρ_s is the density of sand assumed to be 2650 kg m^{-3}.

In order to predict the potential of wind to deliver sand towards the fixed foredune segment, Q_b was modified by the angle of wind direction for Q_{T2} and Q_{T4}. Total potential sand transport can then be calculated by summation of the contribution of all wind direction sectors.

$$Q_T = \sum_{b=1}^{36} Q_b \times \cos(\alpha)$$

Eq. 5.4

Where Q_T is the total sand deposition per metre length of the foredune (m^3 m^{-1}), α is the angle of wind direction relative to shore perpendicular (alongshore winds strictly parallel to the coastline, 340° and 160°, are equal to zero).

The proportion of the sand supply from each wind sector contributing to the total foredune inputs was multiplied by the length of the foredune segment exposed, which corresponds to 100 m at both Brickyard Lane (BL) and Theddlethorpe St Helens (TSH) sites; and 98 m at Mablethorpe North End (MNE). For a realistic model of sand input into the foredune, all amounts of sand transported by effective winds have to be estimated. Potential net sand input into the foredune was calculated by summing the contribution of all wind sectors for onshore (Qonsh: 0°- <150°), offshore (Qoffsh: 180°-<330°) and alongshore (Qalongsh: 150°-170°; 330°-350°) wind components.

5.3.4. Estimation of Resultant Sand Drift and Direction Potentials

The four models calculate the maximum amount of sand supply to the foredune from all wind components. However, it is worth determining the resultant wind direction (i.e. net direction in which the sand would be transported by winds from each direction) and also how much sand material moves along the resultant wind direction. These were achieved by using Fryberger and Dean's method (1979). It standardizes wind data to estimate regional aeolian sand drift potential by summing the contribution of sand supply for each wind speed-direction sector. For this study, drift potential was calculated only for the Q_{T4} model because this includes the greatest number of controlling factors. Through vector analysis, the resultant drift potential (RDP in m^3) and the resultant drift direction (RDD orientated to true North) were calculated. The RDP represents the net sand supply from the RDD, thus corresponding to the minimum sand input to the foredune. Additionally, the ratio of RDP/Q_{T4}, an index of the variability of the wind direction defined by Fryberger and Dean (1979), was estimated. An increase in the directional variability of wind will result in a reduction of the RDP/Q_{T4} ratio. For the Q_{T4} model, wind magnitude and directional variability were calculated and compared at the three sites over the seasonal periods.

5.3.5. Comparison of Potential and Measured Sand Supply into the Foredune-Upper Beach Units

Measurements of the actual sand foredune and upper beach volume change can be used to evaluate the four modelling approaches. At each study site, the change in the total volume of sand in the foredunes from season to season was measured using the seasonal DTMs (Chapter 4). This reflects the net change in sand volume during the time period (as no intermediate surveys were conducted). Potential sand supplies into the foredune were compared to the measured sand volume change at the three study sites over the seasonal periods. As only input to the foredune-upper beach is estimated using the models, the DTMs are defined by the landward boundary, c. 10 m inland from the primary foredune toe, and a seaward boundary at z=3.4 m. It is assumed that under non-storm conditions this limit will not be inundated. The seaward boundary is situated higher than the MHWS reference used to extract potential sand transport events. This is because it is expected that a high moisture content due to wave set-up and sea spray will prevent sand transport. These landward and seaward boundaries delimit the established foredune and upper beach zone.

171

5.4. Results

5.4.1. Predicted Seasonal Sand Supply

A. Comparison and assessment of the approaches

The results of predicted sand supply in the foredune-upper beach corresponding to the sum of sand transport rates from onshore, offshore and alongshore winds are given in m^3 for each approach, to enable comparison with the sand volume changes derived from the DTMs over the seasons. The errors of the predicted sand supply approaches were assessed using RMSE which is commonly used as a good indicator of accuracy (Ebdon, 1977). It determines how close the model predicted values are to the actual data. The RMSE was given by:

$$RMSE = \sqrt{\frac{\sum_{i=1}^{n}(A - B)^2}{n}}$$

Where A is the predicted sand supply from the four approaches and B is the actual sand volumes changes derived from DTMs, and divided by the number of seasonal surveys (n).

RMSE was calculated from the squared difference between Hence, the RMSE measures the average magnitude of the error; for which lower values indicate better fit of the model.

A.1. Brickyard Lane (BL)

Table 5.2 presents the predicted sand supply at the BL site obtained for each approach associated with their RMSEs over the seasonal monitoring periods.

Table 5.2. Measured sand volume changes and predicted sand supply to the foredune for the four approaches and RMSE results at BL site. The overall best model is in bold.

Period	Measured sand volume change (m^3)	Predicted sand supply (m^3)			
	DTM	Q_{T1}	Q_{T2}	Q_{T3}	Q_{T4}
S1-S2	-51.12	1107.91	715.88	1013.12	**661.60**
S2-S3	191.08	339.95	211.98	330.52	**204.90**
S3-S4	138.96	345.45	130.71	290.19	**112.51**
S4-S5	259.08	585.11	280.41	576.17	**271.47**
RMSE		615.31	364.69	564.68	**356.72**

The highest RMSE residual was computed for Q_{T1} (615.31 m^3). In contrast, the lowest RMSE residual of 356.72 m^3 was obtained for Q_{T4}, suggesting that this provides the closest prediction of the measured sand volume changes. In S1-S2, the four approaches predicted a significant foredune sand supply whereas a sand loss was measured due to the occurrence of erosive storm surges. For S2-S3, S3-S4, and S4-S5 periods, the predicted sand transport supplies from the approach Q_{T4} correspond reasonably well to the observed sand volume changes (within ±10%). It slightly underestimated sand supply by 26.45 m^3 in S3-S4. However, the Q_{T4} predicted sand supply value was higher by 12.39 m^3 than the measured volume changes in the summer-autumn season (S4-S5).

A.2. *Theddlethorpe St Helens (TSH)*

At TSH site, the lowest RMSE residual of 628.90 m^3 was computed for the Q_{T4} approach (Table 5.3). In general, the Q_{T4} approach predicted a sand gain in the foredune-upper beach system while negative volume changes were measured in S1-S2, S3-S4, and S4-S5. A sand gain was measured in S3-S4 and the Q_{T4} approach did predict a positive sand supply, however the prediction is less than half that which was measured. For this period, the Q_{T3} approach gave the best prediction with a slight difference of 20.12 m^3. Overall models performed considerably worse for this site than at BL.

Table 5.3. Measured sand volume changes and predicted sand supply to the foredune for the four approaches and RMSE results at TSH site. The overall best model is in bold.

Period	Measured sand volume changes (m^3)	Predicted sand supply (m^3)			
	DTM	Q_{T1}	Q_{T2}	Q_{T3}	$\mathbf{Q_{T4}}$
S1-S2	-470	1071.04	692.07	979.41	**639.59**
S2-S3	-178.56	322.21	200.92	313.27	**194.20**
S3-S4	264.22	344.49	130.34	284.34	**112.19**
S4-S5	-160.03	591.64	283.53	582.60	**274.49**
RMSE		894.01	653.66	850.67	**628.90**

A.3. Mablethorpe North End (MNE)

The most accurate approach was obtained for Q_{T4} with a RMSE residual of 270.59 m^3 (Table 5.4), and this was also the lowest predicted error compared to the two other sites. Over the S1-S2 period, the Q_{T4} approach overestimated the measured sand gain by 45.53 m^3 (8%). A reduction in sand volume was measured from S2-S3, however the Q_{T4} approach predicted a gain in foredune sand volume of 190.28 m^3. Over the S3-S4 and S4-S5 periods, the best estimates are from the Q_{T3} approach, while Q_{T4} approach underestimated the sand supply up to 317.67 m^3.

Table 5.4. Measured sand volume changes and predicted sand supply to the foredune for the four approaches and RMSE results at MNE site. The overall best model is in bold.

Period	Measured sand volume changes (m^3)	Predicted sand supply (m^3)			
	DTM	Q_{T1}	Q_{T2}	Q_{T3}	Q_{T4}
S1-S2	567.81	1049.00	677.83	940.07	**613.91**
S2-S3	-227.08	320.71	199.98	306.55	**190.28**
S3-S4	235.32	338.43	128.05	283.42	**110.27**
S4-S5	582.96	583.48	279.62	563.07	**265.29**
RMSE		368.19	272.95	326.36	**270.59**

In general, the comparison and assessment between measured sand volume changes and the predicted sand supply to the foredune-upper beach system indicates that the Q_{T4} approach is the most reliable at the three sites. It was thus selected to conduct more detailed investigations at the seasonal scale.

B. Seasonal magnitude and frequency of sand transport using the Q_{T4} model

Based on the Q_{T4} model, Table 5.5 presents the seasonal predicted sand supply into the foredune-upper beach at the three sites from the different wind components at the three sites. For visualizing the pattern of wind components, seasonal sand roses are presented for BL which was similar to the other sites (Figure 5.3).

Table 5.5. Total and wind component of predicted sand input to the foredune (Q_{T4}) and Fryberger indices at the three sites. RDP=resultant drift potential, RDD=resultant drift direction and RDP/Q_{T4} is an index of the variability of the wind direction.

	Measured sand volume changes (m³)				All			Onshore			Offshore			Along S			Along N		
	BL	TSH	MNE		BL	TSH	MNE	BL	TSH	MNE	BL	TSH	MNE	BL	TSH	MNE	BL	TSH	MNE
S1-S2	-51.12	-470	567.81	Q_{T4}	661.60	639.59	613.91	390.69	377.69	362.52	249.39	241.1	231.41	8.53	8.25	7.92	12.99	12.55	12.05
				RDP	139.69	135.04	129.62												
				RDD		262			231			32			344			170	
				RDP/Q_{T4}		0.21			0.87			0.94			0.99			0.99	
S2-S3	191.08	-178.56	-227.08	Q_{T4}	204.90	194.21	190.28	119.49	113.25	111.32	79.88	75.71	73.85	0.98	0.92	0.90	4.55	4.32	4.21
				RDP	46.94	44.49	43.64												
				RDD		206			224			55			348			166	
				RDP/Q_{T4}		0.23			0.86			0.76			0.99			0.99	
S3-S4	138.96	264.22	235.32	Q_{T4}	112.51	112.19	110.27	84.25	84.02	81.0	15.23	15.19	14.63	0	0	0	13.02	12.98	12.51
				RDP	74.07	73.87	71.85												
				RDD		199			209			49			X			164	
				RDP/Q_{T4}		0.66			0.88			0.73			X			0.99	
S4-S5	259.08	-160.03	582.96	Q_{T4}	271.47	274.49	265.29	130.62	129.18	126.24	115.39	116.67	112.76	2.17	2.19	2.12	24.73	25.00	24.16
				RDP	24.08	24.36	23.54												
				RDD		236			251			60			336			165	
				RDP/Q_{T4}		0.09			0.78			0.69			0.99			0.99	

Assuming that all blown sand, regardless of wind direction, ends up in the foredune-upper beach unit, the maximum sand input (Q_{T4}), corresponding to the combination of onshore, offshore and alongshore supplies, ranged between 1.52 (S3-S4) and 11.3 (S4-S5) times the values of the RDP. During the 12-month monitoring period, the RDD varied between 199° and 262° (blowing onshore winds), suggesting that net sand transport is from the beach to the foredune (Figure 5.3).

Seasonal estimates of sand supplies were similar at the three sites. The greatest seasonal sand supply up to 661.6 m^3 was estimated over the S1-S2 period (autumn), when effective onshore winds blowing up to 13.93% of the time (Table 5.1) contributed a potential sand supply of 391 m^3 at BL and 363 m^3 at MNE (Table 5.5). Up to 250 m^3 and 22 m^3 of sand were supplied by offshore and alongshore winds respectively. Between S2-S3, the potential sand supply ranged from 204.9 m^3 at BL to 190.28 m^3 at MNE which was approximately one third that of the previous period. Although these periods were characterized by a similar wind directional variability of <0.25, the frequency of effective winds in S2-S3 was much lower than the previous season (Table 5.1). The lowest estimate of sand supply was over the S3-S4 period (spring-summer) when effective onshore winds blowing 9.35% of time were the main suppliers, while both offshore and alongshore winds contributed to <5.19% of total sand supply. This is reflected in the low wind directional variability (RDP/Q_{T4} of 0.66). During S4-S5, the main potential sand supply is from onshore and offshore winds blowing up to 6.80% and 7.49% of the time respectively. These wins each contributed a relatively similar amount of sand to the foredune-upper beach (>110 m^3), however more than 26 m^3 was also supplied by effective alongshore winds blowing 4.30% of time. This results in a high wind directional variability (RDP/Q_{T4} of 0.09) during the S4-S5 period.

A) S1-S2
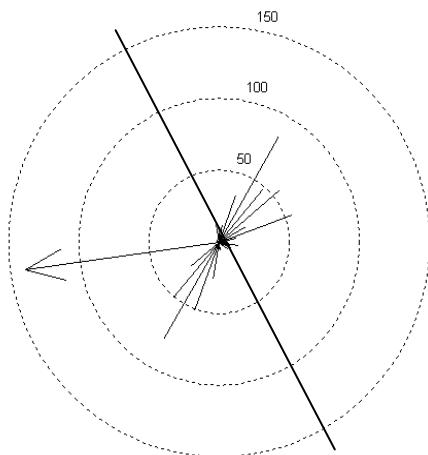
B) S2-S3
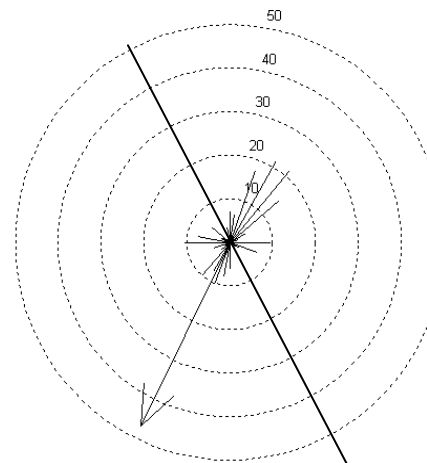
C) S3-S4
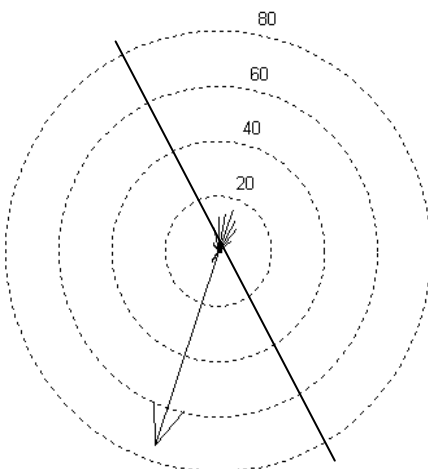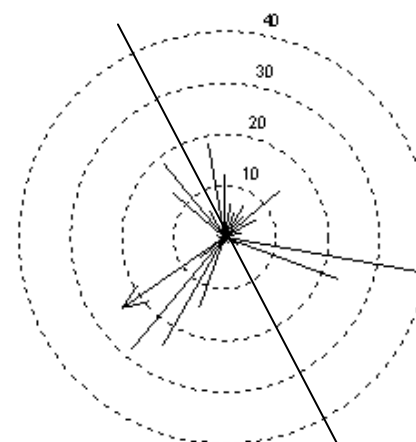
D) S4-S5

Figure 5.3. Seasonal sand roses based on the Q_{T4} at BL for (A) S1-S2, (B) S2-S3, (C) S3-S4 and (D) S4-S5. Sand roses show vectors of potential sand transport from 10°- directions and the resultant drift potential towards the direction of movement (arrow). Black line corresponds to the foredune orientation.

5.5. Discussion

The purpose of this chapter was to develop a model that enables the prediction of sand supply into the foredune-upper beach system from season to season. The occurrence and magnitude of sand transport events over seasonal scales were also investigated.

5.5.1. Modelling Sand Supply to the Foredune

In general, the sand supply simulated using the four modelling approaches is overestimated compared to the actual foredune-upper beach sand budget. Such overestimation is common where predictions based on meteorological data are compared with measured changes (e.g. Sarre, 1989, Davidson-Arnott and Law, 1990, Arens, 1997, Van der Wal, 2000, Delgado-Fernandez, 2011). Typically, the overestimation occurs because variables that limit sediment transport such as moisture content are not accounted for or are poorly parameterized.

In the models, the shear velocity was estimated before the start of saltation process. However this would be more likely to underestimate the calculation of the potential amount of sand supply, compared to applying the impact threshold velocity after sand entrainment. The calculation of the shear velocity could have been improved by parameterizing the fluid shear velocity adjusted for each seasonal foredune grain size at the three sites. Also the roughness length (Z_0), controlling the shear velocity, was considered to be only influenced by the grain size although the vegetation over the foredunes is more likely to increase it. The fetch distance controlled by the beach inundation was considered to exceed the critical fetch distance. This may overestimate the amount of sand supply, but this assumption is reasonable given that the fetch length generally exceeds 50 m. The modelling approach assumes that the amount of sand transported is equal for all wind directions, however the vegetation is likely to reduce it during offshore winds. In general, it is difficult to know the precise impacts of each assumption that was made; some of the assumptions reinforce one another whereas others will balance each other out.

Results have shown that the Q_{T1} model considering only the wind regime (speed and direction) and grain size was the least accurate. In addition to the wind regime, the Q_{T2} model further incorporating the angle of wind approach (cosine effect) gives better estimates than the Q_{T3} model which only considers wind speed and the beach inundation. This suggests that the directed wind angle is more important than water

inundation. Unsurprisingly, the best model is the one that incorporates the greatest number of factors, the Q_{T4} model – wind speed, wind direction, grain size, beach inundation and cosine effect. The modelling results thus illustrate the fact that sand input to the foredune cannot be satisfactorily modelled if only the frequency and magnitude of sand transport wind events are considered. This study agrees with other coastal studies (e.g. Sarre, 1989, Nordstrom and Jackson, 1992, Davidson-Arnott and Law, 1996, Delgado-Fernandez, 2011) which underlined the importance of filtering wind events that do not result in sand transport due to beach inundation. Finally, the results have underlined that all onshore, offshore and alongshore effective winds must be considered to calculate sand supply to the foredune-upper beach system.

5.5.2. Wind Regime and Potential Sand Transport

Measured sand budget reflects net onshore/offshore sand inputs so to assess the models it is necessary to understand the balance between onshore and offshore winds. Seasonal variability of wind regime was observed over 1-year, when onshore effective winds prevailed but also associated with offshore sand transporting winds and less often alongshore winds. Autumn (surveys S1-S2) was the most energetic period for sand transport to the foredune-upper beach.

In general, the seasonal measured sand volume changes at BL and MNE are well predicted by the Q_{T4} model summing onshore, offshore and alongshore sand supply (Table 5.5). It thus suggests that these wind components are complementary in foredune development. Based on the Fryberger and Dean (1979) method, wind regimes can be classified as 'unimodal' when either the onshore or offshore component is the dominant wind resultant (the ratio of the sand supply (Q_{T4}) of these two components is >8) and 'bimodal' when the ratio is <8. Wind regime is classified as 'equal bimodal' when onshore and offshore are nearly equal characterized by a ratio between 1:1 and 3:2 (Wal and McManus, 1993). In this study, the seasonal wind regimes in autumn (S1-S2) was classified as low 'equal bimodal' with a ratio (Q_{T4}) between onshore and offshore components of 8:5 and high resultant predicted sand supply ranging from 614 m^3 at MNE to 662 m^3 at BL. While a strict 'equal bimodal' wind regime characterized both the S2-S3, S4-S5 periods with a ratio of 3:2 and 11:10 respectively. For this latter period, high magnitude and frequent alongshore winds occurred resulting in an increase of directional variability (RDP/Q_{T4} of 0.09). For S3-S4, wind regime was classified as weak 'bimodal' (ratio of 17:3). Overall, the seasonal resultant drift direction (RDD) was directed to 260° (W) or 200° (SSW) resulting in onshore sand transport.

Figure 5.4 compares the seasonal predicted sand supply to the foredune-upper beach system derived from the Q_{T4} model and the measured sand budget at the three sites. Predicted and measured contribution of the foredune-upper beach to budget mobility is also presented. At BL, the annual net predicted sand supply was 1277.37 m^3, while the measured net foredune volume changes over the whole year were around half this value (Figure 5.4A). However, the model estimated reasonably well the observed changes in sand volumes for the S2-S3, S3-S4, and S4-S5 periods. The pattern of the seasonal contribution was similar between the predicted and measured budget changes within the foredune-upper beach at BL from S2 to S5. The annual measured and predicted sand supply into the foredune-upper beach at TSH (Figure 5.4B). This is probably due to the complex morphology of the foredune-beach system characterized by the presence of the embryo dunes on the upper beach which makes it difficult to predict sand input to the foredune. As demonstrated in Chapter 3, the embryo dunes affect sand transport processes by disturbing the near-surface airflow and also by segmenting the fetch distance. It could thus be expected that a fully onshore saturated transport system is likely to cease upon reaching the seaward embryo dunes, and no or little transport takes place on the landward side of the embryo dunes. Under offshore winds, sand is likely to be deposited in the embryo dune field. Because of marine erosion, Christiansen and Davidson-Arnott (2004) stated that the sand stored in embryo dunes may not be supplied to the foredune. At MNE, the model was a good predictor of the annual sand volume changes with a slight overestimation of 20.74 m^3 (Figure 5.6C). The pattern of predicted and measured seasonal contributions was similar over the whole monitoring period. However, a positive sand volume change of 190.28 m^3 was predicted in the foredune-upper beach system between S2-S3 period. This contrasts with a measured sand loss of about the same order of magnitude (-227.08 m^3) due to the occurrence of an erosive storm surge on 28th February (see section 4.3.2).
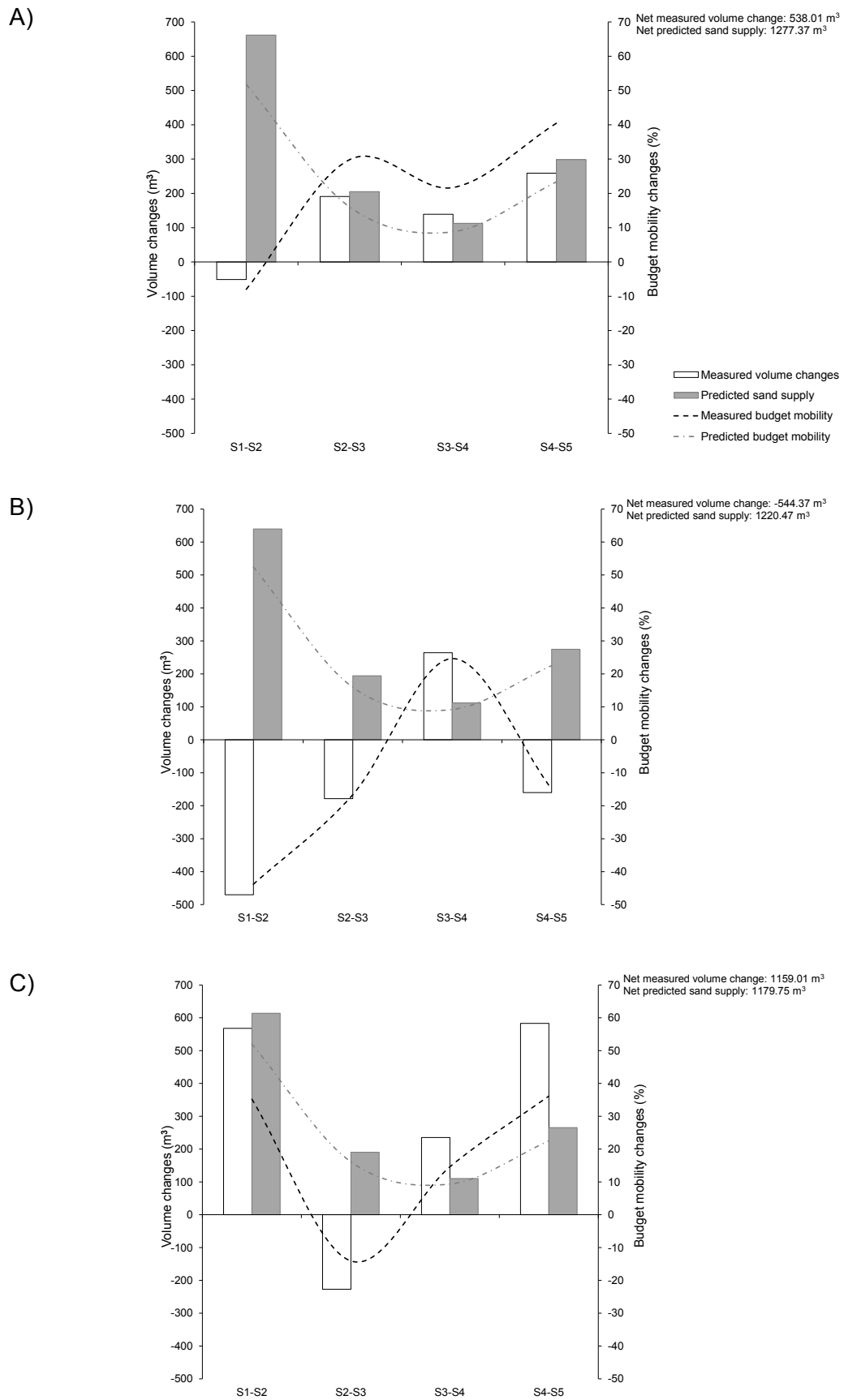
Figure 5.4. Predicted sand supply and measured volume changes of the foredune-upper beach system at: (A) BL, (B) TSH and (C) MNE. The lines are predicted and measured seasonal percentage contribution to the cumulative budget change (100%).

5.5.3. Model Advantages and Suggestions for Refinements at the Seasonal Scale

The developed model simplifies the picture of the complexities of micro-scale aeolian sand transport processes over the foredune. Recently, Delgado-Fernandez (2011) states that an accurate prediction of sand supply to the foredune at the meso-scale cannot be achieved by refinements of each supply-limiting factor, and thus the complex micro-scale sand processes could be reasonably neglected within the foredune-beach system. In the present study, the Q_{T4} model would not give an absolute accurate prediction of aeolian sand supply into the foredune, however it provides an order-of-magnitude estimate which probably mimics the reality of sand supply during periods with no storm surge activity. The model does not take account of the storm surge events which are more likely to remove sand from the foredune- upper beach. Although storm surge events are characterized by higher wind velocities, they often have low probabilities of resulting in sand transport towards the foredune. This is because of the beach width reduction (i.e. beach inundation) caused by wave processes such as storm surge height, wave set-up and run-up during strong onshore winds (Davidson-Arnott and Law, 1990, Delgado-Fernandez and Davidson-Arnott, 2011).

Furthermore, results of the Q_{T4} model suggest several areas for which its performance could be further improved. First, the total of sand transport rate can be better estimated by calculating the beach width resulting from changes in water level for 15-minute records (i.e. frequency of water level measurements). Previously, Davidson-Arnott and Law (1996) reported that successful modelling of sediment supply into the foredune would require explicit inclusion of beach width into predictive models, which in turn necessitates the collection of records on temporal variations in beach width. Then the interactions between beach width, fetch effect and angle of wind approach would be refined, leading to an accurate estimation of the tradeoffs that govern the amount of transported sand into the foredune. Local rainfall should be also considered in the model by filtering sand transport events during precipitation. Second, additional parameters such as spatial distribution of surface moisture content, local topography (slope angle, micro-topography features), and vegetation parameter within the foredune-beach system were not included. As previously mentioned, these controlling factors influence the velocity threshold for sand transport which can be highly dynamic and variable (Wiggs et al., 2004a) so that sand entrainment usually involve the combination of more than one threshold (Davidson-Arnott and Bauer, 2009). It would require to refine a wind threshold for given surface moisture, grain sand size and wind speed conditions which can be used to predict sand transport. Additionally, the omission of the vegetation factor can be a drawback in the applicability of the model,

because vegetated foredunes have strong sediment trapping abilities (Lynch et al., 2008). Therefore, any wind vector component crossing the foredune line might result in the sediment being trapped and deposited in the vegetated foredune. The modelling approach assumes that the amount of sand transported is equal for all directions whether from flat, unvegated beach or from foredunes where the vegetation cover is 100% and tall. Chapter 3 showed that a small quantity of sand transport takes place from the foredunes where vegetation is present. During offshore winds, the vegetation on the dunes would reduce the availability of sediment and also fetch distance, which suggests that offshore sand supply would be lower than for onshore winds of the same magnitude. Given this, it is surprising that seasonal sand supply estimates are as good as they are. This is probably because the net sand transport is onshore (RDP).

A fully accurate model needs to incorporate every factor at the meso-scale, however this is difficult due to the temporal variability of occurrence (e.g. turbulence <1s, tidal cycle-hours). The Q_{T4} model is a relative good indicator at the seasonal scale. The next challenge is to see whether it can be used over longer periods. Chapter 6 presents the measured foredune-beach morphology at the meso-scale. Q_{T4} is tested at this scale in Chapter 8.

5.6. Conclusion

- Over the 1-year monitoring period, wind regime (both speed and direction) was seasonally variable. All the seasonal wind regimes were classified as 'equal bimodal' with the exception of 'weak bimodal' in S3-S4. Strong wind speed conditions characterize autumn season (S1-S2, S4-S5) when the greatest rate of potential sand supply to the foredune-upper beach.

- Onshore sand transporting winds prevailed over the seasonal periods, resulting in a net sand transport directed from the beach to the foredune. Nevertheless, effective onshore, offshore and alongshore winds must be considered to estimate potential sand supply into the foredunes.

- The modelling approaches predict the amount of sand transport into the foredune, based first on wind regime (speed and direction) and grain size, and can be enhanced by incorporating beach inundation and angle of wind approach controlling fetch effect. These are explicitly acknowledged by the effectiveness of the modelling Q_{T4} approach in determining the amount of sand transport within the foredune-upper beach system from seasonal to 1-year periods. However, the application of the model appears to be limited for complex coastal environment such as TSH site.

- The model provides an explicit link between the micro-scale processes and the meso-scale foredune morphological responses without modelling detailed micro-scale airflow and transport processes occurring in the foredune-beach system.

Chapter 6. Meso-scale Foredune Development and Interactions with Beach

6.1. Introduction

Having considered foredune development with relationship to controlling and forcing factors in the previous chapters, Chapter 6 focuses on the meso-scale (from season to two decades) dynamics and evolution of the foredune-beach system.

Controls of short-term foredune development, particularly in response to short-term events, are reasonably well-understood (e.g. Van de Graaf, 1986, 1994, Ruz and Meur-Férec, 2004, Anthony et al., 2006, Houser et al., 2008). However, less attention has been given to the relative importance of controlling factors of foredune development at the meso-scale. Sherman and Bauer (1993) report that the scale dependency is particularly critical over longer timescales because the coastal dunes under investigation may be unrepresentative of the instantaneous measured sediment budget. Systems with similar mean process conditions can have considerable morphological differences due to variation in the ranges of values reached in the process states (Sherman and Bauer, 1993).

At the meso-scale, variations in the magnitude, frequency and duration of storm surges, wind and wave climate, changes in nearshore sediment budget, bathymetry, sea level and human activities are the main controls on foredune morphology and evolution (Psuty, 1988, Anthony, 2000). Storm surge may dramatically erode and cause retreat of the foredunes, because storm surges raise the level of wave attack at the coast; higher water levels enable waves of a given height to shoal and penetrate farther landward. High energy near-bed currents and shear stresses also occur, the effects of which can generate high sediment transport rates and rapid morphological change (Forbes et al., 2004). Greater morphological change can occur as a result of a single, significant storm event than over many years of non-storm conditions (Morton et al., 1995). As discussed in Chapter 4 depending on the magnitude, frequency and return period of the storm, the level of foredune disturbance can have a significant effect on the nature and rate of subsequent foredune recovery (Saunderson and Davidson-Arnott, 1991). Meso-scale changes from decadal to multi-decadal timescales may

determine foredune-beach trend (i.e. accretion or erosion) (Orford et al., 1999), and are therefore important for coastal management.

Pye (1990) considered the main non-storm phase controls on meso-scale coastal dune development and proposed a model which relates coastal dune morphology to foredune-beach sediment budgets controlled by the wind regime/energy and shoreline dynamics. The model also incorporates vegetation characteristics and human disturbance impacts (Figure 6.1).

	Plan View	Beach Sand Budget	Wind Energy	Vegetation
(a) Beach ridge plain — t4 t3 t2 t1	Beach ridge crests — t4 t3 t2 t1 Shoreline position	Positive	Low	Effective sand trapping
(b) Parallel foredune ridges — t4 t3 t2 t1	Foredune ridge crests — t4 t3 t2 t1	Positive	Higher	Effective trapping
(c) Irregular 'hummock' dunes — t4 t3 t2 t1	Irregular assemblage of 'sandhills' with blowouts and incipient parabolic dunes — t4 t3 t2 t1	Positive	Moderate	Uneffective
(d) — t3 t4 t2 t1	Shoreline — High foredune ridge crest — t1 t2 t3	Steady state supply to beach balanced by transfer to dune	Moderate	Effective
(e) Slow beach recession — Slowly migrating parabolic dunes — t1 t2	Shoreline — Parabolic dunes — Blowout — t1 t2	Slightly negative	Moderate	Effective but damaged by beach recession
(f) Rapid beach recession — Wave eroded cliff — Low relief transgressive sand sheet — t1 t2	Shoreline — Transgressive sandsheet — t1 t2	Negative	High	Effective but damaged by beach recession

Figure 6.1. The effect of shoreline dynamics, wind energy, and sand trapping vegetation and resultant different medium to long-term changes (from time 1 to time 4) on coastal dune morphology (Pye, 1990).

High foredune ridges can be expected to develop where the sediment budget of the beach and foredune are in balance, and the position of the shoreline remains constant. An increase of vegetation cover traps more sand and thus a single vertically accreting foredune ridge is formed (Hesp, 1988). In a setting with a positive beach sand budget, moderate wind regime and inefficient vegetation cover, hummock dunes may develop. While under high wind energy conditions, a coastline subject to net erosion may be

characterized by unstable transgressive dune sheets and blowout development (Pye, 1990, Gares, 1992, Hesp, 2002). Wave erosion processes can also initiate blowouts, but more often cause foredune undercutting, which may lead to destabilisation of the foredune scarp slope (Carter et al., 1990). Alongshore foredune morphology can be characterized by rhythmic spatial variations associated with wave processes and foredune sediment supply.

Currently, little is known about foredune behaviour and dynamics over the decadal time span, and the few studies that exist mainly present conceptual insight rather than quantitative information on morphologic variability (Psuty, 1988, Sherman and Bauer, 1993, Arens and Wiersma, 1994). The aim of this chapter is to determine the intra- and inter-annual changes of the foredune-beach system and its evolutionary tendency at the meso-scale (over the last two decades). In parallel, the relative importance of different external factors in driving those changes is investigated. Specifically, the objectives are to:

(1) Analyse topographic data for the foredune-beach system from different periods in time to determine inter- and intra-annual morphological changes;

(2) Determine the relative importance of meso-scale versus seasonal variability in morphology;

(3) Explore the relative importance of different external forcing factors in driving the observed changes with an emphasis on dune response to storm surges.

6.2. Temporal and Geo-Spatial Methodology

The principal approach to characterize and quantify foredune-beach system evolution at the meso-scale, and which is adopted here, is to repeatedly examine its morphology through time in order to develop a picture of the changes that have occurred (Andrews et al., 2002). Three complementary data sources were used:

1) Topographic surveys of cross-shore beach profile (two-dimensional) carried out regularly by the UK Environment Agency (EA);

2) Aerial photographs, to evaluate the alongshore spatial variability (two-dimensional) and produce three-dimensional topographic data;

3) LIDAR data to investigate the three-dimensional changes of the foredune-beach system, and from which were extracted two-dimensional topographic profiles.

In contrast to Chapters 3, 4, 5, and in keeping with the increase in spatial scale of the units, the data relate to a continuous length of coastline (coordinates from 548960, 388655 to 549870, 387320 that incorporates the three discrete study sites – Brickyard Lane (BL), Theddlethorpe St Helens (TSH), and Mablethorpe North End (MNE) (Figure 6.2).
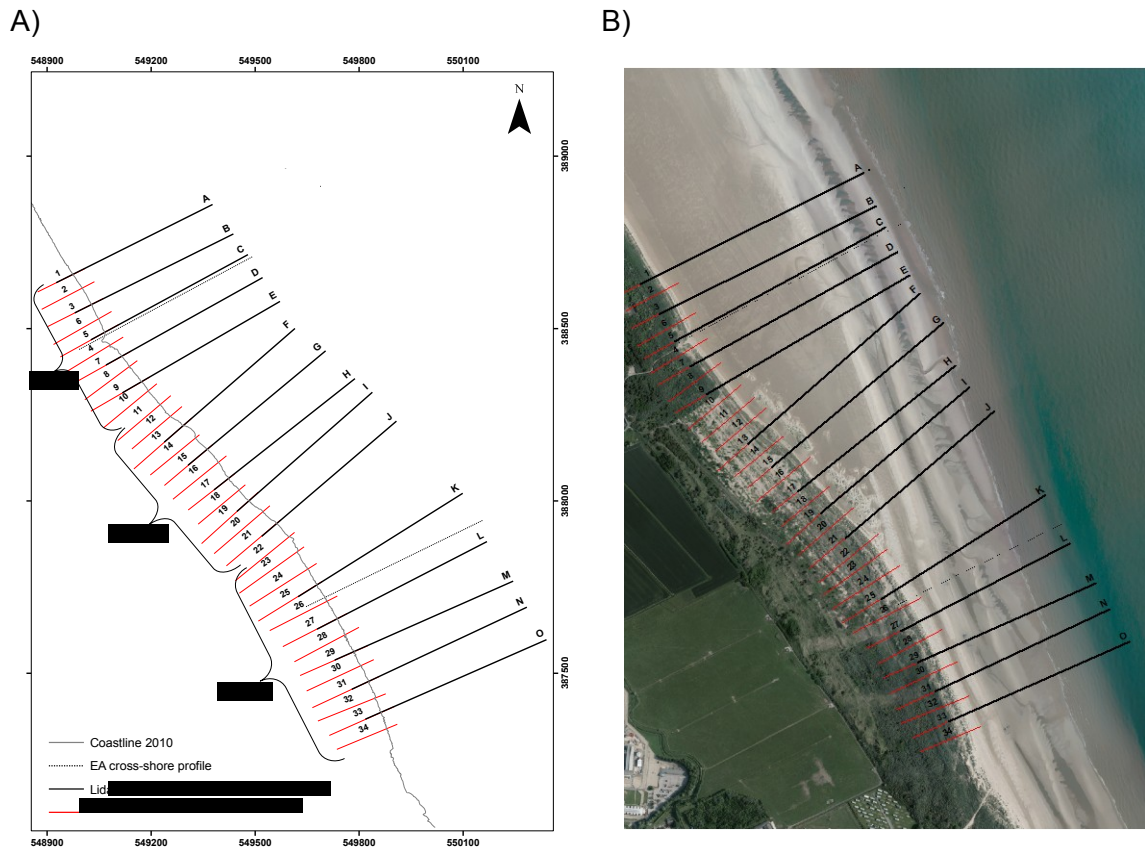
Figure 6.2. (A) Map to show the position and orientation of transects and cross-shore profiles from three data sources with relation to the three study sites, (B) data position superimposed on the 2007 ortho-photograph.

As in Chapter 4, the dynamics and variability of the foredune-beach system were investigated by undertaking morphological measurements (Table 6.1) defined as key indicators (Saye et al., 2005). These objective indicators were determined using the tidal reference and topographic contour levels (Chapter 2 section 2.4). In this Chapter, the foredune unit corresponds to both secondary and primary foredunes delimited by the same seaward boundary presented in Table 4.2. The same boundaries were used for the upper-beach unit, while the lower beach extends from MHWS to the ODN contours. The volume changes of the intertidal zone, covering the upper ridge-runnel system, was also investigated.

Table 6.1. Definitions of indicators to characterize foredune-beach morphologic profile.

Indicator	Definition
Foredune height (m)	Elevation of the secondary foredune crest
Foredune slope-toe position	Contact of the steep foredune face with the gentle upper beach slope
Position of z=3.5 m	Horizontal distance of the z=3.5 m contour from the benchmark, assumed to represent the foredune width
Upper beach width (m)	Horizontal distance from z=3.5 m to MHWS contour
Lower beach width (m)	Horizontal distance between MHWS and ODN contours
Foredune volume ($m^3 m^{-1}$)	Sand volume between benchmark and z=3.5 m contour
Upper beach volume ($m^3 m^{-1}$)	Sand volume between z=3.5 m and MHWS contours
Lower beach volume ($m^3 m^{-1}$)	Sand volume between MHWS and ODN contours
Volume of intertidal beach zone ($m^3 m^{-1}$)	Sand volume between ODN and z=-1 m contours

The Pettitt test presented in Chapter 2 was also applied to the EA summer topographic beach profiles in 1992, 1994, 1997, 2001, 2007, 2009 and 2010, corresponding to the selected aerial photograph years further analysed in this chapter. Only the summer survey profile was used to prevent morphological changes caused by winter storms biasing results. Although the cross-shore distance varied depending on the tidal conditions during the survey, the mean distance between 1992-2010 was used for the Pettitt test.

The results show a general good agreement between the average of the thresholds of the unit boundaries identified for the summer topographic profiles and the limits determined by the tidal reference and contour levels (Figures 6.3A, 6.4A). These reference levels were thus used to carry out the morphometric and volumetric analyses of the foredune-beach system at the meso-scale. Additionally, Figures 6.3B and 6.4B show that the thresholds identified using the Pettitt test confirm a general spatio-temporal persistence of the unit boundaries, in particular the lower beach and intertidal zone through time.

A)

B)
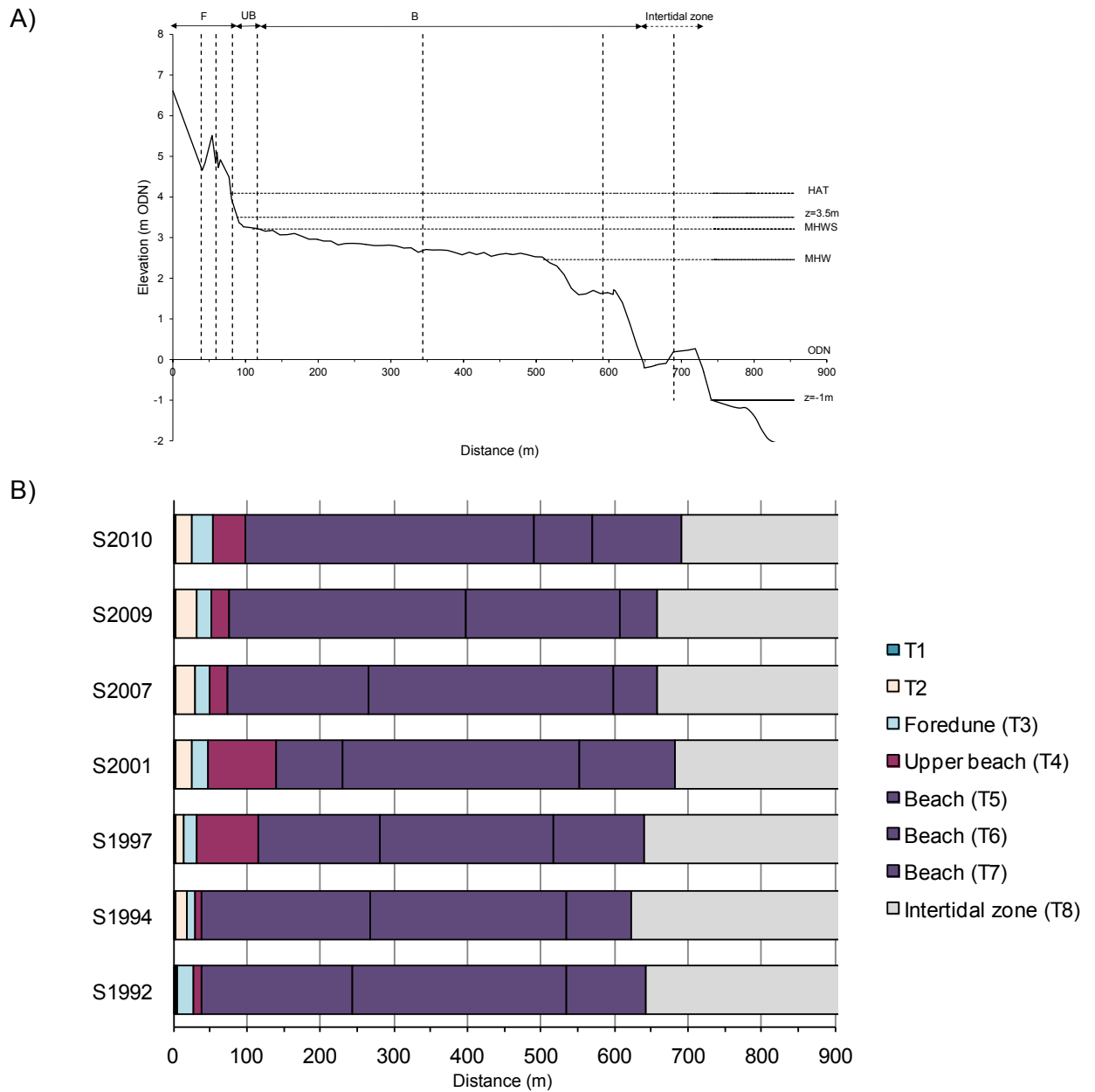
Figure 6.3. Significant (p<0.05, Pettitt test) morphological changes along summer topographic profiles at BL: (A) average of the statistical thresholds (dashed vertical lines) plotted along the profile in 2010. Top arrows indicate sub-units assessed by tidal reference level, F=foredune, UB=upper beach, B=beach corresponding to the middle and lower beach, (B) 1992-2010 showing the thresholds (T).

A)

B)
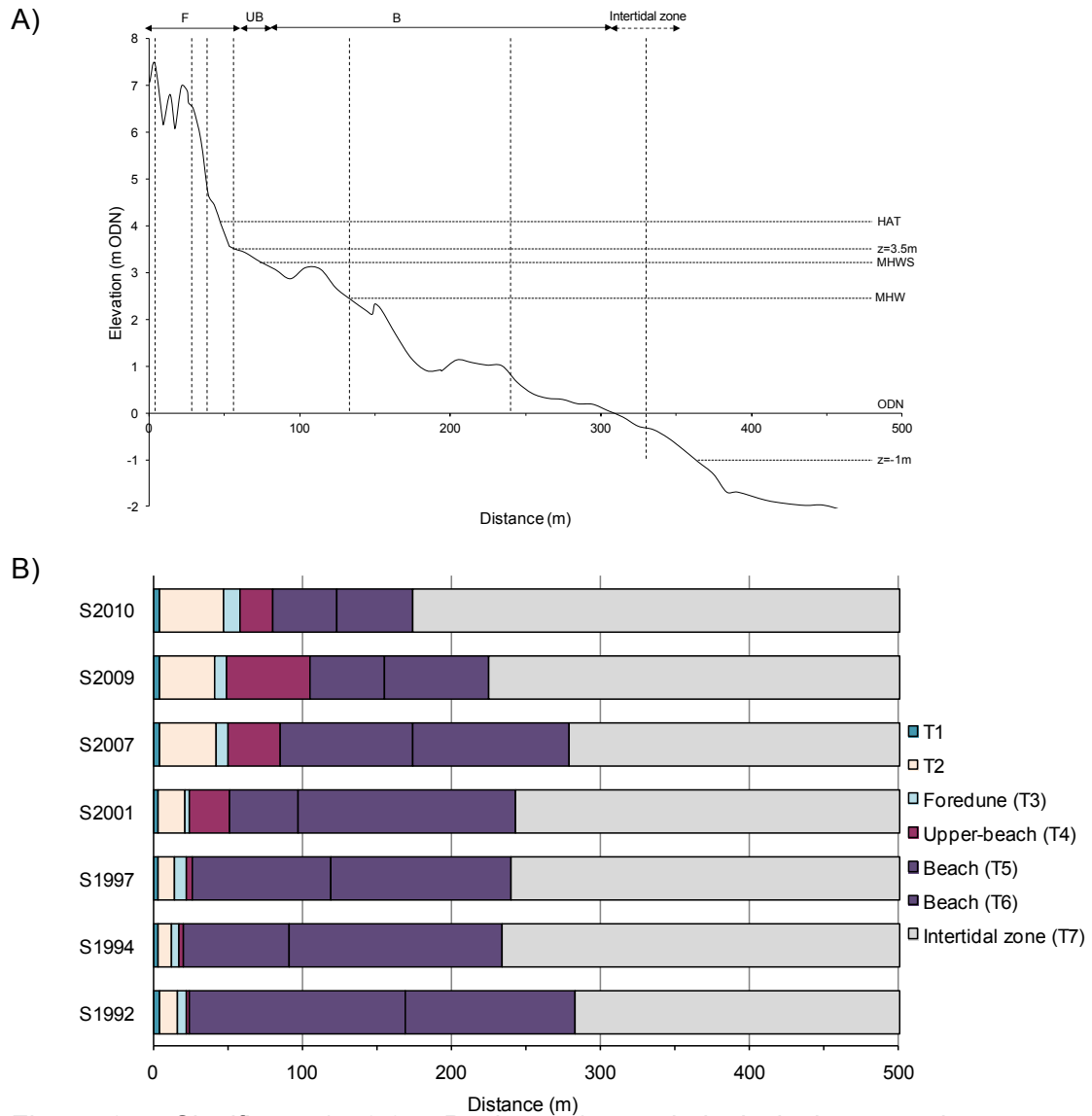
Figure 6.4. Significant (p<0.05, Pettitt test) morphological changes along summer topographic profiles at MNE: (A) average of the thresholds (dashed vertical lines) plotted along the profile in 2010. Top arrows indicate sub-units assessed by tidal reference level, F=foredune, UB=upper beach, B=beach corresponding to the middle and lower beach, (B) 1992-2010 showing the thresholds (T).

Morphological indicators were applied to the foredune, upper beach and beach. For the latter, the lower reference level of z= -1 m was adopted in an attempt to incorporate the landward ridge-runnel system in the analysis. This is because the dynamics of intertidal bar systems have been shown to have a considerable impact on dune sediment budget in other locations (e.g. Aagaard et al., 2004).

6.2.1. Two-Dimensional Morphological Foredune-Beach System Evolution: Methodology

A. Ground topographic profiles

Along the Lincolnshire coast, the Environment Agency (EA) since 1992 has commissioned bi-annual (winter and summer) beach profile surveys. These are conducted at 1 km intervals and two such profiles fall inside the study area (Figure 6.2) The EA profile coded L2E7 lies within the BL site and the profile coded L2D1 lies in the MNE site. These surveys were conducted using a standard total station (horizontal accuracy ±0.1 m and vertical accuracy ±0.01 m) until 2003. Since then a RTK-GPS system (horizontal accuracy ±1 m, vertical accuracy ± 0.15 m) related with reference to Ordnance Survey control points has been used. For this study, topographic profiles were linearly interpolated to 0.1 m and the morphometric and volumetric indicators previously defined in Table 6.1 were calculated. The time series was then used to detect annual changes in morphology.

After de-trending from the averaged elevation, consecutive topographic profiles were cross-correlated with one another to quantify the degree of similarity for which the time interval was half a year (i.e. bi-annual topographic profiles). In addition, cross-correlation analyses with larger time lags were carried out to examine the level of morphological resemblance of the foredune-beach changes over longer timescale. This assumes the bi-annual measurements to be independent, which can be questioned since it is likely that deviations from the time-averaged topographic profile in a certain year are to some extent related to the deviations observed in the previous year.

B. Photogrammetry

Photogrammetry is an effective and useful geomorphological tool (Chandler and Brundsen, 1995). Archival aerial photographs are increasingly being used for terrain modeling and to detect morphological changes through time at the meso- and macro-scales (Chandler, 1999). Photogrammetry has been successfully applied in coastal research for mapping and studying coastal changes and evolution (e.g. Moore, 2000, Hapke, 2005, Chaverot et al., 2008, Thomas et al., 2011). Brown and Arbogast (1999) reported that photogrammetry has improved capabilities for monitoring dunefields by making it possible to reconstruct changes in their morphology through time.

B.1. Data acquisition

Regular aerial photograph surveys are flown along the north Lincolnshire coast between July and October, thus capturing information about the summer state of the foredune-beach system (Table 6.2). Stereo pairs of vertical photographs were provided by the EA for the years 1992, 1994, 1997, 2001, 2007, 2009, and all at a scale of 1:5,000. The paper prints of aerial photographs acquired with different metric cameras in 1992, 1994, 1997, 2001 were scanned at 600 dpi. The scanning process, which is an unavoidable practice for converting historical print image into digital form, can introduce further distortions (Walstra et al., 2010), but these were reduced as far as possible by using a high scanning resolution. For recent years, the aerial photographs were directly obtained using digital cameras. In general, three stereo-pairs of photographs were required to analyze the whole study area. The aerial photographs were chosen for their availability of 60% overlap to minimize systematic errors, and enable accurate identification of ground control points.

Table 6.2. Description of the camera calibration and characteristics of the aerial photographs used.* Paper prints scanned at 600dpi with non-photoscanner. B&W= black and white.

Photo year	Resolution	Camera system	Lens type	Focal length (mm)	Characteristics of photographs
1992	B&W	Metric	Wild Universal Aviogon RC20	153.67	Scanned paper prints*
1994	B&W	Metric	Wild Universal Aviogon RC30	153.61	Scanned paper prints*
1997	B&W	Metric	Wild Universal Aviogon RC30	153.65	Scanned paper prints*
2001	Colour	Metric	Zeiss RMK TOP 15	153.97	Scanned paper prints*
2007	Colour	Digital	UltraCam D, S/N UCD-SU-1-0037	105.20	Original digital photograph
2009	Colour	Digital	UltraCam D, S/N UCD-SU-2-0012	101.40	Original digital photograph
2010	Colour	Digital	UltraCam D, S/N UCD-SU-2-0012	101.40	Original digital photograph

B.2. Photogrammetric processing and analysis

Once the scans have been obtained, the group of image pairs called a block was imported to ERDAS Imagine Leica Photogrammetric Suite system release 9.3 to perform all subsequent photogrammetric processing (Figure 6.5).
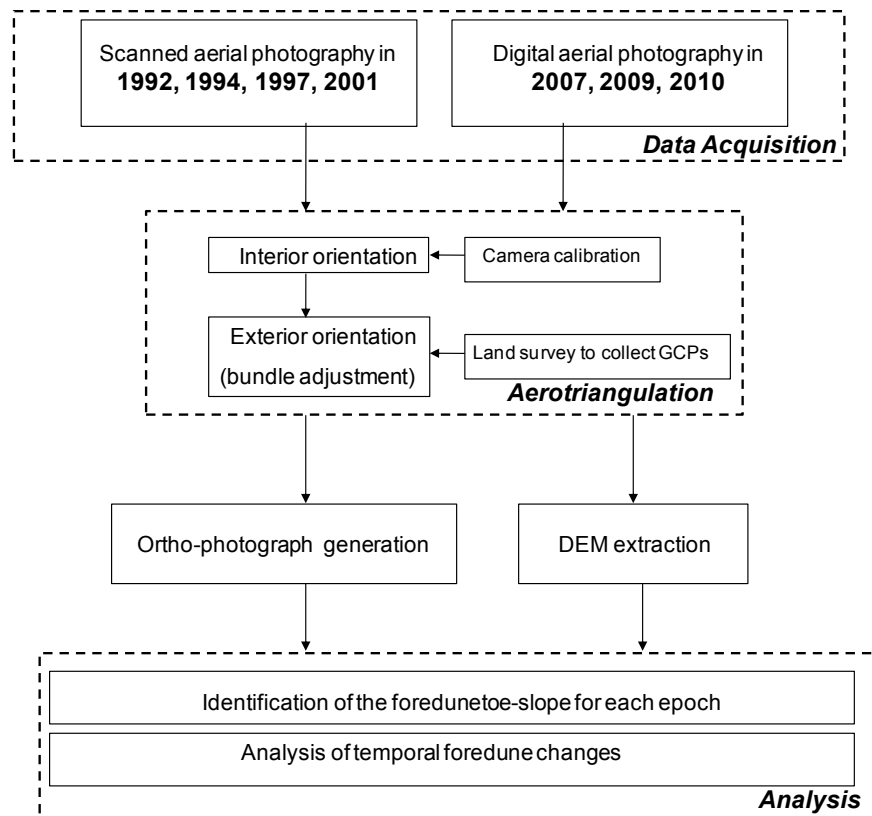
Figure 6.5. Workflow of photogrammetry processing.

Block aerotriangulation process: Interior and exterior orientations

Aerotriangulation, a process relating photograph and ground coordinates, was established through the determination of the interior and exterior orientation of the camera. Interior orientation was applied to restore the internal geometry of the camera at the time of the exposure using fiducial marks on the imagery. They were identified on each image and linked to their photo-locations given by the camera calibration certificates, which also gave information concerning the location of the principal point, focal length, flight height, photo coordinates of the fiducial marks, and measures of lens distortions. Then the exterior orientation step was carried out to define the position and angular orientation of the camera during image capture. This is established by applying an algorithm known as self-calibrating bundle adjustment, in which all photographs in the block are simultaneously adjusted to ground control points (GCP) in one single

least squares solution. This involves linearized collinearity equations in order to establish the relationships between the positions of a set of photographs and a ground coordinate system (Chandler and Brunsden, 1995). GCPs deemed to be ideal were collected throughout the study area for the purpose of exterior orientation. The coordinates (x, y, z) of the GCPs were acquired using a RTK-GPS system, which is sufficiently accurate for measuring the GCPs (Baily et al., 2003) which consisted of buildings, houses or field shelters. The GCPs were identified and where possible were well-distributed across each photograph in each stereo pair in order to solve the camera model parameters. A minimum of 6 GCPs were located along the south of the study area, whereas only 4 were used at the BL site due to a lack of fixed land points. In theory only three GCPs are required, however in practice more points are desirable as redundancy provides appropriate checks and precision (Wolf and Dewitt, 2000). Also tie points, point appearing on more than one photo that serve to connect the photographs together, were automatically added on the stereo model.

Ortho-photograph generation

Ortho-rectified photographs, also called ortho-photographs, combine and display the image characteristics of a photograph with the geometric qualities of a scale map (Wolf and Dewitt, 2000); and are accurate pictorial sources of information about the aerial survey (Krupnik, 2003). Based on the collinearity equations, ortho-photographs were created at a pixel resolution on the ground of 0.25 m for both photographs in each of the stereo pairs through differential rectification in order to remove image displacements caused by the photographic tilt, camera distortion, terrain relief, and scale variations due to changes in altitude along the flight lines. The generated ortho-photographs errors were calculated from all GCPs used in the bundle adjustment, and root mean square error (RMSE) average was generated for each year (Table 6.3). The horizontal RMSE average of the bundle adjustment was 0.29 m in X and 0.26 m in Y. The potential error sources in the aerotriangulation procedure may be due to the distribution of the GCPs because most were located landward of the dunes and there are very few seaward of the dunes. Mills et al. (2003) reports that systematic errors are likely to arise from poorly distributed control points which should be evenly distributed over the images to produce strong geometry, and preferably surround the volume of interest (Chandler, 1999). The horizontal error margin was less than 0.3 m, which is acceptable during the ortho-photograph process (Adams and Chandler, 2002). Finally, all ortho-photographs were directly exported and displayed as a mosaic for analyzing in ArcView 9.3 software (GIS).

Table 6.3. Error analysis of the ortho-photographs.

Photo year	Error analysis of the triangulation process for the ortho-photographs quality control - RMSE (m)		
	X	Y	Z
1992	0.414	0.476	0.765
1994	0.449	0.461	0.592
1997	0.46	0.367	0.758
2001	0.179	0.142	0.122
2007	0.213	0.199	0.118
2009	0.16	0.105	0.08
2010	0.185	0.091	0.083
Average	**0.294**	**0.263**	**0.360**

C. Analysis

The foredune evolution was evaluated by superimposing and comparing the ortho-photographs, allowing a visualisation of dune development and migration over time. Foredune slope-toe was defined as the contact of the steep foredune face with the gentle upper beach slope determined along BL, TSH and MNE sites by generating 10, 11 and 13 transects perpendicular to the foredune, and spaced at approximately 50 m (Figure 6.2).

The coordinates of the foredune slope-toe position were determined by its intersection at each transect. This indicator often corresponded to the limits of the vegetated foredune belt. Quantifying foredune migration can be an uncertain process (Guillén et al., 1999, Battiau-Queney, 2003). In this study, the foredune slope-toe was identified using stereoscopy, which made it possible to visualize clearly the vegetation and the break of slope of the foredune in three-dimensions. To the horizontal RMSE of the ortho-photograph process (±0.3 m), a potential error margin of foredune slope-toe identification ±1 m may be present, resulting in a maximum total error margin of ±1.3 m.

Additionally, the measurements were carried out three times for each photograph block. Measurements were used to calculate foredune position from fixed points (x,y). Figure 6.6 presents the calculation of the distance between the coordinates for consecutive epochs based on the Pythagorean theorem.
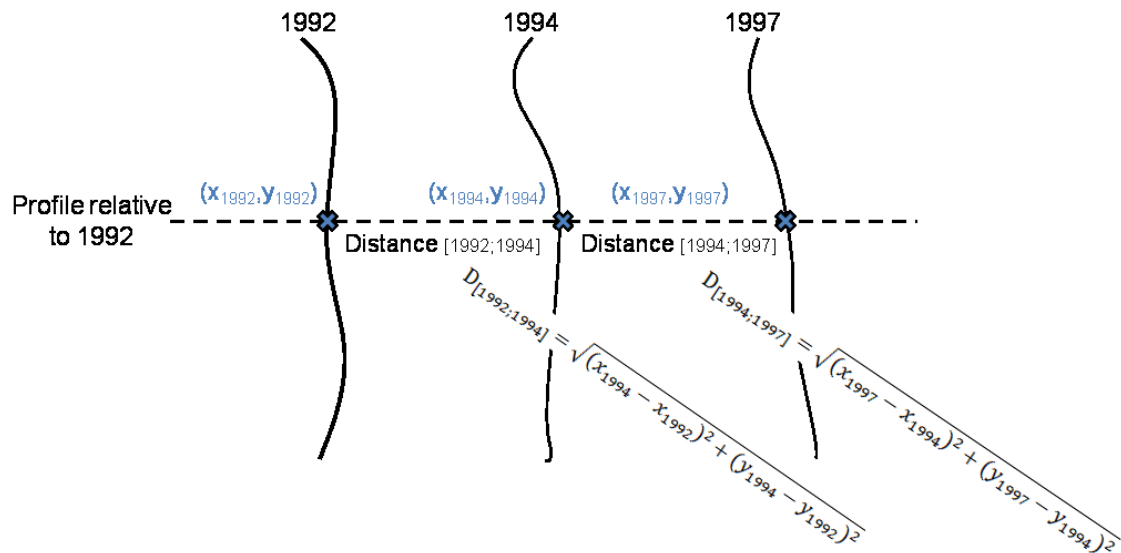
Figure 6.6. Sketch distance calculation for the foredune slope-toe position.

Changes in the rate of foredune evolution, for example in response to different forcing factors were calculated using the end-point-rate (EPR) method (i.e. comparing foredune slope-toe position between 1992 and 1994, 1994 and 1997, 1997 and 2001, 2001 and 2007, 2007 and 2009, and 2009 and 2010) and comparing these results with the long-term trend. The mean of the foredune slope-toe distance changes for each study site was established from the relevant spatial transects and then divided by the time elapsed between the successive years. This method has been suggested to overcome the potential problem of image quality changes over time (Dolan et al., 1991).

Temporal and spatial changes in terrestrial vegetation cover were investigated by undertaking geospatial image thematic classifications, with the aim of automatically categorizing all pixels in an image into thematic classes. The analysis focused on the dune at the three sites because the beach is unvegetated with the exception of the embryo dunes located on the upper beach at TSH. The classification is based on the widely demonstrated notion that the spectral signature of vegetation is different from that of a bare sand surface. The generated ortho-photographs were exported to ERDAS Imagine 9.3 software, and then used to perform an unsupervised classification technique - ISODATA (Iterative Self Organizing Data Analysis Technique) classification, in which the spectral pattern present within the data for each pixel is used as the numerical basis for categorization. The principle of this classification is to gather the

pixels which have similar spectral characteristics into groups by applying the ISODATA clustering algorithm, which is based on spectral distance and iteratively classifies the pixels, by redefining the criteria for each class multiple times to gradually generate the spectral distance patterns. It has been widely used in coastal zone management (e.g. Thompson et al., 1999, Ventura and Irvin, 2000). In this study, a high convergence threshold of 95% was used to maximise the percentage of pixels with cluster assignments and thus decrease the risk of changes between iterations. The classification makes it possible to identify two classes corresponding to vegetated and unvegetated sand surfaces; and to explore the changes in dune vegetation cover.

6.2.2. Three-Dimensional Morphological Foredune-Beach System Change

The shift from a two-dimensional to a three-dimensional representation of morphological changes can enhance our understanding of complex foredune-beach system evolution at meso-scale.

Aerial photography represents the most effective visual source of geographical information for measuring coastline evolution and landforms at meso-scale (Andrews et al., 2002). However more recently LIDAR (Light Detection And Ranging), an active remote sensing technology, has been used to provide comparable data and is often more cost-effective, especially for regional analyses. However, this technology is still recent and historical usually photographic data is required to study coastal foredune evolution at the medium-term. This study uses both data sources to create three-dimensional representations of the study site at different points in time.

Comprehensive visual and quantitative investigations into the spatial and temporal patterns of morphological features have been achieved by producing Digital Surface Models (DSM). These models are a distinct form of digital geographical information, representing the surface of the Earth. In comparison, a Digital Terrain Model (DTM) is a 'bare earth' model generated from a DSM by filtering points into ground (terrain) and non-ground (non-terrain) points such as vegetation, buildings and other objects. Therefore, a DTM should be more appropriate for investigating meso-scale morphological changes in the foredune-beach system. For this research, DTMs derived from LIDAR data were produced for 2001 and 2007, however DSM generation could

only be achieved for the archival aerial photogrammetry due to the problem of vegetation filtering (i.e. spatial variability of vegetation height and density through time). DSMs were assumed to be relevant to extract the height of the foredune slope-toe where the vegetation is likely to be absent.

A. DSM generation from aerial photogrammetry

Having generated a photogrammetric model, DSMs can be extracted automatically by exploiting the spatial quality of the aerotriangulation procedure (Chandler and Brundsen, 1995). Automated DSM extraction from a stereo model comprises three successive steps: digital image matching, interpolation and then quality control. The grid spacing of the DSM is usually limited by the object space pixel dimension and the size of the correlation window used during image matching (Baily et al., 2003), which for the purposes of this analysis was that optimised for a flat study area with a correlation coefficient limit of 0.8. In order to obtain a regular DSM grid, inverse distance weighted (IDW) interpolation was applied and based on an average value from neighbouring data points, weighted according to their distance. The DSM was generated into a regular grid with pixels 1 m × 1 m with each point having x, y and z coordinates; and into a raster format to be directly exported to GIS. DSMs could not be produced at BL and north of the TSH site. This was due to the uneven spatial distribution of the GCPs and also a lack of texture (i.e. low surface roughness), which caused problems for the image matching routines and decreased the probability of the interpolation for DSM generation (Lane, 2000). The accuracy of the generated DSM was quantified by comparing the coordinates of the GCPs used in the bundle adjustment. Table 6.4 presents the accuracy evaluated by computing the global root-mean-square error (RMSE) of independent GCPs, and also the mean error (ME) and mean absolute error (MAE) to distinguish the unwanted systematic error (Chandler et al., 2005). DSMs were also draped onto the ortho-photographs of the same study years to assess the reliability of the DSM.

Table 6.4. Error analysis of DSM generation. RMSE=root-mean-square error, ME=mean error, MAE=mean absolute error.

Photo year	Error analysis of the DSM (m)		
	RMSE	ME	MAE
1992	1.406	-0.210	1.232
1994	0.789	-0.499	0.687
1997	0.567	0.046	0.490
2001	0.804	-0.160	0.692
2007	1.304	-0.985	1.120
2009	0.763	-0.012	0.665
2010	1.338	0.094	0.975

The generated DSMs provide good representation of the elevation of the landward side of the foredunes, but not the beach side due to the lack of GCPs and the influence of surface texture on the automated image matching process. Analysis of sequential DSMs was thus limited to the foredune-upper beach. The ortho-photographs were superimposed on the DSMs to extract the height of the foredune slope-toe for each studied year and along transects from 18 to 34, which covers from the centre of TSH to the south of MNE.

B. DTM generation from LIDAR data

Airborne LIDAR has become a widely used source of digital elevation data. It offers the capability of capturing three dimensional topographic information about the Earth's surface by transmitting pulses of light toward the land surface, and the energy is scattered and reflected back toward the airborne platform, where its return is detected (Wehr and Lohr, 1999, Liu, 2007). The LIDAR system is mounted in an aircraft and is typically composed of a laser scanning mirror unit, a Global Positioning System (GPS) receiver, and an Inertial Navigation System (INS) (Baltsavias, 1999, Brock et al., 2002) providing precise position and attitude, in order to calculate 3D positions of terrain points (i.e. point clouds). The accuracy of LIDAR data is claimed to be ±0.05 m to 0.15 m vertically, with the spatial resolutions ranging from ±0.25 m to 2 m horizontally (Geomatics Group, 2009). This technology provides rapid, high-density and accurate point data (Brock et al., 2002). It is able to penetrate sparse vegetation to map the underlying terrain of interest (Liu, 2008) and can also be used to produce detailed topographic surveys of inaccessible or difficult areas in a single analysis.

LIDAR has been successfully used for large scale mapping and monitoring of coastal landforms above the low water mark including both beaches and coastal dunes (e.g. Stockon et al., 2002, Sallenger, 2003, Woolard and Colby, 2002, White and Wang, 2003, Van Houwelingen et al., 2006, Mitasova et al., 2010). Topographic information can also be compared with data collected using other methods to extend the temporal scope of research (Saye et al., 2005). The high spatial resolution makes it ideal for coastal research at a variety of scales (Woolard and Colby, 2002).

B.1. Data acquisition

LIDAR data collection missions were conducted by the Geomatics Group for the Environment Agency on 21st August 2001 and 13th September 2007 during daylight at low spring tide. The LIDAR surveys were carried out parallel to the coastline and at an altitude of 700 m. The LIDAR system generated 200-300 m wide overlapping ground swaths below the flight path (Askenazi et al., 2000). The airborne position was simultaneously recorded by the onboard GPS, which concurrently received and measured signals from a GPS ground base station, and from which the flight trajectory was determined. The airborne positions were associated with the measurements of slant distances to compute the exact coordinates for each point scanned by LIDAR. LIDAR data cannot provide information below the level of the LAT (Lowest Astronomical Tide) due to a combination of the high turbidity of the sea waters and the type of LIDAR system used.

B.2. Data processing

The LIDAR supplier Geomatics Group carried out two major data processing steps, which were to transform the three dimensional points captured as latitude, longitude, and ellipsoidal height based on the WGS84 reference system to a local coordinate system and then to compute a DSM corresponding to a mathematical representation of the surface of the Earth with a regular grid. The conversion to the local Ordnance Survey system involves two separate processing steps which are the translation of the plan (E, N) coordinates and the conversion of the ellipsoidal GPS heights to orthometric heights based on ODN datum using a local geoid model (Ashkenazi et al., 2000). Using the converted LIDAR data, the DSMs were rasterised by dividing the survey area into a regular grid of bins with a defined spacing, and each scanned point was identified and allocated to one bin. Then the empty bins were filled up using the

IDW interpolation technique, assuming that each input point has a local influence that decreases with distance. DSM grids were filtered to classify the ground (terrain) points from non-ground (non-terrain) points in order to produce DTMs, corresponding to the land topography of the study area at the time of data collection.

B.3. Input and analysis

The LIDAR data sets were supplied as a series of ASCII-files consisting of x, y, z data. They comprise four DTM blocks of data for each survey year, covering 2 by 2 km with a horizontal resolution of 2 m for 2001 and 1 by 1 km with a horizontal resolution of 1 m for 2007. The data set extends c. 4.5 km along the study coast. Lower beach zones covered by water during the LIDAR survey were excluded.

The ASCII files were directly imported to ArcView software and then converted to DTMs using 3D Analyst tool. For each LIDAR survey, DTM blocks were mosaicked together using the Data Management tool. The DTM blocks for 2001 were re-sampled to reduce the cell size from 2 m × 2 m to 1 m × 1 m, by a bilinear interpolation based on the value of the four nearest input cell centres to determine the value of the output raster. Thus, the cell size of the DTM grids in 2001 and 2007 were similar. To facilitate and ensure an identical spatial and temporal analysis, the entire DTM mosaics in 2001 and 2007 were subdivided for examining the three study sites by using masks covering from the intertidal zone to 50 m inland from the HAT contour and approximately 500 m in length at BL and TSH sites and 600 m at MNE. Grids of difference between the study site DTMs in 2001 and 2007 were produced in order to visualize the morphological changes.

In order to facilitate a comparison with transects from other data sources described above, two-dimensional cross-profiles orientated approximately perpendicular to the foredune were generated and then interpolated to 0.1 m. Each study site was segmented into five profiles spaced c.50 m apart (Figure 6.2). Using the generated profiles, analyses of morphometric and volumetric indicators as defined in Table 6.1 were undertaken to characterize temporal and spatial changes. The assessment of sediment budget variability of the foredune-beach system within each study site was also undertaken by calculating the sand volume of the foredune, upper beach, lower

beach and intertidal zone units for the DTMs in 2001 and 2007 and the generated profiles.

6.2.3. External Forcing Factors Methodology

Time series of wind and water level records were examined to investigate the causes of temporal and spatial variability in foredune evolution. This analysis was only undertaken from 1993 to 2010 due to missing wind records at Donna Nook in preceding years. Storm surge was defined as the occurrence of onshore and/or landward-directed alongshore winds (i.e. blowing winds from 350° to 150°) exceeding ≥14 m s^{-1} and a water level ≥3.5 m. Extremely high wind speeds and water level were only considered in order to centre the analysis on energetic and potential foredune modifying events. Along macro-tidal beaches, the water level reached during storms is a primary factor that must be associated with both wind speed and direction and amplitude of surge (e.g. Vasseur and Héquette, 2000).

Wave activity is another important forcing factor controlling foredune erosion during storm events. Long-time series of wave data were not available for the period of this study so a hindcast of significant wave heights was undertaken and based on hourly mean wind data collected at Donna Nook. The parametric wave prediction was determined by using the empirical equation (CERC, 1984) for deep water significant wave heights (Hs):

$$Hs = 5.112 \times 10^{-4} \times U_a \times F^{1/2}$$

Eq 6.1.

Where Ua is a wind-stress factor (m s^{-1}) corresponding to the adjusted wind speed above the seawater. F is the wave fetch length (m), and was calculated for each 20° sector facing the coastline. However, because wave fetch length between 350° and 40° can be defined as unlimited in the North Sea Basin, it was assumed to be equal to the distance between the study area and the shortest distance to the north Basin entrance (c. 450 km).

The first step was to adjust the wind speed recorded at Donna Nook weather station to the wind speed above seawater standardized to 10 m high for wave hindcasting (Kamphius, 2010). The logarithmic velocity profile was assumed:

$$U_a = (\frac{10}{Z_{DN}})^n \times U_{DN}$$

Eq 6.2.

Where Ua is the wind speed above the seawater (m s^{-1}), n is the shear exponent equal to 0.15 by assuming that the ground cover was characterized by low grass or fallow ground, and U_{DN} is the wind speed recorded at the Donna Nook station at the elevation of Z_{DN} (8 m in height).

To characterize each extracted storm surge event and its potential impact on the foredune, the storm erosional susceptibility index (SESI) applied in Chapter 4 was determined by combining the effect of the peak of the water level above the foredune toe, the significant wave height and storm duration. The cumulative effect of storm surges between successive topographic and aerial surveys was investigated by assuming that it was related to the evolution of the foredune-beach profile, and in particular the foredune slope-toe. The annual cumulative SESI (Eq. 4.3) was calculated by totalling the effect of storm surge for the year prior to each analysed survey. This was taken as from July in the year preceding the survey photograph acquisition to the following June because most of the aerial and topographic surveys were taken between July and August. Also, to account for the fact that erosion on the foredune-beach system could reflect storm erosion which occurred months previously, winter and summer cumulative SESIs were determined by summing each specific parameter between 1st July and 31st December and between 1st January and 31st June. The approach assumes that the winter and summer meteorological and marine conditions are reflected in the 1st January and 1st July topographic profiles respectively. This is only an indicative analysis because in reality the winter season covers the months from August to December, and the summer from January to June.

6.3. Results

6.3.1. Topographic Profiles

EA cross-shore topographic profiles were used to examine the foredune-beach morphological changes over the last two-decades at BL and MNE; this could not be achieved for TSH because this site is not monitored by the EA.

A. Brickyard Lane (BL)

Figure 6.7 indicates the seasonal development of the foredune-beach system from the EA cross-shore profiles at the BL site, representing the north of the study area over the period 1992-2010 (excluding winter 1996). The main changes occur in the foredunes, which have grown continuously. The beach characteristics changed very little but in the intertidal zone there was a tendency for ridges to move landwards during the summer.
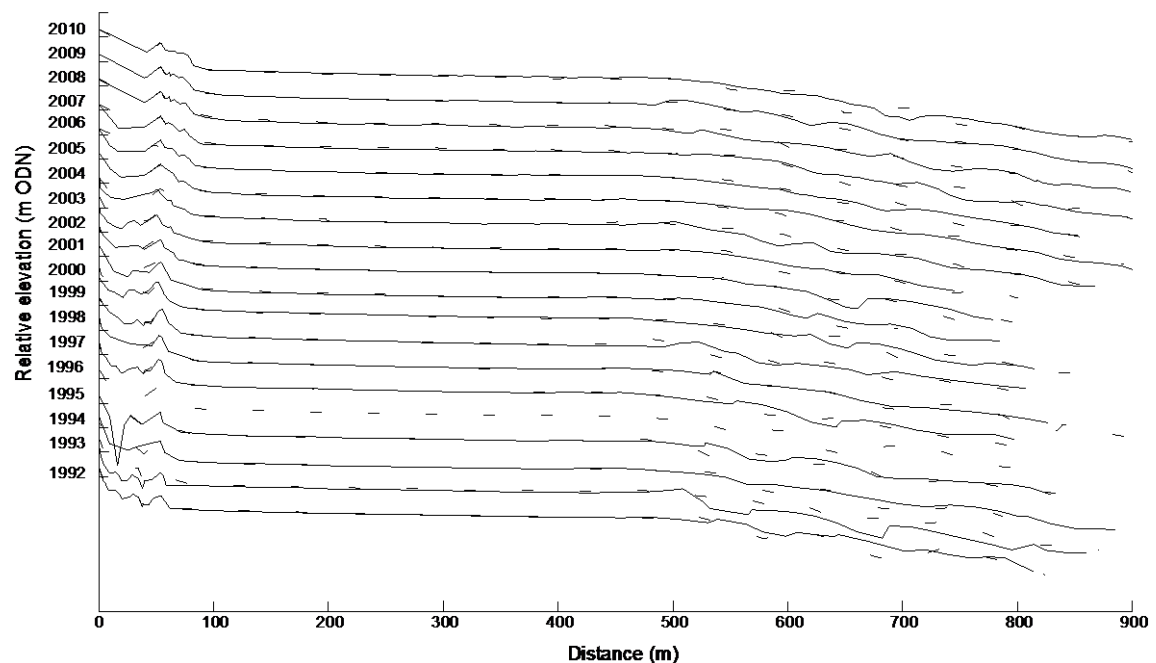
Figure 6.7. Winter and summer foredune-beach profiles at BL in the north of the study area over the period 1992-2010. The annual profiles have been stacked with an offset of 2 m. Solid and dashed lines represent winter and summer profiles respectively.

Table 6.5. Seasonal variability in morphometric indicators along the topographic profile at BL for the foredune (F), upper beach (UB), lower beach (LB) and intertidal (IT) units from 1992 to 2010. In the year column, w and s denote winter and summer profile respectively.

Year	Elevation F (m)	Position z=3.5 m (m)	Width UB (m)	Width LB (m)	Position z=-1 m (m)	Volume F ($m^3 m^{-1}$)	Volume UB ($m^3 m^{-1}$)	Volume LB ($m^3 m^{-1}$)	Volume IT zone ($m^3 m^{-1}$)
w92	6.40	60.0	2.6	626.5	792.1	249.81	8.67	1366.29	46.27
s92	6.40	59.0	5.8	590.4	781.8	258.37	19.30	1308.61	43.32
w93	7.69	67.4	20.5	637.3	772.8	299.97	67.80	1410.30	23.81
s93	6.27	69.0	23.6	657.7	776.3	304.78	78.10	1418.10	13.00
w94	7.00	66.7	15.8	601.4	791.1	307.35	52.12	1351.96	60.74
s94	6.41	64.9	23.5	569.6	779.4	291.31	78.06	1317.58	56.33
w95	6.39	68.3	20.3	581.4	798.0	305.15	66.98	1302.78	50.12
s95	6.36	70.5	15.5	589.3	776.9	309.38	51.71	1293.23	34.14
s96	6.34	72.2	20.8	631.3	761.4	330.19	68.93	1338.98	17.97
w97	6.44	71.2	31.4	593.3	791.5	333.74	105.14	1287.55	39.03
s97	6.17	69.0	31.5	577.7	756.2	317.98	103.86	1293.04	33.46
w98	5.94	75.9	20.2	569.5	773.1	352.48	57.04	1305.60	66.33
s98	6.25	71.6	30.8	583.5	779.1	335.12	102.13	1248.98	57.64
w99	6.53	78.8	33.3	607.8	810.0	367.16	110.90	1301.50	43.99
s99	6.23	75.8	56.5	547.3	785.4	350.46	188.15	1249.24	58.68
w00	6.06	79.7	50.8	573.6	746.9	372.68	168.68	1283.19	17.77
s00	6.30	83.3	31.8	566.4	790.0	388.41	105.60	1316.19	53.61
w01	7.05	84.9	30.0	597.3	792.0	405.42	98.93	1347.67	26.00
s01	6.24	83.5	52.4	555.1	770.8	394.99	173.47	1279.52	47.80
w02	7.04	81.9	34.5	611.8	771.9	391.62	114.11	1339.30	21.75
s02	7.04	84.2	44.6	577.8	741.8	391.61	147.29	1318.87	17.40
w03	7.04	82.5	18.4	602.1	760.0	381.08	61.03	1371.51	26.87
s03	7.00	83.1	33.1	579.5	787.0	402.82	109.36	1279.09	23.44
w04	7.00	80.6	29.6	592.9	758.5	388.72	98.13	1312.54	24.57
s04	6.56	83.4	31.6	600.3	758.2	408.14	105.41	1393.33	23.65
w05	6.48	86.9	32.8	572.6	769.7	415.95	107.82	1327.57	47.05
s05	6.48	84.9	44.6	574.4	780.4	411.53	148.10	1309.50	43.60
w06	6.51	83.7	15.2	575.9	776.6	403.42	51.18	1344.84	62.66
s06	6.51	85.1	30.5	594.5	737.9	412.77	100.50	1367.37	15.42
w07	6.50	85.2	8.5	622.4	744.0	409.55	28.00	1397.43	14.94
s07	6.50	85.3	28.3	574.4	786.9	434.09	94.10	1329.26	60.95
w08	6.50	90.5	11.3	599.1	790.6	456.71	37.88	1296.91	21.93
s08	6.61	96.1	61.5	544.9	781.3	478.66	203.53	1211.47	38.29
w09	6.61	91.3	31.1	559.8	788.0	462.62	102.76	1282.32	46.19
s09	6.61	89.9	23.0	573.3	780.6	460.12	76.62	1304.93	43.71
w10	6.62	88.6	58.6	530.9	776.0	456.86	191.25	1214.44	39.63
s10	6.61	88.8	29.5	606.3	742.5	453.95	96.89	1303.34	67.00

Figure 6.8 shows the changes in sediment volume incorporated into each geomorphological unit.
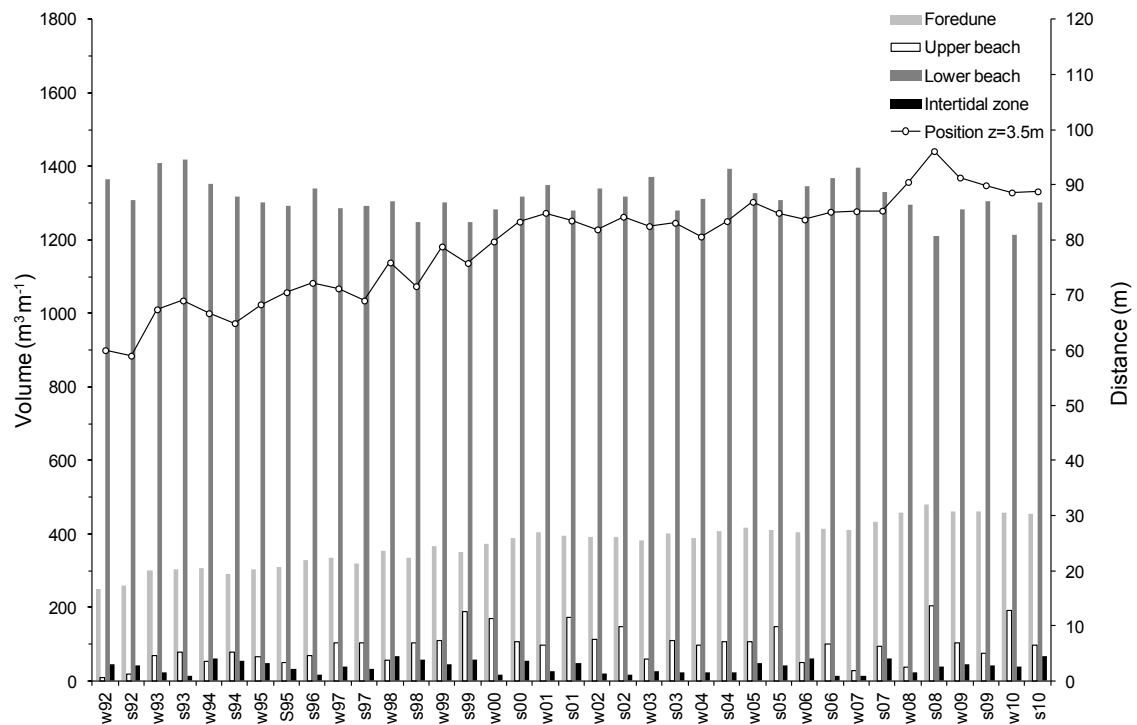
Figure 6.8. Changes in the volume of sand in each geomorphological unit at BL for bi-annual surveys from winter (w) 1992 to summer (s) 2010.

At BL, secondary foredune height was relatively stable from 1992 to 2010 with a mean height of 6.59 m (minimum of 5.94 m in w98; maximum of 7.69 m in w93). However, the position of the foredune toe (z=3.5 m) gradually increased from 60 m to 88.8 m from the benchmark concomitant with an increase in foredune sand volume from nearly 250 m^3 m^{-1} in winter 1992 to 454 m^3 m^{-1} in summer 2010. Figure 6.8 also shows a progressive accretion of the foredune between winter 2007 and the last survey, while no clear trend can be depicted for the upper-beach, lower beach and intertidal zone units.

Cross-correlation between successive topographic profiles indicates that the degree of resemblance between summer and winter is relatively similar to that between winter and summer (Figure 6.9A). The degree of resemblance was defined as the maximum correlation coefficient from cross-correlation analysis and values are on average c.0.64 for both the summer to winter and the winter to summer correlations with standard deviations of c.0.03 and c.0.04 for the former and latter respectively. The high

correlation coefficients indicate that little morphological change occurs over the seasonal periods. Figure 6.9B also shows high correlation coefficients from half year (0.60) to four years (0.65) indicating morphological changes are relatively small over these periods.
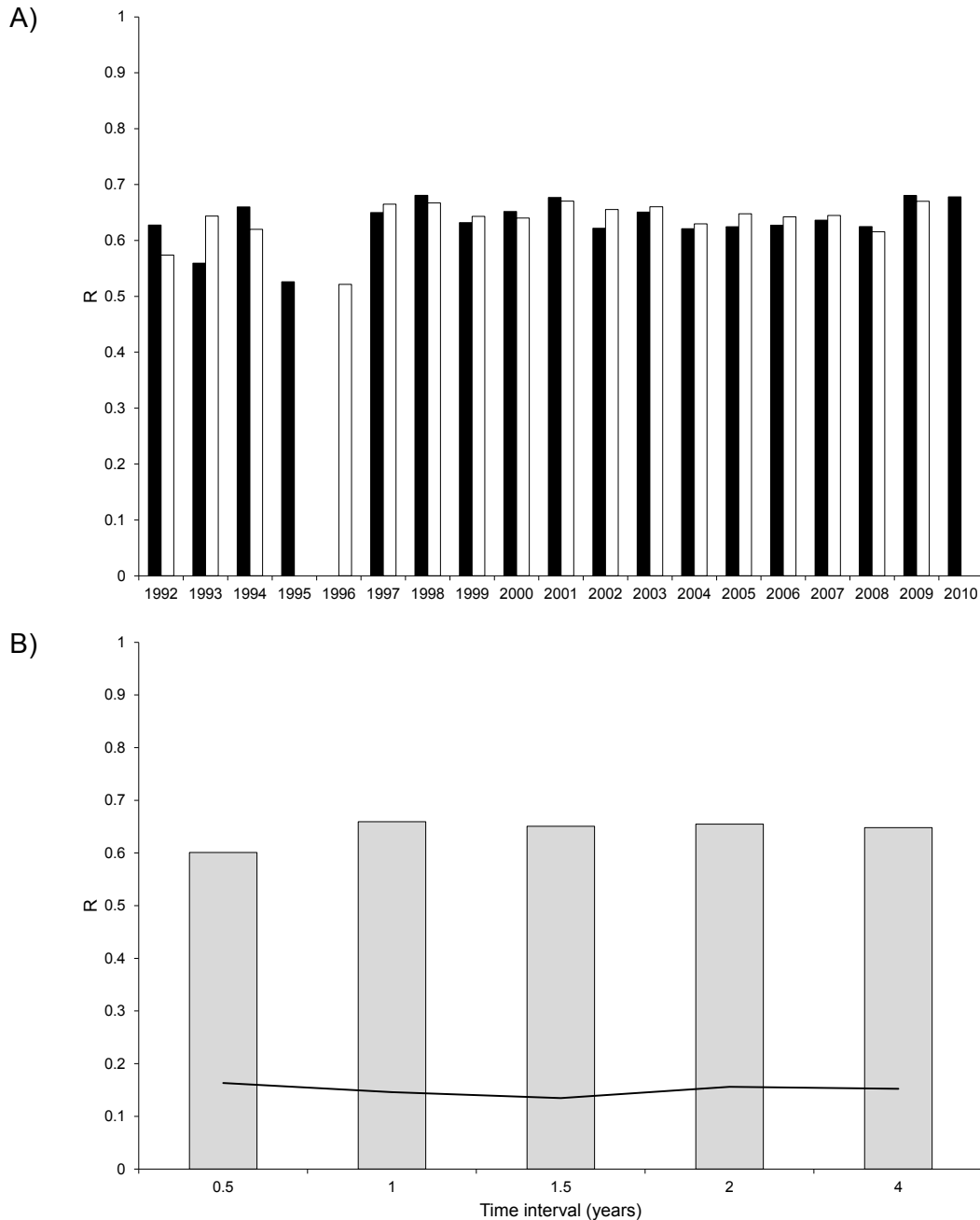
Figure 6.9. Results from cross-correlation between topographic profiles at BL: (A) maximum correlation coefficient from winter to summer (black bars) and from summer to winter (white bars), (B) maximum correlation coefficient in relation to time interval between topographic profiles. Grey bars correspond to the average values for each time interval, and the black line to the standard deviations.

B. Mablethorpe North End (MNE)

Figure 6.10 shows the winter and summer annual variability of the foredune-beach topographic profiles at MNE, located in the south of the study site, from 1992-2010 (with the exception of winter 1992). The most significant changes are observed in the foredune unit, where three foredune crests have formed since 2007. Between winter 1995 and winter 1996, an incipient foredune developed naturally (pers. com. David Welsh, EA), but it then disappeared to nourish the slope and beach units. These latter units seem to experience morphological changes with no clear patterns.
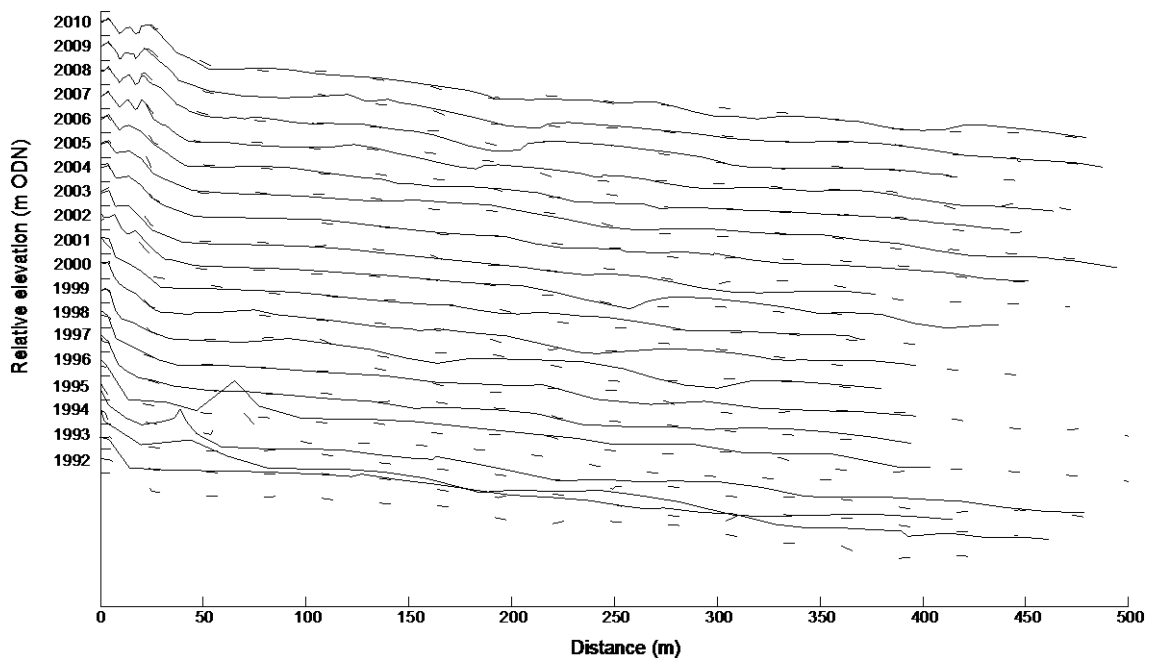
Figure 6.10. Winter and summer foredune-beach profiles at MNE in the south of the study area from 1992-2010. The annual profiles have been stacked with an offset of 2 m. Solid and dashed lines represent winter and summer profiles respectively.

Table 6.6. Seasonal variability in morphometric indicators along the topographic profile at MNE for the foredune (F), upper beach (UB), beach (LB) and intertidal (IT) units from 1992 to 2010. In the year column, w and s denote winter and summer profile respectively.

Year	Elevation F (m)	Position z=3.5 m (m)	Width UB (m)	Width LB (m)	Position z=-1 m (m)	Volume F ($m^3\,m^{-1}$)	Volume UB ($m^3\,m^{-1}$)	Volume LB ($m^3\,m^{-1}$)	Volume IT zone ($m^3\,m^{-1}$)
s92	5.75	22.3	23.6	265.9	317.4	102.36	4.68	415.42	14.54
w93	5.75	13.4	24.9	242.9	318.5	66.07	8.85	470.08	37.67
s93	5.84	18.7	18.9	231.7	297.2	86.92	18.79	377.98	16.82
w94	6.39	18.7	29.2	143.7	270.5	85.47	35.15	170.94	51.89
s94	6.39	17.8	28.2	248.9	357.6	81.02	31.87	356.55	23.52
w95	6.39	42.9	19.2	144.9	218.0	176.45	4.69	157.51	14.54
s95	7.40	78.0	49.4	185.2	373.8	345.74	22.15	279.28	60.71
w96	7.40	77.6	83.8	217.4	373.0	338.92	19.46	288.62	21.03
s96	7.40	27.8	88.5	200.3	335.5	130.58	36.90	320.54	63.08
w97	7.40	28.2	34.1	200.4	373.0	133.29	21.46	309.08	44.61
s97	7.38	26.3	34.8	240.1	347.4	129.60	22.38	366.05	33.48
w98	7.40	25.9	31.0	215.7	373.1	128.22	15.67	340.05	26.82
s98	7.04	25.9	31.0	242.2	302.3	126.07	17.11	319.94	9.96
w99	7.15	26.7	30.3	234.7	376.8	132.97	14.77	373.08	15.76
s99	7.19	26.1	104.5	133.2	366.7	132.76	241.95	153.49	30.70
w00	7.38	26.1	80.7	218	389.9	139.41	177.77	219.39	20.75
s00	7.41	28.1	32.9	273.8	354.9	147.73	22.56	415.96	19.81
w01	7.40	28.0	42.9	234.4	370.0	149.98	48.51	392.42	21.91
s01	7.40	51.5	39.2	182	360.1	244.54	19.70	333.19	31.74
w02	7.40	35.8	58.6	274.8	381.4	195.02	23.82	382.00	18.56
s02	7.40	28.6	34.4	246.5	378.7	154.19	19.69	333.19	27.06
w03	7.40	32.8	32.2	232.6	303.0	175.39	14.08	383.20	15.43
s03	7.49	34.9	39.2	234.7	370.3	193.08	21.80	394.99	20.73
w04	7.46	39.6	39.6	257	369.4	215.35	16.10	376.18	18.20
s04	7.38	37.5	48.7	221.5	394.0	208.26	30.28	349.43	28.97
w05	7.27	41.3	44.6	254.8	381.9	224.36	23.80	404.68	23.65
s05	7.37	40.1	46.2	213.8	370.6	225.21	16.67	391.21	27.69
w06	7.51	39.7	85.5	182.3	385.0	226.35	147.88	223.57	28.33
s06	7.37	44.7	67.7	199.6	391.4	248.54	93.00	298.35	29.14
w07	7.45	41.0	54.7	219.7	382.6	234.02	33.23	338.85	22.35
s07	7.36	43.0	75.6	202.1	389.7	248.73	111.19	268.60	29.56
w08	7.46	48.3	75.3	212.1	384.7	274.50	105.91	253.52	13.32
s08	7.32	53.7	59	217.5	333.8	299.85	35.91	366.07	19.11
w09	7.51	52.5	64.2	223.4	385.7	296.80	35.48	311.24	20.70
s09	7.50	49.8	108.3	180.1	389.0	289.04	171.90	149.83	23.92
w10	7.37	50.1	90.9	191.9	362.8	291.23	135.16	231.45	15.33
s10	7.46	58.2	66.7	233.5	363.0	329.18	56.20	315.99	22.80
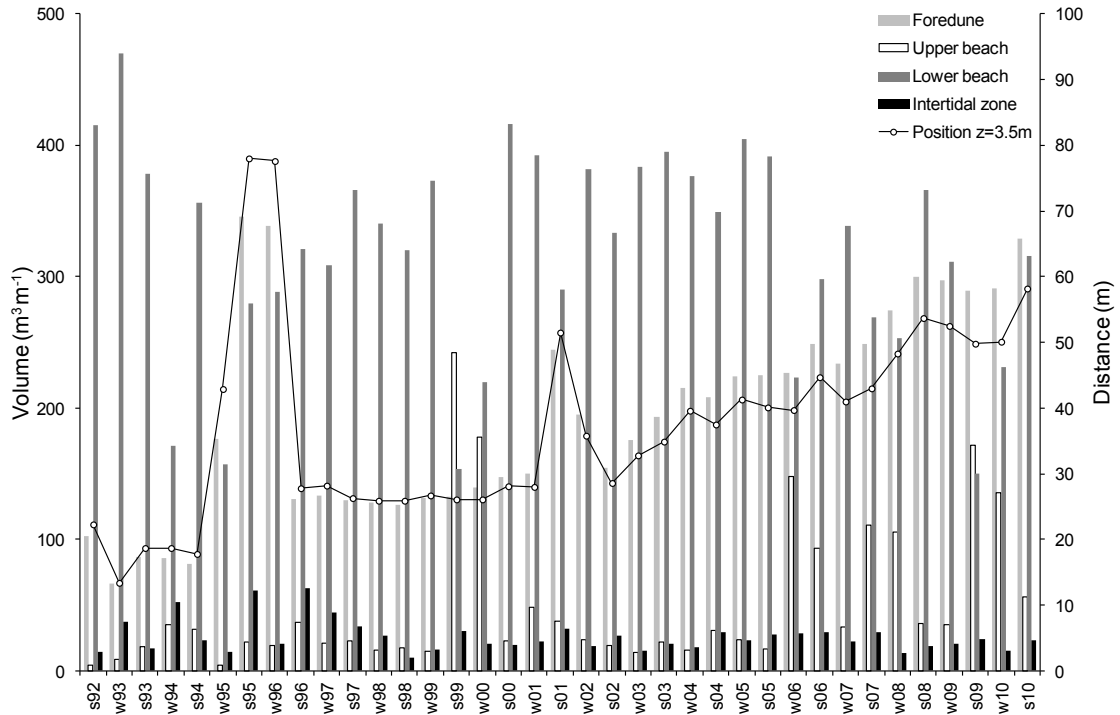
Figure 6.11. Changes in the volume of sand in each geomorphological unit at MNE for bi-annual surveys from winter (w) 1992 to summer (s) 2010.

Topographic profile analysis at MNE indicates that the secondary foredune crest has increased in elevation through time from 5.75 m to 7.46 m (Table 6.6). The relative stability of the foredune toe position (i.e. z=3.5 m contour) from 1996-2001 contrasts with two significant increases in the periods winter 1995-winter 1996 and in summer 2001, following which it gradually advanced seaward (Figure 6.11). Following the same pattern, the foredune unit overall increased in width by 35.9 m and in volume by 226.82 m^3 m^{-1} from summer 1992 to summer 2010. However, as at BL, there are no notable trends in morphological changes of the upper beach, lower beach and intertidal units.

Cross-correlation between successive topographic profiles at MNE indicates that the degree of resemblance between summer and winter is higher compared with that between winter and summer (Figure 6.12A). The values are on average of 0.59 with a standard deviation of 0.15 for the summer-winter correlations. While an average of 0.58 (standard deviation 0.16) was determined for the winter-summer correlations. Figure 6.12B shows a fairly low correlation coefficient over half a year, and thus seasonal morphological variability is relatively significant in the south of the study area. However,

high correlation coefficients from one to four years indicate morphological changes are insignificant over these periods.
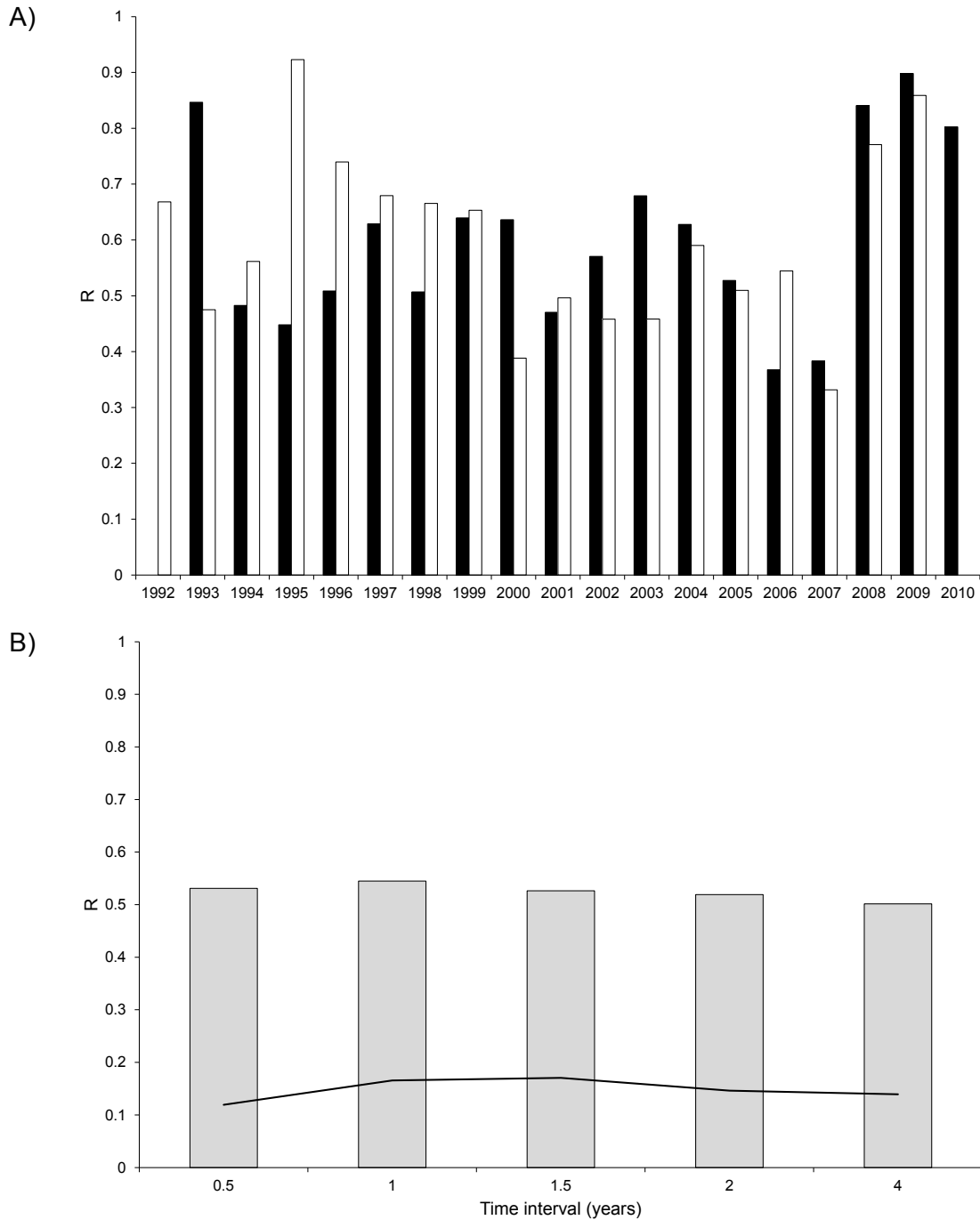
Figure 6.12. Results from cross-correlation between topographic profiles at MNE: (A) maximum correlation coefficient from winter to summer (black bars) and from summer to winter (white bars), (B) maximum correlation coefficient in relation to time interval between topographic profiles. Grey bars correspond to the average values for each time interval, and the black line to the standard deviations.

6.3.2 Aerial Photograph

A. Foredune evolution (1992-2010)

Results from the aerial photograph analysis indicate a mean rate of foredune slope-toe seaward migration of 2.2 m year^{-1} in the study area. This significant and rapid advance over the 18 year period since 1992 varies from 37 m at BL, 42 m at TSH to 46 m at MNE (Figure 6.13). Hence there is a south-north decrease in foredune advance over the studied period, from a mean annual migration rate of almost 2.4 m year^{-1} at MNE to less than 2 m year^{-1} at BL. However, foredune advance was more variable in the south ranging from 22 m to 88 m at different locations at the MNE site compared with a difference between maximum and minimum of 22 m at TSH and 12 m at BL.

At BL, the foredune migrated seaward at 2 m year^{-1} between 1992 and 2010, but this rate varied from 1 m year^{-1} from 2009-2010 to 3.5 m year^{-1} from 1997-2001 (Figure 6.13A). The same trend was observed at TSH, however the mean annual rate of foredune accretion was higher (2.3 m year^{-1}) and ranged from 3.9 m year^{-1} to 1.1 m year^{-1} (Figure 6.13B). The rate of accretion along the MNE foredune varies slightly more than at the other sites from 5.6 m year^{-1} for 1997-2001 to 0.5 m year^{-1} over the period 2007-2009 (Figure 6.13C). At all three sites, most rapid seaward migration of the foredune took place from 1997-2001.
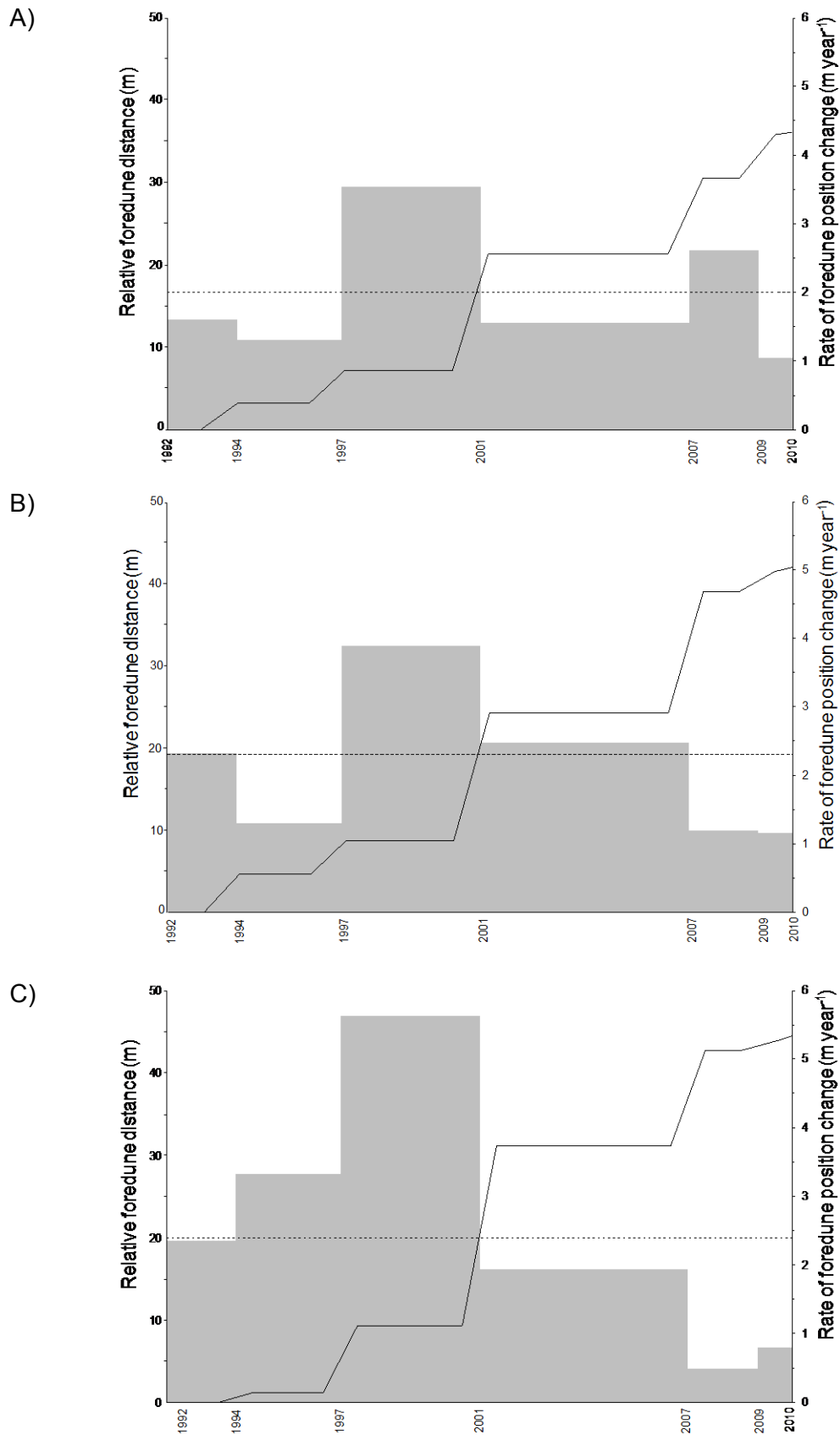
Figure 6.13. Changes in foredune position since 1992 (black line) and in rate of advance between aerial photographs (grey bars) at: (A) BL, (B) TSH and (C) MNE sites. Dashed line represents mean long-term rate of foredune advance.

From 1992-2010, the mean foredune slope-toe elevation was 3.7 m between transects 18 (TSH) and 34 (MNE) (Figure 6.14) which is slightly higher than the seasonal field observations over the monitoring period (refer in Chapter 4). The elevation ranged from nearly 3 m ODN at the transects 25 and 26 in 1992 and 1994 to 4.7 m ODN at the transect 23 in 1994. In general, a low variability of the mean foredune slope-toe elevation was observed over the study period.
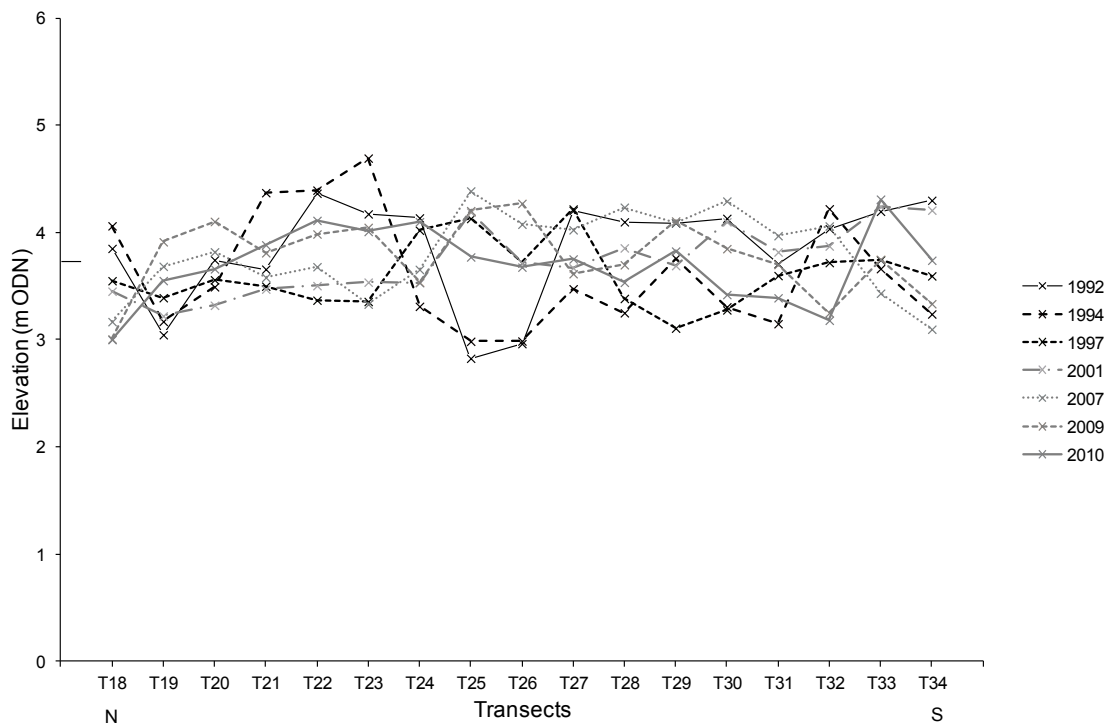
Figure 6.14. Alongshore variation in the elevation of the foredune slope-toe from the southern part of the TSH site (T18) extending to the south of MNE (T34) (see Figure 6.2 transect location) from 1992 to 2010. On the left axis, the horizontal line indicates the mean of foredune slope-toe elevation through time.

B. Vegetation changes (1992-2010)

As mentioned in Chapter 1, vegetation is significant parameter in foredune formation and development (Hesp, 1988, 2002). An unsupervised classification was applied to the ortho-photographs in order to identify vegetation surface changes on the dunes at each site over the period 1992-2010 (section 6.2.1.C)

In 1992, the percentage of vegetation cover on the dunes was 11.55% at BL, 15.41% at TSH, and 2.29% at MNE. Over the last decade, rapid foredune accretion was associated with a slight increase in vegetation cover of 19.51%, 17.41%, and 2.34% at

BL, TSH and MNE respectively between 1992 and 2010 (Table 6.7 and Appendices from 6.1-6.3).

Table 6.7. Dune vegetation changes at the three sites from 1992 to 2010.

	BL		TSH		MNE	
	Vegetated surface (m^2)	Vegetation cover (%)	Vegetated surface (m^2)	Vegetation cover (%)	Vegetated surface (m^2)	Vegetation cover (%)
1992	44113	11.55	49253	15.41	9030	2.29
1994	37389	9.79	40186	12.57	8842	2.24
1997	57740	15.12	48360	15.13	9683	2.45
2001	45180	11.83	45656	14.28	9361	2.37
2007	77236	20.22	79674	24.92	10234	2.59
2009	69517	18.20	61922	19.37	7361	1.86
2010	74519	19.51	55661	17.41	9246	2.34
Mean vegetation cover (1992-2010)		15.17		17.01		2.31

All three sites show similar temporal trends with an increase in dune vegetation cover in 1994-1997 and 2001-2007. The maximum vegetation cover was recorded between 2001 and 2007, and likely to be a response to a high precipitation period, especially in 2007 (Figure 2.10), that favoured vegetation growth. At TSH, this increase is likely to be explained by the formation and development of embryo dunes on the upper beach, while at BL a wedged primary foredune grew rapidly in 2007. Removal management of Sea Buckthorn, an invasive and quickly spreading shrub has been carried out at TSH since 2005. Immediately following removal the dunes are unvegetated however the bare sand is rapidly recolonised by lower order plants such as mosses and by vegetative propagation of plants and shrubs from nearby vegetated dunes. At MNE, vegetation cover is low and varies little, probably because of the foredune is very dynamic and pioneer plants are buried by rapid sand supply.

6.3.3. LIDAR

Changes in foredune-beach morphology and sediment volume were also examined using LIDAR data for 2001 and 2007. Net volumetric change (m^3) was also calculated. In order to compare the different units between sites, a normalized volumetric level (NVL in m^3 m^{-2}) was calculated by dividing the volume by the area for each respective unit in 2001 and 2007, and using this to determine the normalized net volumetric level (NNVL in m^3 m^{-2}) through this period. Using the NNVL makes it possible to determine temporal changes in unit volume and to compare amongst the sites. The fifteen cross-shore profiles that were extracted from the LIDAR data set are shown in Appendices from 6.6-6.8. This set of profiles was used to determine characteristics of foredune-morphology at the three study sites.

A. Brickyard Lane (BL)

A.1. Spatial and temporal morphological variation from 2001-2007

Figure 6.15 shows the LIDAR DTMs for BL generated for 2001 and 2007 as well as a DTM of difference between the two. Most of the morphological changes occur in the foredune and at the seaward side of the tidal beach. There is a clear development of the foredune from discontinuous high spots in 2001 to a clear ridge up to 7 m high in 2007 (Figure 6.15E). Figure 6.15F showing the difference DTM of the foredune and upper beach clearly indicates elevation gain up to 2.5 m. The total sand gain is 8761.35 m^3, equivalent to 1460.2 m^3 $year^{-1}$ (Table 6.8), resulting mainly from the accretion of the secondary foredune in the north and also the linear primary foredune. Between 2001 and 2007, the foredune gained sand. However, the increase of foredune seaward extension was more important than the sand volume gain, resulting in a negative normalized net volumetric level (NNVL) value of -0.60 m^3 m^{-2}. This suggests that vertical accretion was much lower than the horizontal foredune migration. The upper beach unit gained a small, evenly distributed quantity of sand (824.23 m^3) equivalent to 137 m^3 $year^{-1}$. A clear spatial morphological variability of the tidal beach is observed with an elevation loss in the north and gain in the south of the DTM (Figure 6.15C). A total negative volume change in the lower beach unit and tidal zone was up to -2759 m^3 $year^{-1}$ of sand which may have been redistributed in to the upper beach and foredune units. The mobility of the complex intertidal ridges-runnels may have influenced the overall morphological trend in the beach units.
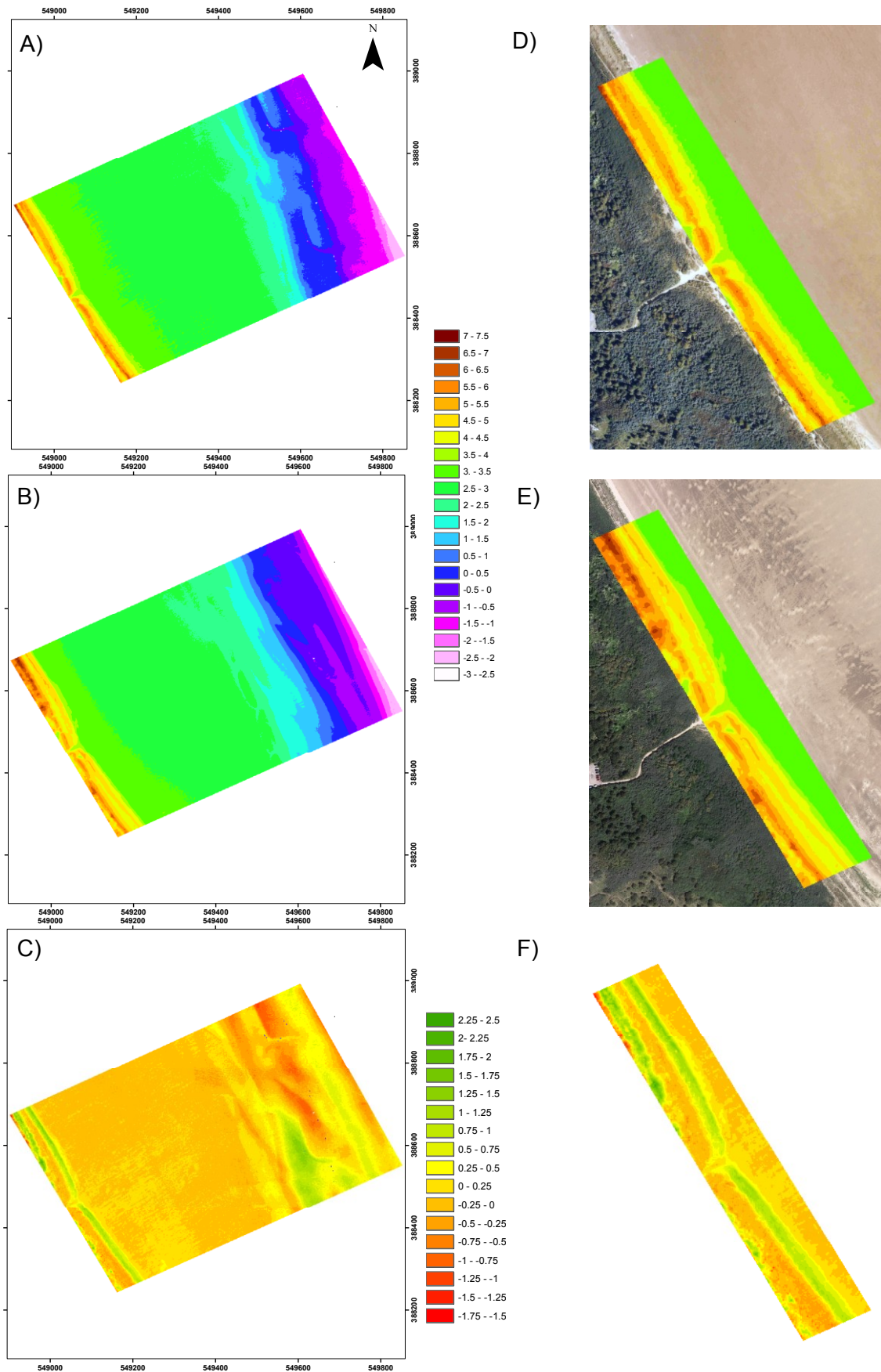
Figure 6.15. DTMs at BL site in: (A) 2001, (B) 2007 and (C) difference DTM derived from LIDAR. Enlargements show the foredune-upper beach in (D) 2001, (E) 2007 and (F) Difference DTM in more detail along the site.

Table 6.8. Sediment volume in different geomorphological units at BL for 2001 and 2007. Total DTM area is 356,108 m^2.

	Foredune		Upper beach		Lower beach		Intertidal zone	
	2001	2007	2001	2007	2001	2007	2001	2007
Volume (m^3)	121251.82	130013.17	30766.57	31590.80	669747.33	655220.38	24013.20	21987.32
Area (m^2)	23777.07	28892.89	9352.48	9335.34	285924.38	280730.28	37054.17	37149.59
Net budget changes (m^3)	8761.35		824.23		-14526.96		-2025.88	
Net budget changes per year (m^3 year^{-1})	1460.23		137.37		-2421.16		-337.65	
Normalized volumetric level (m^3 m^{-2})	5.10	4.50	3.29	3.38	2.34	2.33	0.65	0.59
Normalized net volumetric level (m^3 m^{-2})	-0.60		0 .09		-0.01		-0.06	

A.2. Morphometric and temporal variation

Morphological indicators that can be used to evaluate spatial and temporal changes in the foredune-beach system at BL are summarised in Table 6.9. The alongshore length of the DTM is 500 m at BL extends c. 50 m inland from the HAT contour. Morphological results of the cross-shore profiles extracted from the LIDAR DTMs (presented in Appendix 6.6) show that the secondary foredune height generally decreased slightly in 2007. However, the foredune was subject to a general seaward advance with a mean of 7.36 m and associated with an increase of sand volume corresponding to a mean of c. 41 m^3 m^{-1} (6.83 m^3 m^{-1} per year). The most significant morphological changes occurred in the upper beach and lower beach units, which decreased in volume by -68.73 m^3 m^{-1} in the former, while a relative similar positive volumetric change (72.96 m^3 m^{-1}) was recorded in the lower beach unit from 2001 to 2007. In general, the intertidal zone gained volume with a seaward move of the z=-1 m contour over the study period.

Table 6.9. Comparison of morphological indicators extracted from LIDAR data in 2001 and 2007 along cross-shore profiles at BL (for profile locations see Figure 6.2). Diff=difference.

Profile	Year	Elevation foredune (m)	Position z=3.5 m (m)	Width upper beach (m)	Width lower beach (m)	Position z=-1 m (m)	Volume foredune ($m^3 m^{-1}$)	Volume upper beach ($m^3 m^{-1}$)	Volume lower beach ($m^3 m^{-1}$)	Volume intertidal zone ($m^3 m^{-1}$)
A	2001	6.77	51.3	31.7	609.3	770	253.88	145.29	817.89	21.91
A	2007	6.43	57.2	8.5	584.2	760.3	296.61	56.03	1029.36	69.89
	Diff	-0.34	5.5	-23.2	-25.1	-9.7	42.73	-89.27	211.47	47.98
B	2001	5.53	52.3	45.4	579.5	751.8	236.02	149.44	743.75	32.89
B	2007	5.89	64	7.1	556.5	749.5	304.72	23.86	785.80	85.45
	Diff	0.36	11.7	-38.3	-23	-2.3	68.70	-125.58	42.05	52.56
C	2001	5.67	42.9	24.5	598.9	739.8	195.04	81.27	794.43	27.13
C	2007	5.55	44.8	16.4	572.3	742	207.70	53.88	793.34	70.28
	Diff	-0.12	1.9	-8.1	-26.6	2.2	12.66	-27.39	-1.09	43.15
D	2001	5.74	44.5	13.5	588.3	728.2	206.78	44.70	788.88	35.24
D	2007	5.55	51.1	11.4	546.5	733	241.64	38.38	809.58	79.34
	Diff	-0.19	6.6	-2.1	-41.8	4.8	34.86	-6.32	20.70	44.10
E	2001	5.79	50.5	37.9	541.1	696.7	241.39	125.31	694.70	20.86
E	2007	5.55	61.6	9.1	540.9	720.8	287.25	30.23	786.35	53.72
	Diff	-0.24	11.1	-28.8	-0.2	24.1	45.86	-95.07	91.65	32.86

B. Theddlethorpe St Helens (TSH)

B.1. Spatial and temporal morphological variation in 2001-2007

Morphological variability of the foredune-beach system at the TSH site in 2001-2007 is presented in Figure 6.16, and the associated sediment volume measurements summarized in Table 6.10.

The DTM in 2001 shows that the foredune crest in the south was the highest at 8.5 m. Further north, the foredune elevation is, however, lower characterized by two isolated embryo dunes at the foredune toe up to 4.7 m high. The centre of the foredune unit displayed has a convex outline, contrasting with the flat upper beach morphology which has an elevation of c. 3.3 m. The upper beach has been characterized by a field of embryo dunes, which started to develop in 2001 as observed on the ortho-photograph observations. Between 2001-2007, significant morphological foredune changes occurred with a total accretion of 10,977 m^3 in the form of sand gain on the seaward dune slope. There is also merging and coalescence of the embryo dunes in the north (Figures 6.16B, E).

The area of the foredune unit reduced in 2007, which explains the decrease of the NNVL of -0.63 m^3 m^{-2} (Table 6.10). The foredune unit has only experienced horizontal accretion. The upper beach featured two well-developed embryo dune fields reaching up to 3.5 m in height in 2007. The difference DTM clearly shows the development of these embryo dunes on the upper beach, which gained nearly 2000 m^3 of sand between 2001 and 2007 (Figure 6.16C, F). The NNVL indicates a gain in elevation of the upper beach unit of 0.78 m^3 m^{-2}, corresponding to a vertical sand accumulation of 0.13 m^3 m^{-2} $year^{-1}$. Alongshore and continuous variation of accretion and erosion can be seen in the beach and tidal units which is attributed to cross-shore movement of ridges and runnels. A positive net budget change of 10,877.32 m^3 occurred in the lower beach unit with a NNVL of 0.13 m^3 m^{-2} (Table 6.10). However, the tidal zone lost twice as much as was gained on the lower beach.
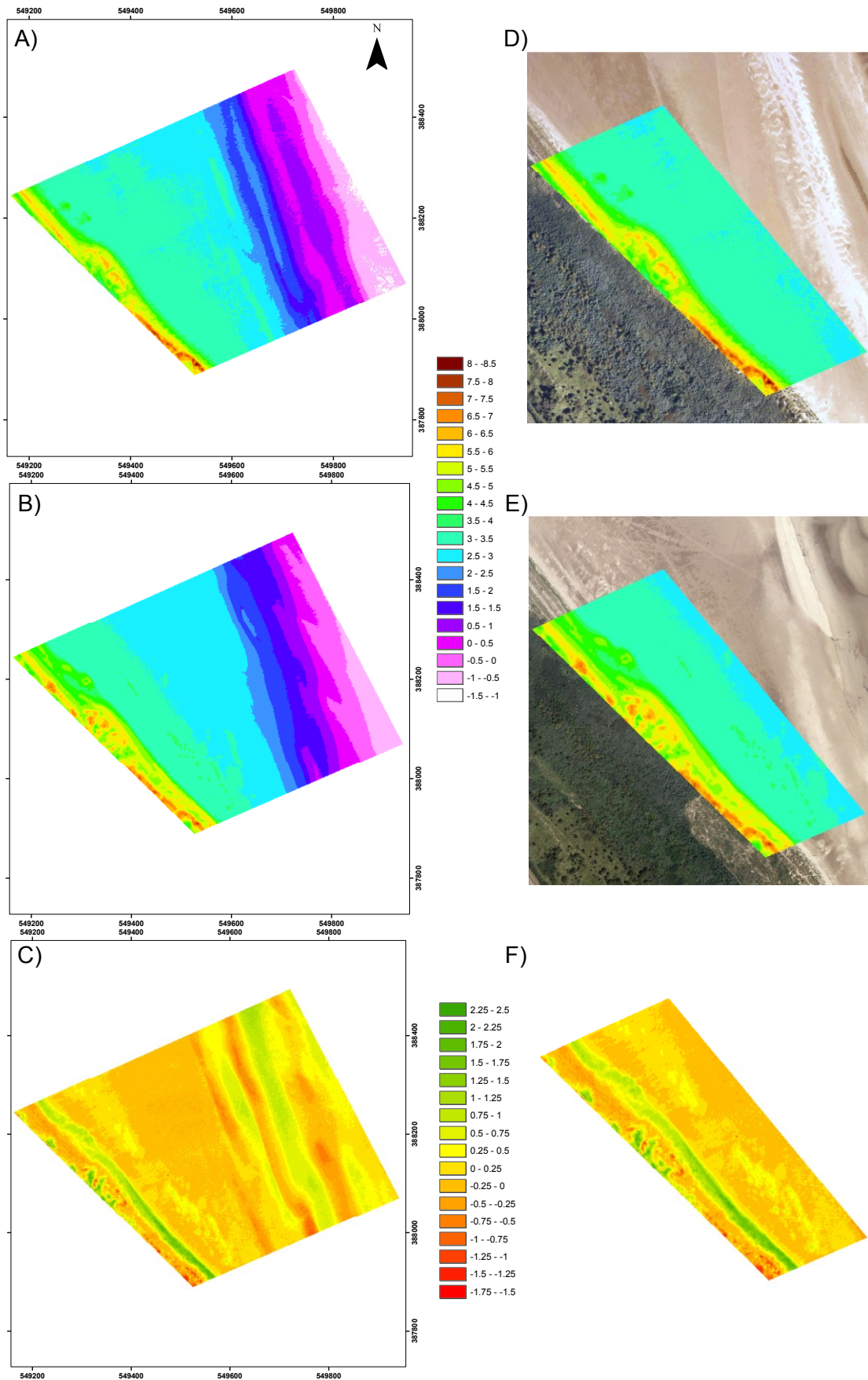
Figure 6.16. DTMs at TSH site in: (A) 2001, (B) 2007 and (C) difference DTM derived from LIDAR. Enlargements show the foredune-upper beach in (D) 2001, (E) 2007 and (F) Difference DTM in more detail along the site.

Table 6.10. Sediment volume in different geomorphological units at TSH for 2001 and 2007. Total DTM area is c.250,050 m^2.

	Foredune		Upper beach		Lower beach		Tidal zone	
	2001	**2007**	**2001**	**2007**	**2001**	**2007**	**2001**	**2007**
Volume (m^3)	136650.78	147628.11	42694.49	44694.44	394798.73	405676.05	16772.07	10798.42
Area (m^2)	25452.62	31183.29	12921.85	10936.51	186012.36	179950.04	25663.02	27979.16
Net budget changes (m^3)	10977.33		1999.95		10877.32		-5973.65	
Net budget changes per year (m^3 $year^{-1}$)	1829.56		333.33		1812.89		-995.61	
Normalized volumetric level (m^3 m^{-2})	5.37	4.73	3.3	4.09	2.12	2.25	0.65	0.39
Normalized net volumetric level (m^3 m^{-2})	-0.63		0.78		0.13		-0.27	

B.2. Morphometric and temporal variation

Table 6.11 summarises the morphometric and volumetric measurements along cross-shore profiles at TSH between 2001 and 2007 (presented in Appendix 6.7).

Results show a spatial variability of the foredune height with an increase in the north of the TSH but decrease in the south. The foredune unit accreted an average of 60.4 m^3 m^{-1}. Significant morphological change occurred in the upper beach unit with a sand gain ranging from 21.67 m^3 m^{-1} up to 197 m^3 m^{-1}, mainly due to the development of the embryo dunes on the upper beach. However, the lower beach unit experienced sand loss (mean of volumetric changes of -229.44 m^3 m^{-1}) associated with a decrease of its width. Overall the intertidal zone gained in sand from 2001 to 2007.

Table 6.11. Comparison of morphological indicators extracted from LIDAR data in 2001 and 2007 along cross-shore profiles at TSH (for profile locations see Figure 6.2). Diff=difference.

Profile	Year	Elevation foredune (m)	Position z=3.5 m (m)	Width upper beach (m)	Width lower beach (m)	Position z=-1 m (m)	Volume foredune (m^3 m^{-1})	Volume upper beach (m^3 m^{-1})	Volume lower beach (m^3 m^{-1})	Volume intertidal zone (m^3 m^{-1})
F	2001	6.08	40	25.1	497.5	668	227.86	133.07	615.99	36.15
F	2007	6.94	71.8	6.8	422.4	699.6	338.54	329.92	381.95	41.38
	Diff	**0.85**	**31.8**	**-18.3**	**-75.1**	**31.6**	**110.68**	**196.85**	**-234.04**	**5.23**
G	2001	5.53	66.6	34.7	450.2	598.1	321.98	55.06	731.15	36.29
G	2007	6.84	71.8	55.5	430.1	654.3	401.17	196.96	280.03	35.74
	Diff	**1.31**	**5.2**	**20.8**	**-20.1**	**56.2**	**79.19**	**141.90**	**-451.11**	**-0.54**
H	2001	5.56	49.6	31.7	312.1	515.4	238.05	340.8	300.31	24.77
H	2007	6.11	74.4	50.4	233	494.5	254.51	379.62	69.12	40.52
	Diff	**0.55**	**24.8**	**18.7**	**-79.1**	**-20.9**	**16.46**	**38.82**	**-231.19**	**15.75**
I	2001	7.56	38.5	38.5	376.1	501.2	197.47	75.93	476.51	32.51
I	2007	7.09	48.7	46.7	312.5	552	256.93	233.14	339.35	58.72
	Diff	**-0.47**	**10.2**	**8.2**	**-63.6**	**50.8**	**59.46**	**157.21**	**-137.16**	**26.21**
J	2001	8.41	46	28	296.8	503.4	253.51	179.31	300.17	28.27
J	2007	7.59	52.4	33.4	283.9	499.1	289.69	200.98	206.46	40.75
	Diff	**-0.82**	**6.4**	**5.4**	**-12.9**	**-4.3**	**36.18**	**21.67**	**-93.71**	**12.48**

C. Mablethorpe North End (MNE)

C.1. Spatial and temporal morphological variation in 2001-2007

Figure 6.17 and Table 6.12 indicate a spatial morphological variability of the different units at MNE between 2001 and 2007.

The foredune height in 2001 ranged from 8.7 m to 3.4 m tall whereas by 2007 it had become wider but lower. Comparison of the volume of sand incorporated in the foredune and upper beach units in 2001 and 2007 indicates a net sand gain of c. 18,741.69 m^3 and 1,709.09 m^3 respectively. The foredune gained more sand between 2001 and 2007 than any other unit. Much of this may be associated with the installation of sand trapping fences in 2000. Vertical deposition and seaward advance of the foredune is apparent and regular along the site (Figure 6.17C), and confirmed by an increase of its area and NNVL of 0.3 m^3 m^{-2} equivalent to an elevation gain of 0.05 m^3 m^{-2} $year^{-1}$. The upper beach increased in both sand volume and extended seaward in 2007, but the low NNVL value of 0.02 m^3 m^{-2} suggests that the vertical accretion was lower than horizontal sand gain. Figure 6.17C displays remarkable continuous alongshore variations of accretion and erosion controlled by the inland ridge-runnel at the top of the beach unit. However, this continuity became less obvious on the beach due to the presence of tidal drainage channels dissecting ridge-runnels. In general, sand loss dominated the lower beach unit, where volume change of -5,053.41 m^3 was recorded. The difference DTM indicates an accretion of the tidal zone where a positive net budget change was recorded of 3,514.16 m^3 (Table 6.12).
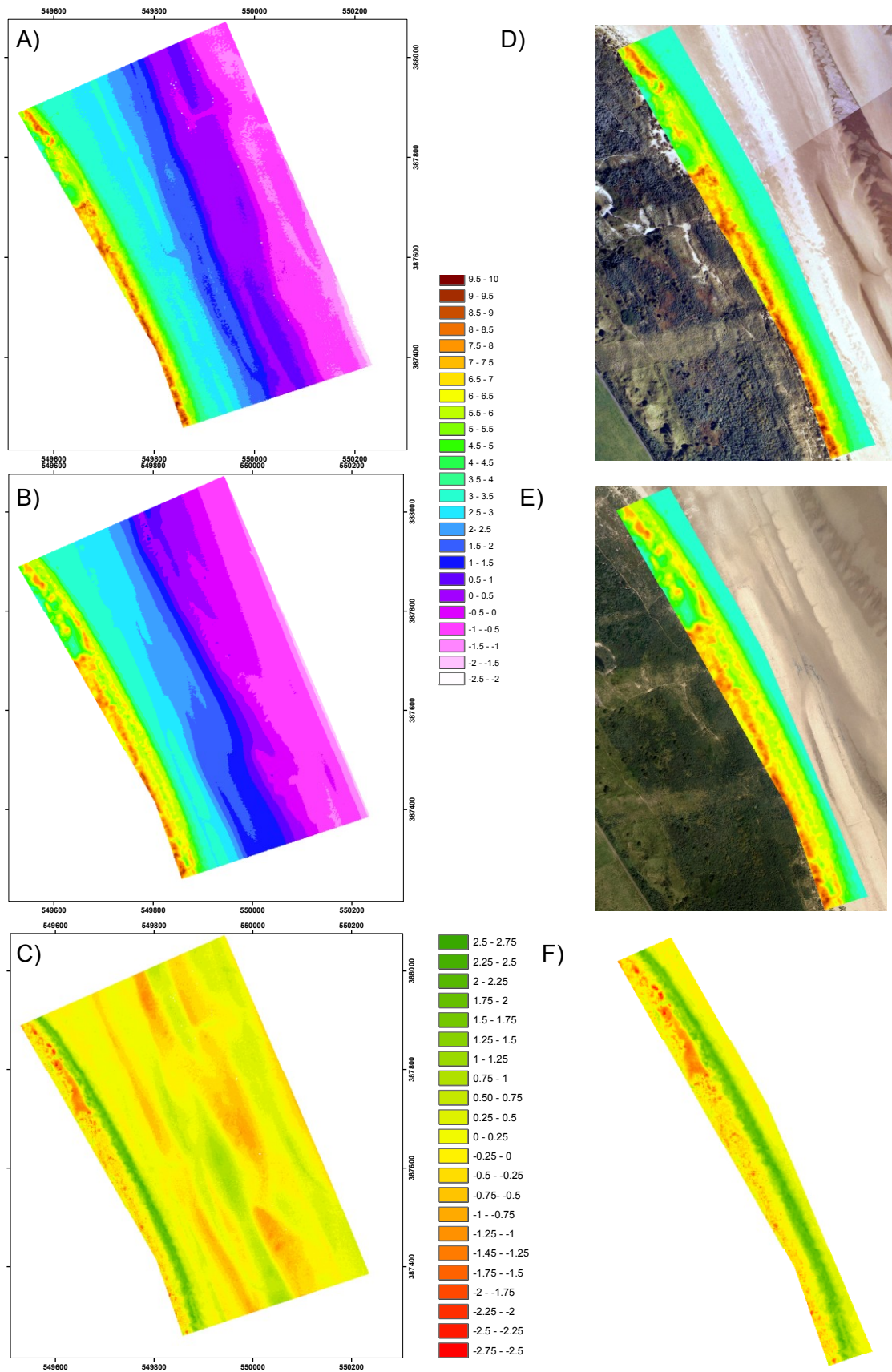
Figure 6.17. DTMs at MNE site in: (A) 2001, (B) 2007 and (C) difference DTM derived from LIDAR. Enlargements show the foredune-upper beach in (D) 2001, (E) 2007 and (F) Difference DTM in more detail along the site.

Table 6.12. Sediment volume in different geomorphological units at MNE for 2001 and 2007. DTM size is 310,260 m^2.

	Foredune		Upper beach		Lower beach		Tidal zone	
	2001	2007	2001	2007	2001	2007	2001	2007
Volume (m^3)	234487.70	253229.39	30001.58	31710.67	250060.67	245007.26	44361.09	47875.25
Area (m^2)	39379.6	40504.5	9232.96	9692.41	172338.65	169825.00	89309.21	90238.51
Net budget changes (m^3)	18741.69		1709.09		-5053.41		3514.16	
Net budget changes (m^3 year^{-1})	3123.62		284.85		-842.23		585.69	
Normalized net budget (m^3 m^{-2})	5.95	6.25	3.25	3.27	1.45	1.44	0.50	0.53
Normalized net budget level (m^3 m^{-2})	0.3		0.02		-0.01		0.03	

C.2. Morphometric and temporal variation

Analysis of the cross-shore profiles (presented in Appendix 6.8) indicated a general decrease of the foredune height between 2001 and 2007 with the exception of the northern profile (Table 6.13). However, the foredune unit increased in width and gained c. 76.5 m^3 m^{-1} of sand. Although the morphological changes in the upper beach unit were variable, accretion of 11.5 m^3 m^{-1} took place. By contrast, the measurement of the lower beach unit show a decrease of the width associated with a sand gain with a mean of 13.7 m^3 m^{-1} so that an increase of the elevation of the beach probably occurred from 2001 and 2007. A mean accretion of c. 40 m^3 m^{-1} was observed in the intertidal zone.

Table 6.13. Comparison of morphological indicators extracted from LIDAR data in 2001 and 2007 along cross-shore profiles at MNE (for profile locations see Figure 6.2). Diff=difference.

Profile	Year	Elevation foredune (m)	Position z=3.5m (m)	Width upper beach (m)	Width lower beach (m)	Position z=-1m (m)	Volume foredune ($m^3 m^{-1}$)	Volume upper beach ($m^3 m^{-1}$)	Volume lower beach ($m^3 m^{-1}$)	Volume intertidal zone ($m^3 m^{-1}$)
K	2001	6.37	59.9	11.9	272.2	411.2	291.89	39.87	186.741	33.44
K	2007	7.32	71.6	7.5	251.8	427.7	348.81	24.88	201.814	46.93
	Diff	**0.95**	**11 .7**	**-4.4**	**-20.4**	**16.5**	**56.92**	**-14.99**	**15.07**	**13.49**
L	2001	8.48	57.7	27.1	240.5	357.7	344.02	90.43	116.63	11.31
L	2007	7.53	73.8	26.2	155.5	427.6	440.29	85.52	153.14	92.07
	Diff	**-0.95**	**16 .1**	**-0.9**	**-85**	**69.9**	**96.27**	**-4.91**	**36.50**	**80.76**
M	2001	8.71	58.5	4.7	241.5	355.5	340.69	15.59	118.31	18.64
M	2007	8.16	69.6	9.5	178.5	390.1	416.18	31.84	168.05	59.35
	Diff	**-0.55**	**11 .1**	**4.8**	**-63**	**34.6**	**75.49**	**16.25**	**49.74**	**40.72**
N	2001	9.07	49	43.5	180	345.3	282.69	135.89	51.46	26.66
N	2007	8.31	57.8	35.7	168.2	375.6	352.03	113.93	79.86	44.20
	Diff	**-0.76**	**8.8**	**-7.8**	**-11.8**	**30.3**	**69.34**	**-21.96**	**28.40**	**17.53**
O	2001	8.66	46.9	6.5	215	357.4	269.37	22.25	130.73	22.81
O	2007	8.51	59	33.5	135.4	373	354.01	105.22	69.50	68.28
	Diff	**-0.15**	**12.1**	**27**	**-79.6**	**15.6**	**84.65**	**82.97**	**-61.23**	**45.47**

6.3.4. Comparison of Morphological Change Using the Three Data Sources

The different estimates of foredune height and toe position and height using the three data sources described were compared (Figure 6.18). Linear regression was applied to compare the foredune distance at L2E7 and L2D1 profiles all referenced to its position in 1992. Further transects were generated to match to the location of the EA profiles (Figure 6.2).
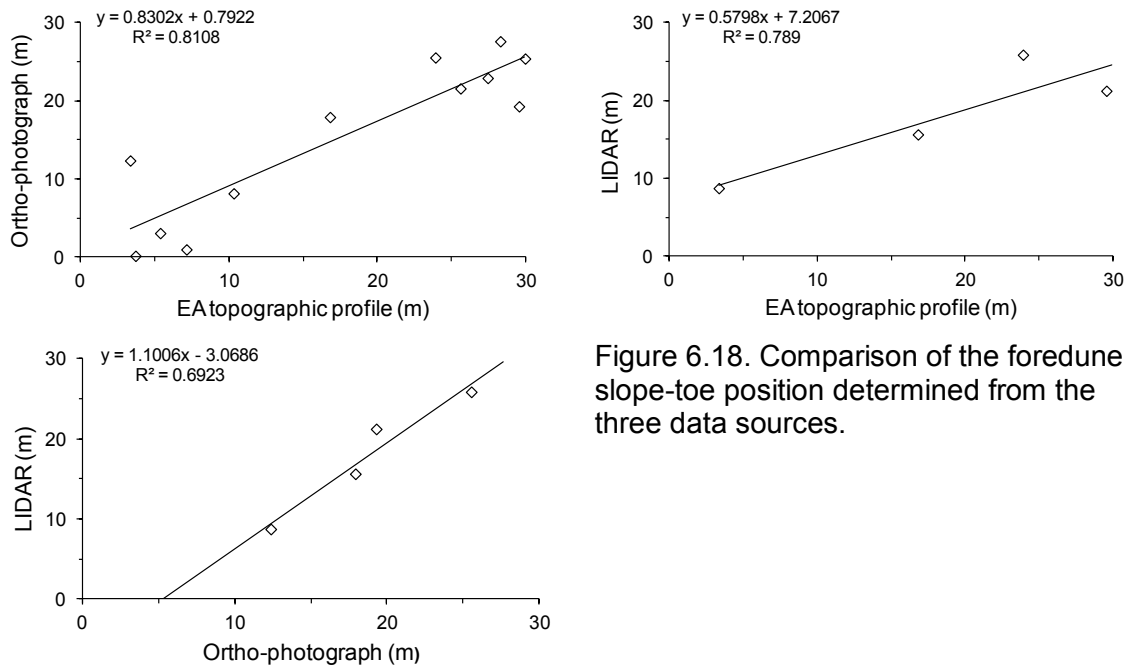
Figure 6.18. Comparison of the foredune slope-toe position determined from the three data sources.

A significant relationship is found between the estimates of the foredune position between EA topographic profiles and ortho-photographs (R^2=0.811). Although the number of data points was limited for the comparison between LIDAR and EA topographic profiles or ortho-photographs, the results show some consistencies. Vertical comparisons between the data sources were also undertaken by determining the average of the difference of the foredune toe-slope elevation estimates. The difference was relatively small ranging from 0.02 m (between EA topographic profile and DEMs derived from aerial-photograph) to 0.19 m (between DEMs and LIDAR data).

6.3.5. External Forcing Factors

Strong onshore and/or landward-directed alongshore winds coinciding with an astronomical high tide result in storm surges that could be responsible for substantial changes in coastal foredune evolution, in particular with regards to the overall annual accretion rates. The analysis of forcing factors for the period 1993-2009 reveals a low occurrence of high wind speeds exceeding 14 m s^{-1} and water levels above 3.5 m. Results indicated that 32 storm surges occurred from 1993 to 2010 (Appendix 6.4), but none were recorded in 1994, 1995, 2002 or 2003. The highest annual storm surges are presented in Table 6.14. For the study period, most storm surges resulted from only 1 to less than 3 hours of observations of potentially eroding high water levels, but this does not mean that the storm surge events were limited to this short duration. It may be due to the fact that the large tidal range restricted the time during which the foredune toe could be reached during a storm surge.

Over the study period, the highest water level during a storm surge event occurred in 1998. The average wind speed recorded at Donna Nook during the 1998 storm event was 15.52 m s^{-1} with a dominant wind direction of 10° (oblique onshore). In response to this strong wind speed, water level attained a height of 4.32 m with a surge of 0.13 m. The hindcast significant wave height reached a peak of 6.3 m, and the SESI was 12.92. The storm surge in 1993 was also violent with the highest mean wind speed up to 21 m s^{-1} and oriented at 30°; a low atmospheric pressure of 998hPa and a recorded water level of 4.16 m with a surge of c. 0.7 m gave a SESI value of 14.02. However, the most significant SESI of 16.07 was calculated for a storm event in 1996 when the storm surge duration was nearly 3 hours characterized by a water level of 4.22 m, a surge of 0.4 m and wind speeds reaching 20 m s^{-1} oriented at 10°. The greatest annual frequency of 8 storm surges was recorded in 1996, and caused significant foredune erosion along the study area (pers. com. John Walker, Natural England) (Appendix 6.5). Between 1996-2001, the mean of water level ≥3.5 m occurred more than four times per year, and exceeded that level by several tens of centimetres each time. Over the period 2004-2010, water level ≥3.5 m is exceeded at least once every year, however three and two storm events occurred in 2007 and 2008 respectively. Over the recent period from 2004 to 2010, the potential foredune erosion events diminished with lower SESI values ranging from 6.92 to 0.15.

Table 6.14. Summary of the number of storm surge events per year and parameters of the annual highest storm event over the period 1993-2009.

Year	Number of storms	Duration of all storm events (hour)	Duration of the highest storm event (hour)	Highest water level (m)	Surge (m)	Wind speed at Donna Nook (m s^{-1})	Adjusted wind speed (m s^{-1})	Wind direction (°)	Hs (m)	Pressure (hPa)	SESI
1993	2	3.5	2.5	4.16	0.68	20.87	21.54	30	8.46	998	14.02
1996	8	10.75	2.75	4.22	0.39	20.00	20.65	10	8.33	1014	16.07
1997	3	2.5	1.5	3.74	0.22	17.13	17.69	90	5.48	1022	1.93
1998	4	5.25	2.5	4.32	0.13	15.52	16.03	10	6.29	1026	12.92
1999	1	0.25	0.25	3.64	0.09	14.39	14.86	60	5.83	1020	0.41
2000	2	2	1.75	3.80	0.37	17.73	18.31	360	7.19	1005	3.74
2001	2	3.5	2.25	4.12	-0.01	17.13	17.69	350	6.93	1007	9.63
2004	1	0.5	0.5	3.84	0.39	15.42	15.92	360	6.25	1020	1.07
2005	1	2	2	3.96	0.44	18.76	19.37	350	7.61	1012	6.92
2006	1	0.75	0.75	3.98	0.13	15.42	15.92	360	6.25	1002	2.23
2007	3	2.75	1	3.88	0.30	17.99	18.57	350	7.29	1006	2.80
2008	2	1.5	0.75	3.79	0.35	15.42	15.92	350	6.25	1023	1.34
2009	1	0.50	0.50	3.67	0.39	14.39	14.86	20	5.83	990	0.50
2010	1	0.75	0.75	3.53	0.36	15.43	15.93	350	6.26	1012	0.15

Comparison of the values of the SESI indicates that foredune erosion events are likely to occur with direct or slightly oblique onshore winds (10°-30°) which seem to be associated with the longest storm surge duration and significant wave heights. Therefore, time series records reveal an inter-annual variability of storm activity characterized by high frequency in 1996-2001 and a low frequency in 2004-2010. However storm surge impact will differ from one storm to another, depending on wind conditions, water level, fetch, wave characteristics and also the morphology of the foredune-beach system.

A. Drivers of potential seasonal and spatial variability of the foredune

The temporal series of extracted storm surges and the SESI parameter indicates the potential cumulative impacts of storms in winter and summer that may affect foredune-beach topographic profiles at BL and MNE.

A.1. Storm surges affecting the winter profile

Figure 6.19A shows 14 storm surges occurring over the seasonal periods 1st July to 31st December from 1993 to 2010, but highest seasonal SESI values were in 1993, 1996 and 1998. The foredune experienced relative stability or a slight accretion at BL between 1993-1998, however volumetric variability characterized the upper beach, varying from 48.50 m^3 m^{-1} to -46.82 m^3 m^{-1}, with the lower beach varying from 101.69 m^3 m^{-1} to -66 m^3 m^{-1} (Figure 6.19B). In the south at MNE, the foredune was likely affected by the storm surge events in 1993 as the z=3.5 m contour retreated landward by 9 m, and -36.30 m^3 m^{-1} of sand was removed (Figure 6.19C). The greatest morphological changes were observed at MNE in 1995 with a significant seaward advance of 25 m of the z=3.5 m contour and an accretion of the foredune by 95.42 m^3 m^{-1} due to the development of the incident foredune (see section 6.3.1.B). A high temporal morphological variability also occurred in the upper beach and lower beach units dominated by a sand loss between 1994-1995. The high storm surge activity in 1996-1997 affect the upper beach at MNE, however sand loss in the foredune was only recorded in 1996. At BL, the foredune and upper beach experienced accretion of 3.55 m^3 m^{-1} and 36.20 m^3 m^{-1} in 1997, while sand loss of -51.42 m^3 m^{-1} was recorded in the lower beach.
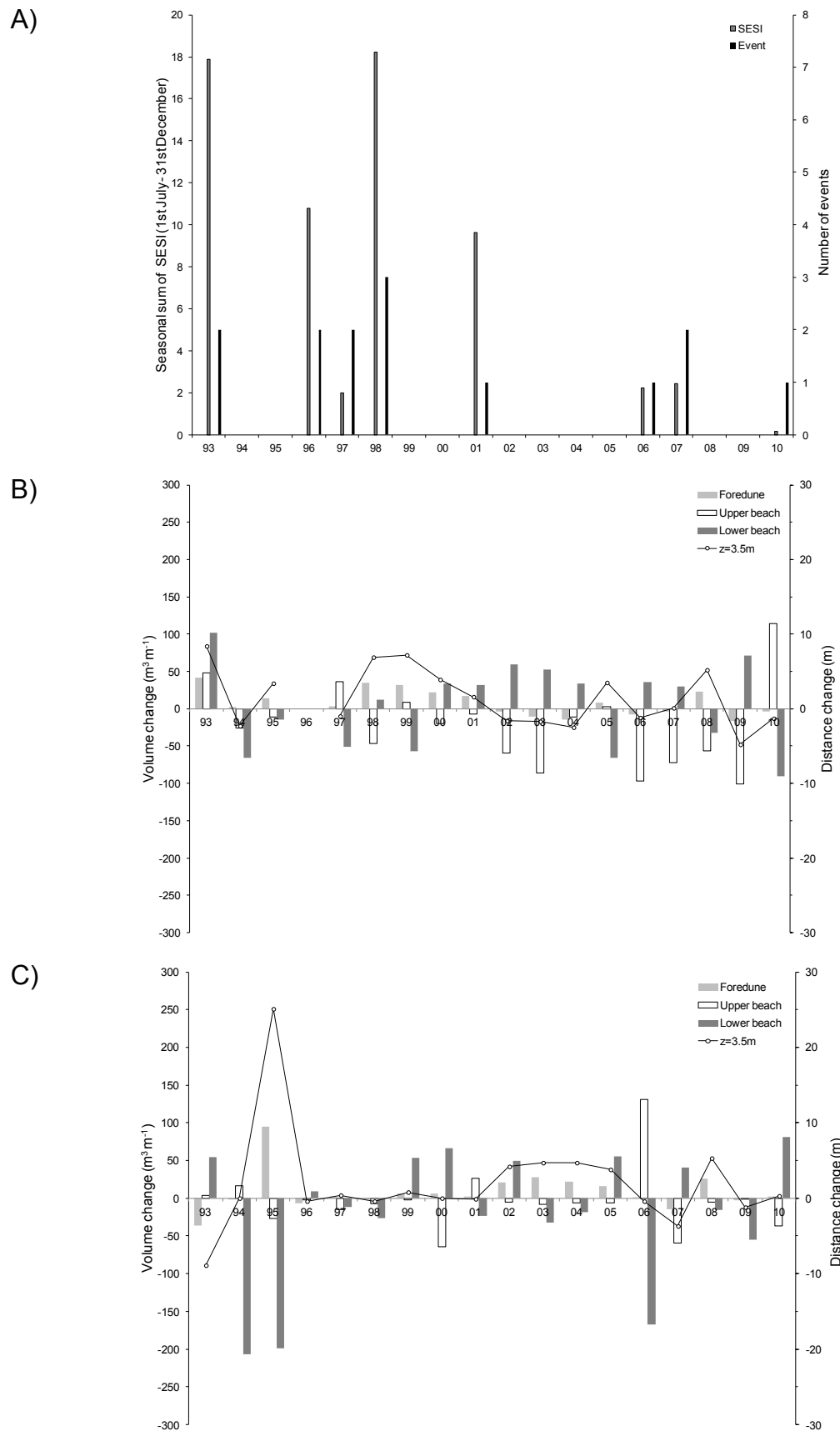
Figure 6.19. (A) Winter SESI parameters determined along the study coast and volume changes of the foredune, upper beach and lower beach units, and foredune distance change (i.e. position of z=3.5 m) representative of: (B) BL and no survey was recorded in Winter 1996 and (C) MNE. Initial survey in summer 1992.

By contrast, no storm surge potentially affecting the winter profile occurred over the period 2002-2005, and both accretion and erosion were observed in the foredune at BL. The upper beach lost sand whilst the lower beach unit gained sand in 2002-2004. This calm period is reflected in the accretion of the foredune at MNE. However, the upper beach was subject to a slight sand loss, and no clear trend can be observed for the lower beach unit. Storm surge events occurred over the seasonal period between July-December in 2006 and 2007 with a small SESI value, possibly causing a slight sand loss in the foredune, however the morphological changes were greater for the upper-beach at both sites. Erosion exceeded -170 m^3 m^{-1} for the upper-beach at BL over this period. Over the recent years, only one winter storm surge event occurred in 2010 with a low SESI value of 0.15, possibly causing a slight sand loss for the foredune at BL. However, accretion and erosion occurred at the upper beach and lower beach respectively. At MNE, the major morphological changes were sand loss from the upper beach and gained on the lower beach, whereas the foredune was relative stable.

A.2. Storm surges affecting the summer profile

Figure 6.20A shows 18 storm surges occurred over the seasonal periods from 1st January to 30th June from 1993 to 2010, but none was recorded from 1993-1995, from 2002-2003 or in 2010.

The greatest cumulative SESI value of 43 was estimated in 1996, which incorporates 6 storm surge events mainly from 10°-30° direction. Storm impacts do not appear to have affected BL, because accretion dominated each unit. However, a significant sand foredune loss of -208 m^3 m^{-1} took place in the south of the study area at MNE.

A)

B)

C)
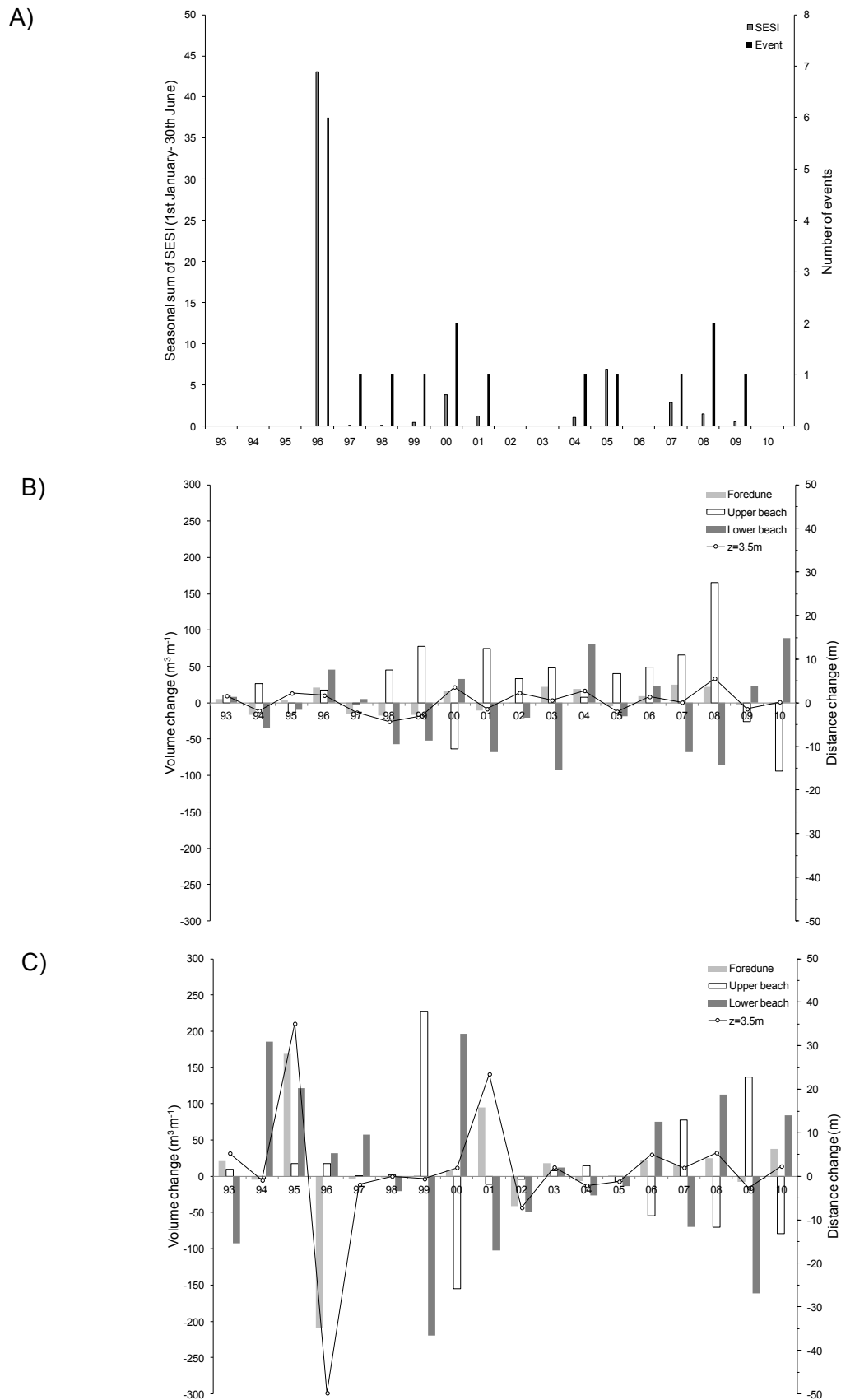
Figure 6.20. (A) Summer SESI parameters determined along the study coast and volume changes of the foredune, upper beach and lower beach units, and foredune distance change (i.e. position of z=3.5 m) at: (B) BL and (C) MNE. Initial survey in winter 1993.

From 1997-2001, a minimum of one storm event per 6-months occurred with SESI ranging from 0.11 to 3.75. The foredune unit was subject to erosion and retreat of the $z=3.5$ m contour over the pre-summer surveys in 1997 and 1998 at both BL and MNE (Figure 6.20B, C). From 2002 to 2003, no storm surge events were recorded over the seasonal period from January to July. An accretion of the foredune and upper beach units dominated at BL, while positive morphological change of the foredune and upper beach was only recorded at MNE in 2003. An average of one storm event per year occurred in 2004 and 2005 associated with a SESI values of 1 and 7 respectively. However sand loss from both the foredune and lower beach units, and also a retreat in foredune toe position were recorded at BL in 2005, while the upper beach experienced accretion. The opposite occurred at MNE, where sand loss of -7.09 m^3 m^{-1} and -26.75 m^3 m^{-1} took place in the foredune and lower beach respectively.

Before the summer survey, storm surge events were recorded once or twice per year from 2007 to 2009. Along both sites, the foredune unit did not seem to be affected, however significant morphological changes occurred on the upper and lower beach units with gained and lost sand respectively. These trends were similar in 2010, where foredune and beach units were relatively stable or in accretion, whereas the upper beach was subject to erosion.

A.3. Years

As previously presented, annual storm surge analysis shows two distinct periods of high storm activity between 1996 and 2001, and between 2004 and 2010, and an isolated year in 1993. Two years of relaxation time separated each storm surge period (1994-1995, and 2002-2003) the second year of which was dominated by accretion at BL and MNE (Figure 6.21B, C).
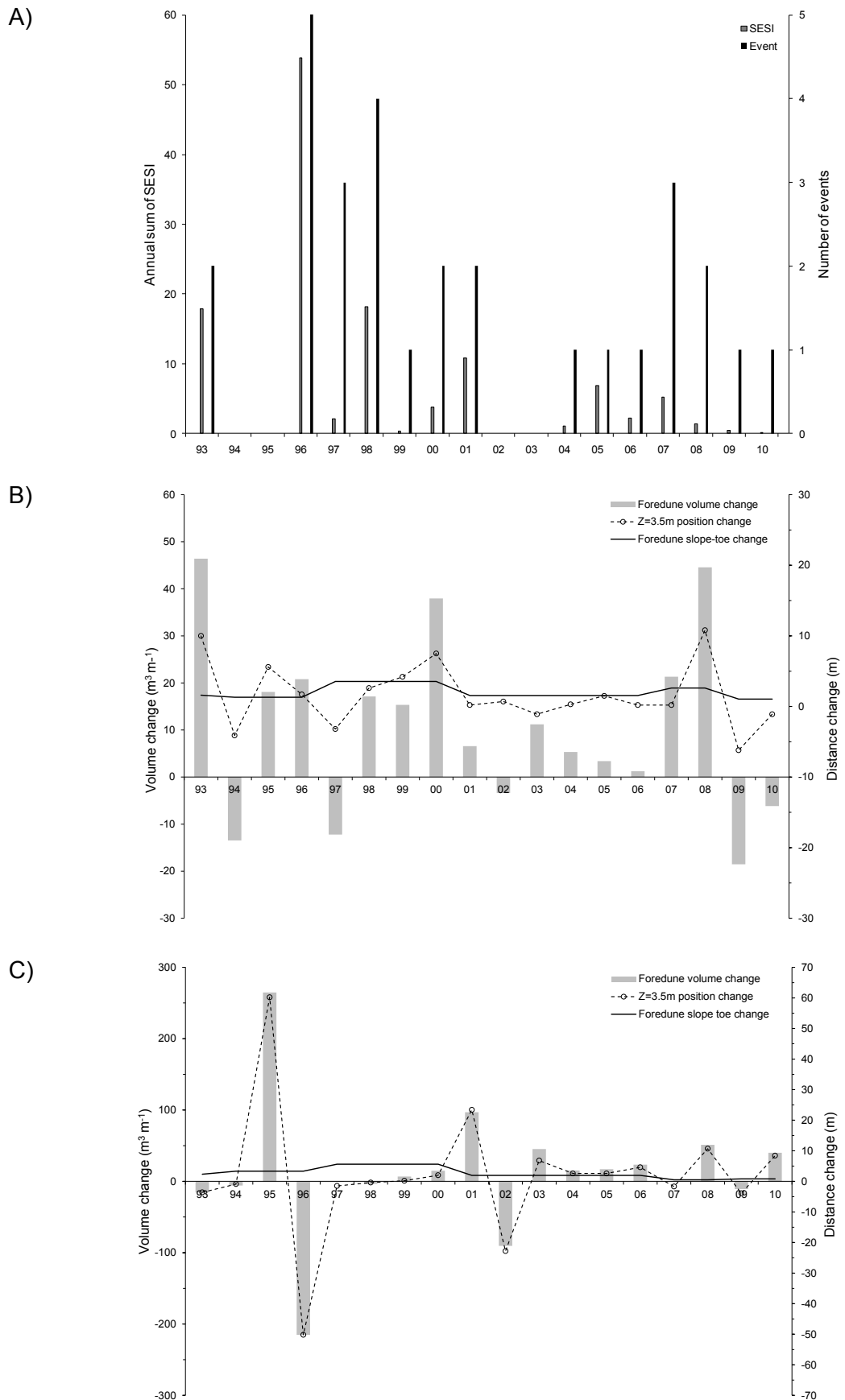
Figure 6.21. (A) Annual cumulative SESI, and cross-shore topographic changes of foredune volume and HAT position, and alongshore changes of the foredune toe-slope at: (B) BL and (C) MNE. Note the difference of the vertical axes.

Between 1996-2001, 20 storm surges occurred with a SESI value ranging from 54 in 1996 to 0.4 in 1999 (Figure 6.21A). The high SESI value in 1996 suggests a high potential foredune impact. Although the greatest foredune slope-toe seaward migration was recorded at both sites from 1997-2001, topographic profiles have indicated a sand loss in the foredune unit at BL in 1997 and at MNE in 1996. However, this was followed by accretion and relative stability for the northern and the southern sites respectively. For the recent years (2002-2010), accretion generally dominates the foredune at BL. Foredune sand gain was recoded at MNE over the recent years with the exception in 2002 and 2009. This is also reflected in the foredune slope toe changes migrating seaward at a rate of c. 2 m year^{-1} along the study sites. The cross-shore topographic profiles indicated that the position of z=3.5m contour was temporally variable at both sites. Between 2004 and 2010, 10 storm surges were recorded, and had lower cumulative SESI values ranging from 0.15 to 7. Over this period, sand gain dominated at BL with an important accretion of c. 45 m^3 m^{-1} and seaward advance of the z=3.5 m in 2008. The foredune experienced a sand gain or relative stability along the cross-shore profiles associated with the lowest rate of foredune toe-slope seaward advance at MNE. In 2010 there was further volume loss at the northern site, whereas at MNE there was a gain in sand volume.

6.4. Discussion

Bi-annual topographic profiles have provided useful data concerning changes in morphology and sand volume at the study sites over two-decades. Data resolution is high but analysis is limited to cross-shore profiles. A useful complement to these profiles is aerial photograph analysis which although less accurate, provides more information about the spatial variability of foredune-beach morphology, and LIDAR data which provide more detailed, accurate three-dimensional data but for only two occasions. A small difference amongst the foredune morphology measurements from the three data sources suggests that they could be combined.

6.4.1. Foredune-Beach System Morphological Changes at Intra- and Inter-Annual Scales

Seasonal morphological changes of the foredune-beach system were examined by splitting topographic profiles and forcing factors between summer (January-June) and winter (July-December). This also attempts to observe the impacts of the storm surge on the system; and is further discussed in section 6.4.2. Over the 1992-2010 period, the cross-shore topographic profiles at BL have shown a clear gradual sand accretion and seaward advance of the foredune, contrasting with variable trends in morphology of the upper beach unit and a slight decrease in size of the lower beach unit. At MNE in the south, foredune morphology was also dominated by a rapid seaward advance and sand gain. However, the morphological trends of beach units are less clear due to temporal fluctuations in sand budgets. Cross-correlation analyses of the topographic profiles have also indicated little morphological change at BL over the seasonal and annual periods (Figure 6.9). However, intra-annual (summer versus winter) morphological changes have been shown to be slightly greater than at the inter-annual scale at MNE (Figure 6.12). While it was not possible to identify any clear seasonal patterns in upper beach or intertidal zone characteristics, foredune accretion was more likely to occur during the summer than in winter. Such a trend has been identified elsewhere (Morton, 1991, Crowell et al., 1991, Ruz and Meur-Férec, 2004, Suanez and Stéphan, 2006, Anfuso et al., 2007) and is linked to constructive wave processes under fair-weather conditions in summer.

Temporal and spatial variability of the foredune slope toe elevation was low along the south of the study area (Figure 6.14), however a spatial south-north variability in foredune seaward migration was observed from a mean annual rate of almost 2.4 m year^{-1} at MNE to less than 2 m year^{-1} at BL. Although the BL site is characterized by a large beach which may reduce wave energy, a lower long-term seaward foredune migration took place over the last decades. It is possible that the foredune at BL may be a transferring path to the southern section of the coast and not a final deposition zone. At TSH, a recent well-developed and vegetated embryo dunefield has developed on the upper beach since 2001 and appears to protect the foredunes from storm erosion allowing rapid and sustained accretion. The embryo dunes are also a potential sand source for foredune post-event recovery. At MNE, the greatest foredune accretion has probably been enabled by the presence of nearshore sand banks and coastline orientation reducing wave energy and storm surge impacts. The presence of fences, located just south of the site, has also probably promoted sand storage. This alongshore variability is thus probably attributable to differences in morphological and environmental characteristics which influence the process-interaction within the foredune-beach system, and also shoreface morphology influenced by nearshore processes and littoral drift (Horn, 2002, Houser, 2009). Data concerning bathymetric changes will be presented in Chapter 7 and further discussed in Chapter 8.

Spatial and temporal vegetation patterns are closely linked to process-response relationships of foredune morphodynamics (Jackson and Cooper, 2011). Olivier and Garland (2003) reported that sand movement occurred at a rate that allowed vegetation on the foredune crests to grow in tandem with the establishment and growth of the pioneer plants, fixing the lateral position and favouring vertical foredune growth. In this study, geospatial vegetation classification analysis has revealed that the rapid foredune accretion and migration was associated with a slight and gradual increase of the vegetation cover. These observations suggest that the vegetation cover is an important parameter but it reflects as much as contributes towards the foredune accretion observed and is unlikely to be the main driver of foredune height gain and migration.

Three dimensional topographic (DTM) analysis was important for examining alongshore morphological variability. Volume changes determined from LIDAR surveys in 2001 and 2007 confirm that the foredune experienced a rapid and significant accretion at the three sites over this period. A relatively similar negative normalized net volumetric level value was measured in the foredune unit at BL and TSH. This suggests that the seaward migration of the foredune was associated with a decrease in its elevation. In contrast both sites experienced a positive NNVL of the upper beach unit. Specifically at TSH, the significant positive morphological change in the upper beach unit up to 0.80 m^3 m^{-2} is mainly due to the development of the embryo dunefield. Both horizontal and vertical accretion dominated the foredune and upper beach units at MNE site, suggesting an important sand transfer from the beach. Overall the sediment volume in the lower beach unit varied little suggesting that any sand exported to the dunes was compensated for by sediments arriving through cross-shore or alongshore transport.

At the three sites, changes in volume of the intertidal units were mainly attributed to alongshore variability of the ridge and runnel systems, and also the presence of a drainage channel observed on the LIDAR DTMs. In the study area, Van Houwelingen et al. (2006) reported that the multiple intertidal ridge and runnel system is permanent and very dynamic in the alongshore dimension at inter-annual timescales. Alongshore variability can also be dominated by the variation in drainage channel density and spacing related to the amount of water that needs to be drained during the falling tide. Further studies on intertidal barred beaches have underscored that the bedforms of channel can migrate alongshore and entrench the ridge-runnel systems (e.g. Anthony et al., 2005, Sedrati and Anthony, 2007). It is reasonable to argue that the significant volume changes observed in the lower beach unit and intertidal zone are unlikely to represent sand loss over the long-term, but rather are temporary changes caused by the alongshore movement of ridges and runnels, which were likely dissected by the development of the drainage channel between 2001 and 2007.

6.4.2. Influence of External Forcing Factors

The most appropriate approach to evaluating the impacts of storm surges on foredune morphology is clearly to obtain data concerning foredune-beach shape and volume immediately before and after a storm event and then to monitor subsequent recovery. This has been achieved very effectively by Morton et al. (1994, 1995), Houser and Hamilton (2009), Suanez et al. (2012) for specific events and suggests that the magnitude, frequency and recurrence intervals of storm surges are key determinants of their long-term impacts on foredunes. However for longer term studies, where secondary data and routine monitoring data sets are available at fixed time intervals such as bi-annually or annually, the probability of the image or data set being obtained immediately pre- or post- storm is low. At this meso-scale, where a variety of data sets is combined to determine longer-term patterns of foredune evolution it is therefore not usually possible to examine dune response to specific storm surge events but it may be possible to evaluate broad impacts. For example, if several high magnitude storm surges occur between one six-monthly survey and the next, some evidence of foredune erosion such as decrease in volume or slowing of the rate of seaward migration would be expected compared with a profile measured after 6-months of relatively calm conditions. Along the study coast, seasonal forcing factor analysis has shown that storm surge events were more frequent and of greater magnitude from January-June than July-December. No clear relationship was found between foredune-beach profile characteristics and storm surge occurrence over the preceding 6-months. This is most likely due to the 6-month survey interval which reveals a 'typical' mid-summer or mid-winter profile whereas for the purposes of this analysis an end-of-winter and end-of-summer would have been preferable.

Rapid accretion of the foredune is most likely to be a direct geomorphic response to the low frequency, high magnitude storm surges. Storm surge investigation based on water level, strong onshore wind speed and hindcast of significant wave height was undertaken with an estimation of the impacts of storm surge on coastal dunes through a storm erosion susceptibility index, depending on the intensity and duration of the storm surge and also the offshore significant wave height. Results indicated that 32 storm surges occurred from 1993 to 2010, 11 of which occurred in 1996-1997 and some of them were associated with high SESI values. Overall storm surges were more frequent during the earlier decade of interest suggesting coastal dunes potentially underwent erosion more often during more recent years. Storm surges from 1993-2001

were not only more frequent than in more recent years but were also of longer duration with higher water levels (Table 6.15). This was due to the occurrence of strong highly oblique onshore winds from 10°-30° related to the longest wave fetch. Additionally, higher frequency of strong winds and water level were observed in 1996. The use of the SESI index validated the higher storminess in 1996, and also permitted a better identification of individual years during which coastal foredune erosion was potential important. This storm surge activity period explains the observed foredune retreat at BL and decrease of mean rate of seaward migration at TSH and MNE. However, differences may occur between the frequency of high water levels and potential erosion for several years. For example, a high value of 18 in 1993 is not explained by more frequent high water levels, but by great magnitude of the storm surge events. Although the 1997-2001 period was characterized by high storm surge events, a high rate of foredune accretion was recorded at the three sites between this period.

Over the recent years (2002-2010), storm surge events were rare associated with low SESI values, which can be partly explained by the alongshore orientation of the storm surges and decrease in event duration. The morphological consequences of the storm surge events between 2002 and 2010 were temporally and spatially variable, however the rate of foredune migration decreased at the three sites over recent years. Spatial variability of the sediment volume availability and wave processes induce a localized pattern of coastal responses during a storm surge event (Cooper et al., 2004).

Several studies have suggested that there are no linear relationships between storm surge severity and the rate of foredune erosion due to the influence of various controlling and environmental factors (e.g. Morton, 2002, Chaverot et al., 2008, Houser, 2009). This is consistent with the present study, for which no clear seasonal and annual relationships were observed between SESI and meso-scale foredune development. The main reason is that the SESI integrates external forcing factors that occur at short timescales (episodic event). The morphological response of the foredunes depends on the occurrence of storm surge events, but also on controlling factors such as fair-weather induced constructive wave processes, wave- and tide-induced marine sediment transport; and efficient wind-induced aeolian sediment transport which can all positively influence sediment budget (e.g. Psuty, 1988, Saye et al., 2005).

At the meso-scale, the potential storm surge impact on coastal dunes is difficult to determine because it is not only dependent on the magnitude and frequency of external forcing factors, but is also significantly influenced by the antecedent beach state (Morton et al., 1995, Ruz and Meur-Férec, 2004). Recent research has suggested that extreme single storms may cause substantial foredune erosion, however consecutive storm surges often exceed the damage of one severe storm (Ferreira, 2005, Anfuso et al., 2007) due to lack of recovery time. Estimation of foredune response to storm surge events thus faces several difficulties related to the intrinsic short-and long-term morphology and behaviour of the beach. All phases of erosion and accretion are obviously not depicted from the aerial photograph analysis. However the EA cross-shore profiles at BL and MNE attempted to fill the gap between studied periods, although they only represent a specific location along the study area. Quantifiable records of coastal morphology rarely inform on the foredune positions recorded immediately before and after storm events. Analysis of the historical geomorphological record may therefore not provide definitive conclusions regarding the role and impact of storm surge in coastal foredune evolution. This is mainly due to the long intervals between records representative of the entire site and also caused by the inter-storm foredune reworking (Cooper et al., 2004). It is therefore quite challenging to predict foredune response to storm surge events.

At both BL and MNE, accretion was recorded during the 12-month monitoring (Chapter 4) and at the annual scale, whilst net erosion occurred at TSH. However, over the long-term (18-years) TSH has been shown to be accreting. The one year study of TSH was strongly affected by seasonal activity, but when examined over the long-term, erosion is shown to be short-lived (refer section 4.3.2.B). The foredune-beach system at TSH was likely subject to a seasonal variability in morphological changes, while its balance is reflected at medium- and long-terms. Previous studies have suggested that one year of monitoring only represents short-term foredune behaviour which could also reflect post-storm re-adjustment whether or not events occur during the same year (Morton, 1991, 2002, Cooper et al., 2004). Morton (1991) further suggests that monthly monitoring surveys over a long period make it possible to distinguish between seasonal variability and foredune trends. Sherman and Bauer (1993) reported that the meso-scale variations of foredune response may integrate the annual and decadal sequences of morphological attenuation and recovery. In Chapter 1, meso-scale was considered to range from months to decades, however this longer data set suggests

that it should be divided into short meso-scale (months- year) and long meso-scale (>1 year).

6.5. Conclusion

- Intra-annual (storm surge affecting summer topographic profile versus winter profile) morphological variability compared to the inter-annual variation is relatively similar at BL, but the latter is slightly higher at MNE.

- From 1992-2010, coastal foredunes in the study area underwent an average rapid seaward migration of 2.2 m year^{-1}. Accretion rates were more rapid in the south than the north of the area. Three-dimensional morphological analysis has also shown that the foredune became wider and lower at BL and TSH in 2007 compared to 2001, while both horizontal and vertical accretion took place at MNE.

- Analysis of historical meteorological and marine external forcing factors revealed high storm surge activity characterized the period from 1993-2001, while more recent years were relatively calm.

- Assessment of the storm erosion susceptibility index (SESI) suggests that the greatest impacts of storm surge on coastal dunes may occur during conditions of oblique onshore winds (10°-30°) which are likely to be associated with the longest storm surge duration and significant wave heights enhanced by long wave fetch. In general, no clear relationship was observed between SESI and foredune morphological changes.

- Storm surges do not appear to substantially slow down the rate of seaward migration which suggests rapid recovery and short relaxation time follows any eroding event.

Chapter 7. Macro-scale Foredune Evolution

7.1. Introduction

After demonstrating that the foredunes have experienced a significant accretion at the meso-scale in Chapter 6, this chapter up-scales to assess the long-term foredune evolution at the three study sites over a ~120 year period. Coastal changes are evaluated, in conjunction with climate and marine conditions with a view to characterizing the spatial and temporal trends occurring at the sediment cell scale.

Long-term coastal changes occur in response to a variety of factors including sea-level change (Orford et al., 1995), large-scale morphological self-organization (Cooper et al., 2007), changes in sediment budget associated with sources (e.g. rivers, cliff erosion), sinks (e.g. sand banks, submarine canyons) and alongshore transport (Pye, 1983), variations in storminess and wave climate (Zhang et al., 2001, Pye and Blott, 2008), and coastal management (Iskander et al., 2007, Kaminsky et al., 2010). The importance of littoral sediment budget as a control on the direction of coastline movement (i.e. accretion or regression) is widely recognized and is typically linked to the concept of the sediment cell. Ideal sediment cells are sections of coast that are relatively self-contained and include defined sources, transport pathways and sinks of sediment.

The delimitation and operation of coastal sediment cells reflects processes interacting at a range of spatial and temporal scales and in many areas coastal morphology and dynamics still reflect and are recovering from the impact of Holocene sea-level changes and deglaciation (May and Hansom, 2003). The concept of sediment cells focuses on wave-driven transport of non-cohesive sediments but within the cell boundaries many coastlines also include landforms dominated by cohesive material such as saltmarshes.

The coastline of England and Wales has been divided into eleven main coastal cells (Figure 7.1A), some of which also contain sub-cells (DEFRA, 2006). The study area is located in cell 2 which is divided into sub-cell 2a extending from Flamborough Head to Spurn Head, sub-cell 2b including the Outer Humber Estuary and sub-cell 2c extending along the Lincolnshire coast from Donna Nook to Gibraltar Point and mainly characterized by coastal dunes and also saltmarshes at Saltfleetby (Figure 7.1B). In the north of the sediment cell (sub-cell 2a), the Holderness glacial-till cliffs extend 60 km along the coast of East Riding and range in height from 3 m to 40 m. Significant erosion of these cliffs takes place through repeated landslide activity, caused mainly by waves undercutting the base of the cliffs and removal of beach material (Dossor, 1955). At main coastal towns this cliff line is fronted by lengths of sea defences (mainly sea walls and groynes). Coarse and fine sediment eroded from these cliffs and the shore platform are transported southwards to Spurn Head and to nearshore and offshore sand banks by the littoral drift and wave currents.

In this chapter, in addition to expanding the temporal scale of the research from two decades to over a century, the spatial scale is also expanded where possible to include the whole sediment cell, and seawards to the LAT and z=-5m contour levels to capture changes in bathymetry. Previous studies in sediment cell 2a, the Holderness coast have shown this area to be undergoing long-term retreat (e.g. Valentin, 1971, Posford-Duvivier, 1992, Balson et al., 1996, Quinn et al. 2009). The north Lincolnshire coast data presented in Chapter 6 of this thesis shows that it is undergoing accretion, whereas south of Mablethorpe there is another zone of coastal erosion caused in part by the lack of protective offshore sand banks (Dugdale and Vere, 1993). Sea defences have been built to protect against coastal flooding. To further counter this long-term erosion, a major beach renourishment plan began from Mablethorpe to Skegness in 1994 in order to replenish lost sediment along the frontage and continues to date (EA, 2004). Just south of Skegness, the coastline changes orientation providing a sheltered coast for accretive coastal dunes and saltmarshes at Gibraltar.
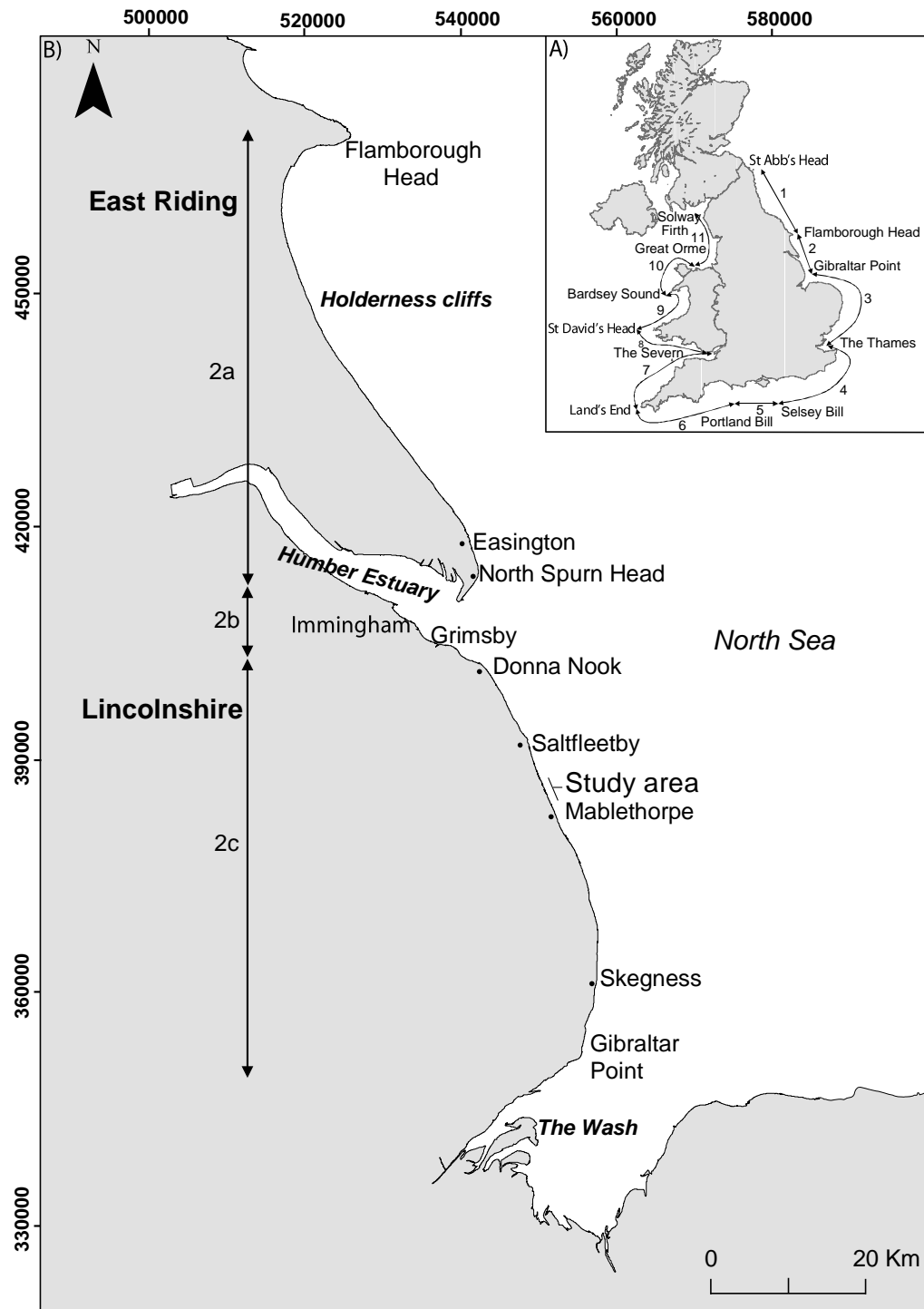
Figure 7.1. (A) Distribution of coastal cells around the coast of England and Wales, (B) boundaries and major features of sediment cell 2, east coast of England.

Controls on coastal morphology which operate within the whole sediment cell, and on a macro-scale have been rarely quantified (Pye and Blott, 2008). However, any study of coastal geomorphology changes without consideration of the interactions within the whole sediment cell is liable to be incomplete and any resulting resource management decisions compromised. The aim of this chapter is to investigate the inter-linkages between coastline and nearshore evolution within the whole sediment cell and their responses to climate forcing in order to get more insight about the long-term evolution of the foredune along the North Lincolnshire coast. The specific objectives are:

(1) Examine coastal trends of accretion or erosion within a whole sediment cell;

(2) Determine long-term foredune evolution over a ~120 year period (1891-2010);

(3) Develop a storm climatology catalogue to explore the long-term variability of the occurrence of potential forcing factors;

(4) Investigate the potential linkages between climate forcing trends and long-term foredune evolution.

7.2. Methodology

7.2.1. Coast and Nearshore Changes along Cross-Shore Profiles (from mid-1990s to 2010)

For the whole sediment cell, topographic surveys were used from the mid-1990s (either 1994, 1996 or 1997), 1999, 2005, 2008 and 2010 and were supplied for the Holderness coast by the East Riding of Yorkshire Council, and for Lincolnshire by the Environment Agency. For each year, a total of 160 profiles was analysed with spacing between profiles of 500 m along the East Riding coast and 1 km along the Lincolnshire coast. The profiles analysed for this study were generally surveyed during the summer or early autumn. Early surveys were conducted using standard total station equipment (horizontal accuracy ±0.1 m and vertical accuracy ±0.01 m) located over Ordnance Survey control points and referenced to the ODN datum as described in Chapter 6. However since 1999 and 2003 (East Riding and Lincolnshire coasts respectively), surveys have been made using a RTK GPS system. LIDAR surveys have been undertaken along the East Riding coast since 2008 (accuracy ranging from ±0.25 m to 2 m horizontally and from ±0.05 m to 0.15 m vertically). From these cross-shore topographic profiles were extracted along the same line used in the initial survey. Near-shore changes were determined using bathymetric profile surveys made as seaward extensions of the terrestrial cross-shore topographic profiles, and carried out by Gardline under contract to the EA in 1999, 2005 and 2008 along the Lincolnshire coast. The surveys employed single multi-beam echo-sounders, the accuracy of which has been estimated to be ±1m in the horizontal and ±0.005 m in the vertical (Gardline, 2008).

Scaling-up makes it difficult to examine the morphological changes in the same number of sub-units as Chapter 6 because the long-term data are not sufficiently detailed, so the focus here is on the coastline position defined as the foredune-beach interface or the cliffline. High resolution cross-shore profiles have proven reliable for determining two dimensional morphological changes through time and they were further linearly interpolated to 0.1 m for accurate identification of the HAT, ODN, LAT and z=-5 m levels (Table 7.1) for the sandy beaches at Spurn Head and along the Lincolnshire coast. As shown in Chapters 2 and 6, tidal reference and topographic contour levels can provide an objective, repeatable, robust way of identifying morphological sub-unit boundaries. However these are not necessarily appropriate along cliffed coastlines so along the East Riding sector, the top of cliff/cliff base position has been measured from

field or airborne surveys, and was assumed to provide a better representation of a cliffed coastline (Brooks and Spencer, 2010).

Table 7.1. Tidal levels and tidal ranges, expressed in metres above Ordnance Datum Newlyn (ODN). Tide level for East Riding coast derived from Spurn Head data taken from Admiralty Tide Tables (Admiralty, 2009) and from tidal statistics at Skegness derived from POLTIPS 3 software developed by the National Oceanography Centre Liverpool (NOC, 2009).

	Topographic domain				Bathymetric domain	
Coastal region	HAT	MHWS	MHWN	MLWN	MLWS	LAT
East Riding	3.80	3.00	1.60	-1.20	-2.70	-3.70
Lincolnshire	4.09	3.21	1.70	-1.09	-2.59	-3.57

7.2.2. Analysis of Long-Term foredune Foredune Evolution (1891-2010)

Historical foredune line change was estimated at Brickyard Lane (BL), Theddlethorpe St Helens (TSH), and Mablethorpe North End (MNE) for different time periods over the past ~120 years (Table 7.2). Historic OS maps surveyed in 1891 and 1910 were acquired from the Edina-Digimap website (Digimap, 2011). They were supplemented with ortho-photographs from 1953 to 1983, and printed aerial photographs from 1989 acquired from different suppliers (Table 7.2). Aerial survey acquisitions were generally during summer months, but a few flights were undertaken in autumn. The aerial photograph in 1989 was ortho-rectified by applying the same methodology described in Chapter 6. Changes post-1989 were analysed in Chapter 6 and the data presented there are used to bring the time series up to 2010.

Table 7.2. Map and aerial photograph source documents and characteristics.

Year	Document type	Source	Document type	Camera system	Lens type	Scale
1891	Map	Edina	OS map			1:10,560
1910	Map	Edina	OS map			1:10,560
1953	Aerial photograph	Natural England	Black+White ortho-photograph	Metric		1:7,500
1966	Aerial photograph	Natural England	Black+White ortho-photograph	Metric		1:7,500
1976	Aerial photograph	Natural England	Black+White ortho-photograph	Metric		1:7,500
1983	Aerial photograph	Natural England	Black+White ortho-photograph	Metric		1:7,500
1989	Aerial photograph	Cambridge University	Black+White paper prints scanned at 600dpi	Metric	Wild Universal Aviogon 311/1 with a focal length of 152.74 mm	1:7,500

The use of historical data and the combination of different data sources can be subject to a range of uncertainties and errors (Thomas et al., 2011, James et al., 2012) which were minimized where possible, as detailed below. The geo-referencing errors were evaluated by determining the RMSE for the generated ortho-photograph in 1989, and by calculating the positional difference of well-distributed and stable ground control points (GCP) such as buildings, road junctions and crop field limits visually identifiable on maps and the ortho-photographs, against the 2010 ortho-rectified photographs (i.e. used as a higher accuracy geo-referenced model). The RMSE in 1989 based on the four GCPs used for aero-triangulation was ±3 m. To estimate the error of the earlier documents, calculation of the positional difference of six ground control points, on every map and ortho-photograph and the same features on the 2010 ortho-rectified photographs was carried out. The average difference for the OS maps ranges between 5.7 m and 7.3 m, while the errors of ortho-photographs are estimated to be 3.4 m in 1953, 3 m in 1966 and below 2 m for all others. In addition to the error margin of the ortho-photograph rectification, a potential error margin of ±1 m should be added for foredune slope-toe position identification, resulting in a maximum total error range of ±4.5 m on the photographs (1953-1989). Therefore, the maximum error range generated from OS maps and ortho-photographs used in this study is deemed to be within acceptable limits (Battiau-Queney et al., 2003, Chaverot et al., 2008). Although the potential errors associated with historical map and ortho-photograph analyses are greater than those for contemporary sources, it was necessary to use both in order to reconstruct coastal changes over the longest time period possible (~120 years). Most coastal studies, examining long-term coastline evolution, do not consider the errors associated with different data sources (e.g. Jungerius and Van der Meulen, 1989, Morton et al., 1995, Anfuso et al., 2007), however these should be kept in mind.

As in Chapter 6, the end-point-rate (EPR) method, determining the distance between the earliest and the most recent coastlines divided by the time periods between surveys, was used to obtain rates of coastline change. Additionally, linear regression (LR) is another method widely and successfully applied in shoreline change and prediction by coastal researchers (Dolan et al., 1991, Crowell et al., 1997). Linear regression was applied to investigate the long-term net trend of foredune evolution for each study site. LR has the advantage of being related to statistical techniques to test and measure the quality of the straight-line fit equation (Crowell et al., 1997). It also minimizes potential random error and short term variability using the regression coefficient (R^2) of foredune slope-toe position (dependent variable) with time (independent variable) which can reveal if a relationship exists (Dolan et al., 1991).

Thus EPR takes into account the variability in rate of foredune migration, while LR assumes a constant rate of foredune advance.

7.2.3. Analysis of Long-Term Climate Forcing

Wind direction is a major control on coastal dune response during storm surges. Although tide gauge records for this area are available since 1956, a complete analysis of historical forcing factors associated with strong onshore winds and high water level could not be undertaken due to an absence of instrumental weather data. For pre-instrumental records suitable proxies (indicators) were used to examine climate influences on coastal dune changes and evolution.

A. Climate forcing analysis

One possible proxy for weather conditions is the occurrence of depressions or synoptic scale storms in the region. These events are usually associated with strong winds due to intense pressure gradients and their occurrence may therefore have a detectable impact on foredunes over the long-term.

A method of classifying the daily circulation or daily weather type patterns of the British Isles (50°–60°N, 2°E–10°W) was originally developed by Lamb (1972) and has been applied to a range of west European climatological and environmental studies (e.g. El-Kadi and Smithson, 1992, Wilby et al., 1997, Buchanan et al., 2002). Lamb's subjective classification used daily atmospheric surface pressure charts to examine the surface airflow pattern and steering of the circulation system (Jones et al., 2012). Eight main directional types are recognized as the cardinal points, and there are three main non-directional types: anticyclonic, cyclonic, and unclassified. Days not characterized by a single weather type can be classified into one of nineteen hybrid combinations of the main types. Jenkinson and Collinson (1977) subsequently designed a reliable objective and automated version of Lamb's classification (Jones et al., 1993). The Jenkinson daily weather type (JWT) catalogue is based on a 16-point grid of mean sea level pressure data over the British Isles to determine numerical values or indices of geostrophic wind total flow and cardinal direction at 0.1° intervals.

In this study, the Jenkinson daily synoptic indices from 1st January 1871 to 31st December 2010 were used as a climate proxy provided by the Climate Research Unit (CRU) at the University of East Anglia, UK (CRU, 2011a). The geostrophic wind flow expressed in pressure units was first converted to m s^{-1}, for which each unit is equivalent to 0.617 m s^{-1}. Although the geostrophic wind is idealized flow unaffected by surface friction, it was assumed to represent the wind conditions in open-sea. The JWT was then used to determine the number of days when strong onshore, offshore, and alongshore winds exceeding 14 m s^{-1} occurred and these records were used to evaluate the annual variability in wind storminess at the synoptic scale.

B. North Atlantic Oscillation index analysis

Previous research has suggested that long-term coastal evolution in Western Europe may be linked to the North Atlantic Oscillation (NAO) (Woolf et al., 2002, Thomas et al., 2011, O'Connor et al., 2011) and so was also explored in terms of influence on the East coast of England. The NAO is a major source of inter-annual variability in the atmospheric circulation affecting the mid-latitudes (Walker and Bliss, 1932). Its monthly index corresponds to the difference between normalized atmospheric surface pressure between the Icelandic low (65°N) and the Azores high (40°N) (Wallace and Gutzler, 1981). Specifically, this oscillation is one of the most dominant modes of winter climate variability in the North Atlantic region (Hurrell et al., 2001), as it influences the pathways of storms or low-pressure cells. A high positive winter phase of the index is characterized by a large pressure gradient over the North Atlantic because the Icelandic low and the high at the Azores are both enhanced, which effectively strengthens westerly winds over northern Europe, while both pressure centres are weakened during its negative winter phase, leading to weaker westerly winds (Hurrell, 1995). Therefore, variations in pressure gradient from one phase to another produce large changes in the mean wind speed and direction over Europe, and also affect the magnitude, intensity and paths of winter storms. Additionally, recent research suggests that the NAO is a major forcing factor for wave climate and sea-level variability in the northeastern Atlantic (Bacon and Carter, 1993, Woolf et al., 2002, Lozano et al., 2004).

The NAO index data was acquired from the CRU website from 1825 to 2010 (CRU, 2011b). The impacts of climate variability along the study area was investigated using the winter NAO (from December to March), which corresponds to the seasonal period

with the most pronounced pressure difference between Iceland and the Azores (Doblas-Reyes et al., 2002).

7.3. Results

7.3.1 Changes in Coastline Position within the Sediment Cell (from mid-1990s to 2010)

Within the coastal cell, analysis of recent topographic profiles clearly highlights the variation in coastline position from the mid-1990s to 2010. There is a clear contrast between the eroding Holderness cliffs of East Riding, and the accreting coast along the north and south Lincolnshire coast. Retreating sectors account for ~50.1 km out of 98.5 km (50.8%) of the coastline, whereas naturally accreting sectors extend for ~25.4 km (25.8%) and artificially (nourished) accreting or stable sectors represent ~23 km (23.4%).

Along the East Riding coast, the change in coastline position is spatially variable ranging from a retreat (erosion) of -89.8 m at the P97 profile to an advance (accretion) of +36.9 m at the P127 profile between 1997 and 2010 (Figure 7.2). On average, the Holderness cliffs retreated -28 m between the initial survey and 2010, but this varies from near stability in the north (profiles P8, P9) due to the presence of coastal defences and gradually increases southwards where a maximum retreat of nearly -90 m is reached north of Easington (from P96-98). The average rate of retreat of the Holderness cliffs is -1.88 m year^{-1} but this varied over the survey period from -1.67 m year^{-1} (initial survey-2005), followed by more rapid erosion of -2.65 m year^{-1} (2005-2008) which then decreased to -1.71 m year^{-1} (2008-2010). Along Spurn Head, the coastline position is delimited by the HAT elevation level; this varied from 1997 to 2010 with parts of the spit extending seawards (e.g. accretion in profile P127) and other parts eroding (narrowing). At some points the spit is lower than the HAT so coastline changes can not be identified using this method (e.g. P123 and P124). The mean rate of change along Spurn Head varies from $+2.84$ m year^{-1} at P127 (centre of the spit) to -3.14 m year^{-1} at P131 (south) over the period 1997-2010.
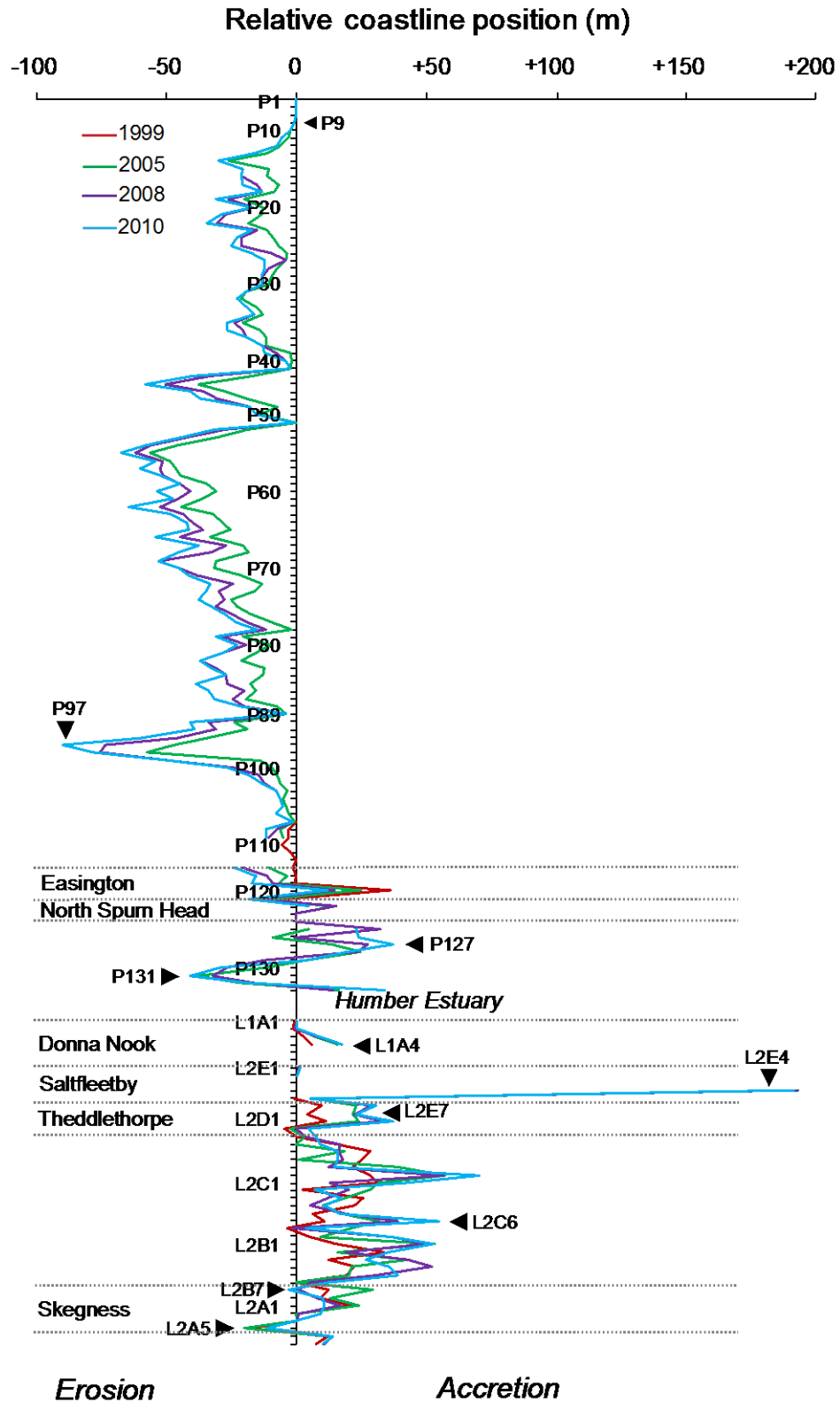
Figure 7.2. Changes in coastline position within sediment cell 2 from Flamborough Head (P1) to Gibraltar Point (L2A7) from the initial survey to 2010 (longshore spacing not to scale). Coastline represented by the cliff base (East Riding; P1-134) or HAT (Lincolnshire coast; L1A1-L2A7). Profile labels correspond to original data sources (East Riding Yorkshire Council or EA). Profiles perpendicular to coastal defences and lagoons are excluded because they are assumed to not represent the natural coastline evolution (P3-P7, P42-P44, P90-P93, P115-P118, P133, L2A4).

Along the Lincolnshire coast, Figure 7.2 shows that the position of the HAT contour was variable between 1994 and 2010, ranging from retreat of -11.3 m at the L2A5 profile to an advance of +191.3 m at the L2E4 profile due to the extension of the saltmarsh at Saltfleetby. At Donna Nook the greatest seawards advance was +17.6 m (L1A4) whilst it is was +37.3 m at Theddlethope (L2D1). Further south, changes range from -2.9 m at the profile L2B7 to +54.6 m at the L2C6 (just north of Skegness) between 1994-2010.

Cross-shore bathymetric survey profiles (only available for cell 2c) show a high spatial variability of LAT and z=-5 m contour levels, but the two indicators show a relatively similar pattern along the Lincolnshire coast (Figures 7.3, 7.4). Their distances relative to the coast (benchmark) are large at Donna Nook and Saltfleetby (up to 2898.9 m at L1A2 and 4233.9 m at L1A1 for LAT contour and z=-5m contour levels in 2008 respectively), but progressively decrease to become closer to the coast at Theddlethorpe (L2E5-L2D1). This spatial variation may be explained by the presence of a low gradient shelf adjoining to the ebb-tidal-delta of the Humber estuary at Donna Nook and a subtidal bank extending from south of Saltfleetby to the north of Mablethorpe. Between 1999-2008, the positions of the bathymetric contour levels were relatively stable and close to the coast from L2D2 to L2A4 due to the absence of a subtidal bank. However, the position of the LAT and z=-5m contour levels increase seaward at Gibraltar Point (L2A5-L2A7) which is likely associated with the nearshore sand banks.
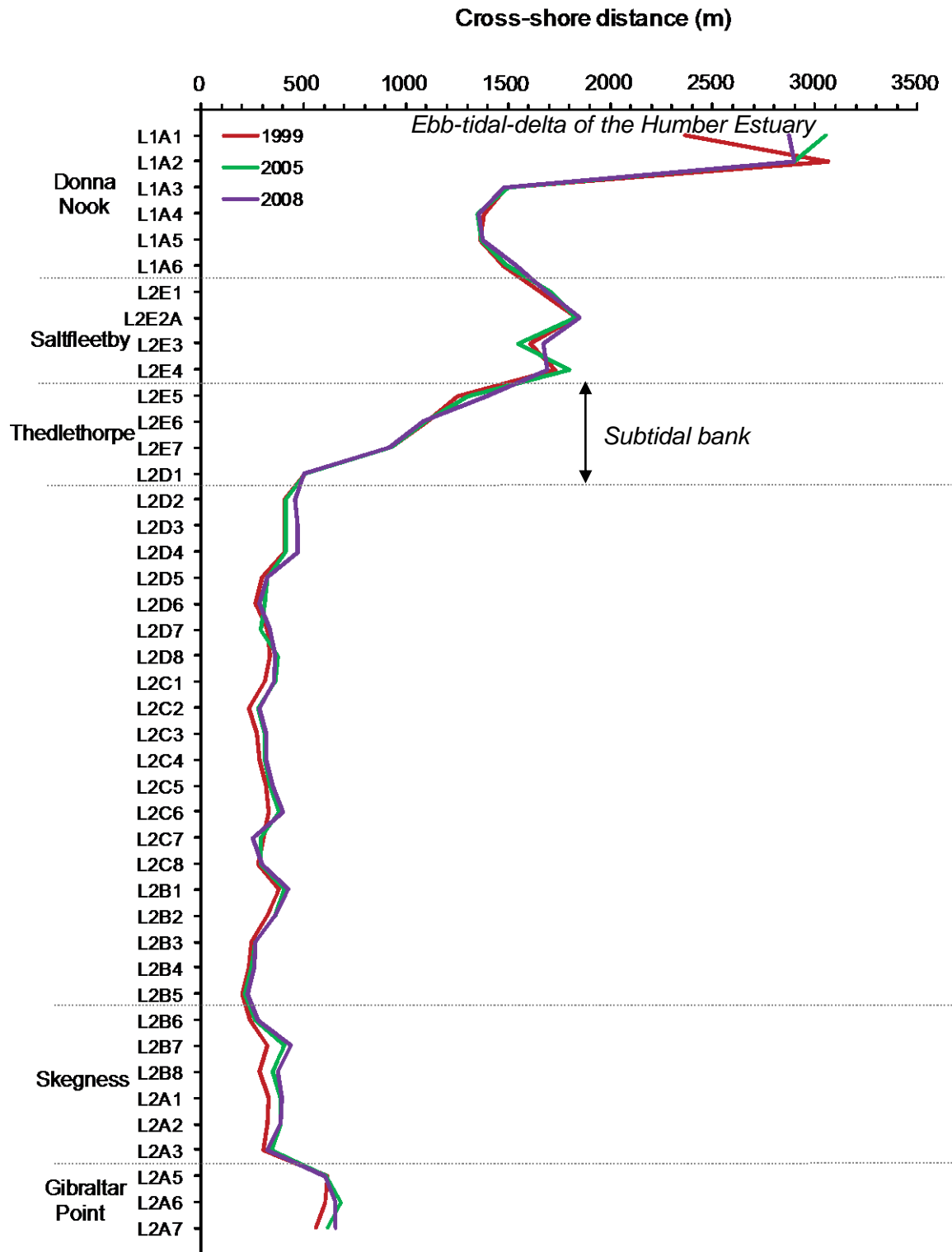
Figure 7.3. Plan view of the Lincolnshire coast where the bathymetric profiles intersect LAT level. The zero line corresponds to the benchmark position. No survey carried out at L2A4.
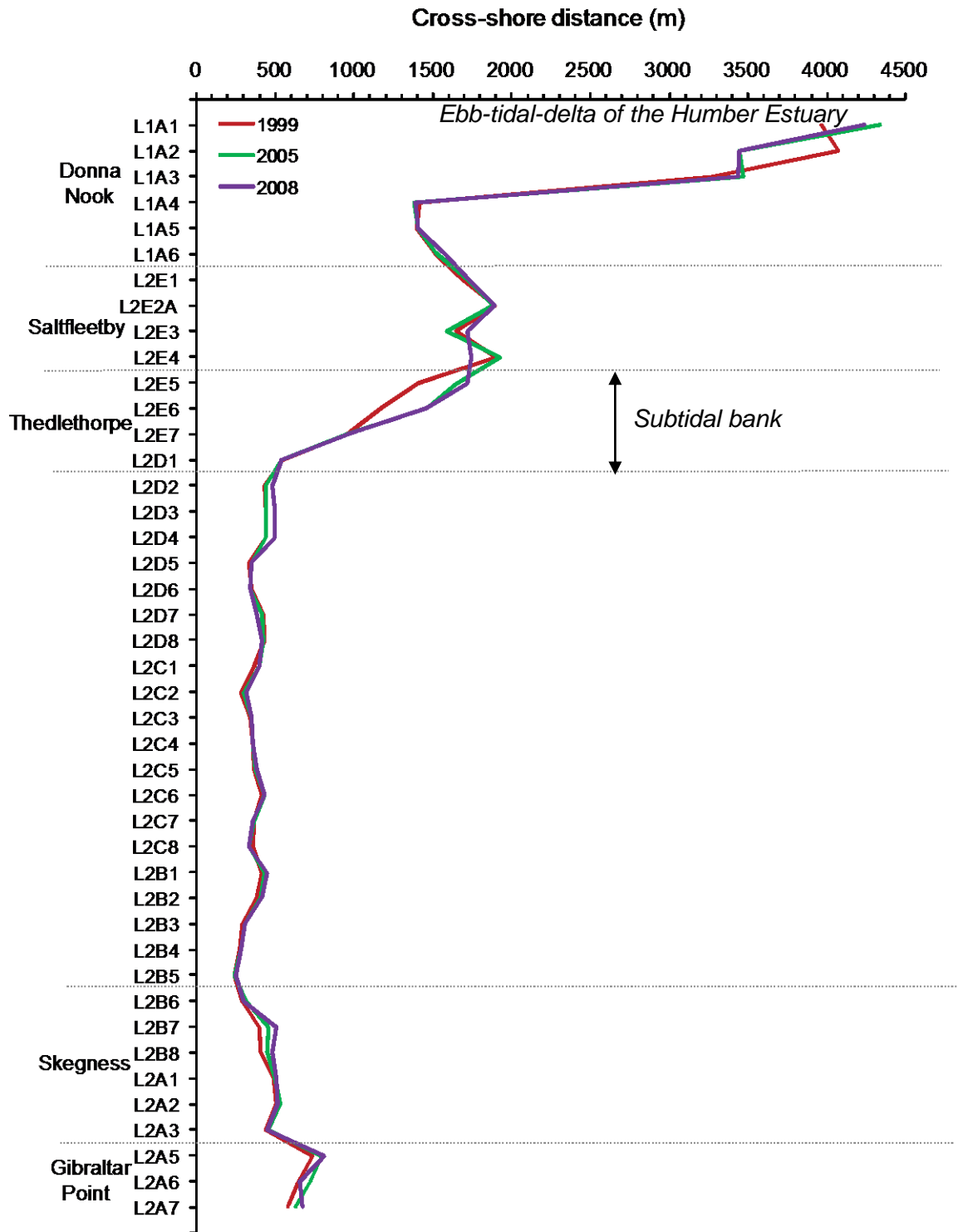
Figure 7.4. Plan view of the Lincolnshire coast where the bathymetric profiles intersect z=-5m level. The zero line corresponds to the benchmark position. No survey carried out at L2A4.

7.3.2 Long-Term Foredune Evolution

Long-term foredune evolution was determined for the three main study sites over a ~120 year period (1891-2010). The overall coastal orientation of the study area did not change. The EPR method, comparing the mean rates of change in foredune slope-toe position established for distinct epochs was used to assess the foredune movement through time, and makes it possible tentatively to evaluate the influence of episodic storm surge events. Linear regression was used to obtain the long-term trends.

A. Brickyard Lane (BL)

Over the long-term, the coastline is accreting at BL site with a positive mean rate of foredune change of 1.82 m year^{-1} for the period 1891 and 2010 (Figures 7.5 and 7.6).
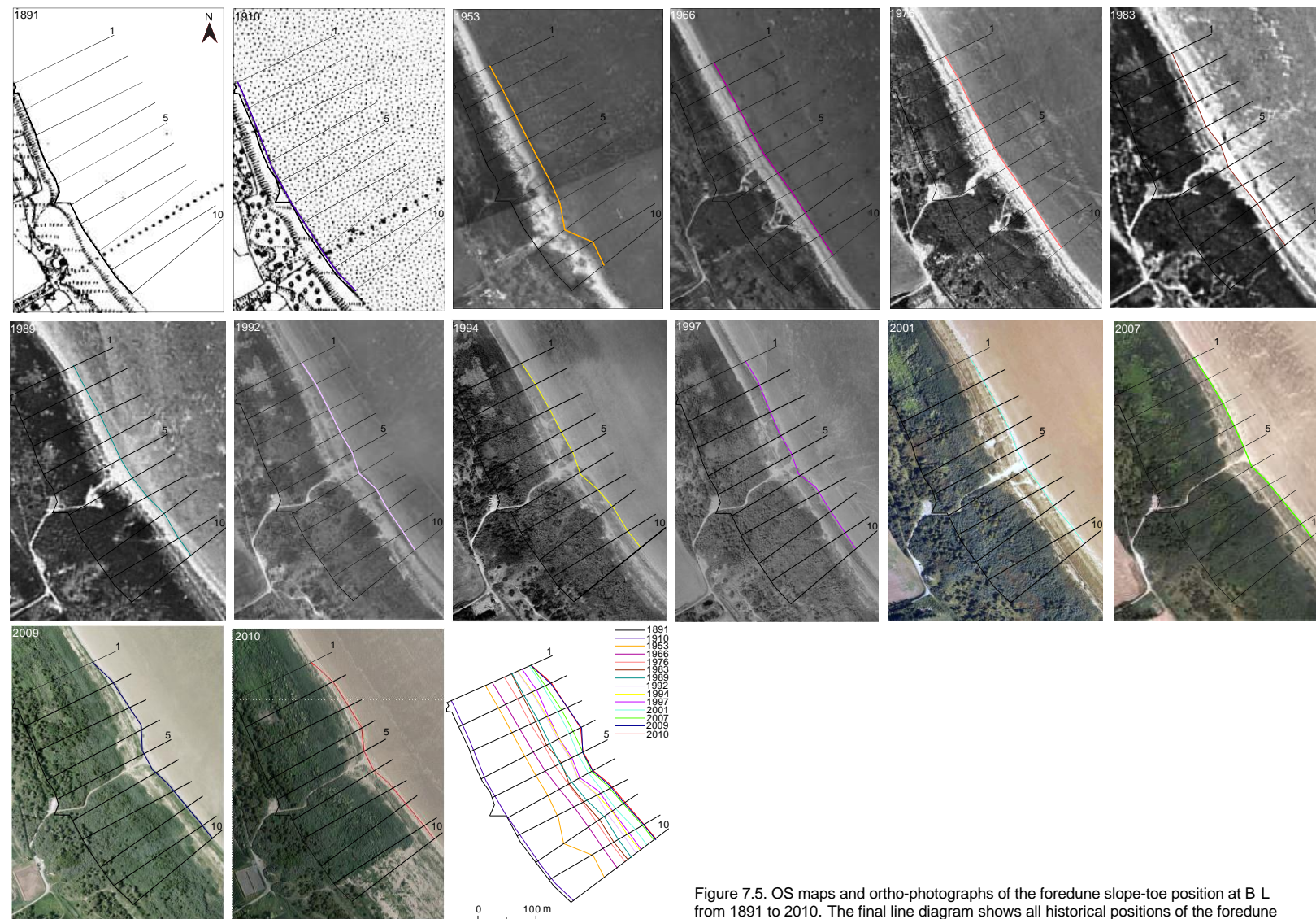
Figure 7.5. OS maps and ortho-photographs of the foredune slope-toe position at B L from 1891 to 2010. The final line diagram shows all historical positions of the foredune slope-toe overlaid. The sea is displayed on the right-hand side.
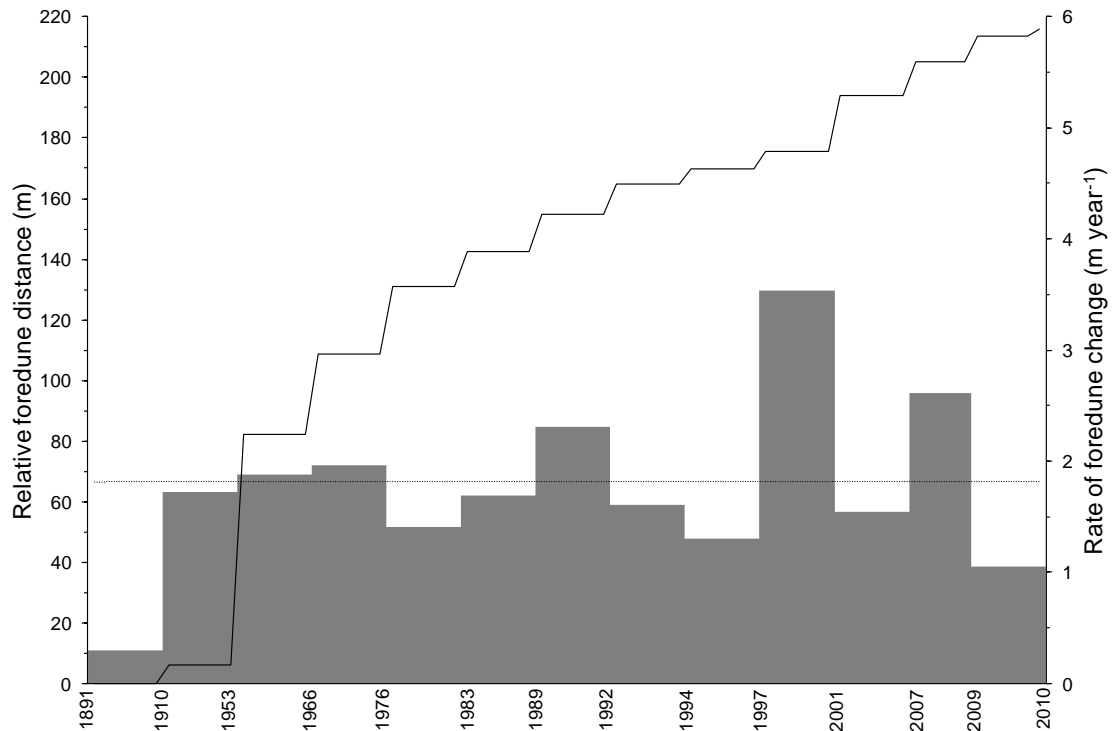
Figure 7.6. Evolution of the foredune position relative to 1891 (black line curve) and mean rates of foredune position change for the studied periods (grey bars) at BL. Dashed line corresponds to mean long-term rate of shoreline evolution (1891-2010). Note the unscaled X-axis.

Annual rate of foredune accretion did vary over time. The lowest rate of accretion measured was 0.3 m year^{-1} between 1891 and 1910. This was followed by a relatively constant period of seaward migration between 1910 and 1997 with a slight increase up to 2.3 m year^{-1} over the period 1989-1992. The highest rate of accretion was 3.5 m year^{-1} between 1997 and 2001. In 2007-2009, foredune accretion was also significant with a rate of 2.6 m year^{-1}, while it decreased to 1.1 m year^{-1}over the period 2009-2010. Results also indicate a south-north variability of the overall foredune prograding with a seaward advance in 2010 ranging from c. 195 m (transects 9 and 10) to 162.2 m (transect 1) relative to 1891 (Figure 7.5).
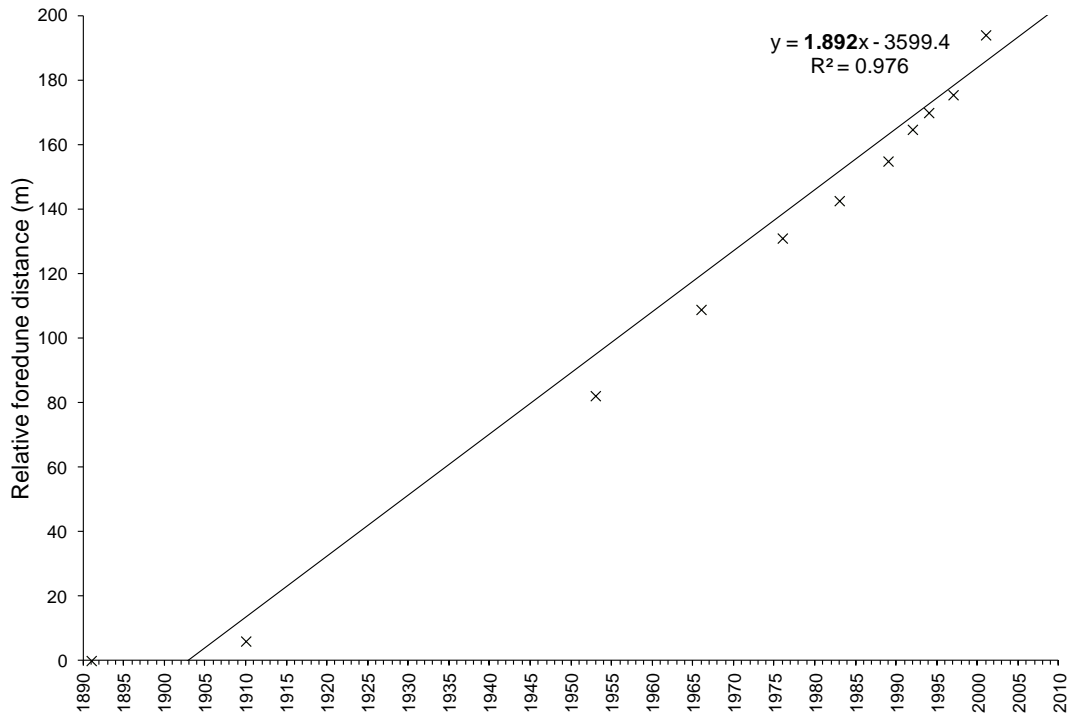
Figure 7.7. Linear regression of the foredune evolution at BL. The black line corresponds to the linear regression.

As previously mentioned, the mean rate of coastline advance calculated using the EPR method is 1.82 m year^{-1} at BL. An alternative and widely used method for predicting long-term and future coastline change is regression analysis between time and distance. The regression line is shown in Figure 7.7 and the mean rate of foredune advance (gradient of line) is 1.89 m year^{-1}. It also shows a significant positive relationship. The foredune change rate determined from the LR was used to extrapolate future foredune position to the year 2020 and 2050. This projects an advance of 243.8 m and 300.5 m relative to 1891 respectively.

B. Theddlethorpe St Helens (TSH)

Figure 7.8 reveals a long-term extensive seaward foredune displacement. The annual mean rate of foredune accretion measured was 1.93 m year^{-1} between 1891-2010 (Figure 7.9).
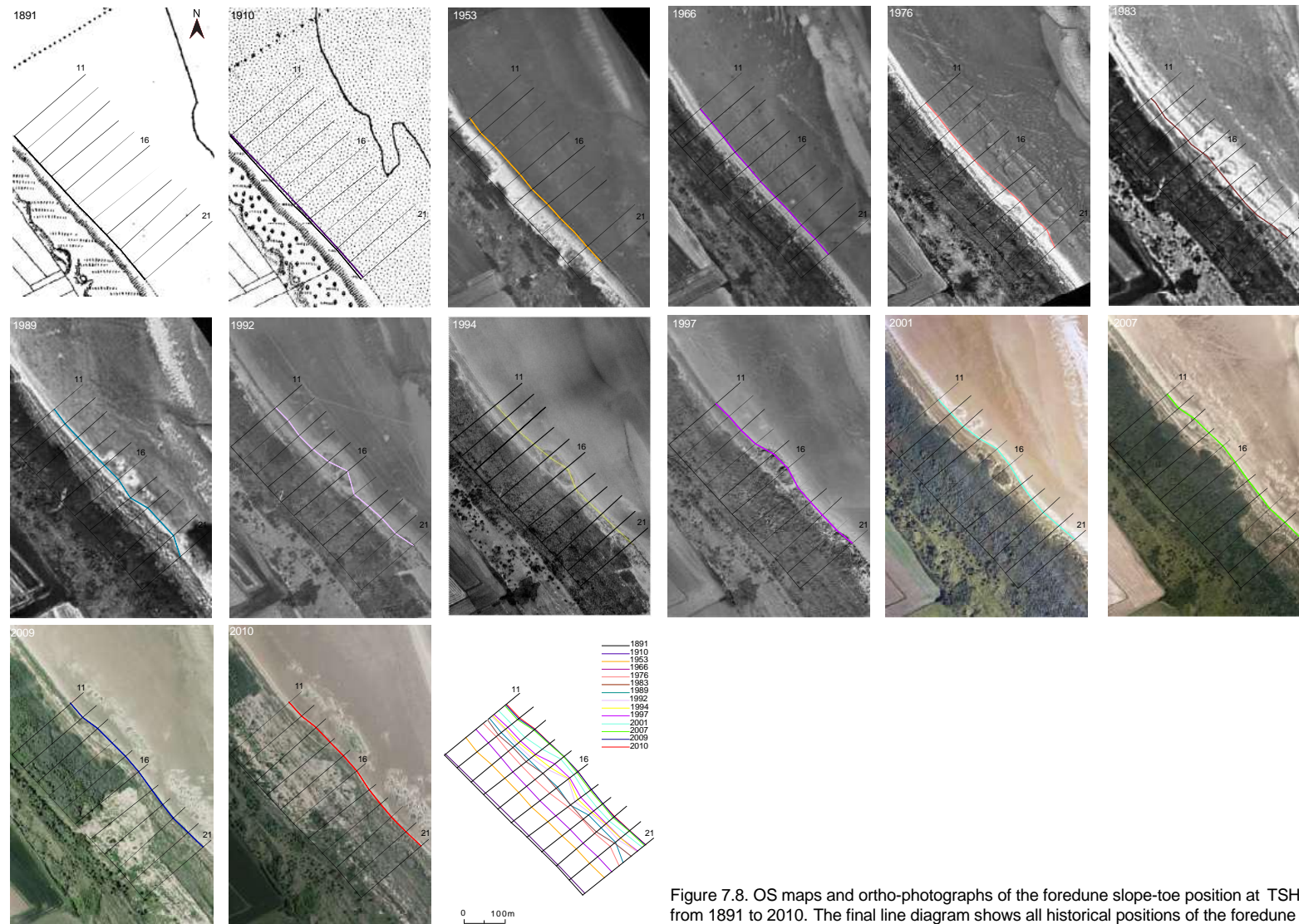
Figure 7.8. OS maps and ortho-photographs of the foredune slope-toe position at TSH from 1891 to 2010. The final line diagram shows all historical positions of the foredune slope-toe overlaid. The sea is displayed on the right-hand side.
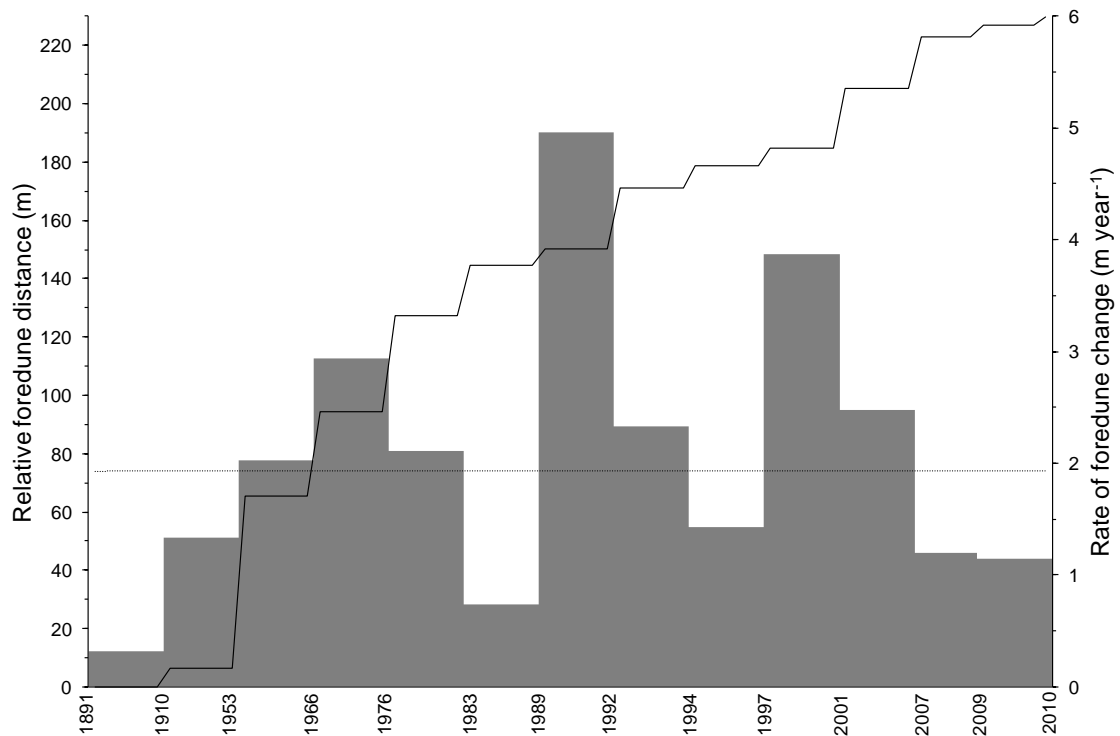
Figure 7.9. Evolution of the foredune position relative to 1891 (black line curve) and mean rates of foredune position change for the studied periods (grey bars) at TSH. Dashed line corresponds to mean long-term rate of shoreline evolution (1891-2010). Note the unscaled X-axis.

This significant and rapid foredune migration relative to 1891 ranges from c. 202.9 m (transect 15) to 184.1 m (transect 19) in 2010, suggesting that relatively uniform accretion occurs across the study site (Figure 7.8). Seaward foredune migration continued from 1891-1966, accretion rates are temporally variable ranging from 0.3 m year^{-1} between 1891 and 1910 to 4.9 m year^{-1} over the period 1989-1992. Since 2001, the foredune accretion rate has decreased to 1.2 m year^{-1} in 2010. The foredune position is plotted against time of data acquisition in Figure 7.10 and indicates a strong positive relationship (R^2=0.94).

The linear regression method estimates a mean rate of foredune advance of 2.04 m year^{-1} which is slightly greater than the EPR estimate (1.93 m year^{-1}). Based on the LR method, the potential foredune position would be 263.2 m in 2020 and 324.4 m in 2050 relative to 1891.

271
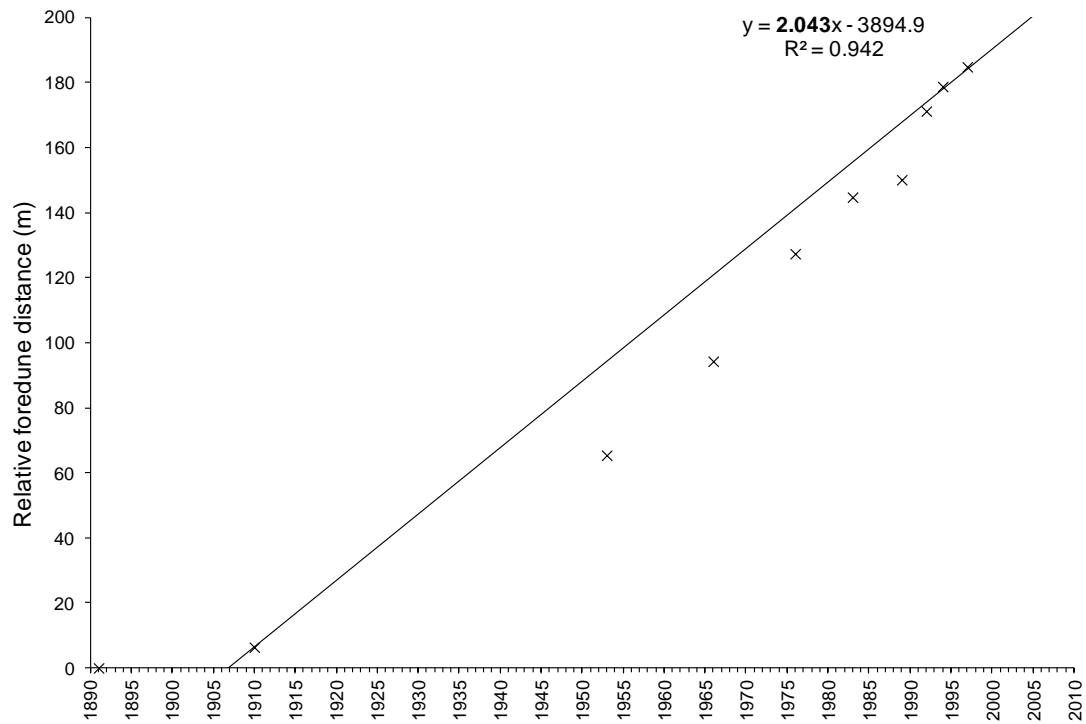
Figure 7.10. Linear regression of the foredune evolution at TSH. The black line corresponds to the linear regression.

C. Mablethorpe North End (MNE)

Figure 7.11 indicates that a seaward advance of the foredune with a mean rate of 1.80 m year^{-1} occurred between 1891 and 2010 (Figure 7.12).

272

Figure 7.11. OS maps and ortho-photographs of the foredune slope-toe position at MNE from 1891 to 2010. The final line diagram shows all historical positions of the foredune slope-toe overlaid. The sea is displayed on the right-hand side.
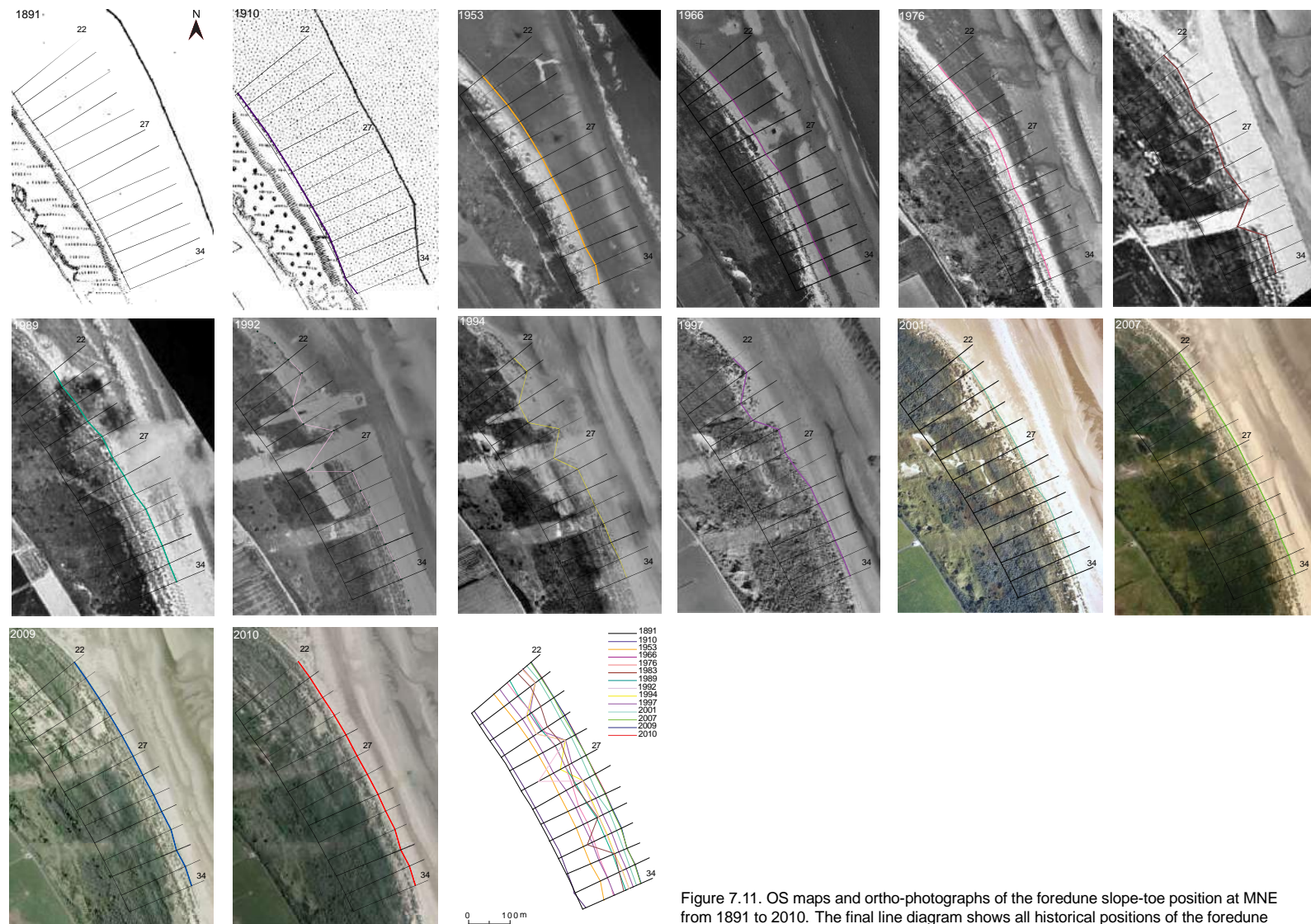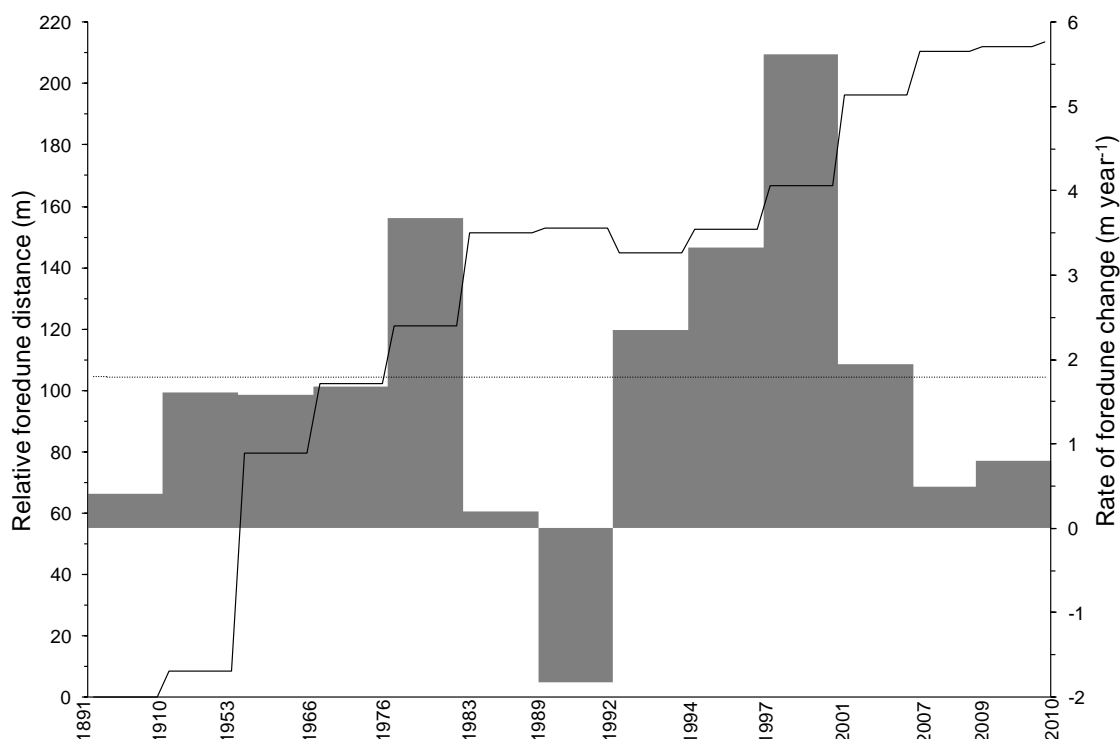
Figure 7.12. Evolution of the foredune position relative to 1891 (black line curve) and mean rates of foredune position change for the studied periods (grey bars) at MNE. Dashed line corresponds to mean long-term rate of shoreline evolution (1891-2010). Note the unscaled X-axis.

This significant and rapid foredune advance since 1891 ranges from 166.1 m at transect 34 to 201.8 m at transect 23 in 2010 (Figure 7.11). Hence, there is south-north variability in the overall foredune position at MNE over the studied period. The rate of foredune movement also does vary over time with a relatively constant accretion rate of c. 1.6 m year^{-1} from 1910-1976, followed by variable rates of change from -1.8 m year^{-1} between 1989-1992 to 5.6 m year^{-1} for the period 1997-2001. The lowest accretion rate of 0.2 m year^{-1} between 1983 and 1989 and observed development of blowouts may be due to the construction of a pipeline for the Theddlethorpe Gas Terminal in 1982 and 1987 near transects 30 and 31 (Figure 7.11). This was likely amplified by the digging of three tunnels and trenched pipelines in spring-summer 1990 along transects 22-31 causing foredune retreat. However, this was followed by a rapid foredune propagation related to a seaward re-colonisation of the vegetation through natural and human actions (pers. com. John Walker, Natural England). One aftermath of the dug pipelines is the presence of an inland blowout c. 118 m long and at distance of 30 m from the foredune slope-toe (near transects 24 and 25, Figure 7.11). Since 2007, the rate of foredune accretion has decreased.

The long-term foredune evolution derived from the LR method is presented in Figure 7.13 indicating a strong positive relationship between time and foredune advance (R^2= 0.95). The mean rate of foredune advance of 1.85 m year^{-1} determined by the LR was similar to the EPR method. The foredune position projection is approximately 238.7 m in 2020 and 294.2 m in 2050.
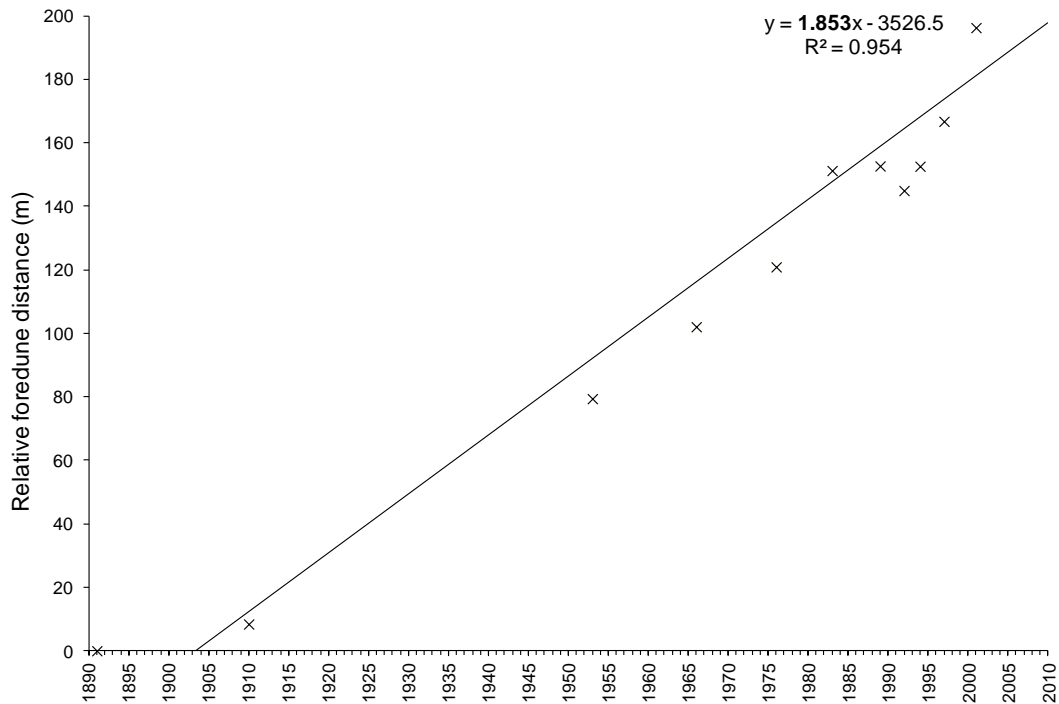
Figure 7.13. Linear regression plot of the foredune evolution at MNE. The black line corresponds to the linear regression.

7.3.2. Historical Records of Storm Surges and Long-Term Trends in Climate Forcing

A. Long-term weather pattern and climate forcing

The lack of availability of continuous wind records of sufficient length has limited the investigation of historical external forcing factors. However, given that the passage of synoptic scale storms is associated with strong winds due to intense pressure gradients (Carnell et al., 1996), it may be possible to use climate forcing proxies to estimate long-term storminess. To assess the potential utility of the JWT catalogue and NAO as proxies for storm surge, correlation analyses were undertaken between the frequency of storm surges per year using recorded wind and tide data from 1993 to 2010 and the incidence of onshore wind events exceeding 14 m s^{-1} predicted by JWT records, and the winter NAO index for the same period. Table 7.3 summarises the Pearson coefficient correlation between external forcing factors and climate forcing indicators.

Table 7.3. Correlation table between annual measured external forcing factors and climate forcing indicators from 1993 to 2010: (1) Number of storm surges recorded; (2) Number of daily onshore wind events extracted from JWT catalogue (3) winter NAO index; and (4) annual minimum atmospheric pressure at Donna Nook. Correlation values above ±0.5 are in bold.

		1 N_{SS}	2 N_{JWT}	3 NAO	4 P_{min}
1	N_{SS}				
2	N_{JWT}	**0.51**			
3	NAO	-0.36	-0.03		
4	P_{min}	0.23	-0.19	-0.48	

The relative temporal patterns of storm surge frequency is similar to the frequency of JWT wind events (Figure 7.14) and there is a significant positive correlation between the number of recorded storm surges and daily onshore events from the JWT catalogue (r=0.51 p<0.05). This suggests the Jenkinson weather catalogue may be a useful proxy for long term storminess. The correlation established between the winter NAO and the annual frequency of storm surges is low (r=-0.36 p<0.05), however a coefficient of correlation of r=-0.48 (p<0.05) is found between NAO and the minimum atmospheric pressure suggesting a potential influence of the NAO on the regional

atmospheric circulation (Table 7.3). The NAO index is a decadal phase of atmospheric variability (Hurrel, 1995) so that its relationship could have been limited in the correlation analysis which covers less than two decades from 1993 to 2010. In general, the correlation results suggest that the annual frequency of high wind speed derived from the JWT catalogue can be used to examine long-term trends of climate forcing. Although no clear relationships were observed with the winter NAO over the period 1993-2010, its potential influence on coastal morphological changes was investigated.
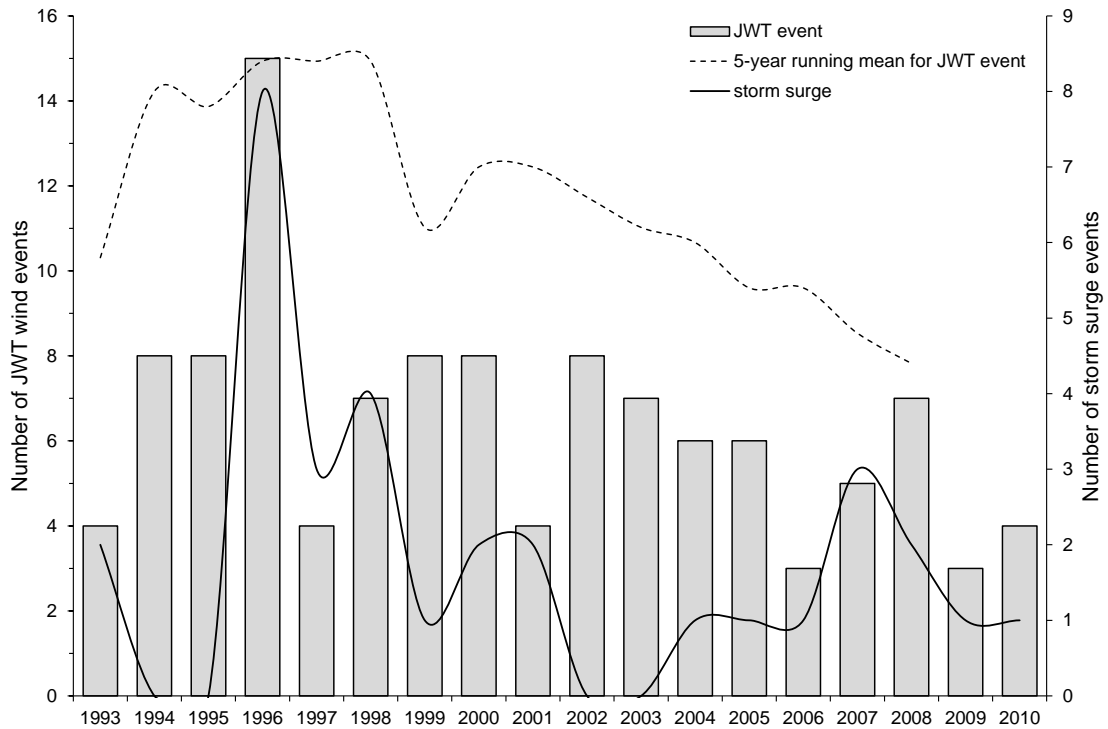
Figure 7.14. Time series of JWT annual strong wind events and storm surge between 1993 and 2010.

A.1. Jenkinson weather catalogue

Figure 7.15 shows the occurrence of days with high wind speeds (storms) from 1871 to 2010 over the British Isles indicated by JWT. Prevailing winds are offshore and coincide with strong westerly winds in winter. The long-term trend of strong offshore winds appears relatively stable (Figure 7.15B). However, offshore winds are not likely to be associated with significant storm surges. Rather storm surge will be associated with strong onshore winds. From 1871-2010 the annual frequency of onshore winds ≥ 14 m s^{-1} varies from zero in 1932 to 19 in 1917 (Figure 7.15A). Three peaks in the onshore storm event record are also observed in 1876, 1878, and 1883 while the 5-year running mean indicates that the highest peak in 1917 was followed by a relatively stable period of 35 years (between late 1920-1955). Three distinct onshore stormy periods occurred in 1955-1970, 1975-1988 and 1994-2000. Strong alongshore winds typically occur on fewer than 6 days per year with no clear long-term trends (Figure 7.15C).
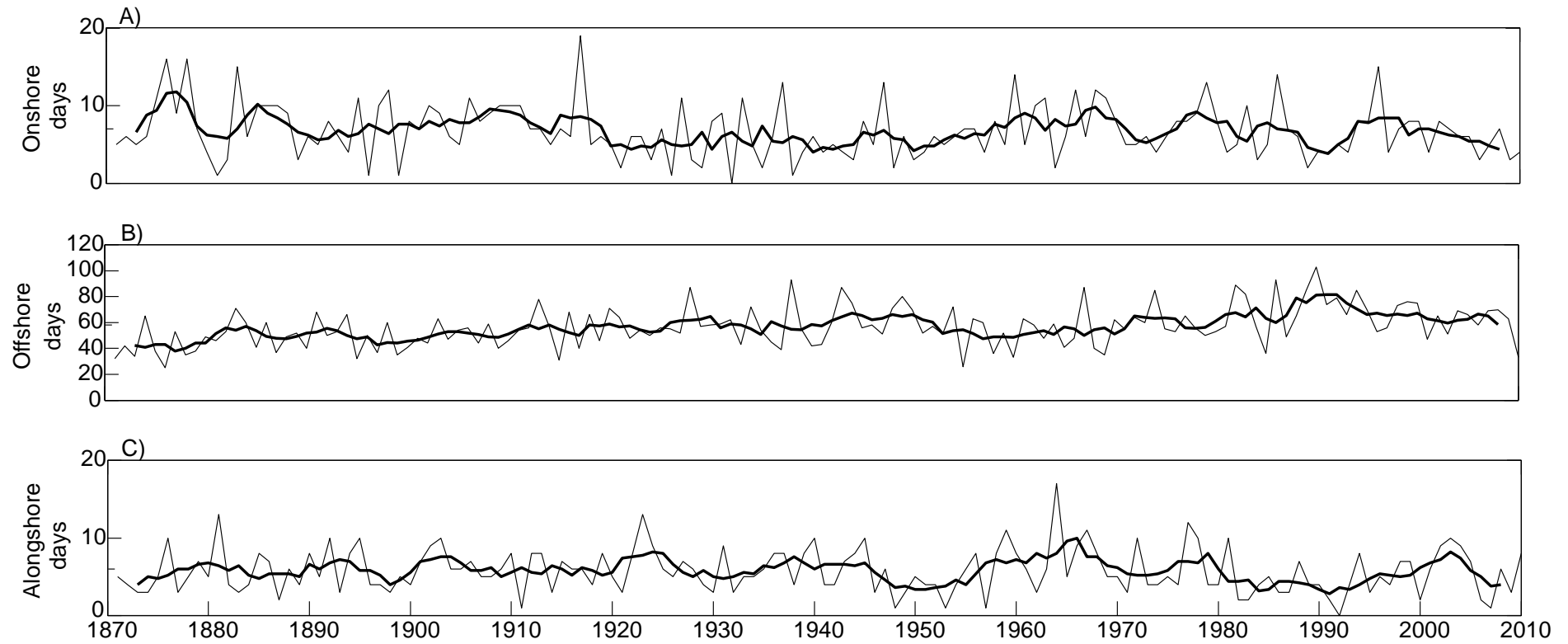
Figure 7.15. Time series from 1871 to 2010 of annual number of days (black line) with winds 14m s^{-1} for: (A) onshore, (B) offshore and (C) alongshore winds. The bold line corresponds to the 5-year running mean and the short bar on the Y-axis to the mean over the entire period.

A.2. North Atlantic Oscillation

The trend and pattern of winter NAO index data was examined (Figure 7.16).
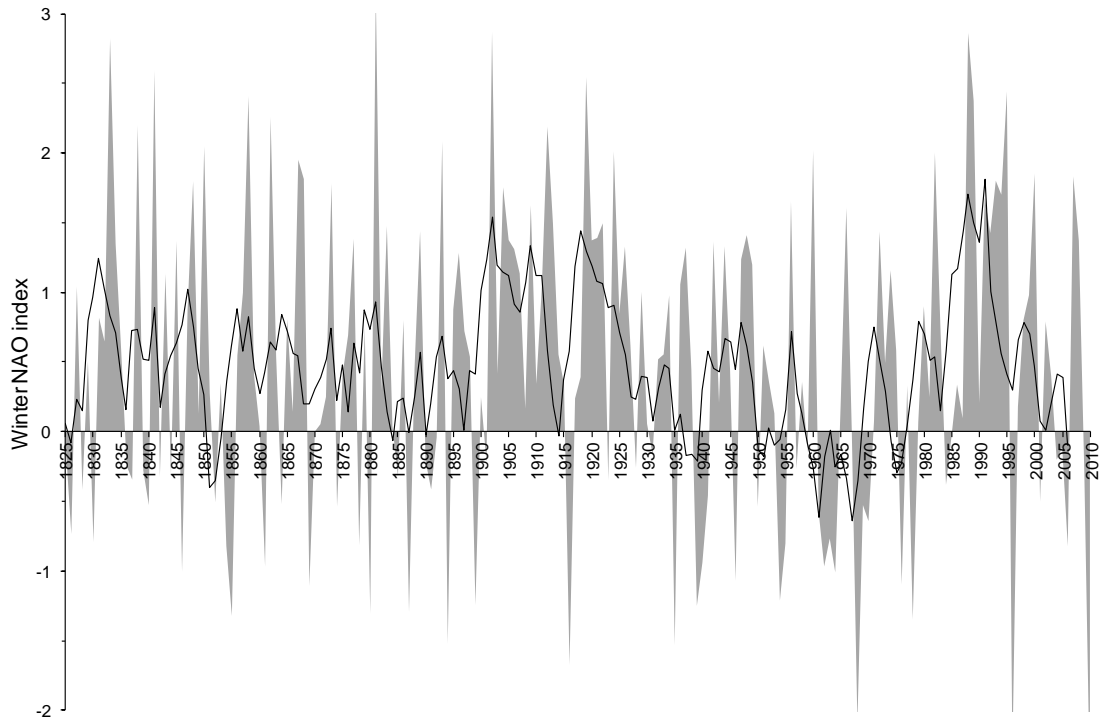
Figure 7.16. Time series of the winter (December to March average) NAO index between 1825 -2010. The black line corresponds to the 5-year running mean.

The period between 1825 and the 1940s is one of high energy conditions implied by a strong winter NAO phase, in particular from 1900 to 1915 and 1919-late 1920s (Figure 7.16). From the early 1950s until the early 1970s, the winter NAO index exhibited a downward trend (exceptions are in 1957, 1961 and 1967) and likely corresponded to a period of calm conditions over North West Europe. By contrast, a strong and persistent positive winter NAO index prevailed between 1980 and 2000, which included the greatest value of 2.44 in 1995 but also a highly negative NAO index in 1996. This general trend suggests that more frequent and stronger winds occurred over the North Atlantic during this 20-year period. The last ten years have fluctuated between positive and negative NAO phases.

7.4. Discussion

An examination of detailed records over the past two decades has demonstrated clear trends in erosion and accretion within the whole sediment cell – from Flamborough Head to Gibraltar Point. These trends can be ascribed to factors such as natural antecedent conditions, relative position within the sediment cell (i.e. updrift/downdrift) and human activities. The long term historical records have indicated a long-term accretion of the coastal dunes in the study area.

7.4.1. Coastline and Nearshore Changes from the mid-1990s-2010

Topographic profiles have provided quantitative information on coastline and nearshore dynamics from the mid-1990s to 2010. Changes along the Holderness cliffs proved to be variable in space and time, but the overall trend was rapid and significant erosion. The loosely-consolidated soft sand and clay cliffs are easily eroded by wave action, and collapse into the sea in significant landslips. The variability of coastline retreat shown in Figure 7.2 suggests periods of rapid cliff retreat alternating with periods of relative stability. This accords with observations by Pye and Blott (2010), and is likely to be a result of rhythmic phases of cliff collapse and subsequent erosion (Pringle, 1985, Posford-Duvivier, 1992, Quinn et al. 2009). Rates of cliffline recession are also spatially very variable. This is likely due to the presence or absence of offshore sand banks and the pattern of submarine contours. For example, where sand banks are present they are likely to reduce inshore wave energy (Eurosion, 2003).

Halcrow and Geosea (1990) modeled the wave-driven littoral drift along the East Riding coast, and found that Easington marks the point at which the southwards travelling sand derived from erosion along the total length of the cliffs moves offshore, although the precise transport pathways of eroded sediments will depend on their mineralogy and grain size (Newsham et al., 2002). This offshore transport is a result of a combination of the change in both the orientation of the coast and the direction of the tidal currents at this point. Some of the littoral drift is transported to the southern end of Holderness to form and maintain the Spurn spit whilst the remainder is likely to be deposited in the nearshore sand banks of The Binks, which act as a sand reservoir for Spurn Head and a buffer to erosion under energetic hydrodynamic conditions (HR Wallingford, 2002). The littoral drift moves in an extended pathway under the influence of successive flood and ebb tidal actions towards the south of the sediment cell

(Dugdale 1980), while it has been estimated that 1% of the total sediment enters and circulates into the Humber estuary in a clockwise direction to be then expelled back in to the North Sea (Halcrow and GeoSea, 1990, Black and Veatch, 2004).

Robinson (1968) released seabed drifters as indicators of sediment movement from the Binks 60% of which were recovered from the south shore of the Humber Estuary and further southwards down the Lincolnshire coast. This confirms a sediment transport pathway between Spurn Head and the Lincolnshire coast across the mouth of the Humber estuary. Much of this sediment is deposited at Donna Nook (Steers, 1966, Tonk, 2000) and is reflected in this study through the dominance of seaward advance (accretion) in both the coastline and nearshore contours (LAT and z=-5 m ODN) at this location. This is consistent with Leggett et al. (1998) who further documented accreting beach profiles along the north Lincolnshire coast up to Mablethorpe with a positive change of 2% (by volume) from 1991-1996. From the mid-1990s to 2010, the coastlines at Saltfleetby and Theddlethorpe including the three sites focused on in this thesis have been accreting. The seaward position of the LAT and z=-5 m levels were stable between 1999 and 2008. They have also shown a similar spatial pattern becoming closer to the coast in the south of Theddlethorpe due to the absence of subtidal banks. As previously mentioned in Chapters 4 and 6, nearshore bathymetry plays an important role in reducing wave energy at the coast. In the literature, relationships have been reported between coastal dunes and shoreface and nearshore bathymetric variations; typically accreting (eroding) foredunes are characterized by areas of seafloor aggradation (starvation) (Houser, 2009, Sabatier et al., 2009, Héquette and Aernouts, 2010). Along the three study sites, long-term morphodynamics of the foredune-beach systems thus function under conditions of largely unlimited sand supply from the shoreface reflecting the abundant stocks of sand in the subtidal bank.

In contrast at Mablethorpe, the coastline switches from one of accretion to one of erosion (Schans et al., 2001) driven by a combination of exposure to wave activity due to the absence of protective nearshore bathymetry (Dugdale and Vere, 1993) and human/tourism pressures (Robinson, 1964, Pye, 1995). Between Mablethorpe and Skegness, coastline changes have been affected by beach nourishment since 1994, and in general indicate signs of seaward extension. The EA (2011) suggests that accretion of the upper beach in this location can be attributed to a better retention of renourishment material due to the wind blowing newly deposited sediment up the

beach. Along the sandy beach backed by coastal dunes at Gibraltar Point the coastline is accreting as evidenced by seawards movement of the LAT and z=-5m contour levels. This is likely due to sediment input from the sand banks and the fact that the coastline changes orientation to be more sheltered (EA, 2011). Some of the sediment inputs to Gibraltar Point may have been gained as a result of the nourishment programme updrift.

7.4.2. Coastal Foredune Evolution from 1891 to 2010

Standard approaches using historical maps and ortho-photographs (Bryant, 1988, Orford et al., 1999, Chaverot et al., 2008, Thomas et al., 2011) were used to reconstruct long-term evolution of the foredune. As previously mentioned, the potential analyzing error between the different data sources should keep in mind. The long-term foredune changes at the three study sites are, however, characterized by high rates of mobility exceeding these potential errors. No long term climate and tidal data were available, so the use of the Jenkinson Daily Weather Type as a proxy was assessed and found to be a reasonable proxy for storminess. Frequencies of events identified using JWT data are much higher than the measured storm surges (Figure 7.15); this is because there was not any differentiation between onshore energetic events associated with high tides, where storm surges would be likely, from those associated with low tides where little or no impact would be expected due to the lower overall water level (Chaverot et al., 2008). Accounting for water level over the longer term will be explored in more detail in Chapter 8. The winter NAO index was also examined because other long-term studies of coastline change have found it a useful proxy. For the Lincolnshire coast, the relationship between storm events and NAO was low and negatively correlated. While a moderate negative correlation was found between the measured storm surge and the winter NAO index. Although the influence of the NAO has been widely studied around the north Atlantic European coasts (e.g. Wakelin et al., 2003, Tsimplis et al., 2005, O'Connor et al., 2011), some uncertainties remain in the North Sea basin (Woolf et al., 2002).

Based on the EPR method, the results have shown that the foredunes have been dominated by a rapid and significant accretion of 1.80 m year^{-1} at MNE, 1.82 m year^{-1} at BL up to 1.93 m year^{-1} at TSH from 1891 to 2010. The result agrees with previous studies which indicated a long-term accretion trend (King, 1972, Robinson, 1984, Halcrow, 1988, Leggett et al., 1998, EA, 2008). One of the sediment sources for these

beaches is, as mentioned above, material eroded from the Holderness coast (Steers, 1966), but in addition there is onshore movement of material from sand banks (Halcrow, 1988, ABP, 1996, HR Wallingford, 2002). The present results did not indicate any general coastline retreat caused by the severe 31st January-1st February 1953 North Sea storm surge, however the intervals between maps and ortho-photographs probably hides some remarkable short-term coastline recession. The storm surge impacts in 1953 are also likely to have been reduced by the presence of coastal dunes and the higher, wide beach along the North Lincolnshire coast (Robinson, 1953, Brampton and Bevan, 1987).

The long record shows the frequency of JWT onshore wind storms was variable from 1871 to the 1920s (1-19 events per year), but was slightly higher than the long term mean of 7 events per year. This was followed by a relatively calm period of up to 35 years (Figure 7.17A). Peak periods of wind storm events occurred during 1955-1970, 1975-1988, and from the mid-1990s to 2000 suggesting an increase in wind speeds likely to generate greater significant wave heights. Greatest rates of coastline accretion were recorded between 1997-2001 period at the three study sites, and also over the periods 1966-1976, 1989-1992 at BL and TSH sites (Figure 7.17B, C, D). These results are concurrent with a high recession rate of the Easington cliffs (Montreuil and Bullard, submitted – Appendix 8). In contrast, the recent decrease in the rate of cliff retreat in 2005-2008 and 2008-2010 appears to relate to the relative reduction of coastline seaward movement at the three sites.

In this study, weather climate results are consistent with recent research suggesting considerable changes of wind storms in Western of Europe throughout the past century, and characterized by important variations on a quasi-decadal timescale (e.g. WASA, 1998, Alexandersson et al., 2000, Lozano et al., 2004). Matulla et al. (2007) reported an increase of storminess from the 1960s and 1990s, which has been suggested to return to calm conditions since the mid-1990s (Alexandersson et al., 2000). An important number of studies have also reported an increase in the magnitude, frequency and durations of storm surges (Vasseur and Héquette, 2000, Lowe et al., 2001, Lowe and Gregory, 2005), wave heights (Bouws et al., 1996, Woolf et al., 2002), and mean sea levels in North Sea over the last decades (Tsimplis et al., 2006).

Within the data set, one particular period of interest is that between the 1900s and 1953 where rates of coastline change throughout the sediment cell were very low. This broadly coincides with a long period of low frequencies of annual wind storms (1920-1955). Both the geomorphological and climatological records suggest there was a period of quiescence lasting ~35 years in the first half of the 20th century. Between the 1900s and 1940s, winter NAO phase was positive with consecutive strong positive phases between 1900-1915 and 1915-1930 (Figure 7.17A). Over this period, the occurrence of storm events, affecting the North Atlantic west-facing coast would be expected to have increased, whereas the east coast would have been relatively sheltered. This could suggest, therefore, that although positive NAO phase may not indicate storminess on the east coast of England, it may provide a useful proxy for quiescence.

The evolution of the foredune has also proved to be spatially variable at the three sites. From 1989 to 1992, foredune propagation dominated at the BL and TSH sites, showing a good agreement with a low annual frequency of energetic onshore winds days associated with a dominance of positive winter NAO phases. This further supports the argument of quiescence period along the east coast of British Isles during positive winter NAO phase. In contrast, a significant annual foredune retreat was recorded at MNE site over this period. This is more likely to be related to local human interferences through construction of gas pipelines.
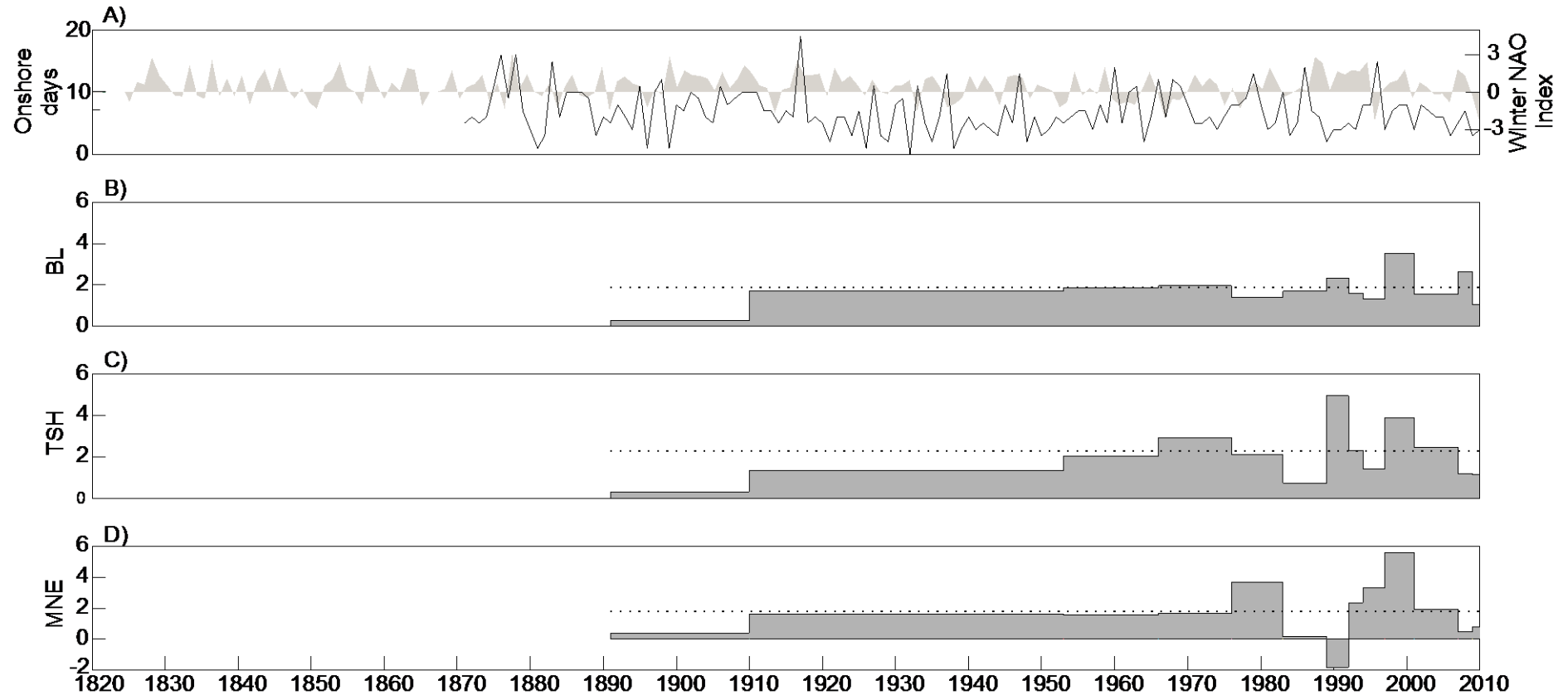
Figure 7.17. Time series between 1825 and 2010 of: (A) the number of onshore wind storm determined by the JWT (black line) and winter NAO index (grey), and evolution of the foredune at: (B) BL, (C) TSH and (D) MNE sites. The dotted line corresponds to the annual mean rate of foredune change.

7.5. Conclusion

- The studied coastal sediment cell reflects processes operating at a range of scales. Rapid erosion of the updrift Holderness cliffs has been counterbalanced with accretion in the shore and nearshore zones along the downdrift Lincolnshire coast.

- The analysis of foredune evolution from 1891 to 2010 indicated temporal and spatial variability, with the study sites characterized by a net and rapid accretion ranging from c. 1.80 m year^{-1} at MNE and BL to 1.93 m year^{-1} at TSH.

- An exploration of storm impact on erosion and accretion rates showed no clear relationship between storm frequency and change in coastal foredune position, however this may be in part due to the relative timing of the rare severe storm occurrence and data acquisition.

- The Jenkinson Daily Weather Type classification was found to be a reasonable proxy for the occurrence of strong onshore winds which may offer scope for further investigation of the role of forcing factors over time periods beyond the length of the meteorological and tidal station records. Winter North Atlantic Oscillation phase was not a good indicator of storminess on the east coast of England but may be a useful proxy for quiescence.

Chapter 8. General Discussion and Conclusion

8.1. Introduction

Chapter 1 of this thesis discussed the challenges associated with understanding the behaviour of coastal dunes and dunefields at a range of scales. In particular, it was concluded that scale was a useful framework for analyzing complex coastal geomorphic systems where relatively low-order scale processes or phenomena could be considered as noise and large-scale processes as boundary conditions (Horn, 2002). This thesis was designed to try and address one of the principal challenges that has faced geomorphologists, and which is to understand how processes operating over different temporal and spatial scales are related, which is one of the main limitations of the reductionist principle (Bauer et al. 1999, Baas, 2002). Following Sherman (1995), the approach therefore was to study the same coastal geomorphic system at different scales (Figure 8.1) and try systematically to identify the key controls on dune formation. In this final thesis chapter, the knowledge and understanding gained at the different scales is synthesized to understand the past and present morphodynamics of the field site. In this, as in most other previous studies, moving from the small spatial scale, where several variables are measured over short-timescales, to the meso- and macro-scales, it is necessary to reduce the number of parameters that are considered, or change the way in which they are measured. This is due primarily to data availability and logistical constraints. However, in some cases data collected at one scale (e.g. grain size) can be used to inform models or predictions of behaviours at a different scale (section 8.2)
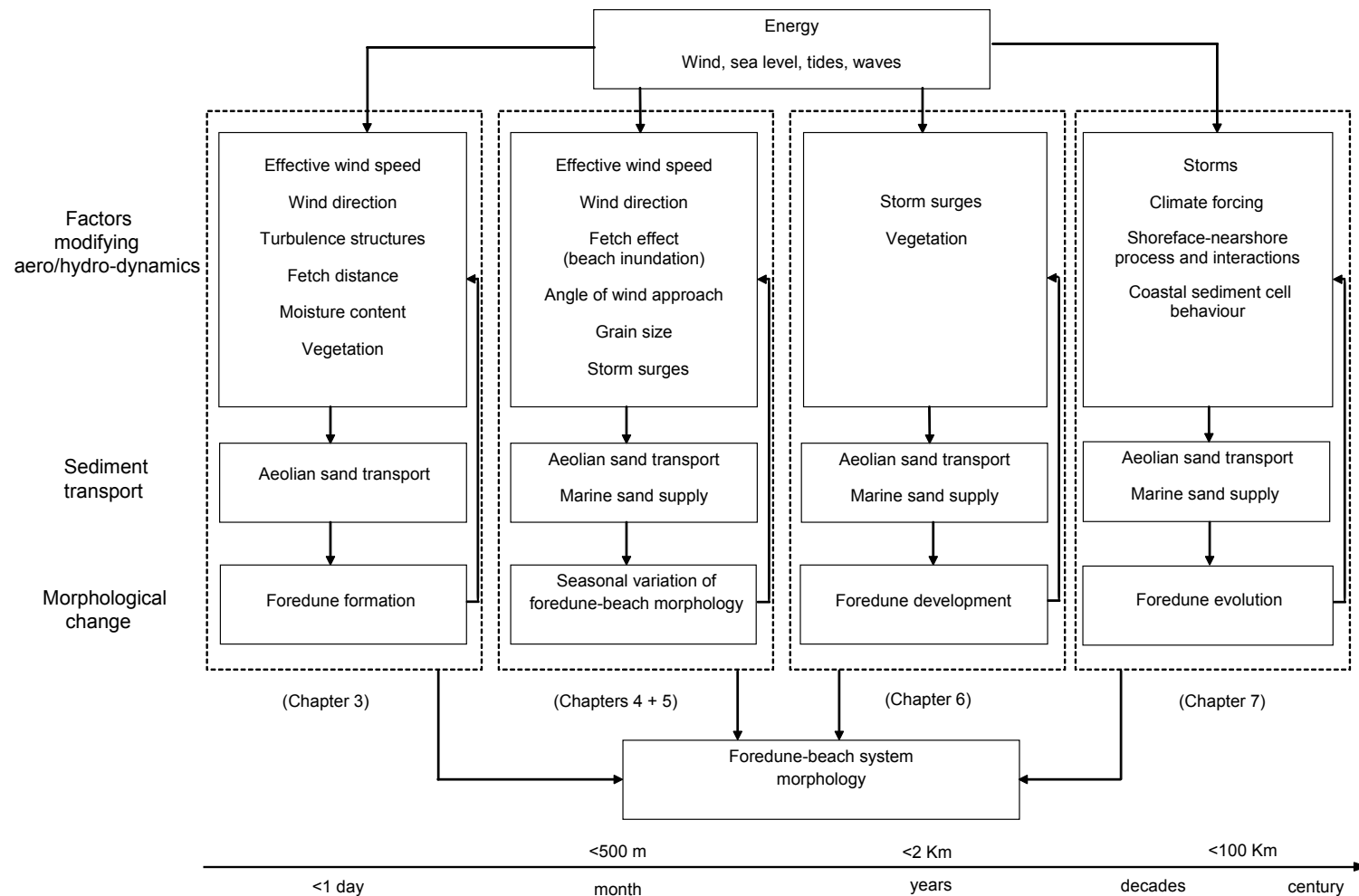
Figure 8.1. Foredune-beach morphodynamic system and component (interaction process) examined in this thesis.

8.2. Up-scaling from Micro to Macro-Scales

The short-term field experiments for this study were designed to determine the relationship between topography and near-surface airflow at the field site under a range of wind conditions. During the experiments, wind speeds were generally low which meant that sediment transport measurements in relation to wind speed were limited because wind rarely exceeded the required threshold velocity. To accommodate this limitation, wind speed variations over the dunes are considered here not as absolute values, but instead the focus is on relative values, referred to as 'sand transport capacity' (e.g. Kocurek and Lancaster, 1999). A decrease in wind speed causes a reduction in potential sand transport capacity that is likely to cause deposition as less sediment can be transported by slower winds. An increase in wind speed causes an increase in potential sand transport capacity such that additional sediment can be entrained (erosion). Two key assumptions are made; the first is that the pattern of increased/decreased sand transport capacity is consistent regardless of the overall wind speed; the second is that sand supply is unlimited. The first assumption may not be the case for very weak winds so some caution is required when using this technique to infer patterns where wind speed during the experiments was very low (13th October 2009, 14th October 2009, 15th October 2009, 26th January 2010, 29th April 2010). The second assumption is considered further later on in the developed model of sand supply into the foredune.

Factors other than wind speed are also important, as demonstrated in section 3.5.3, turbulence (u'- and w'- fluctuating components) is strongly correlated to the shear stress velocity although the relationship between shear stress velocity and the net horizontal airflow (U-component) was weak. This suggests that turbulence has a greater influence on sediment transport than the net wind velocity. This can be factored into a general summary of flow conditions by differentiating turbulent flow (T) from steady flow (S). Turbulent flow in combination with increasing wind speeds would further enhance potential sand transport. Under steady flow no enhancement takes place. Variation in grain-size is incorporated in to the calculation of the sand-transport threshold, however because overall wind speeds were low and actual sediment transport therefore low it is difficult to determine the sand-trapping effectiveness of vegetation, so this is not considered further at the meso-scale.

The data presented in Chapter 3 show that both the velocity and direction of airflow are modified by the foredunes through topographic forcing and steering effects at the three study sites. The nature of this modification varies according to position on the foredune-beach referred to as 'spatial compartmentation' by Nordstrom et al., 1996, and angle of approach of the winds, or airflow deflection (Mikkelsen, 1989, Sweet and Kocurek, 1990, Hesp, 2005, Walker et al., 2009, Lynch et al., 2010). Topographic forcing and steering are shown to be slightly different in detail at the three sites, but there are some common characteristics that can be identified and are summarized in Figure 8.2.

Direct offshore winds typically remain attached and undeflected as they pass over the dunes with a seaward aspect ratio of less than 0.167 (Figure 8.2A). Under these conditions, wind speed is decelerated as it passes over the secondary foredune and starts to expand but begins to accelerate over the primary foredune, continuing to increase in velocity over the beach. However, the deceleration zone expands to the primary foredune toe at Brickyard Lane (BL) probably due to the convex-concave-convex-concave dune profile (Figure 8.2A). At the three sites, unsteady turbulent airflow was generally recorded over the foredunes with a maximum at the primary foredune crest and toe. This suggests a localized development of turbulence structures; airflow becomes steady across the beach. Recently, Lynch et al. (2009) observed airflow separation associated with a turbulent multi-directional flow and a recirculation cell on the lee side of a sharp foredune crest with a distinct brink at an elevation of c. 11 m in Northern Ireland. The authors suggested that the morphology of the lee foredune slope is the primary determinant of the lee-side secondary airflow adjustment.

A)

N

Regional wind
+
-
T: Turbulence
S: Steady

BL

S

T+

T-
TSH: T+

T+

T

Sea

SFC   SFT   PFC   PFT   Beach

B)

T

T-

T+

T-

S

Sea

SFC   SFT   PFC   PFT   Beach

C)

S
T+

S
TSH: T

S

S

S

Sea

SFC   SFT   PFC   PFT   Beach

Figure 8.2. General findings of topographic forcing and steering over the foredune-beach for: (A) offshore, (B) oblique offshore and (C) onshore winds. The symbols (+) and (-) indicate an increase and decrease respectively.

As observed elsewhere, flow deflection is most likely to occur when wind approach direction is oblique to the dune crest (Sweet and Kocurek, 1990, Arens et al., 1995, Lynch et al., 2010). On the Lincolnshire coast oblique offshore winds are deflected as they pass over the foredunes with a seaward aspect ratio ranging between 0.013 and 0.06 to become near-parallel to the dune crest before returning to the upwind (regional) direction when they reach the beach (Figure 8.2B). Under relatively slow sand-transporting winds sediment deposition would be expected on the dunes, however for faster sand-transporting winds sediment would be transported alongshore. The main geomorphological implications are sediment deposition on the secondary foredune crest up to its toe during both oblique and direct offshore winds. Erosion is likely to be increased by the effects of turbulence over the primary foredune. Sand will be transported seaward across the beach where it will be deposited mainly due to high surface moisture content and micro-topography. This agrees with Wal and McManus (1993) who state that offshore winds indirectly contribute to the development of foredunes by transporting sand on to the beach where is temporally stored, before onshore winds then move it back to the foredunes. The authors also found that offshore winds contributed directly to the development of foredunes through the formation of seaward-dipping wind shadow structures on the seaward side of the main coastal dunes.

Under onshore winds, velocity is highest on the beach and decelerates over the primary foredune before accelerating or maintaining speed over the secondary foredune (Figure 8.2C). Similarly, turbulence slightly increases from the primary foredune toe to the secondary foredune crest. This is a well-established spatial pattern and has been observed in coastal dune systems in the Netherlands (Arens et al., 1995, Arens, 1996b), Canada (Hesp et al., 2005, Walker et al., 2009), and also desert dunes (Frank and Kocurek, 1996a, Wiggs et al., 1996, McKenna Neuman et al., 1997). The main geomorphological implication is sand transport across the beach and sand deposition on the primary foredune, although high levels of turbulence localized over the foredunes may make sand transport possible. In Lincolnshire, topographic forcing during onshore winds causes deviations in the velocity properties of near-surface airflow but not in direction (i.e. undeflected).

The schematic diagrams in Figure 8.2 are the generalized results from several experiments under the same wind regime. Highly oblique onshore winds above the wind velocity threshold only occurred once at Mablethorpe North End (MNE) during one experiment (27th April 2010) which makes it difficult to infer any general patterns,

however overall flow decelerates from the beach to the foredunes and deflects parallel to the crestline mainly due to the smooth topography (refer in section 3.4.3). This topographic steering may not have been observed at BL due to low wind speed conditions during the experiment. Deflection of oblique onshore winds (<30°) to the crestline has been previously observed in the field (e.g. Arens et al., 1995, Walker, 1999, Hesp et al., 2005, Walker et al., 2006). Walker et al. (2009) associated such a deflection with increased turbulence along the seaward foredune slope.

These general patterns are clearly observed where the geomorphological characteristics of the foredunes and beach are relatively simple, such as the low gradient beach and simple primary and secondary foredunes at BL and MNE. Where the foredune-beach system has more complex geomorphology, such as at Theddlethorpe St Helens (TSH) where a field of embryo dunes has developed on the upper-beach expanding seaward, the sediment transfer patterns are disrupted. At TSH there is evidence that the embryo dunes limit the transfer of sediment between the beach and the main coastal dunes by trapping sediment under offshore, onshore and also alongshore winds. At the three sites, the airflow pattern has been shown to be relatively simple across the beach, however this study has not monitored airflow within the intertidal zone characterized by ridge-runnel systems. Recently, Anthony et al. (2009) reported spatial variations in airflow over the intertidal zone due to ridge and runnel topography. Runnels can also reduce the fetch distance due to a high surface moisture content and the presence of micro-topography thus limiting aeolian sand transport across the intertidal zone (Vanhée et al., 2002, Anthony et al., 2009).

By examining relative sand transport capacity it is possible to suggest the most likely geomorphological processes that will take place in different units of the foredune-beach. Figure 8.2 indicates, for example that during offshore winds accretion would be expected in the lee of the secondary foredune and on the beach whilst erosion of the primary foredune may take place, reducing its height and possibly width. For onshore winds, beach volume would be expected to decrease whilst the width and volume of the foredunes would increase. The results agree with Hesp et al. (2005) who suggest that onshore winds encourage vertical accretion of the foredune and also play an important role in the scarp filling process of the dune toe for post-storm recovery.

At this stage, some consideration needs to be given to the timescale over which such changes can be detected. In many coastal environments it is not unusual for wind direction to be very variable over a period of only a few days and unless wind speeds are very strong it may be difficult to detect geomorphological change. The field sites used in Chapter 3 were visited each season (every ~3 months) and detailed topographic measurements were made to determine changes in morphometry. During the period between surveys a range of wind conditions occurred including both offshore and onshore winds with varying degrees of obliquity. Ignoring other variables at this stage, the gap between surveys means that the changes in sub-unit characteristics (height, width, volume) will reflect the net result of all the winds occurring. If onshore winds occur with higher magnitude and frequency the net change in topography should reflect that expected during onshore winds such as an increase in foredune width, whereas geomorphology following periods where offshore winds dominate should show a decrease in foredune width. Table 8.1 compares the predicted geomorphological changes expected as a result of the wind regime (transport footprint) occurring between surveys with those observed in terms of simple changes in the width and volume of the foredune and beach. The latter corresponds to the combined morphological changes of the upper and lower beach at BL and MNE sites. However, the morphological results of the lower beach were only considered at TSH due to the presence of the embryo dunes on the upper beach where in-situ sand reworking takes place. Also, embryo dunes are supplied in sand by alongshore winds (Montreuil and Bullard, 2010) which were excluded in the model.

Table 8.1. Seasonal comparison between predicted (P) and measured morphological changes at BL, TSH and MNE. Ratio onshore/offshore corresponds to the frequency of effective winds, and wind classification is based on the ratio of onshore and offshore sand supply derived from the Q_{T4} model. Grey cells indicate that the predicted and measured relative morphological changes are the same.

Survey	Q_{T4} model Frequency ratio Onsh/Offsh	Wind classification	Foredune width (m)				Foredune volume (m^3)				Beach width (m)				Beach volume (m^3)			
			P	BL	TSH	MNE	P	BL	TSH	MNE	P	BL	TSH	MNE	P	BL	TSH	MNE
S1-S2	14:13	Equal bimodal	+	-	-	+	+	-	+	+	-	-	+	-	-	+	+	-
S2-S3	9:7	Equal bimodal	+	+	+	+	+	+	+	-	-	+	+	+	-	-	+	+
S3-S4	9:2	Weak bimodal	+	-	-	-	+	-	+	+	-	+	-	-	-	+	+	-
S4-S5	7:8	Equal bimodal	-	+	-	+	-	+	-	-	+	-	-	-	+	-	-	-

Whilst in some cases the predicted and observed patterns are the same, for example at MNE, period S1-S2, in more cases the patterns are different. Out of the 48 morphological changes predicted from the wind regime, only 42% were actually observed. This approach was most reliable at MNE (9/16) and least reliable at the BL site (4/16). This is a very simple approach and there are several possible factors that can cause mismatch between the predictions and the observations. First, the ratio of onshore to offshore winds for most seasons was very balanced, thus the net geomorphological change would not be very pronounced. Using this argument the best predictions should be for the S3-S4 period when onshore effective winds were clearly the most frequent, however the performance of the predictions is similar to that for S1-S2, S2-S3 and S4-S5 when offshore and onshore winds were equally effective. Second, the role of alongshore winds is not considered while oblique winds of 10° can potentially supply sand to the foredune (section 5.4.1.B). Third, to most effectively detect geomorphological change in relation to a specific wind regime the foredune-beach geomorphology should be surveyed following a period of winds from a constant direction (e.g. 10-days of onshore winds); Van Houwelingen (2005) reported monthly variations in wind regime along the Lincolnshire coast (2001-2002), so overall, this suggests that the topographic surveys should be more frequent. Fourth, no account is made here of the impact of high magnitude and low frequency events such as storm surge which often induce erosion and foredune retreat. Previous studies have shown that highly energetic marine conditions can be capable of driving sand on the upper-beach or depositing it by swash processes to the foredune (e.g. Anthony et al., 2006, Houser, 2009). Finally, as previously mentioned, sediment supply has been assumed to be unlimited across the foredune-beach, however this is unlikely due to the limiting effect of the vegetation on foredunes (offshore winds) and high surface moisture content often associated with bedforms on the beach (onshore winds). These are further discussed later on.

The simple predictive model in Table 8.1 is based on wind regime and potential areas of erosion and deposition on the dunes. However in Chapter 5, a more complex suite of models was developed and tested that can, in part address some of the limitations outlined above. The models were used to predict the volume of sediment transported into the foredune-upper beach system and tested against actual measurements of the volume of sand from digital elevation models. Model Q_{T4} was found to be the best performing model, probably because it includes the most key factors such as wind speed and direction, grain size, and fetch effect controlled by beach inundation and angle of the wind approach. The improvements of this model are the input value in m^3

unit and the consideration of the beach inundation factor. However, there is a loss of spatial resolution because only two geomorphological sub-divisions are used, foredune and beach, rather than the detailed sub-units used previously.

The data used in Q_{T4} have the advantage of being widely available in many locations and over long time periods because they are standard data sets. This means it should be possible to apply and test the model at a variety of locations and over different timescales. In this thesis no attempt was made to apply the model in any other locations, however it can be tested on longer timescales. Q_{T4} predicted sediment budgets were calculated for the foredunes at the Lincolnshire coast sites for 1994-2010 to see whether the model performs better at longer timescales than for a single year. A variety of geomorphological data in this thesis can be used to test performance, notably the aerial photograph analysis and LIDAR data both surveyed in summer and presented in Chapter 6. The average of grain size in the foredune unit measured over the overall monitoring period was used to parameterize the model at each site. From ortho-photograph analysis, the measured sand budget was determined by multiplying the foredune rate changes, by the length of the foredune section (500 m at BL and TSH and 600 m at MNE) and the foredune height (the average of the foredune height obtained from the EA topographic profiles at BL and MNE) for the chosen time period. Because there is no EA profile at TSH, the average of the foredune height surveyed over the 12-month period in 2009-2010 was used. Additionally, predicted sand budget was compared with the LIDAR data derived from the analysed transects for the available years in 2001 and 2007.

Table 8.2 shows that for four scenarios the predicted sand volume change was within 10% of that measured using aerial photographs or LIDAR data. The model was a good predictor of sand supply to the foredune at BL in 1994-2001 and 2007-2010, and in 2001-2007 at TSH and MNE. However, for some time periods and sites the predicted change is considerably higher or lower than the measured sand volume change. Between 1994-2001 the predicted sand supply to the foredune at MNE was less than half that measured. This is probably due to the landward retreat of the coastal dunes causing by the digging of gas pipelines in 1987 and 1990 with impacts still visible on the ortho-photographs in 1994. Following this disruption period, coastal dunes recovered through human actions (i.e. planting of Marram Grass) associated with natural re-colonization of the vegetation likely favoured by environmental conditions such as high precipitation and effective onshore winds enabling a rapid vegetated dune development (see section 7.3.2.C). Between 2001-2007, the measured foredune sand

volume change at MNE determined from both aerial photographs and LIDAR was lower than that predicted. However, the sand gain difference of 6345 m^3 may be explained by the fact that the surveys were not carried out at the same time and perhaps due to an additional error between these geospatial technologies.

Table 8.2. Comparison between measured and predicted potential foredune sand supply at the meso-scale. Predictions within ±10% are in bold.

Site	Period	Measured sand volume changes from foredune rate changes (m^3)	Measured sand volume from LIDAR surveys (m^3)	Predicted sand supply (m^3)
BL	1994-2001	**52327**		49843
	2001-2007	30707	24362	49244
	2007-2010	**20670**		20475
TSH	1994-2001	60327		44988
	2001-2007	**45363**	**47824**	44448
	2007-2010	10807		18481
MNE	1994-2001	141042		57310
	2001-2007	**51744**	**53102**	56621
	2007-2010	7984		21581

From the Q_{T4} model applied at the meso-scale and also the simple sub-unit predictions inferred from seasonal scale data (Table 8.2), predicted sand supply is sometimes very close to that measured but on occasion considerably higher, or lower which indicates erosion where deposition actually occurred. One of the key factors affecting sand budget that is not accounted for in any of the models is sand output due to storm surge events. Over the seasonal monitoring periods (2009-2010), 6 events with the potential to affect dune morphology occurred (water level ≥ 3.5 m combined with onshore or seaward alongshore wind speed 10 m s^{-1} – see section 4.3.2). The highest cumulative Storm Erosion Susceptibility Index (SESI), incorporating the storm surge intensity, the duration and the significant wave height, was measured between summer and autumn 2010 (S4-S5) due to the occurrence of three consecutive storm surges, the last of which was orientated from the north with an unlimited wave fetch and with winds exceeding 15 m s^{-1}. The expectation was that these events would cause foredune erosion which could be detected in the S5 survey. However of the three sites, erosion was only detected on the foredune-upper beach at TSH (comparing S4 and S5 surveys) whilst accretion occurred at BL and MNE.

At the meso-scale, any event characterized by a water level ≥3.5 m coinciding with onshore or seaward alongshore wind speed ≥ 14 m s^{-1} was considered to have a potential impact on the foredune. Over the period 1994-2001, a high frequency of

storm surge activity occurred with an average of nearly 3 storm surges per year contrasting with an average of only one event per year from 2002-2010 (section 6.3.4). No storm surges were recorded in 2002 and 2003 and during this time the foredune-beach system would be expected to recover from any storm damage (relaxation time). There were 3 storm surge events in 2007 (March, September and November) and 2 in 2008, two of which reached 3.8 m (i.e. 0.3 m higher than the foredune toe), and one event per year in 2009-2010. During the high storm activity period (1994-2001), it would be expected that sediment would be eroded from the foredune. The measured sand budget should thus be lower than the prediction (with the exception of MNE due to human interferences). However, measured and predicted values were relatively similar at BL and measured was higher than predicted at TSH. From 2001 to summer 2007, the model provides a good estimate of the sand supply to the foredune at TSH and MNE but not at BL during the period with few storm surges. A lower measured sand budget than predicted at TSH and MNE can be explained by an increase of storm surges coming from the north (unlimited wave fetch) in 2007 and 2008.

The timing, track, and meteorological and oceanographic characteristics of storm surges and their interaction with hydro-dynamics are key elements in determining foredune impacts (Zhang et al., 2001, Forbes et al., 2004, Cooper et al., 2007). Foredune-beach response to an individual storm event can vary spatially and is a function of coastal sediment budget (Héquette and Aernouts, 2010, Houser and Mathew, 2011), beach antecedent conditions (Morton, 2002, Ruz and Meur-Férec, 2004), coastline orientation and associated nearshore circulation processes (Masselink and Pattiaratchi, 2001), and local shoreface and nearshore morphodynamics (Anthony et al., 2006).

One of the assumptions of the Q_{T4} model is unlimited sediment supply, however the surface moisture content and vegetation on the foredunes which are not incorporated in the model are important supply-limiting factors. Surface moisture on the beach is generally short-lived and is difficult to predict. Sarre (1989) reported that the main factor limiting aeolian sand transport across the foredune-beach is the level of the seawater whereas amount and duration of precipitation have little effect. Additionally, it is reasonable to state that long-term impact of moisture content must be reflected in the vegetation on coastal dunes. However, vegetation density has been relatively stable at the three sites between 1994 and 2010 (refer in section 6.3.2.B).

The Q_{T4} model underestimated the measured foredune sand budget at TSH between 1994 and 2001, however the preceding argument suggests that, due to the high frequency of storm surges, in fact predicted sand transport should have been higher than that which was measured. The measured high accumulation of sand may therefore reflect processes operating along the coastline such as marine inputs. Onshore sand supply processes from the shoreface into the foredune-beach system can occur through different processes such as upper-beach shore-attachment of tidal sand banks after a major storm event (Anthony et al., 2006), a cycle of welding intertidal bars on the beach (Aagaard et al., 2004), and the supply of intermittent and diffuse packets of sand driven by energetic hydro-dynamic conditions (Sabatier et al., 2009). The first process is unlikely to have occurred because the high positive sand budget is only seen at TSH and would have been expected to be recorded at the two others nearby sites. In Chapter 6, the bi-annual EA cross-shore topographic profiles at BL and MNE have not indicated any long-term cyclic onshore migration of intertidal bars over the last 18 years. The third and local mechanism probably took place due to the presence of the subtidal bank acting as a major sediment store (Robinson, 1968a, 1968b, Tonk, 2000, EA, 2008) and decreasing the wave energy at the coast (IECS, 1994). Onshore sand supply would be more likely to be delivered to the shoreface and lower beach, and then incorporated into the foredune by aeolian sand transport processes. However, significant swash deposition of sand on the interface of the upper beach and the foredune toe at high tide can occur if the upper beach flat becomes flooded by large spring tides combined with water level set-up caused by strong onshore winds (Anthony et al., 2006). Further the embryo dunes formed on the upper beach in 2001 may have reduced wave energy during storm surges.

During the early stage of the embryo dune formation between 2001-2007, the model was accurate to within 10% (Table 8.2). However for the late stage from 2007-2010, the model overestimated sand supply to the foredunes, probably due to the retained sand in the embryo dunes on the upper beach depriving the foredune.

As previously suggested in 6.4.1, the foredune-beach system at BL may be a transferring path to the southern section of the coast and not a final deposition site. Sand material from BL may be transported by littoral drift to the south and perhaps to the foredune-beach system at MNE. The mean littoral drift attains a maximum velocity of 0.25 m s^{-1} during spring tides and is c. 0.15 m s^{-1} during neap tides (Kroon and Masselink, 2002). Depending on grain size influences on the mode of transport, sediment material at BL can potentially reach and nourish the coastal section at MNE

after less than 2 hours. Along the Polish Baltic coast, Borówka and Rotnicki (2001) suggested that aeolian sand transport plays an important role in nourishing the alongshore current; they found that the quantity of sand supplied to the sea by aeolian transport from the beach is similar to the amount of eroded sand material from dune cliffs caused by storm surges.

The model prediction was accurate to within ±10% for 6 out of 12 of the foredune sand budget estimates at the meso-scale. A key variable influencing foredune sediment budget is the magnitude and frequency of storm surge events which was not factored in to the model, but may explain the model-observation mismatch on three occasions. The Q_{T4} model performance depends on the variability of both external forcing factors and surplus of marine sand supply to the foredune. However, it can still provide an order-of-magnitude estimate and be used to indicate the occurrence of external positive (amount of marine supply) or negative (storm surge) morphological factors. It is not possible, at present to extend the application of the model to longer periods at these sites due to a lack of long-term wind data. The model would need revisiting if an attempt was to be made to predict long-term changes using the JWT because at present the input data required are hourly whereas JWT is a daily-data set. Additional variables that may confound the model at the multi-decadal scale are sea-level change, and sediment budget with in the coastal cell.

8.3 Top-Scale: Coastal Dune Evolution

Several studies have emphasized that coastal dune evolution is controlled by the shoreface morphodynamics and nearshore processes along many coasts (e.g. Aagaard et al., 2004, Houser et al., 2006, Héquette and Aernouts, 2010), which are to some extent governed by onshore and alongshore drifts (Lapinskis, 2005, Aagaard, 2011).

The deviation from the mean rate of foredune change, corresponding to 1.82 m year^{-1} at BL, 1.93 m year^{-1} at TSH and 1.80 m year^{-1} at MNE, between 1891 and 2010 is plotted in Figure 8.3. Thick marks on the left-axis show the mean rate of foredune change from 1992-2010; mean accretion for this shorter, more recent period is slightly higher than the long-term. At all three sites, the lowest rate of foredune advance was from 1891-1910 and one of the highest rates from 1997-2001, while rates were close to the long-term average between 1953-1976 (with the exception at TSH from 1966-1976). At BL, the difference was generally less than 0.8 m year^{-1}, however rates of

change at the two other sites were more variable. At MNE, the rate of accretion was minimal from 1983-1989 and erosion occurred from 1989-1992.

In Chapter 7, energetic wind events extracted from the JWT catalogue, were shown to be a potentially valuable resource for examining climate influences on coastal morphological trends in the study area. High frequency of onshore wind storm events exceeding 14 m s^{-1} was recorded during 1871-1920, 1955-1970 and 1975-1988 (see Figure 7.17) which may explain the low rate of foredune accretion along the study coast during these periods. The period from the mid-1990s to 2000 was also associated with a high frequency of onshore storms, however a high seaward foredune migration occurred. This can suggest that onshore storm events took place during low tide when little or no foredune impact occur. Storm surge events also affect the Holderness cliffs and often increase the rate of erosion there. Eroded sand material is likely to be supplied to the foredunes by the southern alongshore drift. This also could explain with foredune accretion occurs following a storm surge period.

Although coastal dune erosion is often an area of focus, especially around the UK shoreline, coastal dune accretion is occurring in various coastal settings in Western Europe. For example, east of Calais in the north of France, the foredune advanced seaward more than 300 m from 1949 to 2000, corresponding to extremely rapid rates of c. 6 m year^{-1} (Héquette and Aernouts, 2010). This advance has probably been caused by the nearshore bathymetry and interruption of the littoral drift due to the construction of Calais harbour (Héquette and Aernouts, 2010). Along the east coast of England, coastal dunes at west Brancaster Bay are also undergoing long-term accretion of up to 2 m year^{-1} (Halcrow, 1988, Bristow et al., 2000), favoured by a wide and low angled beach and also influenced by active and reclaimed saltmarshes (Saye et al., 2005). Along a coast with prevailing offshore winds, Ferentinos and McManus (1981) observed a long-term accretion of the coastal dunes at Tentsmuir in Scotland which are the result of a complex interplay of aeolian, wave and tidal processes (Wal and McManus, 1993).
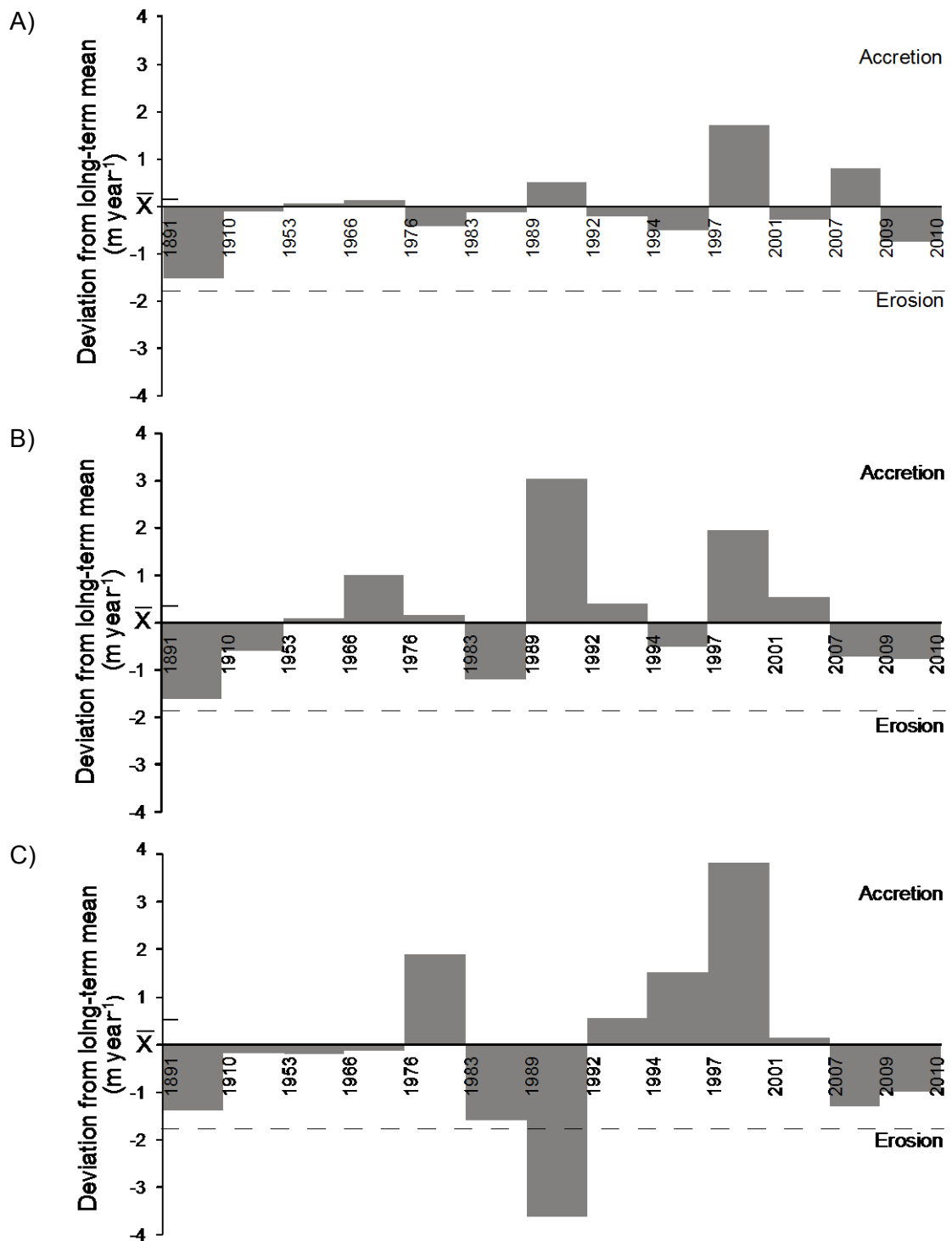
Figure 8.3. Deviation from long-term foredune mean change ($\bar{X}$) between 1891 and 2010 at: (A) BL, (B) TSH and (C) MNE. The mark of the vertical axis shows the mean rate of foredune range determined from aerial photographs from 1992-2010.

The foredune toe morphological changes, determined at the seasonal scale using cross-shore profiles and the long-term using ortho-photographs, suggest a minimum of 2 years of monitoring data make it possible to depict the trend of the dune morphology at BL (Table 8.3). However, a longer data set is necessary for more complex sites such as TSH and MNE. Clearly, the spatial resolution (and spatial averaging) and positional accuracy of the data sets will also have an impact on the length of record required to generate an accurate assessment; in this case the oldest map sources (119 years in Table 8.3) are likely to be less reliable than the more modern aerial photographs. Thus, whilst short temporal topographic data set can reveal seasonal variability, it may lead to a misinterpretation of the long-term foredune trend. Morphology data should further be combined with meterological and marine records to have a complete understanding of foredune-beach trend and evolution. These would also help to predict future foredune-beach morphology.

Table 8.3. Estimates of annual rate of foredune toe position change based on different data sets. Note: where measurements are over period of <1 year rate of change is assumed to be constant for 12-months. Cross-shore profile data are effectively 1-dimensional 'at-a-point' estimates whereas map and ortho-photograph data are 2-dimensional (mean) alongshore (see section 6.2.1 for details). * human interferences

	Cross-shore profiles			**Maps and ortho-photographs**									
	month			year									
Site	3	6	12	1	2	9	13	18	27	44	57	100	119
BL	-4.00	8.60	1.10	1.05	2.62	2.08	2.81	1.83	1.88	1.81	1.84	1.78	1.04
TSH	23.20	22.20	4.40	1.15	1.20	1.84	2.86	2.23	2.17	2.54	2.28	1.81	1.06
MNE	11.60	-3.60	12.00	0.80	0.50	1.22	3.42	2.86	0.36*	1.85	1.72	1.66	1.04

At the Lincolnshire coast, despite considerable short-term/seasonal differences, long-term foredune accretion is remarkably uniform at the three sites studied (Table 8.4). These results agree with Guillén et al. (1999) who studied the foredune toe position along a 120 km stretch of the Dutch coast and found a lower foredune-beach mobility at long-term (decades) than at short-term due to seasonal cycles of storm wave events. The authors further suggested that foredune morphology is controlled by different processes acting simultaneously on the coast but at different timescales. Ruessink and Jeuken (2002) further reported a uniform alongshore trend of the foredune related to the periodicity of storm surge occurrence and a non-uniform trend that closely followed alongshore changes in beach width attributed to the aperiodic addition of material to the beach. Availability of sediment supply within the coastal cell and local nearshore processes control the sand budget of the beach, which turn influences the foredune morphology (Psuty, 1988).

Table 8.4. Alongshore variability of the annual rate of foredune changes between 1891 and 2010 at the three sites.

Site	Number of transect	Average (m year^{-1})	Range (m year^{-1})
BL	10	1.82	1.79-2.21
TSH	11	1.93	1.72-2.48
MNE	13	1.80	1.74-1.97

Chapter 7 demonstrated the inter-linkages between the foredune-beach systems and the nearshore processes within the coastal sediment cell. Erosion of the Holderness cliffs supplies around 1,004,755 m^3 yr^{-1} of sediment to the southerly littoral drift (Montreuil and Bullard, submitted – Appendix 8). Assuming no additional sources out of the coastal sediment cell, the total volumetric changes from the foredune to the beach quantified from the topographic profiles along the whole cell suggests that 29% of the material eroded from the Holderness cliffs is transported 'directly' by the littoral drift to the Lincolnshire coast. Specifically, the total volume of accretion along the study area and extending 2 km north represents 1.24% of the total estimated cliff erosion, while most of the sediment supply along the Lincolnshire coast is deposited in the subtidal or nearshore sand banks. However, the sediment in the banks is transported later to the shoreface by cross-shore currents (Robinson, 1968b, Posford-Duvivier, 1996, EA, 2008) and then potentially supplied to the foredune-beach system.

8.4. Future changes

In the future, a rise of eustatic sea level is expected and may accelerate with global warming (IPCC, 2007). Climate change may also result in an increase in extreme climate events, including an increase in intensity and frequency of storms (storminess), causing high waves to reach the coast (McCarthy et al., 2001, Debernard et al., 2002, Hall et al., 2006, De la Vega-Leinert and Nicholls, 2008). It is well recognized that rising sea level increases the risk of adverse coastal impacts, while accelerations in the rate of rise may initiate profound alterations in geomorphological configurations within coastal sediment cells and their associated sediment dynamics (Church et al., 2001, Pye and Blott, 2006, Nicholls et al., 2007). However, the nature and magnitude of the impact on coastal dunes are difficult to evaluate because the responses of coastal dunes to changes in the magnitude and frequency of such events is hard to predict due to regional and local factors (Carter, 1991, Lee, 2001, Psuty and Silveira, 2010). Bruun (1962) proposed a geometrical adjustment-model, in which the recession of the foredune is proportional to the rise in mean sea level. However, the Bruun model

ignores many major variables including the foredune sediment budget, sediment supply from littoral drift and offshore sources (Cooper and Pilkey, 2004, Davidson-Arnott, 2005). An important number of physical responses may thus occur with a three-dimensional redistribution of large volumes of cross-shore and alongshore sediment controlling the foredune-beach response to the sea level and climate changes.

Along the east coast of England, probabilistic projections of changes in 30-year mean wind speeds relative to 1961-1990 suggest a change of less than 3% by the 2080s (Jenkins et al., 2009). Sea level rise is c.1 mm year^{-1} determined from the measurements at Immingham over the period between 1960 and 2006 (HECAG, 2009), however Woodworth et al. (2009) suggested an average of 0.54 mm year^{-1} using a linear trend regression analysis. Based on these present rates, sea level will rise between c. 0.27 m and 0.50 m by 2050 along the study coast, however it may be greater if there is an increase in the rate of sea level rise in the future. The extrapolation of the future foredune position relative to 2010 projects an advance of 84.4 m at BL, 97.8 m at TSH and 80.4 m at MNE in 2050 corresponding to a seaward migration of 330.5 m, 324.4 m and 294.2 m at the respective sites relative to 1891 (section 7.3.2), however the future coastal change should take account of the potential effects of sea level rise. Future scenarios also suggest that the Holderness cliffs will still be dominated by recession (Quinn et al., 2009). Between 1997-2010, the cliff recession rate was of -2.2 m year^{-1} (section 7.3.1) but predicted regional changes in sea-level and storminess are likely to accelerate it up to -3 m year^{-1} (Pye and Blott, 2010). Eroded sediment from the cliffs would be thus further transported and partly supplied to the north Lincolnshire coast. In addition to the sedimentary inputs, pathways within the coastal cell and cross-shore connections between the nearshore sand banks and the coast will be essential. Along the study area, it is expected that coastal dune evolution would be similar to now through an equilibrium-adjustment in morphology in response to climate change and sea level rise.

As previously presented in section 6.1, Pye's model (1990) incorporates dynamics and continuous relationships between beach-dune sediment budgets, wind regime and vegetation to explain long-term foredune evolution under static sea level rise. The long-term accretion occurring at the three sites is in agreement with Pye's scenario 'b' of seaward coastal propagation under conditions with positive sediment availability, effective wind energy, vegetation trapping and under a static sea level (Figure 6.1). Recently, the author expanded this model by taking account of rising sea level trends (Pye et al., 2007). However, the model only considers transgressive scenarios and

does not suggest what the impacts of sea level rise might be on accreting dune systems. Lee (2001) reported that the storms might lead to the formation of new ridges of sand and shingle which could act as nuclei for dune development and extend the coastal dune field. In the future, it is reasonable to expect coastal dune accretion to continue at the three sites. However, this depends on continued sand supply combined with the absence of frequent and severe storm surge events.

8.5. Improvements and Future Research Considerations

The research reported in this thesis investigated foredune development and evolution on a macro-tidal beach using an up-scaling approach.

Several improvements and considerations became apparent while conducting the present research. Firstly, during the field experiments wind speeds were generally low so that sediment transport measurements were limited. To overcome this limitation, 'sand transport capacity' was considered, however further experiments should be undertaken to validate the present findings for a range of different wind speeds. Secondly, a comparison between airflow measurements and computational simulations of fluid dynamics would validate and enhance insight into the airflow and sand transport processes over the foredune. Simulations would also extend the range of investigated wind conditions which could be confirmed by further field experiments. Thirdly, where the wind regime is complex, if the role of the wind in foredune-beach morphology is to be assessed, topography needs to be measured more frequently than in areas where wind regime is simple (i.e. onshore). Ideally the time interval would be variable according to wind conditions but monthly surveys may be sufficient (section 8.3.2). Finally, the development of a model of foredune sand input and output including storm impacts and supply to the littoral drift will improve the estimate of the actual sand budgets. This should also consider the presence and characteristics of the vegetation on the foredune, and its effect on sand trapping and fetch distance limitation. During offshore winds, vegetation is likely to reduce sand transport and thus supply to the beach whereas this effect is likely to be less important different under onshore wind conditions. Recently, Delgado-Fernandez (2011) suggested that instead of applying a deterministic procedure, adopting a probabilistic approach commonly used in meteorological modelling can offer some benefits and improve modelling of sand supply to the coastal dunes at the meso-scale. The probabilistic approach determines the potential of an event occurrence/magnitude based on historical and long-term data

while including information on the uncertainty of the prediction. Evaluating the performance of the model also might be more critical than measuring its absolute accuracy.

Moreover, directions for further research can be suggested. First, a useful extension of this study would be to investigate the morphological relationships between the foredune-beach system and intertidal ridges-runnels in response to meteorological and oceanographic forcing factors. Previous research has suggested that the intertidal bars are sediment stores and potentially available for onshore aeolian transport, thus controlling the long-term foredune evolutionary trends (Aagaard et al., 2004). Van Houwelingen et al. (2006) described a complex morphological behaviour of the intertidal ridge-runnels along the north Lincolnshire coast, which varies at spatial and temporal scales in response to a combination of external forcing factors. Undertaking seasonal topographic monitoring of the foredune-beach combined with detailed high resolution bathymetric surveys would make it possible to get more insights about the process-responses between the foredune and the beach composed of intertidal bars, and the nearshore zones, thus providing information on the potential sediment availability for aeolian transport delivery to the foredunes. These insights could be further combined into a numerical model to simulate disturbances of the ridges-runnels and impacts on the coastal dunes under various external forcing conditions. Availability of such data presents an opportunity to appreciate the range of morphological behaviours and changes of the foredune-beach system at various timescales (Thom and Hall, 1991). This type of foredune-beach system is quite common, occurring not only around UK coast but also in France, Belgium, The Netherlands and along other macro-tidal coasts characterized by a gentle beach gradient, a short wave fetch and a surplus of sediment (King, 1972). Second, a higher resolution temporal study of the impacts of storm surge events would be useful. Most research in to storm impacts has focused on high magnitude events and found that it is necessary to quantify the foredune-beach state immediately before and after the event occurs as well as regular monitoring of recovery. For coasts where storm surges are typically of lower magnitude, but still of potential geomorphological significance, such pre- and immediate post-storm evaluation is even more important because geomorphological impacts are less obvious. Detailed information on the storm surge return period and also foredune recovery period would be useful for coastal managers and planners.

Finally, ground-penetrating radar has been demonstrated to be a successful technique for examining the internal structure of coastal dunes and is often associated with

luminescence dating for determining the timing of their formation and evolution (Clemmensen at al., 2001, Wilson et al., 2001). Such data sets would extend the temporal scale and make it possible to elucidate foredune storm-recovery. Bristow et al. (2000) undertook ground-penetrating radar surveys of the dunes at Brancaster approximately 50 km south of the present study area and found records of the severe storm surge in the 1950s, probably the 1953 severe storm surge. The authors also reported that coastal dune development is linked to the beach state, with dune development associated with shoreline propagation, which has dominated at Brancaster where offshore winds also prevail and are suggested be reducing the landward migration of the coastal dunes.

8.6. General Conclusion

The overall aim of this research was to improve understanding of the ways in which foredune-beach interactions occur under a complex wind regime at a range of overlapping temporal and spatial scales. This study contributes to the existing literature by presenting the characteristics of the foredune morphodynamics coupled with the beach as a coastal geomorphic system. It also addressed the process-response at various temporal and spatial scales, ranging from micro-scale airflow and sand transport processes to the macro-scale evolution of foredunes over the last century. Results have also demonstrated that the interaction of processes at different temporal and spatial scales, in addition to the occurrence of external forcing factors and feedback-dominated morphological responses, increases the complexity of the dynamics of the foredune-beach system. Findings were embedded to propose an up-scaling foredune-beach morphodynamic model.

More specifically, the conclusions relating to the defined objectives in this thesis are:

(1) "Identify near-surface airflow processes operating on the foredune-beach systems under different wind regimes at the micro-scale" – Airflow over the foredunes experiences alterations in velocity and direction that can be remarkable and vary spatially depending on wind direction at the three sites, while steady and undisturbed airflow prevails on the beach. For direct offshore and onshore winds, the airflow stays attached and undeflected over the foredune, while it is deflected parallel along the foredunes during oblique offshore winds.

(2) "Use the findings from (1) to develop a conceptual model describing the patterns of sand transport and deposition under different wind conditions" – During offshore winds, near surface airflow decelerates over the secondary foredunes favouring sand deposition while it progressively recovers over the primary foredune to accelerate across the beach. Erosion is thus likely to occur superimposed by the turbulence effect at the primary foredune. Sand is then transported across the beach to reach its seaward side where it is probably deposited due to high surface moisture content and presence of micro-topography features. A similar near-surface airflow pattern takes place on the beach during onshore winds, however the airflow is subject to deceleration over the primary foredune leading to sand deposition. The secondary foredune topographically induces airflow acceleration which potentially allows sand to reach its crest. The spatial variability of the near surface airflow processes control the transport capacity and pathways, which in turn control foredune morphodynamics.

(3) "Compare seasonal measured and predicted rates of sediment supply in order to define the roles of different wind directions in foredune formation at the meso-scale" – Over the seasonal monitoring periods, effective onshore transporting winds prevailed resulting in a potential net sand transport directed from the beach to the foredune. The comparison between the measured and developed model of sand supply has however demonstrated that effective offshore and alongshore sand transporting winds must also be considered as contributors to the foredune-upper beach system.

(4) "Generate a time series of digital terrain models of the dunefield and of historical foredune position to determine the annual changes and long-term evolutionary tendency and to investigate the relative importance of different external factors in driving those changes" – Foredune evolution has been dominated by a rapid and significant accretion of c. 2 m year^{-1} at the three sites over the last 120 years. This reflects a synchronizing balance between significant marine sediment supply availability and effective wind regime. Along the study coast, the occurrence of storm surge event is low leading to an efficient relaxation time for a complete post-storm recovery.

5) "Up-scale from micro- to macro-scales to contribute to the wider understanding of the foredune-beach geomorphological system" – The up-scale approach, combined with overlapping timescales, has made it possible to have a better understanding of the foredune-beach geomorphic system. Micro-scale airflow and sand transport processes were measured under different wind conditions to characterize the near-surface airflow

and transport capacity across the foredune-beach profile. The findings were used to simulate morphological development and then compared to the seasonal measured foredune-beach changes in order to interpret the morphological implications and sediment patterns of the different wind components. Using a deterministic procedure, a model of sand supply was developed at the seasonal time frame, and tested against the measured foredune-upper beach sand volume changes. This model was then extrapolated and compared with the rate of foredune changes at the meso-scale determined using aerial photographs and LIDAR data. The sand supply model does not always accurately predict sand supply, because it does not include the potential influence of storm surges. At the macro-scale, coastal dune evolution is strongly controlled by the availability of sediment material, transfer processes and pathways occurring within the sediment cell. In this study, the modelling approach for resolving aeolian transport to coastal dunes has been shown to predict approximately the same order of magnitude of change as measured sand deposition into the coastal dunes. The model incorporated wind speed and direction, grain size, fetch effect controlled by the beach inundation and angle of wind approach. These have some implications for modelling and management, and highlight that micro-scale airflow process could be neglected to predict long-term sand supply to the coastal dunes. This thesis has also shown that the Jenkinson Daily Weather Type classification was found to be a reasonable proxy for the occurrence of strong onshore winds along the study coast which may offer scope for further investigation of the role of forcing factors over time periods beyond the length of the meteorological and tidal station records. Winter North Atlantic Oscillation phase however was not a good indicator of storminess on the study coast but may be a useful proxy for quiescence. Although these environmental conditions are similar along the study sites, local morphology of the foredune-beach plays an important in the long-term evolution. The determined dominant processes and morphological changes at each scale level were synthesized to contribute to the understanding of the foredune-beach morphodynamic system.

This study approach has provided invaluable information about the foredune-beach system at both temporal and spatial scales. It is hoped that this research project may serve as a useful comparative resource for any future coastal dune studies and management. In a coastal environment with a complex wind regime, all wind components may contribute to sand supply into the foredune and thus to its development. Offshore winds thus have the potential to be an important driver in foredune-beach morphodynamics and evolution and should be taken into account

when compiling foredune sand budgets. This factor should be considered by coastal managers developing foredune management plans.

A key variable influencing foredune-beach sand volume is the magnitude and frequency of storm surge events and this was not, however, factored in to the model. Since coastal dunes evolve as a consequence of gradual changes but also respond to the occurrence of episodic disturbing events, it would be important to consider both sand input and output of the coastal dunes. The fundamental steps for the adequate prediction of foredune development and storm response should be based on the understanding of storm climatology and the nature of their impacts.

Moreover, this study reinforces that temporal scale of interest has an impact on the foredune behaviour and the estimated rate of foredune change. Short-term study (from 3-months to 1 year) is likely to show short-temporal changing trends of the foredune-beach system (i.e. cycle of accretion/erosion) whereas its evolutionary trend would be depicted after a minimum of 2 years depending on the morphological complexity of the site. This demonstrates the problem of the limitation of topographic data availability associated with meteorological and oceanographic measurements to fully understand foredune-beach behaviour. The lack of a comprehensive view of the dynamics of the foredune-beach is a main limitation to providing managers and planners with a suitable set of tools for decision-making (Sherman et al., 1995).

Finally, the complexity of morphodynamic processes and the dynamic foredune-beach system present a challenge for coastal management (Thomas, 1999). Preserving or enhancing the morphodynamics of the foredune-beach system necessitates innovative designs rooted in geomorphological and aeolian research (Jackson and Nordstrom, 2011). Predictions of accelerated sea level rise and possible increased storminess related to global warming over the next century have been shown to markedly alter sediment budget regimes and behaviours in foredune-beach systems. Therefore, it is necessary to have a better understanding of the foredune processes and morphological changes from micro- to macro-scales in order to review future management options and subsequently to implement the most suitable strategies that also consider the uncertainties related to possible future coastal change.

References

Aagaard, T., 2011. Sediment transfer from beach to shoreface: the sediment budget of an accreting beach on the Danish North Sea coast. Geomorphology, 135, 143-157.

Aagaard, T., Orford, J., and Murray, A.S., 2007. Environmental controls on coastal dune formation : Skallingen Spit, Denmark. Geomorphology, 83, 29-47.

Aagaard, T., Davidson-Arnott, R., Greenwood, B., and Nielsen, J., 2004. Sediment supply from shoreface to dunes: linking sediment transport measurements and long-term morphological evolution. Geomorphology, 60, 205-224.

ABP (Associated British Ports), 1996. Southern North Sea sediment transport study, literature review and conceptual sediment transport model. Report R.546. ABP Research and Consultancy Ltd, Southampton, 80p.

Adams, J.C., and Chandler, J.H., 2002. Evaluation of lidar and medium scale photogrammetry for detecting soft Cliff Coastal change. Photogrammetric Record, 17 (99), 405-418.

Admiralty, 2009. Admiralty Tide Tables. Volume 1. United Kingdom and Ireland, including European Channel Ports. Hydrographic Office, Tauton, 440p.

Admiralty Tidal Stream Atlas, 1962. (eds). Tidal Stream Atlas, North Sea, Southern Portion. Hydrographic Office, Taunton.

Alexandersson, H., Tuomenvirta, H., Schmith, T. and Iden, K., 2000. Trends of storms in NW Europe derived from an updated pressure data set. Climate Research 14, 71-73.

Anderson, R.S and Haff, P.K., 1991. Wind modification and bed response during saltation of sand in air. Acta Mechanica Supplementum, 1, 21-52.

Andrews, B.D, Gares, P.A. and Colby, J.D., 2002. Techniques for GIS modeling of coastal dunes. Geomorphology, 48, 289-308.

Anfuso, G., Dominguez, L. and Gracia, F.J. 2007. Short and medium-term evolution of a coastal sector in Cadiz, SW Spain. Catena, 70, 229-242.

Anthony, E.J., Ruz, M.H. and Vanhée, S., 2009. Aeolian sand transport over complex intertidal bar-trough beach topography. Geomorphology, 105, 95-105.

Anthony, E.J, Vanhée, S. and Ruz, M-H., 2006. Short-term beach-dune sand budgets on the north sea coast of France: sand supply from shoreface to dunes, and the role of wind and fetch. Geomorphology, 81, 316-329.

Anthony, E.J., Levoy, F. and Degryse-Kulkami, C., 2005. Short-term intertidal bar mobility on a ridge-and-runnel beach, Merlimont, northern France. Earth Surface Processes and Landforms, 30, 81-93.

Anthony, E.J., 2000. Marine sand supply and Holocene coastal sedimentation in northern France between the Seine estuary and Belgium. In: Pye, K. and Allen, J.R.L. (eds). Coastal and Estuarine Environments, Sedimentology, Geomorphology and Geoarchaeology. Geological Society Special Publication 175, London, 87-97.

Arens, S.M., 1997. Transport rates and volume changes in a coastal foredune on a Dutch Wadden Island. Journal of Coastal Conservation, 3, 49-56.

Arens, S.M., 1996a. Rates of aeolian transport on a beach in a temperature humid climate. Geomorphology, 17, 3-18.

Arens, S.M., 1996b. Patterns of sand transport on vegetated dune. Geomorphology, 17, 339-350.

Arens, S.M., 1995. Air flow over foredunes and implications for sand transport. Earth surface processes and landforms, 20, 315-332.

Arens S.M., Van Kaam-Peters H.M.E. and Van Boxel, J.H., 1995. Air flow over foredunes and implications for sand transport. Earth Surface Processes and Landforms, 20, 315-332.

Arens, S.M. and Van der Lee, G.E.M., 1995. Saltation sand traps for the measurement of aeolian transport into the foredunes. Soil Technology, 8, 61-74.

Arens, S. M., 1994. Aeolian Processes in the Dutch Foredunes. PhD-thesis, University of Amsterdam, 150p.

Arens, S.M. and Wiersma, J., 1994. The Dutch foredunes; inventory and classification. Journal of Coastal Research, 10, 189-202.

Arnold, S., 2002. Development of the saltation system under controlled environmental conditions. Earth Surface and Landforms, 27, 817-829.

Ashkenazi, V. Dumville, M., Bingley, R. and Dodson, A., 2000. The use of remote sensing in climate change, R&D technical Report E82. Environment Agency R&D Dissemination Centre, Swindon, 24p.

Atherton, R.J., Baird A.J. and Wiggs G.F.S., 2001. Inter-tidal dynamics of surface moisture content on a meso-tidal beach. Journal of Coastal Research, 17, 482-489.

Baas, A.C.W., 2008. Challenges in aeolian geomorphology: Investigating aeolian streamers. Geomorphology, 93, 3-16.

Baas, A.C.W., 2007. Complex systems in aeolian geomorphology. Geomorphology, 91, 311-331.

Baas, A.C.W., 2002. Chaos, fractals and self-organization in coastal geomorphology: simulating dune landscapes in vegetated environments. Geomorphology, 48, 309-328.

Bacon, S., and Carter, D.J.T., 1993. A connection between mean wave height and atmospheric pressure gradient in the North Atlantic. International Journal of Climatology, 13, 423-436.

BADC, 2009. British Atmospheric Data Centre. [online] Available at: <http://badc.nerc.ac.uk/home/index.html> [access 12th November 2011].

Bagnold, R.A., 1954. Experiments on the gravity-free dispersion of large spheres in a Newtonian fluid under shear, Proceedings of the Royal Society London, 225, 49-63.

Bagnold, R.A. 1941. The Physics of blown sand and desert dunes. Methuen, London, 265p.

Baily, B., Collier, P., Farres, P. Inkpen, R. and Pearson, A., 2003. Comparative assessmenet of analytical and digital photogrammetric methods in the construction of DEMs of geomorphological forms. Earth Surface Process and Landforms, 28, 307-320.

Balson, S., and Jeffery, D.H., 1991. The glacial sequence of the southern North Sea. In Ehlers, J., Gibbard, P. L. and Rose, J. (eds). Glacial deposits in Great Britain and Ireland. Balkema, Rotterdam, 245-254.

Balson, P.S. and Harrison, D.J., 1988. Marine aggregate survey Phase 1: Southern North Sea. British Geological Survey, Marine report 86/38.

Baltsavias, E.P., 1999. Airborne Laser Scanning: basic Relations and Formulas. ISPRS Journal of Photogrammetry & Remote Sensing, 54, 199-214.

Battiau-Queney, Y., Billet, J-F., Chaverot, S., and Lanoy-Ratel, P., 2003. Recent shoreline mobility and geomorphologic evolution of macrotidal sandy beaches in the north of France. Marine Geology, 194, 31-45.

Bauer, B.O. and Davidson-Arnott, R.G.D., Hesp, P.A., Namikas, S.L., Ollerhead, J. and Walker, I.J., 2009. Aeolian sediment transport on a beach: surface moisture, wind fetch and mean transport. Geomorphology, 105, 106-116.

Bauer, B.O. and Davidson-Arnott, R.G.D., 2002. A general framework for modeling sediment supply to coastal dunes including wind angle, beach geometry, and fetch effects. Geomorphology, 49, 89-108.

Bauer, B.O. and Sherman, D.J., 1999. Coastal dune dynamics: problems and prospects. In: Goudie, A.S., Livingstone, I. and Stokes, S. (eds). Aeolian Environments, Sediment and Landforms. Wiley and Sons, Chichester, 325p.

Bauer, B.O., Yi, J., Namikas, S.L. and Sherman, D.J., 1998. Event detection and conditional averaging in unsteady aeolian systems. Journal of Arid Environments, 39, 345-375.

Bauer, B.O., Davidson-Arnott, R.G.D., Nordstrom, K.F., Ollerhead, J. and Jackson, N.L., 1996. Indeterminacy in aeolian sediment transport across beaches. Journal of Coastal Research, 12, 641-653.

Belly, P.Y., 1964. Sand movement by wind (with Addendun II by A.A. Kadid). U.S. Army, Corps of Engineering Coastal Engineering Research Center, Technical Memorandum, 1, 79p.

Birds, E., 2000. (eds). Coastal Geomorphology: An introduction. Wiley, Chichester, 322p.

Black & Veatch, 2004. Humber Estuary shoreline management plan phase 2, summary of geomorphology studies. Report produced for Environment Agency, Surrey, 45p.

BODC, 2009. British Oceanographic Data Centre, UK Tide Gauge Network. [online] Available at:
< https://www.bodc.ac.uk/data/online_delivery/ntslf/processed/>
[access 20th November 2011].

Bórowka, I.M and Rotnicki, K., 2001. Budget of the eolian sand transport on the sandy barrier beach, a case study of the Leba Barrier, southern Baltic coast, Polan. Zeitschrift für Geomorphologie, 45, 55-79.

Bott, S. and Hart, H., 1990. Particle size analysis utilizing polarization intensity differential scattering, Coulter Electronics. New England, 17-18.

Bouws, E., Janninxk, D. and Komen, J., 1996. The increasing wave height in the North Atlantic Ocean. Bulletin of the American Meteorological Society, 77, 2275-2277.

Brampton, A.H. and Bevan, S.M., 1987. Beach Changes along the coast of Lincolnshire, UK. (1959-1985). Proceedings on Coastal Sediments' 87, ASCE, 539-554.

Bray, M. and Hooke, J., 1997. Prediction of soft-cliff retreat with accelerating sea-level rise. Journal of Coastal Research, 13, 453-467.

Bristow, C.S., Chroston, P.N., Bailey, S.D., 2000. The structure and development of foredunes on a locally prograding coast: insights from ground-penetrating radar surveys, Norfolk, UK. Sedimentology, 47, 923-944.

Brock, J.C., Wright, C.W., Sallenger, Jr. A.H., Krabill, W.B. and Swift, R.N., 2002. Basis and methods of NASA airborne topographic mapper LIDAR surveys for coastal studies. Journal of Coastal Research, 18, 1-13.

Brooks, S.M. and Spencer, T., 2010. Temporal and spatial variations in recession rates and sediment release from soft rock cliffs, Suffolk coast, UK. Geomorphology, 124, 26-41.

Brown, D.G. and Arbogast, A.F., 1999. Digital photogrammetric change analysis as applied to active coastal dunes in Michigan. Photogrammetric Engineering and Remote Sensing, 65, 467-474.

Bruun P., 1962. Sea-level rise as a cause of shore erosion. Journal Waterways Harbors Division. ASCE, 88, 117-130.

Bryant, E., 1987. Storminess and high tide beach change Stanwell Park, Australia, 1943-1978. Marine Geology, 79 (3), 171-187.

Buchanan, C.M., Beverland, I.J. and Heal, M.R., 2002. The influence of weather-type and long-range transport on airborne particle concentrations in Edinburgh. UK. Atmospheric Environment, 36, 5343-5354.

Buckley, R., 1987. The effect of sparse vegetation on the transport of dune sand by wind. Nature, 325, 426-428.

Burrough, P.A. and McDonnell, R.A., 1998. Principles of geographical information systems. Oxford University Press, England, 333p.

Butterfield, G.R., 1991. Grain transport rates in steady and unsteady turbulent airflows. Acta Mechanica, 1, 97-122.

Butterfield, C.P., 1989. Aerodynamic pressure and flow visualization measurements from a rotating wind turbine blade, Proceedings of the 8th ASME Wind Energy Symposium, 7, 245-255.

Campbell Scientific, 2009. Wind speed and direction sensors A 100R anemometer and W200P-1 windvane. Campbell Scientific, Loughborough, 2p.

Campbell Scientific, 2007. CSAT3 three dimensional sonic anemometer user guide. Campbell scientific, Loughborough, 42p.

Carnell, R.E., Senior, C.A. and Mitchell, J.F.B., 1996. An assessment of measures of storminess: simulated changes in northern hemisphere winter due to increasing CO2, Climate Dynamics, 12, 467-476.

Carter, R.W.G., 1991. Near-future sea level impacts on coastal dune landscapes. Landscape Ecology, 6, 29-39.

Carter, R.W.G., Hesp, P.A. and Norsdtrom, K.F., 1990. Erosional landforms in coastal dunes, In: Nordstrom, K.F. and Psuty, N.P., (eds). Coastal Dunes, Form and Process. John Wiley & Son Ltd., Chichester, 217-250.

Carter, R.W.G., Devoy, R.J.N. and Shaw, J., 1989. Late Holocene sea levels in Ireland. Journal of Quaternary Science, 4, 7-24.

Carter, R.W.G., 1988. Coastal Environments, An introduction to the physical, ecological and cultural systems of coastlines. Academic Press, London, 301-333.

CERC (Coastal Engineeering Research Center), 1984. Shore protection manual (in 2 Volumes) (eds). US Army Corps of Engineers, Coastal Engineering Research Center, Washington DC.

Chandler, J.H., 1999. Effective application of automated digital photogrammetry for geomorphological research. Earth Surface Process and Landforms, 24, 51-63.

Chandler, J.H. and Brunsden, D., 1995. Steady state behaviour of the Black Ven Mudslide: the application of archival analytical photogrammetry to studies of landform change. Earth Surface Process and Landforms, 20, 255-275.

Chapman, C.A., Walker, I.J., Hesp, P.A., Bauer, B.O. and Davidson-Arnott, R.G.D., 2012. Turbulent Reynolds stress and quadrant event activity in wind flow over a coastal foredune, Geomorphology, 151-152, 1-12.

Chaverot, S., Héquette, A. and Cohen, O., 2008. Changes in storminess and shoreline evolution along the northern coast of France during the second half of the 20th century. Zeitschrift für Geomorphologie, 52 (3), 1-20.

Chaverot, S., Héquette, A. and Cohen, O., 2005. Evolution of climatic forcing and potentially eroding events on the coast of Northern France. Coastal Dynamics 2005_State of the Practice Proceedings of the 5th International Conference, ASCE, 214-225.

Clarke, M.L., Rendell, H.M., Tastet, J-P., Clavé, B. and Lassé, L. 2002. Late Holocene sand invasion and North Atlantic storminess along the Aquitaine coast, southwest France. The Holocene, 12, 231-238.

Chepil, W.S., Siddoway, F.H. and Armbrust, D.V., 1964. Prevailing wind erosion direction. Journal of Soil and Water Conservation, 19, 67-71.

Christiansen, M.B. and Davidson-Arnott, R.G.D., 2004. Rates of landward sand transport over the foredune at Skallingen, Denmark and the role of dune ramps. Danish Journal of Geography, 104, 1, 31-43.

Church, J.A., Gregory, J.M., Huybrechts, P., Kuhn, M., Lambeck, K., Nhuan, M.T., Qin, D., Woodworth, P.L., 2001. Changes in Sea Level, Chapter 11. In Houghton, J.T., Jenkins, G.J. and Ephraums, J.J. (eds). in International Panel on Climate Change, Climate Change 2001, the Scientific Basis, Cambridge University Press, Cambridge, 639-693.

Claudino-Sales, V., Wang, P. and Horwitz, M.H., 2008. Factors controlling the survival of coastal dunes during multiple hurricane impacts in 2004 and 2005: Santa Rosa barrier island, Florida. Geomorphology, 95, 295-315.

Clemmensen, L.B., Pye, K., Murray, A. and Heinemeiers, J., 2001. Sedimentology, stratigraphy and landscape evolution of a Holocene coastal dune system, Lodbjerg, NW Jutland, Denmark. Sedimentology, 48, 3-27.

Clemmensen, L.B., Andreasen, F., Nielsen, S.T., and Sten, E., 1996. The late Holocene dunefield at Vejers, Denmark: characteristics, sand budget and depositional dynamics. Geomorphology, 17, 79-98.

Coates, M.J., Folkard, A.M., 2009. The effects of littoral zone vegetation on turbulent mixing in lakes. Ecological Modelling, 220, 20, 2714-2726.

Cooper, J.A.G., McKenna, J., Jackson, D.W.T. and O'Connor, M., 2007. Mesoscale coastal behavior related to morphological self-adjustment. Geological Society America Geology, 35 (2), 187-190.

Cooper, J.A.G, Jackson, D.W.T., Navas, F., McKenna, J. and Malvarez, G., 2004. Identifying storm impacts on an embayed, high energy coastline: examples from western Ireland. Marine Geology, 210, 261-280.

Cooper, J.A.G. and Pilkey, O.H., 2004. Sea-level rise and shoreline retreat: time to abandon the Bruun Rule. Global and Planetary Change, 43, 157-171.

Cornelis, W.M., Oltenfreiter, G., Gabriels, D. and Hartmann, R., 2004. Splash-saltation of sand due to wind-driven rain: horizontal flux and sediment transport rate. Soil Science Society America Journal, 68, 41-46.

Crowell, M., Douglas, B.C. and Leatherman, S.P., 1997. On forecasting future U.S. shoreline positions: a test of algorithms, Journal of Coastal Research, 13, 1245-1255.

Crowell, M., Leatherman, S.P. and Buckley, M.K., 1991. Shoreline change rate analysis: long-term versus short term data. Shore and Beach, 61, 13-20.

CRU (Centre Research Unit), 2011a. Lamb weather types. University of East Anglia. [online] Available at:
http://www.cru.uea.ac.uk/cru/data/lwt/ [access 22nd March 2011].

CRU (Centre Research Unit), 2011b. North Atlantic Oscillation (NAO). University of East Anglia. [online] Available at:
<http://www.cru.uea.ac.uk/cru/data/nao/>[access 25th March 2011].

Davidson-Arnott, R.G.D and Bauer, B.O., 2009. Aeolian sediment transport on a beach: Thresholds, intermittency, and high frequency variability. Geomorphology, 105, 117-126.

Davidson-Arnott, R.G.D., Yang, Y., Ollerhead, J., Hesp, P.A. and Walker, I.J., 2008. The effects of surface moisture on aeolian sediment transport threshold and mass flux on a beach. Earth Surface Processes and Landforms, 33, 55-74.

Davidson-Arnott R.G.D., 2005. Conceptual model of the effects of sea level rise on sandy coasts. Journal of Coastal Research 21, 1166–1172.

Davidson-Arnott, R.G.D. and Dawson, J.D., 2001. Moisture and fetch effects on rates of aeolian sediment transport, Skallingen, Denmark. Proceedings Canadian Coastal Conference, CCSEA, 309-321.

Davidson-Arnott, R.G.D. and Law, M.N., 1996. Measurement and prediction of long-term sediment supply to Coastal Foredunes. Journal of Coastal Research, 12, 654-663.

Davidson-Arnott, R.G.D. and Law, M.N. 1990. Seasonal patterns and controls on sediment supply to coastal foredunes, Long Point, Lake Erie. In: Nordstrom, K.F. and Psuty, N.P. (eds). Coastal Dunes, Form and Process, John Wiley & Son Ltd., Chichester, 177-199.

Davies, J.I., 1964. A morphogenic approach to world shorelines. Zeitschrift für Geomorphologie, 8, 127-142.

Debernard, J., Sætra, Ø. and Røed, L.P., 2002. Future wind, wave and storm surge climate in the northern North Atlantic. Climate Research, 23, 39-49.

De Boer, D.H., 1992. Hierarchies and spatial scales in process geomorphology: a review, Geomorphology, 4, 303-318.

DEFRA (Department for Environment, Food, Rural Affairs), 2006. Shoreline management plan guidance Volume 1: aims and requirements. DEFRA, London, 44p.

De la Vega-Leinert, A.C. and Nicholls, R.J., 2008. Potential implications of sea-level rise for Great Britain. Journal of Coastal Research, 24, 342-357.

Delgado-Fernandez, I., 2011. Meso-scale modelling of Aeolian sediment input to coastal dunes. Geomorphology, 130, 230-243.

Delgado-Fernandez, I. and Davidson-Arnott, R.G.D., 2011. Meso-scale Aeolian sediment input to coastal dunes: the nature of Aeolian transport events. Geomorphology, 126, 217-232.

Delta-T Devices. 1999. Theta Probe Soil Moisture Sensor Type ML2x User Manual. Delta-T Devices, Ltd, Cambridge, 22p.

Department of Energy, 1989. Wave Climate Atlas of the British Isles. OTH 89 303. HMSO, London.

De Vriend, H.J., 1991. Mathematical modeling and large scale coastal behaviour. Part 1. Physical Progress. Journal of Hydraulic Research, 29 (6) 727-740.

Digimap, 2011. Historic Digimap, historical OS maps from the 1840s to the 1990s. [online]. Available at: <http://digimap.edina.ac.uk/main/services.jsp?collection=historic>[access 6th March 2011].

Doblas-Reyes, F.J., Casado, M.J. and Pastor, M.A. 2002. Sensitivity of the Northern Hemisphere blocking frequency to the detection index. Journal Geophysical Research D, 107, ACL 6, 1-22.

Dolan, R., Fenster, M.S. and Holmes, J., 1991. Temporal analysis of shoreline recession and accretion. Journal of Coastal Research, 3, 723-744.

Doody, J.P., 1991. (eds). Sand Dune Inventory of Europe. Joint Nature Conservation Committee/European Union for Coastal Conservation, Peterborough.

Dossor, J., 1955. The coast of Holderness: the problem of erosion, Proceedings of the Yorkshire geological society, 30 (2), 133-145.

Dugdale, R.E. and Vere, A., 1993. Saving Lincolnshire's beaches. East Midland Geographer, 16 (1), 31-32.

Dugdale, R.E., 1980. Nearshore sandbanks and foreshore accretion on the south Lincolnshire coast. East Midland Geographer 7 (2), 49-63.

Dyer, K.R. and Moffat, T.J., 1998. Fluxes of suspended matter in the East Anglian plume Southern North Sea. Continental Shelf Research, 18, 1311-1331.

EA (Environment Agency), 2011. Anglian coastal monitoring programme, Lincshore coastal morphology report 2006-2011. Shoreline Management Group, Peterborough, 37p.

EA (Environment Agency), 2008. Anglian coastal monitoring programme, Coastal trend analysis, Lincolnshire, Subcells 2b-c_Grimsby to Gibraltar Point. Shoreline Management Group, Peterborough, 63p.

EA (Environment Agency), 2004. Lincshore 2005 to 2010 PAR Volume 1, Strategy for approval. Report to Environment Agency, Anglian Region, Peterborough. Halcrow, Swindon.

Eastwood, D.A. and Carter, R.W.G., 1981. The Irish dune consumer: a preliminary investigation of motivations and perceptions of coastal recreation visitors as a potential aid to management decision marketing. Journal of Leisure Research, 14, 278-281.

Ebdon, D., 1977. (eds). Statistics in Geography. Wiley-Blackwell, Orford, 232p.

El-Kadi, A.K.A. and Smithson, P.A., 1992. Atmospheric classifications and synoptic climatology, Progress in Physical Geography, 16 (4), 432-455.

Ellis, J.T., Li, B., Farrell, E.J. and Sherman, D.J., 2009. Protocols for characterizing Aeolian mass-flux profiles. Aeolian Research, 1, 19-26.

Eurosion, 2003. Holderness coast, UK, Eurosion case study, DHV group, 22p.

Fairbanks, R.G., 1989. A 17,000-year glacio-eustatic sea level record: Influence of glacial melting rates on the Younger Dryas event and deep-ocean circulation. Nature, 342, 637-642.

Ferentinos, G. and McManus, J., 1981. Nearshore processes and shoreline development in St Andrews Bay, Scotland, UK. In: Nio, S.D., Shittenhelm, R.T.E. and Van Weering, T.C.E. (eds) Holocene marine sedimentation in the North Sea Basin. Special Publication International Association of Sedimentologists, 5, 161-174.

Ferreira, Ó., 2005. Storm groups versus extreme single storms: predicted erosion and management consequences. Journal of Coastal Research 42, 221-227.

Forbes, D.L., Parkes, G.S., Manson, G.K. and Ketch, L.A., 2004. Storms and shoreline retreat in the southern Gulf of St Lawrence. Marine Geology, 210, 169-204.

Frank, A. and Kocurek, G., 1996a. Toward a model for airflow on the lee side of aeolian dunes. Sedimentology, 43, 451-458.

Frank, A.J. and Kocurek, G., 1996b. Airflow up the stoss slope of sand dunes: limitations of current understanding. Geomorphology, 17, 47-54.

Fryberger, S.G., 1979. Dune forms and wind regime. In: McKee, E.D. (eds). A Study of Global Sand Seas, USGS Professional Paper, 1052. US Geological Survey and United States National Aeronautics and Space Administration, Washington, 137-169.

Fryrear, D.W., 1986. A field dust sampler. Journal of Soil and Water Conservation, 41, 117-119.

Gardline, 2008. Lincolnshire coastline bathymetric/beach survey, summer 2008, survey report Ref 7689, 19p.

Gares, P.A. , Nordstrom , K.F., Sherman , D.J., Bauer, B.O., Davidson-Arnott, R.G.D. Carter, R.W.G., Jackson, D.W.T and Gomes, N., 1993. Aeolian sediment transport under offshore wind conditions: implications for aeolian sediment budget calculations. In: Hildebrand, L.P. (eds). Coastlines of Canada. New York, ASCE, 59-72.

Gares, P.A., 1992. Topographic changes associated with coastal dune blowouts at Island beach park, New Jersey. Earth Surface Processes and Landforms, 17, 589-604.

Gares, P.A. 1988. Factors affecting eaolian sediment tra,nsport in beach and dune environments. Journal of Coastal Research, SI3, 121-126.

Geomatics Group, 2009. Lidar, Integrated spatial data. Environment Agency, Bath, 2p.

Gillette, D.A. Herbert, G. Stockton, P.H. and Owen, P.R., 1996. The fetch effect in wind erosion. Earth Surface Processes and Landforms, 21, 641-659.

Goldsmith, V., 1985. Coastal dunes. In: Davis, R.A. (eds). Coastal Sedimentary Environments. Springer-Verlag, New York, 303-378.

Gomes, N., Andrade, C. and Romariz, C., 1992. Sand transport rates in the Tróia-Sines arc, S.W. Portugal. In: Carter, R.W.G., Curtis, T.G.F. and Sheely-Skeffington, M.J. (eds). Coastal dunes, Balkena, Rotterdam, 33-42.

Goossens, D., Offer, Z.Y. and London, G., 2000. Wind tunnel and field calibration of five aeolian sand traps, Geomorphology, 35, 233-252.

Guillén, J., Stive, M.J.F. and Capobianco, M., 1999. Shoreline evolution of the Holland coast on a decadal scale. Earth Surface Processes and Landforms, 24, 517-36.

Halcrow and GeoSea, 1990. The Anglian Sea defence management study - Phase III. Field Survey Report. V3. Estuary Sediment Trends. GeoSea Consulting, Cambridge.

Halcrow, 1988. The sea Defence Management Study for the Anglian Region Study report and Atlas. Sir William Halcrow & Partners Ltd, Swindon.

Hall, J.W., Sayers, P.B., Walkden, M.J.A. and Panzeri, M., 2009. Impacts of climate change on coastal flood risk in England and Wales: 2030-2100. Philosophical Transactions of the Royal Society, 364, 1027-1049.

Hapke, C.J., 2005. Estimation of regional material yield from coastal landslides based on historical digital terrain. Earth Surface Processes and Landforms, 30, 679-697.

Haxel, J.H. and Holman, R.A., 2004. The sediment response of a dissipative beach to variations in wave climate. Marine Geology, 206, 73-99.

HECAG (Humber Estuary Coastal Authorities Group), 2009. Flamborough Head to Gibraltar Point Shoreline Management Plan, Scott 1022 Wilson, 182p.

Héquette, A. and Aernouts, D., 2010. The influence of nearshore sand bank dynamics on shoreline evolution in a macrotidal coastal environment, Calais, northern France. Continental Shelf Research, 30, 1349-1361.

Hesp, P.A., 2005. Flow reversal and dynamics of foredunes and climbing dunes on a leeward east coast, New Zealand. Zeitschrift Fur Geomorphologie, Coasts under Stress II, 141, 123-134.

Hesp, P.A., Davidson-Arnott, R., Walker, I.J. and Ollerhead, J., 2005. Flow dynamics over a foredune at Prince Edward Island, Canada. Geomorphology, 65, 71-84.

Hesp, P.A., 2004. Coastal dunes in the Tropics and Temperate Regions: Location, formation, morphology and vegetation processes. In: Martinez, M. and Psuty, N. (eds). Coastal Dunes, Ecology and Conservation. Ecological Studies. Springer-Verlag, Berlin, 29-49.

Hesp, P.A., 2002. Foredunes and blowouts: initiation, geomorphology and dynamics. Geomorphology, 48, 245-268.

Hesp, P.A., 1999. The beach, backshore and beyond, In: Short A.D. (eds). Handbook of Beach and Shoreface Dynamics. Wiley and Sons, Chichester, 145-169.

Hesp, P.A., 1991. Ecological processes and plant adaptations on coastal dunes. Journal of Arid Environments, 21, 165-191.

Hesp, P.A., 1989. A review of biological and geomorphological processes involved in the initiation and development of incipient foredunes. Proceedings of the Royal Society of Edinburgh, 96B, 181-201.

Hesp, P.A., 1988. Surf zone, beach, and foredune interactions on the Australia South east, coast. Journal of Coastal Research, 3, 15-25.

Hesp P.A., 1983. Morphodynamics of incipient foredunes in New South Wales, Australia. In: Brookfield, M.E. and Ahlbrandt, T.S. (eds). Eolian Sediments and Processes. Elsevier, Amsterdam, 325-342.

Hesp, P.A., 1981. The formation of shadow dunes. Journal of Sedimentary Research, 51, 101-112.

Horn, D.P., 2002. Mesoscale beach processes, Progress in Physical Geography, 26 (2), 272-289.

Houser, C. and Mathew, S., 2011. Alongshore variation in foredune height in response to transport potential and sediment supply: South Padre Island, Texas. Geomorphology, 125, 62-72.

Houser, C., 2009. Synchronization of transport and supply in beach-dune interaction. Progress in Physical Geography, 33 (6), 733-746.

Houser, C. and Hamilton, S., 2009. Sensitivity of post-hurricane beach and dune recovery to event frequency. Earth Surface Processes and Landforms, 34, 613-628.

Houser, C., Hapke, C. and Hamilton, S., 2008. Controls on coastal dune morphology, shoreline erosion and barrier island response to extreme storms. Geomorphology, 100, 223-240.

Houser, C., Greenwood, B. and Aagaard, T., 2006. Divergent response of an intertidal swash bar. Earth Surface Processes and Landforms, 31, 1775-91.

HR Wallingford, 2002. Southern North Sea sediment transport study, phase 2, Sediment Transport report, Wallingford, 94p.

Hsu, S.A., 1974. Computing aeolian sand transport from routine weather measurements. Proceedings of the 14th Coastal Engineering Conference, Copenhagen, 2, 1619-1626.

Hughes, S.A., 1983. Movable-bed modeling law for coastal dune erosion during erosion. Journal of Waterway, Port, Coastal and Ocean Engineering, 109 (2), 164-179.

Hurrell, J.W., Kushnir, Y., and Visbeck, M., 2001. The North Atlantic Oscillation, Science, 291, 603-605.

Hurrell, J.W., 1995. Decadal trends in the North Atlantic Oscillation and relationships to regional temperature and precipitation. Science, 269, 676-679.

IECS (Institute of Estuarine and Coastal Studies), 1994, Humber estuary and coast, report for the Environment Sub-Committee of Humberside County, 47p.

IPCC (Intergovernmental Panel on Climate Change), 2007. Climate Change 2007. The Physical Science Basis. Cambridge University Press, Cambridge.

Illenberger, W.K. and Rust, I.C., 1988. A sand budget for the Alexandria coastal dunefield, South Africa. Sedimentology, 35, 513-521.

Iskander, M.M., Frihy, O.E., El Ansary, A.E., El Mooty, M.M. and Nagy, H.M., 2007. Beach impacts of shore-parallel breakwaters backing offshore submerged ridges, Western Mediterranean Coast of Egypt. Journal of Environmental Management, 85, 1109-1119.

Jackson, D.W.T. and Cooper, J.A.G., 2011. Coastal dune fields in Ireland: rapid regional response to climate change. Journal of Coastal Research, SI 64, 293-297.

Jackson, D.W.T., Cooper, J.A.G. and Del Rio, L., 2005. Geological control on beach State. Marine Geology, 216, 297-314.

Jackson, D.W.T. and Cooper, J.A.G., 1999. Beach fetch distance and aeolian sediment transport. Sedimentology, 46, 517-522.

Jackson, D.W.T. and McCloskey, J. 1997. Preliminary results from a field investigation of aeolian sand transport using high resolution wind and transport measurements. Geophysical Research Letters, 24 (2), 163-166.

Jackson,N.L. and Nordstrom, K.F., 2011. Aeolian sediment transport and landforms in managed coastal systems: a review. Aeolian Research, 3, 181-196.

Jackson, N.L. and Nordstrom, K.F., 1998. Aeolian transport of sediment on a beach during and after rainfall, Wildwood, NJ, USA. Geomorphology, 22, 151-157.

Jackson, P.S. and Hunt, J.C.R., 1975. Turbulent flow over a low hill. Quarterly Journal of the Royal Meteorological Society, 101, 925-955.

Jackson, R.G., 1976. Sedimentological and fluid-dynamic implications of the turbulent bursting phenomenon in geophysical flows. Journal of Fluid Mechanics, 77, 531-560.

James, L.A., Hodgson, M.E., Ghoshal, S. and Latiolais, M.M., 2012. Geomorphic change detection using historic maps and DEM differencing: the temporal dimension of geospatial analysis. Geomorphology, 137, 181-198.

Jenkins, G.J., Murphy, J.M., Sexton, D.S., Lowe, J.A., Jones, P. and Kilsby, C.G., 2009. UK Climate Projections: Briefing report. Met Office Hadley Centre, Exeter, UK.

Jenkinson, A.F. and Collinson, B.P., 1977. An initial climatology of gales over the North Sea. Synoptic Climatology Branch Memorandum 62, Meteorological Office, Bracknell.

Jensen, J. and Sorensen, M., 1986. Estimation of some aeolian saltation thransport parameters: a re-analysis of Williams's data. Sedimentology, 33, 547-558.

Jungerius, P.D. and Van der Meulen, 1989. The development of dune blowouts, as measured with erosion pins and sequential air photos. Catena, 16, 369-376.

Jolliffe, I.T., 2002. Principal components analysis. Springer and Verlag, New York, 502p.

Jones, P.D., Harpham, C. and Briffa, K.R., 2012. Lamb weather types derived from reanalysis products. International Journal of Climatology, DOI: 10.1002/joc.3498.

Jones, P.D., Hulme, M., and Briffa, K.R., 1993. A comparison of Lamb circulation types with an objective classification scheme. International Journal of Climatology, 13, 655-663.

Kadib, A.A., 1965. Calculation procedure for sand movement by wind on natural beaches, US Army Corps of Engineers, Misc. Paper 2-64.

Kaimal, J.C. and Finnigan, J.J., 1994. Atmospheric Boundary Layer Flows. Oxford Univ. Press, New York.

Kaminsky, G.M., Ruggiero, P., Buijsman, M.C., McCandless, D. and Gelfenbaum, G., 2010. Historical evolution of the Columbia River littoral cell. Marine Geology, 273, 96-126.

Kamphius, J.W., 2010. (eds). Introduction to coastal engineering and management, World Scientific, London, 437p.

Kawamura, R., 1951. Study of sand movement by wind. Translated (1965) as University of California Hydraulics Engineering Laboratory Report HEL 2-8, Berkeley.

King, C.A.M., 1972. Dynamics of beach accretion in south Lincolnshire, England. In: Coastes, D.R. (eds). Proceedings of the 3rd Annual Geomorphology Symposia Series, Binghampton, Allen & Unwin, London, 73-98.

King, C.A.M. 1972. Beaches and Coasts. Edward Arnold, London, 570p.

King, C.A.M. and Barnes, F.A., 1964. Changes in the configuration of the inter-tidal beach zone of part of the Lincolnshire coast since 1951. Zeitschrift für Geomorphologie, 8, 105-126.

Kocurek, G. and Lancaster, N., 1999. Aeolian system sediment state: theory and Mojave Desert Kelseo dune field. Sedimentology, 46, 505-515.

Kostaschuk, R., Shugar, D.H., Best, J.L., Parsons, D.R., Lane, S.N. and Hardy, R.J., 2008. Suspended sediment transport over a dune. In: Parsons, D.R., Best, J.L., and Garlan, T. (eds). Marine Sandwave and River Dune Dynamics III, University of Leeds, UK, 197-201.

Kroon, A. and Masselink, G., 2002. Morphodynamics of intertidal bar morphology on a macrotidal beach under low-wave energy conditions, north Lincolnshire, England. Marine Geology, 190, 591-608.

Kroon, A., 1994. Sediment transport and morphodynamics of the beach and nearshore zone near Egmond, the Netherlands. PhD-thesis, Utrecht University, 275p.

Krupnik, A., 2003. Accuracy prediction for ortho-image. Photogrammetric Record, 18 (101), 41-58.

Lamb, H.H., 1972. British Isles weather types and a register of daily sequences of circulation patterns, 1861-1971. Geophysical Memoir 116, HMSO, London, 85p.

Lancaster, N., 1985. Variations in wind velocity and sand transport rates on the windward flanks of desert sand dunes. Sedimentology, 32, 581-593.

Lane, S.N., James, T.D. and Crowell, M.D., 2000. Application of digital photogrammetry to complex topography for geomorphological research. Photogrammetric Record, 16 (95), 793-821.

Lapinskis, J., 2005. Long-term fluctuations in the volume of beach and froedune deposits along the coast of Latvia. Baltica, 18 (1), 38-43.

Lassettre, N.S., Piégay, H., Dufour, S. and Rollet, A.J., 2008. Decadal changes in distribution and frequency of wood in a free meandering river, the Ain River, France. Earth Surface Processes and Landforms, 33, 1098-1112.

Lee, M., 2001. Coastal defence and the Habitats Directive: predictions of habitat change in England and Wales. Geographical Journal, 167, 39-56.

Lee, Z.S. and Bass, A.C.W., 2012. Streamline correction for the analysis of boundary layer turbulence. Geomorphology, 171-172, 69-82.

Leeder, M. R., 1983. On the interactions between turbulent flow, sediment transport and bedform mechanics in channelizedjows, Special Publications of the International Association of Sedimentologists, 6, 5-18.

Leenders, J., Vanboxel, J. and Sterk, G., 2005. Wind forces and related saltation transport. Geomorphology, 71, 357-372.

Leggett, D.J., Lowe, J.P. and Cooper, N.J., 1998. Beach evolution on the Souther North Sea coast. Conference Engineering Proceeding, ASCE, 2759-2772.

Lettau, K. and Lettau, H.H., 1977. Experimental and micrometeorological field studies of dune migration. In: Lettau, K. and Lettau, H.H. (eds). Exploring the World's Driest Climate. Institute for Environmental Studies, University of Wisconsin, Madison, 110-147.

Liu, X., 2008. Airborne LIDAR for DEM generation: some critical issues. Progress in Physical Geography, 32 (1), 31-49.

Liu, X., Zhang, Z., Peterson, J. and Chandra, S., 2007. LIDAR-derived high quality ground control information and DEM for image orthorectification. Geoinformatica, 11, 37-53.

Livingstone, I. and Warren, A., 1996. Aeolian geomorphology, an introduction, Longman, England, 204p.

Logie, M., 1982. Influence of roughness elements and soil moisture on the resistance of sand to wind erosion. Catena, SI1, 161-173.

Lowe, J.A. and Gregory, J.M., 2005. The effects of climate change on storm surges around the United Kingdom. Philosophical Transactions of the Royal Society, A363, 1313-1328.

Lowe, J.A., Gregory, J.M. and Flather, R.A., 2001. Changes in the occurrence of storm surges around the United Kingdom under a future climate scenario using a dynamic storm surge model driven by the Hadley Centre climate models. Climate Dynamics, 18, 179-188.

Lozano, I., Devoy, R.J.N., May, W., and Andersen, U., 2004. Storminess and vulnerability along the Atlantic coastlines of Europe: analysis of storm records and of a greenhouse gases induced climate scenario. Marine Geology, 210, 205-225.

Lyles, L. and Krauss, R.K., 1971. Threshold velocities and initial particle motion as influenced by air turbulence, Transactions of the American Society of Agricultural Engineers, 14, 563-566.

Lynch, K., Jackson, D.W.T. and Cooper J.A.G., 2010. Coastal foredune topography as a control on secondary airflow regimes under offshore winds. Earth Surface Processes and Landforms, 35, 344-353.

Lynch, K., Jackson, D.W.T., and Cooper, J.A.G., 2009. Foredune accretion under offshore winds. Geomorphology, 105, 139-149.

Lynch, K., Jackson, D.W.T. and Cooper J.A.G., 2008. Aeolian fetch distance and secondary airflow effects: the influence of micro-scale variables on meso-scale foredune development. Earth Surface Processes and Landforms, 33, 991-1005.

Lynch, K., Jackson, D.W.T. and Cooper, J.A.G., 2006. A remote-sensing technique for the identification of aeolian fetch distance. Sedimentology, 53, 1381-1390.

Masselink, G., Kroon, A. and Davidson-Arnott, R.G.D, 2006. Morphodynamics of intertidal bars in wave-dominated coastal settings, a review. Geomorphology, 73, 33-49.

Masselink, G. and Anthony, E.J., 2001. Location and height of intertidal bars on macrotidal ridge and runnel beaches. Earth Surface Processes and Landforms, 26, 759-774.

Masselink, G. and Pattiaratchi, C.B., 2001. Seasonal changes in beach morphology along the sheltered coastline of Perth, Western Australia. Marine Geology, 172, 243-263.

Masselink, G. and Short, A.D., 1993. The effect of tide range on beach morphodynamics and morphology: a conceptual beach model. Journal of Coastal Research, 9, 785-800.

May, V. and Hansom, J., 2003. Coastal geomorphology of Great Britain. No. 28 in Geological Conservation Review Series. Joint Nature Conservation Committee, Peterborough.

McCarthy, J.J., Canziani, O.F., Leary, N.A., Dokken, D.J. and White, K.S. (eds) 2001. Climate change 2001, impacts, adaptation, and vulnerability. Intergovernmental Panel on Climate Change. Cambridge University Press, Cambridge.

McKenna-Neuman, C.,Lancaster, N. and Nickling, W.G., 2000. Effect of unsteady winds on sediment transport intermittency along the stoss slope of a reversing dune. Sedimentology, 47, 211-226.

McKenna Neuman, C., Lancaster, N. and Nickling, W.G., 1997. Relations between dune morphology, air flow, and sediment flux on reversing dunes, Silver Peak, Nevada. Sedimentology, 44, 1103-1113.

McKenna-Neuman, C. and Nickling, W.G., 1989. A theoretical and wind tunnel investigation of the effect of capillary water on the entrainment of soil by wind. Canadian. Journal of Soil Science, 69, 79-96.

Meur-Férec, C. and Ruz, M-H., 2002. Observed and predicted rates of aeolian sand transport on the upper beach and dune top, Wissant beach, Northern France. Géomorphologie: relief, processus, environnement, 4, 321-334.

Miccadei, E., Mascioli, F., Piacentini, T. and Ricci, F., 2011. Geomorphological features of coastal dunes along the central Adriatic coast (Abruzzo, Italy). Journal of Coastal Research, 27, 1122-1136.

Mikkelsen, H.E., 1989. Wind flow and sediment transport over a low coastal dune. GeoSkrifter 32, Institute of Geology, University of Aarhus, Denmark, 60p.

Mills, J.P., Buckley, S.J. and Mitchell, H.L., 2003. Synergistic fusion of GPS and photogrammetrically generated elevation models. Photogrammetric Engineering & Remote Sensing 69, 4, 341-349.

Mitasova, H., Hardin, E., Overton, M. F. and Kurum, M. O., 2010. Geospatial analysis of vulnerable foredune-beach systems from decadal time series of LIDAR data. Journal of Coastal Conservation, 14, 161-172.

Montreuil, A-L., Bullard, J.E., submitted. A 150 year record of coastline dynamics within a large-scale sediment cell: eastern England, Geomorphology.

Montreuil, A.L. and Bullard, J.E., 2011. Meso-scale foredune development on a macro-tidal coast with a complex wind regime. Journal of Coastal Research, SI 64, 265-268.

Moore, L.J., 2000. Shoreline Mapping Techniques. Journal of Coastal Research, 16, 111-124.

Morton, R.A., 2002. Factors controlling storm impacts on coastal barriers and beaches_a preliminary basis for near real-time forecasting. Journal of Coastal Research, 18, 486-501.

Morton, R.A., Gibeaut, J.C. and Paine, J.G., 1995. Meso-scale transfer of sand during and after storms: implications for prediction of shoreline movement. Marine Geology, 126, 161-179.

Morton, R.A., Gibeaut, J.C. and Paine, J.G., 1994. Stages and durations of post-storm beach recovery, southeastern Texas coast, USA. Journal of Coastal Research, 10, 884-908.

Morton, R., 1991. Accurate shoreline mapping: past, present, and future. In: Kraus, N.C., Gingerinch, K.J. and Kriebel, D.L. (eds). Coastal Sediments '91. ASCE, Seattle, 997-1010.

Motyka, J.M., 1986. A Macro Review of the Coastline of England and Wales. Volume 2: The East Coast, the Tees to the Wash. Report SR107, HR Wallingford Ltd.

Navarro, M., Muñoz-Pérez, J.J., Romàn-Sierra, J., Tsoar, H., Rodríguez, I. and Gómez-Pina, G., 2011. Assessment of highly active dune mobility in the medium, short and very short term. Geomorphology, 129, 14-28.

Neumeier, U., 2007. Velocity and turbulence variations at the edge of saltmarshes. Continental Shelf Research, 27, 1046-1059.

Newsham, R., Balson, P.S., Tragheim, D.G. and Dennis, A.M., 2002. Determination and prediction of sediment yields from recession of the Holderness coast, NE England. Journal of Coastal Conservation, 8, 49-54.

Nicholls, R.J., Wong, P.P., Burkett, V.R., Codignotto, J.O., Hay, J.E., McLean, R.F., Ragoonaden, S. and Woodroffe, C.D., 2007. Coastal systems and low-lying areas. In: Parry, M.L. (eds). Climate change 2007: impacts, adaptation and vulnerability. Contribution of working group II to the fourth assessment report of the intergovernmental panel on climate change. Cambridge University Press, Cambridge, 315-356.

Nickling, W.G. and McKenna Neuman, C., 1995. Development of deflation lag surface. Sedimentology, 42, 403-414.

Nickling, W.G. and Davidson-Arnott, R.G.D., 1990. Aeolian sediment transport on beaches and coastal sand dunes. Proceedings Canadian symposium on coastal sand dunes, National Research Council of Canada, Ottawa, 1-36.

NOC (National Oceanography Centre), 2009. Tidal statistics for Skegness, Proudman Oceanographic Laboratory, Liverpool.

Nordstrom, K.F, Bauer, B.O., Davidson-Arnott, R.G.D., Gares, P.A., Carter, R.W.G., Jackson, D.W.T. and Sherman, D.J., 1996. Offshore Aeolian Transport across a Beach: Carrick Finn Strand, Ireland. Journal of Coastal Research, 12, 3, 664-672.

Nordstrom, K.F and Jackson, N.L., 1993. The role of wind direction in eolian transport on a narrow sandy beach. Earth Surface Processes and Landforms, 18, 675-685.

Nordstrom, K.F. and Jackson, N., 1992. Effect of source width and tidal elevation changes on Aeolian transport on an estuarine beach. Sedimentology, 39, 769-779.

North, G. R., Bell, T. L., Cahalan, R. F. and Moeng, F. J., 1982. Sampling errors in the estimation of empirical orthogonal functions, Mon. Weather Rev., 110, 699– 706.

O'Connor, M.C., Cooper, J.A.G. and Jackson, D.W.T., 2011. Decadal behavior of tidal inlet-associated beach systems, northwaest Ireland in relation to climate forcing, Journal of Sedimentary Research, 81, 38-51.

Olivier, M.J. and Garland, G.G., 2003. Short-term monitoring of foredune formation on the east coast of South Africa. Earth Surface Processes and Landforms, 28 (1), 1143-1155.

Orford, J.D., Forbes, D.L. and Jennings, S.C., 2002. Organisational controls, typologies and time scales of paraglacial gravel-dominated coastal systems. Geomorphology, 48, 51-85.

Orford, J.D, Wilson, P., Wintle, A.G., Knight, J. and Braley, S., 2000. Holocene coastal dune initiation in Northumberland and Norfolk, eastern England: climate and sea level changes as possible forcing agents for dune initiation. In: Shennan, I. and Andrews, J. (eds). Holocene land-ocean interaction and environmental change around the North Sea. Geological Society Special Publication 166, London, 197-217.

Orford, J.D., Cooper, J.A.G. and McKenna, J. 1999. Mesoscale temporal changes to foredune at Inch Spit, south-west Ireland. Zeitschrift für Geomorphologie, 43, 439-461.

Orford, J.D., Carter, R.W.G., Jennings, S.C. and Hinton, A.C., 1995. Processes and timescales by which a coastal gravel-dominated barrier responds geomorphologically to sea-level rise: Story Head barrier, Nova Scotia. Earth Surface Processes and Landforms 20, 21-37.

Overton, M.F. and Fisher, J.S., 1988. Laboratory investigation of dune erosion. Journal of Waterway, Port, Coastal, and Ocean Engineering, 114, 367-373.

Owen, P.R., 1964. Saltation of uniform grains in air. Journal of Fluid Mechanics, 20, 225-242.

Parsons, D.R.,Walker, I.J. and Wiggs, G.F.S., 2004a. Numerical modelling of flowstructures over idealized transverse aeolian dunes of varying geometry. Geomorphology, 59, 149-164.

Parsons, D.R., Wiggs, G.F.S., Walker, I.J., Ferguson, R.I. and Garvey, B.G., 2004b. Numerical modelling of airflow over an idealised transverse dune. Environmental Modelling & Software, 19 (2), 153-162.

Pearce, K.I. and Walker, I.J., 2005. Frequency and magnitude biases in the Fryberger model with implications for characterizing geomorphically effective winds, Geomorphology, 68, 39-55.

Pethick J., 2001. Coastal management and sea-level rise. Catena, 42, 307-322.

Pethick, J., 1984. An Introduction to coastal geomorphology. Edward Arnold, London, 127-143.

Pettitt, A.N., 1979. A non-parametric approach to the change-point problem. Journal of Applied Statistics, 28 (2), 126-135.

Phillips, J.D., 2003. Sources of nonlinearity and complexity in geomorphic systems. Progress in Physical Geography, 27 (1), 1-23.

Phillips, J.D., 1992. The end of equilibrium ?. Geomorphology, 5, 195-201.

Pond, S. and Pickard, G. L., 1983. (eds). Introductory Dynamical Oceanography. Pergamon, Oxford, 329p.

Posford-Duvivier, 1996. Lincolnshire shoreline management plan. Internal report of Environment Agency, Anglian Region. Rightwell House, Bretton Centre, Peterborourgh, 87p.

Posford-Duvivier, 1992. Easington coast protection. Report to Holderness Borough Council. Posford Duvivier, Peterborough, 92p.

Pringle, A.W., 1985. Holderness coast erosion and the significance of ords. Earth Surface Processes and Landforms, 10, 107-124.

Psuty, N.P. and Silveira, T.M., 2010. Global climate change: an opportunity for coastal dunes ??. Journal of Coastal Conservation, 14, 153-160.

Psuty, N.P., 1992. Spatial variation in coastal foredune development, In: Carter, R. W.G., Curtis, T.G.F. and Sheehy-Skeffington, M. (eds). Coastal Dunes: Geomorphology, Ecology and Management for Conservation. The Hague, Balkema, 3-13.

Psuty, N.P., 1990. Foredune mobility and stability, Fire Island, New York. In: Nordstrom, K.F., Psuty, N. P. and Carter, R. W. G. (eds). Coastal Dunes: Form and Process. John Wiley & Son Ltd., Chichester, 159-176.

Psuty, N.P., 1989. An application of science management problems in dunes along the Atlantic coast of the USA. In: Gimingham, C. H., Ritchie, W., Willetts, B. B. and Willis, A. J. (eds). Coastal Sand Dunes. Royal Society of Edinburgh, Scotland, 96B, 289-307.

Psuty, N.P., 1988. Sediment budget and dune/beach interaction, Journal of Coastal Research, SI 3, 1-4.

Pye, K. and Blott, S.J., 2010. Aldbrough gas storage project: geomorphological assessment of impact of propsed cliff protection works on adjoining areas, Kenneth Pye Associate Ltd, External investigation report No. EX1214, 16p.

Pye, K. and Blott, S.J., 2008. Decadal-scale variation in dune erosion and accretion rates: An investigation of the significance of changing storm tide frequency and magnitude on the Sefton coast, UK. Geomorphology, 102, 652-666.

Pye, K., Saye, S.E. and Blott, S.J., 2007. Sand dune processes and management for flood and coastal defence. Part 1: Project Overview and Recommendations. Joint

DEFRA/EA Flood and Coastal Erosion Risk Management R & D Programme R & D Technical Report FD1302/TR. DEFRA/EA, London, 35p.

Pye, K. and Blott, S.J., 2006. Coastal processes and morphological change in the Dunwich-Sizewell area, Suffolk, UK. Journal of Coastal Research, 22, 453-473.

Pye K., 1995. Controls on long-term saltmarsh accretion and erosion in the Wash, Eastern England. Journal of Coastal Research, 11, 337-356.

Pye, K., 1993. Introduction: the nature and significance of aeolian sedimentary systems. The dynamics and environmental context of aeolian sedimentary systems. Geological Society Special Publication 72, London, 1-4.

Pye, K. and Neal, A., 1994. Coastal dune erosion at Formby Point, north Merseyside, England: causes and mechanisms. Marine Geology, 119, 39-56.

Pye, K. and Neal, A., 1993b. Late Holocene dune formation on the Sefton coast, northwest England. In: Pye, K. (eds). The dynamics and environmental context of aeolain sedimentary systems. Geological Society Special Publication 72, London, 210-217.

Pye, K., 1990. Physical and human influences on coastal dune development between the Ribble and Mersey estuaries, northwest England. In: Nordstrom, K.F., Psuty, N.P. and Carter, R.W.G. (eds). Coastal Dunes: Form and Process. John Wiley & Son Ltd., Chichester, 339-359.

Pye, K. and Tsoar, H., 1990. Aeolian sand and sand dunes. Unwin Hyman, London, 396p.

Pye, K., 1983. Coastal dunes. Progress in Physical Geology, 31, 249-266.

Quinn, J.D., Philip, L.K. and Murphy, W., 2009. Understanding the recession of the Holderness Coast, east Yorkshire, UK: a new presentation of temporal and spatial patterns. Quarterly Journal of Engineering Geology and Hydrogeology, 42, 165-178.

Ranwell, D.S., 1972. Ecology of Salt Marshes and Sand Dunes. Chapman & Hall, London, 258p.

Rasmussen, K.R., 1989. Some aspects of flow over coastal dunes. Proceedings of the Royal Society of Edinburgh, 96B, 126-147.

Reynolds, O., 1895. On the dynamical theory of incompressible viscous fluids and the determination of the criterion. Philosophical Transactions, 186, 123-64.

Robert, A., Roy, A.G. and De Serres, B., 1996. Turbulence at a roughness transition in a depth limited flow over a gravel bed. Geomorphology, 16, 175-187.

Robinson, A.H.W., 1968a. The submerged glacial landscape on the Lincolnshire, Transactions of the Institute of British Geographers, 44, 119-132

Robinson, A.H.W., 1968b. The use of the sea bed drifter in coastal studies with particular reference to the Humber, Zeitschrift für Geomorphologie, 7, 13-16.

Robinson, A.H.W., 1964. The inshore waters, sediment supply and coastal changes of part of Lincolnshire. East Midland Geographer 3 (6), 22, 307-321.

Robinson, D.N., 1984. The Saltfleetby-Theddlethorpe coastline. Transactions of the Lincolnshire Naturalists' Union, 21, 1-12.

Robinson, D.N., 1981. The book of the Lincolnshire Seaside, the story of the coastline from the Humber to the Wash. Barracuda Books Ltd, Buckingham, England, 172p.

Robinson, D.N., 1953. The storm surge 31st January-1st February, 1953 and the associated meterological and tidal conditions. Geography, 38, 134-141.

Rogerson, P.A., 2004. Statistical methods for Geography: a student's guide. (eds). Sage, London, 368p.

Ruessink, B.G. and Jeuken, M.C.J.L., 2002. Dunefoot dynamics along the Dutch coast, Earth Surface Processes and Landforms, 27, 1043-1056.

Ruggiero, P., Komar, P.D., McDouglas, W.G., Marra, J.J. and Beach, R.A., 2001. Wave runup, extreme water levels and the erosion of properties backing beaches. Journal of Coastal Research, 17, 407-419.

Ruz, M.H. and Meur-Férec, C., 2004. Influence of high water levels on Aeolian sand transport: upper beach/dune evolution on a macrotidal coast, Wissant Bay, northern France. Geomorphology, 60, 73-87.

Sabatier, F., Anthony, E.J., Héquette, A., Suanez, S., Musereau, J., Ruz, M-H. and Regnauls, H., 2009. Morphodynamics of beach/dune systems: examples from the coast of France, Géomorphologie: relief, processus, environnement, 1, 3-22.

Sallenger, Jr., A.H., Krabill, W.B., Swift, R.N., Brock, J., List, J.,Hansen, M., Holman, R.A., Manizade, S., Sontag, J., Meredith, A., Morgan, K., Yunkel, J.K., Frederick, E.B. and Stockton, H., 2003. Evaluation of airborne topographic LIDAR for quantifying beach changes. Journal of Coastal Research, 19, 125-133.

Sanderson, P.G., Eliot, I. and Fuller, M., 1998. Historical development of a foredune plain at Desperate Bay, Western Australia. Journal of Coastal Research, 14, 1187-1201.

Sarre, R., 1989. Aeolian sand drift from the intertidal zone on a temperate beach: potential and actual rates. Earth Surface Processes and Landforms, 14, 247-258.

Sarre, R., 1987. Aeolian sand transport. Progress in Physical Geography, 11 (2), 157-182.

Saunders, K.E. and Davidson-Arnott, R.G.D., 1990. Coastal dune response to natural disturbances, In: Davidson-Arnott, R. (eds). Symposium on Coastal Sand Dunes, Guelph Ontario, National Research Council of Canada, Ottawa, 321-346.

Saye, S.E., Van der Wal, D., Pye, K., and Blott, S. J., 2005. Beach-dune morphological relationships and erosion/accumulation: An investigation at five sites in England and Wales using Lidar data. Geomorphology, 72, 128-155.

Schans, H., Möller, I. and Spencer, T., 2001. Large-scale classification of the East Anglian coastline, UK. Proceedings of the 4th International Conference on Coastal Dynamics' 01, ASCE, 683-692.

Sedrati, M. and Anthony, E.J., 2008. Sediment dynamics and morphological change on the upper beach of a multi-barred macrotidal foreshore, and implications for mesoscale shoreline retreat Wissant Bay, northern France. Zeitschrift für Geomorphologie, 53 (3), 91-106.

Sedrati, M. and Anthony, E.J., 2007. Storm-generated morphological change and longshore sand transport in the intertidal zone of a multi-barred macrotidal beach. Marine Geology, 244, 209-229.

Shao, Y., McTainsh, G.H. and Leys, J.F., 1993. Efficiencies of sediment samplers for wind erosion measurement. Australian Journal of Soil Research, 31, 519-532.

Shao, Y. and Raupach, M.R., 1992. The overshoot and equilibrium of saltation. Journal of Geophysical Research, 97, 20559-20564.

Sherman, D. J., Jackson, D.W.T., Namikas, S.L. and Wang, J., 1998. Wind-blown sand on beaches: an evaluation of models. Geomorphology, 22, 113-333.

Sherman, D.J., 1995. Problems of scale in the modeling and interpretation of coastal dunes. Marine Geology, 124, 339-349.

Sherman, D.J. and Lyons, W., 1994. Beach state controls on Aeolian sand delivery to coastal dunes. Physical Geography, 15, 381-395.

Sherman, D.J. and Bauer, B. O., 1993. Dynamics of beach-dune sytems. Progress in Physical Geomorphology, 17, 413-447.

Sherman, D.J. and Hotta, S., 1990. Aeolioan sediment transport: theory and measurements. In Nordsrtom, K.F., Psuty, N.P. and Carter, R.W.G. (eds). Coastal Dunes, Form and Process. John Wiley & Son Ltd., Chichester, 16-38.

Short, A.D. and Trembanis, A.C., 2004. Decadal scale patterns in beach oscillation and rotation Narrabeen beach, Australia—time series, PCA and wavelet analysis. Journal of Coastal Research, 20, 523-532.

Short, A.D. and Hesp, P.A., 1982. Wave, beach and dune interaction in southeast Australia. Marine Geology 48, 259-284.

Simpson, J.H., 1993. The North Sea Project: an overview and way forward. Philosophical Transactions of the Royal Society, 343 (1669), 585-596.

Siniscalchi, F., Nikora, V. I., Aberle, J. Plant patch hydrodynamics in streams: mean flow, turbulence and drag forces, Water Resources Research, 48, W01513-1527.

SNH (Scottish Natural Heritage), 2000. A guide to managing coastal erosion in beach/dune systems, Scottish Natural Guide. [access 12th February 2012] Available at: <http://www.snh.org.uk/publications/online/heritagemanagement/erosion/1.shtml> [].

Southgate, H.N. and Beltran, L.M., 1998. Self-organisational processes in beach morphology. Proceedings of the 8th International Biennial Conference on Physics of Estuaries and Coastal Seas, 409-416.

Steers, J.A., Stoddart, D.R., Bayliss-Smith, T.P., Spencer, T. and Durbidge, P.M., 1979. The storm surge of 11th January 1978 on the east coast of England. The Geographical Journal, 145, 192-205.

Steers, J.A., 1966. Holderness, Lincolnshire and the Fenland. In: Steers, J.A. (eds) The coastline of England and Wales. Cambridge University Press, Cambridge, 406-440.

Sterk, G., Jacobs, A.F.G. and Van Boxel, J.H., 1998. The effect of turbulent flow structures on saltation sand transport in the atmospheric boundary layer. Earth Surface Processes and Landforms, 23, 877-887.

Stockdon, H.F., Sallenger, Jr. A.H., List, J.H. and Holman, R.A., 2002. Estimation of shoreline position and change from airborne scanning LIDAR data. Journal of Coastal Research, 18, 502-513.

Stout, J.E., 1998. Effect of averaging time on the apparent threshold for aeolian transport. Journal of Arid Environments, 39, 395-401.

Stout, J. E. and Zobeck T.M., 1997 Intermittent saltation. Sedimentology, 44, 959-970.

Suanez, S., Cariolet, J-M., Cancouët, R., Ardhuin, F. and Delacourt, C., 2012. Dune recovery after storm erosion on a high-energy beach: Vougot beach, Brittany (France). Geomorphology, 139, 16-33.

Suanez, S. and Stéphan, P., 2006. Meteo-marine forcings and seasonal morphosedimentary dynamic of dunes. Example of the bay of Saint-Michel-en-Grève (Côtes d'Armor, Bretagne). Géomorph.: relief, processus, environnement, 2, 91-110.

Summerfield, M.A., 1991. Global Geomorphology, London, Longman Scientific & Technical, England, 537p.

Svasek, J. and Terwindt, J., 1974 Measurements of sand transport by wind on a natural beach. Sedimentology, 21, 311-322.

Sweet, M.L. and Kocurek, G. 1990. An empirical model of Aeolian dune lee face air flow. Sedimentology, 37, 1023-1038.

Swinnerton, H.H., 1936. A monograph of the British Lower Cretaceous belemnites. Monograph of the Palaeontographical Society, London, 86p.

Tennekes, H. and Lumley, J.L., 1972. A first course in turbulence. MIT Press, Massachusetts, 300p.

Terwindt, J.H.J and Wijnberg, K.M., 1991. Thoughts on large scale behaviour, Proceedings Coastal Sediments '91, ASCE, 1476-1487.

Thom, B.G. and Hall, W., 1991. Behaviour of beach profiles during accretion and erosion dominated periods. Earth Surface Processes and Landforms, 16, 113-127.

Thomas, T., Phillips, M.R., Williams A.T. and Jenkins, R.E., 2011. A multi-century record of linked nearshore and coastal change. Earth Surface Processes and Landforms, 36, 995-1006.

Thomas, D.S.G. and Wiggs, G.F.S., 2008. Aeolian system responses to global change: challenges of scale, process and temporal integration. Earth Surface Processes Landforms, 33, 1396-1418.

Thomas, D.S.G., 1999. Coastal and Continental Dune Management into the Twenty-first century. In Goudie, A.S., Livingstone, I., and Stokes, S. (eds). Aeolian environment, sediments and landforms. John Wiley & Son Ltd., Chichester, 105-127.

Thompson, A.G., Eastwood, J.A., Yates, M.G., Fuller, R.M., Wadswoth, R.A., and Cox, R., 1998. Airborne remote sensing intertidal biotopes: BIOTA I. Marine Pollution Bulletin, 37, 3-7, 164-172.

Tonk, A.M., 2000. Monitoring changes in coastal morphology. North Lincolnshire, report to Environment Agency, Loughborough, 44p.

Toone, J., 2009. Geomorphological discountinuities and ecological organisation: a case study of the river Drôme. PhD-thesis, Loughborough University, 187p.

Trenhaile, A.S., 1997. Coastal dynamics and Landforms. Clarendon Press, Oxford, 143-169.

Trimble, 2009. Trimble R8 GNSS and R6/5800 GPS receivers_User guide, Trimble Navigation Ltd., Ohio, 88p.

Tsimplis, M.N., Shaw, A.G.P., Flather, R.A. and Woolf, D.K., 2006. The influence of the North Atlantic Oscillation on the sea level around the northern European coasts reconsidered: the thermosteric effects. Phil. Trans. R. Soc., 364, 845-856.

Tsimplis, M.N., Woolf, D.K., Osborn, T.J., Wakelin, S., Wolf, J., Flather, R., Shaw, A.G.P., Woodworth, P., Challenor, P., Blackman, D., Pert, F., Yan, Z. and Jevrejeva, S., 2005. Towards a vulnerability assessment of the UK and northern European coasts: the role of regional climate variability. Phil. Trans. R. Soc., 363, 1329-1358.

Udden, J.A., 1914. Mechanical composition of clastic sediments. Bulletin of the Geological Society of America, 25, 655-744.

Valentin, H., 1971. Land loss at Holderness. In: Steers, J.A. (eds). Applied coastal geomorphology. Macmillan, London, 116-137.

Van Boxel, J.H., Sterk, G. and Arens, S.M. 2004. Sonic anemometers in aeolian sediment transport research. Geomorphology, 59, 131-147.

Van Boxel, J.H., Arens, S.M. and Van Dijk, P.M., 1999. Aeolian processes across transverse dunes. I: Modelling the air flow. Earth Surface Processes and Landforms, 24, 255-270.

Van de Graaff, J., 1994. Coastal dune erosion under extreme conditions: Coastal hazards; perception, susceptibility and mitigation. Journal of Coastal Research, 12, 253-262.

Van de Graaff, J. and Koster, M.J., 1990. Dune and beach erosion and nourishment, In: Pilarczyk, K.W. (eds). Coastal Protection, Balkema, Rotterdam.

Van de Graaff, J., 1986. Probabilistic design of dunes, an example from The Netherlands. Coastal Engineering, 9, 479-500.

Van der Wal, D., 2000. Modelling aeolian sand transport and morphological development in two beach nourishment areas, Earth Surface Processes and Landforms, 25, 77-92.

Van der Wal, D., 1999. Aeolian transport of nourishment sand in beach-dune environments. PhD-thesis, University of Amsterdam, 157p.

Vanhée, S., Anthony, E.J. and Ruz, M.H., 2002. Aeolian sand transport on a ridge and runnel beach: Preliminary Results from Leffrinckoucke Beach, Northern France. Journal of Coastal Research, SI 36, 732-740.

Van Houwelingen S.T., Masselink, G. and Bullard, J.E., 2008. Dynamics of multiple intertidal bars over semi-diurnal and lunar tidal cycles, North Lincolnshire, England, Earth Surface Processes and Landforms, 33, 1473-1490.

Van Houwelingen S.T., Masselink, G. and Bullard, J.E., 2006. Characteristics and dynamics of multiple intertidal bars, north Lincolnshire, England. Earth Surface Processes and Landforms, 31, 428-443.

Van Houwelingen, S.T., 2005. Temporal and Spatial Variability in the Ridge and Runnel Morphology along the North Lincolnshire Coast, England, PhD-thesis, Loughborough University, 174p.

Vasseur, B., and Héquette, A., 2000. Storm surges and erosion of coastal dunes between 1957 and 1988 near Dunkerque (France) southwestern North Sea. In: Pye,K. and Allen, J.R.L. (eds.), Coastal and Estuarine Environments. Geological Society Special Publication 175, London, 99-107.

Vellinga, P., 1982. Beach and dune erosion during storm surges, Delft Hyfraulics Lab, 276p.

Ventura, S.J. and Irvin, B.J., 2000. Automated landform classification methods for soil landscape studies. In: Wilson, J.P. and Gallant, J.C. (eds). Terrain Analysis: Principles and Applications. Wiley and Sons Ltd., Chichester, 267-294.

Vespremeanu-Stroe, A. and Preoteasa, L., 2007. Beach-dune interactions on the dry-temperate Danube delta coast. Geomorphology, 86, 267-282.

Wakelin, S.L., Woodworth, P.L., Flather, R.A. and Williams, J.A., 2003 Sea-level dependence on the NAO over the NW European Continental Shelf. Geophysical Research Letters, 30 (7), 561-564.

Wal, A. and McManus, J. 1993. Wind regime and sand transport on a coastal beach-dune complex, Tentsmuir, eastern Scotland. In: Pye, K. (eds). The dynamics and environmental context of aeolian sedimentary systems. Geological Society Special Publication 72, London, 159-171.

Walker, G.T. and Bliss, E.W., 1932. World weather. Memoirs of the Royal Meteorological Society, 4, 53-84.

Walker, I.J., Hesp, P.A., Davidson-Arnott, R.G.D., Bauer, B.O., Namikas, S.L. and Ollerhead, J., 2009. Responses of three-dimensional flow to variations in the angle of incident wind and profile form of dunes: Greenwich Dunes, Prince Edward Island, Canada. Geomorphology, 105, 127-138.

Walker, I.J., Hesp, P.A., Davidson-Arnott, R.G.D. and Ollerhead, J., 2006. Topographic steering of alongshore airflow over a vegetated foredune: Greenwich Dunes, Prince Edward Island, Canada. Journal of Coastal Research, 22, 1278-1291.

Walker, I.J., 2005. Physical and logistical considerations of using ultrasonic anemometers in aeolian sediment transport research. Geomorphology, 68, 57-76.

Walker, I.J. and Nickling, W.G., 2003. Simulation and measurement of surface shear stress over isolated and closely spaced transverse dunes in a wind tunnel. Earth Surface Processes and Landforms, 28, 1111-1124.

Walker, I.J. and Nickling, W.G., 2002. Dynamics of secondary airflow and sediment transport over and in the lee of transverse dunes. Progress in Physical Geography, 26 (1), 47-75.

Walker, I.J., 2000. Secondary airflow and sediment transport in the lee of transverse dunes. PhD-thesis, University of Guelph, 256p.

Walker, I.J., 1999. Secondary airflow and sediment transport in the lee of a reversing dune. Earth Surface Processes and Landforms, 24, 437-448.

Wallace, J.M., and Gutzler, D.S., 1981. Teleconnections in the geopotential height field during the northern hemisphere winter season. Monthly Weather Review, 109, 784-812.

Walstra, J., Chandler, J.H., Dixon, N. and Wackrow, R., 2010. Evaluation of the controls affecting the quality of spatial data derived from historical aerial photographs. Earth Surface Processes and landforms, 36, 853-863.

WASA, 1998. Changing waves and storms in the North Atlantic, Bulletin of the American Meteorological Society, 79 (5), 741-760.

Wehr, A. and Lohr, U., 1999. Airborne laser scanning_an introduction and overview, Photogrammetry & Remote Sensing, 54, 68-82.

Wentworth, C.K., 1922. A scale of grade and class terms for clastic sediments, Journal of Geology, 30, 377-392.

Wheater C.P. and Cooke A.C., 2000. Using statistics to understand the environment. Routledge, Oxford, 245p.

White, S.A. and Wang, Y., 2003. Utilizing DEMs derived from LIDAR data to analyze morphologic change in the North Carolina coastline. Remote Sensing of Environment, 85 (1), 39-47.

White, B.R., 1979. Soil transport by wind on Mars. Journal of Geophysical Research, 84, 4643-4651.

Wiggs G.F.S., Atherton R.J. and Baird A.J., 2004a. Thresholds of aeolian sand transport: establishing suitable values. Sedimentology, 51, 95-108.

Wiggs G.F.S., Baird A.J., Atherton, R.J., 2004b. The dynamic effects of moisture on the entrainment and transport of sand by wind. Geomorphology, 59, 13-30.

Wiggs, G.F.S., Livingstone, I. and Warren, A., 1996. The role of streamline curvature in sand dune dynamics: evidence from field and wind tunnel measurements. Geomorphology, 17, 29-46.

Wiggs, G.F.S., 1993. Desert dune dynamics and the evaluation of shear velocity: an integrated approach. In: Pye, K. (eds). The dynamics and environmental context of aeolian sedimentary systems. Geological Society, London, 37-48.

Wilby, R.L., Dalgleish, H.Y. and Foster, I.D.L., 1997. The impact of weather patterns on historic and contemporary catchment sediment yields. Earth Surface processes and landforms, 22, 353-363.

Williams, J.J., Thorne, P.D. and Heathershaw, A.D., 1989. Measurements of turbulence in the benthic boundary layer over a gravel bed. Sedimentology, 36, 959-971.

Willmarth, W.W. and Lu, S.S., 1972. Structure of the Reynolds stress near the wall. Journal of Fluid Mechanics, 55, 65-92.

Wilson, P., Orford, J.D., Knight, J., Braley, S.M. and Wintle, A.G., 2001. Late-Holocene (post-4000 year BP) coastal dune development in Northumberland, northeast England, The Holocene, 11 (2), 215-229.

Wolf, P.R. and Dewitt, B.A., 2000. Elements of photogrammetry (eds). McGraw-Hill, London. 663p.

Wolfe, S.A. and Nickling, W.G., 1993. The protective role of sparse vegetation in wind erosion, Progress in Physical Geography, 17 (1), 50-68.

Woodworth, P.L., Teferle, F.N., Bingley, R.M., Shennan, I. and Williams, S.D.P., 2009. Trends in UK mean sea level revisited. Geophysical Journal International, 176, 19-30.

Woolard, J. W. and Colby, J.D., 2002. Spatial characterization, resolution, and volumetric change of coastal dunes using airborne LIDAR: Cape Hatteras, North Carolina. Geomorphology, 48, 269-287.

Woolf, D.K., Challenor, P.G., and Cotton, P.D., 2002. Variability and predictability of the north Atlantic wave climate. Journal of Geophysical Research Oceans, 107, 3145-3159.

Wright, L.D and Thom, B.G., 1977. Coastal depositional landforms: A morpho-dynamic approach. Progress in Physical Geography, 1 (3), 412-459.

Yang, Y. and Davidson-Arnott, R.G.D., 2005. Rapid measurement of surface moisture content on a beach. Journal of Coastal Research, 21, 447-52.

Zhang, K., Douglas, B.C. and Leatherman, S.P., 2001. Beach erosion potential for severe Nor'easters. Journal of Coastal Research, 17, 309-321.

Appendices

Appendix 2. Major coastal dune localities in UK.

Appendix 3.1. Rotation of the sonic frame reference.
Appendix 3.2. Summary of airflow properties during direct offshore winds estimated from the ultrasonic anemometers.
Appendix 3.3. Summary of airflow properties during oblique offshore winds estimated from the ultrasonic anemometers.
Appendix 3.4. Summary of airflow properties during onshore winds estimated from the ultrasonic anemometers.

Appendix 4.1. Synoptic situations in: (A) 17th October 2009, (B) 20th October 2009.
Appendix 4.2. Synoptic situation in 28th February 2010.
Appendix 4.3. Synoptic situations in: (A), (B) 13th-26th August and (C) 24th September 2010.

Appendix 6.1. ISODATA classification for vegetation analysis at BL.
Appendix 6.2. ISODATA classification for vegetation analysis at TSH.
Appendix 6.3. ISODATA classification for vegetation analysis at MNE.
Appendix 6.4. Storm surge events recorded between 1993-2010.
Appendix 6.5. Severe foredune erosion after cumulative storm surges in February 1996
Appendix 6.6. Lidar cross-shore profiles in 2001 and 2007 at BL site from north (A) to south (E).
Appendix 6.7. Lidar cross-shore profiles in 2001 and 2007 at TSH site from north (F) to south (J).
Appendix 6.8. Lidar cross-shore profiles in 2001 and 2007 at MNE site from north (K) to south (O).

Appendix 7. Bathymetric EA profiles at BL and MNE in 1999, 2005 and 2008

Appendix 8. Journal paper.

Appendix 2. Major coastal dune localities in UK (Doody, 1991).

Site	Location	Size (km^2)	Habitats
	England		
1	North Northumberland Dunes	5.54	Sand flats
2	Saltfleetby-Theddlethorpe	3.67	Saltmarshes and sand beach
3	Gibraltar Point	2.79	Saltmarshes and sand beach
4	North Norfolk Coast	7	Beach and sand flat
5	Winterton	3	Beach and sand flat
6	Sandwich and Pegwell Bay	4.8	Saltmarshes and sand beach
7	Studland Heath	2.04	Saltmarshes
8	Penhale	5.42	Sand beach
9	Braunton Burrows	8.8	Sand beach
10	Sefton Coast	21.09	Beach and sand flat
11	North Walney	3.4	Sea inlets
12	Drigg Point	3.44	Saltmarshes and sand flat
	Wales		
13	Kenfig	4.8	Saltmarshes and sand flat
14	Owich	1	Sand beach
15	Whitefored Burrows	1.5	Sand beach
16	Tywyn Gwendraeth	17	Sand beach
17	Stackpole Warren	1.5	Sand beach
18	Ynyslas	1.25	Beach and sand flat
19	Morfa Dyffryn	3	Beach and sand flat
20	Morfa Harlech	4.5	Saltmarshes and sand beach
21	Newborough Warren	5.25	Sand beach
22	Tywyn Aberffraw	2.5	Sand beach
	Scotland		
23	Torrs Warren	7.7	Sea inlets
24	Killinallan (Islay)	2.5	Sand beach
24a	Oronsay Machair	3.4	Sand beach
25	Hough Bay & Ballavullin Machair (Tirree)	2.5	Wetland and sand beach
26	Crossapol & Gunna Machair (Coll)	2	Sand beach
27	South Uist Machair	4	Beach and sand flat
28	Howmore Estuary Machair	9	Sea inlets
29	Loch Bee Machair	8.5	Beach and sand flat
30	Baleshare & Kirkibost Machair	3.5	Beach and sand flat
31	Monarch Isles Machair	4	Sea inlets
32	Berneray Machair	6.5	Sand beach
33	Northon Bay Machair	1	Sand beach
34	Sandwood Bay	0.75	Sand beach
35	Faraid Head & Balnakeil Bay	1.7	Sand beach
35a	Invernaver	2.95	Sand beach
36	Dunnet Links	8	Sand beach
37	Morrich More	15	Beach and sand flat

38	Loch of Strathbeg	5	Saltmarshes and sand beach
39	Sands of Forvie	7.5	Sand beach
40	St. Cyrus	4	Sand beach
41	Barry Links	7.9	Sand beach
42	Tentsmuir and Earshall Muir	7	Beach and sand flat
	Isle of Man		
43	Point of Ayre	0.5	Sand beach
	Channel Islands		
44	Le Quennevais	1	Sand beach

Appendix. 3.1. Rotation of the sonic frame of reference.

Recorded velocity data were rotated for yaw and pitch to correct for potential ultrasonic misalignment to the local streamlines for each experiment as described by Walker (2005).

The first rotation, the yaw rotation, orients the u-component (streamwise) into the wind direction. The rotation can be achieved by requiring that the average spanwise velocity is zero ($\overline{v_1}=0$).

$$\theta = \arctan(\frac{\overline{v_0}}{\overline{u_0}})$$

$$u_1 = u_0 cos\theta + v_0 sin\theta$$

$$v_1 = -u_0 sin\theta + v_0 cos\theta$$

$$w_1 = w_0$$

Where u_0, v_0, w_0 are the recorded components of wind speed and u_1, v_1, w_1 are components after rotation. The overbar denotes the time-averaged value. The orientation of the ultrasonic anemometer relative to the wind direction can range any angle between 0° and 360°, however the result of arctan gives an angle between -90° and 90°, so that the angle has to be increased by 180° whether the average of u-component is negative.

The second rotation, pitch rotation, orients the u-components into the direction of the sloping streamlines and the w-components (vertical lift) to the streamlines. This rotation requires that the average of vertical lift is zero ($\overline{w_2}=0$).

$$u_2 = u_1 cos\varphi + w_1 sin\varphi$$

$$v_2 = v_1$$

$$w_2 = -u_1 sin\varphi + w_1 sin\varphi$$

Where φ is the streamline slope, u_2, v_2, w_2 are components after the second rotation.

Appendix 3.2. Summary statistics of airflow properties during **direct offshore winds** estimated from the ultrasonic anemometers at 0.8 m high including: fluctuating velocity of u'- and w'-components (m s^{-1}) at the reference (Ref) and mobile masts during offshore winds. Note that maximum (max) and minimum (min) corresponds to the two extreme values over the 20-min experiment. The mean of the u' and v' component are zero.

| | | u' | | | | | | w' | | | | | |
| | | Ref | | | Mobile | | | Ref | | | Mobile | | |
		Max	Min	σ	Max	Min	σ	Max	Min	σ	Max	Min	σ
BL Exp-4	SFC	1.42	0.76	0.21	1.30	0.74	0.17	0.54	-0.44	0.11	0.77	-0.77	0.06
	SFT	1.28	0.62	0.20	1.27	0.55	0.19	0.44	-0.33	0.04	0.75	-0.68	0.10
	PFC	1.52	0.82	0.23	1.59	0.84	0.20	0.51	-0.44	0.05	0.88	-0.88	0.11
	PFT	1.78	0.87	0.25	1.89	0.84	0.22	0.64	-0.45	0.09	0.88	-0.67	0.11
	MB	1.45	0.70	0.17	1.40	0.68	0.21	0.54	-0.45	0.06	0.50	-0.39	0.07
	LB	1.53	0.69	0.22	1.34	0.76	0.17	0.59	-0.47	0.07	0.49	-0.35	0.04
TSH Exp-4	SFC	1.20	0.57	0.14	1.19	0.51	0.16	0.37	-0.25	0.04	0.78	-0.53	0.10
	SFT	1.47	0.52	0.22	1.20	0.51	0.16	0.38	-0.26	0.04	0.75	-0.68	0.10
	PFC	1.55	0.49	0.23	1.06	0.57	0.14	0.42	-0.22	0.05	0.65	-0.57	0.07
	PFT	1.73	0.54	0.27	1.07	0.63	0.14	0.48	-0.33	0.07	0.72	-0.63	0.08
	UB	1.50	0.33	0.23	1.30	0.38	0.23	0.36	-0.30	0.05	0.64	-0.52	0.11
	SED	1.01	0.47	0.16	1.11	0.41	0.15	0.39	-0.27	0.04	0.63	-0.37	0.10
MNE Exp-4	SFC	0.83	0.39	0.14	0.79	0.42	0.10	0.41	-0.25	0.05	0.55	-0.37	0.08
	SFT	1.14	0.31	0.18	0.61	0.36	0.08	0.34	-0.28	0.04	0.41	-0.34	0.05
	PFC	1.10	0.45	0.18	1.01	0.41	0.15	0.45	-0.38	0.06	0.56	-0.47	0.07
	PFT	2.02	0.46	0.38	1.28	0.42	0.24	0.54	-0.38	0.08	0.66	-0.46	0.09
	UB	1.01	0.43	0.15	1.06	0.45	0.14	0.51	-0.30	0.07	0.53	-0.53	0.08
	LB	1.27	0.56	0.18	1.12	0.56	0.15	0.47	-0.37	0.05	0.42	-0.34	0.05

The mean of u'-and w'-components are zero.

Appendix 3.3. Summary statistics of airflow properties during **oblique offshore winds** estimated from the ultrasonic anemometers at 0.8 m high including: fluctuating velocity of u'- and w'-components (m s^{-1}) at the reference (Ref) and mobile masts during oblique offshore winds. Note that maximum (max) and minimum (min) corresponds to the two extreme values over the 20-minutes experiment. The mean of the u' and v' component are zero.

| | | u' | | | | | | w' | | | | | |
| | | Ref | | | Mobile | | | Ref | | | Mobile | | |
		Max	Min	σ	Max	Min	σ	Max	Min	σ	Max	Min	σ
BL Exp-2	SFC	1.01	0.52	0.14	1.26	0.70	0.15	0.34	-0.22	0.05	0.58	-0.46	0.06
	SFT	1.05	0.46	0.17	0.89	0.47	0.12	0.34	-0.24	0.05	0.65	-0.56	0.08
	PFC	1.26	0.53	0.21	1.33	0.62	0.19	0.35	-0.27	0.04	0.74	-0.89	0.12
	PFT	1.17	0.60	0.17	1.17	0.59	0.13	0.42	-0.42	0.06	0.57	-0.52	0.06
	MB	0.83	0.35	0.12	0.66	0.37	0.09	0.29	-0.25	0.04	0.28	-0.24	0.03
BL Exp-3	SFC	1.45	0.75	0.20	1.77	0.74	0.28	0.52	-0.48	0.06	0.80	-0.69	0.12
	SFT	1.54	0.68	0.21	1.44	0.61	0.21	0.64	-0.44	0.09	0.94	-0.83	0.11
	PFC	1.26	0.62	0.18	1.28	0.69	0.16	0.45	-0.39	0.04	0.71	-0.71	0.08
	PFT	1.23	0.60	0.18	1.24	0.76	0.15	0.52	-0.27	0.06	0.60	-0.47	0.08
	MB	0.85	0.47	0.10	0.77	0.40	0.11	0.32	-0.32	0.03	0.30	-0.30	0.03
	LB	0.74	0.43	0.08	0.84	0.42	0.10	0.28	-0.23	0.02	0.28	-0.27	0.03
TSH Exp-2	SFC	1.11	0.62	0.12	1.41	0.85	0.14	0.48	-0.36	0.05	0.96	-0.70	0.11
	PFC				2.24	1.26	0.24				0.79	-0.64	0.08
	PFT	1.22	0.66	0.25	1.62	0.66	0.15	0.42	-0.32	0.04	0.76	-0.71	0.09
	UB	1.41	0.93	0.17	1.52	0.61	0.22	0.87	-0.33	0.08	0.45	-0.73	0.04
	SED	1.01	0.62	0.09	1.15	0.57	0.16	0.45	-0.29	0.03	0.36	-0.48	0.04
TSH Exp-3	SFT	0.47	0.20	0.06	0.62	0.19	0.07	0.18	-0.18	0.02	0.53	-0.32	0.04
	PFC	0.73	0.26	0.15	0.94	0.17	0.19	0.32	-0.25	0.05	0.59	-0.49	0.12
	PFT	0.77	0.29	0.12	0.78	0.28	0.11	0.33	-0.18	0.05	0.54	-0.37	0.07
	UB	0.71	0.38	0.09	0.77	0.39	0.13	0.40	-0.22	0.05	0.29	-0.40	0.03
	SED	0.76	0.24	0.12	0.90	0.39	0.17	0.36	-0.29	0.06	0.45	-0.26	0.07
	LB	0.83	0.40	0.17	0.85	0.35	0.11	0.30	-0.30	0.04	0.27	-0.20	0.03

		u'						w'					
			Ref			Mobile			Ref			Mobile	
		Max	Min	σ	Max	Min	σ	Max	Min	σ	Max	Min	σ
MNE Exp-1	SFT	0.64	0.32	0.08	0.59	0.33	0.05	0.44	-0.42	0.07	0.40	-0.37	0.06
	PFC	0.55	0.32	0.06	0.73	0.27	0.14	0.45	-0.28	0.05	0.37	-0.32	0.06
	PFT	0.76	0.31	0.12	0.77	0.30	0.11	0.50	-0.20	0.07	0.33	-0.18	0.04
	UB	0.68	0.38	0.08	0.72	0.35	0.08	0.42	-0.33	0.06	0.26	-0.21	0.03
	MB	0.71	0.39	0.09	0.70	0.35	0.09	0.41	-0.35	0.06	0.27	-0.27	0.03
	LB	0.72	0.42	0.09	0.65	0.34	0.08	0.40	-0.41	0.07	0.24	-0.19	0.03

The mean of u'-and w'-components are zero.

Appendix 3.4. Summary statistics of airflow properties during **onshore winds** estimated from the ultrasonic anemometers at 0.8 m high including: fluctuating velocity of u'- and w'- components (m s^{-1}) at the reference (Ref) and mobile masts during onshore winds. Note that maximum (max) and minimum (min) corresponds to the two extreme values over the 20-minutes experiment. The mean of the u' and v' component are zero.

| | | u' | | | | | | w' | | | | | |
| | | Ref | | | Mobile | | | Ref | | | Mobile | | |
		Max	Min	σ	Max	Min	σ	Max	Min	σ	Max	Min	σ
BL Exp-1	SFT	0.80	0.44	0.09	0.73	0.46	0.06	0.43	-0.29	0.04	0.36	-0.26	0.03
	PFC	0.68	0.48	0.05	0.62	0.38	0.08	0.39	-0.32	0.03	0.26	-0.22	0.03
	PFT	0.66	0.45	0.05	0.51	0.32	0.05	0.38	-0.34	0.03	0.22	-0.16	0.02
	UB	0.47	0.42	0.09	0.39	0.31	0.05	0.27	-0.34	0.04	0.17	-0.15	0.01
	MB	0.48	-0.48	0.04	0.35	-0.35	0.04	0.28	-0.23	0.03	0.15	-0.21	0.02
	LB	0.43	-0.34	0.05	0.31	-0.33	0.04	0.24	-0.10	0.03	0.13	-0.19	0.01
TSH Exp-1	SFT	0.47	0.24	0.06	0.37	-0.31	0.04	0.23	-0.15	0.02	0.20	-0.17	0.02
	PFC	0.35	0.18	0.04	0.39	-028	0.05	0.21	-0.17	0.02	0.20	-0.16	0.02
	PFT	0.28	0.13	0.04	0.35	0.16	0.05	0.17	-0.14	0.02	0.17	-0.11	0.02
	UB	0.54	0.26	0.10	0.43	0.28	0.07	0.34	-0.28	0.06	0.21	-0.11	0.04
	SED	0.49	0.13	0.08	0.48	0.17	0.09	0.31	-0.18	0.05	0.22	-0.22	0.03
	LB	0.37	0.17	0.05	0.43	0.13	0.06	0.23	-0.20	0.02	0.13	-0.07	0.02
MNE Exp-2	PFC	0.20	0.08	0.04	0.31	0.10	0.05	0.09	-0.05	0.01	0.10	-0.09	0.02
	PFT	0.32	0.15	0.04	0.36	0.18	0.05	0.12	-0.07	0.01	0.16	-0.10	0.02
	UB	0.48	0.18	0.07	0.39	0.16	0.07	0.19	-0.10	0.02	0.20	-0.10	0.03
MNE Exp-3	SFC	0.57	0.44	0.04	0.84	0.54	0.08	0.25	-0.23	0.02	0.37	-0.31	0.04
	PFC	0.62	0.34	0.08	0.68	0.39	0.08	0.29	-0.18	0.03	0.32	-0.22	0.03
	PFC	0.59	0.38	0.06	0.86	0.51	0.10	0.29	-0.23	0.03	0.38	-0.28	0.04
	PFT	0.58	0.40	0.08	0.71	0.43	0.09	0.30	-0.22	0.03	0.34	-0.32	0.04

The mean of u'-and w'-components are zero.

Appendix 4.1. Synoptic situations in: (A) 17th October 2009, (B) 20th October 2009.
Source: http://www.wetterzentrale.de/
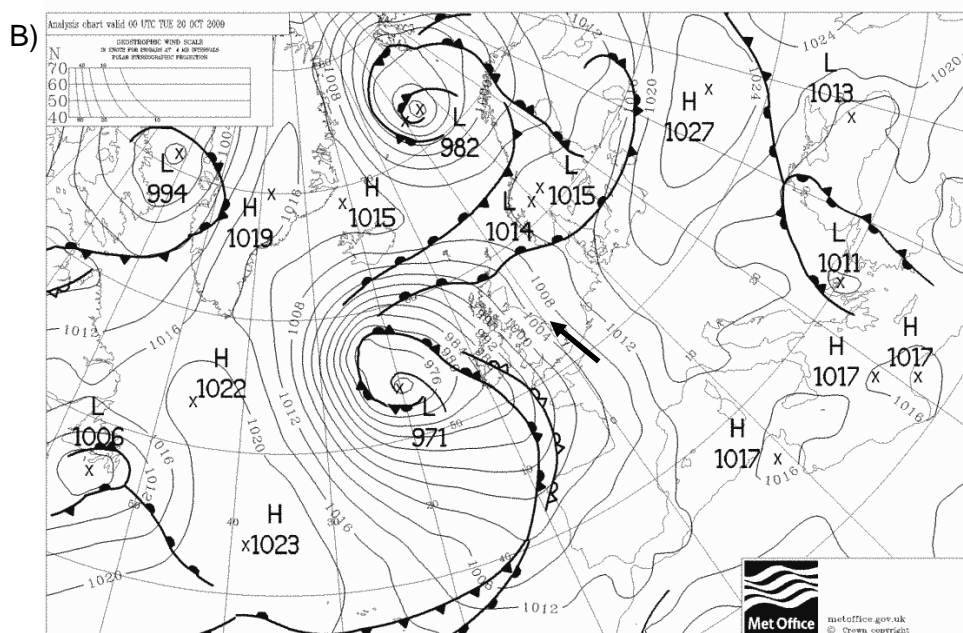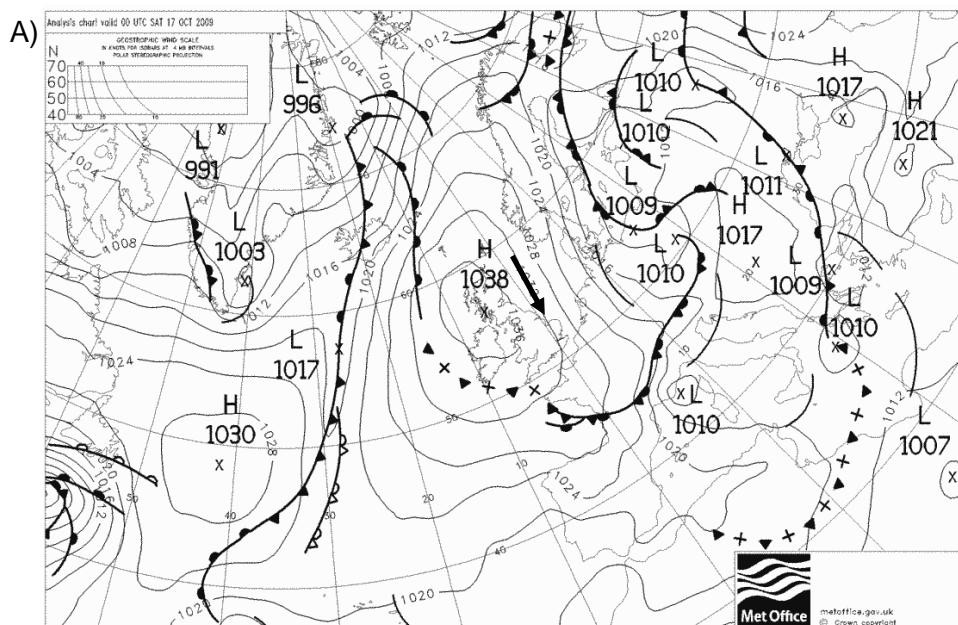
——— Mean seal level Pressure (hPa)　　➡ Flow orientation at the study area

Appendix 4.2. Synoptic situation in 28th February 2010.
Source: http://www.wetterzentrale.de/

Mean seal level Pressure (hPa)   Flow orientation at the study area
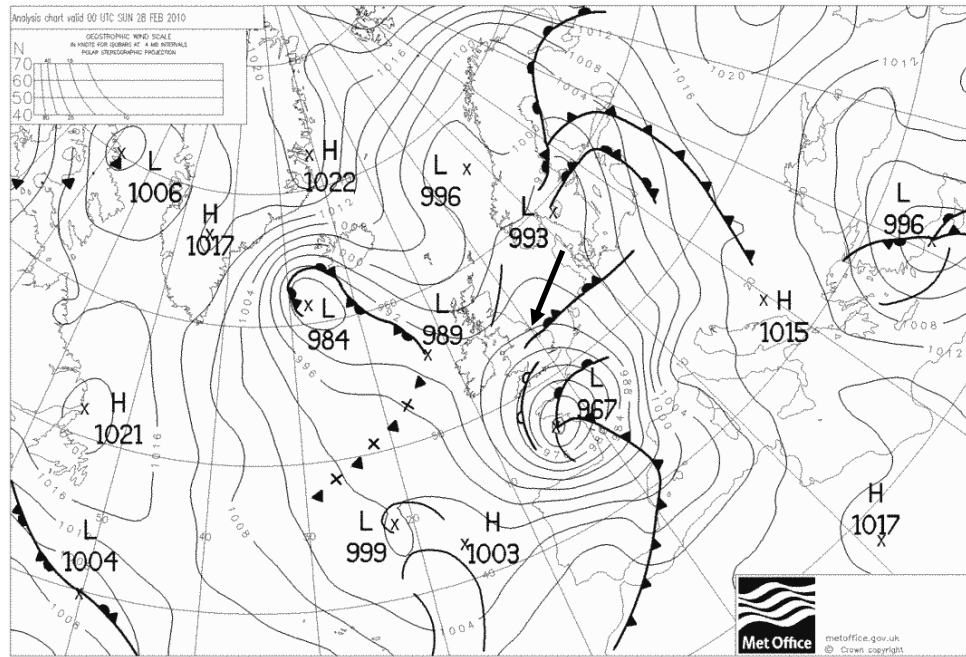
Appendix 4.3. Synoptic situations in: (A), (B) 13th-26th August and (C) 24th September 2010. Source: http://www.wetterzentrale.de/
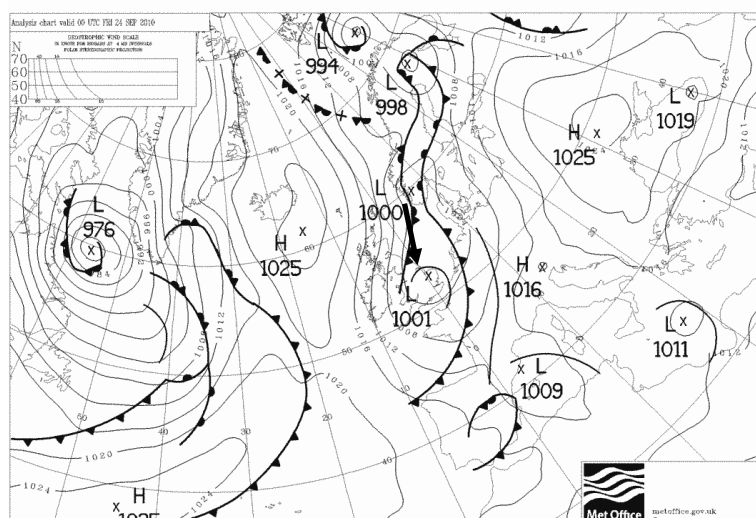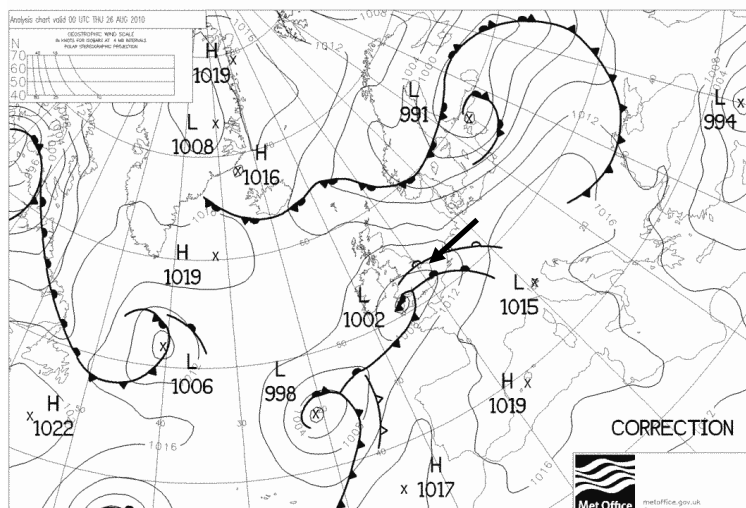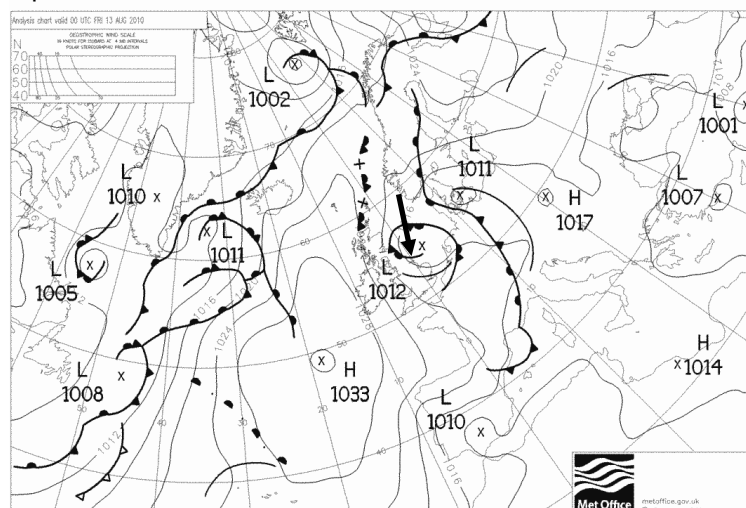
——————— Mean seal level Pressure (hPa) ➤ Flow orientation at the study area

Appendix 6.1. ISODATA classification for vegetation analysis at BL. Dashed and black lines correspond to the foredune position in 1891 and the study year respectively. Red polygon shows the study site analysed.

1992

1994

1997

2001

2007

2009

2010

Appendix 6.2. ISODATA classification for vegetation analysis at TSH. Dashed and black lines correspond to the foredune position in 1891 and the study year respectively. Red polygon shows the study site analysed.

1992

1994

1997

2001

2007

2009

2010
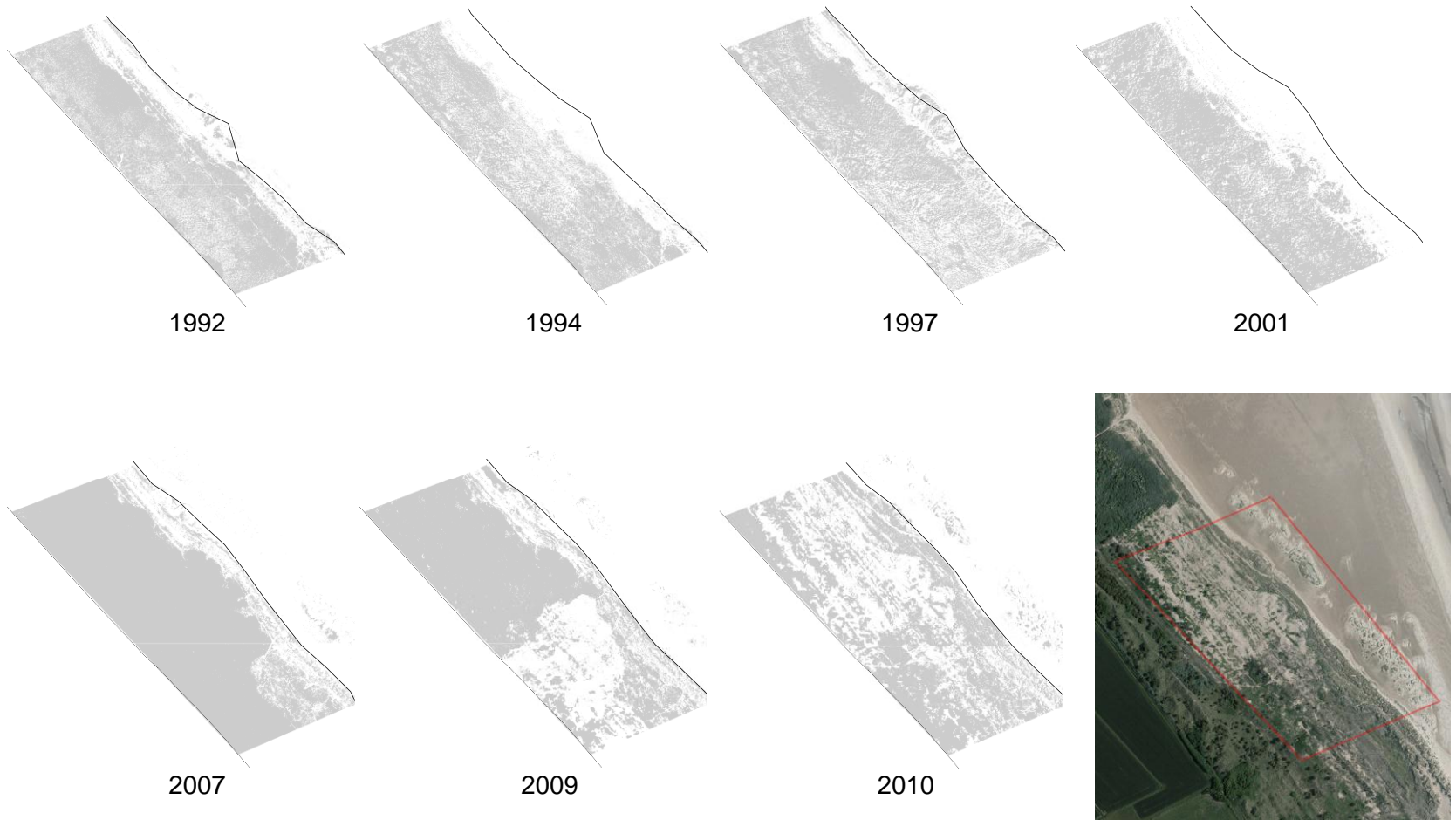
Appendix 6.3. ISODATA classification for vegetation analysis at MNE. Dashed and black lines correspond to the foredune position in 1891 and the study year respectively. Red polygon shows the study site analysed.

1992

1994

1997

2001

2007

2009

2010

Appendix 6.4. Storm surge events recorded between 1993-2010.

Year	Duration of the storm events (hour)	Highest water level (m)	Surge (m)	Wind speed at Donna Nook (m/s)	Adjusted wind speed (m/s)	Wind direction (°)	Hs (m)	Pressure (hPa)	SESI
14/10/1993	1	3.65	0.12	15.42	15.92	20	6.25	1004	3.85
13/12/1993	2.5	4.16	0.68	20.87	21.54	30	8.46	998	14.02
18/02/1996	0.25	3.58	0.16	22.62	23.35	10	9.17	990	0.18
19/02/1996	0.25	3.59	0.76	19.53	20.16	20	7.92	1023	0.17
19/02/1996	1.25	4.15	0.59	19.02	19.63	30	7.71	1012	6.26
19/02/1996	2.75	4.22	0.39	20.00	20.65	10	8.33	1014	16.07
20/02/1996	1.75	3.83	-0.02	14.91	15.39	30	6.04	1030	20.36
03/05/1996	0.5	3.52	0.26	15.93	16.45	360	6.45	1005	0.04
12/11/1996	2	3.76	0.33	19.4	20.03	20	7.87	1005	5.54
12/11/1996	2	3.87	0.32	17.28	17.84	360	7.01	1008	5.24
26/06/1997	0.5	3.53	0.23	16.45	16.98	10	6.67	998	0.09
16/12/1997	1.5	3.74	0.22	17.13	17.69	90	5.48	1022	1.93
16/12/1997	0.5	3.52	0.12	14.91	15.39	70	6.33	1033	0.06
11/06/1998	0.5	3.53	0.31	15.93	16.45	10	6.46	1002	0.11
07/10/1998	1	3.87	0.04	14.39	14.86	10	5.83	1023	2.15
08/10/1998	2.5	4.32	0.13	15.52	16.03	10	6.29	1026	12.92
03/11/1998	1.25	3.88	0.25	16.26	16.78	20	6.59	988	3.16
18/05/1999	0.5	3.64	0.09	14.39	14.86	60	5.83	1020	0.41
04/04/2000	0.25	3.51	0.37	19.02	19.63	10	7.71	995	0.02
04/04/2000	1.75	3.80	0.37	17.73	18.31	360	7.19	1005	3.74
11/01/2001	1.25	3.66	0.04	14.39	14.86	60	5.83	1023	1.19
19/09/2001	2.25	4.12	-0.01	17.13	17.64	350	6.93	1007	9.63
22/02/2004	0.5	3.84	0.39	15.42	15.92	360	6.25	1020	1.07
13/02/2005	2	3.96	0.44	18.76	19.37	350	7.61	1012	6.92
13/08/2006	0.75	3.98	0.13	15.42	15.92	360	6.25	1002	2.23
20/03/2007	1	3.88	0.3	17.99	18.57	350	7.29	1006	2.80
26/09/2007	0.75	3.61	0.14	15.93	16.45	350	6.46	1022	0.51
23/11/2007	1	3.79	0.39	14.39	14.86	350	5.83	1014	1.91
10/03/2008	0.75	3.56	0.18	14.73	15.21	150	2.1	970	0.1
05/04/2008	0.75	3.79	0.35	15.42	15.92	350	6.25	1023	1.34
10/02/2009	0.5	3.67	0.39	14.39	14.86	20	5.83	990	0.5
24/09/2010	0.75	3.53	0.35	15.43	15.93	350	6.26	1012	0.15

Appendix 6.5. Severe foredune erosion after cumulative storm surges in February 1996.

A)

B)

C)

Appendix 6.5. Severe foredune erosion after cumulative storm surges in February 1996.

Appendix 6.6. Lidar cross-shore profiles in 2001 and 2007 at BL from north (A) to South (E).

D)

E)
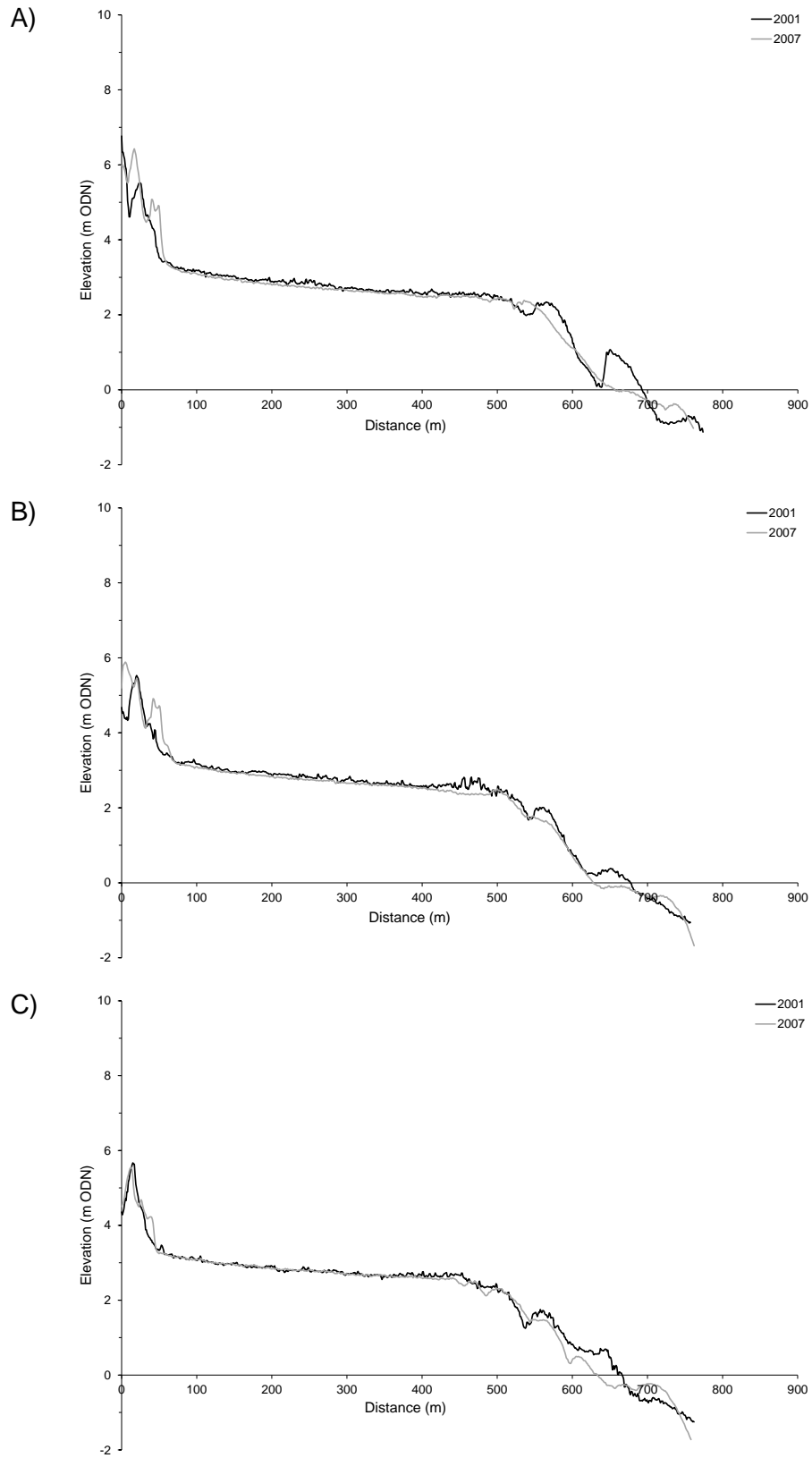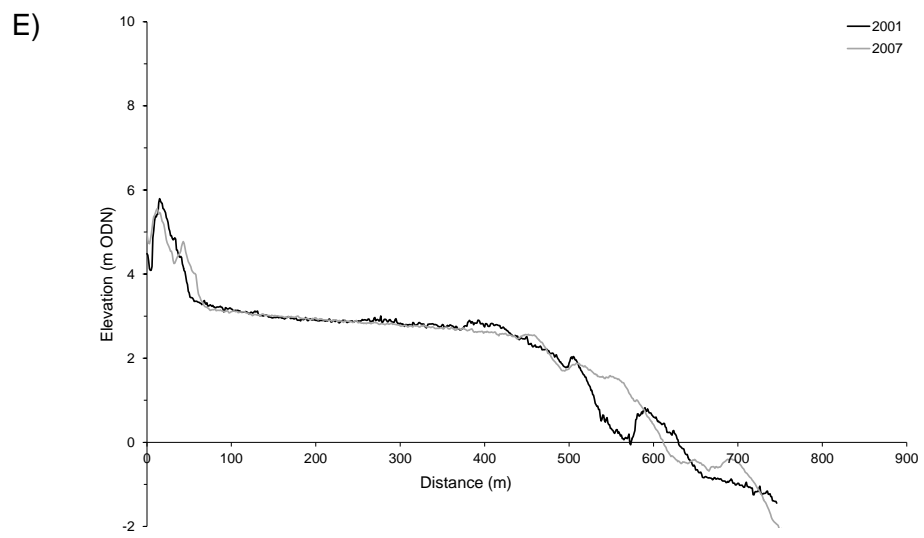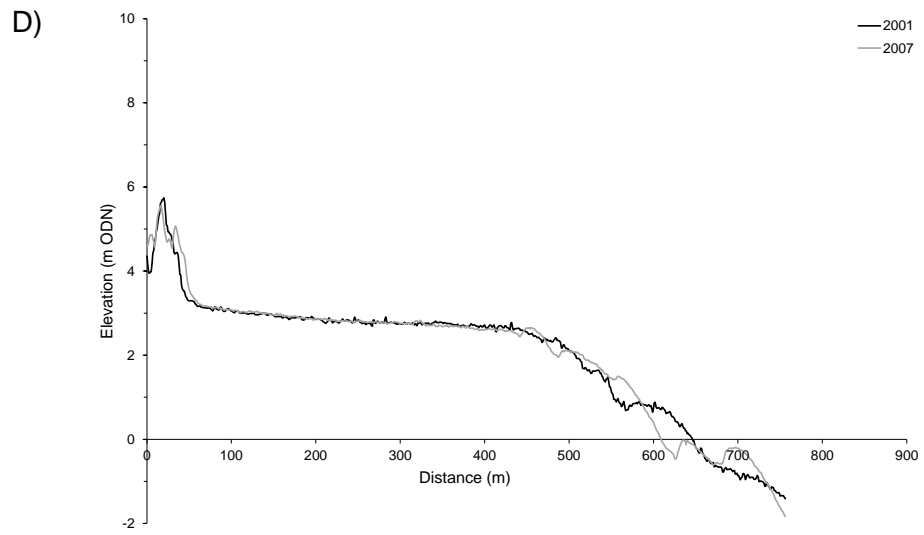
Appendix 6.7. Lidar cross-shore profiles in 2001 and 2007 at TSH from north (F) to south (J).

I)

J)
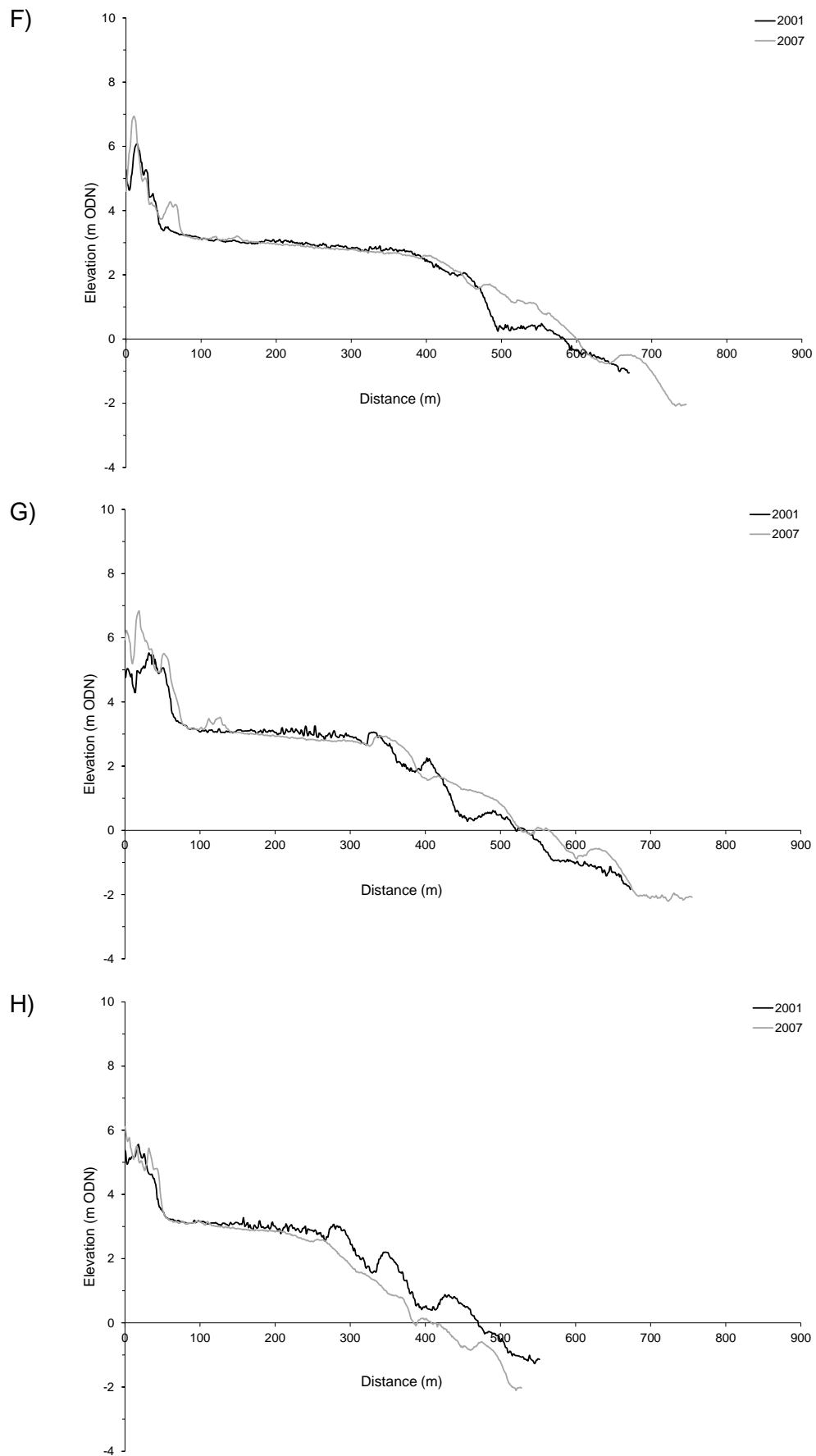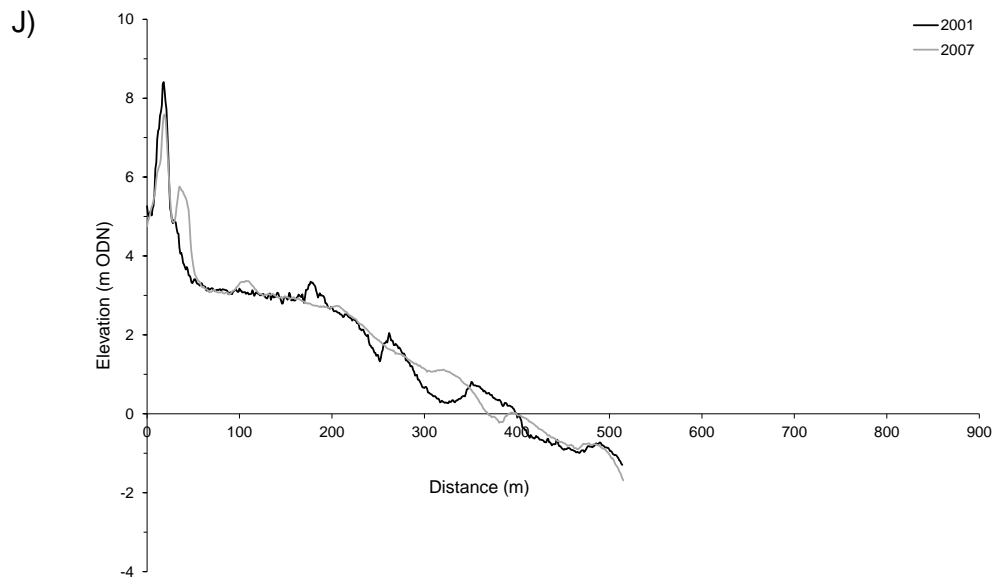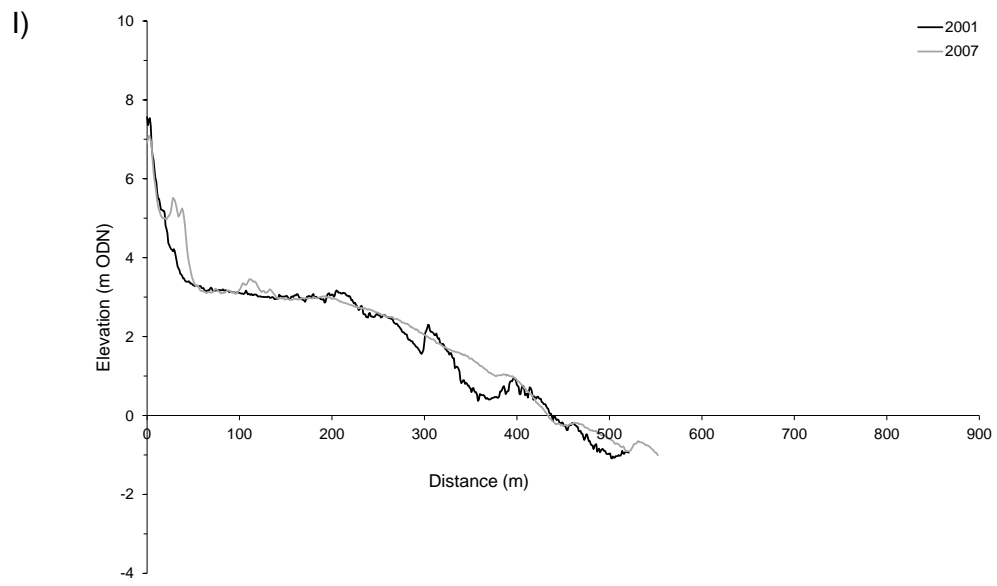
Appendix 6.8. Lidar cross-shore profiles in 2001 and 2007 at MNE from north (K) to south (O).

N)

O)
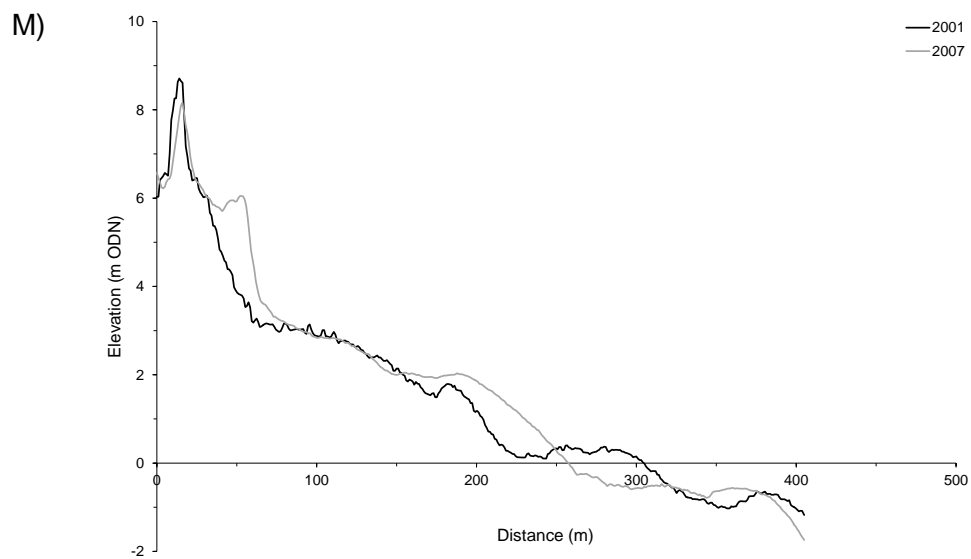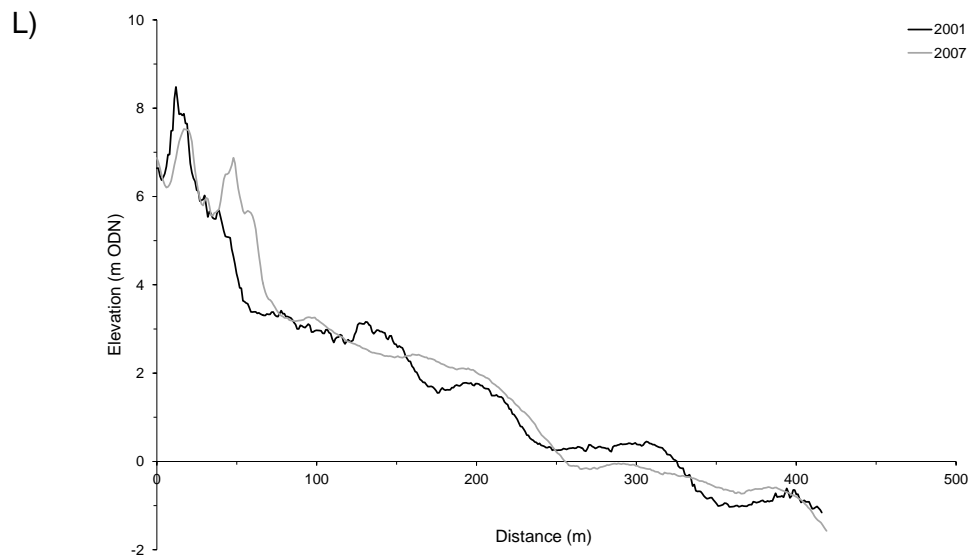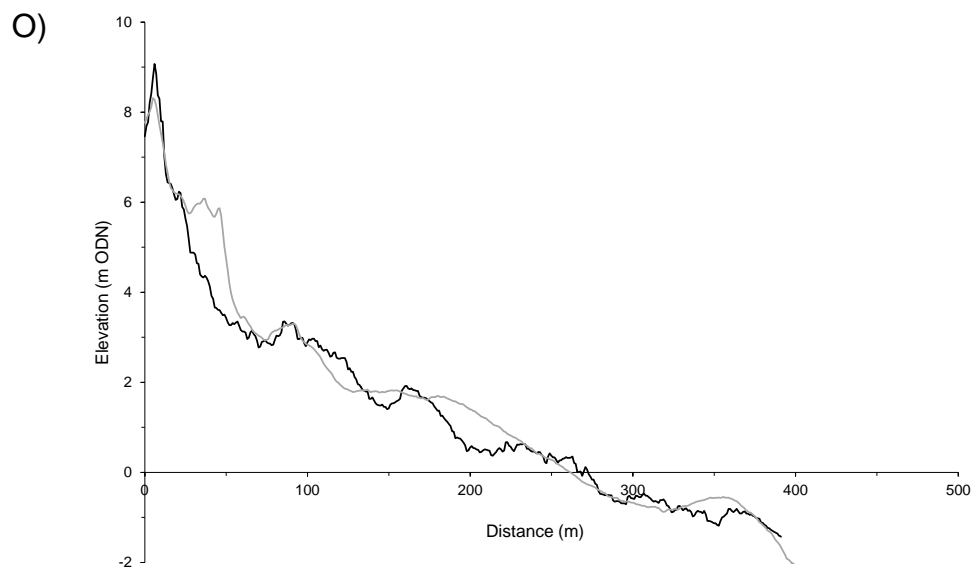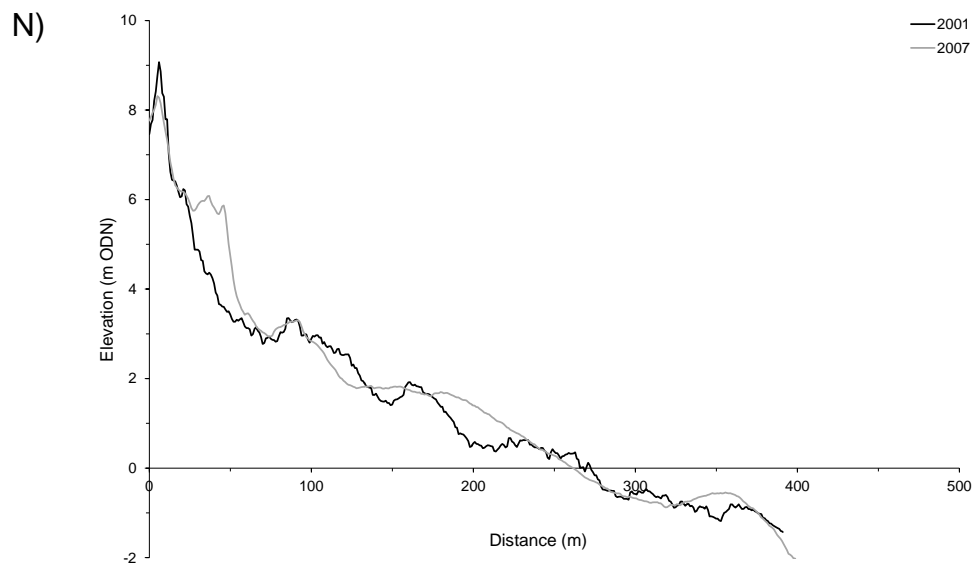
Appendix 7. Bathymetric EA profiles at: (A) BL – L2E7, (B) MNE – L2D1.

Appendix 8. Journal paper.

Elsevier Editorial System(tm) for Geomorphology
Manuscript Draft
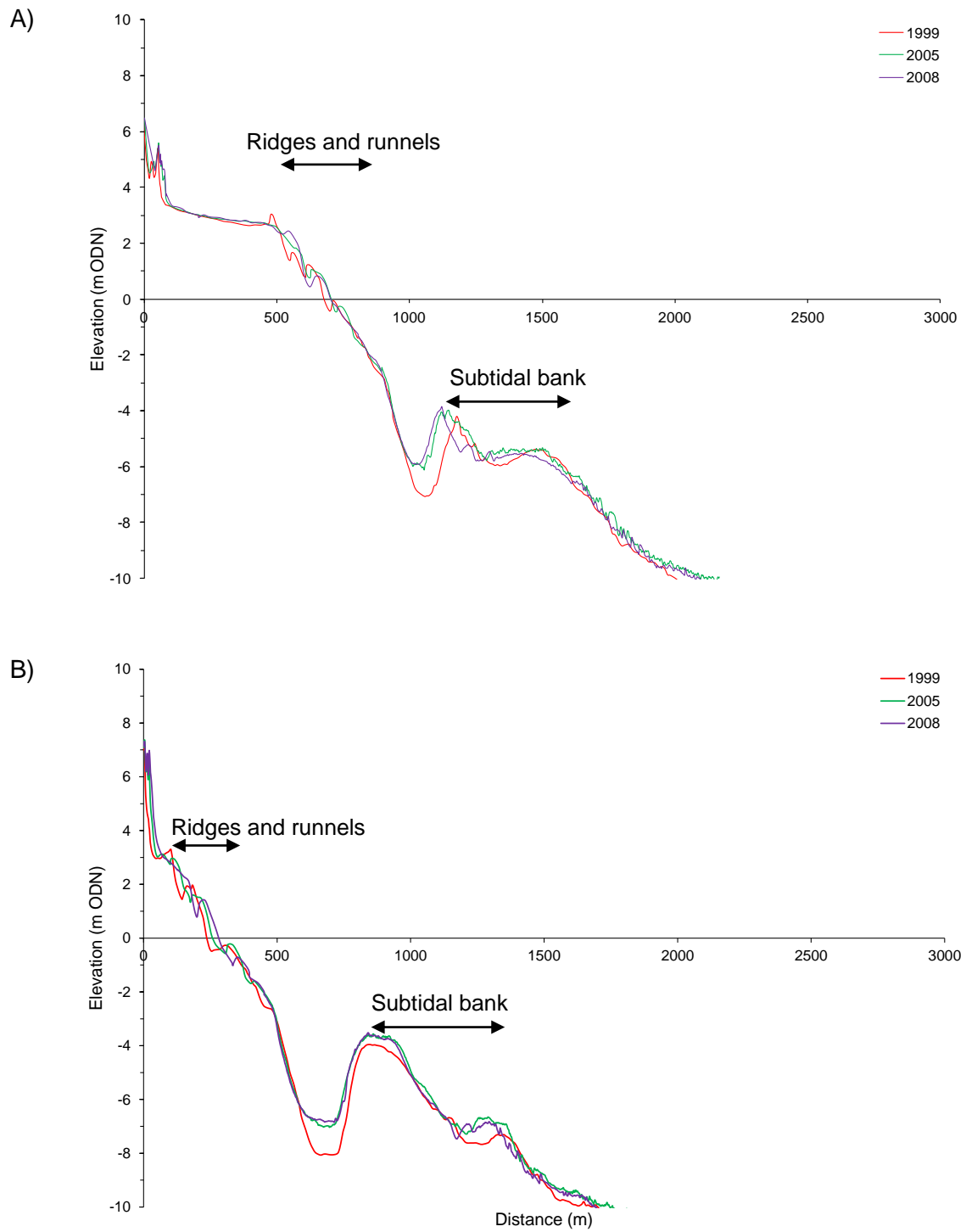
Title: A 150 year record of coastline dynamics within a sediment cell: eastern England

Article Type: Research Paper

Corresponding Author: Dr. Joanna Bullard,

Corresponding Author's Institution: Loughborough University

First Author: Anne-Lise Montreuil

Order of Authors: Anne-Lise Montreuil; Joanna E Bullard, PhD

Abstract: Coastal sediment cells reflect processes operating at a range of scales, but it is the medium spatial and temporal scales (decades to centuries) that are of greatest interest for coastal management. This paper focuses on coastline position change within a single sediment cell over 150 years where the geomorphology includes cliffs, beaches and saltmarshes. The focus is the east coast of England from Flamborough Head to Gibraltar Point. Although the updrift sector of this sediment cell has been studied for well over a century, the downdrift sector has attracted significantly less attention. Using topographic profiles, bathymetric profiles, aerial photographs and historical maps we mapped coastline erosion and accretion using the Digital Shoreline Analysis System (DSAS) and calculated volumetric changes for different morphometric units. Rapid erosion of the updrift Holderness cliffs has been counterbalanced with accretion on beaches along the downdrift Lincolnshire coast. The amount of accretion in Lincolnshire corresponds to around 29% of the volume of sediment eroded from Holderness. Much of the eroded cliff material is likely to be deposited temporarily into nearshore and offshore sand banks before being redistributed by cross-shore currents. An exploration of storm surge impact on long term erosion and accretion rates showed no clear relationship between storm surge frequency and change in coastline position, however this may be in part due to the relative timing of storm occurrence and data acquisition. The Jenkinson Daily Weather Type classification was found to be a reasonable proxy for the occurrence of strong onshore winds which may offer scope for further investigation of the role of forcing factors over time periods beyond the length of the meteorological and tidal station records. Winter North Atlantic Oscillation phase was not a good indicator of storminess on the east coast of England but may be a useful proxy for quiescence.

1   A 150-year record of coastline dynamics within a sediment cell: eastern England.

2

3

4   Anne-Lise Montreuil[1], Joanna E. Bullard[1*]

5

6   [1]Department of Geography, Loughborough University, Leicestershire, LE11 3TU, UK.

7   Email: j.e.bullard@lboro.ac.uk

8   Tel: +44(1)509 222794

9   Fax: +44(0)1509 223930

10

11   *Corresponding author

12

13 **Abstract**

14 Coastal sediment cells reflect processes operating at a range of scales, but it is the medium

15 spatial and temporal scales (decades to centuries) that are of greatest interest for coastal

16 management. This paper focuses on coastline position change within a single sediment cell

17 over 150 years where the geomorphology includes cliffs, beaches and saltmarshes. The

18 focus is the east coast of England from Flamborough Head to Gibraltar Point. Although the

19 updrift sector of this sediment cell has been studied for well over a century, the downdrift

20 sector has attracted significantly less attention. Using topographic profiles, bathymetric

21 profiles, aerial photographs and historical maps we mapped coastline erosion and accretion

22 using the Digital Shoreline Analysis System (DSAS) and calculated volumetric changes for

23 different morphometric units. Rapid erosion of the updrift Holderness cliffs has been

24 counterbalanced with accretion on beaches along the downdrift Lincolnshire coast. The

25 amount of accretion in Lincolnshire corresponds to around 29% of the volume of sediment

26 eroded from Holderness. Much of the eroded cliff material is likely to be deposited

27 temporarily into nearshore and offshore sand banks before being redistributed by cross-

28 shore currents. An exploration of storm surge impact on long-term erosion and accretion

29 rates showed no clear relationship between storm surge frequency and change in coastline

30 position, however this may be in part due to the relative timing of storm occurrence and data

31 acquisition. The Jenkinson Daily Weather Type classification was found to be a reasonable

32 proxy for the occurrence of strong onshore winds which may offer scope for further

33 investigation of the role of forcing factors over time periods beyond the length of the

34 meteorological and tidal station records. Winter North Atlantic Oscillation phase was not a

35 good indicator of storminess on the east coast of England but may be a useful proxy for

36 quiescence.

37

38

39 **Keywords** Sediment cell, Coastline change, sediment budget, storm surge, Jenkinson

40 Weather Types

41

42

43 **Highlights**

44 1) Trends in the balance of sediment supplies and sinks in a littoral cell are examined.

45 2) Long-term erosion dominates cliffs updrift and reaches rates of up to 2 m year^{-1}

46 3) Accretion up to 2.7 m yr^{-1} dominates on sandy beaches at the centre of the cell.

47 4) The Jenkinson Daily Weather Type is a useful proxy for UK east coast storminess.

48

1. Introduction

Coastlines are inherently dynamic landscape components and significant alterations in their position and alignment have been documented worldwide. These changes occur in response to factors such as sea-level change (Orford et al.,1995), large-scale morphological self-organization (Cooper et al., 2007), changes in sediment budget associated with sources (e.g. rivers, cliff erosion), sinks (e.g. sand banks, submarine canyons) and longshore transport (Pye, 1983; Aagaard et al., 2004), variations in storminess and wave climate (Zhang et al., 2001; Pye and Blott, 2008), and coastal management (Iskander et al., 2007; Kaminsky et al., 2010). Along any stretch of coastline, variations in the rate and direction (erosion or accretion) of change are common, associated with local sediment budget and coastal characteristics such as the distribution of headlands, cliffs and beaches; records of such dynamics are typically used to plan coastal management strategies. The importance of littoral sediment budget as a control on the direction of coastline movement is widely recognized and is typically linked to the concept of the sediment (or littoral) cell. Ideal sediment cells are sections of coast that are relatively self-contained and include defined sources, transport pathways and sinks of sediment. The concept was first applied to the California coast (Bowen and Inman, 1966; Inman and Frautschy, 1966) but is now widely used in countries such as the USA, Canada, New Zealand and the UK for coastal management planning, where cell boundaries define the planning units (e.g. Motyka and Brampton, 1993; Hooke and Bray, 1995; Cooper and Pontee, 2006).

The delimitation and operation of sediment cells reflect processes interacting at a range of spatial and temporal scales, and in many areas coastal morphology and dynamics still reflect and are recovering from the impact of Holocene sea-level changes and deglaciation (May and Hansom, 2003). It is the medium spatial (≥10 km) and temporal (decades to centuries) scales that are usually of greatest interest for coastal management and forward planning

4

75   (Cooper et al., 2001; Pethick, 2001; Orford and Pethick, 2006; Gelfenbaum and Kaminsky,

76   2010), but there is often a lack of systematic information concerning decadal-scale changes

77   in interacting landforms within a single cell (e.g. Lee, 2001; Ruggiero et al., 2005; Pye et al.,

78   2007). The aim of this paper is to quantify the spatial and temporal variability in coastline

79   position, rate of change and sediment budget within a single sediment cell. Particular

80   attention has been given to six areas of interest characterised by different coastal landforms

81   (e.g. cliffs, beaches) or management intervention. We use complementary data sources

82   including maps, aerial photographs and topographic profiles to document change over

83   timescales up to 150 years. A preliminary examination of the relationship between

84   morphological change and forcing factors is also presented. The area of interest is the east

85   coast of England between Flamborough Head and Gibraltar Point. Whilst the northern part of

86   this region has been widely-studied, the downdrift, southern sector has attracted significantly

87   less attention.

88

89   **2. Regional setting**

90   Prior to the 1980s, coastal management in Britain was typically local in focus and

91   determined by administrative bodies such as local authorities. Increasing recognition in the

92   1980s that management at one location can impact the coastline elsewhere led to various

93   authorities combining interests to develop more integrated coastal management plans

94   (Hooke and Bray, 1995). These coastal groups recognised the importance of understanding

95   sediment transport patterns for effective management (e.g. Hooke and Bray, 1995; Hooke et

96   al., 1996). Since the 1990s, the coastline of England and Wales has been divided in to

97   eleven coastal cells (Motyka and Brampton, 1993) (Fig. 1). Each of these cells represents a

98   defined natural sedimentary system and for each there is a Shoreline Management Plan

99   (SMP) used to guide sustainable coastal defence decision-making processes (MAFF, 1994;

100   DEFRA, 2006). SMPs involve numerous partner organisations and stakeholders including

101   local authorities, government agencies and business and community groups, and their

102 introduction marked a strategic step towards integrated management of the coastline within

103 natural rather than purely administrative boundaries that is both long term and considers the

104 impact of local-scale coastal management elsewhere (Hooke and Bray, 1995; O'Connor et

105 al., 2009).

106

107 *2.1. Geomorphology of the coastal cell*

108 This paper focuses on sediment cell 2 along the East Riding and Lincolnshire coastlines,

109 which is divided into three sub-cells (2a Flamborough Head to Spurn Head; 2b Outer

110 Humber Estuary; 2c Donna Nook to Gibraltar Point: Fig. 1). Net longshore sediment

111 transport is from north to south. The concept of sediment cells focuses on wave-driven

112 transport of non-cohesive sediments (Motyka and Brampton, 1993) and is harder to apply to

113 fine sediments in suspension (Hooke and Bray, 1995). However, many sediment cells

114 include a variety of landforms including both those formed from non-cohesive sediments

115 (such as sandy beaches) and those dominated by cohesive material such as saltmarshes.

116 In the study area, coastal geomorphology within the cell is varied and includes chalk and

117 glacial till cliffs, wide sandy beaches, saltmarshes, sand dunes, coastal spits and nearshore

118 and offshore sand banks. Coastal management strategies include engineered defences built

119 over the last two centuries and beach nourishment programmes, although large stretches of

120 the coastline have no man-made defences. The main cell boundaries are Flamborough

121 Head to the north, a fixed chalk headland, and Gibraltar Point spit in the south, which is a

122 partial boundary with sediment transfer continuing in to The Wash and southern North Sea.

123

124 <Fig. 1>

125

In the north of the sediment cell, glacial till cliffs 3-40 m high extend 60 km along the Holderness coast and are rapidly retreating (recently reviewed by Quinn et al., 2009). The cliff erosion occurs through repeated landslide activity, caused mainly by waves undercutting the base of the cliffs and removing beach material (Dossor, 1955; Quinn et al., 2009). Sea defences are present near some coastal towns. Sediment eroded from these cliffs and the shore platform are transported southwards to Spurn Head and to offshore sand banks by littoral drift and wave currents. Spurn Head is a narrow sand and gravel spit that extends 5.5 km into the mouth of the Humber Estuary (sub-cell 2b). The Humber Estuary mouth stretches from Spurn Head to Donna Nook and is influenced both by the tide and flow from the river. Strong tidal flows intersect the north-south sediment transport pathway along the open coast, limiting the entry of gravels and sands into the estuary mouth.

In contrast, the low-lying Lincolnshire coast, south of the Humber, comprises superficial deposits left by retreating ice sheets (Swinnerton and Kent, 1949; Brampton and Beven, 1987) and is characterized by sandy beaches and saltmarshes (sub-cell 2c). Offshore sand banks are present from Donna Nook to Mablethorpe, and not only protect the shore against wave attack, but also provide a source of sand to the beaches which are up to 3.5 km wide and backed by dunes (van Houwelingen et al., 2006). Extensive saltmarshes at Saltfleetby are sheltered by broad beaches. This section of the Lincolnshire coastline is typically accreting (HR Wallingford, 2002). South of Mablethorpe the sediment budget changes and coastal erosion dominates in part due to the absence of offshore sand banks (Dugdale and Vere, 1993). Sea defences have been built to protect against coastal flooding and, following a severe storm surge in 1953, extensive 'hard' defences were built such as seawalls, groynes and revetments particularly near Skegness. Historically, during high storms, the thin sand cover on the beach moved seaward and the underlying glacial till was exposed and eroded. To counter this erosion, a major beach renourishment plan began in 1994 and continues to date (Environment Agency, 2004). Just south of Skegness, the coastline

153 changes orientation slightly providing a sheltered coast for the development of coastal dunes

154 and saltmarshes at Gibraltar Point (National Nature Reserve).

155

156 *2.2. Marine and climatic setting*

157 Along this coast, tides are semi-diurnal and macro-tidal, with a mean spring tidal range of 6

158 m; tidal currents flow southward during the flood and northward during the ebb (Table 1).

159 The dominant incident wave approach is from the north to east quadrant (corresponding to

160 the longest wind fetch). Offshore significant wave conditions are characterized by a 50%

161 exceedence significant wave height of 0.5 m and a modal wave period of 4s, but wave

162 heights can reach 2.5 m in winter (van Houwelingen et al., 2008). Wave-driven processes

163 and flood residual tidal currents are the main drivers of alongshore sediment transport which

164 is directed towards the south (Pye, 1995; van Houwelingen et al., 2006). Storm surges are

165 relatively rare, but the most severe recent events occurred in 1953 (Barnes and King, 1953;

166 Brampton and Beven, 1987) and in 1978, and significantly affected the Lincolnshire coast

167 (Steers et al., 1979; Blott and Pye, 2004). Severe storm surges are the result of combined

168 high tidal level and energetic wave activity, caused by deep depressions tracking eastward

169 toward the North Sea and moving around the North Sea basin in an anticlockwise circulation

170 (Dolata et al., 1983). Consequently, surge levels increase southwards along the east coast

171 of England caused by the funnelling effect of the narrowing North Sea. Winds prevail from

172 the southwest (i.e. offshore) and wind speeds are modest (<8 m.s^{-1}) for the majority of the

173 time (73%). During winter months, however, the development of high pressure systems over

174 the British Isles and the North Sea can lead to prolonged strong northwesterly and easterly

175 winds (Steers, 1966).

176

177 <Table 1>

178

179 Global average sea level rose at approximately 1.8 mm year^{-1} between 1961 and 2003, but

180 has accelerated to 3.1 mm year^{-1} over recent years (IPCC, 2007). Along the east coast of

181 England, sea-level rise is lower than this global average at c.1 mm year^{-1} (HECAG, 2009,

182 Woodworth et al., 2009). For the purposes of this study sea level is considered to have been

183 negligible from 1850 to 2010.

184

185 **3. Methods and Approach**

186 Changes in coastline position (section 3.2) from the mid-1990s for the whole sediment cell

187 were determined using cross-shore topographic surveys. From these, we identified 6 specific

188 areas of interest (AOIs) within the sediment cell representing a range of coastal

189 geomorphological features (Table 2). These 6 AOIs were examined in more detail to

190 determine:

191   1. the changing position and relative rate of retreat or accretion of the coastline from the

192   mid- to late-1800s to date;

193   2. changes in the volume of sediment in backshore and beach/foreshore from the mid-

194   1990s to date;

195   3. changes in nearshore bathymetry from 1999 (for AOIs 3-6 only).

196 A preliminary exploration of the key environmental factors affecting rates of coastline change

197 was made using climate and tidal data, including the potential for using a proxy dataset to

198 explain long-term geomorphological changes.

199

200 <Table 2>

201

202 *3.1. Geomorphological data sources*

3.1.1. Topographic and bathymetric profiles

The temporal frequency of cross-shore topographic surveys around the UK is variable and for this study dates were selected that were: a) available for all AOIs, b) corresponded to aerial photograph coverage, and c) maximized the length of the record. Surveys were used from the mid-1990s (one of 1994, 1996 or 1997), 1999, 2005, 2008 and 2010 and were supplied for the Holderness coast by the East Riding of Yorkshire Council, and for Lincolnshire by the UK Environment Agency. For each year, a total of 160 profiles, surveyed in summer or early autumn, was analysed (profile spacing 0.5 km and 1 km along the East Riding and Lincolnshire coasts, respectively). Initially surveys were conducted using a standard total station (horizontal accuracy ±0.1 m and vertical accuracy ±0.01 m) located over Ordnance Survey (OS) control points and referenced to the ODN datum. However, since 1999 and 2003 (East Riding and Lincolnshire, respectively), surveys have been made using a RTK-GPS system. Detailed topographic airborne laser surveys have been undertaken along the East Riding coast since 2008 (horizontal accuracy ±1 m; vertical accuracy ±0.15 m). From these we extracted cross-shore topographic profiles along the same lines used in earlier surveys.

Nearshore changes were determined using bathymetric surveys made as seaward extensions of the terrestrial cross-shore topographic profiles, and carried out by Gardline under contract to the UK Environment Agency in 1999, 2005 and 2008 along the Lincolnshire coast only. The surveys employed single multi-beam echo-sounders, the accuracy of which has been estimated to be ±1 m in the horizontal and ±0.005 m in the vertical (Gardline, 2008).

3.1.2. Maps and Aerial Photographs

228 For each AOI, coastline change was estimated over a ~150-year period using historic OS

229 maps (1854-1951: Table 3) and aerial photographs (1953-2010: Table 3 - available data

230 vary by site). Analysis of the historical OS maps can often experience a delay between field

231 survey dates and the publication dates, so that it is difficult to establish specifically when

232 surveys were undertaken. Aerial survey acquisitions were generally during summer months.

233 The use of historical data and combining different data sources can be subject to

234 uncertainties and errors (Thomas et al., 2011; James et al., 2012) which were minimized

235 where possible. Aerial photographs were individually registered against the 2010 ortho-

236 rectified photographs using the British National Grid (OSGB36) reference system, and

237 ArcMap 9.3 software. Registration was based upon eight stable ground control points (e.g.

238 buildings, road junctions) visually identifiable on all photographs; an average error of ±1.5 m

239 is considered acceptable (Dolan et al., 1991; Chaverot et al., 2008). The root mean square

240 error (RMSE; Maune, 2007) associated with the geo-referencing process was less than 3.5

241 m for each aerial photograph. Independent error estimates were also undertaken by

242 measuring the positional difference of six additional ground control points, on every map and

243 aerial photograph and the same features on the 2010 ortho-rectified photograph. The

244 average difference for the OS maps ranges between 6.6 m and 7.3 m, while the errors of

245 ortho-photographs are estimated to be 3.4 m in 1953, and below 2 m for all others and

246 deemed to be within acceptable limits (Longley et al., 2005).

247

248 <Table 3>

249

250 The coastline (section 3.2) on each map and aerial photograph was digitized using ArcView

251 9.3 software. The Digital Shoreline Analysis System (DSAS) enables calculation of rate of

252 change statistics from multiple shoreline positions (Thieler et al., 2009; Brooks and Spencer,

253 2010;) and was used in combination with ArcView to calculate coastline change between

254 consecutive maps and aerial photographs. For this study, transects were generated every

255 100 m perpendicular to the reference coastline, defined as 1854 and 1891 for the East

256   Riding and Lincolnshire coast AOIs respectively (Table 2). At Saltfleetby, the number of

257   transects was reduced due to a lack of ground control points in part of the AOI and historical

258   coastal change was only estimated from ortho-photographs. This is because when

259   measured using the above technique there was a difference in the coastline position

260   depicted on the 1951 OS map and that interpreted from the 1953 aerial photographs of 625

261   m. In the context of other coastline changes, such high rates of accretion are highly unlikely

262   and are attributed to errors and uncertainties in the mapping process (James et al., 2012).

263   Within DSAS, the End Point Rate (EPR) method, determining the distance between the

264   earliest and the most recent coastlines divided by the time between surveys, was used to

265   obtain rates of coastline change. This also reduces the potential problem of image quality

266   over time (Dolan et al., 1991).

267

268   *3.2. Definition of morphological parameters*

269   Defining a consistent reference point along a dynamic coastline is challenging due to

270   variations in tide levels, meteorological or marine conditions (Pajak and Leatherman, 2002;

271   Thieler and Danforth, 1994), and limitations of spatial resolution during data acquisition

272   (Cracknell, 1999). Here, the coastline was defined from the topographic profiles using a fixed

273   reference plane at HAT (highest astronomical tide) level for the sandy beaches along Spurn

274   Head and the Lincolnshire coast; for precision, cross-shore profiles were linearly interpolated

275   to 0.1 m. The HAT level often coincides with the seaward limit of vegetated coastal

276   foredunes and can provide an objective, repeatable way of identifying morphological sub-unit

277   boundaries (Guillén et al., 1999). However, along the East Riding coast the top of cliff/cliff

278   base position identified from field or airborne surveys was assumed to provide a better

279   representation of the coastline (Brooks and Spencer, 2010). Coastline changes were

280   investigated relative to the initial survey if profiles did not reach the HAT level (with first

281   measureable survey being the zero, or reference, line).

283 The topographic profiles were also used to quantify sediment budget changes in the AOIs

284 (1997-2010 East Riding; 1994-2010 Lincolnshire). Cross-shore profiles were divided into

285 three morphological units - backshore, foreshore and nearshore – and sediment volume was

286 determined using simple trapezoidal area calculations under the survey line for one unit

287 length (m^3 m^{-1}) of coastline. The reference base for the backshore was +MHWS (mean high

288 water spring) height (Fig. 2), and thus corresponds to the sediment unit which is only

289 affected by marine processes during energetic events. The boundaries of the foreshore unit

290 are MHWS and ODN heights (z=0 m). In both these units volume is calculated above ODN.

291 The nearshore zone was divided using ODN to MLWS (sub-unit 1) and from MLWS to z = -5

292 m (sub-unit 2). The baseline of z = -5 m was used to compute the sediment volume (Fig. 2).

294 <Fig. 2>

296 Although it has been argued that the HAT level gives a good approximation of coastline

297 (Halcrow, 1988; Saye et al., 2005; Pye et al., 2007), it is worth noting that across different

298 data sources (aerial photographs, topographic profiles) there is no significant correlation

299 between the coastline and HAT level positions (Table 4). There are several possible reasons

300 for this; first the coastline derived from aerial photographs corresponds to the crest of the

301 foredune on sandy beaches, while the HAT level often represents the foredune slope-toe,

302 which is likely to be a more dynamic morphologic feature (Ruessink and Jeuken, 2002).

303 Second, the terrestrial and airborne surveys were not carried out simultaneously so some

304 morphological change may have occurred between survey periods. Coastline position is

305 related to the sand volume of the backshore and, unsurprisingly, there is a negative

306 relationship between sand volume in the backshore and in the foreshore. Recent studies

307 elsewhere in the North Sea Basin have suggested that significant quantities of sand can be

308   supplied from the nearshore zone to the shoreface during energetic hydrodynamic

309   conditions (Aagaard et al., 2004; Anthony et al., 2006).

310

311   <Table 4>

312

313   *3.3. Climate and tidal data sources*

314   Coastline position reflects processes operating at a range of magnitudes and frequencies. It

315   has been demonstrated, for example, that the coastline can recover relatively rapidly

316   following a single storm event, however sequences of storm events can cause major and

317   sustained alterations due to insufficient recovery time (Douglas and Crowell, 2000; Morton

318   and Sallenger, 2003; Stockdon et al., 2007). Detailed examination of the impact of climate

319   and tidal conditions on the coastline would require continuous records of all variables

320   including coastline position. Whilst coastline position data are only available every few years

321   over the long term and every few months more recently, there are higher temporal resolution

322   records of wind and water level and atmospheric conditions. These data can be used to

323   identify the occurrence and frequency of high magnitude events, such as storms, that are

324   likely to have a significant influence on the coastline.

325

326   *3.3.1. Modern records*

327   Wind and water level records were examined from 1994 to 2010 to investigate the causes of

328   temporal and spatial variability in coastline dynamics. Hourly mean wind speed and direction

329   were obtained from Donna Nook weather station and fifteen-minute measurements of the

330   water level at Immingham tide gauge were supplied by the British Meteorological Data

331   Centre and the British Oceanographic Data Centre (BODC) respectively. Data relating to

332   water levels obtained in Chart Datum were converted to Ordnance Datum using the

333 conversions at Spurn Head and Skegness given by BODC (www.bodc.ac.uk). Within macro-

334 tidal environments, the primary factor controlling storm impacts is the water level reached

335 during storm surges, and it must be associated with both wind speed and direction, and

336 amplitude of surge (Vasseur and Héquette, 2000). Storm surge impact will only occur during

337 high tides. To identify energetic events with potential impact on the coastline a storm surge

338 was defined as the occurrence of onshore winds (i.e. winds from 350° to 150°) $\geq$ 14 m s^{-1}

339 combined with a water level $\geq$ 3.5 m (ODN). Offshore winds are in the range 180° to 320°,

340 with all other winds defined as alongshore. The mean of the monthly extreme water levels

341 from 1994 to 2010 was 3.88 m and 3.74 m (ODN) at Spurn Head and Skegness,

342 respectively. However, tide gauge measurements do not always reflect the hydrodynamic

343 processes operating near the coast (Masselink and Hughes, 2003; Parker and Foden,

344 2009), particularly the run-up (set-up and wave up-rush) which can reach tens of centimetres

345 along a macro-tidal beach during a storm surge. Therefore, a threshold of 3.5 m, slightly

346 lower than the mean monthly extreme water level, was selected. This also corresponds

347 approximately to the height of the interface between the foredune toe and the gentle beach

348 slope along the Lincolnshire coast.

349

350 *3.3.2. Proxy records of wind strength*

351 The lack of long, continuous wind records has limited exploration of the impacts of long-term

352 variations in storminess. However, given that the passage of synoptic scale storms is

353 associated with strong winds due to intense pressure gradients (Carnell et al., 1996) it may

354 be possible to use historical records of synoptic conditions to estimate long-term storminess

355 (Alexandersson et al., 2000; Wang et al., 2009; Donat et al., 2010). Studies have suggested

356 that the North Atlantic Oscillation (NAO) may control the occurrence of storm surge in the

357 Atlantic and thus potentially influence coastal morphological changes (Woolf et al., 2002;

358 O'Connor et al., 2011; Thomas et al., 2011). However, no clear associations have been

359   found between NAO and the extreme wind and water climate in the North Sea (Woolf et al.,

360   2003; Tsimplis et al., 2005), probably due to the sheltering effect of the British Isles land

361   mass.

362

363   A method of classifying the daily circulation patterns of the British Isles (50°–60°N, 2°E–

364   10°W) was developed by Lamb (1972) and has been applied to a range of west European

365   climatological and environmental studies (El-Kadi and Smithson, 1992; Wilby et al., 1997;

366   Buchanan et al., 2002). Lamb's subjective classification used daily atmospheric pressure

367   charts to examine the surface airflow pattern and steering of the circulation system. Eight

368   main directional types are recognized as the cardinal points, and there are three main non-

369   directional types: anticyclonic, cyclonic, and unclassified. Days not characterized by a single

370   weather type can be classified into one of nineteen hybrid combinations of the main types.

371   Jenkinson and Collinson (1977) subsequently designed an objective, automated version of

372   Lamb's classification (Jones et al., 1993) to produce the Jenkinson daily weather type (JWT)

373   catalogue (also known as Circulation Weather Type; CWT). JWT is based on a 16-point grid

374   of mean sea level pressure data over the British Isles to determine numerical values or

375   indices of geostrophic wind total flow (F) and cardinal direction (D) at 0.1° intervals.

376

377   In this study, the Jenkinson daily synoptic indices from 1871 to 2010 were used as a climate

378   proxy (provided by the Climate Research Unit, University of East Anglia, UK). Wind flow

379   expressed in pressure units was converted to m s^{-1} (1 unit = 0.617 m s^{-1}) and the JWT was

380   then used to determine the number of days when onshore, offshore, and alongshore winds

381   exceeding 14 m s^{-1} occurred. These records were used to evaluate the annual variability in

382   wind storminess at the synoptic scale.

383

384

385 **4. Results**

386 *4.1. Coastal morphological changes*

387 *4.1.1. Flamborough Head to Gibraltar Point*

388 Topographic profiles clearly highlight recent changes in coastline position (Fig. 3). There is a

389 marked contrast between the eroding Holderness cliffs of East Riding, and the accreting

390 Lincolnshire coast. Retreating sectors account for ~50.1 km out of 98.5 km (50.8%) of the

391 coastline, whereas naturally accreting sectors extend for ~25.4 km (25.8%) and artificially

392 (nourished) accreting or stable sectors represent ~23 km (23.4%).

393

394 <Fig. 3 >

395

396 On average, the Holderness cliffs retreated -28 m between the initial survey (mid-1990s) and

397 2010, but changes along this stretch of the coast varied from cliff retreat (erosion) of -89.8 m

398 at the P97 profile to an advance (accretion) of +36.9 m at the P127 profile near Spurn Head

399 between 1997 and 2010. In the north (P8-9) the coastline is near-stable due to sea defences

400 (Fig. 3: where positive values indicate accretion or seawards extension and negative values

401 indicate retreat or erosion). The mean short-term rate of retreat of the Holderness cliffs is

402 1.88 m year^{-1} but this varied over the survey period from -1.67 m year^{-1} (1990s-2005),

403 followed by more rapid erosion of -2.65 m year^{-1} (2005-2008) then slowing to -1.71 m year^{-1}

404 (2008-2010). Along Spurn Head, parts of the spit extended seawards (e.g. profile P127

405 showed accretion of +37 m) and other parts eroded (narrowed). The mean rate of change

406 along Spurn Head varied from +2.84 m year^{-1} at P127 (centre of the spit) to -3.14 m year^{-1} at

407 P131 (south) between 1997 and 2010.

408

409 Along the Lincolnshire coast, coastline change (1994-2010) varied from retreat of -11.3 m at

410 the L2A5 profile to an advance of +191.3 m at the L2E4 profile due to the extension of the

411 saltmarsh at Saltfleetby (Fig. 3). At Donna Nook the greatest seawards advance was +17.6

412 m (L1A4) whilst at Theddlethorpe it was +37.3 m (L2D1). Further south, changes range from

413 -2.9 m at the profile L2B7 to +54.6 m at the L2C6 (just north of Skegness) between 1994

414 and 2010.

415

416 *4.1.2. Specific areas of interest – trends in coastline position 1800s-2010*

417 Within the sediment cell, the AOIs have very different spatial and temporal dynamics. Over

418 the past 150 years the Easington cliffs have been eroding (Fig. 4). Mean cliff retreat rate is -

419 2 m year^{-1} but it exceeded -3 m year^{-1} for the periods 1854-1890, and 1969-2005. The

420 annual rate of cliff erosion decreased to -1.36 m year^{-1} between 2005 and 2010. The highest

421 rates of retreat occur along the southern urbanized coastal sections and locally reached -3.9

422 m yr^{-1} from 2008-2010 and -5.6 m yr^{-1} from 1952 to 1969. Over the long-term North Spurn

423 Head is eroding with a mean rate of coastline change of -1.56 m year^{-1} for the period 1854-

424 2010 (Fig. 4). As at Easington, the highest rate of erosion measured (-4.9 m year^{-1}) occurred

425 between 1951 and 1969. Since 1969, data from the aerial photograph analysis indicate that

426 the mean annual rate of retreat is slowing down.

427

428 <Fig. 4>

429

430 The downdrift sector of the sediment cell (2c – Lincolnshire) is dominated by sandy beaches

431 and saltmarshes (Table 2). At Donna Nook map and aerial photograph analyses indicate a

432 seaward advance of the coastline of 2.7 m year^{-1} (Fig. 5A). Since 1951 the rate of accretion

433   has been relatively constant. This AOI stretches 5.1 km alongshore but coastline advance

434   since 1891 has varied from +46 m in the north to +449 m at the southern end of the site.

435

436   <Fig. 5>

437

438   At Saltfleetby, coastline evolution was only investigated between 1994 and 2010 (section

439   3.1.2). Results indicate erosion of -1.1 m year^{-1} between 1994 and 2008, followed by a more

440   recent phase of accretion (Fig. 5E). The Saltfleetby AOI is characterized by extensive

441   saltmarsh partially bounded on the seaward side by sand dunes. These dunes have been

442   very dynamic and their development appears to be linked to that of the saltmarsh. Aerial

443   photograph analysis indicates both an inland migration and decrease in size of these dunes.

444   Taking the Saltfleetby AOI as a whole, the overall erosion trend reflects the morphological

445   changes of these coastal dunes. By excluding transects intersecting the dunes, the results

446   indicate that where saltmarsh dominates it is accreting at a rate of +1.15 m year^{-1}. A gradual

447   increase in the rate of accretion was also observed from +1.36 m year^{-1} (1999-2005) to

448   +2.64 m year^{-1} (2008-2010).

449

450   South of Saltfleetby, at the Theddlethorpe AOI there is no saltmarsh, but a wide beach with

451   well-developed dunes. Within the AOI overall coastline position advanced +126 m in the

452   north increasing to c..+185 m in the south. Here the coastline is accreting rapidly at a mean

453   rate of 2 m year^{-1} (1891-2010). As with the other AOIs, the rate of coastline change has

454   varied through time and between 1951 and 1953 an accretion rate as high as +7.67 m year^{-1}

455   is suggested by our analysis; however this may be over-estimated due to the change in data

456   source from the OS map (1951) to aerial photographs (1953). From the photo-interpretation

457   analysis, the rate of accretion varied with a mean annual rate from c.+3.1 m year^{-1} for 1976-

458   1983 to just +0.97 m year^{-1} over the period 2005-2008. By considering the photo-

459   interpretation results only, the mean rate of coastline accretion was of +1.9 m year^{-1} between

460   1953-2010, which is similar to the average estimated for the 119-year study period.

461

462   No detailed analyses of the coastline changes were undertaken along the Skegness coast

463   because it has been protected by sea defences which were installed following the 1953

464   floods and are well maintained (HECAG, 2009). Sea defences prevent or alter interactions

465   between inland and tidal zones, however since 1994 the data show accretion seaward of the

466   defences along a vegetated line which has extended both alongshore and towards the sea

467   (Fig. 6). This may be a response to a major sand nourishment programme undertaken just to

468   the north along the beach at the L2B6 profile of 210,000 m^3 in 1994, with subsequent

469   replenishment in 2006 and 2007 (Environment Agency, 2008).

470

471   <Fig. 6>

472

473   *4.1.3. Specific areas of interest – changes in sediment budget 1990s-2010*

474   Tables 5 and 6 present the net sediment budget calculated individually for the backshore,

475   foreshore and nearshore (bathymetric) units in each of the AOIs (Fig. 2). The data shown

476   are the total gain (+) or loss (-) of sediment in m^3 x 10^3 between successive surveys, and

477   cumulative change through time. Annual rate of change in m^3 year^{-1} is also estimated.

478

479   <Table 5>

480   <Table 6>

481

482   At Easington, from 1997 to 2010 there was a cumulative sand loss of c. -66.9 $\times 10^3$ m^3 for the

483   combined backshore and foreshore units (Table 4). The majority of this is accounted for by

484   cliff erosion in the backshore which is twenty-two times greater than losses from the

485   foreshore unit. North Spurn Head was also affected by overall sand loss with an erosion rate

486   of c. -1.5$\times 10^3$ m^3 year^{-1} although during specific periods both the backshore (1997-1999) and

487   foreshore (1999-2005) did gain sediment (c. -8.3$\times 10^3$ m^3 and 0.8 x 10^3 m^3 respectively).

488

489   As might be expected from the long-term coastline trends described above, the Lincolnshire

490   coast overall gained sediment from 1994-2010. At Donna Nook the results indicate an

491   annual positive budget of 49.9 $\times 10^3$ m^3 year^{-1}. The backshore displayed the greatest mean

492   accretion rate of 30.5$\times 10^3$ m^3 year^{-1}, however net volume gain has fallen since 2005 with

493   sand losses between 2005 and 2008. Similarly at Saltfleetby there were volumetric gains in

494   both the backshore and foreshore from 1994 to 2005 followed by overall sediment losses

495   from 2005 to 2010. Overall Theddlethorpe gained on average c. 47.6$\times 10^3$ m^3 year^{-1} from

496   1994 to 2010 but all of the increase in sediment volume was on the backshore (c. 63. $\times 10^3$

497   m^3 year^{-1}) whilst the foreshore actually lost c. -15.4$\times 10^3$ m^3 year^{-1}. At Skegness there was a

498   total mean accretion of c. 21.5$\times 10^3$ m^3 year^{-1} with the greatest changes recorded in the

499   backshore unit.

500

501   For the nearshore units (Table 5) there were overall sediment gains at Donna Nook and

502   Skegness but sediment losses at Saltfleetby (-6.3$\times 10^3$ m^3 year^{-1}) and Theddlethorpe (-

503   35.1$\times 10^3$ m^3 year^{-1}). At Theddlethorpe, interestingly the nearshore sub-unit 1 from ODN to

504   MLWS experienced a significant sand loss, whilst accretion took place in the seaward

505   nearshore unit. At Skegness the nearshore zone gained sediment in sub-unit 1 but lost

506   sediment in sub-unit 2.

507

508   *4.2   Forcing factors*

509   *4.2.1. Twenty-year record*

510   Strong onshore winds occurring during astronomical high tides result in storm surges that

511   could be responsible for coastline erosion and retreat. The analysis of forcing factors for the

512   period 1993-2009 shows water levels above 3.5 m are infrequent and no storm surge events

513   were recorded in 1994-1995 and 2002-2003 (Fig. 7). Although storm surge frequency was

514   variable, the mean rate of coastline retreat at Easington was relatively constant from 1994-

515   2010. At North Spurn Head storm activity (1-5 events yr^{-1}) from 1997-2001 coincided with a

516   phase of accretion (Fig. 7) whilst from 2002-2006 storms were less frequent and this

517   included a phase of coastline erosion of up to -1.3 m yr^{-1}.

518

519   \<Fig. 7>

520

521   Along the Lincolnshire coast, at Donna Nook (Fig. 7C) up to 8 storm surges per year

522   occurred between 1994 and 1998 and this coincided with coastline accretion of c. +4 m year^{-}

523   ^{1}. Coastal propagation subsequently continued at a slower but relatively constant rate. A

524   stormy phase from 1996-1998 coincided with saltmarsh retreat at Saltfleetby AOI of -2.3 m

525   year^{-1} however this slowed down to less than -0.3 m year^{-1} between 1999 and 2004 before

526   accelerating back to -2.3 m year^{-1} from 2005-2007, another storm phase. However, where it

527   is unconstrained by the coastal dunes, the saltmarsh shows significant seaward advance

528   over the last twelve years, with no clear relationships with the occurrence of storm surge

529   events. At Theddlethorpe the highest rates of coastline accretion (+2.5 m year^{-1}) occurred

530   between 1994 and 1998 (Fig. 6E) when up to 8 storms per year were recorded. The rapid

531   coastline advance continued in the absence of frequent storm events between 1999 and

532   2004 and continued, but at a slower rate until 2010. This decrease in the rate of advance

533   coincided with a period of slightly higher storm surge activity. At Skegness from 1999-2004

534   the coastline (HAT level) prograded at a rate of +1 m year^{-1} but changed to a retreat of -2 m

535   year^{-1} between 2008 and 2010, possibly in response to storms in 2008.

536

537   *4.2.2. Long-term record*

538   Fig. 8 shows the occurrence of days with high wind speeds (storms) from 1871 to 2010 over

539   the British Isles indicated by JWT. The most frequent winds are offshore, coinciding with

540   strong westerly winds in winter. The long-term trend of strong offshore winds appears

541   relatively stable although with a slight fall in frequency in the 1960s. However, offshore winds

542   are not likely to be associated with significant storm surges. Rather storm surge will be

543   associated with strong onshore winds. From 1871-2010 the annual frequency of onshore

544   winds ≥14 m s^{-1} varies from zero in 1932 to 19 in 1917. The 5-year running mean indicates

545   three peaks in the onshore storm event record in 1876, 1878, and 1883. This last peak was

546   followed by a relatively stable period of 35 years. Three distinct stormy periods occurred in

547   1955-1970, 1975-1988 and 1994-2000 (Fig. 8). Strong alongshore winds typically occur on

548   fewer than 6 days per year.

549

550   <Fig. 8>

551

552   To assess the utility of the Jenkinson weather catalogue as a proxy for storm surge, a

553   correlation analysis was undertaken between the frequency of storm surges predicted per

554   year using recorded wind and tide data from 1994 to 2010 and the incidence of onshore

555   wind events exceeding 14 m s^{-1} predicted by JWT records for the same period. The temporal

556   patterns of storm frequency are broadly similar (Fig. 9) and high correlation coefficients are

557   obtained for both Skegness (r=0.52, p<0.05) and Spurn Head (r=0.58 p<0.05) suggesting

558   the Jenkinson weather catalogue may be a useful proxy for long-term storminess.

559

560   <Fig. 9>

561

562   **5. Discussion**

563   An examination of detailed records over the past two decades and longer historical records

564   demonstrates clear trends in erosion and accretion along the Flamborough Head to Gibraltar

565   Point coast. These trends can be ascribed to factors such as natural antecedent conditions,

566   relative position within the sediment cell (i.e. updrift/downdrift) and human activities. In this

567   discussion, we consider the short-term changes in coastline position and sediment budget

568   and their relationships with environmental forcing factors, the long term historical coastline

569   changes and finally possible response of the coastline to sea level rise.

570

571   *5.1. Coastline changes from mid 1990s-2010*

572   Unsurprisingly, the topographic profile data indicate rapid and significant erosion of the

573   Holderness cliffs since the mid-1990s. Spatially-averaged retreat rates suggest more rapid

574   erosion from 2005-2008 (>2.6 m yr^{-1}) compared with preceding and following years (c. 1.7 m

575   yr^{-1}). However, rates of cliffline recession are spatially very variable (Fig. 3). This reflects

576   localised occurrence of landslips, which typically cause a few years of increased recession

577   followed by a period of below average retreat (Pringle, 1985; Posford Duvivier, 1992), such

578   as described for profiles P78 and P95 by Quinn et al. (2009), the location of intertidal

579   sandbars which accelerate cliff erosion rates (Pringle, 1985; Pethick, 1996; Moore et al.,

580   1998) and the presence or absence of offshore sand banks which reduce inshore wave

581   energy and hence slow retreat rates (Eurosion, 2003). Changes in the HAT level indicate

582   that, downdrift of Holderness, the north Lincolnshire beaches are accreting. Leggett et al.

583   (1998) also documented accreting beach profiles along the north Lincolnshire coast with a

584   positive change of 2% (by volume) from 1991-1996. Between Mablethorpe and Skegness,

585   the coastline has been affected by beach nourishment since 1994, and overall the HAT level

586   has undergone seaward extension. The UK Environment Agency (2011) suggests accretion

587   of the upper-beach in this location can be attributed to retention of renourishment material

588   blown up the beach.

589

590   Using topographic profiles for all the cliffed sections of the East Riding coast, we calculated

591   that the retreating cliffs have lost 1,004,755 m^3 yr^{-1} (1000x10^3 m^3 yr^{-1}) of sediment since the

592   initial survey in the mid-1990s. This rate is comparable to the estimate of 1000×10^3 m^3 year^{-1}

593   (from 1852-1952) by Valentin (1971). ABP (1996) predicted a slightly higher cliff erosion rate

594   of up to 1400×10^3 m^3 year^{-1}. The combined sediment losses from both the cliffs and the

595   shoreface along the Holderness coast are estimated to be in the region 2500-3000 ×10^3 m^3

596   year^{-1} (ABP, 1996; Balson et al., 1996, 1998; Eurosion, 2003), which increases to 3900-4700

597   x10^3 m^3 year^{-1} if the lower seabed to the limit of erosion is included (Wingfield and Evans,

598   1998). Of this eroded material 60-80% is clays and silts, while the rest is predominantly sand

599   and gravels (Balson and Harrison, 1988; Blewett and Huntley, 1998; Townend and

600   Whitehead, 2003). Balson et al. (1998) estimated that 33% of the sediment is eroded from

601   the cliff, and 67% from the shorefaces and seabed.

602

603   Calculations for the AOI at Easington for this paper suggest the cliffs here have yielded

604   approximately 66.9×10^3 m^3 year^{-1} (Table 5). Posford Duvivier (1992) modeled the wave-

605   driven littoral drift at Easington (including both sediments being transported from the

606   northern cliffs and input from Easington itself) and predicted a southward longshore sand

607   transport of 157-310×10^3 m^3 year^{-1} from this area. Easington marks the point at which the

608   southwards travelling sand derived from erosion along the total length of the cliffs moves

609   offshore (Halcrow and Geosea, 1990), although the precise transport pathways of eroded

610   sediments will depend on their mineralogy and grain size (Newsham et al., 2002). This

611   offshore transport is a result of a combination of the change in both the orientation of the

612   coast and the direction of the tidal currents at this point. Previous studies suggest 3-6% of

613   the eroded cliff material is transported to the southern end of Holderness and incorporated in

614   to the Spurn Head spit whilst the remainder is deposited in the nearshore and offshore

615   zones (Valentin, 1971; Ciavola, 1997).

616

617   Whilst the littoral drift may input 30-60 x 10^3 m^3 yr^{-1} to the spit (Valentin, 1971; Ciavola,

618   1997), our results show that erosion from North Spurn Head has the potential to supply

619   1.5×10^3 m^3 year^{-1} to areas downdrift (Table 5). The principal pathway of bedload sediment

620   material is southwards towards the nearshore sand banks of The Binks, which act as a sand

621   reservoir for Spurn Head and a buffer to erosion under energetic hydrodynamic conditions.

622   The littoral cell of interest has three sub-cells, the central one (2b; Fig. 1) being defined by

623   the Humber Estuary. The sediment budget of the Humber Estuary is complex but whilst total

624   sediment flux through the estuary mouth is very high, the net exchange between the estuary

625   and the North Sea is low (Townend and Whitehead, 2003) with estimates of sediment input

626   to the North Sea ranging from 100-255 kt yr^{-1} (compared with 1400-2610 kt yr^{-1} eroded from

627   Holderness; McCave, 1987; HR Wallingford, 1992). Only around 1% of the total sediment is

628   estimated to enter and circulate into the Humber estuary before being expelled back in to the

629   North Sea (Halcrow and GeoSea, 1990; Black and Veatch, 2004). Fine sediments eroded

630   from the updrift Holderness cliffs are transported into the estuary by the flood tide and

631   coarser sand-sized materials are moved in to the marine environment (ABP, 2000). Strong

632   tidal flows can prevent gravels and sands from crossing the Humber Estuary (HECAG,

633   2009), however, Robinson (1968) released seabed drifters from The Binks near Spurn Head,

634   60% of which were recovered from the south shore confirming a sediment transport pathway

635   across the mouth. Medium and fine sands can be transported across the estuary mouth

636   especially during storm conditions and build up in offshore sand banks at Donna Nook

637   (Steers, 1966; Tonk, 2000; HECAG, 2009). This deposition is reflected in this study through

638   the dominance of accretion in both the back/fore shore and nearshore zones at Donna Nook

639   where the volume of accretion is equivalent to 5.8% of the total estimated Holderness cliff

640   erosion (Tables 5, 6). Additional sediment supply to this area can come from The Binks

641   during storm surge conditions (HR Wallingford, 2002).

642

643   From the mid-1990s to 2010 the back and fore shore units at Saltfleetby and Theddlethorpe

644   have been accreting, while erosion has characterized the nearshore zone (Tables 5, 6). The

645   total annual sediment supply at Saltfleetby and Theddlethorpe is equivalent to 4.7% of that

646   eroded from the East Riding coast. At Mablethorpe, the coastline switches from accretion to

647   erosion (Schans et al., 2001) driven by a combination of exposure to wave activity (Dugdale

648   and Vere, 1993) and anthropogenic pressures (Robinson, 1964; Pye, 1995). The artificially

649   nourished coastal section from Mablethorpe to Skegness was assumed not to accumulate

650   sediment from the Holderness cliffs. Data from topographic and bathymetric profiles at

651   Gibraltar Point indicate that sediment input has been approximately 181.9×10^3 m^3 year^{-1}.

652   Assuming no additional sources, this quantity would represent 18.7% of the cliff material

653   eroded to the north. Again assuming no additional sediment sources or sinks along the

654   coastline, when combined with the 5.8% input to Donna Nook and 4.7% input at Saltfleetby-

655   Theddlethorpe, this suggests that only 29% of the material eroded in sediment sub-cell 2a is

656   transported 'directly' by the littoral drift to the Lincolnshire coast (sub-cell 2c). The majority of

657   sand material eroded from the Holderness cliffs can therefore be assumed to move offshore,

658   however the division is likely to be less clear-cut as material transported offshore to the

659   Binks and other sand banks along the Lincolnshire coast, will be redistributed by cross-shore

660 wave currents (Halcrow, 1988; ABP, 1996). Sediments introduced to the system during the

661 nourishment programme may also form some of the inputs to Gibraltar Point.

662

663 Over the short-term there were few storm surges where wind speed was ≥14 m s^{-1} and water

664 level was ≥3.5 m ODN, but the highest frequencies occurred between 1996-2001. This was

665 followed by two very calm years and then by a period of medium activity between 2004-2010

666 (Fig. 7). At Easington, retreat rates were remarkably constant whereas they varied far more

667 at North Spurn Head and along the Lincolnshire coast. Our data show a positive correlation

668 between storm surge occurrence and coastline position and between storm surge and sand

669 volume in the backshore, whereas there is a negative relationship with the sand volume in

670 the foreshore (Table 4). However, there are no clear relationships between coastline change

671 and storminess. A limitation of our data set is the relative timing of data acquisition in that it

672 rarely includes the coastline position recorded immediately before or after a storm surge,

673 however it may represent the beach morphology in calm weather conditions, and thus the

674 post-storm recovery state.

675

676 *5.2. Coastal evolution from the 1800s to 2010*

677 Although coastline changes determined from maps and historical aerial photographs are

678 likely to be less reliable than recent field surveys, they are necessary to determine the long-

679 term evolutionary tendency of the coastline. The changes that have taken place in the

680 northern part of this sediment cell (2a) along the Holderness coast have been the subject of

681 numerous previous studies (e.g. Reid, 1885; Valentin, 1954, 1971; Dosser, 1955; Steers,

682 1966; Mason and Hansom, 1988; HECAG, 2009; Quinn et al., 2009), and beach

683 development in the far south around Gibraltar Point has also received some attention (e.g.

684 King, 1964, 1968, 1973; Barnes and King 1955; King and Barnes, 1964). There has,

685 however, been considerably less research in the south-central sector of the cell along the

686 north Lincolnshire coast.

687

688 In the north of the sediment cell, we determined that the southern Holderness cliffs have, on

689 average, been eroding at 2 m yr^{-1} since 1854 (Fig. 11). This is in agreement with previous

690 estimates of 1-2 m yr^{-1} over 150 years (Valentin, 1954; Mason and Hansom, 1988; Quinn et

691 al., 2009). Some research indicates that towards Flamborough Head, parts of the north of

692 the Holderness coast underwent aggradation from 1852-1952 (Valentin, 1954; Bird, 1984)

693 but analysis of recent topographic profiles (1994-2010) suggest that currently erosion is

694 taking place along the whole cliffed coastline albeit at a much more rapid rate towards the

695 south. Spurn Head has long been recognized as a very dynamic feature undergoing cyclic

696 breaching, destruction and reformation (De Boer, 1964). This paper has reported significant

697 variability in rates of erosion on North Spurn Head ranging from nearly -5 m yr^{-1} (1951-1969)

698 to <-0.7 m yr^{-1} (1890-1951 2005-2010). This most recent decrease in rates of erosion was

699 also observed by Saye et al. (2005).

700

701 In contrast, the beaches of north Lincolnshire have undergone accretion up to +2.7 m year^{-1}

702 over the past 120 years (Fig. 11). The result agrees with the study by Halcrow (1988) which

703 indicated accretion from the late 19th century to 1970. Robinson (1984) also reported that by

704 the early 19th century the Saltfleetby-Theddlethorpe coastline was characterized by an

705 accreting coastline. One of the sediment sources for these beaches is, as mentioned above,

706 material eroded from the Holderness coast (Steers, 1946), but in addition there is onshore

707 movement of material from sand banks (Halcrow, 1988; ABP, 1996; HR Wallingford, 2002).

708 Our analysis did not indicate any general coastline retreat caused by the severe 31st

709 January-1st February 1953 North Sea storm surge, however the intervals between maps and

710 aerial photographs probably hides some short-term coastline recession. The storm surge

711 impacts in 1953 are also likely to have been reduced by the presence of coastal dunes and

712 the higher, wide beach along the North Lincolnshire coast (Robinson, 1953; Brampton and

713 Beven, 1987).

714

715 <Fig. 11>

716

717 *5.3 Proxies for storminess*

718

719 Pressure-based circulation weather types, such as the JWT used here, have been widely

720 used to examine general trends and variability in long-term storminess in Europe (e.g.

721 Alexandersson et al., 2000; Donat et al., 2011; Wang et al., 2011) and are generally more

722 reliable proxies over sea than over land (Krueger et al., 2012). We suggest JWT may

723 provide a reasonable proxy for storminess on the east coast of England. Frequencies of

724 storm events identified using JWT data are much higher than those of measured storm

725 surges (Fig. 9); this is because we have not differentiated onshore energetic events

726 associated with high tides, where storm surges would be likely, from those associated with

727 low tides where little or no impact would be expected due to the lower overall water level

728 (Chaverot et al., 2008). Accounting for water level over the longer term is something that

729 could be explored in future. Over long time periods other studies have successfully used

730 similar proxy measures of storminess, such as variations in the NAO, to explain temporal

731 patterns of coastline evolution (Vespremeanu-Stroe et al., 2007; Thomas et al., 2011;

732 O'Connor et al., 2011) which suggests analysis of the JWT data set may be worth pursuing

733 further.

734

735 Overall temporal patterns of storminess (all directional sectors) in the NE Atlantic and North

736 Sea since the 1870s determined using the JWT/CWT approach have shown variable, but

737 typically low, levels of storminess in the late nineteenth century and first half of the twentieth

738 century (Alexandersson et al., 2000; Wang et al., 2009) although in the central North Sea

739 (55°N 5°E) total gale days indicate high storminess in the early twentieth century (Donat et

740 al., 2011). Minimum storm activity has been put at around 1960 with maximum storminess

741 during the 1990s followed by a decline to long-term average conditions in the early 2000s

742 (Wang et al., 2009; Donat et al., 2011). This is broadly in accordance with patterns

743 determined in this paper, however due to the geomorphological research questions being

744 addressed we deconstructed the total record into specific directional sectors (onshore,

745 offshore and alongshore) and events meeting specific wind speed conditions, and these

746 components show some differences to the overall pattern. For example, the frequency of

747 JWT onshore wind storms was variable from 1871 to the 1920s (1-19 events per year), but

748 was slightly higher than the long term mean of 7 events per year. This was followed by a

749 relatively calm period of up to 35 years (Fig. 10A). Peak periods of onshore wind storm

750 events occurred during 1955-1970, 1975-1988, and from the mid-1990s to 2000. The first of

751 these peak periods contrasts with more widely-observed low levels of overall storminess

752 (which can be seen in the offshore record in Fig. 8). These peaks indicate an increase in

753 wind speeds likely to generate greater significant wave heights and these energetic periods

754 are broadly coincident with the highest rates of coastal erosion recorded between 1854-1890

755 and 1951-1969 at Easington and North Spurn Head (Fig. 10). The JWT storm event

756 frequency decreased after 2005, which coincides with a decrease of coastline recession

757 rates at these sites. Within a littoral sediment cell with a defined sediment budget, erosion of

758 material in one part of the cell should lead to accretion elsewhere within the cell; accordingly

759 high recession rates along the Easington cliffs between 1891-1910 and 1976-1983 were

760 concomitant with the highest rates of coastline accretion recorded at Donna Nook (1891-

761 1910) and Theddlethorpe (1976-1983), and from 1994-2005 at both sites (Fig. 10). In

762 contrast, the recent decrease in cliff retreat from 2005-2010 may be the cause of the lower

763   rates of seaward accretion along the North Lincolnshire sandy beaches over the same

764   period. In the study region our long-term data set only provides reliable information

765   concerning longshore coastal changes, however, as discussed in section 5.1, the short-term

766   (decadal) data indicate cross-shore sediment transport to and from offshore stores such as

767   sand banks is substantial. As with other regions, such as the Columbia River Littoral Cell

768   (Ruggiero et al., 2005), lack of cross-shore transport data makes it difficult to make long-

769   term sediment budget calculations.

770

771   Within our data, one particular period of interest is that between the 1900s and 1951 where

772   rates of coastline change throughout the sediment cell were very low. This broadly coincides

773   with a long period of low frequencies of annual wind storms (1920-1955). Both the

774   geomorphological and climatological records suggest there was a period of quiescence

775   lasting ~35 years in the first half of the 20th century. Previous research has identified strong

776   correlations between storminess in the NE Atlantic (including the North Sea) and NAO (e.g.

777   Wang et al., 2009), but in the methods we indicated that winter NAO was not a good

778   indicator of storminess on the east coast of England. Positive winter NAO phase leads to

779   enhanced westerlies due to a stronger than usual sub-tropical high pressure centre and a

780   deeper than normal Icelandic low (Hurrel, 1995) and most storms identified using CWT are

781   associated with westerly flow (Donat et al., 2010). Between 1900s and 1950, winter NAO

782   phase was positive with consecutive strong positive phases between 1900-1915 and 1915-

783   1930 (Fig. 10B). Over this period, the occurrence of storm events, affecting the North

784   Atlantic west-facing coast would be expected to have increased, whereas the east coasts

785   would be relatively sheltered. It can be suggested, therefore, that although positive NAO

786   phase may not indicate storminess on the east coast of England, it could provide a useful

787   proxy for quiescence. The advantage of using JWT/CWT data sets is that they can be

788   focused on specific directional sectors (in this case winds from the north and the eastern

789   sector (N, NE, E, SE) which is important in the context of understanding the impact of events

790   on the coastline. Although the JWT approach was originally developed for the British Isles

791   (Lamb, 1972) it has been successfully applied to other regions including the Netherlands

792   (Buishandt and Brandsma, 1997), Spain (Goodess and Palutikof, 1998, Lorenzo et al.,

793   2008), Portugal (Trigo and Dacamara, 2000) and Morocco (Born et al., 2010) in research

794   focusing primarily on precipitation and catchment scale flooding. This paper, and other

795   recent studies using circulation weather types to examine wind storms (e.g. Wang et al.

796   2009; Donat et al., 2011), suggest that they could provide a valuable data source for

797   interpreting long-term coastal geomorphological change throughout northwest Europe.

798

799   The use of JWT/CWT data merits further exploration but low levels of storminess are not

800   likely to explain fully the relatively static nature of the coastline from 1900 to 1950. Other

801   possibilities are a redistribution of sediments, for example there was a natural extension of a

802   barrier located seaward of the centre of the Spurn spit during the 18th and 19th centuries

803   (Halcrow, 2002) which may have lead to a reduction in sand volume reaching beaches in

804   north Lincolnshire as the barrier extended (Pye and Blott, 2010). In addition, this coast has a

805   long history of defence. Hard coastal defences were built on sections of the Holderness

806   coast such as Hornsea, Mappleton, Withernsea and Easington in the late 19th century and

807   may have temporarily reduced or stopped the cliff retreat; the construction of a groyne field

808   is also likely to have impeded the littoral drift of sediment (Pye and Blott, 2010). In 1883/84,

809   further groynes and timber revetments were built to prevent breaching and erosion along

810   Spurn Head. Spurn Head was a military stronghold during the second world war and coastal

811   defences were built along the seaward side (De Boer, 1981), which are likely to have

812   reduced alongshore sand transport to the south. These were abandoned and fell in to

813   disrepair in the 1960s.

814

815

816   *5.4. Response of the coastline to sea-level rise*

There are number of challenges associated with predicting the response of sediment cell

and landform dynamics to climate change and sea-level rise. One of the most important is

obtaining historical records over sufficiently long time periods for accurate change detection,

particularly given that in many littoral cells short-term changes can occur at a very different

rate, or even show the opposite trend, to long-term change (Ruggiero et al., 2005; Brooks

and Spencer, 2012). In addition, as demonstrated here, because both cliff and beach

systems can exhibit considerable alongshore variability in rates of change, and because

sediment processes acting over a larger area can influence local scale change, the spatial

scale needs to extend over at least the sub-cell and ideally the whole coastal cell (Ruggiero

et al., 2005; Neill et al., 2008; Quinn et al., 2009). In this study, the time interval between

data sets (years to decades) and the length of time between the earliest and the most recent

data set (>110 years) means the impact of short-term change is minimised; there are clear

directional changes at most of the AOIs examined (with the exception of Spurn Head). Over

the historical period coastline dynamics in the downdrift sector of the sediment cell (2c) have

been controlled by the supply of sand material from the updrift section of the cell (2a), the

eroding Holderness coast. During periods of more rapid cliff retreat, rates of coastline

progradation have been higher on the Lincolnshire coast; when cliff retreat is slowed, such

as during the early twentieth century, rates of accretion downdrift are reduced. For the

central sub-cell (2b) historical data used to reconstruct changes in the volume of the Humber

estuary since 1851 suggest an overall period of infilling prior to 1940 followed by erosion up

to 2000 (although data sources prior to 1936 were incomplete) however there has been no

significant change in average flow rates over the last century (Townend et al., 2007).

A number of studies has examined and modelled the likely response of other sectors of the

east coast of England (notably sediment cell 3; East Anglia) to future environmental change

(Dickson et al., 2007; Dawson et al., 2009; Brooks and Spencer, 2012). Sea level is

predicted to rise at an accelerated rate in future (IPCC, 2007) and there is a range of

844   possible responses of cliffs to sea-level rise varying from increased retreat rate to decreased

845   retreat rate or no change (Ashton et al., 2011), but sea-level rise is not the only controlling

846   factor on cliff retreat (e.g. Lim et al., 2010). Storm frequency and magnitude are also

847   predicted to increase and will probably heighten coastal erosion as well as flooding on low-

848   lying coasts (Webster et al., 2005; Bindoff et al., 2007; Chini et al., 2010). Dickson et al.

849   (2007) and Brooks and Spencer (2012) used historical data for retreating sectors of the East

850   Anglian coast (Norfolk and Suffolk respectively; both sediment cell 3) to test models for

851   predicting coastline response to sea level rise. Brooks and Spencer (2012) found that the

852   longer the time period for which historical (baseline) data were available, the better the

853   predictions, but importantly found that a single spatially-averaged estimate of retreat

854   performed poorly because the alongshore variation in retreat rates was not accounted for.

855   On the Norfolk coast, models of historical change captured the measured patterns of erosion

856   in the cliffed sectors (e.g. from Weybourne to Eccles) and deposition along the

857   unconsolidated coastline from Eccles to Winterton Ness, and a similar pattern of cliff

858   recession and beach volume increase is predicted under a variety of sea level change and

859   management scenarios (Dickson et al., 2007). In sediment cell 2, it could be assumed that

860   the future rate of cliff erosion and sediment supply will be similar to present day rates

861   (Newsham et al., 2002; Black and Veatch, 2004), although whilst this may be an appropriate

862   assumption at Easington where rates of erosion have been relatively stable for 150 years, at

863   sites such as Spurn Head future behaviour is likely to be harder to predict (Scott and Wilson,

864   2009). Spurn Head above the upper-intertidal zone is expected to migrate westward, but it

865   is unlikely to extend further south due to the forcing effects of tidal flows and overwashing

866   events that occur during storm surges (East Riding Council, 2004). Models applied to cell 3

867   suggest that broad spatial patterns of erosion and retreat are likely to continue over the

868   twenty-first century and, similarly; in cell 2 sand eroded from the Holderness cliffs is likely to

869   continue to supply the North Lincolnshire coastline causing ongoing accretion. At present,

870   whilst the Holderness coast has some coastal defences these are insufficient to prevent cliff

871   erosion and the current Shoreline Management Plan recommends letting natural processes

872 continue except in localised areas where town frontages and infrastructure require protection

873 (HECAG, 2009). Similarly, along the Lincolnshire coast defences are minimal north of

874 Mablethorpe and continued coastal progradation will likely allow this to continue during the

875 current century even under predicted sea-level rise. A largely unknown factor, and one for

876 which there are fewer long-term historical records from which to make predictions, is the

877 impact of cross-shore sediment transport to and from the offshore sand banks. As indicated

878 in section 5.1 offshore sediment transport is substantial and the offshore sand banks play an

879 important role not only in supplying sand to the coastline, but also in reducing wave energy

880 (Steers, 1966; Motyka and Brampton, 1993; Blott and Pye, 2004, Brooks and Spencer,

881 2012) which may impact both coastline recession and progradation rates.

882

883 **6. Conclusions**

884 Spatial and temporal variability in coastline position, rate of change and sediment budget

885 were assessed within a single sediment cell. There have been clear trends in erosion and

886 accretion from Flamborough Head to Gibraltar Point over the past 150 years and the

887 different parts of the sediment cell are clearly connected. High rates of erosion updrift (2a)

888 are associated with high rates of accretion downdrift (2c) and periods of relative stability in

889 these two sections of the sediment cell are broadly coincident. The volume of sediment

890 incorporated in to the accreting beaches represents around 29% of that eroded from the

891 Holderness cliffs. The results highlight the importance of understanding the variable

892 dynamics of different types of landform occurring within a single sediment cell (e.g. cliffs,

893 dune-backed beaches). Erosion on sandy beaches is often an outcome of storm surges,

894 however where the storm causes the release of large quantities of sediment updrift within

895 the sediment cell, this erosion may be mitigated or, in the case of north Lincolnshire, result in

896 accretion due to the increased sediment supply to areas downdrift.

897

898 Overall temporal patterns of storminess in the north Atlantic and North Sea can be identified

899 using pressure-based continental weather types. An exploration of the use of the Jenkinson

900 Daily Weather Type as a proxy for storm surges over the historical record suggests that by

901 deconstructing the data into specific directional sectors, to account for onshore-, offshore-

902 and alongshore-directed events, useful information on long-term patterns of storminess and

903 its potential impacts on specific coasts can be obtained. The performance of such weather

904 type data for predicting the geomorphological impacts of storm surges would probably be

905 improved by incorporating information about water level with the wind record.

906

907

908

References

Aagaard, T., Nielsen, J., Gro Jensen, S., Friderichsen, J., 2004. Longshore sediment transport and coastal erosion at Skallingen, Denmark. Danish Journal of Geography 104, 5-14.

ABP, 1996. Southern North Sea Sediment Transport Study, Literature review and conceptual sediment transport model. Report R546, ABP Research and Consultancy Ltd, Southampton.

Alexandersson, H., Tuomenvirta, H., Schmith, T., Iden, K. 2000. Trends of storms in NW Europe derived from an updated pressure data set. Climate Research 14, 71-73.

Anthony, E.J., Ruz, M.H., Vanhée, S., 2006. Morphodynamics of intertidal bars on a megatidal beach, Merlimont, northern France. Marine Geology 208, 73–100.

Ashton, A.D., Walkden, M.J.A., Dickson, M.E. 2011. Equilibrium responses of cliffed coasts to changes in the rate of sea level rise. Marine Geology 284, 217-229.

Balson, P.S., Tragheim, D., Newsham, R., 1998. Determination and prediction of sediment yields from recession of the Holderness coast, eastern England. Proceedings of the 33rd MAFF Conference River and Coastal Engineers, London, pp. 4.5.1-4.6.2.

Balson, P.S., Tragheim,D., Newsham, R., 1996. A photographic technique to determine the potential sediment yield from recession of the Holderness coast, UK, in Taussik, J., Mitchell, J. (Eds.) Partnership in Coastal Zone Management. Samara Publishing Ltd, Cardigan, pp. 507-514.

Balson, P.S., Harrison, D.J., 1988. Marine aggregate survey Phase 1: Southern North Sea, British Geological Survey, Marine report 86/38.

Barnes, F.A., King, C.A.M., 1953. The storm flood of 1st February, 1953 II, The Lincolnshire coastline and the 1953 storm flood. Geography 38, 141-160.

Barnes, F.A., King, C.A.M., 1955. Beach changes in Lincolnshire since the 1953 storm surge. East Midland Geographer 1, 18-28.

Bindoff, N.L., Willebrand, J., 2007. Observations: Oceanic Climate Change and Sea Level. in: Solomon, S., D. Qin, M. Manning, Z. Chen, M. Marquis, K.B. Averyt, M. Tignor and H.L. Miller. (Eds.), Climate Change 2007: The Physical Science Basis. Contribution of Working Group I to the Fourth Assessment Report of the Intergovernmental Panel on Climate Change. Cambridge University Press, pp. 387-429.

951   Bird, E., 1984. Coasts. Basil Blackwell, New York.

952   Black and Veatch Ltd., 2004. Humber Estuary Shoreline management plan phase 2,
953   summary of geomorphology studies. Report produced for Environment Agency.

954   Blewett, J., Huntley, D. 1998. Measurement of suspended sediment transport processes in
955   shallow water off the Holderness coast, UK. Marine Pollution Bulletin 37, 134-143.

956   Blott, S.J., Pye, K., 2004. Morphological and sedimentological changes on an artificially
957   nourished beach, Lincolnshire, UK. Journal of Coastal Research 20, 241-233.

958   Born, K., Fink, A.H., Knippertz, P. 2010. Meteorological processes influencing the weather
959   and climate of Morocco. In: Speth, P., M. Christoph, B. Diekkruger, M. Bollig, A.H. Fink, H.
960   Goldbach, T. Heckelei, T., G. Menz, B. Reichert, M. Rossler (eds). Impacts of Global
961   Change on the Hydrological Cycle in West and Northwest Africa. Springer, Berlin, 150-163.

962   Bowen, A.J., Inman, D.L., 1966. Budget of littoral sands in the vicinity of Point Arguello,
963   California. Coastal Engineering Research Centre. Technical Memorandum 19, 41 pp.

964   Brampton, A.H., Beven, S.M., 1987. Beach changes along the coast of Lincolnshire, U.K
965   (1959-1985). Proceedings on Coastal Sediments 87. Am. Society of Civil Engineers, 539-
966   554.

967   Brooks, S.M., Spencer, T., 2010 Temporal and spatial variations in recession rates and
968   sediment release from soft rock cliffs, Suffolk coast, UK. Geomorphology 124, 26-41.

969   Brooks, S.M., Spencer, T. 2012. Shoreline retreat and sediment release to accelerating sea
970   level rise: measuring and modeling cliffline dynamics on the Suffolk Coast, UK. Global and
971   Planetary Change 80-81, 165-179.

972   Bryant, E.A., 1988. Storminess and high tides beach change, Stanwell Park, Australia, 1943-
973   1978. Marine Geology 79, 171-187.

974   Buchanan, C.M., Beverland, I.J., Heal, M.R., 2002. The influence of weather-type and long-
975   range transport on airborne particle concentrations in Edinburgh, UK. Atmospheric
976   environment 36, 5343-5354.

977   Buishand, A., Brandsma, T. 1997. Comparison of circulation classification schemes for
978   predicting temperature and precipitation in the Netherlands. International Journal of
979   Climatology 17, 875-889.

980 Carnell, R.E., Senior, C.A., Mitchell, J.F.B., 1996. An assessment of measures of
981 storminess: simulated changes in northern hemisphere winter due to increasing CO_2.
982 Climate Dynamics 12, 467-476.

983 Chaverot, S. Héquette, A., Cohen, O., 2008. Changes in storminesss and shorline evolution
984 along the northern coast of France during the second half of the 20th century. Zeitschrift fuer
985 Geomorphologie 52, 1-20.

986 Chini, N., Stansby, P., Leake, J., Wolf, J., Roberts-Jones, J., Lowe, J. 2010. The impact of
987 sea level rise and climate change on inshore wave climate: a case study for East Anglia
988 (UK). Coastal Engineering 57, 973-984.

989 Ciavola, P., 1997. Coastal dynamics and impact of coastal protection works on the Spurn
990 Head spit (UK). Catena 30, 369-389.

991 Cooper, J.A.G., McKenna, J., Jackson, D.W.T, O'Connor, M., 2007. Mesoscale coastal
992 behavior related to morphological self-adjustment. Geology 35, 187-190.

993 Cooper, N.J., Hooke, J.M., Bray, M.J. 2001. Predicting coastal evolution using a sediment
994 budget approach: a case study from southern England. Ocean and Coastal Management 44,
995 711-728.

996 Cooper, N.J., Pontee, N.I., 2006. Appraisal and evolution of the littoral 'sediment cell'
997 concept in applied coastal management: experiences from England and Wales. Ocean and
998 Coastal Management 49, 498-510.

999 Cracknell, A.P., 1999. Remote sensing techniques in estuaries and coastal zones an update.
1000 International Journal of Remote Sensing 19, 485–496.

1001 Dawson, R.J., Dickson, M.E., Nicholls, R.J., Hall, J.W., Walkden, M.J.A., Stansby, P.K.,
1002 Mokrech, M., Richards, J., Zhou, J., Milligan, J., Jordan, A., Pearson, S., Rees, J., Bates,
1003 P.D., Koukoulas, S., Watkinson, A.R. 2009. Integrated analysis of risks of coastal flooding
1004 and cliff erosion under scenarios of long term change. Climatic Change, 95, 249-288.

1005 De Boer, G., 1964. Spurn head, its history and evolution. Transactions of the Institute of
1006 British Geographers 34, 71-89.

1007 De Boer, G., 1981. Spurn Point since 1849, in: Neale, J., Flenley, J. (Eds.), The Quaternary
1008 in Britain. Pergamon Press, Oxford, pp. 206-215.

1009 DEFRA, 2006. Shoreline management plan guidance Volume 1: aims and requirements, 44
1010 pp.

1011 Dickson, M.E., Walkden, M.J.A., Hall, J.W. 2007. Systemic impacts of climate change on an
1012 eroding coastal region over the twenty-first century. Climatic Change 84, 141-166.

1013 Dolan, R., Fester, M.S., Holme, S.J., 1991. Temporal analysis of shoreline recession and
1014 accretion. Journal of Coastal Research 7, 723–744.

1015 Dolata, L.F., Roeckner, E., Behr, H., 1983. Prognostic storm surge simulation with a
1016 combined meteorological/oceanographic model. North Sea Dynamics, in: Sündermann, J.,
1017 Lenz, W. (Eds.), North Sea Dynamics. Springer-Verlag, pp. 266–278.

1018 Donat, M.G., Leckebusch, G.C., Pinto, J.G., Ulbrich, U. 2010. Examination of wind storms
1019 over Central Europe with respect to circulation weather types and NAO phases. International
1020 Journal of Climatology 30, 1289-1300.

1021 Donat, M.G., Renggli, D., Wild, S., Alexander, L.V., Leckebusch, G.C., Ulbrich, U. 2011.
1022 Reanalysis suggests long-term upward trends in European storminess since 1871.
1023 Geophysical Research Letters 38, L14703.

1024 Dossor, J., 1955. The coast of Holderness: the problem of erosion, Proceedings of the
1025 Yorkshire Geological Society 30, 133-145.

1026 Douglas, B. C., Crowell, M., 2000. Long-Term Shoreline Position Prediction and Error
1027 Propagation'. Journal of Coastal Research 16, 145–152.

1028 Dugdale, R. E., Vere, A., 1993. Saving Lincolnshire's beaches. East Midland Geographer
1029 16, 31-32.

1030 Dugdale, R.E., 1980. Nearshore sandbanks and foreshore accretion on the south
1031 Lincolnshire coast. East Midland Geographer 7, 49-63.

1032 East Riding Council, 2004 Coastal processes, pp. 1-4.

1033 El-Kadi, A.K.A., Smithson, P.A., 1992. Atmospheric classifications and synoptic climatology.
1034 Progress in Physical Geography 16, 432-455.

1035 Environment Agency, 2004. Lincshore 2005 to 2010 PAR Volume 1, Strategy For Approval.
1036 Report to Environment Agency, Anglian Region, Peterborough. Halcrow, Swindon.

1037 Environment Agency, 2008. Anglian Coastal Monitoring Programme, Coastal Trend
1038 Analysis, Lincolnshire Subcells 2b-c _Grimsby to Gibraltar Point, 63 pp.

1039 Environment Agency, 2011. Anglian coastal monitoring programme, Lincshore coastal
1040 morphology report 2006-2011, 35 pp.

1041   Eurosion, 2003. Holderness coast, UK, Eurosion case study, DHV group, 22 pp.

1042   Gardline, 2008. Lincolnshire coastline bathymetric/beach survey, summer 2008, survey
1043   report Ref 7689, 19 pp.

1044   Gelfenbaum, G., Kaminsky, G.M. 2010. Large-scale coastal change in the Columbia River
1045   littoral cell : an overview. Marine Geology 273, 1-10.

1046   Goodess, C.M., Palutikof, J.P. 1998. Development of daily rainfall scenarios for southeast
1047   Spain using a circulation-type approach to downscaling. International Journal of Climatology
1048   10, 1051-1083.

1049   Guillén, J., Stive, M.J.F., Capobianco, M., 1999. Shoreline evolution of the Holland coast on
1050   a decadal scale. Earth Surface Processes and Landforms 24, 517-536.

1051   Halcrow and GeoSea Consulting, 1990. The Anglian Sea Defence Management Study -
1052   Phase III. Field Survey Report. Volume 3. Estuary Sediment Trends. GeoSea Consulting,
1053   Cambridge.

1054   Halcrow, 1988. The sea defence management study for the Anglian region, study report Sir
1055   William Halcrow & Partner Ltd, Swindon, UK.

1056   HECAG, 2009. Flamborough Head to Gibraltar Point Shoreline Management Plan, Scott
1057   Wilson, 182 pp.

1058   Hooke, J.M., Bray, M.J. 1995. Coastal groups, littoral cells, policies and plans in the UK.
1059   Area 27, 358-368.

1060   Hooke, J.M., Bray, M.J., Carter, D.J. 1996. Sediment transport analysis as a component of
1061   coastal management – a UK example. Environmental Geology 27, 347-357.

1062   HR Wallingford, 1992. Particulate pollutants in the North Sea. Report SR 292. Hydraulics
1063   Research Wallingford.

1064   HR Wallingford, 2002. Southern North Sea Sediment transport Study Phase, Sediment
1065   Transport Report EX 4526, 93 pp.

1066   Hurrel, J.W., 1995. Decadal trends in the North Atlantic Oscillation: regional temperatures
1067   and precipitation. Science 269, 678-679.

1068   Inman, D.L., Frautschy, J.D., 1966. Littoral processes and the development of shorelines.
1069   Proceedings Coastal Engineering Conference, ASCE, pp. 511-536.

1070 IPCC, 2007. Climate Change 2007: Impacts, Adaptation and Vulnerability. in: M.L. Parry,
1071 O.F. Canzioni, J.P. Palutikof, J.P. van der Linden, C.E. Hanson (eds) Contribution of
1072 Working Group II to the Fourth Assessment Report of the Intergovernmental Panel on
1073 Climate Change. Hanson, Cambridge University Press., pp. 7-22.

1074 Iskander, M.M., Frihy, O.E., EL Ansary, A.E., El Mooty, M.M.A., Nagy, H.M., 2007. Beach
1075 impacts of shore-parallel breakwaters backing offshore submerged ridges, Western
1076 Mediterranean Coast of Egypt. Journal of Environmental Management 85, 1109–1119.

1077 James, L.A., Hodgson, M.E., Ghoshal, S., Megison Latiolais, M., 2012. Geomorphic change
1078 detection using historic maps and DEM differencing: the temporal dimension of geospatial
1079 analysis. Geomorphology 137, 181-198.

1080 Jenkinson, A.F., Collinson, B.P., 1977. An initial climatology of gales over the North Sea.
1081 Synoptic Climatology Branch Memorandum 62, Meteorological Office, Bracknell.

1082 Jones, P.D., Hulme, M., Briffa, K.R., 1993. A comparison of Lamb circulation types with an
1083 objective classification scheme. International Journal of Climatology 13, 655–663.

1084 Kaminsky, G. M., Ruggiero, P., Buijsman, M.C., McCandless, D., Gelfenbaum, G., 2010.
1085 Historical evolution of the Columbia River littoral cell. Marine Geology 273, 96-126.

1086 King, C.A.M., 1964. The character of the offshore zone and its relationship to the foreshore
1087 near Gibraltar Point, Lincolnshire. East Midland Geographer 3, 230-243.

1088 King, C.A.M., 1968. Beach measurements at Gibraltar Point, Lincolnshire. East Midland
1089 Geographer 4, 295-300.

1090 King, C.A.M., 1973. Dynamics of beach accretion in south Lincolnshire, England. In: D.R.
1091 Coates (ed) Coastal Geomorphology. Proceedings of the 3rd Annual Geomorphology
1092 Symposium Series, Binghampton, New York. 73-98.

1093 King, C.A.M., Barnes, F.A., 1964. Changes in the configuration of the inter-tidal beach zone
1094 of part of the Lincolnshire coast since 1951. Zeitschrift für Geomorphologie 8, 105-126.

1095 Krueger, O., Von Storch, H., 2012. The informational value of pressure-based single-station
1096 proxies for storm activity. Journal of Atmospheric and Oceanic Technology 29, 569-580.

1097 Lamb, H.H., 1972. British Isles Weather Types and a Register of the Daily Sequence of
1098 Circulation Patterns, 1861–1971. Geophysical Memoir 116, HMSO, London, 85 pp.

1099   Lee, M., 2001. Coastal defence and the Habitats Directive: predictions of habitat change in
1100   England and Wales. Geographical Journal 167, 39-56.

1101   Leggett, D.J., Lowe, J.P., Cooper, N.J., 1998. Beach evolution on the Southern Sea coast.
1102   Coastal Engineering 26, 2759-2772.

1103   Lim, M., Rosser, N.J., Allison, R.J., Petley, D.N. 2010. Erosional processes in the hard rock
1104   coastal cliffs at Staithes, North Yorkshire. Geomorphology 114, 12-21.

1105   Longley, P.A., Goodchild, M.F., Maquire, D.J., Rhind, D.W., 2005. Geographic Information
1106   Systems and Science 2nd edition, Wiley, London.

1107   Lorenzo, M.N., Taboada, J.J., Gimeno, L. 2008. Links between circulation weather types and
1108   teleconnection patterns and their influence on precipitation patterns in Galicia (NW Spain).
1109   International Journal of Climatology 28, 1493-1505.

1110   McCave, I.N. 1987. Fine sediment sources and sinks around the East Anglian coast. Journal
1111   of the Geological Society of London 144, 149-152.

1112   MAFF 1994. Shoreline Management Plans: a guide for operating authorities. Ministry of
1113   Agriculture, Fisheries and Food and the Welsh Office, London.

1114   Mason, S.J., Hansom, J.D., 1988. Cliff erosion and its contribution to a sediment budget for
1115   part of the Holderness coast, England. Shore and Beach 56 (4), 30-38.

1116   Masselink, G., Hughes, M.G., 2003. Introduction to Coastal Processes and Geomorphology,
1117   Hodder Arnold, Hodder Headline Group, London.

1118   Maune, D.F. 2007. Digital Elevation Model Technologies and Applications: The DEM Users
1119   Manual 2nd edition. American Society for Photogrammetry and Remote Sensing, Bethesda.

1120   May, V., Hansom, J., 2003. Coastal Geomorphology of Great Britain. No. 28 in Geological
1121   Conservation Review Series. Joint Nature Conservation Committee, Peterborough

1122   Moore, T., Morris, K., Blackwell, G., Gibson, S., Stebbing, A., 1998. An expert system for
1123   integrated coastal zone management: a geomorphological case study. Marine Pollution
1124   Bulletin 37, 361-370.

1125   Morton, R.A., and Sallenger, A.H., Jr., 2003. Morphological impacts of extreme storms on
1126   sandy beaches and barriers. Journal of Coastal Research 19, 560-573.

1127   Motyka, J.M., Brampton, A.H., 1993. Coastal mapping-mapping of Littoral cells, Technical
1128   report SR 328, HR Wallingford Ltd, 102 pp.

1129 Neill, S.P., Elliott, A.J., Hashemi, M.R. 2008. A model of interannual variability in beach
1130 levels. Continental Shelf Research 28, 1769-1781.

1131 Newsham, R., Balson, P.S., Tragheim, D.G., Denniss, A.M., 2002. Determination and
1132 prediction of sediment yields from recession of the Holderness Coast, NE England. Journal
1133 of Coastal Conservation 8, 49-54.

1134 O'Connor, M.C., Cooper, J.A.G., Jackson, D.W.T., 2011. Decadal behavior of tidal inlet-
1135 associated beach systems, northwest Ireland in relation to climate forcing. Journal of
1136 Sedimentary Research 81, 38-51.

1137 O'Connor, M.C., Lymberry, G., Cooper, J.A.G., Gault, J., McKenna, J. 2009. Practice versus
1138 policy-led coastal defence management. Marine Policy 33, 923-929.

1139 Orford, J.D., Carter R.W.G., Jennings S.C., Hinton A.C. 1995. Processes and timescales by
1140 which a coastal gravel-dominated barrier responds geomorphologically to sea-level rise:
1141 Story Head barrier, Nova Scotia. Earth Surface Processes and Landforms 20, 21-37.

1142 Orford, J.D., Cooper, A.G., McKenna, J., 1999. Mesoscale temporal changes to foredunes at
1143 Inch Spit, south-west Ireland. Zeitschrift für Geomorphologie 43 (4), 439-461.

1144 Orford, J.D., Pethick, J., 2006. Challenging assumption of future coastal habitat development
1145 around the UK. Earth Surface Processes and Landforms 31, 1625-1642.

1146 Pajak, M.J., Leatherman, S., 2002. The high water line as shoreline indicator. Journal of
1147 Coastal Research 18, 329-337.

1148 Parker, J.A., Foden, D., 2009. High-resolution measurement of a North Sea storm surge.
1149 Journal of Coastal Research SI 56, 1656-1660.

1150 Pethick, J., 2001. Coastal management and sea-level rise. Catena 42, 307-322.

1151 Pethick, J S., 1994. Humber estuary and coast – management issues. Report by: Institute of
1152 Estuarine and Coastal Studies, University of Hull, for Humberside County Council.

1153 Pethick, J.S. 1996. Coastal slope development: temporal and spatial periodicity in the
1154 Holderness cliff recession. In Anderson, M.G., Brooks, S.M. (eds). Advances in Hillslope
1155 Processes. Wiley, Chichester, vol. 2, 897-917.

1156 Posford Duvivier, 1992. Easington Coast Protection. Report to Holderness Borough Council.
1157 Posford Duvivier, Peterborough.

1158   Pringle, A.W., 1985. Holderness coast erosion and the significance of ords. Earth Surface
1159   Processes and Landforms 10, 107-124.

1160   Pye, K., 1983. Coastal dunes. Progress in Physical Geography, 31, pp 249-266.

1161   Pye, K., 1995. Controls on long-term saltmarsh accretion and erosion in the Wash, Eastern
1162   England. Journal of Coastal Research 11, 337–356.

1163   Pye, K., Blott, S.J., 2008. Decadal-scale variation in dune erosion and accretion rates: an
1164   investigation of the significance of changing storm tide frequency and magnitude on the
1165   Sefton coast, UK. Geomorphology 102, 652-666.

1166   Pye, K., Blott, S.J., 2010. Aldbrough gas storage project: geomorphological assessment of
1167   impact of proposed cliff protection works on adjoining areas, report no EX1214, 16 pp.

1168   Pye, K., Saye, S.E., Blott, S.J., 2007. Sand Dune Processes and Management for Flood and
1169   Coastal Defence. Part 1: Project Overview and Recommendations. RandD Technical Report
1170   FD1302/TR/1, Department for Environment, Food and Rural Affairs, London, 35pp.

1171   Quinn, J.D., Philip, L.K., Murphy, W., 2009. Understanding the recession of the Holderness
1172   Coast, east Yorkshire, UK: a new presentation of temporal and spatial patterns. Quarterly
1173   Journal of Engineering Geology and Hydrogeology 42, 165-178.

1174   Reid, C. 1885. Memoirs of the Geological Survey of England and Wales. The Geology of
1175   Holderness, and the Adjoining Parts of Yorkshire and Lincolnshire. HMSO, London.

1176   Robinson, A.H.W., 1964. The inshore waters, sediment supply and coastal changes of part
1177   of Lincolnshire. East Midland Geographer 3, 22,307-22,321.

1178   Robinson, A.H.W., 1968. The use of sea bed drifter in coastal studies with particular
1179   reference to the Humber. Zeitschrift für Geomorphologie 7, 1-23.

1180   Robinson, D.N., 1953. The storm surge 31st January-1st February, 1953 and the associated
1181   meterological and tidal conditions. Geography 38, 134-141.

1182   Robinson D.N., 1984. The Saltfleetby-Theddlethorpe coastline. Transactions of the
1183   Lincolnshire Naturalists' Union 21, 1–12.

1184   Ruessink, B.G., Jeuken, M.C.J.L.L., 2002. Dunefoot dynamics along the Dutch coast. Earth
1185   Surface Processes and Landforms 2, 1043-1056.

1186   Ruggiero, P., Kaminsky, G.M., Gelfenbaum, G., Voigt, B. 2005. Seasonal to interannual
1187   morphodynamics along a high-energy dissipative littoral cell. Journal of Coastal Research
1188   21, 553-578.

1189   Saye, S.E., van der Wal, D., Pye, K., Blott, S.J. 2005. Beach–dune morphological
1190   relationships and erosion/accretion: an investigation at five sites in England and Wales using
1191   LIDAR data. Geomorphology 72, 128–55.

1192   Schans, H., Möller, I., Spencer, T., 2001. Large-scale classification of the East Anglian
1193   coastline, UK. Coastal Dynamics '01. Proceedings of the 4th International Conference on
1194   Coastal Dynamics, Lund, Sweden. ASCE, 683 – 692.

1195   Scott Wilson, 2009. Flamborough Head to Gibraltar Point Shoreline Management Plan.
1196   Appendix C - Assessment of Coastal Behaviour and Baseline Scenarios. Scott Wilson,
1197   Basingstoke.

1198   Steers, J.A., 1946. The Coastline of England and Wales. Cambridge University Press,
1199   Cambridge. 644 pp.

1200   Steers, J.A., 1966. Holderness, Lincolnshire and the Fenland, in: Steers, J.A. (Eds) The
1201   coastline of England and Wales. Cambridge University Press, Cambridge, pp. 406-440.

1202   Steers, J.A., Stoddart, D.R., Bayliss-Smith, T.P., Spencer, T., Durbridge, P.M. 1979. The
1203   storm surge of 11 January 1978 on the east coast of England. The Geographical Journal
1204   145, 192-205.

1205   Stockdon, H.F., Sallenger Jr., A.H., Holman, R.A., Howd, P.A., 2007. A simple model for the
1206   spatially-variable coastal response to hurricanes. Marine Geology 238, 1–20.

1207   Swinnerton, H.H., Kent, P.E. 1949. The Geology of Lincolnshire. Lincolnshire Naturalists
1208   Union, Lincoln.

1209   Thieler, E. R., Danforth, W.W., 1994. Historical shoreline mapping (I): Improving technique
1210   and reducing position errors. Journal of Coastal Research 19 (3), 549-563.

1211   Thieler, E.R., Himmelstoss, E.A., Zichichi, J.L., Ergul, A., 2009, Digital Shoreline Analysis
1212   System (DSAS) version 4.0—An ArcGIS extension for calculating shoreline change: U.S.
1213   Geological   Survey   Open-File   Report   2008-1278.   Available   online   at
1214   http://pubs.usgs.gov/of/2008/1278/.

1215 Thomas, T., Phillips, M.R., Williams, A.T., Jenkins, R.E., 2011. A multi-century record of
1216 linked nearshore and coastal change. Earth Surface Processes and Landforms 36, 995-
1217 1006.

1218 Tonk, A.M., 2000. Monitoring changes in coastal morphology. North Lincolnshire, report to
1219 Environmnent Agency, 44 pp.

1220 Townend, I., Whitehead, P. 2003. A preliminary net sediment budget for the Humber
1221 Estuary. The Science of the Total Environment 314-316, 755-767.

1222 Townend, I., Wang, Z.B., Rees, J.G. 2007. Millenial to annual volume changes in the
1223 Humber Estuary. Proceedings: Mathematical, Physical and Engineering Sciences 463, 837-
1224 854.

1225 Trigo, R.M., Dacamara, C.C. 2000. Circulation weather types and their influence on the
1226 precipitation regime in Portugal. International Journal of Climatology 20, 1559-1581.

1227 Tsimplis, M.N., Woolf, D.K., Osborn, T.J., Wakelin, S., Wolf, J., Flather, R., Shaw, A.G.P.,
1228 Woodworth, P., Challenor, P., Blackman, D., Pert, F., Yan, Z., Jevrejeva, S., 2005. Towards
1229 a vulnerability assessment of the UK and northern European coasts: the role of regional
1230 climate variability. Philosophical Transactions of the Royal Society 363, 1329–1358.

1231 Valentin, H., 1971. Land loss at Holderness, in Steers, J.A. (Eds.), Applied Coastal
1232 Geomorphology, Macmillan, London, pp. 116-137.

1233 Valentin, H., 1954. Der landverlust in Holderness, Ostengland, von 1852-1952. Die Erde 6,
1234 296-315.

1235 van Houwelingen, S.T., Masselink, G., Bullard, J. 2006. Characteristics and dynamics of
1236 multiple intertidal bars, north Lincolnshire, England. Earth Surface Processes and
1237 Landforms, 31, 428-443.

1238 van Houwelingen, S.T., Masselink, G., Bullard, J. 2008. Dynamics of multiple intertidal bars
1239 over semi-diurnal and lunar tidal cycles, North Lincolnshire, England. Earth Surface
1240 Processes and Landforms, 33, 1473-1490.

1241 Vasseur, B., Héquette, A., 2000. Storm surges and erosion of coastal dunes between 1957
1242 and 1988 near Dunkerque (France), southwestern North Sea. Coastal and Estuary
1243 Environments. Geological Society. Sp. Publ., 175, 99-107.

1244 Vespremeanu-Stroe, A., Constantinescu, S., Tătui,F., Giosan, L., 2007. Multi-decadal
1245 evolution and North Atlantic Oscillation influences on the dynamics of the Danube delta
1246 shoreline. Journal of Coastal Research SI 50, 157-162.

1247 Wang, X.L., Zwiers, F.W., Swail, V.R., Feng, Y. 2009. Trends and variability of storminess in
1248 the Northeast Atlantic region, 1874-2007. Climate Dynamics 33, 1179-1195.

1249 Wang, X.L., Wan, H., Zwiers, F.W., Swail, V.R., Compo, G.P., Allan, R.J., Vose, R.S.,
1250 Jourdain, S., Yin, X. 2011. Trends and low-frequency variability of storminess over western
1251 Europe, 1878-2007. Climate Dynamics 37, 2355-2371.

1252 Webster, P. J., Holland, G. J., Curry, J. A., Chang, H-R., 2005. Changes in tropical cyclone
1253 number, duration and intensity in a warming environment. Science 309, 1844-1846.

1254 Wilby, R.L., Dalgleish, H. Y., Foster, I.D.L., 1997. The impact of weather patterns on historic
1255 and contemporary catchment sediment yields. Earth Surface processes and landforms 22,
1256 353–363.

1257 Woodworth, P.L., Teferle, F.N., Bingley, R.M., Shennan, I., Williams, S.D.P., 2009. Trends in
1258 UK mean sea level revisited, Geophysical Journal International 176, 19-30.

1259 Woolf, D.K., Cotton, P.D., Challenor, P.G., 2003. Measurements of the offshore wave
1260 climate around the British Isles by satellite altimeter, Philosophical Transactions of the Royal
1261 Society 361, 27-31.

1262 Woolf, D.K., Challenor, P.G., Cotton,P.D., 2002. The variability and predictability of the North
1263 Atlantic wave climate. Journal of Geophysical Research 107 (C10), 3145-3159.

1264 Zhang, K., Douglas, B. C. and Leatherman, S. P., 2001. Beach Erosion Potential for Severe
1265 Nor'easters. Journal of Coastal Research 17, 309-321.

1266

1267
1268

Table 1　　Tidal levels and tidal ranges, expressed in metres above Ordnance Datum Newlyn (ODN). Tide level for East Riding coast derived from Spurn Head data taken from Admiralty Tide Tables (Admiralty, 2009) and from tidal statistics at Skegness derived from POLTIPS 3 software developed by the National Oceanography Centre Liverpool (NOC, 2009). Abbreviations: HAT – Highest Astronomical Tide; MHWS – Mean High Water Spring; MHWN – Mean High Water Neap; MLWN – Mean Low Water Neap; MLWS – Mean Low Water Spring; LAT – Lowest Astronomical Tide.

Table 2　　Summary characteristics of the six areas of interest (AOIs) examined in detail. Profile labels correspond to original data sources (East Riding Yorkshire Council or UK Environmental Agency).

Table 3　　Summary of map and aerial photograph source documents and characteristics for each AOI. Abbreviations: B&W – black and white, EA – UK Environment Agency. For AOI information, see Table 2.

Table 4.　　Correlation table between morphology parameters and forcing factors at the sandy beaches between surveys (AOIs 2, 3, 5): CI - Relative coastline position, C_{HAT} - HAT level position, V_B - sand volume in backshore, V_F – sand volume in foreshore, SS - storm surge. Correlation values above ±0.5 are in bold.

Table 5　　Estimated inter-survey and cumulative sediment volume changes for the periods 1994/97-1999, 1999-2005, 2005-2008, 2008-2010, by shore units (see Fig. 2). Positive values indicate accretion, and negative values erosion.

Table 6　　 Estimated inter-survey and cumulative volumetric changes for the periods 1994/97-1999, 1999-2005, 2005-2008, 2008-2010, by nearshore sub-unit (see Fig. 2). Positive values indicate accretion, and negative values erosion.

Figure Captions

Figure 1   Inset: Distribution of coastal cells around the coast of England and Wales, Main figure: Boundaries and major features of sediment cell 2, east coast of England.

Figure 2   Schematic diagram defining the limits of the backshore, foreshore and nearshore zones used to calculate sediment budget.

Figure 3   Changes in coastline position within sediment cell 2 from Flamborough Head (P1) to Gibraltar Point (L2A7) over the period from mid-1990 to 2010 (longshore spacing not to scale). Coastline represented by the cliff base (East Riding; P1-121) or HAT (Spurn Head; P122-P134 and Lincolnshire coast; L1A1-L2A7). Zero line represents the initial survey in 1994/96/97 along East Riding coast and 1997 along Lincolnshire coast. Profile labels correspond to original data sources (East Riding Yorkshire Council or UK Environmental Agency). Notation of AOIs is indicated - see Table 2. Profiles perpendicular to coastal defences and lagoons are excluded (P3-P7, P42-P44, P90-P93, P115-P118, P133, L2A4).

Figure 4   Position of coastlines from 1854/91 to date for: A) Easington, B) North Spurn Head superimposed on ortho-photographs in 2010. Evolution of the coastline position (line curve) relative to OS maps in 1854 at C) Easington, D) North Spurn Head. Dashed line corresponds to mean long-term rate of shoreline evolution (1854-2010).

Figure 5   Position of coastlines from 1891 to date for: A) Donna Nook, B) Saltfeetby, C) Theddlethorpe superimposed on ortho-photographs in 2010. Evolution of the coastline position (line curve) relative to OS maps in 1891 at D) Donna Nook, F) Theddlethorpe and in 1994 at E) Saltfeetby. Dashed line corresponds to mean long-term rate of shoreline evolution over the timeframe.

Figure 6   Position of coastline from 1891 to date for Skegness: A) North, B) South.

Figure 7   Annual frequency of storm surge and coastline evolution between 1994/97-2010 at: A) Easington, B) North Spurn Head, C) Donna Nook, D) Saltfleetby, E) Theddlethorpe, and F) Skegness.

Figure 8   Time series of JWT annual strong wind events and storm surge measured at tide gauges between 1994 and 2010

1333	Figure 9	Time series of JWT annual storm wind events between 1871-2010 for A) onshore winds, B) alongshore winds and C) offshore winds. In each case daily frequency and 5-year running mean are shown. Note: vertical scales differ.
1337	Figure 10	Time series of: A) JWT annual strong onshore wind events between 1871-2010, B) winter NAO values (Dec-March) between 1850-2010 and coastline evolution at C) Easington, D) North Spurn Head, E) Donna Nook, and F) Theddlethorpe from 1854/91 to 2010.
1341	Figure 11	Long-term morphodynamic trends in the coastal cell along East Riding and Lincolnshire coasts at the studied AOIs since 1850/81.

1343

Response to Reviewers

Thank you for the editorial comments.

We have accepted all the minor typos and clarified minor points where requested and cross-checked the references and citations.

We have added in appropriate references by Swinnerton & Kent (1949) and Steers et al. (1979) where suggested.

As far as we can ascertain, most of the work by King and Barnes on the Lincolnshire coast is in the far south, around Gibraltar Point (Ed. comment on line 581). It was remiss of us not to acknowledge some of this in the paper, but our point that the northern Lincolnshire coast (Donna Nook to Skegness) has been relatively unstudied is valid. We have therefore not added refs to King and Barnes around line 581, but have instead rephrased lines 682-686 to acknowledge their contribution.

We have expanded the conclusion to highlight general points of wider interest from the study.

Table 1

1   Table 1   Tidal levels and tidal ranges, expressed in metres above Ordnance Datum

2   Newlyn (ODN). Tide level for East Riding coast derived from Spurn Head data taken from

3   Admiralty Tide Tables (Admiralty, 2009) and from tidal statistics at Skegness derived from

4   POLTIPS 3 software developed by the National Oceanography Centre Liverpool (NOC,

5   2009). Abbreviations: HAT – Highest Astronomical Tide; MHWS – Mean High Water Spring;

6   MHWN – Mean High Water Neap; MLWN – Mean Low Water Neap; MLWS – Mean Low

7   Water Spring; LAT – Lowest Astronomical Tide.

8

Coastal region	HAT	MHWS	MHWN	MLWN	MLWS	LAT
East Riding	3.80	3.00	1.60	-1.20	-2.70	-3.70
Lincolnshire	4.09	3.20	1.70	-1.09	-2.59	-3.57

9

10

11

Table 2

1 Table 2 Summary characteristics of the six areas of interest (AOIs) examined in detail.

2   Profile labels correspond to original data sources (East Riding Yorkshire

3   Council or UK Environmental Agency).

AOI	Sediment cell	Location	Geomorphology		Alongshore length (km)	Profiles	No. Transects used in DSAS
			Landward features	Near/ Offshore features			
1	2a	Easington (E)	Clay strata and cliff from 9m to 5.3m high		5.2	P113-P121	43
2	2a	North Spurn Head (NSP)	Sand spit of c. 5km length	Glacial ridge of clay banks	1.4	P122-P124	17
3	2b	Donna Nook (DN)	Coastal dunes and clay embankment	Sand banks of morainic material	5.1	L1A1-L1A6	34
4	2c	Saltfleet-by (SA)	Saltmarsh	Sand banks of morainic material	4.1	L2E1-L2E4	30
5	2c	Theddle-thorpe (TH)	Coastal dunes	Sand banks of morainic material	4.9	L2E5-L2D1	44
6	2c	Skegness (SK)	Engineering defences Erosive clay strata		5	L2B6-L2A3	57

4

Table 3

1   Table 3   Summary of map and aerial photograph source documents and
2   characteristics for each AOI. Abbreviations: B&W – black and white. For AOI
3   information, see Table 2.

4

AOI	Year	Type	Source	Document type	Scale
EA, NSH	1854, 1890, 1951	OS map	Edina	Geo-referenced	1:10 560
DN, SA, TH, SK	1891, 1910, 1951	OS map	Edina	Geo-referenced	1:10 560
EA, NSH	1966	B&W Aerial photo	English Heritage and EA	Scan from print photograph (600dpi)	1:7 500
EA, NSH	2005, 2008, 2010	Colour Aerial photo	East Riding Yorkshire Council	Digital ortho-georeferenced	1:5 000
DN	1970	B&W Aerial photo	English Heritage	Scan from print photograph (600dpi)	1:7 500
TH	1953, 1966, 1976, 1983	B&W Aerial photo	Natural England	Scan from print photograph (600dpi)	1:7 500
DN, SF, TH, SK	1994, 1999	B&W Aerial photo	Environment Agency	Scan from print photograph (600dpi)	1:5 000
DN, SF, TH, SK	2005, 2008, 2010	Colour Aerial photo	Environment Agency	Digital ortho-georeferenced	1:5 000

5

6

Table 4

1   Table 4.   Correlation table between morphology parameters and forcing factors at the

2   sandy beaches between surveys (AOIs 2, 3, 5): CI - Relative coastline position, C_{HAT} - HAT

3   level position, V_B - sand volume in backshore, V_F – sand volume in foreshore, SS - storm

4   surge. Correlation values above ±0.5 are in bold.

5

	CI	C_{HAT}	V_B	V_F	SS
CI		-0.112	**0.538**	-0.011	**0.733**
C_{HAT}			0.073	0.072	-0.019
V_B				**-0.528**	**0.656**
V_F					**-0.508**

6

7

8

Table 5

1   Table 5   Estimated inter-survey and cumulative sediment volume changes in

2   backshore and foreshore units (see Figure 2). Positive values indicate

3   accretion, and negative values erosion.

AOI	Period	Inter-survey change (m^3 x 10^3)			Cumulative change (m^3 x 10^3)		
		Backshore	Foreshore	Total	Backshore	Foreshore	Total
Easington	1997/1999	-161.3	-20.8	-182.1	-161.3	-20.8	-182.1
	1999/2005	-175.9	-60.0	-235.9	-337.2	-60.0	-397.2
	2005/2008	-367.8	-59.3	-427.1	-705.0	-59.3	-764.3
	2008/2010	-127.2	-37.8	-165.0	-832.3	-37.8	-870.0
	Rates of change (m^3 $year^{-1}$)				-64.0	-2.9	-66.9
North Spurn Head	1997/1999	8.4	-1.9	6.5	8.4	-1.9	6.5
	1999/2005	-11.0	0.8	-10.2	-2.7	-1.9	-4.5
	2005/2008	-13.0	-22.8	-35.9	-15.7	-1.9	-17.6
	2008/2010	-1.4	-0.3	-1.7	-17.1	-1.9	-19.0
	Rates of change (m^3 $year^{-1}$)				-1.3	-0.1	-1.5
Donna Nook	1994/1999	96.3	91.2	187.5	96.3	91.2	187.5
	1999/2005	497.5	-109.0	388.6	593.8	-17.7	576.1
	2005/2008	-132.1	-105.3	-237.4	461.7	-123.0	338.6
	2008/2010	26.5	432.7	459.2	488.1	309.7	797.8
	Rates of change (m^3 $year^{-1}$)				30.5	19.4	49.9
Saltfleetby	1994/1999	349.5	129.6	479.1	349.5	129.6	479.1
	1999/2005	66.4	173.7	240.1	415.9	303.3	719.2
	2005/2008	-21.2	-26.6	-47.8	394.7	276.7	671.4
	2008/2010	-24.2	12.7	-11.5	370.6	289.4	659.9
	Rates of change (m^3 $year^{-1}$)				23.2	18.1	41.2
Theddlethorpe	1994/1999	681.8	-435.4	246.4	681.8	-435.4	246.4
	1999/2005	276.0	358.2	634.1	957.8	-77.3	880.5
	2005/2008	423.0	-330.3	92.7	1380.8	-407.6	973.3
	2008/2010	-372.1	160.6	-211.5	1008.8	-247.0	761.8
	Rates of change (m^3 $year^{-1}$)				63.0	-15.4	47.6
Skegness	1994/1999	153.1	-51.6	101.5	153.1	-51.6	101.5
	1999/2005	48.6	107.6	156.2	201.7	56.0	257.7
	2005/2008	-7.8	65.1	57.3	193.8	121.2	315.0
	2008/2010	67.9	-38.3	29.6	261.7	82.9	344.6
	Rates of change (m^3 $year^{-1}$)				16.4	5.2	21.5

4

5

Table 6

1   Table 6   Estimated inter-survey and cumulative volumetric changes by nearshore sub-

2   unit (see Figure 2). Positive values indicate accretion, and negative values erosion.

3

		Nearshore inter-survey change $(m^3 \times 10^3)$			Nearshore cumulative change $(m^3\ 10^3)$		
	Period	Sub-unit1	Sub-unit2	Total	Sub-unit1	Sub-unit2	Total
Donna Nook	1999/2005	219.5	112.8	332.3	219.5	112.8	332.3
	2005/2008	-187.6	-73.0	-260.6	31.9	39.8	71.8
	Rates of change (m^3 year$^{-1)}$)				3.5	4.4	8.0
Saltfleetby	1999/2005	140.3	-223.4	-83.1	140.3	-223.4	-83.1
	2005/2008	-3.9	30.2	26.3	136.3	-193.1	-56.8
	Rates of change (m^3 year^{-1})				15.1	-21.5	-6.3
Theddlethorpe	1999/2005	-286.3	128.2	-158.1	-286.3	128.2	-158.1
	2005/2008	-14.3	70.8	56.4	-572.7	256.5	-316.2
	Rates of change (m^3 year^{-1})				-63.6	28.5	-35.1
Skegness	1999/2005	116.7	12.9	129.6	116.7	12.9	129.6
	2005/2008	25.3	-34.2	-8.9	142.0	-21.3	120.7
	Rates of change (m^3 year^{-1})				15.8	-2.4	13.4

4

5

Figure 2

Figure 3

Figure 5
[Click here to download high resolution image](#)

Figure 11
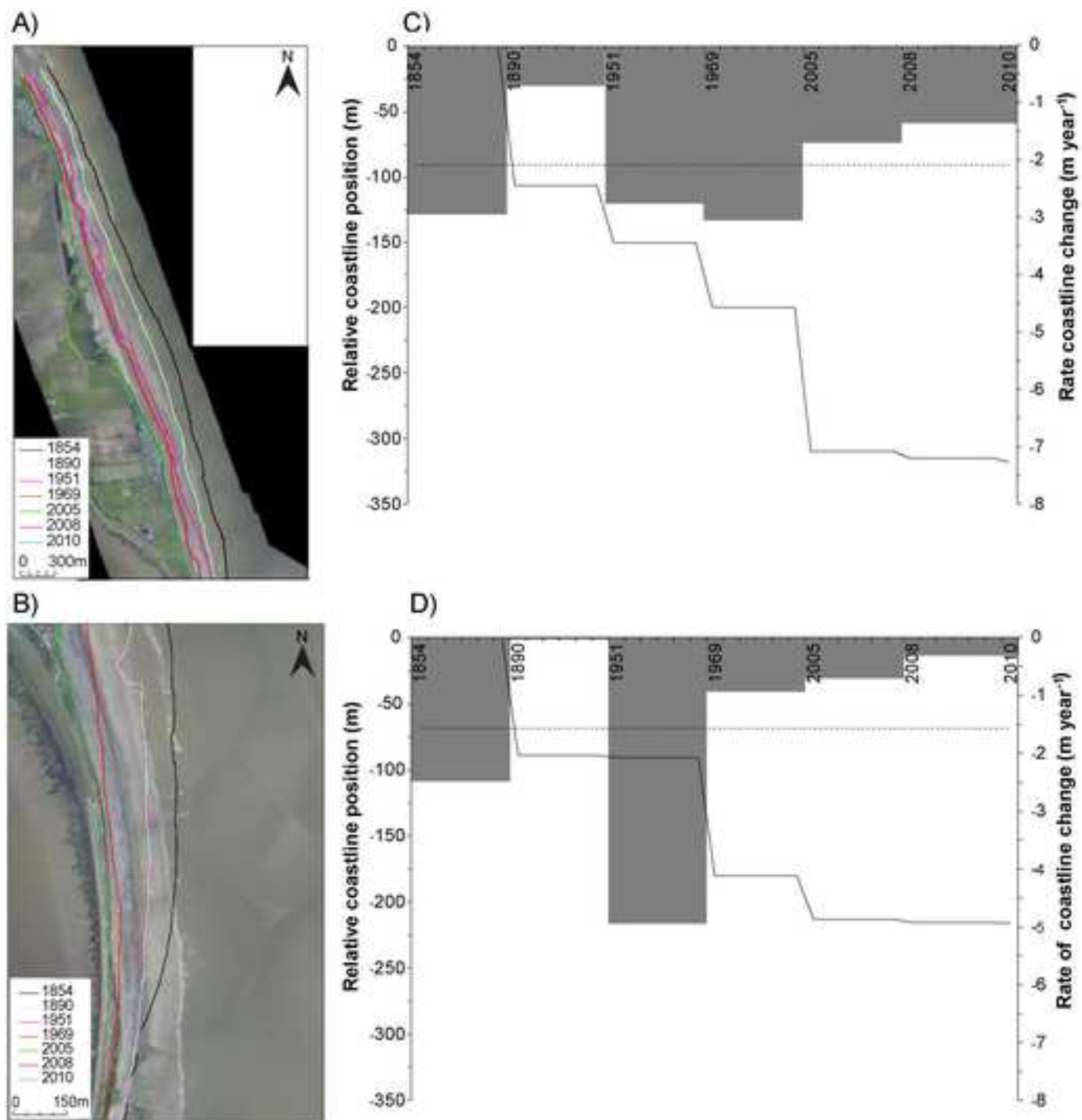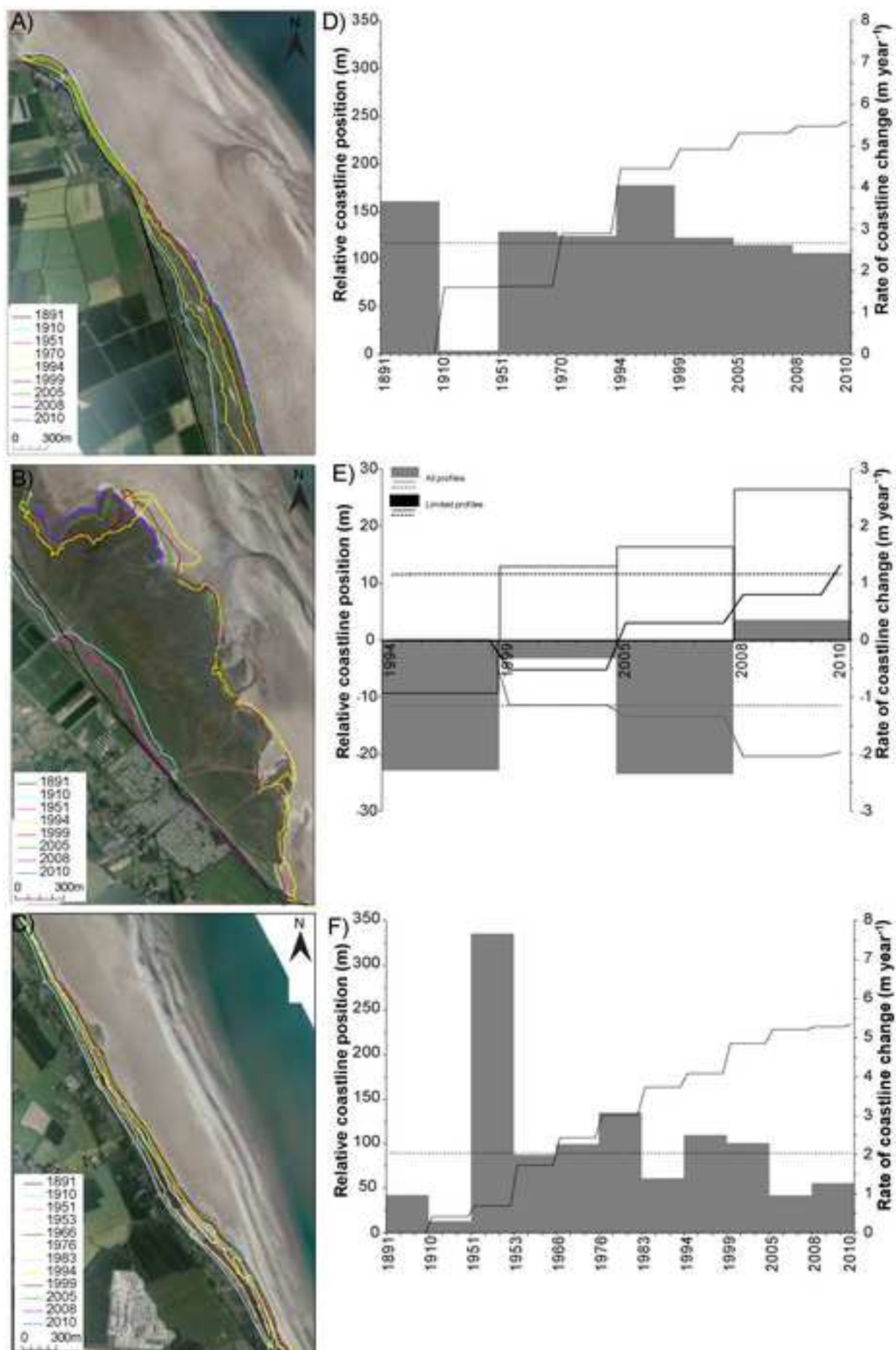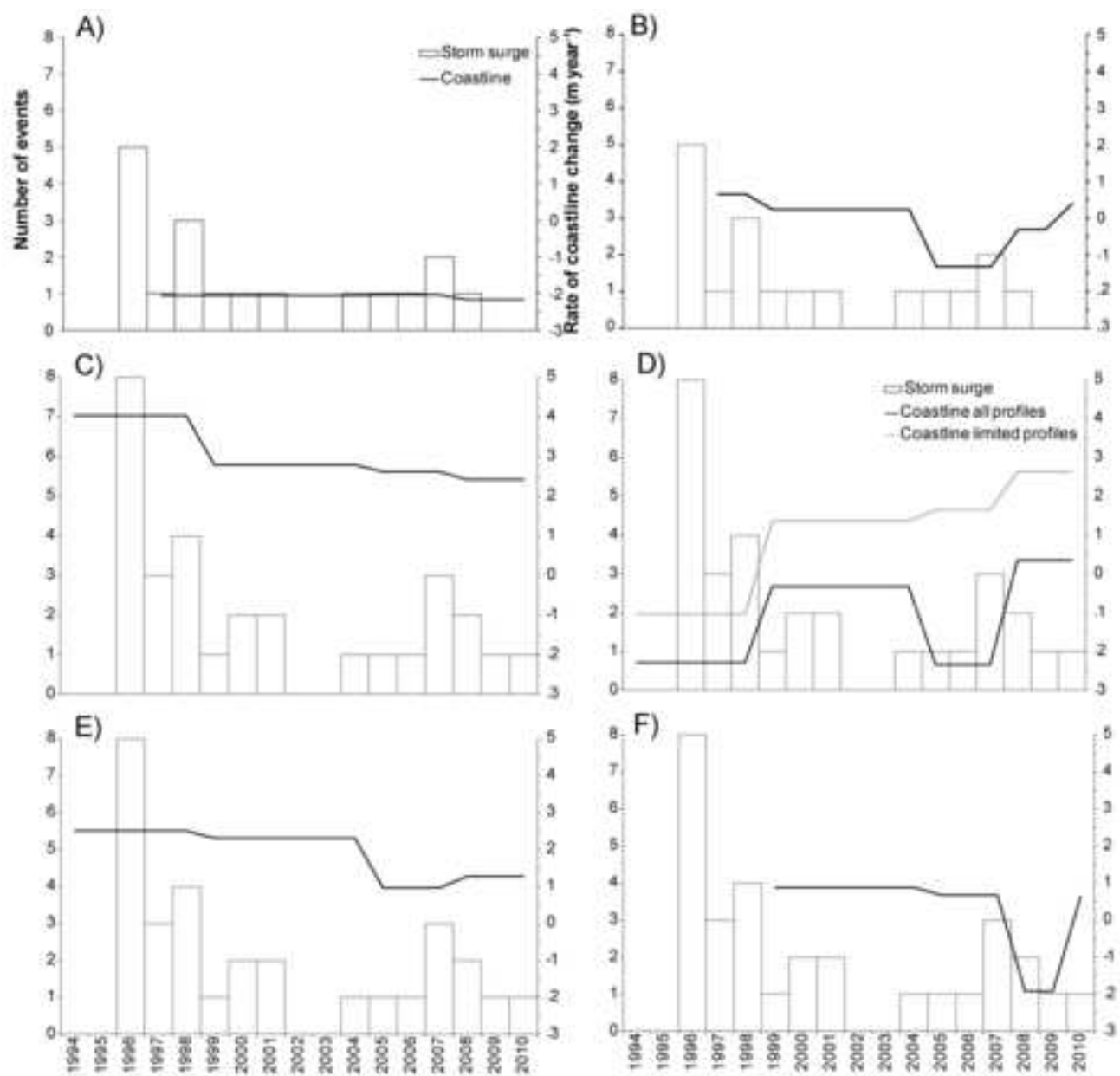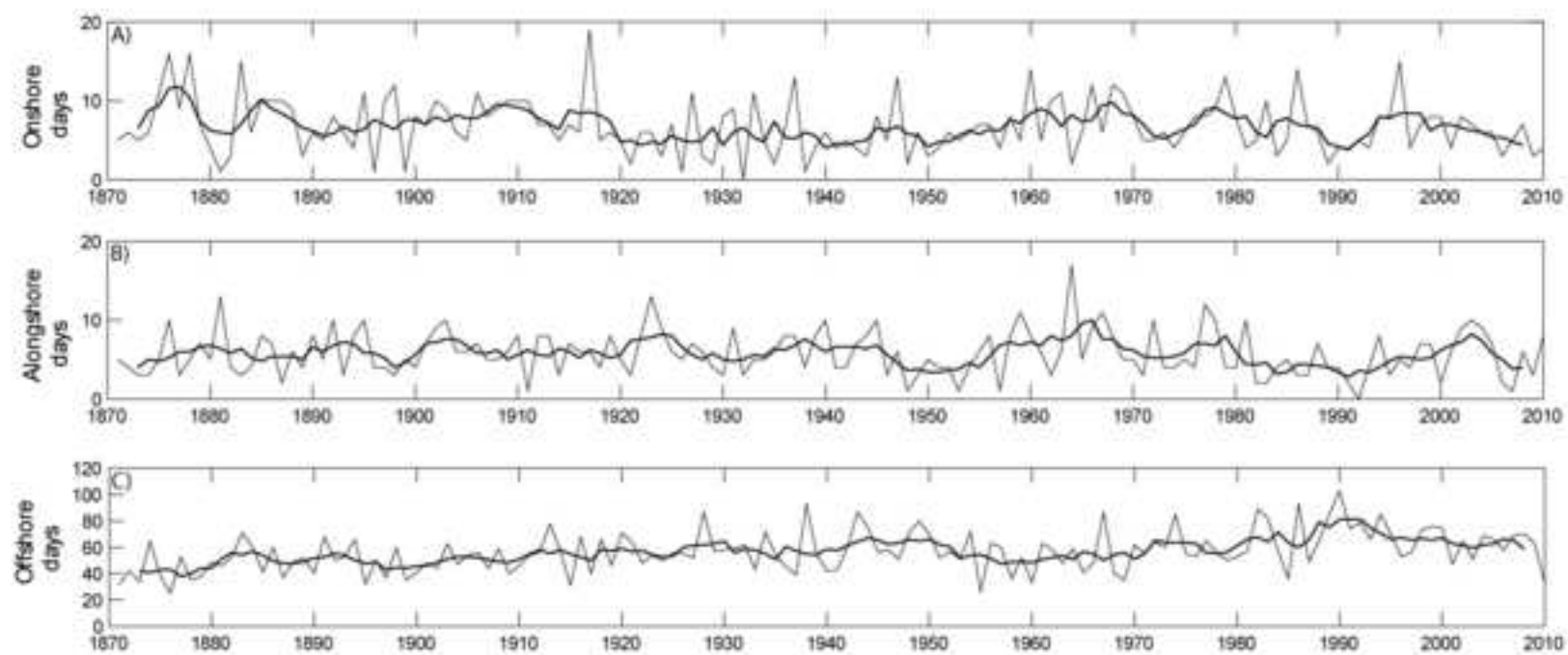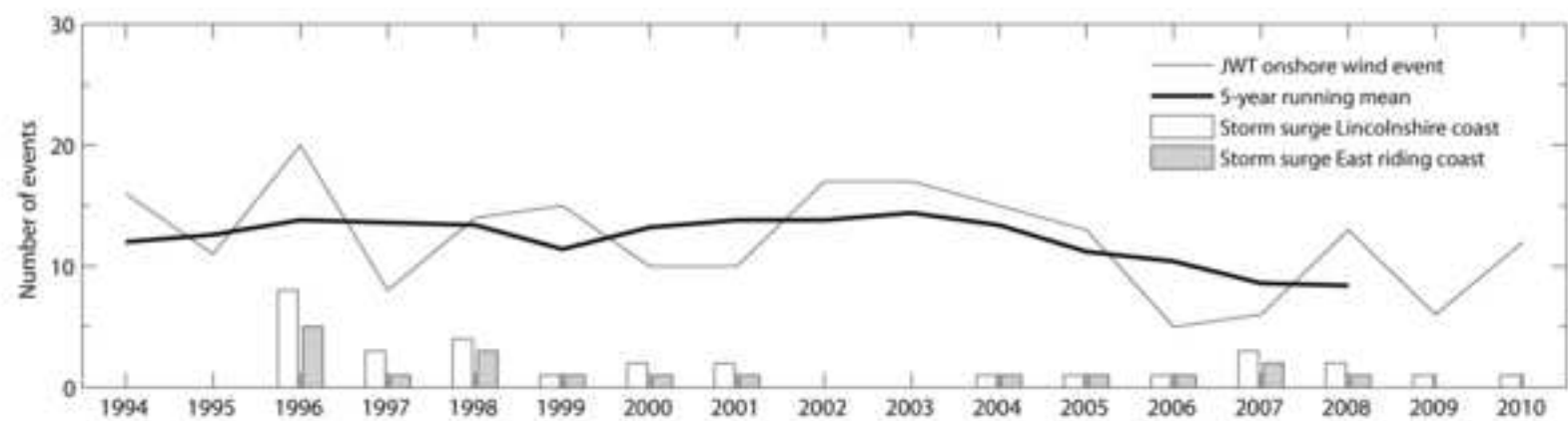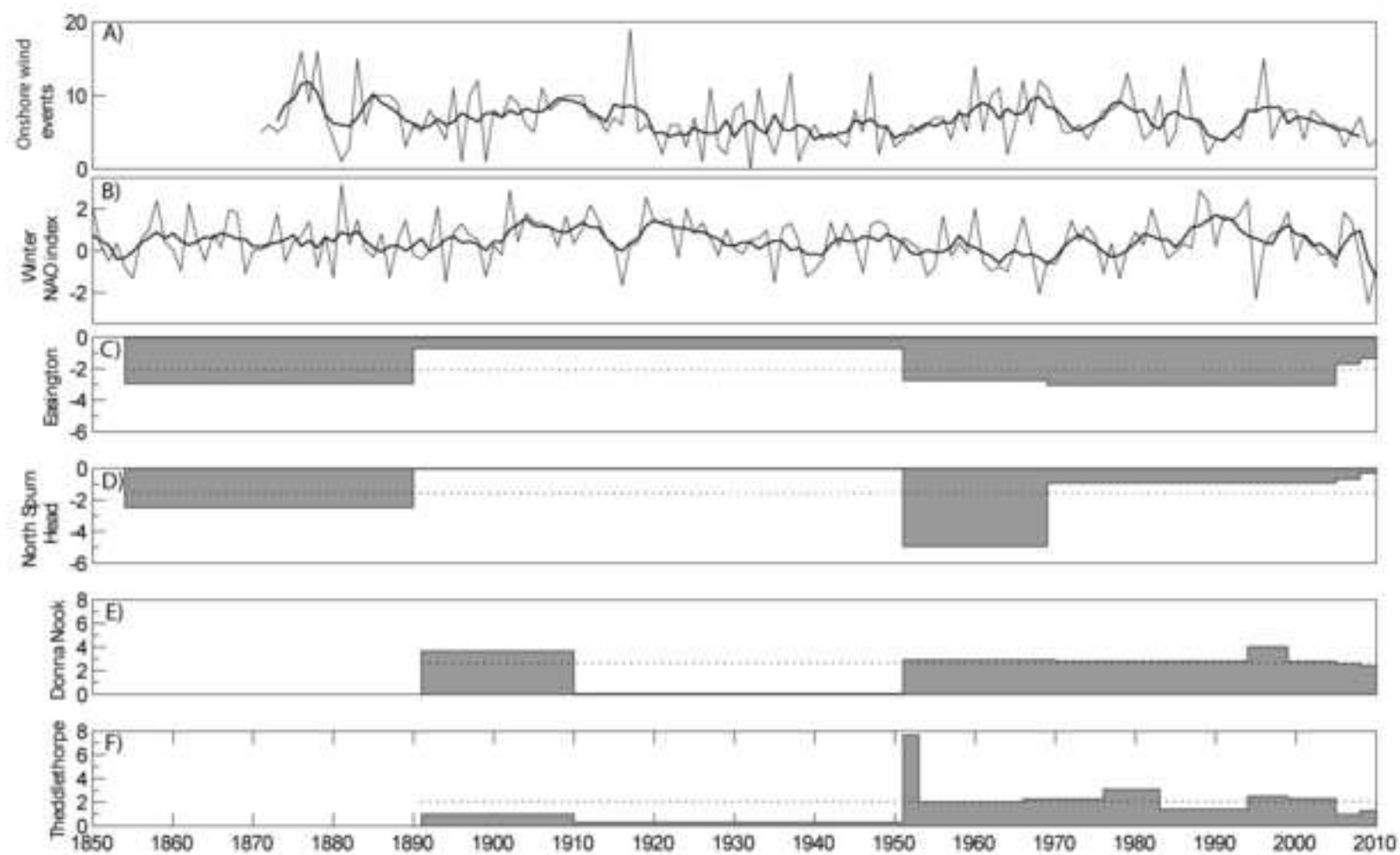[Click here to download high resolution image](#)